2014

Elucidating the reactivity and structure-property relationships of benzobisoxazoles for the rational design of conjugated materials

Brian Charles Tlach
Iowa State University

Elucidating the reactivity and structure-property relationships of benzobisoxazoles for the rational design of conjugated materials

by

Brian C. Tlach

A dissertation submitted to the graduate faculty

in partial fulfillment of the requirements for the degree of

DOCTOR OF PHILOSOPHY

Major: Organic Chemistry

Program of Study Committee:
Malika Jeffries-EL, Major Professor
George Kraus
Javier Vela
Arthur Winter
Sumit Chaudhary

Iowa State University

Ames, Iowa

2014

TABLE OF CONTENTS

ABSTRACT

Benzobisoxazoles are rigid electron deficient aromatic heterocycles with good thermal, environmental, and chemical stability. Much work has been done on the design of new electron rich conjugated materials for organic semiconductors, however, the research on modification or development of electron deficient aromatics has been limited. Our group has developed a mild synthesis of non-halogenated and 4,8-dihalogenated benzobisoxazoles from cheap and readily available starting materials to use as electron deficient moieties in organic semiconductors. Using the halogens as synthetic handles to further functionalize the benzobisoxazoles, the optical, electronic, and physical properties of the system are tuned through inductive, resonance, and/or cross-conjugation effects. Likewise, the halogens can be utilized for direct polymerization through the 4,8-axis which creates polymers with much different properties than those synthesized through the traditional 2,6-axis. These new benzobisoxazoles can be polymerized or functionalized with ease at either axis producing materials with a wide-range of properties from wide band gap, highly fluorescent materials for blue organic light emitting diodes to narrow band gap, broad absorbing materials for organic photovoltaics. In order to expedite the search for new materials, we have used Density functional tTheory (DFT) and time-dependent DFT (TDDFT) to model properties and focus our efforts on the structures with the most desirable properties. This has led us to develop and investigate the properties of a diverse set of benzobisoxazole materials which can be efficiently prepared from common synthetic intermediates for organic semiconducting applications.

CHAPTER 1

GENERAL INTRODUCTION

1.1 Dissertation Organization

This dissertation follows the work completed by the author in the Jeffries-EL research lab over the last six years. The focus of this work is the influence of structural modification on the optical, electronic, and physical properties of conjugated small molecules and polymers. An emphasis of this work is on benzobisoxazole-based systems and the elucidation of structure-property relationships to assist in the rational design of conjugated small molecules and polymers for organic semiconductor devices. Chapter 1 is a general introduction to organic semiconductors and how structural modification can alter and optimize the optical, electron, and physical properties of conjugated materials to improve performance in organic semiconductor applications. An overview of the synthesis and properties of structurally diverse benzobisoxazole-based materials is provided. Finally, a brief overview of computational modeling of conjugated systems is also discussed and its role in reducing cost and time in the design of organic semiconductor materials.

Chapter 2 is a paper that was published in the *Journal of Organic Chemistry* in 2011that details the synthesis, characterization, and structure-property study within a series of alkynyl-substituted benzobisoxazole small molecules and polymers. The author of this dissertation completed a majority of the synthetic work and characterization of the molecules, except for the synthesis of co-monomer 3,4-didodecylthiophene dicarboxaldehyde

which was performed by Achala Bhuwalka. The author of this dissertation also performed a majority of the characterization of the materials. The author of this dissertation wrote the entire experimental section and supplementary information sections along with contributions to the introduction and results and discussion. Dr. Aimée Tomlinson provided the computational modeling of the benzobisoxazole compounds and made major contributions to introduction and results and discussion. Ultraviolet photoelectron spectroscopy was performed by Atta Gueye, Dr. Elena Sheina, and Dr. Christopher Brown of Plextronics, Inc. Dr. Malika Jeffries-EL wrote the remainder of the paper.

Chapter 3 is a paper that was published in the *Journal of Organic Chemistry* in 2013 that details the synthesis, characterization, and structure property study of a series of diaryl and tetraaryl benzobisoxazole small molecules. This paper enables a deeper understanding of the role of axis choice and cross conjugation in benzobisoxazole systems. The author of this dissertation performed all of the synthetic work and performed a majority of the characterization of the materials. The author of this dissertation also wrote the experimental section and supplementary information along with contributions to the introduction and the discussion and results. Dana Drochner developed the initial methodology for the synthesis of 4-dodecyl-1-(triethoxymethyl)benzene. Dr. Aimée Tomlinson, with assistance from Alden Ryno, provided the computational modeling of the benzobisoxazole compounds. Dr Aimée Tomlinson also made major contributions to the introduction and results and discussion. Ultraviolet photoelectron spectroscopy on the materials was performed by Atta Gueye, Dr. Elena Sheina, and Dr. Christopher Brown of Plextronics, Inc. Dr. Malika Jeffries-EL wrote the remainder of the paper.

Chapter 4 is a paper that was published in the *Australian Journal of Chemistry* in 2014 that details the synthesis and characterization of a series of four extended conjugation benzobisoxazole-benzodithiophene copolymers and elucidates the impact of cross-conjugation in conjugated polymers. The author of this dissertation performed all of the synthetic work and a majority of the characterization of the materials. The author this dissertation wrote the experimental section and supplementary information, made major contributions to the results and discussion, and minor contributions to the introduction. Computational modeling of the polymers was performed by Kiley Morgan and Christopher Collins under the guidance of Dr. Aimée Tomlinson. Dr. Aimée Tomlinson also made contributions to the introduction and results and discussion. Thermal studies were performed by Michael Zenner. The remainder of the paper was written by Dr. Malika Jeffries-EL.

Chapter 5 is a paper that will be submitted to *Macromolecules*. This paper focuses on the design of benzobisoxazole-fluorene copolymers with bulky side-chains on the 2,6-positions of benzobisoxazole and phenyl substituents on the 9-position of fluorene. An alternative conjugation axis allows for direct single-bond polymers to be synthesized without any π-spacers. The structural features of these new polymers should allow for higher efficiency and better stability when used in organic light emitting diodes. The author of this dissertation performed all of the synthetic work along with a majority of the characterization for the materials. Quantum yield measurements were performed by Carmen Gott and device fabrication is ongoing. The paper for this work was written entirely by the author of this dissertation.

Chapter 6 draws some general conclusions of the work performed along with possible future research for conjugated materials based on benzobisazoles including asymmetric,

highly functionalized, and two-dimensional benzobisoxazoles. This will be part of a general discussion of what has previously been reported in this area. The author's acknowledgements are also are also included at the end of this chapter.

1.2 Organic Semiconductors

Over the past several decades since the first reports of conductivity in organic materials by Shirakawa in the 1970s,[1,2] there has been a large interest in developing organic semiconductors. Tremendous advancements in the field have been made since the first reports of the conductivity of doped polyacetylene. The development of new conjugated materials over the last few decades has led to their inclusion in organic photovoltaics (OPV)s,[3-7] light emitting diodes (OLED)s,[8-12] organic field-effect transistors (OFET)s,[13-16] polymer batteries,[17-20] sensors,[21-23] and non-linear optics.[24,25] Organic semiconductors have not yet reached the performance level of their inorganic counterparts, however, they offer several other unique advantages. Organic semiconductors do not require high purity raw materials and are derived from petroleum or renewable resources, unlike silicon based semiconductors which require ultra high purity crystalline silicon and have poor efficiencies when defects are present.[26,27] Furthermore, organic semiconductors have the ability to be fabricated using low-cost methods such as spin coating,[28] inkjet printing,[29] or screen printing.[30] The fabricated devices are flexible and lightweight allowing for ease of transport and installation. One of the main advantages of organic semiconductors is the ability to tune the optical, electron, and physical properties through synthetic modification, whereas inorganic materials have properties that are intrinsic to the material and are not easily

modified. By modifying the molecular structure of the organic semiconducting material, the properties of the material can be tailored to fit a specific application.[31]

The main candidates for use as organic semiconductors are conjugated small molecules and polymers. Although the following discussion in this section will focus on conjugated polymers, several of the same principles can be applied to conjugated small molecules as well. Conjugated structures are those which have a backbone consisting entirely of alternating single and double/triple bonds and commonly include aromatic carbocycles and heterocycles. As a result, every atom in the structure has one electron in a π-molecular orbital (π-MO) which creates a system of adjacent π-MOs that is delocalized throughout the backbone of the conjugated polymer and affords their semiconducting nature. As each conjugation unit is added to the polymer, another π-bonding orbital and a π*-antibonding orbital are added and the conjugation length increased. The increase in the conjugation length and the number of π-bonding orbitals increases the energy of the highest occupied molecular orbital (HOMO) while the increase in the number of π*-antibonding orbitals decreases the energy of the lowest unoccupied molecular orbital (LUMO). As conjugation length approaches infinity, the large number of π- and π*-MOs begin resemble a band structure with a definitive energy gap (band gap) between the two. The large number of energetically similar, filled π-orbitals form the valence band while the large number of energetically similar unfilled π*-orbitals form the conduction band. The position and energy of the HOMO, LUMO, and band gap are directly related to the molecular structure and are critical for the design of conjugated polymers for semiconducting applications.[32]

When observing the narrowing of the gap between the HOMO and LUMO as conjugation length is increased, theoretically we would expect to see the band gap diminish

to zero where the valence band and conduction band converge to resemble a conductor as shown for the polyacetylene in Figure 1.1. However, this is not the case as even in the simplest case of polyacetylene, a band gap of 1.5 eV is observed classifying the material as a semiconductor (charge carriers induced thermally, optically, or electrochemically).[33]

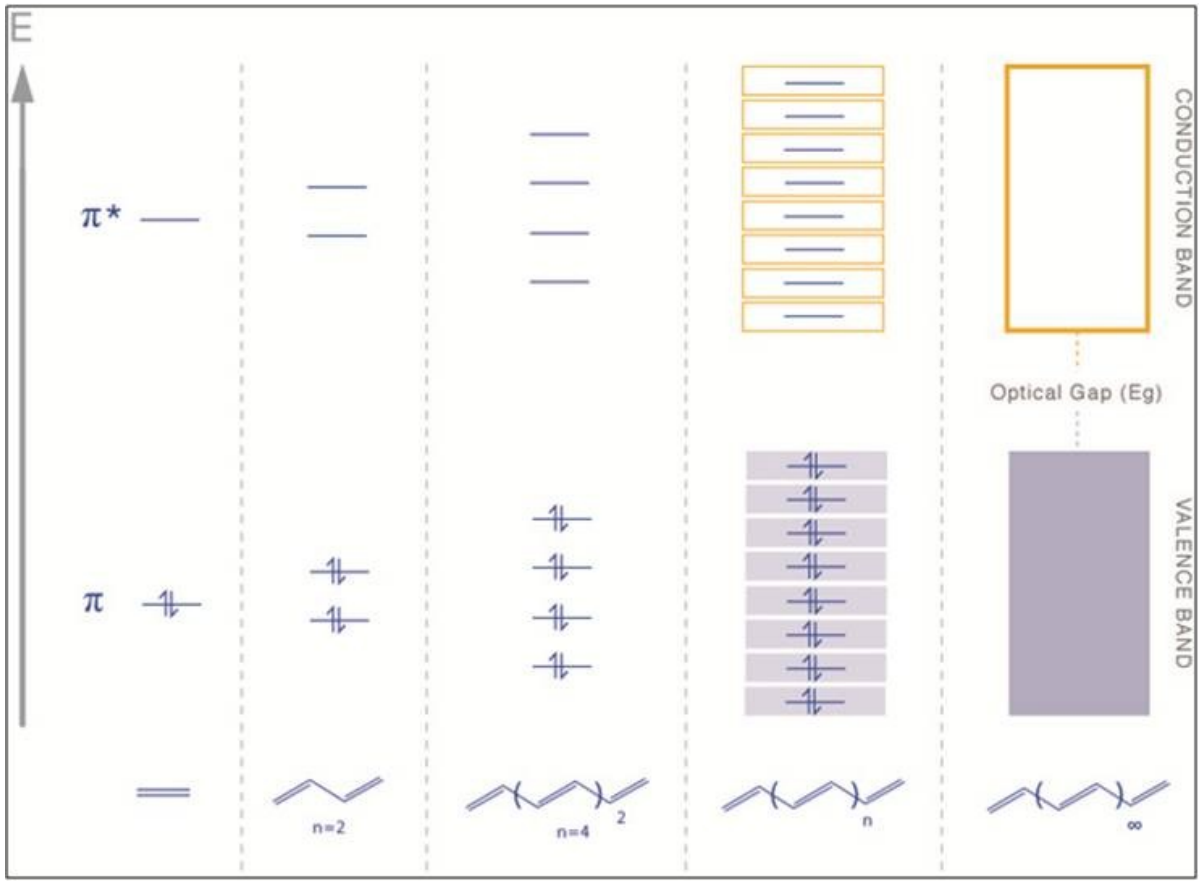

Figure 1.1. Development of conjugated polymer band structure from π-orbitals from monomer to oligomer to infinite polyenes.

This is due to inherent defects in the polymer chains which are induced by the tendency of the polymer backbone to twist over long distances. As a result, complete delocalization across the entire polymer chain does not occur but instead delocalization occurs for a specific length of polymer chain and forms the effective conjugation length. The effective conjugation length is inherent to each polymer system, varies with structure, and gives rise to

the optical and electronic properties of the system.[32] Typically band gap decreases with increasing conjugation length, however, due to Peierls distortions of the alternating short and long bonds, a band gap of zero will never be achieved.[34-36] Synthetically, the effective conjugation length can be tuned by intentionally causing the polymer backbone to twist by introducing steric strain as illustrated in Figure 1.2. This twisting will decrease the effective π-orbital overlap within the conjugated backbone chain, reducing the effective conjugation length. The twisting can be induced by steric interactions between hydrogen atoms on adjacent aromatic units in the polymer backbone such as in poly(*p*- phenylene) (PPP). This effect is decreased when five-membered aromatics such as thiophene or furan are incorporated into the polymer. Alternatively, planarity can be increased by utilizing ladder-type structures and covalently bonding adjacent aromatic rings locking the aromatic rings into a planar position and removing potential hydrogen interactions.

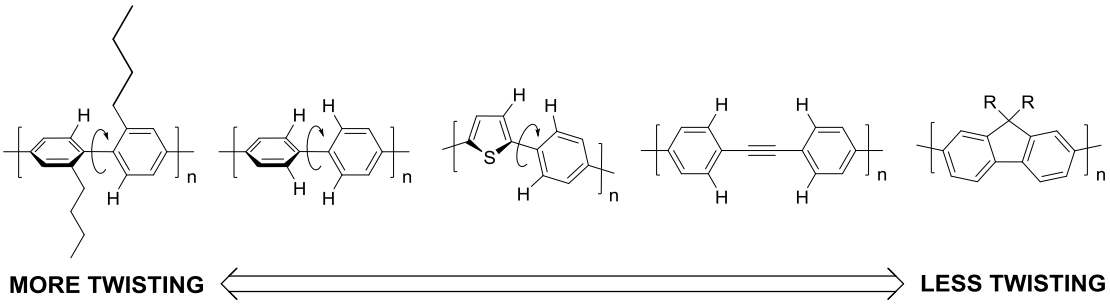

Figure 1.2. Influence of molecular structure on twisting along the conjugated backbone.

By extending the bridge of the ladder system, more planar structures are achieved with concomitant reduction in polymer band gap.[37,38] To further reduce hydrogen-hydrogen interactions, increased rotational freedom can introduced into the polymer backbone by incorporating vinyl or ethynyl groups between aromatic rings such as going from PPP to poly(phenylene-ethynylene) (PPE). Further steric hinderance can be caused by interaction of

side-groups off the polymer backbone, most commonly being solubilizing alkyl chains. This problem is more difficult to solve as the placement of alkyl chains is typically limited. Fortunately, this problem can be circumvented through intelligent placement of alkyl chains during monomer design and/or appropriate alkyl position matching between monomers in the conjugated backbone. In all cases, appropriate molecular design can modulate planarity and band gap based on the desired polymer properties.

Another method of tuning band gap of conjugated polymers is through modulating the stability of the two lowest non-degenerate ground states. These two states are different possible resonance structures of the conjugated material with the lower energy form being the aromatic or benzoid form and the higher energy form being the quinoid form.[6] The benzoid form has all single bonds between adjacent aromatic carbocyclic or heterocyclic rings systems with π-electrons confined within the ring systems. The quinoid form shifts all double bonds to single bonds (and vice versa) creating double bonds between adjacent aromatic ring systems, breaking aromaticity, and delocalizing the π-electrons throughout the conjugated backbone which increases the energy of this state. Due to the double bonds between ring systems, the quinoid form is more planar and has a longer effective conjugation length and thus a narrower band gap. The ratio of benzoid to quinoid form is defined by the parameter bond length alteration (BLA), which is defined as the average difference in bond lengths between adjacent carbon-carbon bonds in the conjugated backbone.[39] When the aromatic stabilization is high, as in PPP, the benzoid state dominates and results in a large BLA and wider band gap. If the quinoid state dominates, the carbon-carbon bonds between ring systems adopt more double-bond character resulting in a decreased BLA and a lower band gap.[6] BLA and band gap are directly related and thus as the system adopts more quinoid

character, the band gap and BLA both decrease (Figure 1.3). By incorporating aromatic ring structures with lower aromatic resonance stabilization (lower degree of aromaticity) such as thiophene (1.26 eV) compared to benzene (1.56 eV), the system has a greater tendency to adopt a more quinoid form and a lower band gap. This leads to poly(thiophene) (PT) having a narrow band gap (2.0 eV) than PPP (3.2 eV). BLA and band gap can also be decreased by diluting the aromaticity of the conjugated backbone by introduction of a vinylene or ethynylene group in the polymer backbone which results in poly(phenylenevinylene) (PPV) having a lower band gap than PPP (2.4 eV versus 3.2 eV, respectively). The most efficient method of decreasing band gap is by incorporating aromatic units in the backbone that prefer the quinoid form, such as in poly(isothianaphthalene), PITN, giving it a band gap around 1 eV.

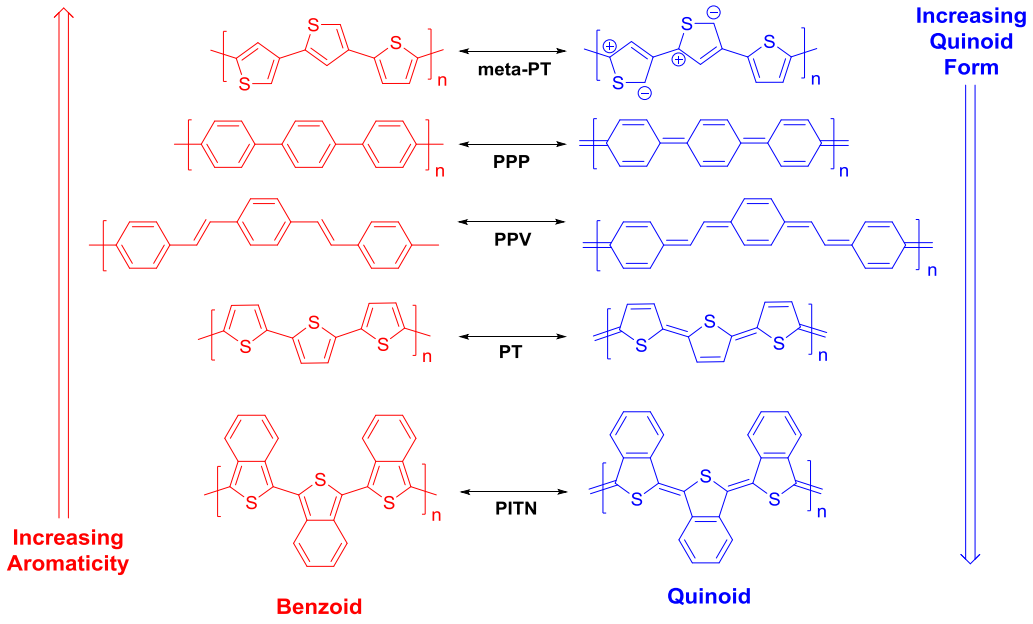

Figure 1.3. Stability of quinoid versus benzoid resonance structures for meta-conjugated poly(thiophene) (meta-PT), PPP, PPV, PT, and PITN. Band gap decreases from top to bottom.

This is due to isothianaphthalene preferring the quinoid form to maintain aromaticity of the benzene ring (large resonance stabilization energy).[40] Conversely to widen the band gap, structures which favor the benzoid form or destabilizes the quinoid form such as the presence of meta-conjugation in the polymer backbone which does not allow delocalization of electrons along the entire polymer backbone.

Controlling the population of the quinoid form in the ground state through synthetic modification of the backbone is a very useful way to engineer the band gap of conjugated polymer. An alternative way of tuning the energy levels of conjugated polymers is through the addition or modification of substituents directly appended to the conjugated backbone that tune properties through inductive and/or resonance effects (Figure 1.4). Through the incorporation of electron withdrawing groups, the electron affinity of the system can be increased leading to a lower LUMO. Inductively, this can be done by incorporating highly electronegative atoms such as fluorine or groups such as trifluoromethyl groups.

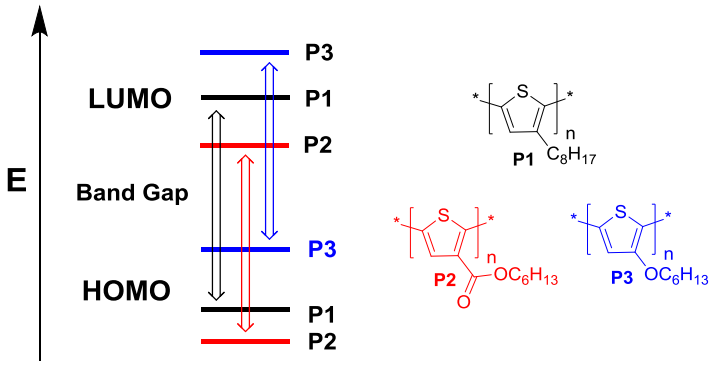

Figure 1.4. Illustration of substituent effect on the energy levels of conjugated polymers.

The resonance effects of electron withdrawing groups such as ketones, imines, esters, amides, nitriles, and alkynes also effectively increase electron affinity of the material. Conversely, the ionization potential of the material can be decreased by addition of electron

donating substituents which leads to a higher HOMO. Increased ionization potential can be achieved through inductive effects of electron donating groups such as alkyl or vinyl groups or electron rich atoms such as Se, S, O, or Si. Similarly, resonance effects of electron donating groups such as alkoxy, alkylthiols, and amines also decrease ionization potential.[41,42] Attaching of new substituents is a challenge of molecular design as useful synthetic handles are typically limited in conjugated systems. This lack of functionality may require the development of new methodology to incorporate functional handles onto the conjugated backbone if further structural modification of the aromatic core is desired. Inclusion of new substituents presents formidable synthetic challenges, however the ability to fine tune the electronic levels of conjugated polymers is very useful and less time consuming than attempting to design sddsssscompletely new and untested aromatic structures.

When modifying the conjugated backbone or substituents, the impact on the electronic properties is not always straightforward and rarely affects a single property. Thus attempting to achieve the optimum properties through structural modification can be highly challenging and sometimes an exercise in futility. An alternative technique that has become very popular for property tuning is through copolymerization of electron deficient (acceptor) electron rich (donor) aromatic moieties with examples shown in Figure 1.5.[43] The push-pull nature of these donor-acceptor (D-A) systems favors delocalization of electrons and increased quinoid nature leading to decreased BLAs and narrower band gaps.[41] Furthermore, the orbital mixing between the donor and acceptor creates a new hybridized HOMO and LUMO which falls in between the HOMO and LUMO levels of the donor and acceptor.

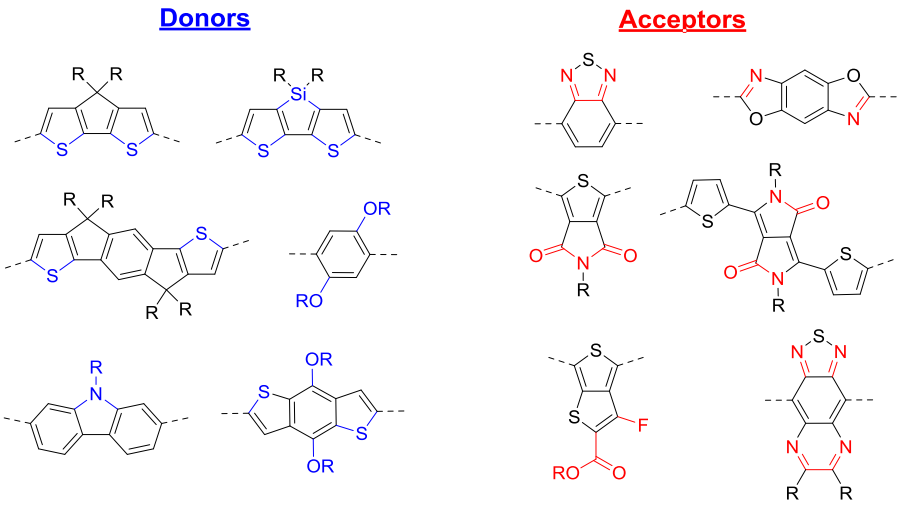

Figure 1.5. Examples of donor and acceptors used in donor-acceptor with important functionality in blue (donor) and red (acceptor).

Similar to how size and energy of molecular orbitals (MO)s resemble the atomic orbitals they are closest in energy to, the HOMO and LUMO of the D-A material will be determined by the donor or acceptor energy level that they are closest in energy to. Therefore the HOMO level of the D-A polymer will be largely determined by the HOMO of the donor while the LUMO level will largely determined by the LUMO of the acceptor (Figure 1.6). This energy level tuning is very useful to position the HOMO and LUMO and can be independently tuned by choosing a different donor and acceptor which ultimately determines the size of the band gap. Using a donor with a deep HOMO level, improves the oxidative stability of the material. This avoids the problem of oxidative instability found in electron rich polymers that have low ionization potential and easily have an electron removed by oxygen.[44] When strong D-A character is present in a polymer, intramolecular charge transfer (ICT) will occur between the donor and acceptor.[42,45] ICT causes a narrowing the band gap of the material and is a low energy excited state causing the polymer to absorb light at lower energies (longer

wavelength) and allows greater absorption of the solar flux for OPVs. This makes the D-A motif very useful for designing improved performance conjugated polymers.

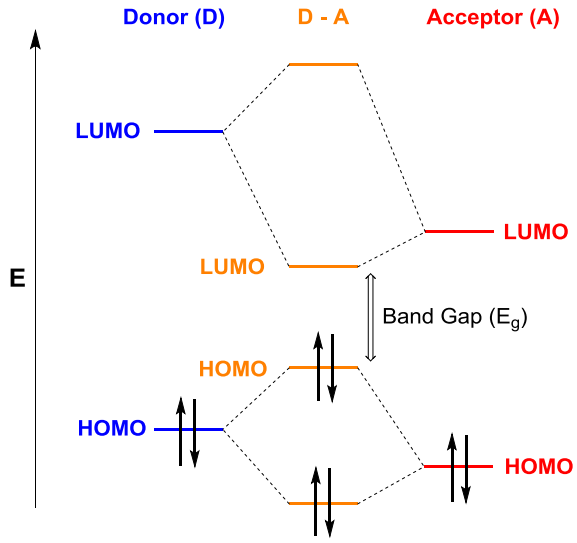

Figure 1.6. Reduction in band gap as a result of orbital mixing between donor (D) and acceptor (A) monomers in D-A polymers.

Due to the aromatic nature of conjugated systems, they typically have very poor solubility in organic solvents as there is very little interaction between the solvent and the aromatic structure. Furthermore, the aromatic structures have strong intermolecular $\pi - \pi$ stacking which prefer crystallinity to dissolution. In order to make organics viable for low-cost and large-scale processing, conjugated polymers must be rendered soluble in common organic solvents. To improve the solubility of conjugated materials, alkyl chains are appended to conjugated backbone to improve interaction with solvent molecules and to disrupt $\pi - \pi$ stacking between the polymer chains. Alkyl chains can also improve molecular weight as higher molecular weight materials are imperative to achieving longer effective conjugation, good film forming properties, and higher charge mobility.[46] Unfortunately appending alkyl chains is not always straightforward or easily done on many conjugated

systems. Alkyl chains are often appended in the early synthetic steps requiring several steps to be repeated when a different alkyl chain is desired. When developing the methodology to new or modified conjugated materials, the placement, number, and size of alkyl chains is imperative.

The type, size, and number of flexible alkyl chains grafted onto the conjugated backbone have a large impact on the physical properties and thin film morphology of conjugated polymers.[47-49] Having too few alkyl chains can lead to low molecular weight materials and solubility issues. Conversely, incorporating too many alkyl chains can prevent close packing of the polymer chains, prevent proper inter-digitation of alkyl chains on separate polymer chains, or cause twisting of the polymer backbone. Improper packing diminishes the charge transport via "chain hopping" or along the conjugated backbone due to decreased effective conjugation length, both of which lower the overall charger mobility of the material. While short, straight alkyl chains such as hexyl or octyl promote greater film order and efficient $\pi - \pi$ stacking, they also limit solubility and the molecular weight of the polymer.[6,50] Although efficient $\pi - \pi$ stacking is necessary for OPVs and OFETs, lower molecular weight polymers tend to have lower charge mobility which can limit polymer performance.[46] Shorter branched alkyl chains such as 2-ethylhexyl or 3,7-dimethyloctyl improve solubility to allow higher molecular materials, however they disrupt $\pi - \pi$ stacking to a larger extent than straight alkyl chains and also disrupt efficient inter-digitation of the alkyl chains. Similarly, long alkyl chains such as 2-butyloctyl or hexadecyl provide much higher solubility but at the cost of heavily disrupted $\pi - \pi$ stacking of the conjugated backbones. These long branched alkyl chains are useful when the number of alkyl chains that can be appended is limited or to solubilize larger π-systems. While bulky branched chains

can be detrimental to the performance of OPVs and OFETs, decreased π – π stacking can be beneficial in some application such as OLEDs to help prevent aggregation induced fluorescence quenching[51] or exciplex formation.[52,53] Furthermore, the thermal properties of the polymers are greatly impacted by the alkyl chain selection and the thermal stability decreased when alkyl chains are appended.[54] This commonly is not a problem as most conjugated polymers have stability above the operating temperatures required in organic semiconductor applications (commonly less than 50 °C). While alkyl chains are highly important to maintain solubility of conjugated polymers, an appropriate balance between solubility and thin film order must be achieved.

1.3 Benzobisoxazoles and Their High Performance Materials

Benzobisazoles are a fused-ring aromatics consisting of a benzene ring flanked on either side by oxazole, thiazole, or imidazole moieties (Figure 1.7). A *cis* and *trans* isomer of benzobisoxazole and benzobisimidazole have been synthesized while only one isomer of benzobisthiazole (BBZT) has been developed as there is currently no known methodology to the *cis*-isomer. The trans-isomer of benzobisoxazole or benzo[1,2-*d*-4,5-*d*′]bisoxazole (BBO) will be the focus of this dissertation.

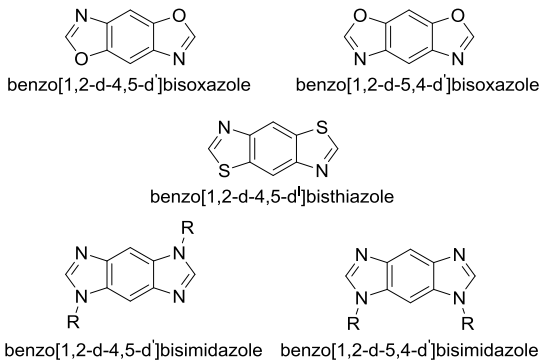

Figure 1.7. Examples of benzobisazoles.

Benzobisazoles are conjugated, electron deficient aromatics that were first investigated by in the early 1970s by Osman, et al. as small molecule dyes in addition to the probing of their mass spectroscopy.[55-58] In the 1980s, Wolfe, et al. began to investigate benzobisazole copolymers as high-performance materials which had very high thermal stability (>300 °C),[59] excellent chemical stability,[60] and great mechanical stability.[61-63] The great mechanical strength of the reported polymers was attributed to the linear nature of the benzobisazole moiety and the lack of hydrogens on the five-membered azole ring. This feature minimizes twisting between the azole and adjacent aromatic moiety forming rigid and regular structures, especially in benzobisoxazoles.[64] The physical properties of these systems led to the mass production of poly(*p*-phenylene-*alt*-2,6-benzobisoxazole) as a high performance material known as Zylon® (Figure 1.8). Roberts, et al. later studied the unique optical and electronic properties of these compounds.[65-67]

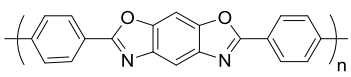

Figure 1.8. Structure of Zylon®.

Although the poly(benzobisazole)s (PBA)s synthesized by Wolfe and others showed great mechanical and thermal stabilities, the lack of solubilizing side-chains rendered them insoluble in organic solvents and required the polymerization and any subsequent solution characterization or processing to be done in strong acids such as PPA or methanesulfonic acid. Alternatively, the polymers were found to be soluble in protic organic solvents when complexed with Lewis acids such as $AlCl_3$.[65] When purifying or casting films of the PBAs, the polymers must be rinsed with water several times to remove residual acid.[68,69] Even with several rinsing cycles, residual acid can dope the polymers, resulting in polymer defects.

More importantly, residual acid accelerates the degradation of the polymers[70,71] which resulted in Kevlar® eventually replacing Zylon® in bullet-proof vests.

One of the main limitations of the early PBAs and benzobisazole small molecules synthesized by Wolfe, et al. was the harsh reaction conditions involving the condensation of 2,5-diaminobenzene-1,4-dithiol (DABDT) or 2,4-diaminoresorcinol (DAR) with 1,4-benzenedicarboxylic acid in PPA at temperatures ~250 °C as shown in Scheme 1.1.[61-63,72-75]

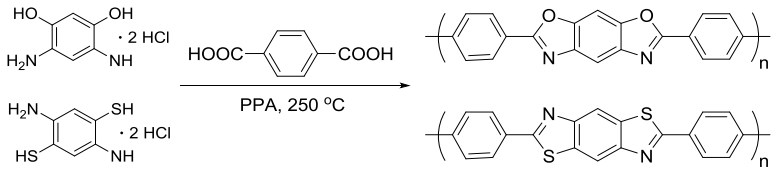

Scheme 1.1. Wolfe polycondensation preparation of poly(benzobisazoles).

A slight variation was used by So, et al. utilizing methanesulfonic acid and P_2O_5 (Eaton's reagent) to form PBAs.[76] Both of these reaction conditions have very little functional tolerance and even alkyl chains can be oxidized under these conditions, causing polymer defects. Regardless of the method used, the starting material for the trans isomer of benzobisoxazole, 2,5-diaminobenzene-1,4-diol (DAHQ), was oxidized to the 1,4-benzoquinone, precluding its polymerization. The limited functional group tolerance of this methodology does not allow appropriate functional groups needed to synthesize conjugated polymers for solution-processed organic semiconductors.

1.4 Milder Benzazole and Benzobisoxazole Syntheses

Many other groups have investigated the synthesis of benzobisazole polymers utilizing a modified polycondensation that was reported by Wolfe with examples shown in

Scheme 1.2. One minor variation includes the use of acid chlorides in place of carboxylic acids.[77] PBAs were also synthesized through a polyamidation with terephthaloyl chlorides to yield poly(*o*-hydroxy-amides) as polymer precursors followed by solution or solid-state cyclodehydration (thermal or acid/base mediated) to yield PBAs.[78,79] A similar method protected the hydroxyl group of the *o*-aminophenol with trimethylsilyl group which then underwent polyamidation with terphthaloyl chlorides followed by cyclodehyradation to yield PBAs.[80-83] This latter method allowed the inclusion of alkoxy or thioalkyl chains on the polymer backbone, however the temperatures required (>250 °C) caused some cross-linking of alkyl chains to occur.[84] Jenekhe, et al. also investigated the synthesis of small molecule BBZTs through a two-step, one-pot imine formation with aromatic aldehydes followed by oxidation to the thiazole.[75,85] The yields of these reactions were poor (less than 12%) and the synthesis of benzobisoxazoles using this method have not been reported.

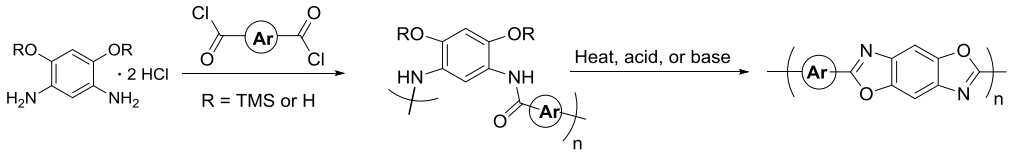

Scheme 1.2. Milder variations of the Wolfe acid condensation.

Recently, several groups have investigated milder syntheses of benzazoles with some examples shown in Scheme 1.3. These include the use of copper catalyzed reactions from amidobenzenes,[86] *o*-bromo-amidobenzenes,[87,88] *o*-dibromobenzene,[89] or *o*-aminobenzene thiols.[90] Iron catalysis has also been investigated using *o*-bromo-amidobenzenes as starting materials.[91] There have also been other reports of the synthesis of benzazoles using palladium catalysis with isocyanides, haloarenes, and *o*-aminophenols.[92] Metal-free methods have also been explored such as the use tertiary amines, *o*-aminophenols, and elemental sulfur.[93]

Unfortunately, the application of these methods has not been reported for benzobisazoles nor has the methodology been developed to the prerequisite starting materials for these methods.

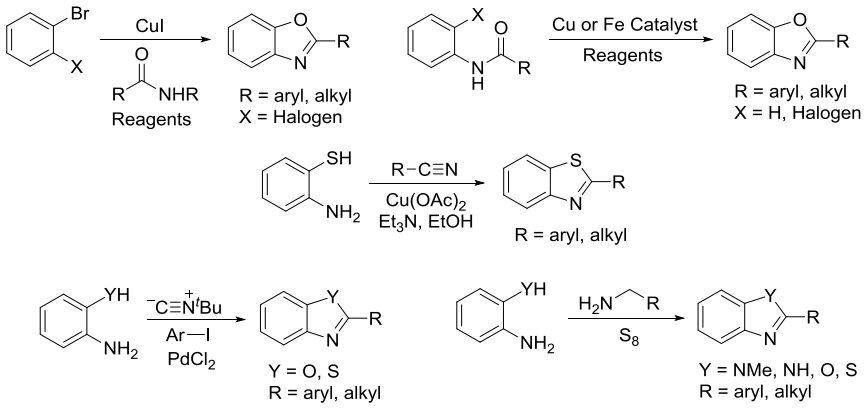

Scheme 1.3. Examples of mild benzazole syntheses.

Our previous group member, Dr. Jared Mike, developed a very mild synthesis of benzobisoxazoles[94] and BBZT[95] by Lewis acid catalyzed condensation of DAHQ, DAR, or DABDT, with functionalized orthoesters as shown in Scheme 1.4.

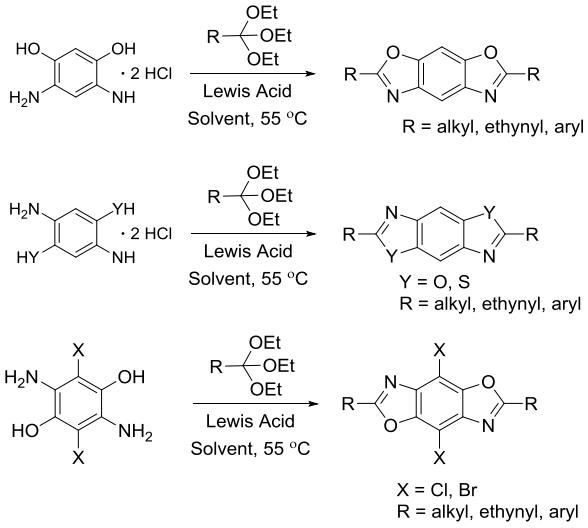

Scheme 1.4. Synthesis of BBO and BBZT monomers through orthoester condensations.

We also have utilized several methods of orthoester syntheses including the method of Tschitschibabin[10,96] or utilizing trithiomethyl intermediates.[97,98] These functionalized

orthoesters are condensed under Lewis acid conditions to yield benzobisazole building blocks for the development of conjugated small molecules and polymers. This mild methodology provides great functional group tolerance including alkyl, trimethylsilylethynyl, chloromethyl, and alkylthienyl groups with much broader synthetic utility compared to other methods.[10,54,99-101]

1.5 Poly(benzobisazole)s for Organic Semiconductors

From the functionalized benzobisazole building blocks, our group has been quite successful at developing new benzobisazole polymers shown in Scheme 1.5. Utilizing the 2,6-dichloromethylbenzobisazoles,[94,95] several vinylene-linked copolymers were synthesized by utilizing a two-step Arbusov reaction to form a diethylphosphonate followed by a Horner-Wadsworth-Emmons reaction with aryl dicarbaldehydes. Using phenyl[54] and thiophene[101] dicarbaldehydes, Dr. Mike was able to synthesize *cis*- and *trans*-BBO polymers which achieved poor efficiency (0.08%) when used as the donor material in bulk heterojunction (BHJ) OPVs. Expanding the same methodology to include 9,9-dialkylfluorene-2,7-dicarboxaldehydes and DABDT, former group member, Dr. Jeremy Intemann, was able to synthesize several wide band gap polymers that were incorporated into blue or blue-green emitting guest-host OLEDs to yield modest efficiencies of up to 0.93 Cd A^{-1}.[102,103] Utilizing a simpler methodology, former group member James Klimavicz was able to synthesize several donor – π – acceptor – π – donor chromophores by a modified aldol reaction between 2,6-dimethylbenzobisoxazoles and aryl aldehydes.[104] These small molecules and polymers provide straightforward routes to a variety of materials, however, the poor performance of

the materials prompted us to develop other develop alternative polymerization methods to avoid the vinylene linkage.

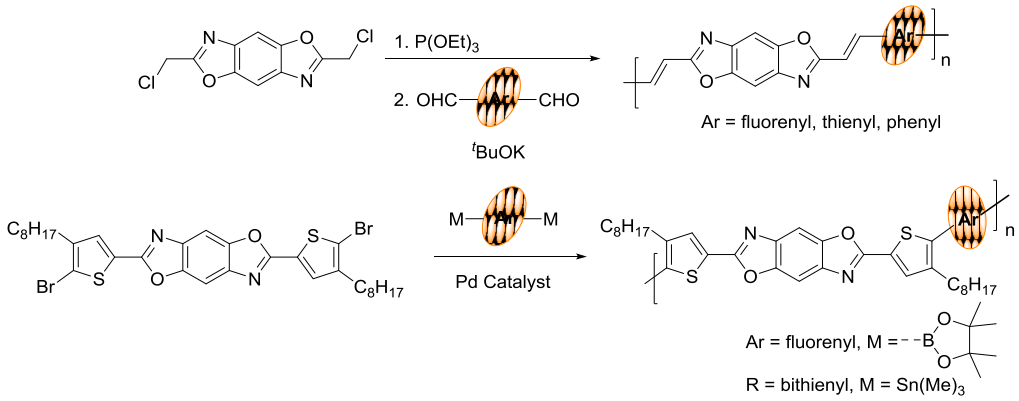

Scheme 1.5. Examples of PBAs for organic semiconductors.

In order to develop new materials without vinylene linkages, we sought to develop aryl orthoesters to synthesize 2,6-diarylbenzobisazoles (Scheme 1.5). Dr. Mike developed the synthesis for 2-bromo-3-octyl-5-(triethoxymethyl)thiophene and condensed this DAHQ, DAR, and DABDT to yield 2,6-bis(5-bromo-4-octylthien-2-yl)benzobisazoles.[10] The bromine atoms at the 5-position of the thiophene provide synthetic handles for Stille or Suzuki cross-coupling polymerizations. Dr. Mike copolymerized this monomer with flourene to yield terpolymers which showed improved efficiencies over previous polymers in guest-host OLEDs of 0.86 Cd A^{-1}.[10] Similarly, group member Achala Bhuwalka copolymerized the same monomers with a dialkyl-bithiophene that were incorporated as the donor material in BHJ solar cells and provided higher efficiencies (1.14%) than we previously reported. Jenekhe and coworkers published a similar BBZT polymer which provided even higher efficiencies of 2.1%.[85] These polymers display the synthetic versatility of the benzobisazole moiety as a single monomer could be used for multiple organic semiconductor applications.

1.6 Halogenated Benzobisoxazoles

By modifying the synthetic methodology developed by Dr. Mike, the author of this dissertation was able to synthesize 4,8-dichloro and 4,8-dibromoBBOs (Scheme 1.4 above).[105] These halogens provide an opportunity to synthesize halogenated BBO small-molecules and polymers,[106] create two-dimensional conjugated systems, and tune solubility, optical, and electronic properties of small molecules and polymers.[11,107] These functional handles increase the synthetic versatility of the BBO system with two potential axes for functionalization or polymerization creating several unique conjugated materials from a common aromatic core as shown in Figure 1.9. Dr. Intemann utilized the 4,8-axis to synthesize ethynyl-linked copolymers through Sonogashira cross-couplings between BBO and carbazole, fluorene, or alkoxybenzenes which showed three-fold increase in the efficiency (3.1 Cd A^{-1}) for guest-host OLEDs compared to our previous reports.[11]

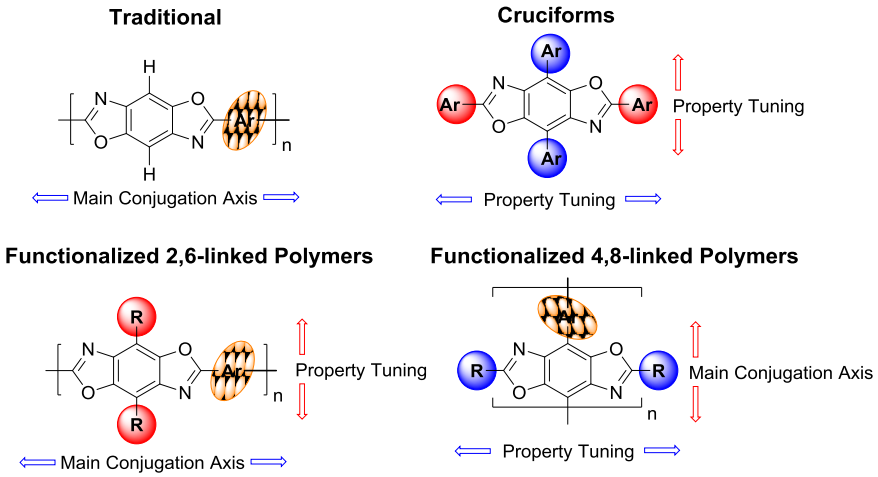

Figure 1.9. Versatility of the 4,8-dibromoBBO aromatic core.

Altering the conjugation axis increases the versatility of the BBO and allows further tuning of properties such as the thermal stability, solubility, solid-state packing, and the optical and electronic properties with differences highlighted in Figure 1.10. Poly(BBO)s

suffer from poor solubility due to their rigid-rod structure, but ease of alkyl chain inclusion on the 2,6-axis could help to increase the solubility and modify solid-state packing of the polymers. The 4,8-polymers should also have a smaller energy difference between the quinoid and benzoid resonance forms compared to the 2,6-polymers. This can be attributed to the oxazole rings remaining aromatic when switching between the quinoid and benzoid resonance forms of the polymer whereas in the 2,6-polymers both the oxazole rings and central benzene ring lose aromaticity, increasing the energy difference between the two forms. This indicates the polymer will have an increased amount of quinodal character which is known to extend the effective conjugation length of the π-system and result in a narrower band gap from an increased HOMO level and decreased LUMO level.[6] However the 4,8-polymers will likely be more twisted as the strain between monomers is greater between the co-monomer and central benzene than the co-monomer and the oxazole moiety.

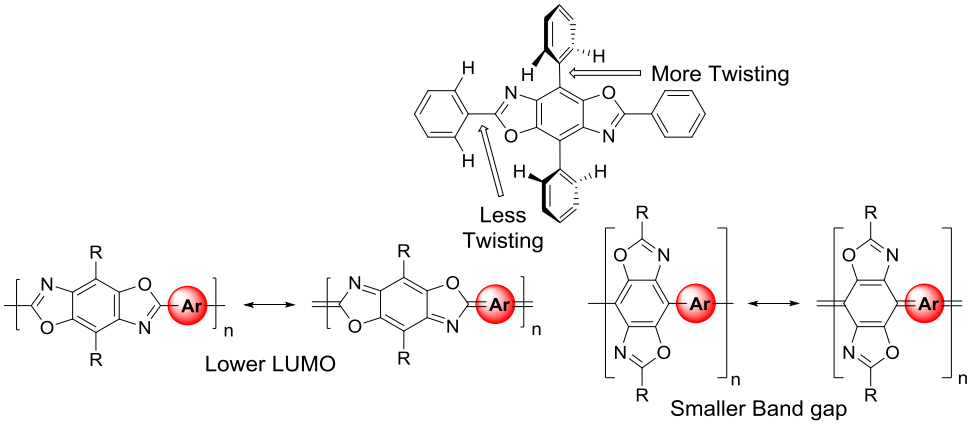

Figure 1.10. Difference between 4,8- and 2,6-conjugation axis in BBO polymers.

This could have a large impact of solid-state packing of the polymer and thermal properties of the polymers which can influence performance in organic semiconductors. However, the increased twisting may be beneficial when designing OLEDs to decrease aggregation-induced quenching.[51] The twisting can also lead to less efficient π – π stacking which can be

detrimental to efficient charge mobility in OPVs and OFETs. Furthermore, the 2,6-axis has the electron-accepting oxazole moieties directly conjugated in the polymer chain which could possibly lead to lower LUMO levels and concomitant decrease band gap.

1.7 Cross Conjugated and Cruciforms

The properties of conjugated polymers are unique in that the optical and electron properties can be tuned through chemical synthesis. However, predictably tuning a single property can be difficult to do even in D-A polymers as structural modification rarely affects a single property. An alternative method of property tuning is through the use of two-dimensional cross-conjugated systems where two conjugation axes intersect at a common core in a small molecule or polymer.[108] The conjugation pathways are spatially separated yielding two independent π-conjugation systems within the molecule. By changing the aryl group, further extending the π-system, or modifying the aryl groups with electron-donating or electron-withdrawing nature, the cross-conjugation can modify the optical and electron properties of the system.[109-116]

Cross-conjugation was first observed to effectively tune the optical and electronic properties in [n]radialenes (alicyclic compounds which all ring carbon atoms are sp^2 hybridized and have an exocyclic double bond)[117] and similar tetraethynyethenes.[118] Additional examples of property tuning via cross-conjugation was observed in PPEs decorated with phenylene-vinylene side-chains to yield polymers that behaved as hybrids of PPEs and PPVs.[109,111] Bunz and co-workers observed the properties of the PPEs were tuned by varying the structure and electronic nature of the phenylenevinylene side groups. In addition to the tunability of the optical and electronic properties of the hybrid PPE/PPVs, the

phenylenevinylene side arms were also found to redistribute the frontier molecular orbitals (FMO)s based on their structure. When 4-(*N*,*N*-dibutylamino)phenylene-vinylene was used as the side arm, the HOMO was fully localized to the phenylenevinylene side-arms while the LUMO was localized to the main PPE backbone.[109]

Although cross-conjugated polymers are possible, the main interest in these systems has been to develop X-shaped small molecule "cruciforms." Cruciforms are cross-conjugated small molecules that have two distinct π-conjugation linear arms of nearly equal conjugation length connected through a central aromatic core.[21,22,106,112,116,119-137] These two distinct arms can be positioned in either *ortho* or *para* to each other on the central core with the different substitution isomers having their own unique properties.[116] The two separate conjugation pathways of the cruciforms give them two spatial separated FMO systems which can be independently tuned by synthetic modification. Through strategic design of each "arm" (4-aminophenyl versus phenyl) or the π-bridge between the arm and the central core of the cruciform (ethynyl versus vinyl), it is possible to isolate the HOMO and LUMO on separate arms in addition to the ability to modify the physical properties of the cruciform. The localization of the HOMO and LUMO on separate axes allows for independent tuning of the HOMO and LUMO through careful synthetic modification of each arm, barring any significant reorganization of the FMOs upon the structural modification. This localization of the HOMOs and LUMOs allows for ICT between the two cruciform arms and is accompanied by narrowing of the band gap, the loss of vibronic features in the fluorescence spectra, a decrease in fluorescence quantum yield, and the appearance of a low energy shoulder in the UV-Vis absorption.[22] Several examples of cruciforms have been developed (Figure 1.11) which include distryl-bis(arylethynyl)benzenes,[22,116,119-122] tetra

(arylethynyl)benzenes,[123-128] tetrastyrylbenzenes,[135,136] 2,6-diary-4,8-bis(arylethynyl)BBOs,[21,129-134] and 2,4,6,8-tetraarylBBOs.[106,112,138] The unique properties of these systems make them well-suited for sensors and other organic semiconductor applications.

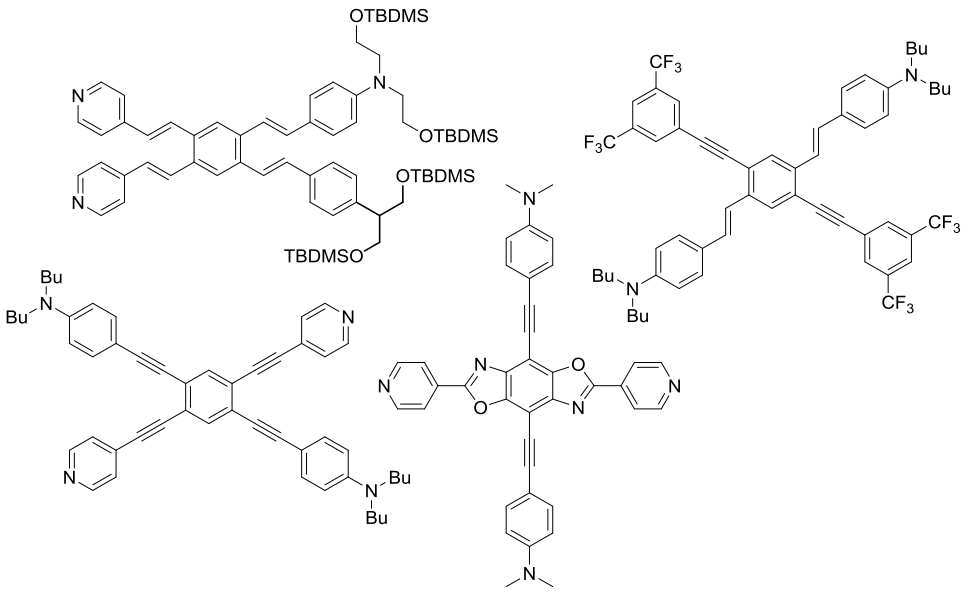

Figure 1.11. Examples of cruciform systems.

Of the cruciforms mentioned previously, there are two possible methods of property tuning through synthetic modification: modifying one or both of the cruciform arms and/or changing the π-bridge (ethynyl, vinyl, or none) between the cruciform arm and central core. BBO-based cruciforms are unique in that of the aforementioned cruciforms, it possesses two non-identical conjugation pathways. The first is through 2,6-axis through the oxazole rings or the 4,8-axis through the central benzene ring giving BBO cruciforms an added dimension of property tuning through changing the substitution pattern on the BBO core. The effect of conjugation pathway on cruciform properties was investigated by Miljaníc in 2,6-diaryl-4,8-diethynylBBO cruciforms[131] and by the author of this dissertation in 2,4,6,8-tetraarylBBO cruciforms.[106] In both cruciform types, it was found that BBO is also unique in that it will

preferentially localize the HOMO along the vertical 4,8-axis even in the absence of electron poor or electron rich cruciform arms (Figure 1.12).[106,131]

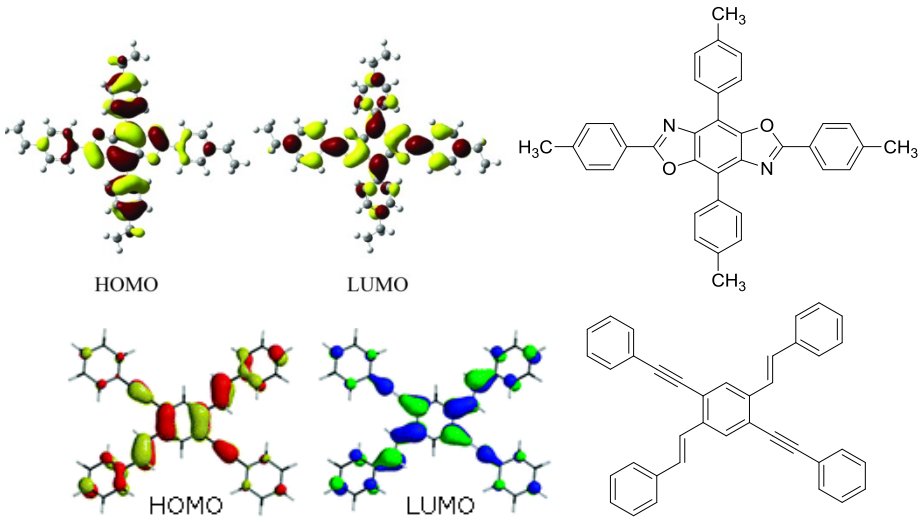

Figure 1.12. Comparison of FMO localization in the absence of donor-acceptor character in BBO cruciforms (top) distyrl-bis(phenylethynyl)benzenes.[108]

The synthesis of the BBO cruciforms has been achieved through the use of three different methodologies with the key arm installation steps shown in Scheme 1.6.[139] Nuckolls and coworkers synthesized 2,4,6,8-tetraarylBBO cruciforms starting from 1,4-dibromo-2,5-dimethoxybenzene utilizing a Negishi cross-coupling and a double Staudinger reaction to synthesize cruciforms intended to study molecular electronics.[138] Although this method is mild, it requires several steps between arm installations with one set of arms being installed in the first step of the synthesis. The author of this dissertation also synthesized 2,4,6,8-tetraarylBBO cruciforms starting from 3,6-diamino-2,5-dibromo-1,4-hydroquinone (Br-DAHQ) utilizing a sequential Lewis acid catalyzed orthoester condensation followed by a Stille or Suzuki cross-coupling to synthesize cruciforms to study the optical and electronic properties of the BBO system. This method is also mild, requires fewer steps, and allows for late installation of the cruciform arms, and the ability to use common intermediates for each

cruciform arm.[106] Using a similar methodology, Miljanić and coworkers synthesized 4,8-bis(arylethynyl)-2,6-diarylBBO cruciforms for use as fluorescent sensors through a two-step Wolfe acid condensation followed by a Sonogashira cross-coupling starting from Br-DAHQ.[130] This method also allows for the late installation of the cruciform and use of common intermediates and ease of variation of the aromatic arms. However, the functional group tolerance is limited to by the harsh nature of the PPA condensation.

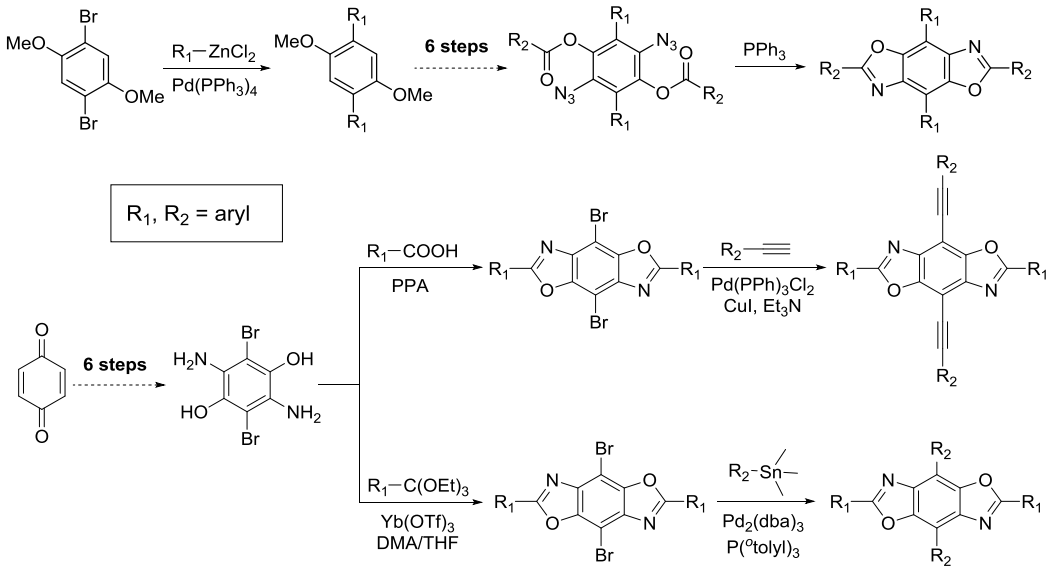

Scheme 1.6. Methods of cruciform arm installation to form BBO cruciforms.

1.8 Material Design Through Computational Modeling

As the field of organic semiconductors continues to grow and advance, so too does the search for new conjugated materials to provide enhanced performance. This search typically involves the synthesis and analysis of new materials to elucidate structure-property relationships. From this data, further fine tuning of the properties can be done through chemical synthesis. This method of development is very time consuming and expensive as typically several derivatives must be synthesized.

One possible method for expediting the development of new materials is the use of theoretical calculations to model the properties of the new materials prior to their bench-top synthesis. Performing theoretical calculations are faster than organic synthesis, and based on the level of theory used, can be less expensive. When developing a new material, theoretical calculations could be used to predict the properties of several structural iterations of the aromatic system and identify the best structures to further pursue. Likewise, when attempting to further tune properties, theoretical calculations could be done to predict whether the synthetic modification would have a beneficial or negative impact on properties such as the HOMO, LUMO, band gap, and UV-Vis absorption or emission. Beyond predicting properties, theoretical calculations can help in elucidating structure property relationships by predicting FMOs, surface potentials, and optimized geometries of the systems.

Of the theoretical methods available, the most common method used for conjugated systems is density functional theory (DFT). DFT is as a semi-empirical method that calculates energy and other molecular properties based on electron density throughout a molecule. This is different than typically *ab inito* methods, such as Hartree-Fock (HF), which calculate one-electron wavefunctions to determine energy and are based solely on computational results. The advantage of DFT over *ab initio* methods for larger conjugated systems is that computing time scales with the third power of molecular size, compared to the fourth power for HF or the fifth power for Møller-Plesset second-order perturbation theory.[140,141] In large molecules, electron density is a much simpler to calculate than complex total wavefunctions required in *ab initio* calculations. Furthermore, the electron correlation effects can be determined with reasonable computational expense.[142] Although theoretical

calculations may have some error, typically the trends are more important in predicting properties than the absolute values.[139]

For theoretical methods, several basis sets and functional are available based on the accuracy desired. In conjugated systems, smaller extended basis sets are commonly used due to the size of the systems being analyzed. The basis set becoming the most popular in conjugated systems is 6–31G* ("6" Gaussian-type orbitals (GTO)s to form one functional for core atomic orbitals, "3" GTOs to form the first functional for the valence electrons, "1" diffuse GTO to form a second functional for valence electrons, and the inclusion of all d orbitals (*)).[33] Linear combinations of GTOs are commonly used in place of more accurate Slater-type orbitals as they are much simpler to calculate and provide similar accuracy.[33] Another common basis set utilized is 3–21G*, a smaller basis set that decreases computational costs by utilizing a fewer number of functionals for the core atomic orbitals and has been utilized on extremely large conjugated systems to reduce computational costs.[140] However, 6–31G* has been shown to be more accurate than 3–21G* on the same molecule or system.[143] When comparing different basis sets in a series of small molecules, larger basis sets such as 6–311G** performed only marginally better than 6–31G*.[144] A basis set that is less common but we have achieved good results in our group is the SVP (split valence, polarization of H-atoms) basis set which requires similar computing time to 6–31G*.[106,107] The SVP basis set is very similar to 6–31G* except in the SVP basis set, polarization of the H-atoms is done to include the 2*p* orbitals on hydrogen[145] which should lead to better results.[146] For most conjugated systems, 6–31G* or SVP basis sets have the optimum balance of computing speed and accuracy that has led to wide usage by scientists to study conjugated materials.[147]

Several DFT functional are available for conjugate materials, but the most widely used is B3–YLP, a hybrid of HF and DFT functionals. The "YLP" indicates the correlation developed by Yang, Lee, Parr for the density functional energy formulation of the Colle – Salvetti correlation energy.[148] The "B3" indicates Becke's three parameter exchange-correlation functional is utilized to more accurately calculate the highly important exchange-correlation term for DFT.[149,150] B3–YLP generates the typical Kohn – Sham orbitals[151,152] found in DFT with these equations originally solved by Pople, et al. Pople, et al. also used the B3–YLP/6–31G* system to calculate a variety of molecular properties[153] and proposed the appropriate grid size for DFT calculations[154] which is quite accurate even for complex molecules.[155] The B3–YLP functional has also been shown to give comparable results to higher levels of theory such as Møller – Plesset 2nd order perturbation theory or HF/6–31G methods[144,156] that require much longer computation times.[157] B3–YLP was also found to yield more accurate results than other DFT methods such as VWN–YLP (YLP with Vosko, Wilk, and Nusair correlation functional[158]) or B–YLP, (YLP with Becke first parameter correlation-exchange correction) with similar computational costs.[141,144] Utilizing the B3–YLP or SVP functional with the 6–31G*, several groups have obtained reliable and accurate results for conjugated systems.[53,140,159-161]

DFT is a great method for modeling the ground-state properties of conjugated systems such as optimized geometries and FMOs. When designing new materials, there is a large advantage to computationally model properties that depend on the molecule's excited states such as optical transitions, HOMO, and LUMO. Although DFT does not have the ability to do so, a time dependent extension of density functional theory (TDDFT) can be used to model excited states with the same scalability and accuracy of DFT.[162] TDDFT has

been shown to be as accurate as more computational intensive *ab initio* methods, but at a much lower computational costs [140] while utilizing the same basis sets and functionals as DFT. The Runge-Gross Theorem[163] is the foundation of TDDFT which solves the time dependent Kohn – Sham system[151] which describes how electron density changes with external potential and calculates the frequency dependent electron density. The modeling of excited states by TDDFT was formally derived by Gross in the 1990s[164] and the accuracy of TDDFT versus other methods in modeling excited states was demonstrated in a series of polyenes.[165] The excited states are calculated by TDDFT from calculating the vertical excitation energies from the DFT calculated optimized geometries.[166] Singlet excited states can be easily calculated without any extra calculations, however, triplet states can also be calculated if the appropriate spin-dependent exchange correlation kernel is applied.[167] Using the oscillator strengths of the transitions, the absorption or emission spectra can be simulated.[168,169]

Many of the important properties of conjugated systems can be predicted utilizing the DFT and TDDFT with the 6–31G* or SVP basis set and has been demonstrated to accurately predict optimized geometries, FMOs, electron densities, HOMO, LUMO, and band gap energies.[170-173] For polymers, a long chain limit must be developed using a set of oligomers such that the energy (E) of the HOMO, LUMO, and band gap are calculated by fitting the oligomer length with the Kuhn expression[166,174] (Equation 1.1)

$$E = E_o \sqrt{1 + 2\frac{k'}{k_o}\cos\frac{\pi}{N+1}} \qquad \text{(Equation 1.1)}$$

where E_o is the transition energy of the double bonds in oligomers, N is the number of double bonds in the oligomer, and k'/k_o is an adjustable parameter. Several of these properties are

influenced by synthetic modification and thus a preliminary structure-property relationship can be developed before any synthesis takes place.

1.9 Conclusions

Organic semiconductors have shown to be useful alternatives to their inorganic counterparts. As the interest in organic semiconductors continues to grow, new research is needed for several reasons:

- Demand for higher performing materials for organic semiconductors
  - Inorganic materials for electronics are limited by purity, cost, and toxicity
  - Conjugated materials need improvement for commercial development
  - Properties of organic semiconductors allow new or niche applications
    - Flexible and lightweight devices allow for niche applications
    - Non-toxic nature allows safe installment and disposal
- Organic electronics have several key properties
  - Optical and electronic properties tunable through chemical synthesis
    - Band gap tunable through population of quinoid form or D-A motifs
    - Energy levels tunable through electron rich or electron poor substituents
    - ICT allows for widened absorption and narrower band gaps
  - Alkyl chains needed for solubility and can modulate thin film morphology
    - Solubility allows for inexpensive large scale solution processing
    - Alkyl chain can be tailored to application to improve performance

Benzobisazoles are conjugated building blocks that have several unique futures that make them useful materials for organic electronics:

- Benzobisazoles are rigid fused ring heterocycles
  - High thermal and oxidative stability yields high-performance materials
  - Oxazole rings provide minimal steric interactions and efficient π – π stacking
  - New milder bisazole formation allows for increased functional group tolerance
    - Allows synthesis of polymers suitable organic semiconductors
    - One core can provide polymers for several applications
    - Synthesis straightforward, scales easily, and functionality easily installed
- Halogenated BBOs provide increased material versatility and potential applications
  - Utilize halogens for as synthetic handles
    - Improve solubility and modify π – π stacking
    - Increase acceptor strength
  - Creates a new polymerization axis
    - Provides direct synthetic handle for cross-coupling polymerization
    - Modifies the acceptor strength and the quinoid resonance structure energy BBO
    - Changes planarity and steric interactions compared to 2,6-axis
    - Utilize 2,6-axis for property tuning or improve solubility
  - Used to develop cross-conjugated cruciforms
    - Creates spatially separated FMOs
    - Localized FMOs allow for ICT, absorption broadening and decreased band gap
    - Delocalized FMOs orbulky groups can lead to highly emissive materials
  - Highly tunable optical, electron, and physical properties

- Monodisperse allowing for traditional purification methods and batch-to-batch reproducibility

Although synthetic modification allows for property tuning, there is a difficulty in predicting how the modification and will fully impact the molecular properties. Synthesis of several structural iterations of a compound can be time-consuming and expensive. To expedite the material development process computational modeling can be powerful and inexpensive tool for material design:

- DFT provides accurate property prediction with manageable computational costs
  - Great scalability with the third power of molecular size great for large systems
  - Variety of basis sets and functional available based on level of accuracy needed
- TDDFT useful for modeling excited states and predicting transitions
  - Structure-property elucidation is more available
    - Determine energy levels and excited state transitions.
    - Predict absorption and emission spectra which is critical for applications
    - Modeled geometries and FMOs assist to elucidate optical, electronic, and physical properties to elucidate structure-property relationships

There is a demand for new conjugated materials for renewable and clean energy or more efficient materials. These materials can satisfy current demands such as OPVs and OLEDs but also offer niche applications to take advantage of their lightweight and flexible nature and ease of processing. Benzobisazoles are excellent building block for conjugated materials as their properties are tunable through synthetic modification and their synthesis is easily scalable making them appropriate for large scale production. However, modifications rarely impact a single property and can have a beneficial or detrimental effect on several

molecular properties. In order to elucidate this prior to material synthesis, computational modeling can be used to focus on the specific materials with the most desirable properties. This tool assists in developing new conjugated materials to provide higher efficiency materials needed for the commercial development of organic semiconductors.

1.10 References

(1) Shirakawa, H.; Louis, E. J.; MacDiarmid, A. G.; Chiang, C. K.; Heeger, A. J. *Journal of the Chemical Society, Chemical Communications* **1977**, 578.

(2) Chiang, C. K.; Druy, M. A.; Gau, S. C.; Heeger, A. J.; Louis, E. J.; MacDiarmid, A. G.; Park, Y. W.; Shirakawa, H. *Journal of the American Chemical Society* **1978**, *100*, 1013.

(3) Tang, C. W. *Applied Physics Letters* **1986**, *48*, 183.

(4) Scharber, M. C.; Muehlbacher, D.; Koppe, M.; Denk, P.; Waldauf, C.; Heeger, A. J.; Brabec, C. J. *Advanced Materials* **2006**, *18*, 789.

(5) Thompson, B. C.; Fréchet, J. M. J. *Angewandte Chemie International Edition* **2008**, *47*, 58.

(6) Cheng, Y.-J.; Yang, S.-H.; Hsu, C.-S. *Chemical Reviews* **2009**, *109*, 5868.

(7) Bhuwalka, A.; Mike, J. F.; He, M.; Intemann, J. J.; Nelson, T.; Ewan, M. D.; Roggers, R. A.; Lin, Z.; Jeffries-El, M. *Macromolecules* **2011**, *44*, 9611.

(8) Tang, C. W.; VanSlyke, S. A. *Applied Physics Letters* **1987**, *51*, 913.

(9) Friend, R. H.; Gymer, R. W.; Holmes, A. B.; Burroughes, J. H.; Marks, R. N.; Taliani, C.; Bradley, D. D. C.; Dos Santos, D. A.; Bredas, J. L.; Logdlund, M.; Salaneck, W. R. *Nature* **1999**, *397*, 121.

(10) Mike, J. F.; Intemann, J. J.; Cai, M.; Xiao, T.; Shinar, R.; Shinar, J.; Jeffries-El, M. *Polymer Chemistry* **2011**, *2*, 2299.

(11) Intemann, J. J.; Hellerich, E. S.; Tlach, B. C.; Ewan, M. D.; Barnes, C. A.; Bhuwalka, A.; Cai, M.; Shinar, J.; Shinar, R.; Jeffries-El, M. *Macromolecules* **2012**, *45*, 6888.

(12) Burroughes, J. H.; Bradley, D. D. C.; Brown, A. R.; Marks, R. N.; Mackay, K.; Friend, R. H.; Burns, P. L.; Holmes, A. B. *Nature* **1990**, *347*, 539.

(13) Dimitrakopoulos, C. D.; Malenfant, P. R. L. *Advanced Materials* **2002**, *14*, 99.

(14) Babel, A.; Jenekhe, S. A. *Advanced Materials* **2002**, *14*, 371.

(15) Babel, A.; Jenekhe, S. A. *The Journal of Physical Chemistry B* **2002**, *106*, 6129.

(16) Yoon, M.-H.; DiBenedetto, S. A.; Facchetti, A.; Marks, T. J. *Journal of the American Chemical Society* **2005**, *127*, 1348.

(17) Meyer, W. H. *Advanced Materials* **1998**, *10*, 439.

(18) Pan, L.; Qiu, H.; Dou, C.; Li, Y.; Pu, L.; Xu, J.; Shi, Y. *International Journal of Molecular Sciences* **2010**, *11*, 2636.

(19) Appetecchi, G. B.; Croce, F.; Persi, L.; Ronci, F.; Scrosati, B. *Electrochim. Acta* **2000**, *45*, 1481.

(20) Mike, J. F.; Lutkenhaus, J. L. *ACS Macro Letters* **2013**, *2*, 839.

(21) Lim, J.; Miljanic, O. S. *Chem. Commun. (Cambridge, U. K.)* **2012**, *48*, 10301.

(22) Zucchero, A. J.; Wilson, J. N.; Bunz, U. H. F. *Journal of the American Chemical Society* **2006**, *128*, 11872.

(23) Zhou, Z.; Shinar, R.; Allison, A. J.; Shinar, J. *Advanced Functional Materials* **2007**, *17*, 3530.

(24) Samyn, C.; Verbiest, T.; Persoons, A. *Macromolecular Rapid Communications* **2000**, *21*, 1.

(25) Nalwa, H. S. *Advanced Materials* **1993**, *5*, 341.

(26) Gribov, B. G.; Zinov'ev, K. V. *Inorganic Materials* **2003**, *39*, 653.

(27) Davis, J. R., Jr.; Rohatgi, A.; Hopkins, R. H.; Blais, P. D.; Rai-Choudhury, P.; McCormick, J. R.; Mollenkopf, H. C. *Electron Devices, IEEE Transactions on* **1980**, *27*, 677.

(28) Chang, J.-F.; Sun, B.; Breiby, D. W.; Nielsen, M. M.; Sölling, T. I.; Giles, M.; McCulloch, I.; Sirringhaus, H. *Chemistry of Materials* **2004**, *16*, 4772.

(29) Sirringhaus, H.; Kawase, T.; Friend, R. H.; Shimoda, T.; Inbasekaran, M.; Wu, W.; Woo, E. P. *Science (Washington, D. C.)* **2000**, *290*, 2123.

(30) Mori, K.; Ning, T.; Ichikawa, M.; Koyama, T.; Taniguchi, Y. *Jpn. J. Appl. Phys., Part 2* **2000**, *39*, L942.

(31) Kim, Y.-G.; Thompson, B. C.; Ananthakrishnan, N.; Padmanaban, G.; Ramakrishnan, S.; Reynolds, J. R. *Journal of Materials Research* **2005**, *20*, 3188.

(32) Bredas, J. L.; Silbey, R.; Boudreaux, D. S.; Chance, R. R. *Journal of the American Chemical Society* **1983**, *105*, 6555.

(33) Anslyn, E. V.; Dougherty, D. A. *Modern Physical Organic Chemistry*; University Sciences: Sausalito, CA, 2004.

(34) Yannoni, C. S.; Clarke, T. C. *Physical Review Letters* **1983**, *51*, 1191.

(35) Jenekhe, S. A. *Nature* **1986**, *322*, 345.

(36) Brédas, J. L.; Chance, R. R.; Silbey, R. *Physical Review B* **1982**, *26*, 5843.

(37) Brisset, H.; Thobie-Gautier, C.; Jubault, M.; Gorgues, A.; Roncali, J. *Journal of the Chemical Society, Chemical Communications* **1994**, 1765.

(38) Blanchard, P.; Verlhac, P.; Michaux, L.; Frère, P.; Roncali, J. *Chemistry – A European Journal* **2006**, *12*, 1244.

(39) Brédas, J. L. *The Journal of Chemical Physics* **1985**, *82*, 3808.

(40) Hoogmartens, I.; Adriaensens, P.; Vanderzande, D.; Gelan, J.; Quattrocchi, C.; Lazzaroni, R.; Bredas, J. L. *Macromolecules* **1992**, *25*, 7347.

(41) van Mullekom, H. A. M.; Vekemans, J. A. J. M.; Havinga, E. E.; Meijer, E. W. *Materials Science and Engineering: R: Reports* **2001**, *32*, 1.

(42) Jenekhe, S. A.; Lu, L.; Alam, M. M. *Macromolecules* **2001**, *34*, 7315.

(43) Yamamoto, T.; Zhou, Z.-h.; Kanbara, T.; Shimura, M.; Kizu, K.; Maruyama, T.; Nakamura, Y.; Fukuda, T.; Lee, B.-L.; Ooba, N.; Tomaru, S.; Kurihara, T.; Kaino, T.; Kubota, K.; Sasaki, S. *Journal of the American Chemical Society* **1996**, *118*, 10389.

(44) Murphy, A. R.; Liu, J.; Luscombe, C.; Kavulak, D.; Fréchet, J. M. J.; Kline, R. J.; McGehee, M. D. *Chemistry of Materials* **2005**, *17*, 4892.

(45) Veldman, D.; Meskers, S. C. J.; Janssen, R. A. J. *Advanced Functional Materials* **2009**, *19*, 1939.

(46) Kline, R. J.; McGehee, M. D.; Kadnikova, E. N.; Liu, J.; Fréchet, J. M. J. *Advanced Materials* **2003**, *15*, 1519.

(47) Li, Y.; Chen, Y.; Liu, X.; Wang, Z.; Yang, X.; Tu, Y.; Zhu, X. *Macromolecules* **2011**, *44*, 6370.

(48) Friedel, B.; McNeill, C. R.; Greenham, N. C. *Chemistry of Materials* **2010**, *22*, 3389.

(49) Gadisa, A.; Oosterbaan, W. D.; Vandewal, K.; Bolsée, J.-C.; Bertho, S.; D'Haen, J.; Lutsen, L.; Vanderzande, D.; Manca, J. V. *Advanced Functional Materials* **2009**, *19*, 3300.

(50) Chu, C.-W.; Yang, H.; Hou, W.-J.; Huang, J.; Li, G.; Yang, Y. *Applied Physics Letters* **2008**, *92*.

(51) Grimsdale, A. C.; Leok Chan, K.; Martin, R. E.; Jokisz, P. G.; Holmes, A. B. *Chemical Reviews* **2009**, *109*, 897.

(52) Jenekhe, S. A.; Osaheni, J. A. *Science* **1994**, *265*, 765.

(53) Egbe, D. A. M.; Carbonnier, B.; Birckner, E.; Grummt, U.-W. *Progress in Polymer Science* **2009**, *34*, 1023.

(54) Mike, J. F.; Makowski, A. J.; Mauldin, T. C.; Jeffries-El, M. *Journal of Polymer Science Part A: Polymer Chemistry* **2010**, *48*, 1456.

(55) Osman, A. M.; Mohamed, S. A. *U. A. R. J. Chem.* **1971**, *14*, 475.

(56) Osman, A. M.; Mohamed, S. A. *U. A. R. J. Chem.* **1971**, *14*, 493.

(57) Osman, A. M.; Khalaf, A. A.; Amer, F. A. K. *Indian J. Chem.* **1974**, *12*, 120.

(58) Osman, A. M.; Metwally, S. A. M. *Indian J. Chem.* **1974**, *12*, 775.

(59) Wolfe, J. F. *Encyclopedia of Polymeric Science and Engineering*; John Wiley and Sons: New York, New York, 1988; Vol. 11.

(60) Allen, S. R.; Filippov, A. G.; Farris, R. J.; Thomas, E. L.; Wong, C. P.; Berry, G. C.; Chenevey, E. C. *Macromolecules* **1981**, *14*, 1135.

(61) Wolfe, J. F.; Loo, B. H.; SRI International, USA . 1980, p 4 pp.

(62) Wolfe, J. F.; Loo, B. H.; Arnold, F. E. *Macromolecules* **1981**, *14*, 915.

(63) Wolfe, J. F.; Arnold, F. E. *Macromolecules* **1981**, *14*, 909.

(64) Welsh, W. J.; Bhaumik, D.; Mark, J. E. *Macromolecules* **1981**, *14*, 947.

(65) Roberts, M. F.; Jenekhe, S. A. *Chemistry of Materials* **1993**, *5*, 1744.

(66) Osaheni, J. A.; Jenekhe, S. A. *Journal of the American Chemical Society* **1995**, *117*, 7389.

(67) Alam, M. M.; Jenekhe, S. A. *Chemistry of Materials* **2002**, *14*, 4775.

(68) Allen, S. R.; Farris, R. J.; Thomas, E. L. *J Mater Sci* **1985**, *20*, 2727.

(69) Feldman, L.; Farris, R. J.; Thomas, E. L. *J Mater Sci* **1985**, *20*, 2719.

(70) Tamargo-Martínez, K.; Villar-Rodil, S.; Paredes, J. I.; Martínez-Alonso, A.; Tascón, J. M. D. *Chemistry of Materials* **2003**, *15*, 4052.

(71) Walsh, P. J.; Hu, X.; Cunniff, P.; Lesser, A. J. *Journal of Applied Polymer Science* **2006**, *102*, 3517.

(72) Chow, A. W.; Bitler, S. P.; Penwell, P. E.; Osborne, D. J.; Wolfe, J. F. *Macromolecules* **1989**, *22*, 3514.

(73) Bhaumik, D.; Welsh, W. J.; Jaffe, H. H.; Mark, J. E. *Macromolecules* **1981**, *14*, 951.

(74) Jois, Y. H. R.; Gibson, H. W. *Journal of Heterocyclic Chemistry* **1992**, *29*, 1365.

(75) So, Y.-H.; Zaleski, J. M.; Murlick, C.; Ellaboudy, A. *Macromolecules* **1996**, *29*, 2783.

(76) So, Y.-H.; Heeschen, J. P. *The Journal of Organic Chemistry* **1997**, *62*, 3552.

(77) Lin, C.-W.; Hsu, S. L. C.; Yang, A. C. M. *Polymer* **2012**, *53*, 1951.

(78) Joseph, W. D.; Mercier, R.; Prasad, A.; Marand, H.; McGrath, J. E. *Polymer* **1993**, *34*, 866.

(79) Joseph, W. D.; Abed, J. C.; Mercier, R.; McGrath, J. E. *Polymer* **1994**, *35*, 5046.

(80) Maruyama, Y.; Oishi, Y.; Kakimoto, M.; Imai, Y. *Macromolecules* **1988**, *21*, 2305.

(81) Tanaka, Y.; Oishi, Y.; Kakimoto, M.-A.; Imai, Y. *Journal of Polymer Science Part A: Polymer Chemistry* **1991**, *29*, 1941.

(82) Itoya, K.; Arata, M.; Kakimoto, M.-A.; Imai, Y.; Maeda, J.; Kurosaki, T. *Journal of Macromolecular Science, Part A* **1994**, *31*, 817.

(83) Kricheldorf, H. R.; Engelhardt, J. *Die Makromolekulare Chemie* **1989**, *190*, 2939.

(84) Kricheldorf, H. R.; Domschke, A. *Polymer* **1994**, *35*, 198.

(85) Ahmed, E.; Kim, F. S.; Xin, H.; Jenekhe, S. A. *Macromolecules* **2009**, *42*, 8615.

(86) Ueda, S.; Nagasawa, H. *The Journal of Organic Chemistry* **2009**, *74*, 4272.

(87) Evindar, G.; Batey, R. A. *J. Org. Chem.* **2006**, *71*, 1802.

(88) Saha, P.; Ali, M. A.; Punniyamurthy, T. *Org. Synth.* **2011**, *88*, 398.

(89) Altenhoff, G.; Glorius, F. *Advanced Synthesis & Catalysis* **2004**, *346*, 1661.

(90) Sun, Y.; Jiang, H.; Wu, W.; Zeng, W.; Wu, X. *Org. Lett.* **2013**, *15*, 1598.

(91) Bonnamour, J.; Bolm, C. *Organic Letters* **2008**, *10*, 2665.

(92) Bochatay, V. N.; Boissarie, P. J.; Murphy, J. A.; Suckling, C. J.; Lang, S. *The Journal of Organic Chemistry* **2013**, *78*, 1471.

(93) Nguyen, T. B.; Ermolenko, L.; Dean, W. A.; Al-Mourabit, A. *Organic Letters* **2012**, *14*, 5948.

(94) Mike, J. F.; Makowski, A. J.; Jeffries-El, M. *Organic Letters* **2008**, *10*, 4915.

(95) Mike, J. F.; Inteman, J. J.; Ellern, A.; Jeffries-El, M. *The Journal of Organic Chemistry* **2009**, *75*, 495.

(96) Tschitschibabin, A. E. *Ber.* **1905**, *38*, 561.

(97) Breslow, R.; Pandey, P. S. *J. Org. Chem.* **1980**, *45*, 740.

(98) Mamane, V.; Aubert, E.; Fort, Y. *Journal of Organic Chemistry* **2007**, *72*, 7294.

(99) Intemann, J. J.; Mike, J. F.; Cai, M.; Bose, S.; Xiao, T.; Mauldin, T. C.; Roggers, R. A.; Shinar, J.; Shinar, R.; Jeffries-El, M. *Macromolecules* **2010**, *44*, 248.

(100) Bhuwalka, A.; Mike, J. F.; He, M.; Intemann, J. J.; Nelson, T.; Ewan, M. D.; Roggers, R. A.; Lin, Z.; Jeffries-El, M. *Macromolecules* **2011**.

(101) Mike, J. F.; Nalwa, K.; Makowski, A. J.; Putnam, D.; Tomlinson, A. L.; Chaudhary, S.; Jeffries-El, M. *Physical Chemistry Chemical Physics* **2011**, *13*, 1338.

(102) Intemann, J. J.; Mike, J. F.; Cai, M.; Barnes, C. A.; Xiao, T.; Roggers, R. A.; Shinar, J.; Shinar, R.; Jeffries-El, M. *Journal of Polymer Science Part A: Polymer Chemistry* **2013**, *51*, 916.

(103) Intemann, J.; Mike, J.; Cai, M.; Bose, S.; Xiao, T.; Mauldin, T.; Roggers, R.; Shinar, J.; Shinar, R.; Jeffries-EL, M. *Macromolecules* **2011**, *44*, 248.

(104) Klimavicz, J. S.; Mike, J. F.; Bhuwalka, A.; Tomlinson, A. L.; Jeffries-El, M. *Pure and Applied Chemistry* **2012**, *84*, 991.

(105) Tlach, B. C.; Tomlinson, A. L.; Bhuwalka, A.; Jeffries-El, M. *The Journal of Organic Chemistry* **2011**, *76*, 8670.

(106) Tlach, B. C.; Tomlinson, A. L.; Ryno, A. G.; Knoble, D. D.; Drochner, D. L.; Krager, K. J.; Jeffries-El, M. *The Journal of Organic Chemistry* **2013**, *78*, 6570.

(107) Tlach, B. C.; Tomlinson, A. L.; Morgan, K. D.; Collins, C. R.; Zenner, M. D.; Jeffries-EL, M. *Australian Journal of Chemistry* **2014**, *67*, 711.

(108) Zucchero, A. J.; McGrier, P. L.; Bunz, U. H. F. *Accounts of Chemical Research* **2009**, *43*, 397.

(109) Wilson, J. N.; Josowicz, M.; Wang, Y.; Bunz, U. H. F. *Chemical Communications* **2003**, 2962.

(110) Ripaud, E.; Olivier, Y.; Leriche, P.; Cornil, J. r. m.; Roncali, J. *The Journal of Physical Chemistry B* **2011**, *115*, 9379.

(111) Wilson, J. N.; Windscheif, P. M.; Evans, U.; Myrick, M. L.; Bunz, U. H. F. *Macromolecules* **2002**, *35*, 8681.

(112) Klare, J. E.; Tulevski, G. S.; Nuckolls, C. *Langmuir* **2004**, *20*, 10068.

(113) May, J. C.; Biaggio, I.; Bures, F.; Diederich, F. *Applied Physics Letters* **2007**, *90*, 251106.

(114) Gao, B.; Liu, Y.; Geng, Y.; Cheng, Y.; Wang, L.; Jing, X.; Wang, F. *Tetrahedron Letters* **2009**, *50*, 1649.

(115) Würthner, F.; Thalacker, C.; Diele, S.; Tschierske, C. *Chemistry – A European Journal* **2001**, *7*, 2245.

(116) Wilson, J. N.; Hardcastle, K. I.; Josowicz, M.; Bunz, U. H. F. *Tetrahedron* **2004**, *60*, 7157.

(117) Hopf, H.; Maas, G. *Angewandte Chemie International Edition in English* **1992**, *31*, 931.

(118) Nielsen, M. B.; Schreiber, M.; Baek, Y. G.; Seiler, P.; Lecomte, S.; Boudon, C.; Tykwinski, R. R.; Gisselbrecht, J.-P.; Gramlich, V.; Skinner, P. J.; Bosshard, C.; Günter, P.; Gross, M.; Diederich, F. *Chemistry – A European Journal* **2001**, *7*, 3263.

(119) Wilson, J. N.; Smith, M. D.; Enkelmann, V.; Bunz, U. H. F. *Chemical Communications* **2004**, 1700.

(120) Wilson, J. N.; Bunz, U. H. F. *Journal of the American Chemical Society* **2005**, *127*, 4124.

(121) Tolosa, J.; Zucchero, A. J.; Bunz, U. H. F. *Journal of the American Chemical Society* **2008**, *130*, 6498.

(122) McGrier, P. L.; Solntsev, K. M.; Miao, S.; Tolbert, L. M.; Miranda, O. R.; Rotello, V. M.; Bunz, U. H. F. *Chemistry – A European Journal* **2008**, *14*, 4503.

(123) Marsden, J. A.; Miller, J. J.; Shirtcliff, L. D.; Haley, M. M. *Journal of the American Chemical Society* **2005**, *127*, 2464.

(124) Spitler, E. L.; Shirtcliff, L. D.; Haley, M. M. *The Journal of Organic Chemistry* **2006**, *72*, 86.

(125) Spitler, E. L.; Shirtcliff, L. D.; Haley, M. M. *The Journal of Organic Chemistry* **2007**, *72*, 86.

(126) Spitler, E. L.; Monson, J. M.; Haley, M. M. *The Journal of Organic Chemistry* **2008**, *73*, 2211.

(127) Ohta, K.; Yamada, S.; Kamada, K.; Slepkov, A. D.; Hegmann, F. A.; Tykwinski, R. R.; Shirtcliff, L. D.; Haley, M. M.; Salek, P.; Gel'mukhanov, F.; Aagren, H. *J. Phys. Chem. A* **2011**, *115*, 105.

(128) Chase, D. T.; Young, B. S.; Haley, M. M. *The Journal of Organic Chemistry* **2011**, *76*, 4043.

(129) Schwaebel, T.; Lirag, R. C.; Davey, E. A.; Lim, J.; Bunz, U. H. F.; Miljanic, O. S. *J. Visualized Exp.* **2013**, e50858.

(130) Osowska, K.; Miljanic, O. S. *Chemical Communications* **2010**, *46*, 4276.

(131) Lim, J.; Albright, T. A.; Martin, B. R.; Miljanić, O. Š. *The Journal of Organic Chemistry* **2011**, *76*, 10207.

(132) Lim, J.; Nam, D.; Miljanic, O. S. *Chemical Science* **2012**, *3*, 559.

(133) Jo, M.; Lim, J.; Miljanic, O. S. *Org. Lett.* **2013**, *15*, 3518.

(134) Martinez-Martinez, V.; Lim, J.; Banuelos, J.; Lopez-Arbeloa, I.; Miljanic, O. S. *Phys. Chem. Chem. Phys.* **2013**, *15*, 18023.

(135) Kang, H.; Zhu, P.; Yang, Y.; Facchetti, A.; Marks, T. J. *Journal of the American Chemical Society* **2004**, *126*, 15974.

(136) Kang, H.; Evmenenko, G.; Dutta, P.; Clays, K.; Song, K.; Marks, T. J. *Journal of the American Chemical Society* **2006**, *128*, 6194.

(137) Klare, J. E.; Tulevski, G. S.; Sugo, K.; de Picciotto, A.; White, K. A.; Nuckolls, C. *Journal of the American Chemical Society* **2003**, *125*, 6030.

(138) Klare, J. E.; Tulevski, G. S.; Sugo, K.; de Picciotto, A.; White, K. A.; Nuckolls, C. *Journal of the American Chemical Society* **2003**, *125*, 6030.

(139) Saeed, M. A.; Le, H. T. M.; Miljanić, O. Š. *Accounts of Chemical Research* **2014**.

(140) De Angelis, F.; Fantacci, S.; Sgamellotti, A. *Theor Chem Account* **2007**, *117*, 1093.

(141) Novoa, J. J.; Sosa, C. *The Journal of Physical Chemistry* **1995**, *99*, 15837.

(142) Magyar, R. J.; Tretiak, S. *Journal of Chemical Theory and Computation* **2007**, *3*, 976.

(143) Zhang, L.; Zhang, Q.; Ren, H.; Yan, H.; Zhang, J.; Zhang, H.; Gu, J. *Solar Energy Materials and Solar Cells* **2008**, *92*, 581.

(144) Scott, A. P.; Radom, L. *The Journal of Physical Chemistry* **1996**, *100*, 16502.

(145) Weigend, F.; Ahlrichs, R. *Physical Chemistry Chemical Physics* **2005**, *7*, 3297.

(146) Zheng, J.; Xu, X.; Truhlar, D. *Theor Chem Account* **2011**, *128*, 295.

(147) Zade, S. S.; Zamoshchik, N.; Bendikov, M. *Accounts of Chemical Research* **2010**, *44*, 14.

(148) Lee, C.; Yang, W.; Parr, R. G. *Physical Review B* **1988**, *37*, 785.

(149) Becke, A. D. *The Journal of Chemical Physics* **1993**, *98*, 1372.

(150) Becke, A. D. *Journal of Chemical Physics* **1993**, *98*, 5648.

(151) Hohenberg, P.; Kohn, W. *Physical Review* **1964**, *136*, B864.

(152) Kohn, W.; Sham, L. J. *Physical Review* **1965**, *140*, A1133.

(153) Johnson, B. G.; Gill, P. M. W.; Pople, J. A. *The Journal of Chemical Physics* **1993**, *98*, 5612.

(154) Gill, P. M. W.; Johnson, B. G.; Pople, J. A. *Chemical Physics Letters* **1993**, *209*, 506.

(155) Masunov, A.; Tretiak, S. *The Journal of Physical Chemistry B* **2003**, *108*, 899.

(156) Møller, C.; Plesset, M. S. *Physical Review* **1934**, *46*, 618.

(157) Osuna, R. M.; Ortiz, R. P.; Okamoto, T.; Suzuki, Y.; Yamaguchi, S.; Hernández, V.; López Navarrete, J. T. *The Journal of Physical Chemistry B* **2007**, *111*, 7488.

(158) Vosko, S. H.; Wilk, L.; Nusair, M. *Canadian Journal of Physics* **1980**, *58*, 1200.

(159) Jin, Z.; Masuda, H.; Yamanaka, N.; Minami, M.; Nakamura, T.; Nishikitani, Y. *The Journal of Physical Chemistry C* **2009**, *113*, 2618.

(160) Angelis, F. D.; Fantacci, S.; Selloni, A. *Nanotechnology* **2008**, *19*, 424002.

(161) Goerigk, L.; Grimme, S. *Physical Chemistry Chemical Physics* **2011**, *13*, 6670.

(162) Fantacci, S.; Migani, A.; Olivucci, M. *The Journal of Physical Chemistry A* **2004**, *108*, 1208.

(163) Runge, E.; Gross, E. K. U. *Physical Review Letters* **1984**, *52*, 997.

(164) Petersilka, M.; Gossmann, U. J.; Gross, E. K. U. *Physical Review Letters* **1996**, *76*, 1212.

(165) Hsu, C.-P.; Hirata, S.; Head-Gordon, M. *The Journal of Physical Chemistry A* **2000**, *105*, 451.

(166) Milian Medina, B.; VanVooren, A.; Brocorens, P.; Gierschner, J.; Shkunov, M.; Heeney, M.; McCulloch, I.; Lazzaroni, R.; Cornil, J. *Chemistry of Materials* **2007**, *19*, 4949.

(167) Liu, K. L.; Vosko, S. H. *Canadian Journal of Physics* **1989**, *67*, 1015.

(168) Fantacci, S.; De Angelis, F.; Sgamellotti, A.; Marrone, A.; Re, N. *Journal of the American Chemical Society* **2005**, *127*, 14144.

(169) De Angelis, F.; Car, R.; Spiro, T. G. *Journal of the American Chemical Society* **2003**, *125*, 15710.

(170) Belletête, M.; Blouin, N.; Boudreault, P.-L. T.; Leclerc, M.; Durocher, G. *Journal of Physical Chemistry A* **2006**, *110*, 13696.

(171) Blouin, N.; Michaud, A.; Gendron, D.; Wakim, S.; Blair, E.; Neagu-Plesu, R.; Belletete, M.; Durocher, G.; Tao, Y.; Leclerc, M. *Journal of the American Chemical Society* **2008**, *130*, 732.

(172) Liu, T.; Gao, J.-S.; Xia, B.-H.; Zhou, X.; Zhang, H.-X. *Polymer* **2007**, *48*, 502.

(173) Pogantsch, A.; Heimel, G.; Zojer, E. In *Journal of Chemical Physics*; American Institute of Physics: 2002; Vol. 117, p 5921.

(174) Gierschner, J.; Cornil, J.; Egelhaaf, H.-J. *Advanced Materials* **2007**, *19*, 173.

CHAPTER 2

TUNING THE OPTICAL AND ELECTRONIC PROPERTIES OF 4,8-DISUBSTITUTED BENZOBISOXAZOLES VIA ALKYNE SUBSTITUTION

Reproduced with permission from *J. Org. Chem.* **2011,** *76,* 8670.

DOI: 10.1021/jo201078w

Brian C. Tlach,[a] *Aimée L. Tomlinson,*[b] *Achala Bhuwalka,*[a] *and Malika Jeffries-EL*[a]*

[a] Department of Chemistry, Iowa State University, Ames IA 50010

[b] Department of Chemistry North Georgia College & State University, GA 30597.

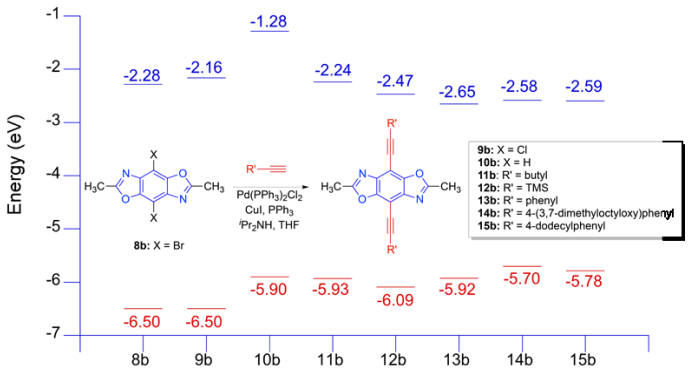

2.1 Abstract

In an effort to design new electron-deficient building blocks for the synthesis of conjugated materials, a series of new *trans*-benzobisoxazoles bearing halogen or alkynyl substituents at the 4,8-positions was synthesized. Additionally, the impact of these modifications on the optical and electronic properties was investigated. Theoretical calculations predicted that the incorporation of various alkynes can be used to tune the energy levels and band gaps of these small molecules. The targeted 4,8-disubstituted benzobisoxazoles were easily prepared in good yields using a two-step reaction sequence: Lewis acid catalyzed orthoester cyclization followed by Sonogashira cross-coupling. The experimentally determined HOMO values for these 4,8-disubstituted benzobisoxazoles ranged from -4.97 to -6.20 eV and showed reasonable correlation to the theoretically predicted values, with a percent deviation that ranged from 2.4 - 12.8%. However, the deviation between actual and predicted HOMO values was reduced to less than 3.5% when the theoretical values were extrapolated to the long chain limit and compared to copolymers containing the 4,8-disubstituted benzobisoxazoles. Collectively, these results indicate that these 4,8-disubstituted *trans*-benzobisoxazoles can be used for the synthesis of new conjugated materials with electronic properties that are variable and predictable.

2.1 Introduction

Conjugated polymers (CPs) are currently being investigated as replacements for traditional inorganic materials in applications such as field effect transistors (FET)s,[1-5] organic light emitting diodes (OLED)s,[6-8] and photovoltaic cells (PVC)s.[9-12] The development of these organic semiconductors is motivated by the potential to reduce the cost

of device fabrication through the use of solution based techniques, and the ability to tune the energy levels for specific applications through chemical synthesis.[13] Currently, a common approach for tuning the properties of CPs is through the synthesis of materials composed of alternating electron-donating and electron-accepting moieties.[14-17] By varying the strength of the donor and acceptor components in the polymer backbone, the highest occupied molecular orbital (HOMO), lowest unoccupied molecular orbital (LUMO), and band gap of the resulting polymer can be readily manipulated.[15,18] Since there are many known π-systems, a wide range of energy levels can be obtained by combining different components. However, in practice certain combinations of properties such as electron-donating and hole-transporting materials (*p*-type) with low lying LUMO levels and narrow band gaps; or electron-accepting and electron-transporting materials (*n*-type) with good solubility are more difficult to attain. Thus, the design of new electron-rich or electron-poor building blocks remains a flourishing area of research.[13]

In this respect, benzobisoxazoles (BBO)s are promising electron-deficient heterocycles for the development of new polymers due to their near-planar structure which can facilitate efficient packing and charge transport.[19-22] Recently, BBOs have been used for the synthesis of donor-acceptor conjugated polymers, however, due to the relatively weak electron-accepting nature of the BBO moiety the resulting materials have had fairly wide bands gaps (1.9 - 2.3 eV).[23-25] Since BBO has two positions on the central benzene ring (4- and 8-) available for structural modification, it may be possible to design new derivatives that are better electron acceptors. In this paper, we evaluate alkyne substitution as an approach to increase electron affinity. We investigated the use of alkynes since, according to the Pauling scale, their electronegativity is similar to that of the cyano group (3.3), which has been

widely used in the synthesis of electron-deficient building blocks.[26] Alkynes have also been utilized to alter the electronic properties of conjugated materials.[27-34] In addition, alkynes offer the advantage of facile installation via Sonogashira cross-coupling. In the case of the BBO moiety, the additional structural variation through substitution facilitates the efficient synthesis of materials with tunable electronic properties by using shared synthetic intermediates. Herein, we examine the influence of alkyne substitution at the central benzene ring on the optical and electronic properties of 4,8-disubstituted benzo[1,2-*d*;4,5-*d'*]bisoxazoles (BBO)s, using a combination of synthetic and computational techniques.

2.3 Results and Discussion

2.3.1 Model Compound Synthesis

The synthesis of 4,8-dihalogenated-2,6-disubstituted BBOs is shown in Scheme 2.2. Recently, we reported a simple method for the synthesis of 2,6-disubstituted BBOs that occurs readily at low temperatures and is tolerant of a number of functional groups.[35] Utilizing this method and the halogenated diaminohydroquinones **5** and **6** we were able to synthesize several 4,8-dichloro and 4,8-dibromo-2,6-disubstituted-BBOs in good yields. The lowest yields were observed when ethyl triethoxyacetate (**7e**) was used for the synthesis of **8e** and **9e**. The reduction in yield is likely due to the poor nucleophilic site adjacent to the ester group. Although this reaction proceeded slowly, the moderate yields obtained (26 - 41%) are higher than previously reported values.[21] We also modified the synthesis of **8d** and **9d** by using THF as the solvent due to the limited solubility of triethyl orthopropiolate (**7d**) in DMA or DMSO. In all cases, the products were easily isolated by precipitation of the reaction mixture in water, filtration, followed by recrystallization from an appropriate

solvent. Due to the scalable nature of the reactions, several compounds were prepared in multi-gram quantities without a decrease in yield.

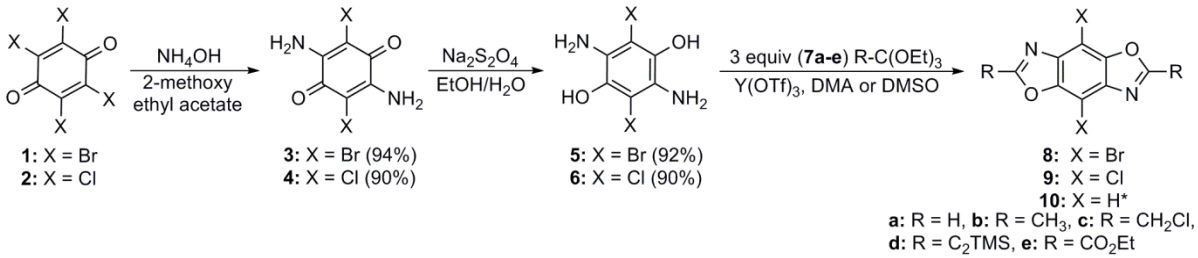

Scheme 2.1. Synthesis of 2,6-disubstituted-4,8-dihalogenated BBOs. ***10b** was synthesized according to literature procedure.[35]

The synthesis of the 4-alkyl and 4-alkoxyphenylacetylenes is shown in Scheme 2.2. The flexible side chains were appended to improve the solubility of the resulting BBOs. The corresponding 4,8-bisalkynyl BBOs **11b**, **13b**, **14b**, **15b**, **15f**, and **16f** were obtained in good yields (73% to 88%) with **12b** in a lower yield (49%), by the Sonogashira cross-coupling reaction of 4,8-dibromo-2,6-dimethyl BBO **8b** and various alkynes as shown in Scheme 2.4.

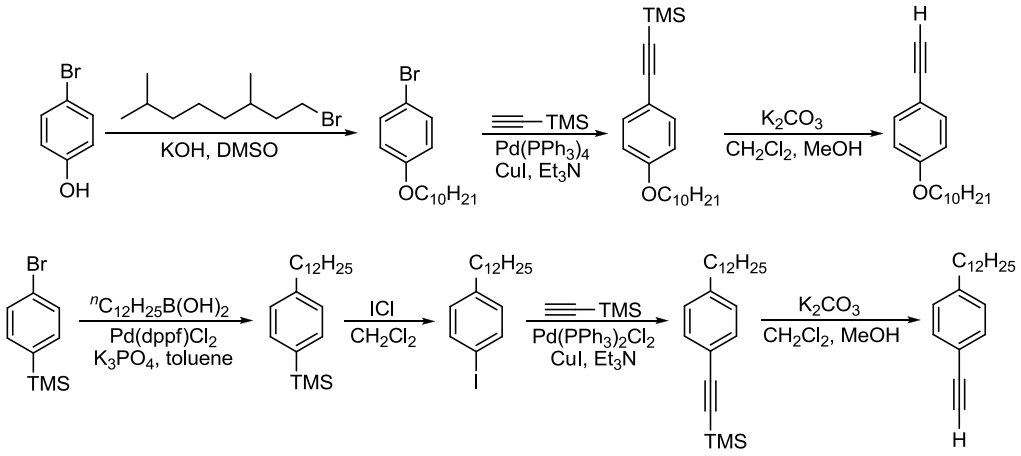

Scheme 2.2. Synthesis of substituted phenylacetylenes.

The resultant substituted BBOs were fully characterized by ^{1}H NMR, ^{13}C NMR and high-resolution mass spectroscopy. For the most part, all attempts to grow crystals of the benzobisoxazoles via recrystallization or slow solvent evaporation produced either powders or small crystals that were unsuitable for X-ray crystallography. However, we were able to obtain suitable crystals of **8c**, **9a**, **9c**, and **10a** (see the crystallographic data in the Supporting Information).

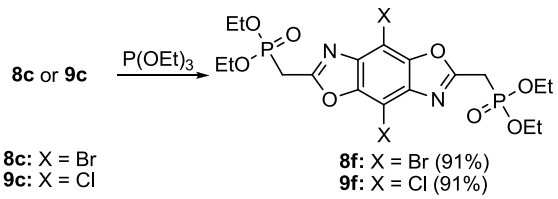

Scheme 2.3. Synthesis of bis(phosphonate) esters by Arbuzov reaction.

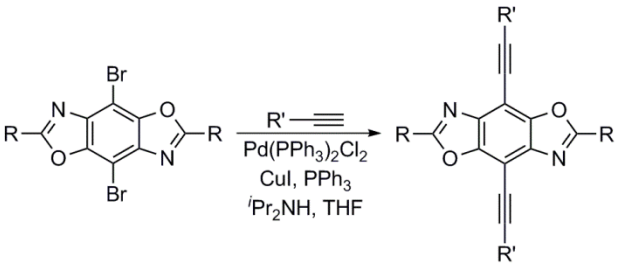

11b: R = CH_3, R' = butyl (88%)
12b: R = CH_3, R' = TMS (49%)
13b: R = CH_3, R' = phenyl (79%)
14b: R = CH_3, R' = 4-(3,7-dimethyloctyloxy)phenyl (84%)
15b: R = CH_3, R' = 4-dodecylphenyl (73%)
15f: R = $CH_2PO(OEt)_2$, R' = 4-dodecylphenyl (65%)
16f: R = $CH_2PO(OEt)_2$, R' = octyl (74%)

Scheme 2.4. Modification of 4,8-dibromobenzobisoxazoles by Sonogashira cross-coupling.

2.3.2 Polymer synthesis

The synthesis of the 4,8-disubstituted poly(arylene vinylene benzobisoxazole)s is shown in Scheme 2.5. The bis(phosphonate) esters **8f** and **9f** were synthesized by the

Arbuzov reaction of the corresponding 2,6-bis(chloromethyl) BBOs **8c** and **9c** and triethylphosphite as shown in Scheme 2.3.[23] The bis(phosphonate) esters **15f** and **16f** were synthesized as shown in Scheme 2.4 by Sonogashira cross-coupling of **8f** with 1-decyne and 4-dodecylphenylacetylene, respectively. The Horner-Wadsworth-Emmons (HWE) polymerization of BBO monomers **8f**, **15f** or **16f** and 2,5-didodecyloxyterephthaldehyde[36] produced polymers **P1**, **P2** and **P3** in yields of 56%, 87%, and 55% respectively. Similarly, the HWE polymerization of BBO monomers **8f** or **9f** and 3,4-didodecylthiophene dicarboxaldehyde[37], yielded the corresponding polymers **P4** and **P5** in yields of 61% and 55%, respectively. **P1**, **P3**, **P5**, and **P6** were polymerized using potassium *tert*-butoxide as the base. The base-sensitive propargyl position on **16f** required the use of a LiBr:Et_3N for selective deprotonation of the phosphonate ester to obtain **P2** in 87% yield.[38] All of the polymers were soluble in several organic solvents, and the structures of the polymers were verified by ^{1}H NMR spectroscopy (see Supporting Information) and gel permeation chromatography, which revealed monomodal molecular weight distributions.

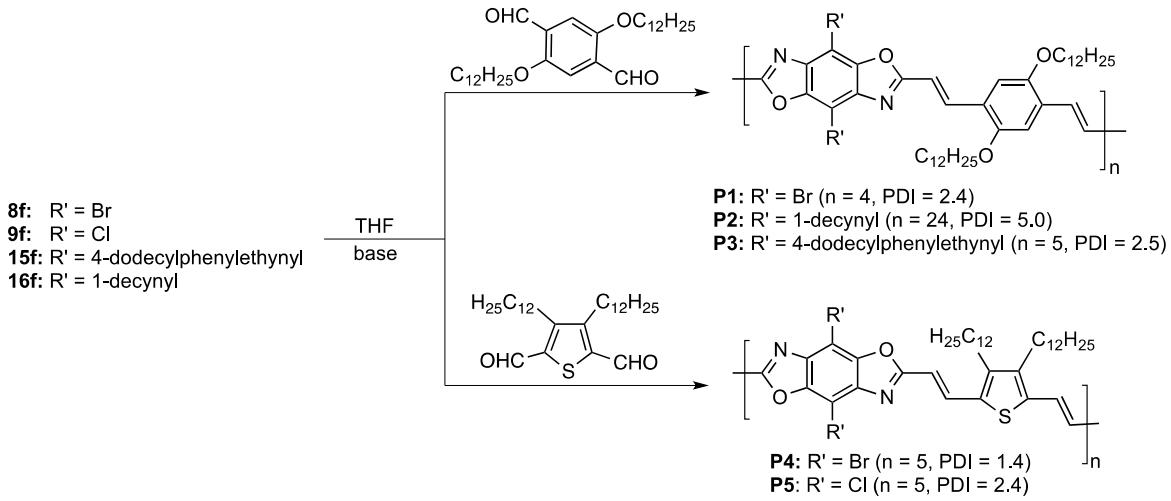

Scheme 2.5. Synthesis of benzobisoxazole polymers.

2.3.3 Spectroscopic Characterization of Model Compounds.

The UV-Vis absorption (Figure 2.1) and photoluminescence (PL) (Figure S2.50 Supporting Information) properties of the BBOs in solution have been investigated, and the spectral data are summarized in Table 2.1. The absorption and PL spectra vary depending on the type of substituents present on the 4,8-position of the BBO core. When excited at their respective λ_{max}, BBOs **8b**, **9b**, and **10b** exhibited very weak fluorescence in solution, whereas all of the other BBOs exhibited strong fluorescence in solution. The lack of fluorescence for **8b** and **9b** is likely due to the heavy-atom effect.

Table 2.1. Optical data of BBO model compounds

	λ_{abs} (nm)[a]	ε ($M^{-1} \cdot cm^{-1}$)[b]	λ_{ems} (nm)[c]
8b	222*, 274	38900	307, 385
9b	219*, 274	23600	313, 385
10b	209, 252*, 285	16200	308, 401
11b	243,304, 317*	38700	348
12b	242, 315*	33600	362
13b	248, 350*, 369	43600	376
14b	226, 259, 362*, 383	45600	397
15b	229, 355*, 376	58600	383

[a] All measurements performed in THF. [b] Extinction coefficients based on absorbance at λ_{max}. [c] Performed at λ_{max}. Asterisk (*) denotes λ_{max}.

The absorbance spectra of the halogen-substituted BBOs **8b** and **9b** displayed intense vibronic coupling with three dominant absorption bands, whereas the unsubstituted BBO **10b**

had two major peaks, each showing strong vibronic coupling. The absorbance spectra of the ethynyl-substituted BBOs **11b-15b** displayed weak vibronic coupling.

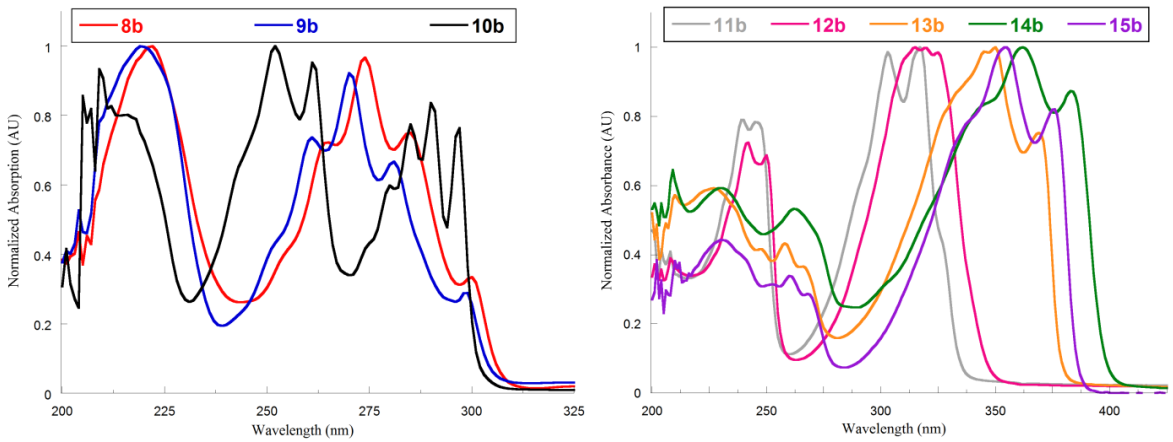

Figure 2.1. UV-Vis spectra of: parent and halogenated BBOs (left) and alkynyl substituted BBOs (right).

All of the substituted BBOs had red-shifted absorbance spectra due to the extended conjugation of the system relative to the unsubstituted BBO **10b** (abs λ_{max} 209, 285 nm). The phenylethynyl benzobisoxazoles **13b-15b** featured longer conjugation lengths and thus absorbed at the longest wavelengths. The introduction of the alkoxy-group onto the *para*-position of the phenyl substituent resulted in a red-shift in the absorbance spectrum; consequently **14b** absorbed at a longer wavelength than **15b**.

The PL and absorption spectra of the polymers in solution (Figure 2.2) and in thin film (Figure S2.52 Supporting Information) were also measured. In solution, **P1** had a PL maximum at 524 nm, with absorption maximum at 476 nm. **P4** had a PL maximum at 563 nm, with an absorption maximum at 506 nm and **P6** had a PL maximum at 560 nm, with an absorption maximum at 510 nm. When replacing the dialkoxyphenyl comonomer with the less aromatic and more electron-rich dialkylthiophene, a red-shift in the absorbance spectra

occurred. In all cases, the PL and absorption spectra were very similar to the analogous non-halogenated polymers: poly(2,5-bisdodecyloxyphenylene vinylene)-*alt*-benzo[1,2-*d*;4,5-*d*′]bisoxazole]-2,6-diyl[23] and poly(3,4-didodecylthiopene vinylene)-*alt*-benzo[1,2-*d*;4,5-*d*′]bisoxazole]-2,6-diyl.[24]

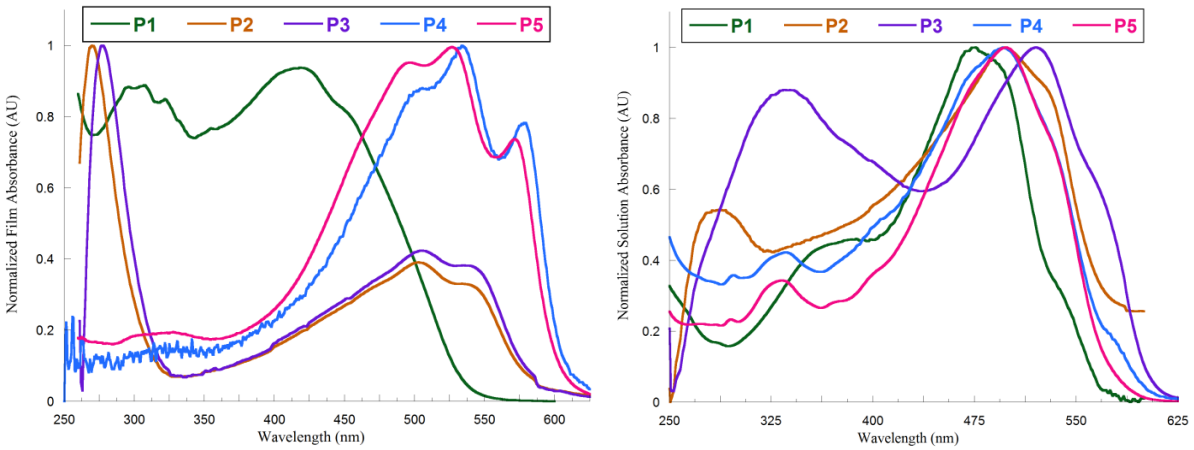

Figure 2.2. UV-Vis spectra of polymers: in solution and as films spun from THF or chloroform/*ortho*-dichlorobenzene solutions (right).

The alkyl-alkyne substituted polymer **P2** had a PL maximum at 576 nm, with absorption maximum at 491 nm, whereas the phenylethynyl substituted **P3** had a PL maximum at 601 nm with an absorption maximum at 520 nm. The bathochromic shift in the absorbance spectra of these polymers relative to their halogenated counterparts was a result of the increased acceptor strength of the substituted BBOs.

The energy levels of the BBO model compounds were investigated and compared to the theoretical data (see Table 2.1). The HOMO values obtained for **8b**-**10b** using cyclic voltammetry had excellent correlation to those predicted by theory, with a percent error of less than 5%. However, we saw a large deviation between the electrochemically determined HOMO values and the predicted values for the other BBOs.

Table 2.2. An experimental and theoretical comparison of the electronic properties of BBO model compounds

	HOMO (eV)			LUMO (eV)			E_g^{opt} (eV)		
	Exp[a]	*Theory*	*% Dev*	*Exp*[b]	*Theory*	*% Dev*	*Exp*[c]	*Theory*	*% Dev*
8b	-6.50	-6.20	4.6	-2.28	-1.45	36.4	4.22 (294)[c]	4.42	4.7
9b	-6.50	-6.30	3.1	-2.16	-1.47	31.9	4.34 (286)	4.52	4.1
10b	-5.90	-6.04	2.4	-1.28	-1.01	21.1	4.62 (296)	4.70	1.7
11b	-5.93	-5.40	8.9	-2.24	-1.43	36.2	3.69 (336)	3.84	4.1
12b	-6.09	-5.70	6.5	-2.47	-1.81	26.7	3.62 (343)	3.74	3.3
13b	-5.92	-5.30	10.5	-2.65	-1.97	25.7	3.27 (379)	3.16	3.4
13b*		-5.67	4.3		-1.67	37.0		3.76	18.0
14b	-5.70	-4.97	12.8	-2.58	-1.74	32.6	3.12 (398)	3.03	2.9
14b*		-5.54	2.9		-1.54	40.3		3.41	9.3
15b	-5.78	n/a	n/a	-2.59	n/a	n/a	3.19 (386)	n/a	n/a

[a] Determined using ultraviolet photoelectron spectroscopy. [b] Calculated from HOMO + E_g^{opt}. [c] Measured from the λ_{max} absorbance. [d] Calculated from lowest energy absorption onset from the intersection of the leading edge tangent with the x-axis. * Based on an optimized geometry of 90º.

As a whole, the electrochemistry of the BBOs was not well behaved and all molecules exhibited non-reversible oxidation cycles. Furthermore, a reduction cycle was not seen for any of the compounds within the solvent window for the acetonitrile/$Bu_4N^+BF_4^-$ (-2.7 to -3.0 eV versus Ag/AgCl). For this reason, we evaluated the BBOs using ultraviolet photoelectron spectroscopy (UPS), which provides an absolute determination of the HOMO level.[39-41] The

UPS HOMO values of the BBOs ranged from -5.70 to -6.50 eV, and the experimentally determined band gaps ranged from 3.19 to 4.62 eV. The LUMO levels ranged from -1.28 to -2.59 eV, and were calculated by adding the optical band gap to the HOMO values. The introduction of electron-withdrawing groups into π-conjugated systems stabilized the LUMO energy and increased the electron-transporting ability.[3] In general, the alkynyl substituted BBOs had deeper HOMOs and smaller band gaps than the halogenated BBOs. When a phenyl ring was added onto the alkynyl substituent, the HOMO level was slightly decreased, and the LUMO level was slightly increased in comparison to the unsubstituted alkynyl group. The HOMO was further raised when electron-donating alkyl or alkoxy substituents were added to the ring.

2.3.4 Computational Studies

To elucidate the influence of structural modification on the optical and electronic properties of the 4,8-disubstituted-BBOs, ground-state geometry optimizations were performed utilizing density functional theory (DFT) employing a B3LYP[42] functional, a 6-31G* basis and the Gaussian 03W software package. DFT/B3LYP/6-31G* is a reliable method that has been widely used for calculating the structural and optical properties of many systems.[43-46] UV-Vis spectra were simulated utilizing the first ten excited states and the time dependent density functional theory (TDDFT) routine with the aforementioned functional and basis set (see Figure 4 and Supporting Information). In addition, the HOMO, LUMO, and optical band gaps (the first excited state) were produced from the TDDFT output. To minimize computational cost, methyl groups were used at the 2 and 6 positions. Also, all alkoxy side chains were truncated to methoxy side chains and alkyl side chains omitted. Hence, the results for structure **15b** are not reported here since it would be a

replication of the prediction for structure **13b**. To evaluate the predictive power of the computational method, a comparison of computed HOMO, LUMO, and optical band gap values to experimental data was made. These results are summarized in Table 2.2.

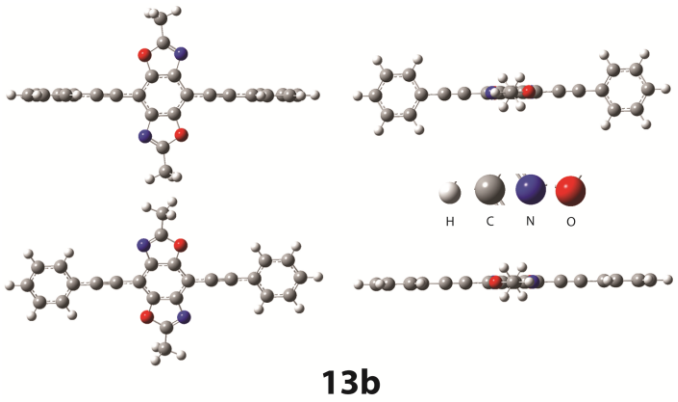

Figure 2.3. A representation for the optimized (bottom) and perpendicular (top) geometries of **13b.**

There was a good correlation for BBOs without conjugated substitutents (**8b-10b**), such that the difference between the theoretical and the experimental values for the HOMOs was less than 0.3 eV. However, the difference between predicted and measured values was as large as 0.8 eV for the optical band gaps. This was not surprising as DFT methods are known to underestimate band gaps.[47-50] The difference between the theoretical and the experimental values for the LUMOs was as large as 0.4 eV. These values possessed the highest amount of deviation (12% – 58%) due to the propagated deviations in the optical band gap and the HOMO values. A larger deviation in theoretical and experimental HOMO values was observed for BBOs bearing alkynyl substituents. The deviation was moderate for structures **11b** and **12b**, (0.53 and 0.39 eV), whereas the variance in structures **13b** and **14b** was much higher (0.62 and 0.73 eV). We hypothesized that the optimized geometry could be the source of error for the phenylethynyl substituted structures. The minimized geometry predicted a

planar configuration whereas it is likely the actual compounds possessed rings that were twisted out of plane. The idea of non-planarity in phenylethynyl side chains is supported by a number of studies.[51,52] To validate this hypothesis, optimized geometries and subsequent excited state calculations were performed on structures in which the phenyl substituent was forced perpendicular to the BBO core (see Figure 2.3). Adapting a twisted geometry reduced the large deviation between the experimental and theoretical HOMO values for **13b** and **14b** from 0.62 to 0.25 eV and from 0.73 to 0.16 eV, respectively.

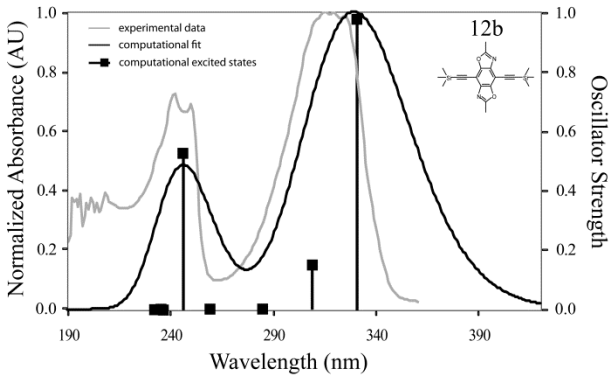

Figure 2.4. A comparison of the experimental UV-Vis spectrum of **12b** with the predicted excited states.

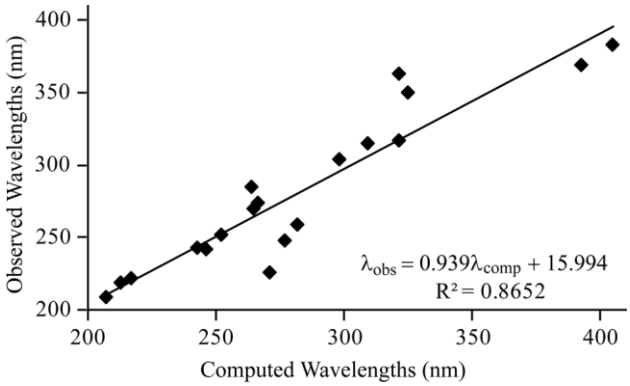

Figure 2.5. A correlation plot of the observed and computed wavelengths.

Strong correlation between the experimental and simulated UV-Vis spectra was also observed. A direct comparison for **12b** is shown in Figure 2.5, and the remaining structures are shown in the Supplemental Information (Figures S2.53 – S2.58). The grey and black lines represented the experimental data and theoretical fit, respectively. The black bars and solid squares were indicative of the oscillator strength and the corresponding excited state. There was a very good agreement between the two data sets especially when one considers that all theoretical computations were performed in vacuum and did not account for solvent stabilization that was present in the experimental sample. This was further demonstrated in an analysis of the contributions of the excited states (see Supporting Information).[53] In all cases, the lowest lying state was primarily due to electronic excitations directly between the HOMO and the LUMO. For **8b**, **9b**, and **12b**, this lowest state was split into two excited states in the computed spectra, whereas the experimental spectra displayed one broad peak. To further evaluate the competency of this method, we generated a correlation plot of the observed and computed wavelengths (see Figure 2.4). For this comparison, an R^2 value of 0.87 was found, indicating good correlation between the experimental and theoretical values.

To examine the influence of substitution on the electron density of the BBO core, the frontier orbitals and electrostatic potential (ESP) maps for each of the model compounds were generated, and are shown in Figure 2.6. The electron-withdrawing nature of the halogens is demonstrated by the frontier orbital HOMOs for **8b** and **9b**, which show a significant amount of electron density that has been drawn away from the BBO backbone. This effect was further exhibited by the ESP maps in which the backbone is slightly greener (less electron rich) than that of the non-substituted core **10b**.

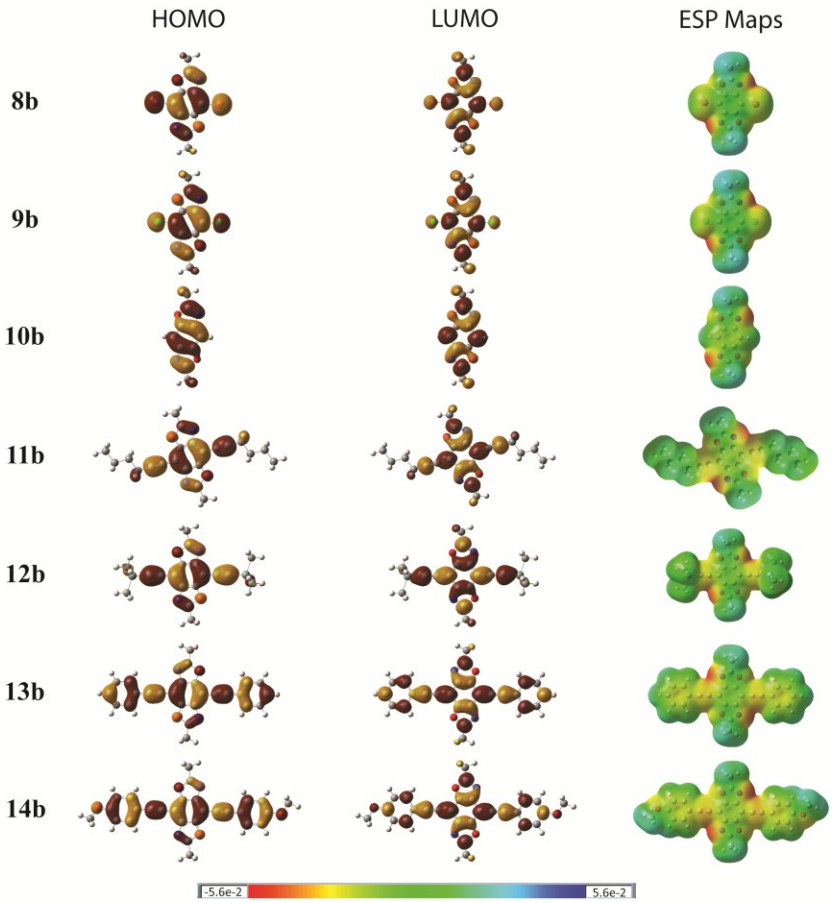

Figure 2.6. Pictorial representations of the frontier orbitals for compounds **8b - 14b** (left) and electrostatic potential maps (right). For the frontier orbitals, the red lobes are positive and the yellow lobes are negative. The charge density within the electrostatic potential maps range from red (electron rich) to blue (electron poor).

Similarly, the electron-withdrawing alkynyl substituents also exhibited a reduction in the density of the BBO core (see **11b**, **12b**, **13b**, and **14b**). However, the addition of substituents bearing phenyl rings led to a large reorganization of electron density from the BBO core (see **13b** and **14b**). This redistribution was so significant that it appears that the BBO core was no longer the primary conjugation axis, which is noteworthy because it suggests that alkynyl substitution can be used in the synthesis of two-dimensional π-delocalized polymers. Such

cruciforms can exhibit interesting optical and electronic properties due to their multiple conjugated pathways.[20,22,54-57]

The ability to accurately predict the electronic properties of polymeric materials is essential for the design new organic semiconductors. To evaluate the ability of our computational methods to predict the properties of 4,8-disubstituted BBO polymers, the geometries of model oligomers (n = 1, 2, 3, and 4) for **P1**, **P2**, **P3**, **P4**, and **P6** were optimized at the density functional theory B3LYP/6-31G* level. In all cases, the bisdodecyl substituents were truncated to methyl groups to reduce computational costs. Unfortunately, **P3** was found to be too large to extrapolate to the long chain limit. The HOMO, LUMO and band gaps for these polymers were obtained by fitting the aforementioned set of oligomers with the Kuhn expression (Equation 2.1)[58,59]

$$E = E_0 \sqrt{1 + 2\frac{k'}{k_0}\cos\frac{\pi}{N+1}} \qquad \text{(Equation 2.1)}$$

where E_0 is the transition energy of a formal double bond, N is the number of double bonds in the oligomer, and k'/k_0 is an adjustable parameter. The results are summarized in Table 2.3. Overall there was excellent correlation between all predicted and experimental values. The largest deviation for both the HOMO and LUMO levels were 1.5% and 4.0%, respectively. This trend was quite an improvement over the small molecule cases where the deviation was quite a bit larger (12.8% for HOMO and 40.3% for LUMO). The polymeric band gaps were found to experience the largest amount of deviation at 10.7%, which was attributed to DFT overestimation.[43,46] As a whole, these results indicated that this level of

theory can be used to accurately predict the HOMO, LUMO, and band gaps for conjugated polymers possessing BBO moieties.

Table 2.3. An experimental and theoretical comparison of the electronic properties of BBO polymers

	HOMO (eV)			LUMO (eV)			E_g^{opt} (eV)		
	Exp[a]	*Theory*	*% Dev*	*Exp*[b]	*Theory*	*% Dev*	*Exp*[c]	*Theory*	*% Dev*
P1	-5.06	-5.23	3.4	-2.91	-2.93	0.7	2.15	2.03	5.6
P2	-5.05	-4.98	1.4	-3.00	-2.78	4.0	2.05	1.98	3.4
P3	-5.00	N/A	N/A	-2.96	N/A	N/A	2.04	N/A	N/A
P4	-5.38	-5.43	0.93	-3.30	-3.23	2.1	2.05	1.92	6.3
P5	-5.38	-5.46	1.5	-3.31	-3.26	1.5	2.07	1.91	7.7

[a] Calculated from the oxidation onset using $-4.8 - E_{ox}^{onset}$. [b] Calculated from the reduction onset using $-(4.8 + E_{red}^{onset})$. [c] Calculated by the energy absorption onset from the intersection of the leading edge tangent with the x-axis.

2.4 Conclusions

In summary, we have demonstrated that alkyne substitution at the central benzene ring of benzo[1,2-*d*;4,5-*d'*]bisoxazoles can be used to modify the optical and electronic properties of these compounds. We were able to synthesize the target compounds in good yields by first synthesizing halogenated benzobisoxazoles and then forming two-dimensional π-systems using Sonogashira cross-coupling. The predicted HOMO values for the small molecules matched well with the experimental results, although as expected, a higher degree

of error was seen for the LUMO and band gap values. In contrast, the predicted energy levels for polymeric materials exhibited excellent correlation for all parameters, further exemplifying the usefulness of the theoretical methods for designing new materials. Although theoretical calculations predicted that attachment of alkynes could be used to vary the energy levels of BBOs by almost 1 eV, smaller changes were observed for the BBO polymers. While it was our intention to minimize computational requirements by using small molecules to evaluate the impact of these structural modifications, this was unfortunately not reasonable as it appears that most of the electronic tuning in BBO small molecules was due to a change in the conjugation axis. Currently, we are designing new BBOs bearing other electron withdrawing groups to further improve the acceptor strength of this group and synthesizing new conjugated polymers based on these alkyne substituted BBOs.

2.5 Experimental Section

2.5.1 General

Unless otherwise noted, reactions were conducted under ambient atmosphere at 18-26 °C. Nuclear Magnetic Resonance (NMR) experiments were carried out in either $CDCl_3$ or DMSO-d_6 at 400 MHz (^{1}H) or 100 MHz (^{13}C). ^{1}H NMR spectra are internally referenced to the residual protonated solvent peak and the ^{13}C NMR are referenced to the central carbon peak of the solvent. In all spectra chemical shifts are given in δ relative to the solvent. Coupling constants are reported in Hertz (Hz). Cyclic voltammetry was performed using a potentiostat, scanning at a rate of 50-100 mV/s. The polymer solutions (2-10 mg/mL) were drop-cast on a platinum electrode and Ag/Ag+ was used as the reference electrode. The reported values are referenced to Fc/Fc^+ (-4.8 eV versus vacuum). All electrochemistry

experiments were performed in dry-degassed CH_3CN under argon atmosphere using 0.1 M tetrabutylammonium hexafluorophosphate as the electrolyte. High-resolution mass spectra were recorded on a double focusing magnetic sector mass spectrometer using electron impact (EI) or electrospray ionization (ESI) at 70 eV. Melting points were obtained using a melting point apparatus, upper temperature limit 260 ºC. Gel permeation chromatography (GPC) measurements were performed on a separation module equipped with three 5µm I-gel columns connected in a series (guard, HMW, MMW and LMW) with a UV-Vis detector. Analyses were performed at 35 °C using THF as the eluent with the flow rate at 1.0 mL/min. Calibration was based on polystyrene standards. Fluorescence spectroscopy and UV-Visible spectroscopy were obtained using polymer solutions in THF, and thin films were spun from THF or $CHCl_3$/*o*-dichlorobenzene solutions. The films were made by spin-coating 25x25x1 mm glass slides, using 10 mg/mL polymer solutions at a spin rate of 5000 rpm on a spin-coater. Ultraviolet Photoelectron Spectroscopy measurements were performed on sample films. X-ray radiation and the detector to crystal distance of 5.03 cm. X-ray crystal structure data for compounds **10a** (734101), **10b** (CCDC 687294), **10c** (CCDC 734103), **10d** (CCDC 734102) and **9c** (CCDC 838477) were deposited with the Cambridge Crystallographic Data Centre, 12 Union Road, Cambridge CB2 1EZ, UK. Triethyl orthochloroacetate (**7c**),[60] trimethylsilyl ethyl orthopropiolate (**7d**)[35], ethyl triethoxyacetate (**7e**),[61] *p*-bromanil,[62] 4-bromo-trimethylsilylbenzene,[5] 2,6-dimethylbenzo[1,2-*d*;4,5-*d'*]bisoxazole (**10b**), [35] 2,5-didodecyloxyterephthaldehyde, [36] and 3,4-didodecylthiophene dicarboxaldehyde[37] were prepared according to literature procedure.[35,63] 3,6-diamino-2,5-dichloro-1,4-benzoquinone was prepared from *p*-chloranil according to literature procedure.[62]

2.5.2 Synthetic Procedures

3,6-diamino-2,5-dibromo-1,4-benzoquinone 3. A 500 mL 3-neck round-bottom flask was equipped with an addition funnel and mechanical stirrer and charged with 42.9 g (100 mmol) of *p*-bromanil **1** and 170 mL of 2-methoxyethyl acetate. The slurry was vigorously stirred while heating to 60 °C. The mixture was removed from the heat source and the addition funnel charged with 43.3 mL (300 mmol) of 27% NH_4OH and added drop-wise over 25 minutes (the reaction exothermed to over 100 °C during the addition). The reaction was allowed to cool to approximately 80 °C and stirred at this temperature for 3 hours and allowed to cool to room temperature overnight. The dark red mixture was filtered and the collected precipitate washed with large portions of distilled water. The collected solid was placed in a flask containing acetone, stirred, and refiltered. The precipitate was then washed with acetone and dried *in vacuo* to yield a brick-red powder (27.9 g, 94% yield). Due to the limited solubility of this compound it was used without further purification or analysis.

3,6-diamino-2,5-dibromo-1,4-hydroquinone 5. A 100 mL round-bottom flask equipped with a large stir bar was charged with 3.26 g (11.0 mmol) 3,6-diamino-2,5-dibromo-1,4-benzoquinone **3**, 33 mL of ethanol, and 7 mL of distilled water. The flask was fitted with an addition funnel and heated to 55 °C with stirring under argon atmosphere. The addition funnel was charged with 4.78 g (27.5 mmol) $Na_2S_2O_4$ dissolved in 50 mL of distilled water and added drop-wise and stirred for 1 hour. The mixture was allowed to cool to room temperature and the precipitate filtered and washed with distilled water and cold ethanol. The resulting solid was dried *in vacuo* to yield a tan powder (3.07 g, 94% yield). Due to the insolubility and air sensitivity of this compound it was used immediately without further purification or analysis.

3,6-diamino-2,5-dichloro-1,4-hydroquinone 6. Prepared analogously to **5** from 3,6-diamino-2,5-dichloro-1,4-benzoquinone **4** (11 mmol) to yield a light tan powder (2.30 g, 90% yield). Due to the insolubility and air sensitivity of this compound it is used immediately without further purification or analysis.

Representative procedure for the preparation of 4,8-dibromobenzobisoxazoles. A dry round-bottom flask was placed under an argon atmosphere and charged with 0.13 g (0.25 mmol) $Y(OTf)_3$, 5 mL DMA and 3 equivalents of orthoester **7(a-e)**. The mixture was warmed to 55 °C and 1.49 g (5.0 mmol) 3,6-diamino-2,5-dibromo-1,4-hydroquinone **5** was added portion-wise over 30 minutes and stirred at 55 °C for 2 hours. The mixture was allow to cool room temperature and diluted with water. The resulting precipitate was collected by filtration and washed with distilled water and cold ethanol.

4,8-dibromo-benzo[1,2-*d*;4,5-*d'*]bisoxazole 8a (X = Br, R = H). Prepared from **5** (5 mmol) and triethyl orthoformate **7a**. Purified by recrystallization from acetic acid to yield white needles, (0.77 g, 48% yield). mp: > 260 °C; ^{1}H NMR (400 MHz, DMSO-d_6): δ 9.05 (2H, s); ^{13}C NMR (100MHz, DMSO-d_6): δ 92.4, 137.7, 145.7, 156.3; HRMS (ESI) Calcd for $C_8H_3N_2O_2Br_2$, 316.8556 $(M+H)^+$; Found, 316.8558.

4,8-dibromo-2,6-dimethylbenzo[1,2-*d*;4,5-*d'*]bisoxazole 8b (X = Br, R = CH_3). Prepared from **5** (20 mmol) and triethyl orthoacetate **7b**. Purified by recrystallization from chloroform/ethanol to yield white needles (5.53 g, 85% yield). mp: > 260 °C; ^{1}H NMR (400 MHz, $CDCl_3$): δ 2.74 (6H, s); ^{13}C NMR (100 MHz, $CDCl_3$): δ 15.1, 92.1, 136.7, 146.8, 165.8; HRMS (EI) Calcd for $C_{10}H_6N_2O_2Br_2$, 343.87960 (M^+); Found, 343.88060.

4,8-dibromo-2,6-bis(chloromethyl)benzo[1,2-*d*;4,5-*d'*]bisoxazole 8c (X = Br, R = CH_2Cl). Prepared from **5** (30 mmol) and triethyl orthochloroacetate **7c**. The crude product was heated in chloroform (500 mL) and filtered. The filtrate was concentrated to 200 mL diluted 1:1 with ethanol to obtain yellow needles (8.33 g, 70% yield). mp: > 260 °C; ^{1}H NMR (400 MHz, $CDCl_3$): δ 4.88 (4 H, s); ^{13}C NMR (100 MHz, $CDCl_3$): δ 36.0, 93.2, 138.3, 147.5, 163.2; HRMS (ESI) Calcd for $C_{10}H_5N_2O_2Cl_2Br_2$, 412.8092 $(M+H)^+$; Found 412.8089.

4,8-dibromo-2,6-bis(trimethylsilylethynyl)benzo[1,2-*d*;4,5-*d'*]bisoxazole 8d (X = Br, R = C_2TMS). Prepared from **5** (3 mmol) and triethyl orthopropiolate **7d** using THF in place of DMA and heated to 50 °C. The solvent was removed *in vacuo* and the crude product purified by recrystallization from heptanes to yield small yellow needles (0.96 g, 63% yield). mp: 245 °C; ^{1}H NMR (400 MHz, $CDCl_3$): δ 0.34 (18 H, s); ^{13}C NMR (100 MHz, $CDCl_3$): δ 0.7, 90.5, 92.4, 105.2, 139.5, 146.6, 148.3; HRMS (ESI) Calcd for $C_{18}H_{19}O_2N_2Si_2Br_2$, 508.9346 $(M+H)^+$; Found, 508.9348.

4,8-dibromo-2,6-bis(ethyl acetyl)benzo[1,2-*d*;4,5-*d'*]bisoxazole 8e (X = Br, R = CO_2Et). Prepared from **5** (5 mmol) and ethyl triethoxyacetate **7e**. Purified by recrystallization from chloroform/heptanes to yield pale yellow needles (0.59 g, 26% yield). mp: > 260 °C; ^{1}H NMR (400 MHz, $CDCl_3$): δ 1.54 (6H, t, *J*=8 Hz), 4.62 (4H, q, *J*=8 Hz); ^{13}C NMR (100 MHz, $CDCl_3$): δ 23.6, 57.0, 93.5, 123.89, 151.1, 154.3, 157.3; HRMS (ESI) Calcd for $C_{14}H_{11}N_2O_6Br_2$ 460.8978 $(M+H)^+$; Found, 460.8975.

Representative procedure for the preparation of of 4,8-dichlorobenzobisoxazoles. A dry round-bottom flask was placed under an argon atmosphere and charged with 0.13 g (0.25 mmol) $Y(OTf)_3$, 5 mL DMSO and 3 equivalents of orthoester

7(a-e). The mixture was warmed to 55 °C and 1.05 g (5.00 mmol) 3,6-diamino-2,5-dichloro-1,4-hydroquinone **6** was added portion-wise over 30 minutes and stirred at 55 °C for 2 hours. The mixture was allowed to cool to room temperature and diluted with water. The resulting precipitate was collected by filtration and washed with water and cold ethanol.

4,8-dichlorobenzo[1,2-*d*;4,5-*d′*]bisoxazole 9a (X = Cl, R = H). Prepared from **6** (5 mmol) and **7a**. Purified by recrystallization from chloroform to yield small white needles (1.56 g, 84% yield). mp: > 260 °C; ^{1}H NMR (400 MHz, DMSO-d_6): δ 9.07 (2H, s); ^{13}C NMR (100MHz, DMSO-d_6): δ 104.4, 136.5, 144.3, 156.6; HRMS (ESI) Calcd for $C_8H_3N_2O_2Cl_2$, 228.9566 $(M+H)^+$; Found, 228.9572.

4,8-dichlorobenzo-2,6-dimethylbenzo[1,2-*d*;4,5-*d′*]bisoxazole 9b (X = Cl, R = CH_3). Prepared from **6** (20 mmol) and **7b**. Purified by recrystallization from chloroform/ethanol to yield white needles (0.78 g, 79% yield). mp: > 260 °C; ^{1}H NMR (400 MHz, $CHCl_3$): δ 2.75 (6 H, s); ^{13}C NMR (100 MHz, $CHCl_3$): δ 15.1, 104.0, 137.5, 145.5, 166.1; HRMS (ESI) Calcd for $C_{10}H_7N_2O_2Cl_2$, 256.9879 $(M+H)^+$; Found, 256.9881.

4,8-dichloro-2,6-bis(chloromethyl)benzo[1,2-*d*;4,5-*d′*]bisoxazole 9c (X = Cl, R = CH_2Cl). Prepared from **6** (20 mmol) and **7c**. Purified by recrystallization from chloroform/ethanol to yield yellow needles (4.69 g, 74% yield). mp: 233-234 °C; ^{1}H NMR (400 MHz, $CHCl_3$) δ 4.84 (4H, s); ^{13}C NMR (100 MHz, $CHCl_3$): δ 23.6, 106.0, 117.6, 138.1, 146.1, 163.4; HRMS (ESI) Calcd for $C_{10}H_5N_2O_2Cl_4$, 324.9103 $(M+H)^+$; Found, 324.9100.

4,8-chloro-2,6-bis(trimethylsilylethynyl)benzo[1,2-*d*;4,5-*d′*]bisoxazole 9d (X = Cl, R = C_2TMS). Prepared from **6** (3 mmol) and **7d** using THF in place of DMSO and heating to 50 °C. The solvent removed *in vacuo* and the crude product purified by recrystallization from

heptanes to yield pale yellow needles (0.73 g, 58% yield). mp: 232-234 °C; ^{1}H NMR (400 MHz, $CDCl_3$): δ 0.34 (18 H, s); ^{13}C NMR (100 MHz, $CDCl_3$): δ 0.2, 90.4, 105.2, 105.3, 138.3, 145.3, 148.6; HRMS (ESI) Calcd for $C_{18}H_{19}N_2O_2Si_2Si_2$,421.0357 $(M+H)^+$; Found, 421.0350.

4,8-dichloro-2,6-bis(ethyl acetyl)benzo[1,2-*d*;4,5-*d'*]bisoxazole 9e (X = Cl, R = CO_2Et). Prepared from **6** and **7e**. Purified by recrystallization from chloroform/ethanol to yield light yellow needles (0.46 g, 41% yield). mp: > 260 °C; ^{1}H NMR (400 MHz, $CDCl_3$): δ 1.52 (6 H, t, *J*=8 Hz), 4.62 (4 H, q, *J*=8 Hz); ^{13}C NMR (100 MHz, $CDCl_3$): δ 14.4, 64.3, 108.2, 139.2, 146.3, 155.0, 155.4; HRMS (ESI) Calcd for $C_{14}H_{11}N_2O_6Cl_2$, 372.9989 $(M+H)^+$; Found, 372.9992.

1-(3,7-dimethyloctyloxy)-4-ethynylbenzene

1-bromo-4-(3,7-dimethyloctyloxy)benzene. A 250 mL round-bottom flask was charged with 100 mL of DMSO, 7.0 g (125 mmol) KOH, and stirred for 1 hour at room temperature. 17.3 g (100 mmol) of 4-bromophenol and 27.6 g (125 mmol) 1-bromo-3,7-dimethyloctane were added successively and the reaction mixture stirred at room temperature overnight. The mixture was poured into 200 mL of water and extracted with dichloromethane (3x). The combined organic layers were washed with 2 N HCl (3x), brine (1x), and dried over $MgSO_4$. The solution was filtered and the solvent removed *in vacuo*. Distillation of the crude product under reduced pressure (185 °C, 260 mtorr) yielded a clear oil (31.0 g, 95% yield). ^{1}H NMR (400 MHz; $CDCl_3$) δ 0.87 (6H, d, *J* = 8 Hz), 0.96 (3H, d, *J* = 8 Hz), 1.15-1.87 (10H, overlapping multiplets), 3.96 (2H, sextet, *J* = 8 Hz), 6.79 (2H, d, *J* = 8 Hz), 7.37 (2H, d, *J* = 12 Hz). ^{13}C NMR (400 MHz; $CDCl_3$) 20.0, 22.8, 28.2, 30.0, 36.3, 37.5, 39.4,

66.7, 112.7, 116.5, 132.3, 158.4. HRMS (EI) Calcd for $C_{16}H_{25}OBr$ 312.1089 (M^+); Found, 312.1084.

1-(3,7-dimethyloctyloxy)-4-(trimethylsilylethynyl)benzene. A dry pressure flask was sealed with a septum, equipped with a stir bar, and purged with argon. The flask was charged with 50 mL of dry/degassed Et_3N and 3.29 g (10.0 mmol) 1-(3,7-dimethyloctyl)oxy-4-bromobenzene. 0.35 g (0.30 mmol) $Pd(PPh_3)_4$ and 0.038 g (0.20 mmol) CuI followed by 1.28 g (13.0 mmol) of trimethylsilylacetylene. The flask was sealed with a Teflon cap and heated to 80 °C for 24 hrs. The solution was cooled to room temperature, diluted with water, and extracted with hexanes (4x). The combined organic extracts were washed with water (2x), brine (2x), and dried over $MgSO_4$. The solution was filtered and the solvent removed *in vacuo*. The product was purified by column chromatography eluting with hexanes/ethyl acetate (98:2) to yield a clear oil (1.62 g, 47% yield). ^{1}H NMR (400 MHz; $CDCl_3$) δ 0.24 (9H, s), 0.88 (6H, d, *J*=8 Hz), 0.94 (3H, d, *J*=8 Hz). 1.15-1.89 (10H, overlapping multiplets), 3.98 (2H, m), 6.82 (2H, d, *J*=12 Hz), 7.39 (2H, d, *J*=12 Hz). ^{13}C NMR (100 MHz; $CDCl_3$) δ 19.9, 22.9, 24.9, 28.2, 30.0, 36.3, 37.49, 39.45, 66.6, 92.4, 105.5, 114.5, 115.16, 133.6, 159.5.

1-(3,7-dimethyloctyoxy)-4-ethynylbenzene. A 50 mL round-bottom flask was charged with 3.04 g (8.80 mmol) 4-(3,7-dimethyloctyl)oxy-1-(trimethylsilylethynyl)benzene, 10 mL CH_2Cl_2, and 10 mL methanol. 0.24 g (1.76 mmol) K_2CO_3 was added and the mixture stirred room temperature overnight. The solvents are removed *in vacuo* and the product purified by column chromatography eluting with hexanes/ethyl acetate (99:1) to yield an orange oil (2.15 g, 95%). ^{1}H NMR (400MHz; $CDCl_3$) δ 0.88 (6H, d, *J*=8 Hz), 0.94 (3H, d, *J*=8 Hz), 1.62-1.85 (10H, overlapping multiplets), 3.0 (1H, s), 4.0 (2H, m), 6.84 (2H, d, *J*=8 Hz), 7.43 (2H, d, *J*=12 Hz. ^{13}C NMR (100 MHz, $CDCl_3$) δ19.9, 22.8, 22.9, 24.9, 28.2, 30.0, 36.3, 37.5, 39.4,

66.5, 75.9, 83.7, 114.0, 114.6, 133.7, 159.7. HRMS (ESI) Calcd for $C_{18}H_{27}O$, 259.2056 $(M+H)^+$; Found, 259.2060.

4-dodecy-1-ethynylbenzene

Dodecylboronic acid. A dry 3-neck 500 mL round-bottom flask was fitted with a reflux condenser, addition funnel, stir bar, septum, and placed under argon atmosphere. The flask was charged with 8.75 g (360 mmol) of magnesium turnings followed by a few crystals of iodine. 300 mL of ether was added and the suspension refluxed until a clear solution developed and the flask was allowed to cool to room temperature. 74.8 g (300 mmol) of $C_{12}H_{25}Br$ was added drop-wise via addition funnel to maintain a gentle reflux and then heated to reflux for 2 hours. A separate dry 3-neck 1 L round-bottom flask was equipped with an addition funnel and mechanical stirrer and charged with 72.7 g (750 mmol) $B(OMe)_3$ and 500 mL of diethyl ether. The flask was cooled to 0 °C in an ice-water bath and the fresh $C_{12}H_{25}MgBr$ solution added via addition funnel. The viscous mixture was allowed to warm to room temperature overnight, cooled back to 0 °C, and quenched with 1 N HCl. The layers were separated and the aqueous layer extracted with diethyl ether (3x) and the combined organic layers washed with water (2x), brine (1x), and dried over $MgSO_4$. The solution was filtered, and the solvent removed *in vacuo*. The crude product was purified by recrystallization from hexanes to yield white needles (24.2 g, 38% yield). ^{1}H NMR (400MHz; $CDCl_3$) δ 1.39 (3H, m), 1.26 (9H, overlapping multiplets), 0.88 (3H, t, *J*=8 Hz). ^{13}C NMR (100 MHz; $CDCl_3$) δ 0.3, 14.4, 22.9, 24.6, 29.6, 29.7, 29.82, 29.86, 29.92, 32.2, 32.6.

4-dodecyl-1-(trimethylsilyl)benzene. A dry 2-neck round-bottom flask was fitted with a reflux condenser, septum, and placed under argon atmosphere. The flask was charged with

7.71 g (36.6 mmol) dodecylboronic acid, 0.43 g (0.6 mmol) $Pd(dppf)Cl_2$, 12.8 g (60.0 mmol) K_3PO_4, and 7.08 g (30.0 mmol) 4-bromo-1-(trimethylsilyl)benzene. The flask was then charged with 60 mL of dry/degassed toluene and the mixture heated to 100 °C for 36 hours then allowed to cool to room temperature. The solids were filtered and the filter cake washed with hexanes and the filtrate concentrated *in vacuo*. The crude product was filtered through a silica gel plug eluting with hexanes. The impurities were removed by careful vacuum distillation to yield a dark yellow oil (7.98 g, 83% yield). ^{1}H NMR (400 MHz; $CDCl_3$) δ 0.41 (9H, s), 1.04 (3H, t, J=8 Hz), 1.45 (18H, overlapped multiplets), 1.77 (2H, m), 2.74 (2H, t, J=8 Hz), 7.32 (2H, d, J=8 Hz), 7.59 (2H, d, J=8 Hz). ^{13}C NMR (100 MHz; $CDCl_3$) 0.8, 14.4, 23.0, 29.7, 29.76, 29.86, 29.93, 29.98, 30.0, 36.3, 128.1, 133.5, 137.2, 143.8.

4-dodecyl-1-iodobenzene. A round-bottom flask was equipped with a stir bar and charged with 4.78 g (15.0 mmol) 4-dodecyl-1-(trimethylsilyl)benzene, 15 mL CH_2Cl_2, and cooled to 0 °C in an ice-bath. A solution of 3.04 g (18.75 mmol) ICl in 6 mL of CH_2Cl_2 was added drop-wise and the solution allowed to warm to room temperature over 1 hour. The reaction was diluted with CH_2Cl_2 and quenched with saturated $NaHSO_3$. The layers were separated and the aqueous layer extracted with CH_2Cl_2 (3x) and the combined organic layers washed with water (1x), brine (3x), and dried over $MgSO_4$. The solution was filtered and the solvent removed *in vacuo*. The crude product was purified by recrystallization at -20 °C from ethanol to yield glistening white flakes. (4.94 g, 88% yield). mp: < 35 °C; ^{1}H NMR (400 MHz; $CDCl_3$) δ 0.88 (3H, t, *J*=8 Hz), 1.28 (18H, overlapped multiplets), 1.57 (2H, m), 2.53 (2H, t, *J*=8 Hz), 6.93 (2H, d, *J*=8 Hz), 7.58 (2H, *J*=8 Hz). ^{13}C NMR (100 MHz; $CDCl_3$) δ 14.4, 22.9, 29.4, 29.6, 29.7, 29.8, 29.9, 31.5, 32.2, 35.7, 90.7, 130.8, 137.4, 142.7.

4-dodecyl-1-(trimethylsilylethynyl)benzene. A dry round-bottom flask was placed under argon atmosphere and charged with 1.87 g (5.0 mmol) 4-dodecyl-1-bromobenzene, 0.0702 g (0.1 mmol) $Pd(PPh_3)Cl_2$, and 0.0095 g (0.05 mmol) CuI. 35 mL of dry/degassed Et_3N was added and the flask cooled to 0 °C in an ice-water bath. 0.58 g (6.5 mmol) trimethylsilylacetylene was added slowly drop-wise syringe over 10 minutes and the mixture stirred for 2 hours at 0 °C then 24 hours at room temperature. The mixture was poured into saturated NH_4Cl and extracted with hexanes (4x). The combined organic extracts were washed with 1 N HCl (3x), water (1x), brine (1x), and dried over $MgSO_4$. The solution was filtered and the solvents removed *in vacuo*. The product was filtered through a silica gel plug eluting with hexanes to yield a pale yellow oil (1.48 g, 87% yield). ^{1}H NMR (400 MHz, $CDCl_3$) δ 0.26 (9H, s), 0.90 (3H, t, *J*=8 Hz), 1.27 (18H, overlapped multiplets), 1.60 (2H, m), 2.60 (2H, t, *J*=8 Hz), 7.11 (2H, d, *J*=8 Hz), 7.39 (2H, d, *J*=8 Hz). ^{13}C NMR (100 MHz; $CDCl_3$) δ 0.3, 14.4, 23.0, 29.4, 29.6, 29.7, 29.9, 29.9, 31.5, 32.2, 93.4, 105.6, 120.4, 128.5, 132.1, 143.8.

4-dodecyl-1-ethynylbenzene. A small round bottom flask was equipped with a stir bar and charged with 1.48 g (4.36 mmol) 4-dodecyl-1-(trimethylsilylethynyl)benzene, 5 mL of CH_2Cl_2, and 5 mL of methanol. 0.17 g (0.87 mmol) K_2CO_3 was added and the mixture stirred at room temperature for 4 hours then diluted with 10 mL of water and 15 mL of CH_2Cl_2. The layers were separated and the aqueous layer extracted with CH_2Cl_2 (3x). The combined organic layers were washed with water (1x), brine (2x), and dried over $MgSO_4$. The solution was filtered and the solvents removed *in vacuo*. The crude product was filtered through a silica plug eluting with hexanes to yield a pale yellow oil (1.16 g, 98% yield). ^{1}H NMR (400 MHz; $CDCl_3$) δ 0.90 (3H, t, *J*=8 Hz), 1.31 (18H, overlapped multiplets), 1.59

(2H, m), 2.60 (2H, t, *J*=8 Hz), 3.04 (2H, s), 7.14 (2H, d, *J*=8 Hz, 7.41 (2H, d, *J*=8 Hz). ^{13}C NMR (100 MHz; $CDCl_3$) δ 14.4, 22.9, 29.5, 29.6, 29.7, 29.8, 29.9, 29.9, 31.5, 32.2, 36.1, 76.6, 84.1, 119.4, 128.6, 132.2, 144.2.

4,8-bis(1-hexynyl)-2,6-dimethylbenzo[1,2-*d*-4,5-*d′*]bisoxazole 11b. A dry pear-bottom flask was placed under argon atmosphere and charged 0.70 g (2.00 mmol) **8b**, 0.0702 g (0.10 mmol) $Pd(PPh_3)_2Cl_2$, 0.019 g (0.10 mmol) CuI, 0.026 g (0.10 mmol) PPh_3, and dissolved in 60 mL of dry/degassed THF. This solution was added to a degassed solution of 0.49 g 1-hexyne (6.00 mmol) and 2.02 g (20.0 mmol) diisopropylamine in 5 mL of dry THF under argon atmosphere in 2-neck round-bottom flask fitted with a reflux condenser. The solution was refluxed for 24 hours. The mixture was allowed to cool to room temperature and the volatile components removed *in vacuo*. The crude product was dissolved in hot hexanes, filtered, and filtrate concentrated *in vacuo*. Further purification by recrystallization from hexanes resulted in white needles (0.62 g, 88% yield). mp: 168-170 °C; ^{1}H NMR (400 MHz, $CDCl_3$): δ 0.98 (6H, t, *J*=8 Hz), 1.55 (4H, m), 1.69 (4H, m), 2.63 (4H, t, *J*=8 Hz), 2.72 (6H, s); ^{13}C NMR (100 MHz, $CDCl_3$): δ 13.8, 15.0, 20.1, 23.3, 30.9, 70.7, 98.1, 101.7, 139.7, 148.8, 165.3; HRMS (ESI) Calcd for $C_{22}H_{25}N_2O_2$, 349.1911 $(M+H)^+$; Found 349.1913.

4,8-bis(trimethylsilylethynyl)-2,6-dimethylbenzo[1,2-*d*-4,5-*d′*]bisoxazole 12b. A dry 3-neck round-bottom flask equipped with a reflux condenser and addition funnel was placed under argon atmosphere and charged with 3.74 g (10.0 mmol) of **8b**, 0.35 g (0.5 mmol) $PdCl_2(PPh_3)_2$, 0.095 g (0.5 mmol) CuI, and 0.13 g (0.5 mmol) PPh_3, 10.1 g (100 mmol) degassed diisopropylamine, and 150 mL of dry/degassed THF. A solution of 2.95 g (30.0 mmol) trimethylsilylacetylene diluted in 12 mL of degassed THF was added drop-wise at room-temperature and the mixture heated to 50 °C overnight. The mixture was allowed to

cool to room temperature and the volatile components were removed *in vacuo*. The crude product was dissolved in hot hexanes, filtered, and the filtrate concentrated *in vacuo*. The product was further purified by recrystallization from ethanol to yield white flakes (1.87 g, 49% yield). mp: > 260 °C; ^{1}H NMR (400 MHz, $CDCl_3$): δ 0.63 (18H, s), 2.75 (6H, s); ^{13}C NMR (100 MHz, $CDCl_3$): δ 0.21, 15.2, 94.0, 98.3, 106.8, 140.0, 149.1, 165.9; HRMS (ESI) Calcd for $C_{20}H_{25}N_2O_2Si_2$, 380.13762 $(M+H)^+$; Found 380.13853.

4,8-bis(phenylethynyl)-2,6-dimethylbenzo[1,2-*d*-4,5-*d′*]bisoxazole 13b. Prepared similarly to **11b** from **8b** and phenylacetylene. Purified by recrystallization from chloroform/ethanol to yield small yellow needles (0.62 g, 78% yield). mp: > 260 °C; ^{1}H NMR (400 MHz, $CDCl_3$): δ 2.78 (6H, s), 7.40 (6H, m) 7.22 (4H, m); ^{13}C NMR (100 MHz, $CDCl_3$): δ 15.2, 79.5, 98.2, 100.1, 122.6, 128.5, 129.3, 132.3, 148.7, 165.9; HRMS (ESI) Calcd for $C_{26}H_{17}N_2O_2$, 389.1285 $(M+H)^+$; Found, 389.1287.

4,8-bis(4-(3,7-dimethyloctyloxy)phenylethynyl)-2,6-dimethylbenzo[1,2-*d*-4,5-*d′*]bisoxazole 14b. Prepared similarly to **11b** from **8b** and 1-(3,7-dimethyloctyloxy)-4-ethynylbenzene. The product was purified by recrystallization from ethanol to yield yellow needles (0.59 g, 84% yield). mp: 163-165 °C; ^{1}H NMR (400 MHz; $CDCl_3$): δ 0.88 (12H, d, *J*=8 Hz), 0.96 (6H, d, *J*=8 Hz), 1.67-1.88 (10H, overlapping multiplets), 2.77 (6H, s), 4.05 (4H, m), 6.91 (4H, d, *J*=8 Hz), 7.64 (4H, d, *J*=8 Hz); ^{13}C NMR (100 MHz, $CDCl_3$): δ 15.2, 19.9, 22.8, 24.9, 28.2, 30.1, 36.3, 37.5, 39.5, 66.6, 78.4, 98.2, 100.3, 114.5, 114.7, 133.9, 139.5, 148.6, 160.0, 165.6; HRMS (ESI): Calcd for $C_{46}H_{57}N_2O_4$,701.4313 $(M+H)^+$; Found, 701.4315.

4,8-bis(4-dodecylphenylethynyl)-2,6-dimethylbenzo[1,2-*d*-4,5-*d′*]bisoxazole 15b.

Prepared similarly to **11b** from **8b** and 4-dodecyl-1-ethynylbenzene. The product was purified by recrystallization from ethanol to yield small white needles (0.53 g, 73% yield). mp: 194-197 °C; ^{1}H NMR (400 MHz, $CDCl_3$): δ 0.88 (6H, d, *J*=8 Hz), 1.27-1.31 (36H, overlapped multiplets), 1.63 (4H, m), 2.64 (4H, t, *J*=8 Hz), 2.75 (6H, s), 7.20 (4H, d, *J*=8 Hz), 7.62 (4H, d, *J*=8 Hz); ^{13}C NMR (100 MHz, $CDCl_3$): 14.4, 15.1, 22.9, 29.5, 29.6, 29.7, 29.8, 29.86, 29.89, 31.4, 32.1, 36.2, 79.0, 98.2, 100.3, 119.8, 128.6, 132.2, 139.6, 144.5, 148.7, 165.7; HRMS (ESI) Calcd for $C_{50}H_{65}N_2O_2$, 725.5041 $(M+H)^+$; Found, 725.5031.

4,8-dibromo-2,6-dimethylbenzo[1,2-*d*-4,5-*d′*]bisoxazole-diethylphosphonate ester 8f. A dry pressure flask was equipped with a stir bar and capped with a septum and placed under argon atmosphere. The flask was charged with 2.68 g (6.46 mmol) **8c**, 3.23 g (19.4 mmol) triethyl phosphate, the flask sealed with a Teflon cap, and the mixture heated to 150 °C for 6 hours. The mixture is allowed to cool to room temperature and the crude product dissolved in a minimal amount of $CHCl_3$ and the product precipitated into 5x the volume of heptanes. The precipitate was collected by filtration and washed with heptanes to yield a yellow-white powder (3.62 g, 91% yield). mp: 163-165 °C; ^{1}H NMR (400MHz, $CDCl_3$): δ 1.40 (12H, t, *J*=8 Hz), 3.66 (4H, d, *J*=28 Hz), 4.23 (8H, m); ^{13}C NMR (100 MHz, $CDCl_3$): δ 16.5 (d, ^{3}J=5 Hz), 27.9 (d, ^{1}J= 138 Hz), 63.4 (d, ^{2}J=7 Hz), 92.0, 138.9, 147.2, 160.9 (d, ^{2}J= 11 Hz); HRMS (EI) Calcd for $C_{18}H_{20}N_2O_8P_2Br_2$, 615.93746 (M^+); Found 615.93965.

4,8-dichloro-2,6-dimethylbenzo[1,2-*d*-4,5-*d′*]bisoxazole-diethylphosphonate ester 9f. Prepared similarly to **8f** from **9c** and triethylphosphite to yield an off-white powder (4.79 g, 91% yield). mp: 164-165 °C; ^{1}H NMR (400MHz, $CDCl_3$): δ 1.38 (12H, t, *J*=8 Hz), 3.67 (4H, d, *J*=28 Hz), 4.25 (8H, m); ^{13}C NMR (100 MHz, $CDCl_3$): δ 16.5 (d, ^{3}J=5 Hz), 29.2 (d,

^{1}J= 138 Hz), 63.4 (d, ^{2}J=7 Hz), 104.8, 137.7, 145.9, 161.3 (d, ^{2}J= 11 Hz); HRMS (ESI) Calcd for $C_{18}H_{25}N_2O_8Cl_2P_2$, 529.0458 $(M+H)^+$; Found, 529.0460.

4,8-bis(decynyl)-2,6-dimethylbenzo[1,2-*d*-4,5-*d'*]bisoxazole-diethylphosphonate ester 16f. A dry 2-neck round-bottom flask was equipped with a stir bar, reflux condenser and placed under argon atmosphere. 140 mL dry/degassed THF, 9.11 g (90.0 mmol) diisopropylamine, and 3.73 g (27.0 mmol) 1-decyne were added and the mixture degassed for 15 minutes. The flask was then charged with 5.56 g (9.00 mmol) **8f**, 0.095 g (0.36 mmol) $PdCl_2(PPh_3)_2$, 0.068 g (0.36 mmol) PPh_3, and 0.25 g (0.36 mmol) CuI. The solution was degassed for 10 minutes and heated to reflux for 24 hrs. The solution was allowed to cool to room temperature and the volatile components removed *in vacuo*. The crude product was filtered through a short silica plug eluting with $Et_2O/CHCl_3$ (4:1). The product was further purified by recrystallization from hexanes to yield a yellow solid (4.87 g, 74% yield). mp: 119-120 °C; ^{1}H NMR (400MHz, $CDCl_3$): δ 1.87 (6H, t, *J*=8 Hz), 1.28-1.35 (16H, overlapping multiplets), 1.36 (12H, *J*=8 Hz), 1.46 (4H, m), 1.69 (4H, quintet, *J*=8Hz), 2.58 (4H, t, *J*=8 Hz), 3.64 (4H, d, *J*=24 Hz), 4.22 (8H, m) ; ^{13}C NMR (100 MHz, $CDCl_3$): δ 14.3, 16.5 (d, ^{3}J=6 Hz), 20.4, 22.9, 27.8 (d, ^{1}J=137 Hz), 28.8, 29.3, 29.35, 29.39, 32.1, 63.3 (d, ^{3}J=6 Hz), 70.6, 98.9, 102.3, 140.0, 149.3, 160.4 (d, ^{2}J=25 Hz); HRMS (ESI) Calcd for $C_{58}H_{83}N_2O_8P_2$, 997.5619 $(M+H)^+$; Found, 997.5631.

4,8-bis-(4-dodecylphenylethynyl)-2,6-dimethylbenzo[1,2-*d*-4,5-*d'*]bisoxazole-diethylphosphonate ester 15f. Prepared similarly to **16f** from **8f** and 4-(dodecyl)-1-ethynylbenzene to yield a bright yellow powder (5.15 g, 65% yield). mp: 110-111 °C; ^{1}H NMR (400MHz, $CDCl_3$): δ 0.89 (6H, t, *J*=8 Hz), 1.27-1.35 (36H, overlapping multiplets), 1.38 (12H, t, *J*=8 Hz), 1.63 (4H, m), 2.64 (4H, t, *J*=8 Hz), 3.67 (4H, d, *J*=28 Hz), 4.25 (8H,

m), 7.21 (4H, d, *J*=8 Hz), 7.57 (4H, d, *J*=8 Hz) ; ^{13}C NMR (100 MHz, $CDCl_3$): δ 14.3, 16.6 (d, ^3J=6 Hz), 22.9, 27.86 (d, ^1J= 138 Hz), 27.9, 29.5, 29.6, 29.7, 29.8, 29.8, 29.9, 29.9, 31.4, 32.1, 63.4 (d, ^2J=6 Hz), 78.9, 99.0, 100.8, 119.8, 128.7, 132.1, 139.9, 144.7, 149.1, 160.6 (d, ^2J= 9 Hz); HRMS (ESI) Calcd for $C_{38}H_{59}N_2O_8P_2$, 733.3741 $(M+H)^+$; Found, 733.3739.

General Polymerization Procedure (P1, P3, P4, and P5). A dry Schlenk flask was placed under argon atmosphere and charged with equimolar amounts of phosphonate ester **8f** (**P1**, **P4**), **9f** (**P5**), or **15f** (**P3**) and 2,5-didodecyloxyterephthaldehyde (**P1**, **P3**) or 3,4-didodecylthiophene dicarboxaldehyde (**P4**-**P5**) dissolved in dry THF to make a 0.06 M solution of phosphonate ester. The mixture was stirred at room temperature while adding 2.5 equiv of potassium *tert*-butoxide (1.0 M in THF) in one portion. The mixture was stirred at room temperature for 3 days and the reaction diluted 1.3 times with dry THF and the reaction stirred 2 additional days before precipitating the polymer into 200 mL of methanol. The precipitated polymer was filtered into a cellulose extraction thimble, placed into a Soxhlet extractor and washed with methanol, hexane, and THF (**P1** and **P3**, and P**5**) or $CHCl_3$ (**P6**). Polymer was recovered from the THF or $CHCl_3$ extract by evaporation of the solvent.

Polymer P1. (0.45 g, 56% yield). ^{1}H NMR δ 0.88 (-CH_3, broad), 1.25-1.96 (-$C_{10}H_{25}$, broad), 4.13 (-OCH_2, broad), 6.9-7.25 (Aryl-H and vinyl protons, broad). UV-Vis (THF) λ_{max} = 476 nm. GPC: M_n = 3,300, M_w = 7900, PDI = 2.4. Fluorescence (THF): λ_{em} = 524 nm (λ_{exc} = 476 nm).

Polymer P3. (0.33 g, 55% yield). ^{1}H NMR (400MHz; $CDCl_3$) δ 0.89, (-CH_3, t), 1.25-1.20 (-$C_{11}H_{25}$, broad) 2.46 (aryl-CH_2, broad), 3.64 (OCH_2, broad). 6.93-7.00-7.25 (aryl, vinyl -CH, broad), 7.25-8.0 (aryl–CH, broad).UV-Vis (THF) λ_{max} = 520 nm. GPC: M_n = 5,708, M_w = 14,120, PDI = 2.5. Fluorescence (THF): λ_{em} = 601 nm (λ_{exc} = 520 nm).

Polymer P4. (0.25 g, 61% yield). ^{1}H NMR (400MHz; $CDCl_3$) δ 0.88, (-CH_3, t), 1.20-1.45 (-$C_{11}H_{25}$, broad), 2.77 (-CH_2, broad), 6.92-7.00 (vinyl –CH, broad), 8.02-8.04 (vinyl –CH, broad). UV-Vis (THF) λ_{max} = 506 nm. GPC: M_n = 4,300, M_w = 6,000, PDI = 1.4. Fluorescence (THF): λ_{em} = 563 nm (λ_{exc} = 506 nm).

Polymer P5. (0.20 g, 55% yield). ^{1}H NMR (400MHz; $CDCl_3$) δ 0.88, (-CH_3, t), 6.93-7.00 (-$C_{11}H_{25}$, broad), 2.78 (-CH_2, broad), 6.92-7.00 (vinyl –CH, broad), 7.98-8.04 (vinyl –CH, broad).UV-Vis (THF) λ_{max} = 510 nm. GPC: M_n = 3,300, M_w = 7,900, PDI = 2.4. Fluorescence (THF): λ_{em} = 560 nm (λ_{exc} = 495 nm).

Polymer P2. A dry Schlenk flask was placed under argon atmosphere and charged with 0.36 g (0.50 mmol) **16f**, 0.25 g (0.50 mmol) 2,5-didodecyloxyterephthaldehyde, 0.11g (1.25 mmol) LiBr, and 9 mL dry THF. The mixture was stirred at room temperature and 0.12 g (2.40 mmol) Et_3N diluted in 1 mL THF was added drop-wise and the reaction stirred for 3 days and the polymer precipitated into 150 mL of methanol. The precipitated polymer was filtered into a cellulose extraction thimble, placed in a Soxhlet extractor and washed with methanol, hexane, and THF. The polymer was recovered from the THF extract by evaporation of the solvent (0.40 g, 87% yield). ^{1}H NMR (400MHz; $CDCl_3$) δ 0.92, (-CH_3, broad), 1.35-1.64 (-$C_{11}H_{25}$, -C_6H_{12}, broad) 2.70 (propargyl-CH_2, broad), 3.25 (-OCH_2, broad), 6.93-7.00 (-$C_{11}H_{22}$, 7.04-7.25 (vinyl,aryl –CH, broad), 7.25-7.75 (aryl –CH, broad).UV-Vis (THF) λ_{max} = 491 nm. GPC: M_n = 22,683, M_w = 113,798, PDI = 5.0. Fluorescence (THF): λ_{em} = 576 nm (λ_{exc} = 491 nm).

2.5.3 Computational Details

All of the calculations on these oligomers studied in this work were studied using the Gaussian 03W with the GaussView 4 GUI interface program package. All electronic ground states were optimized using density functional theory (DFT), B3LYP/6-31G*. Excited states were generated through time dependent density functional theory (TD-DFT) applied to the optimized ground state for each oligomer. The HOMO, LUMO, band gap, first ten excited states, and UV-Vis simulations were generated from these excited computations. Approximations of the molecular orbital contributions for each excited state were obtained using the GaussSum 2.2 freeware package. Finally, electrostatic potential maps were created using a coarse setting and an isovalue of 0.03.

2.6 Acknowledgements

The Acknowledgment is made to the Donors of the American Chemical Society Petroleum Research Fund for support of this research. We also thank the 3M Foundation and the National Science Foundation (DMR-0846607) and Teragrid (TG-CHE100148) for partial support of this work. We thank Dr. Kamel Harrata and the Mass Spectroscopy Laboratory of Iowa State University (ISU) for analysis of our compounds and Dr. Arkady Ellern for X-ray crystallographic analysis. We thank Atta Gueye, Dr. Elena Sheina and Dr. Christopher Brown of Plextronics for providing UPS measurements. We thank Scott Meester for the synthesis of 4-(3,7-dimethyloctyloxy)-1-bromobenzene and Andrew Makowski for the synthesis of 2,5-didodecyloxyterephthaldehyde. We also thank Dr. Toby Nelson and Dr. David Yaron (Carnegie Mellon University) for helpful discussions of this research.

2.7 Supporting Information

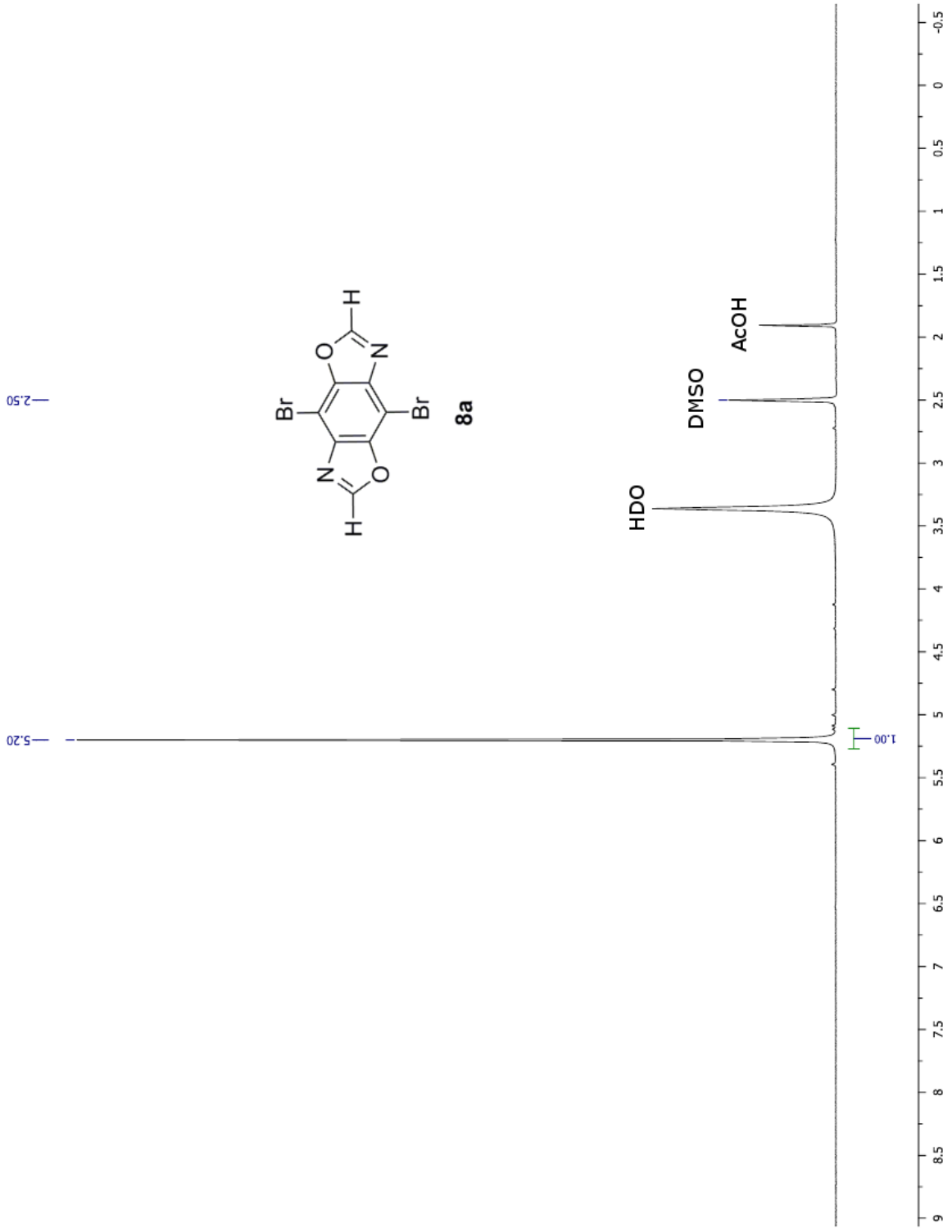

Figure S2.1. ^{1}H NMR of **8a**.

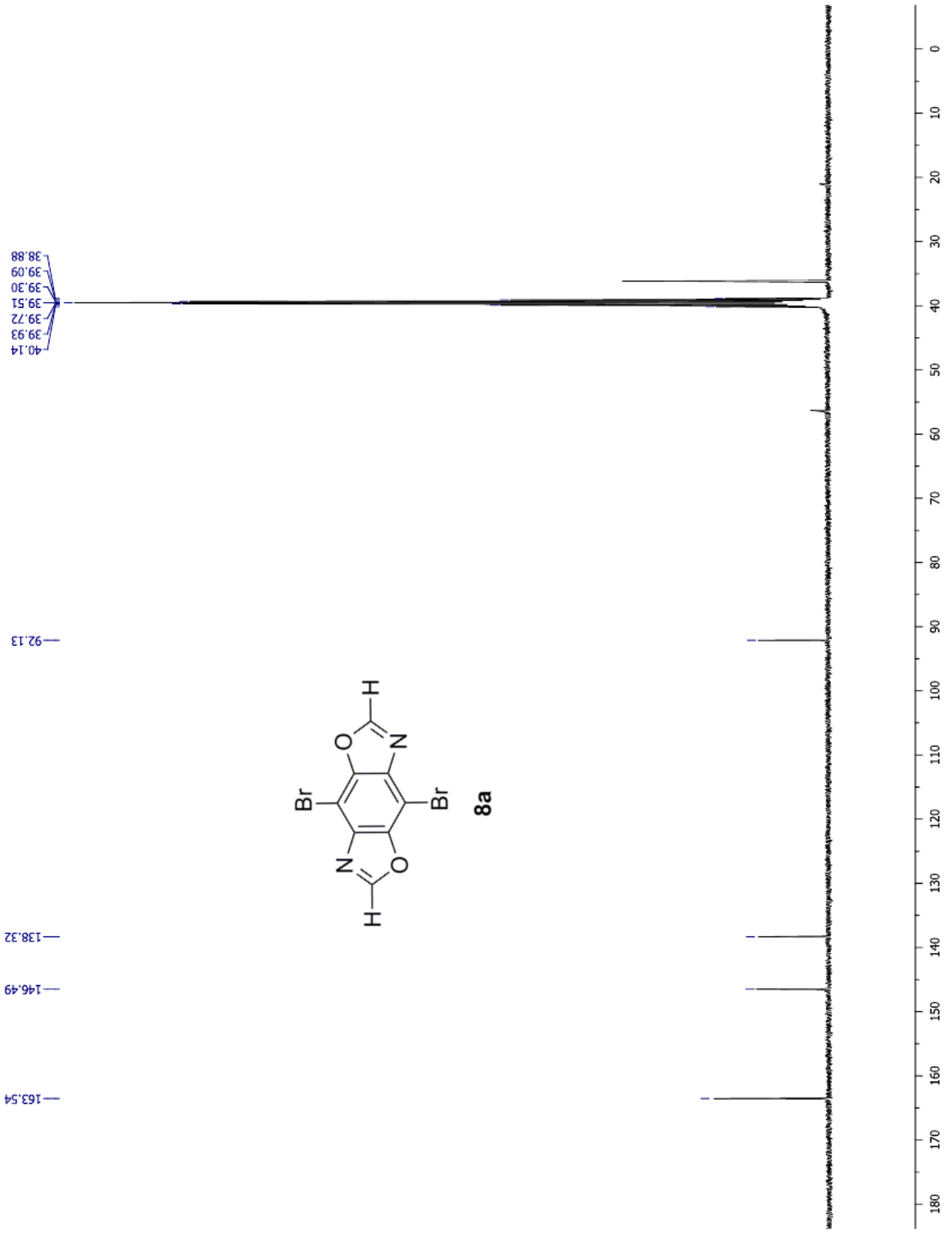

Figure S2.2. ^{13}C NMR of **8a**.

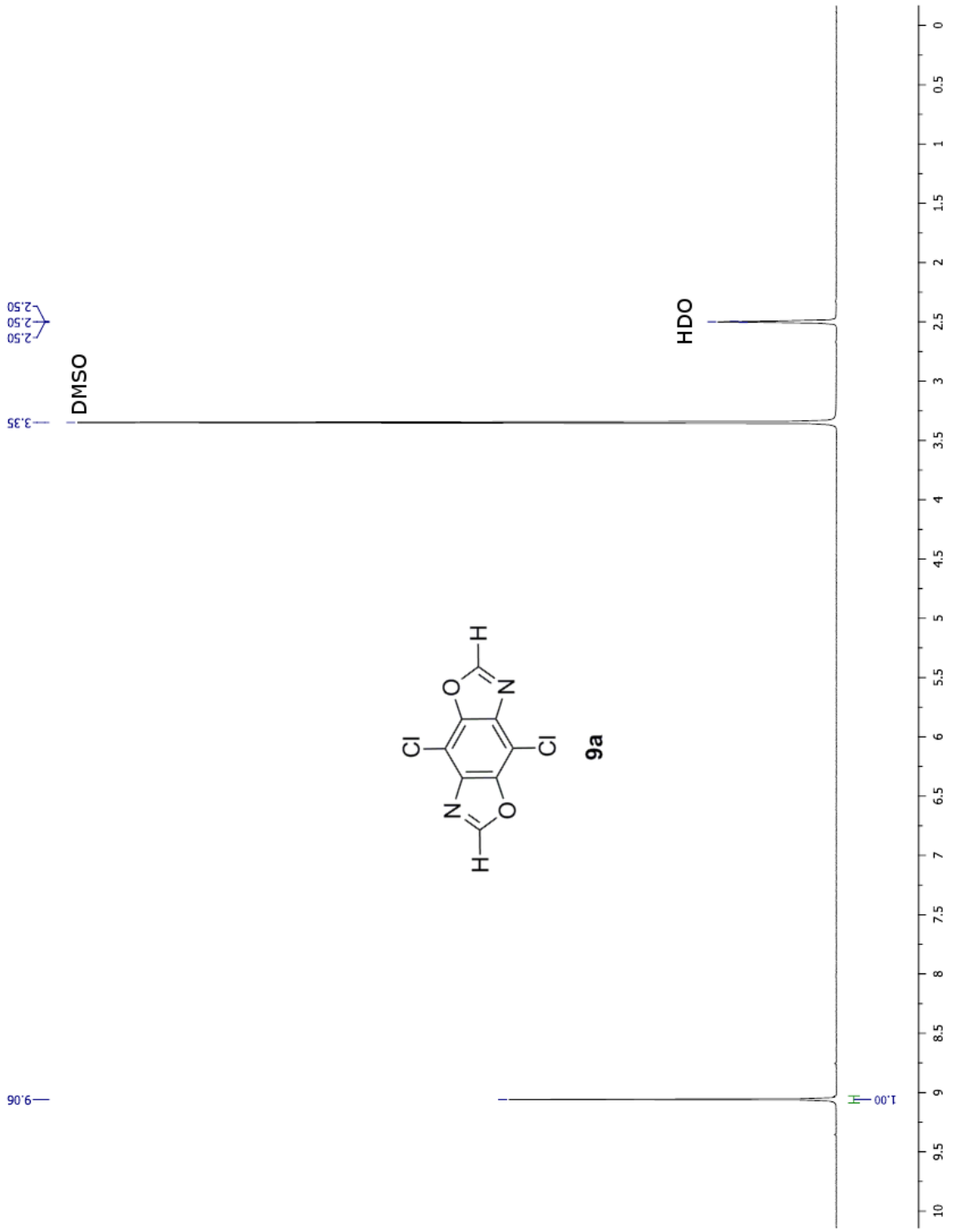

Figure S2.3. ^{1}H NMR of **9a.**

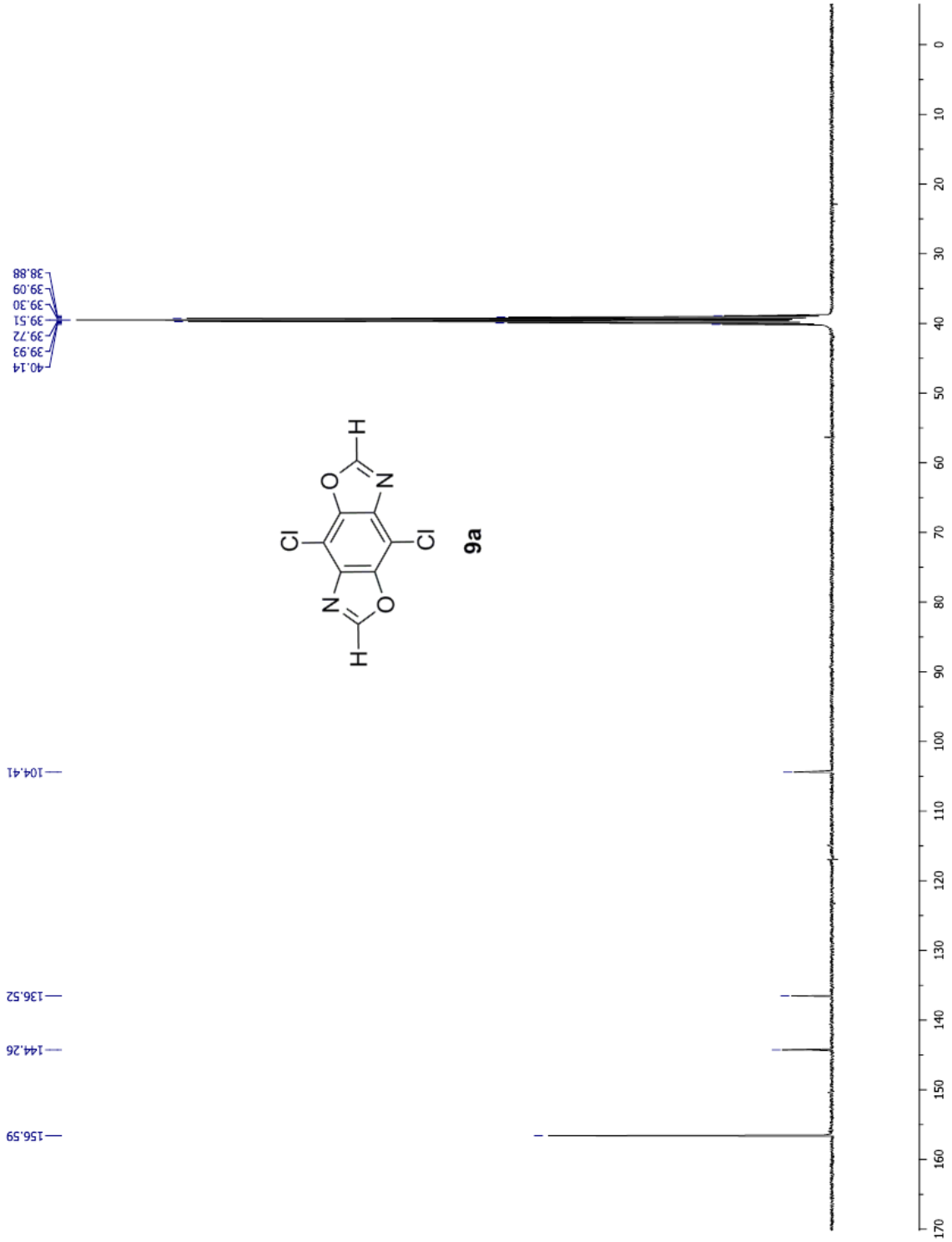

Figure S2.4. ^{13}C NMR of **9a.**

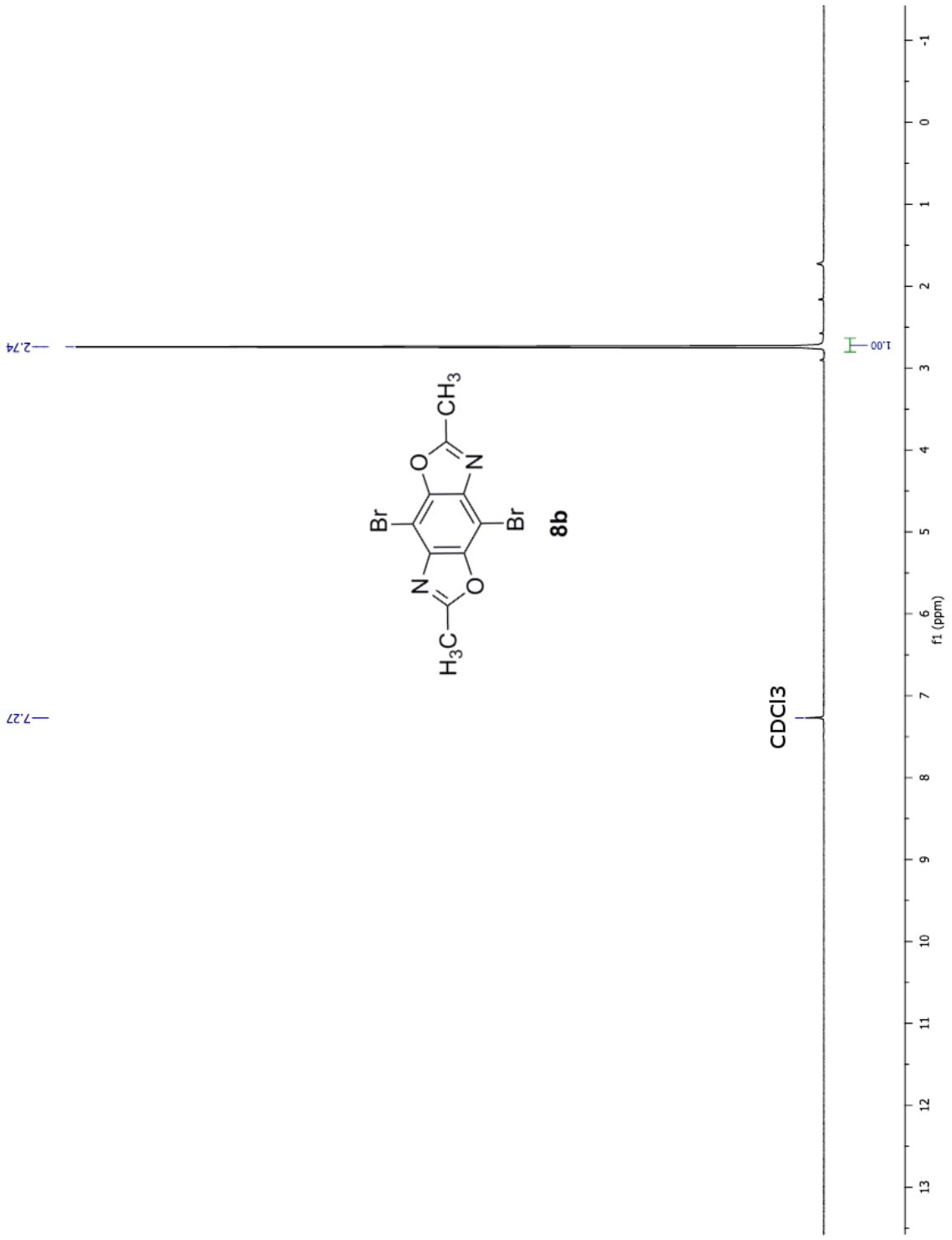

Figure S2.5. ^{1}H NMR of **8b.**

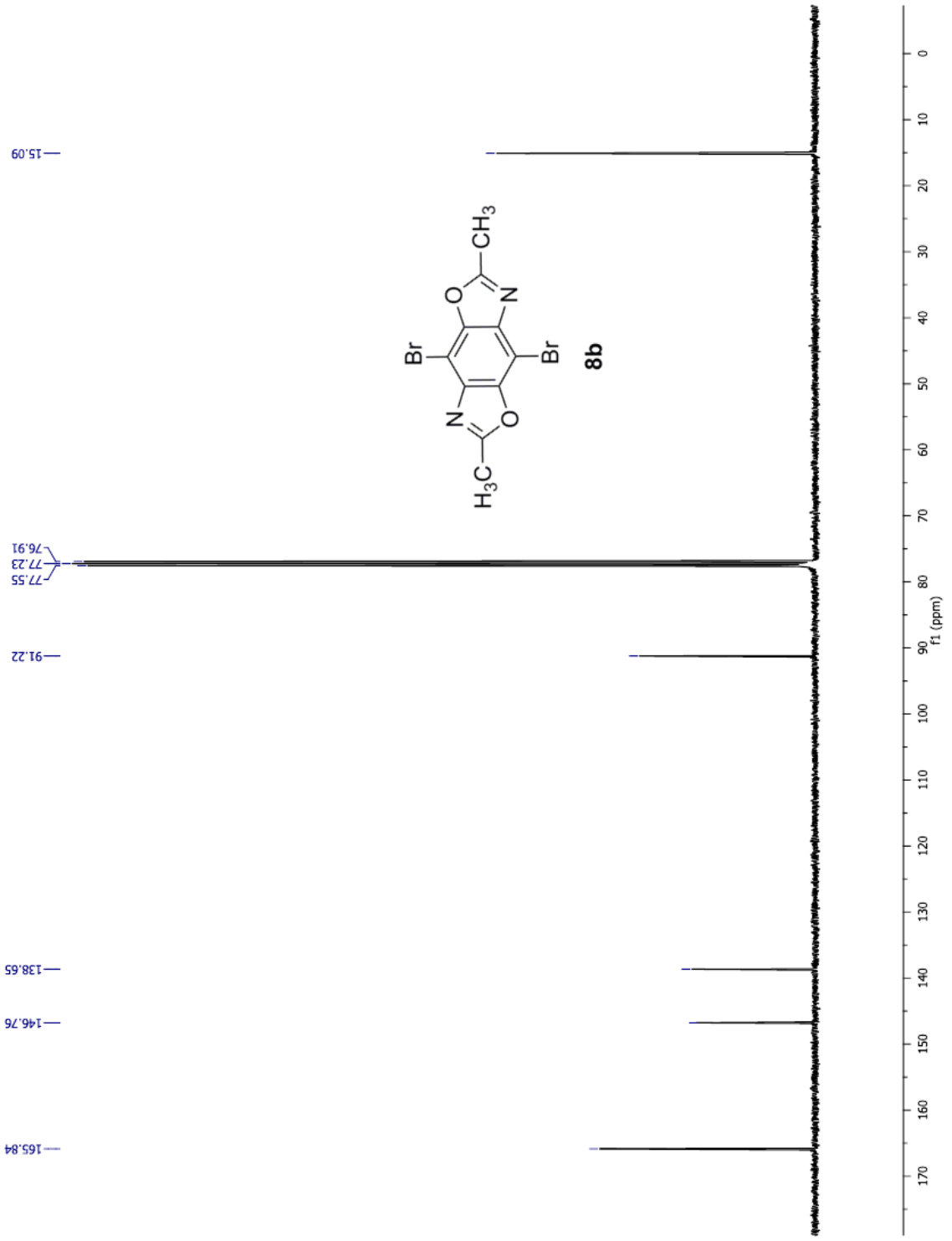

Figure S2.6. ^{13}C NMR of **8b.**

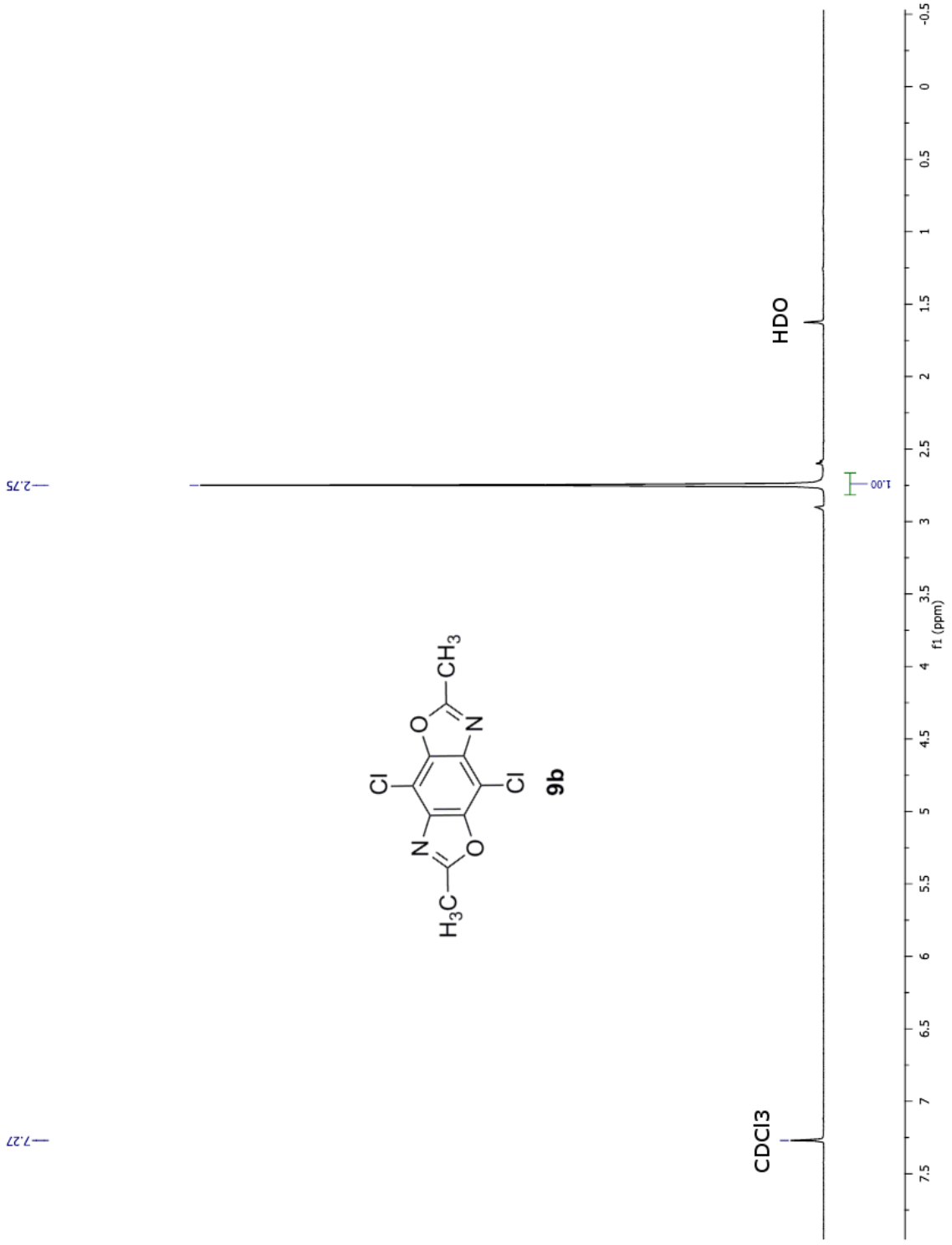

Figure S2.7. ^{1}H NMR of **9b.**

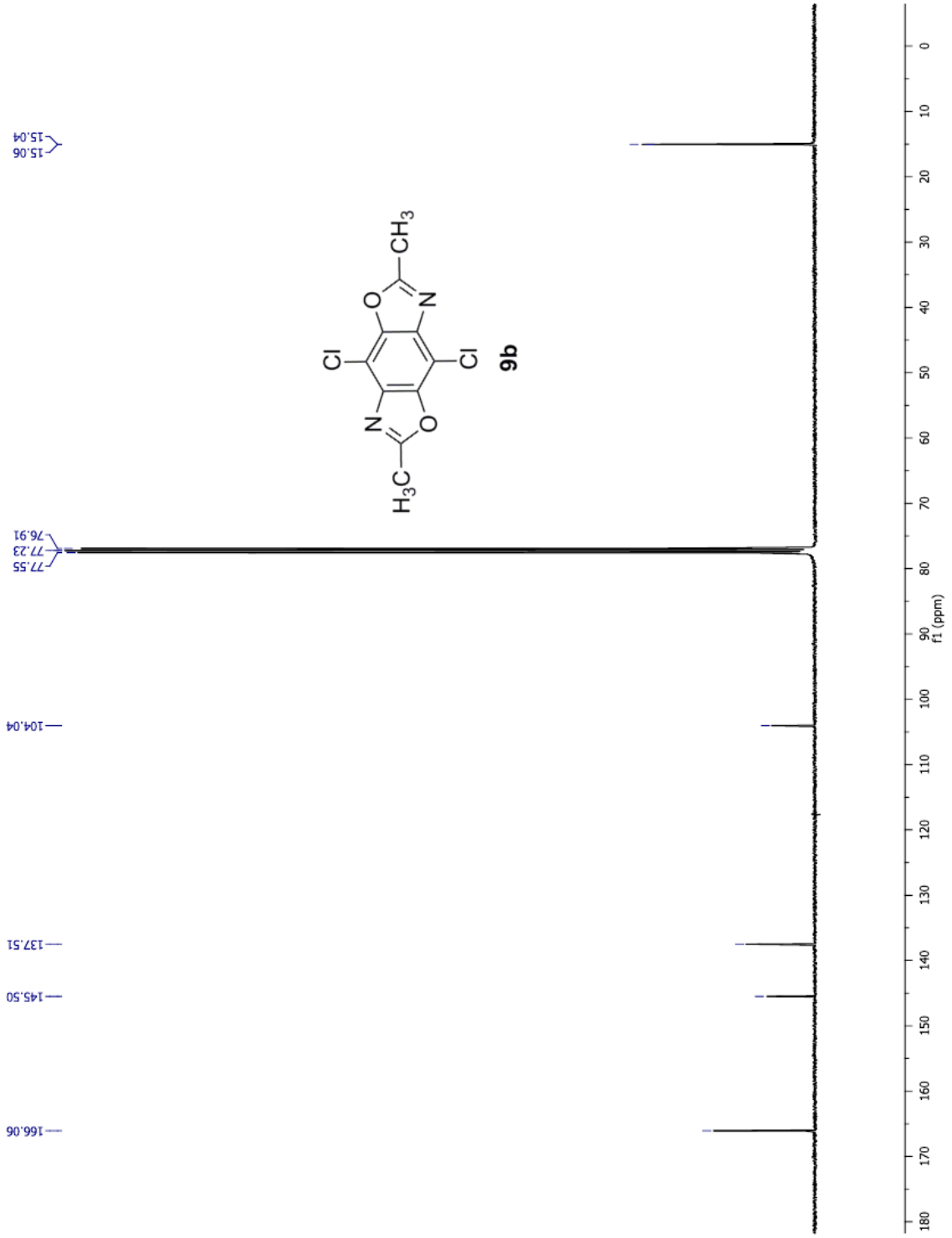

Figure S2.8. ^{13}C NMR of **9b.**

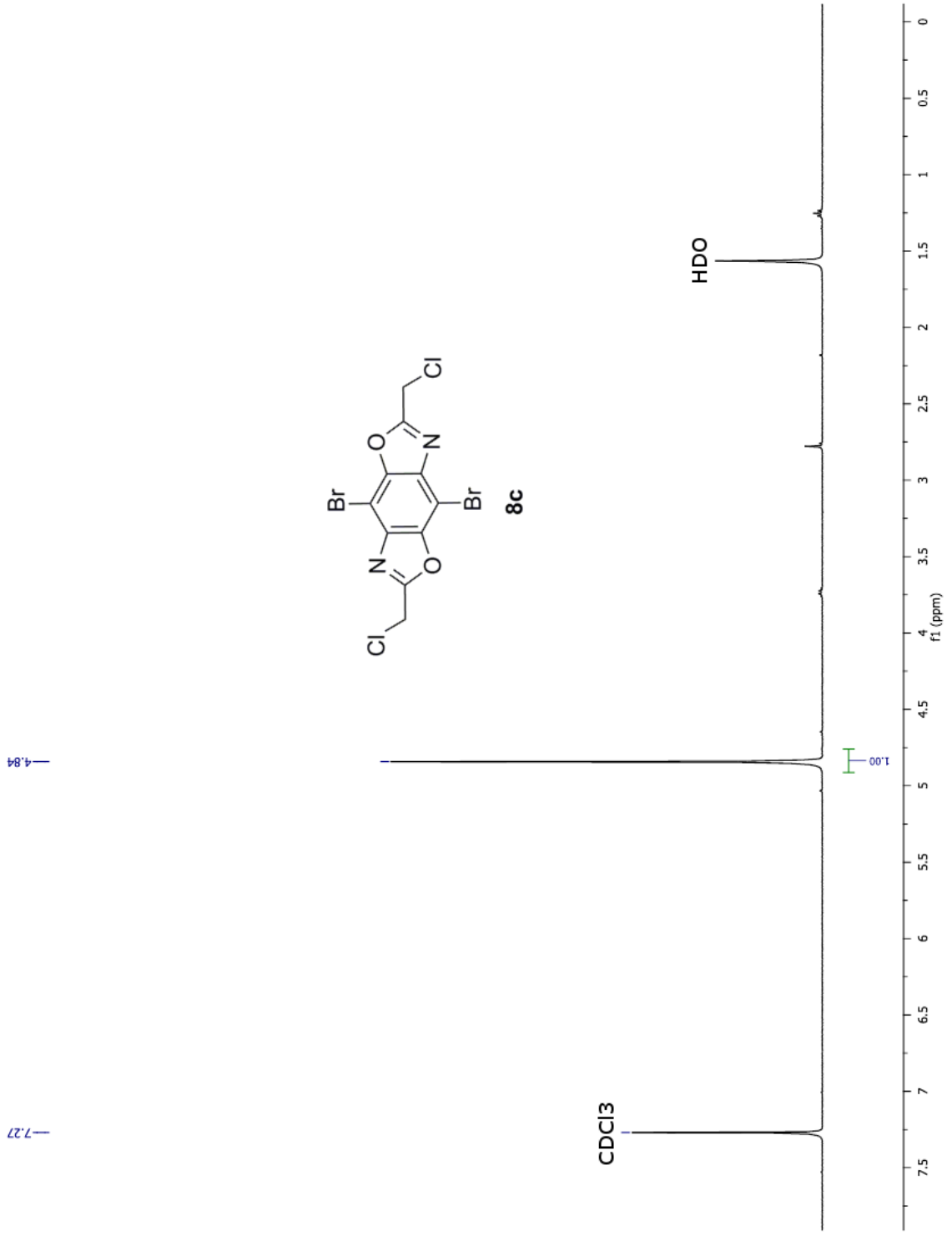

Figure S2.9. ^{1}H NMR of **8c.**

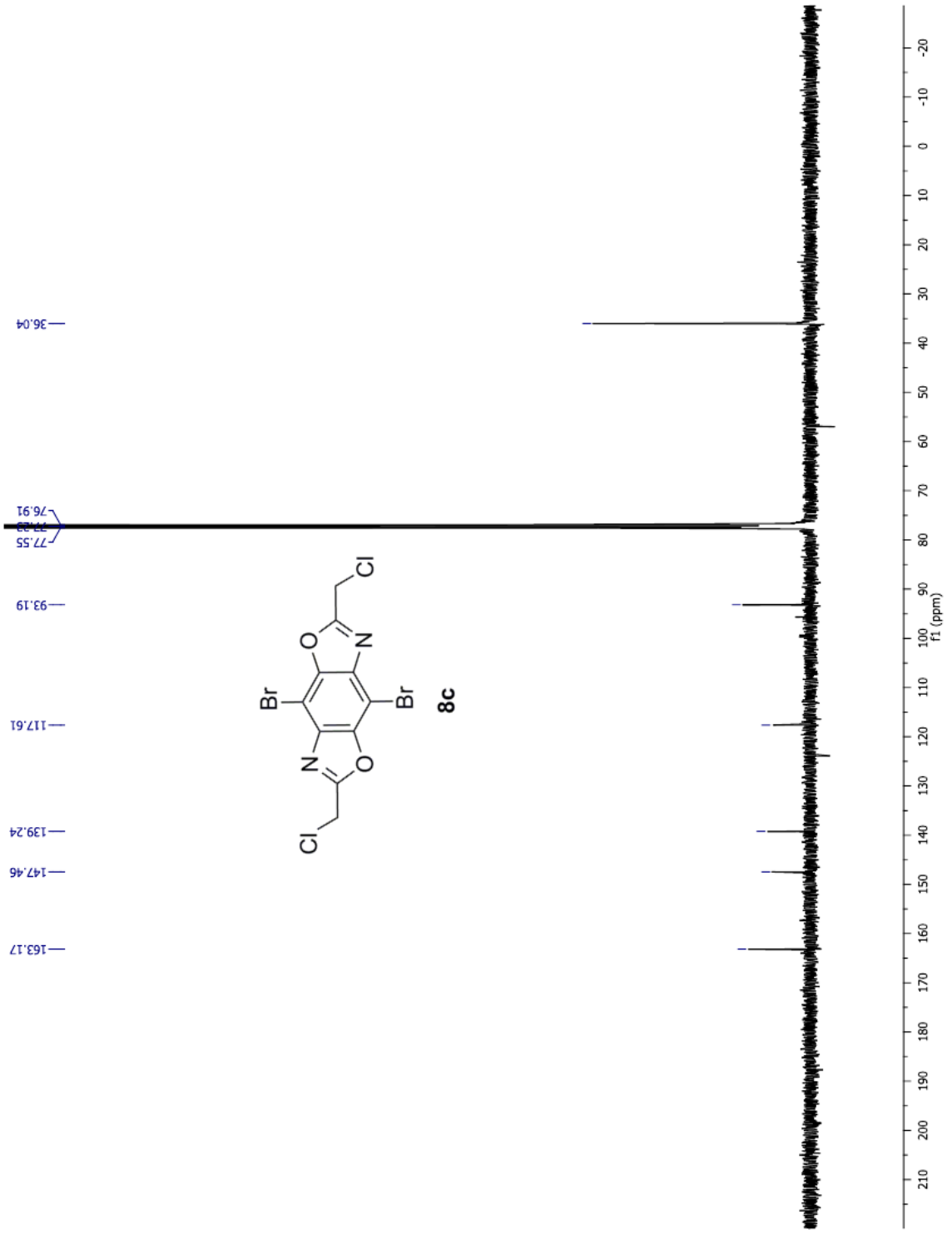

Figure S2.10. ^{13}C NMR of **8c.**

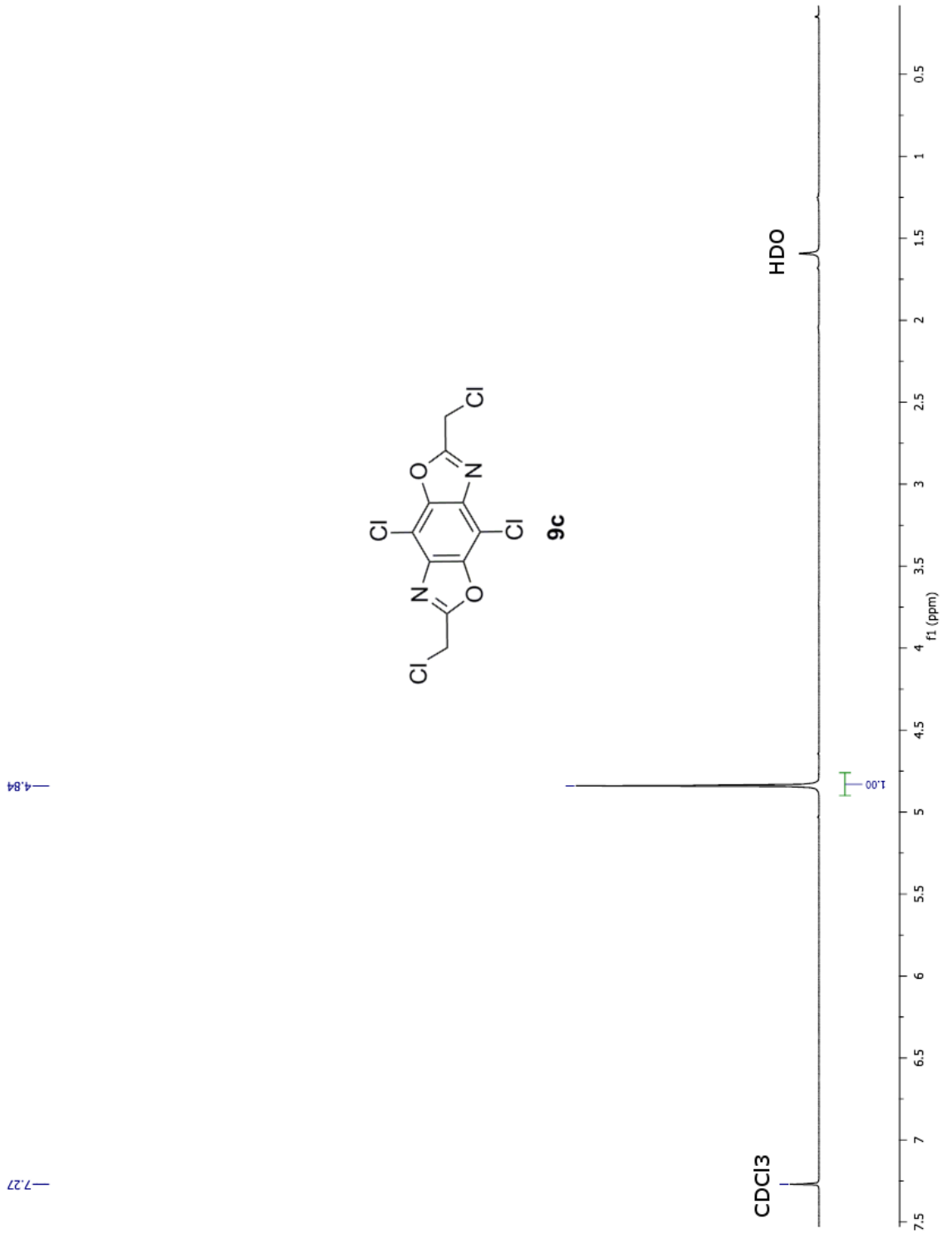

Figure S2.11. ^{1}H NMR of **9c.**

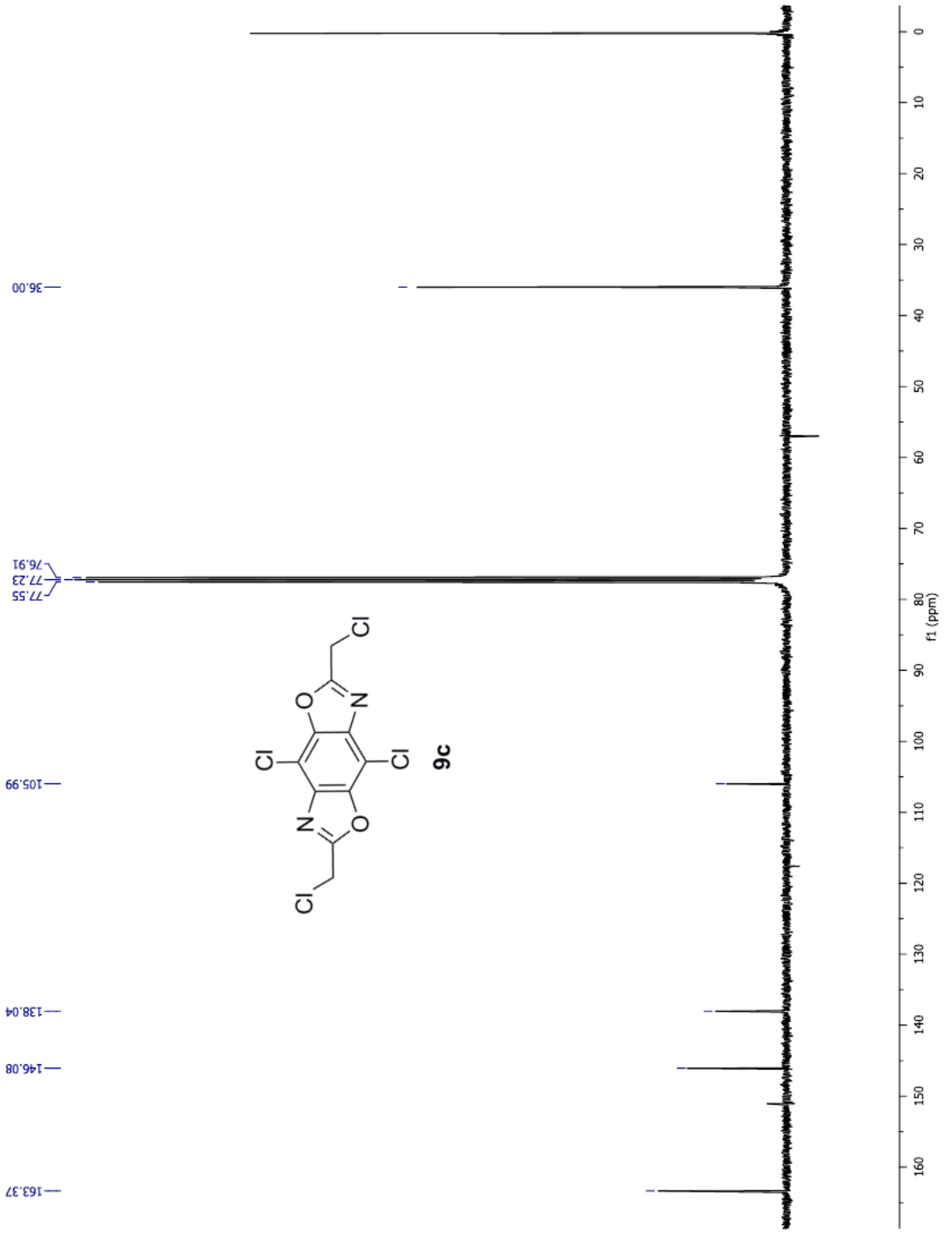

Figure S2.12. ^{13}C NMR of **9c.**

Figure S2.13. ^{1}H NMR of **8d.**

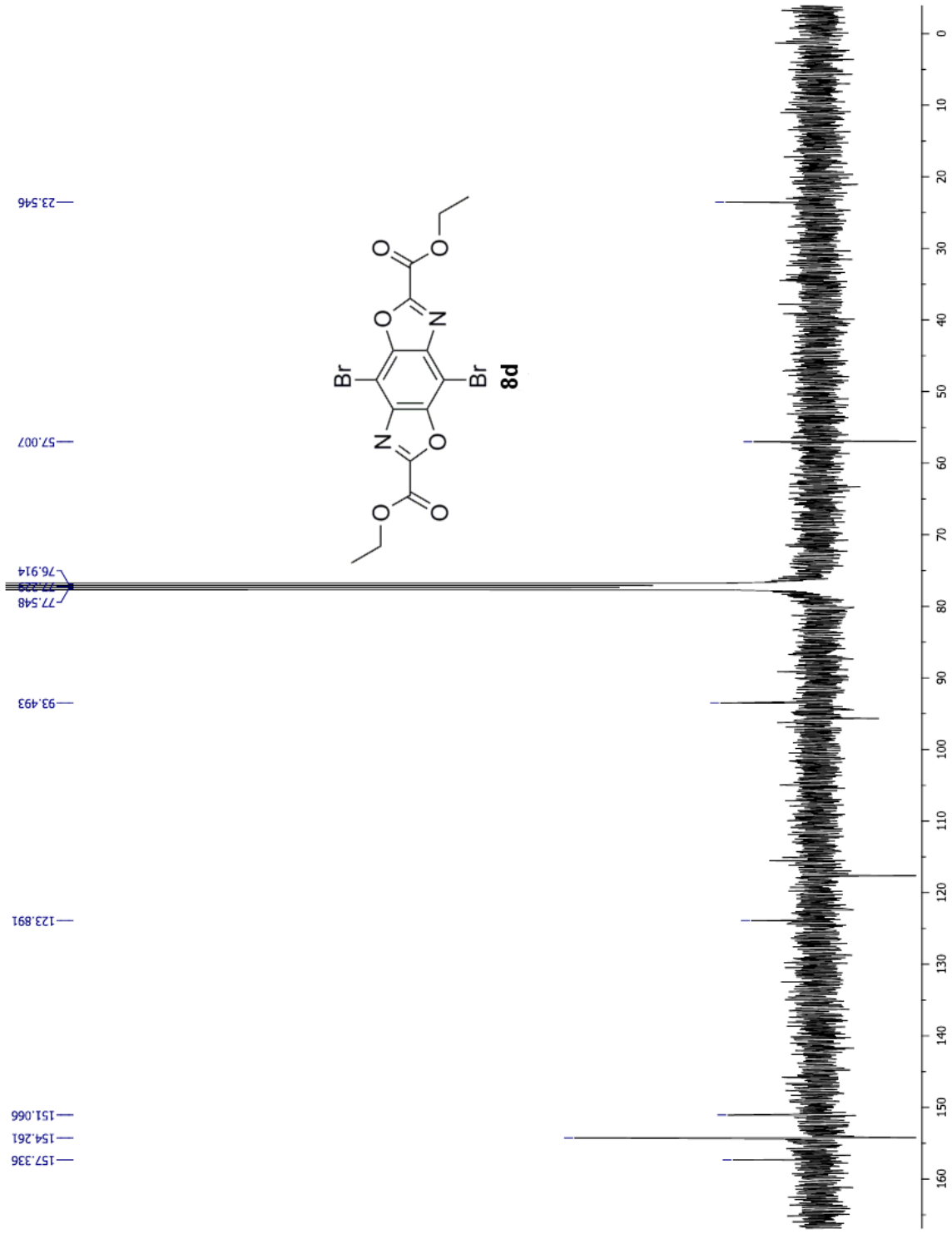

Figure S2.14. ^{13}C NMR of **8d.**

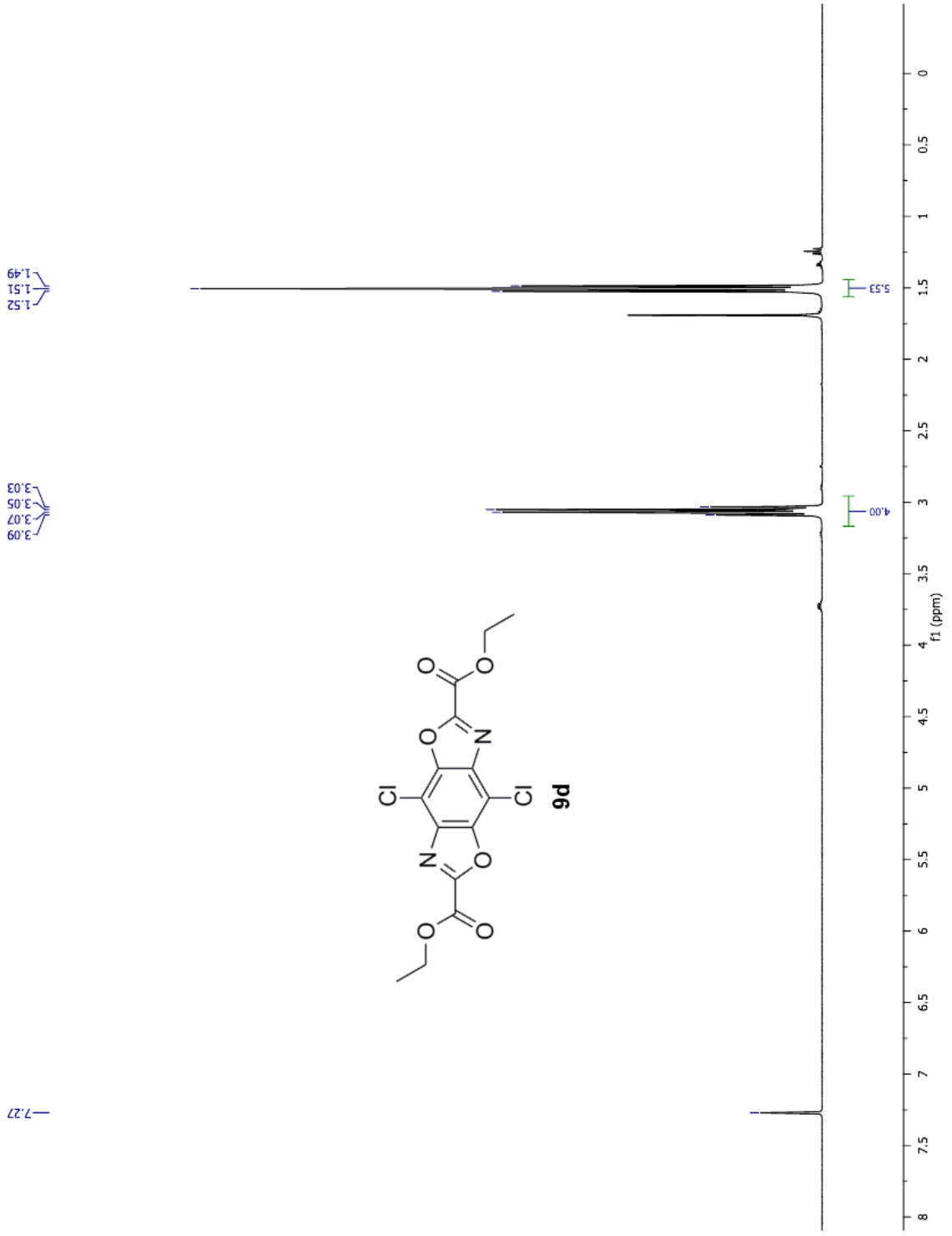

Figure S2.15. ^{1}H NMR of **9d.**

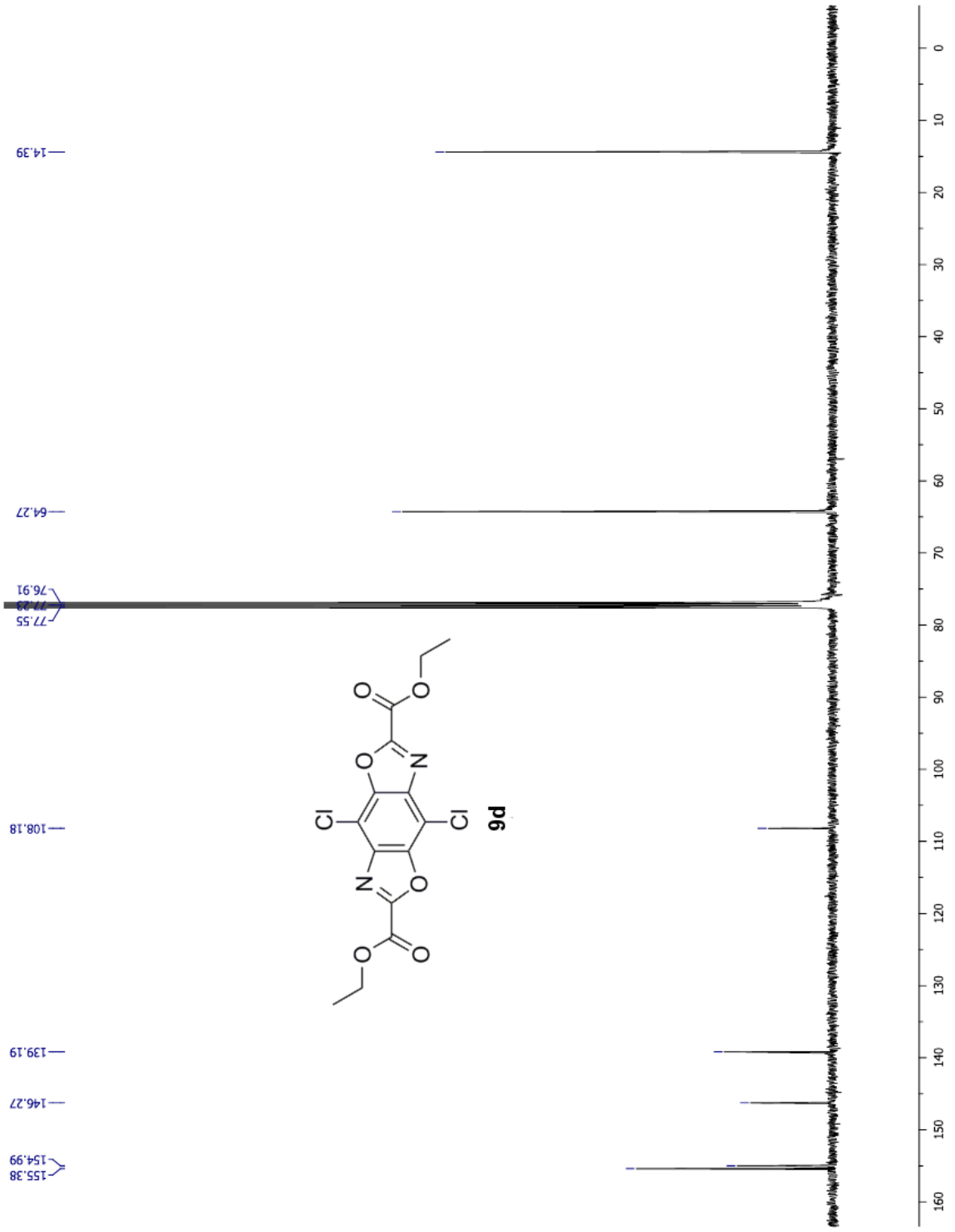

Figure S2.16. ^{13}C NMR of **9d.**

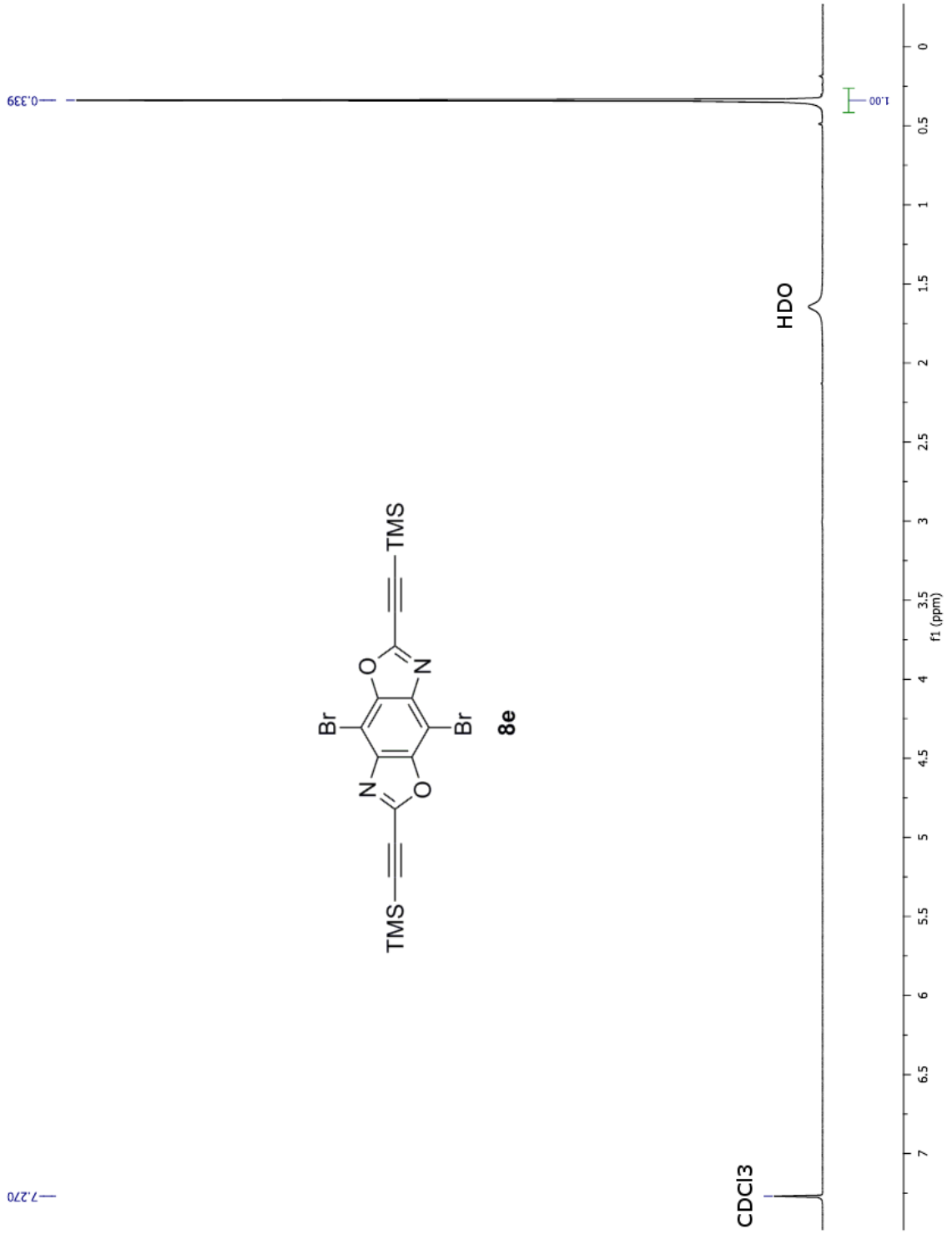

Figure S2.17. ^{1}H NMR of **8e.**

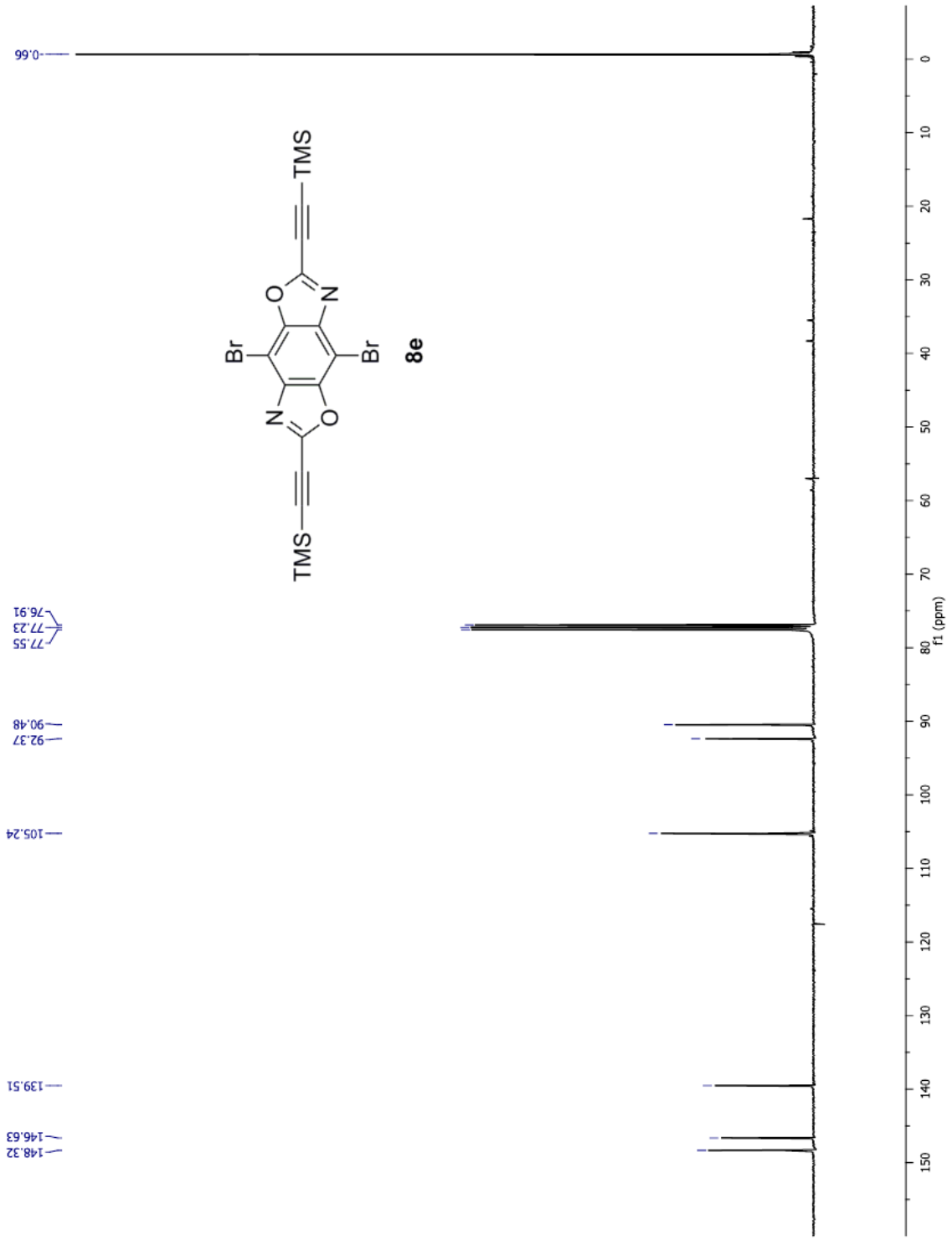

Figure S2.18. ^{13}C NMR of **8e.**

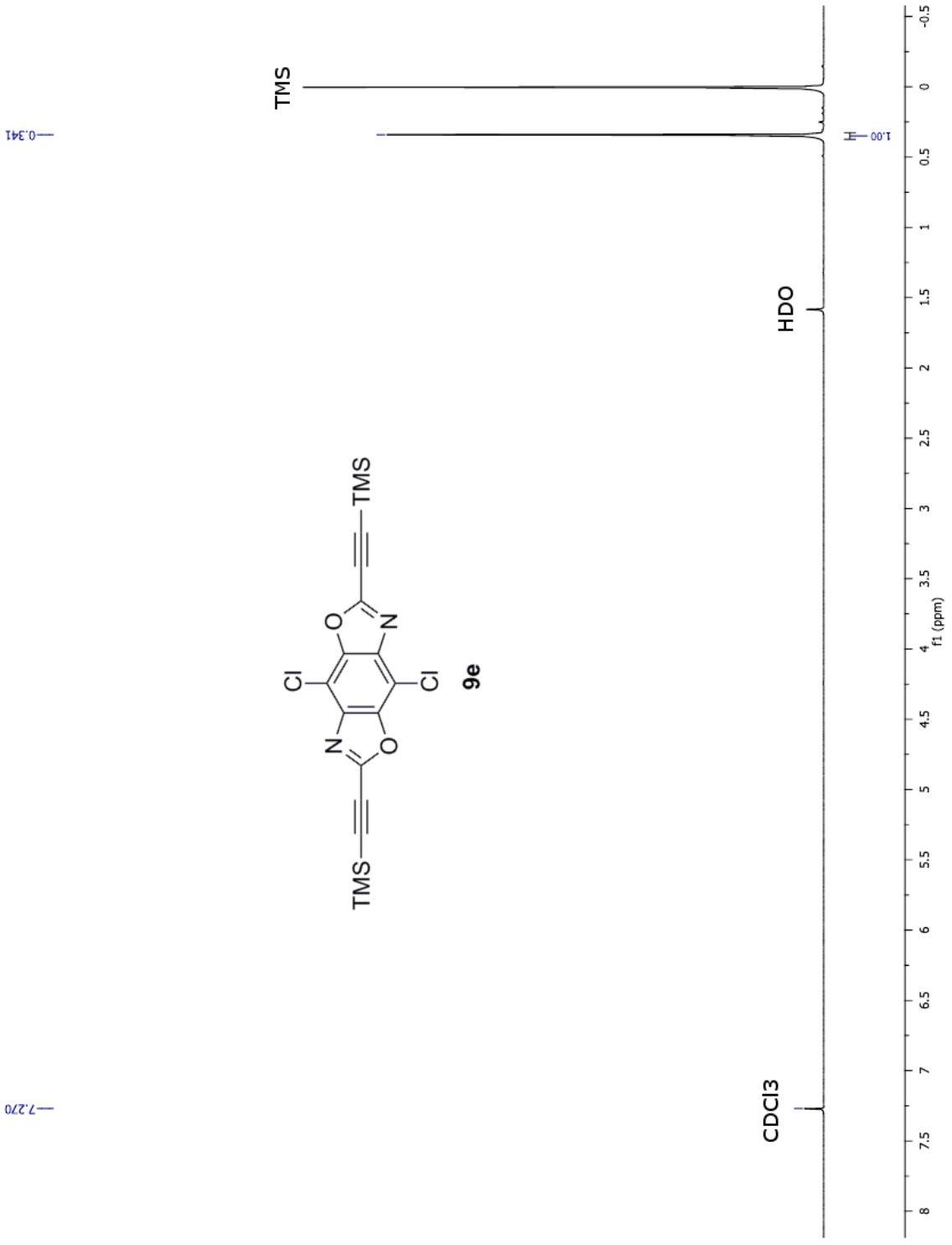

Figure S2.19. ^{1}H NMR of **9e.**

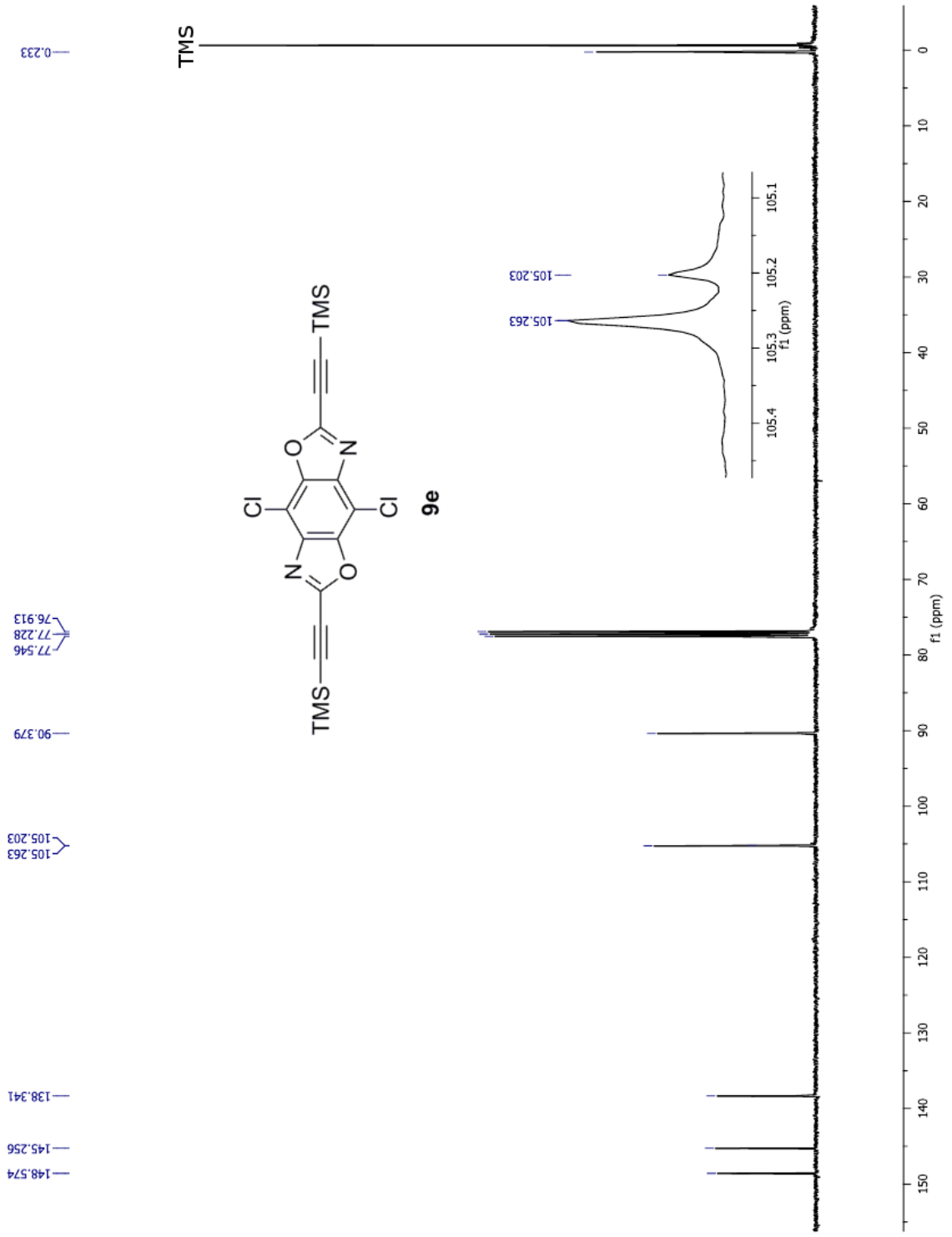

Figure S2.20. ^{13}C NMR of **9e.**

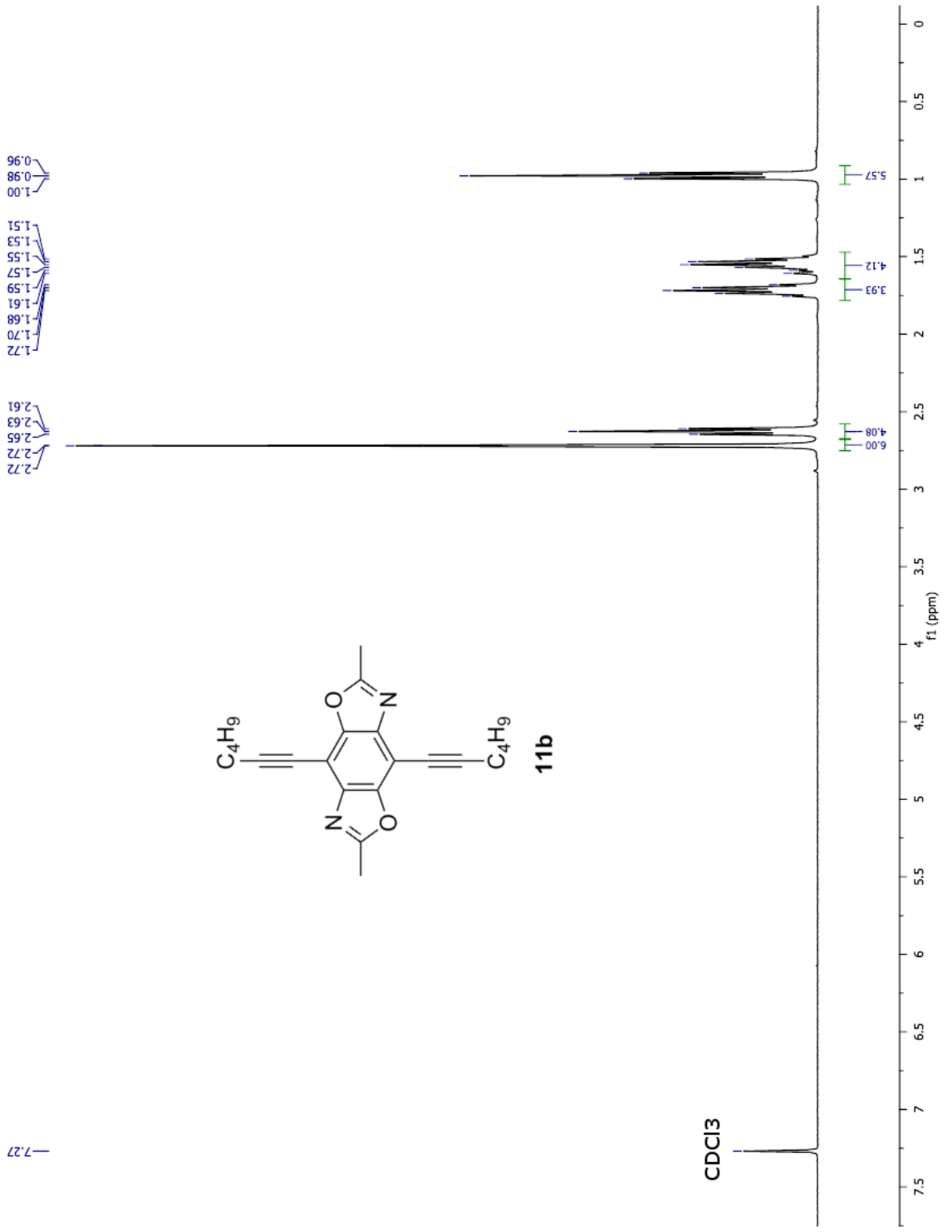

Figure S2.21. ^{1}H NMR of **11b.**

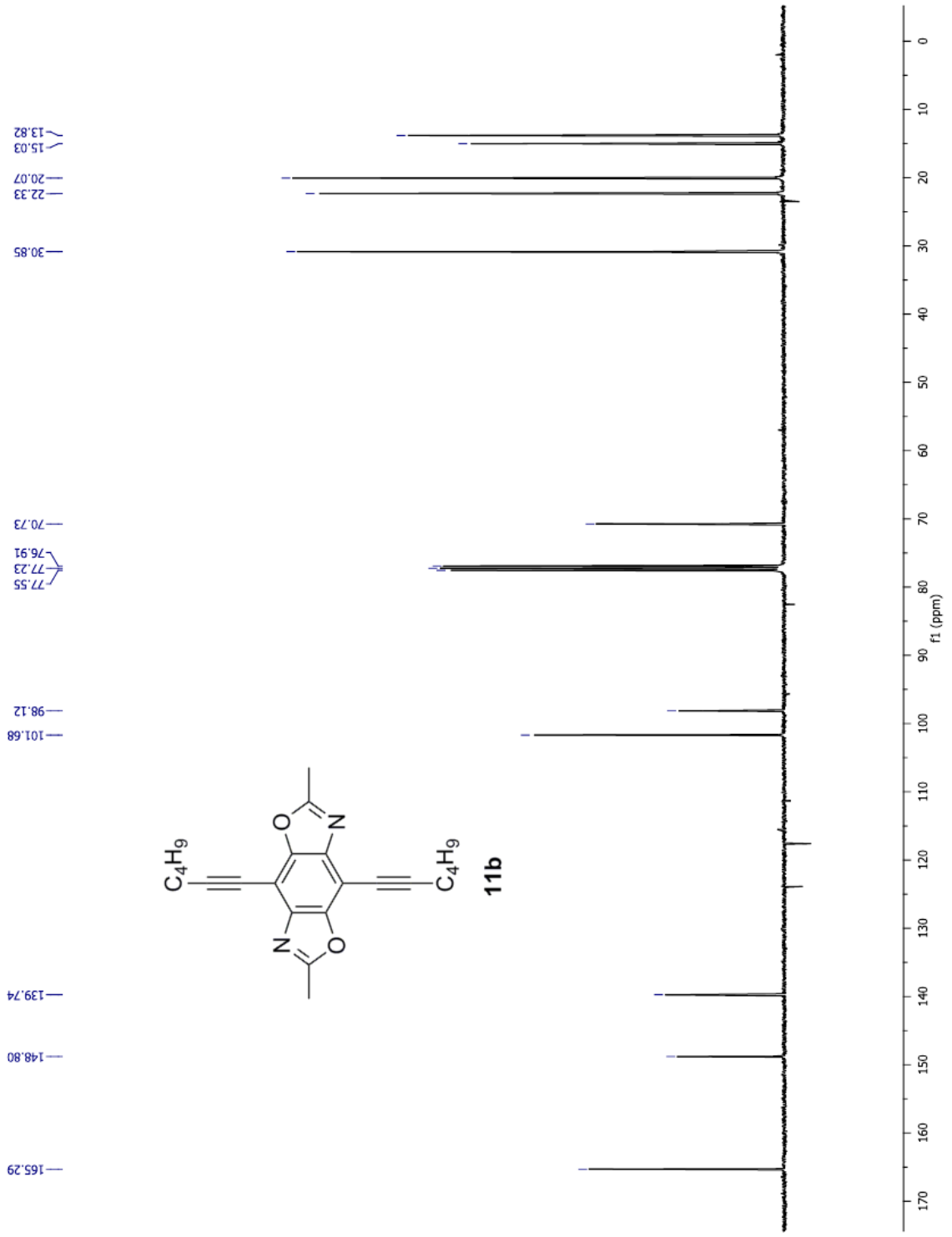

Figure S2.22. ^{13}C NMR of **11b.**

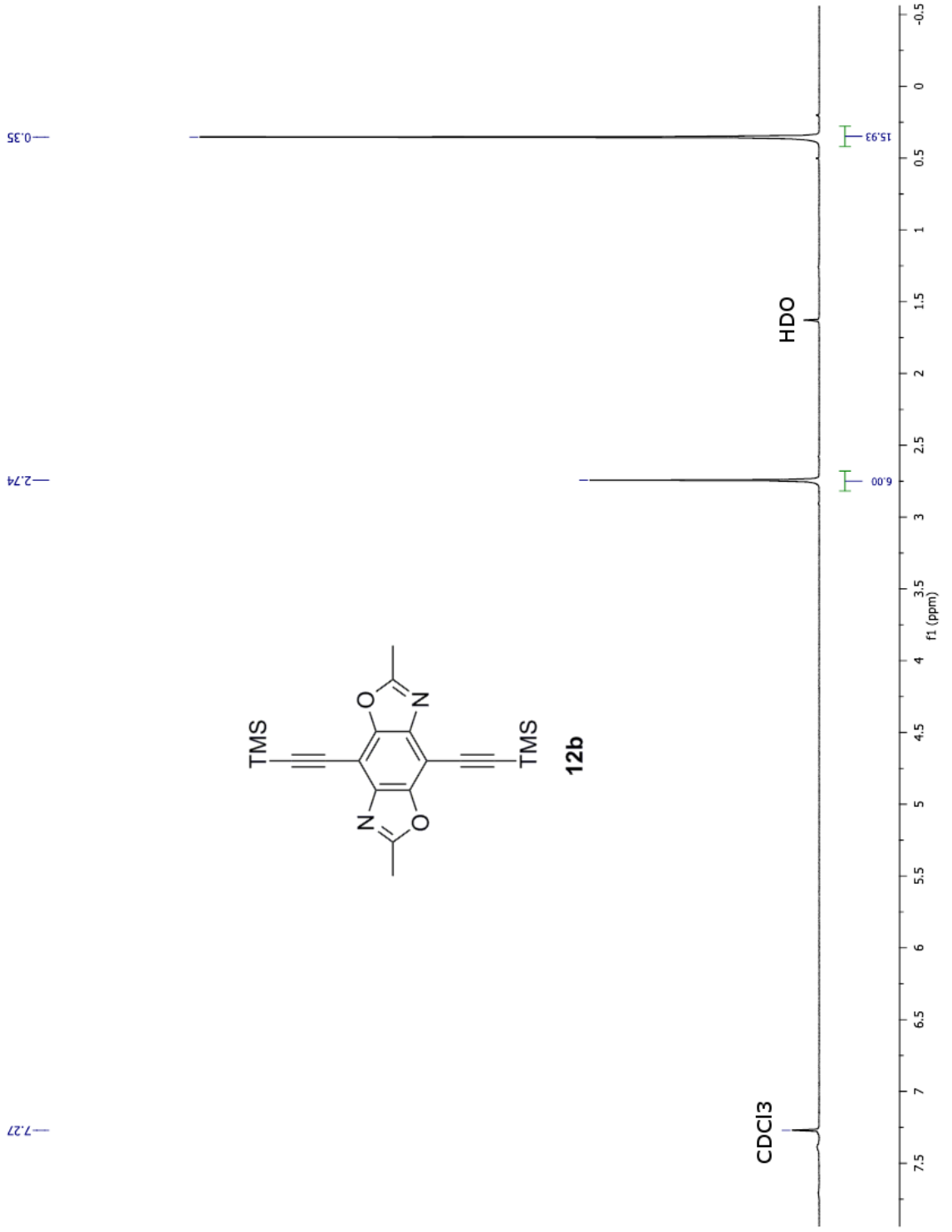

Figure S2.23. ^{1}H NMR of **12b.**

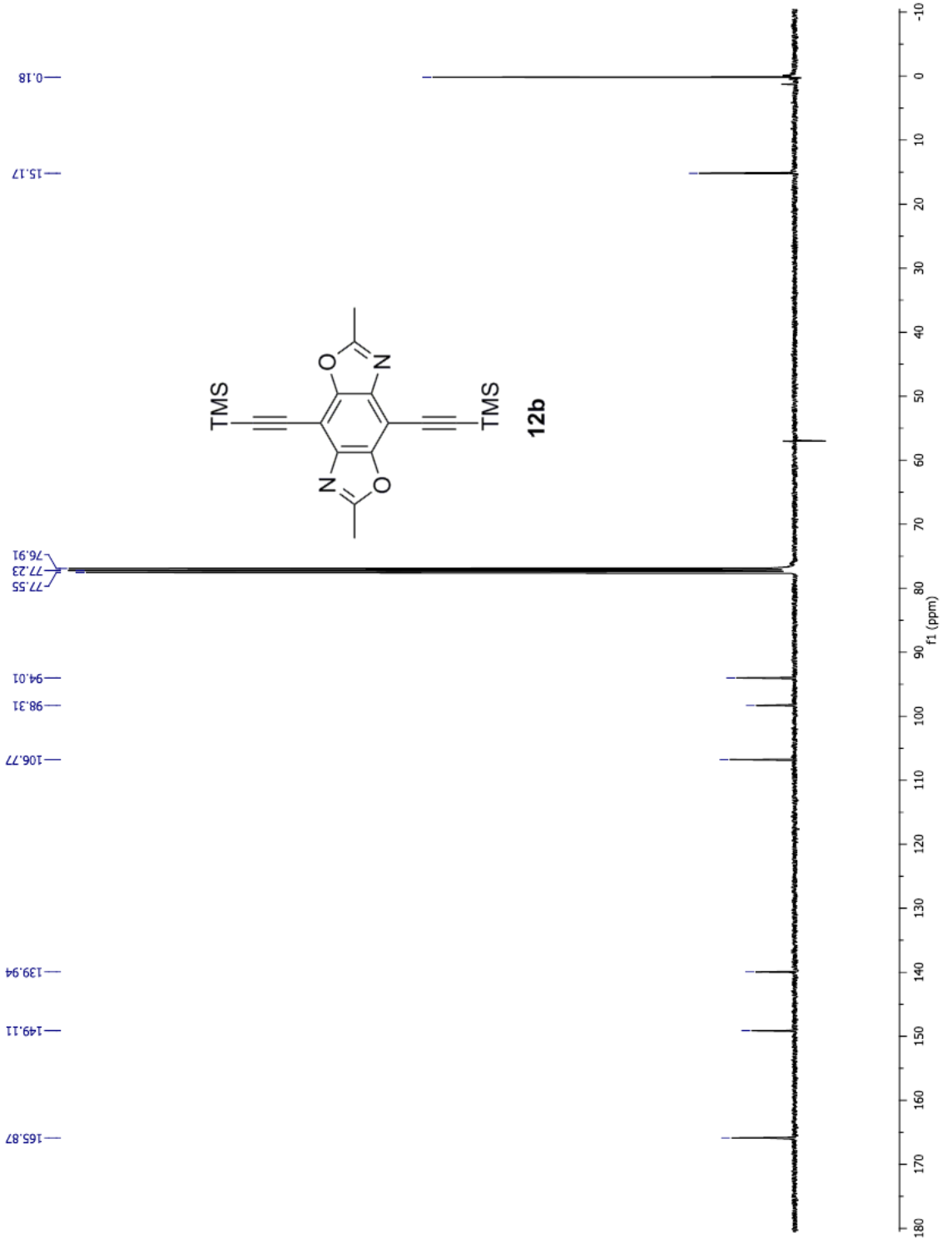

Figure S2.24. ^{13}C NMR of **12b.**

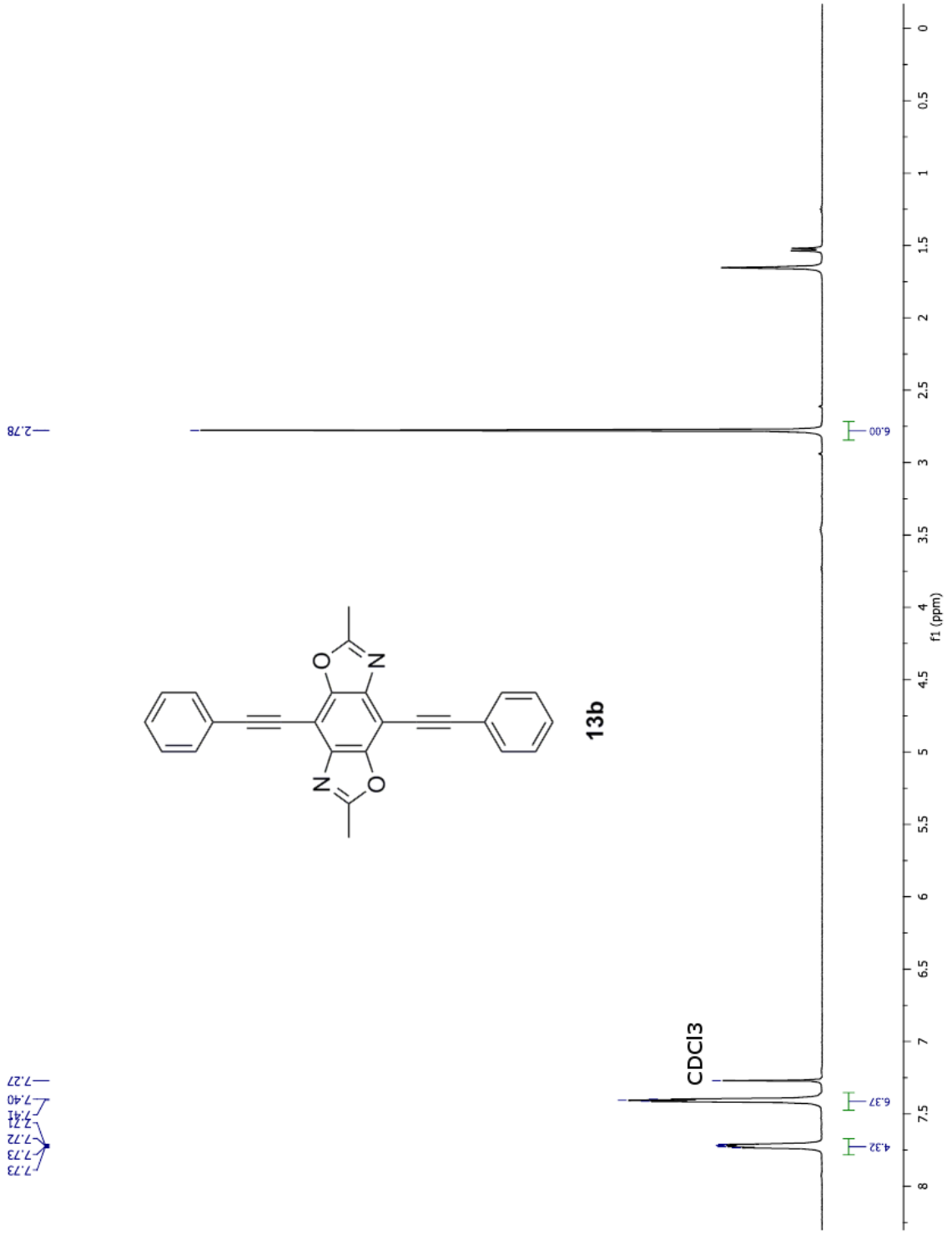

Figure S2.25. ^{1}H NMR of **13b.**

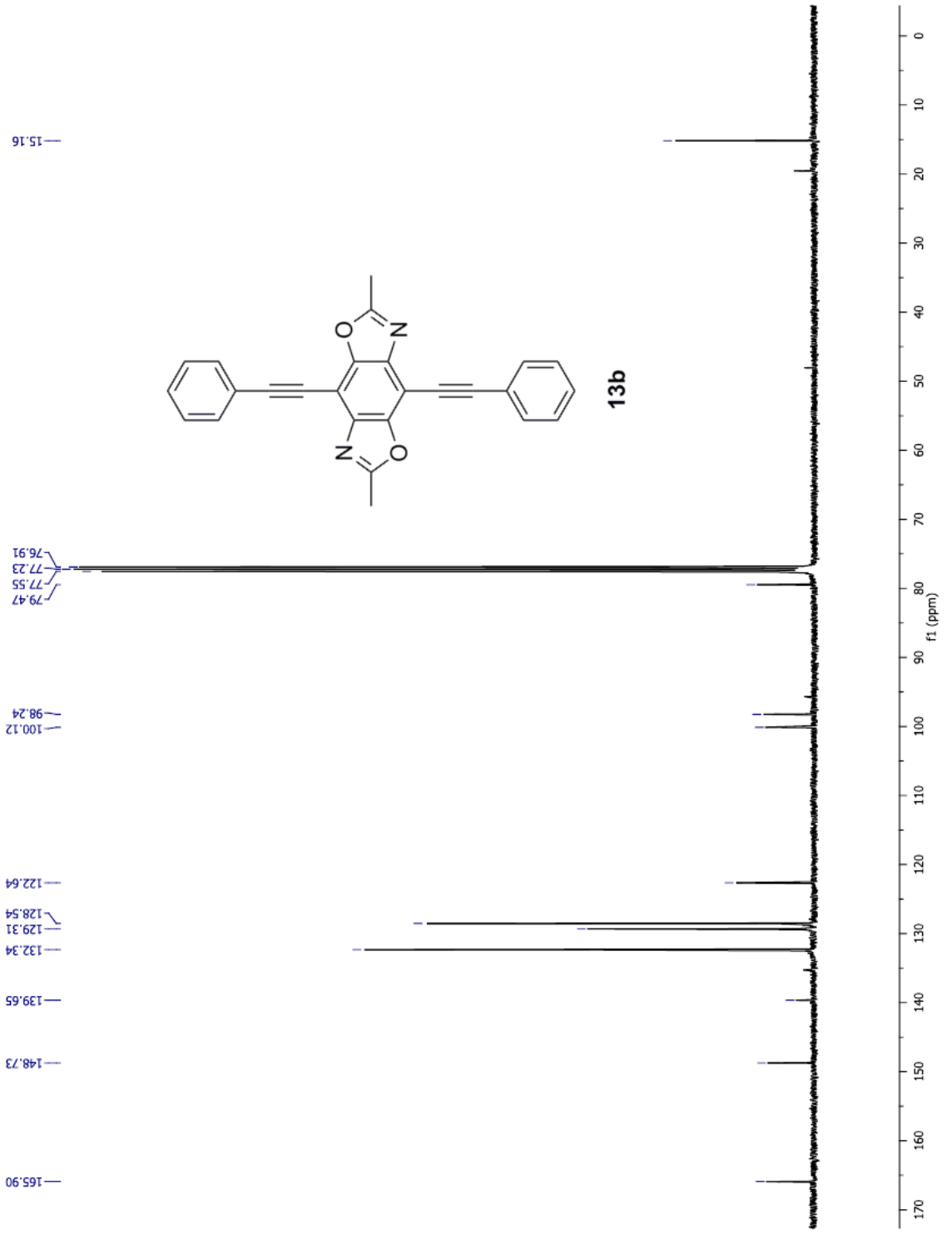

Figure S2.26. ^{13}C NMR of **13b.**

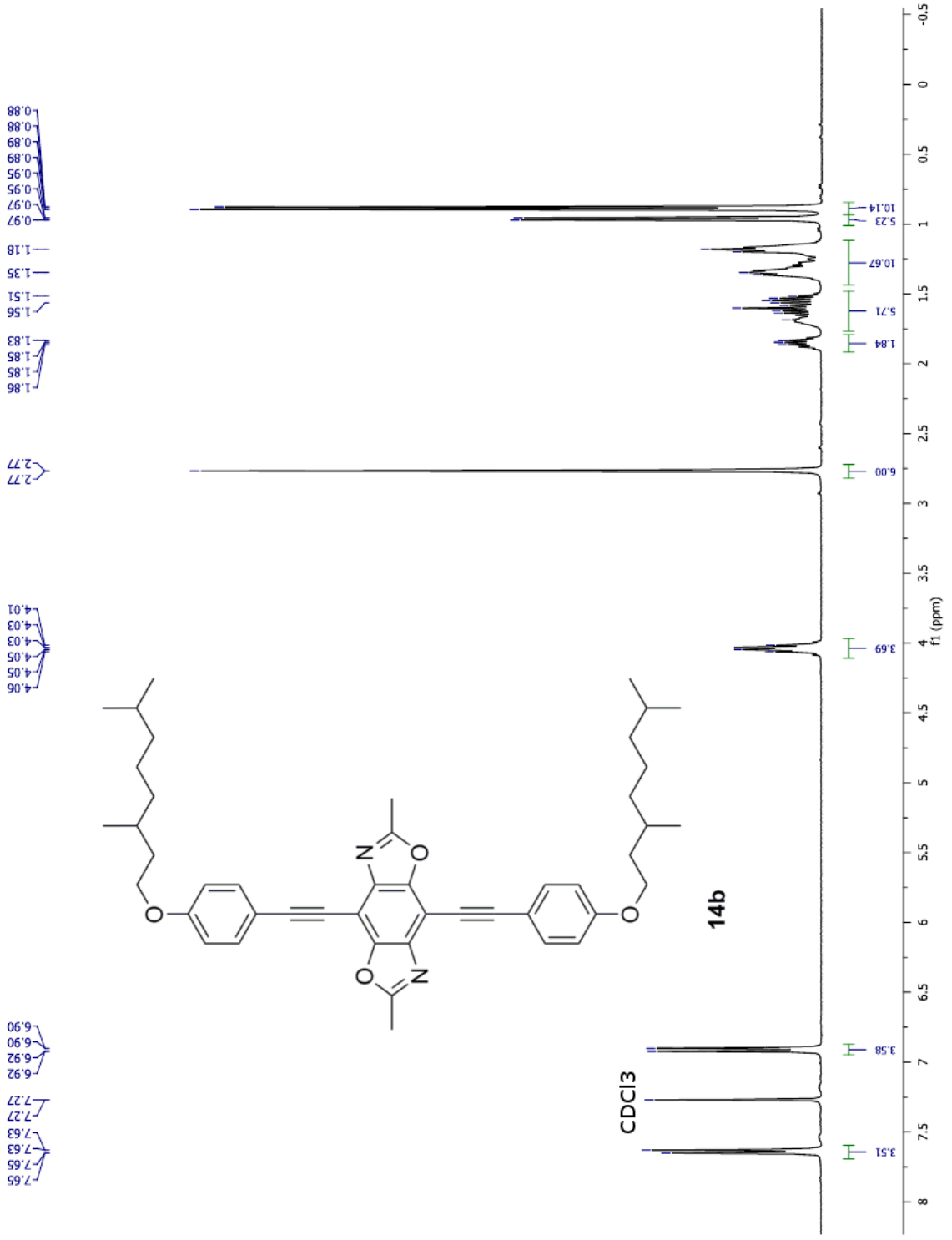

Figure S2.27. ^{1}H NMR of **14b.**

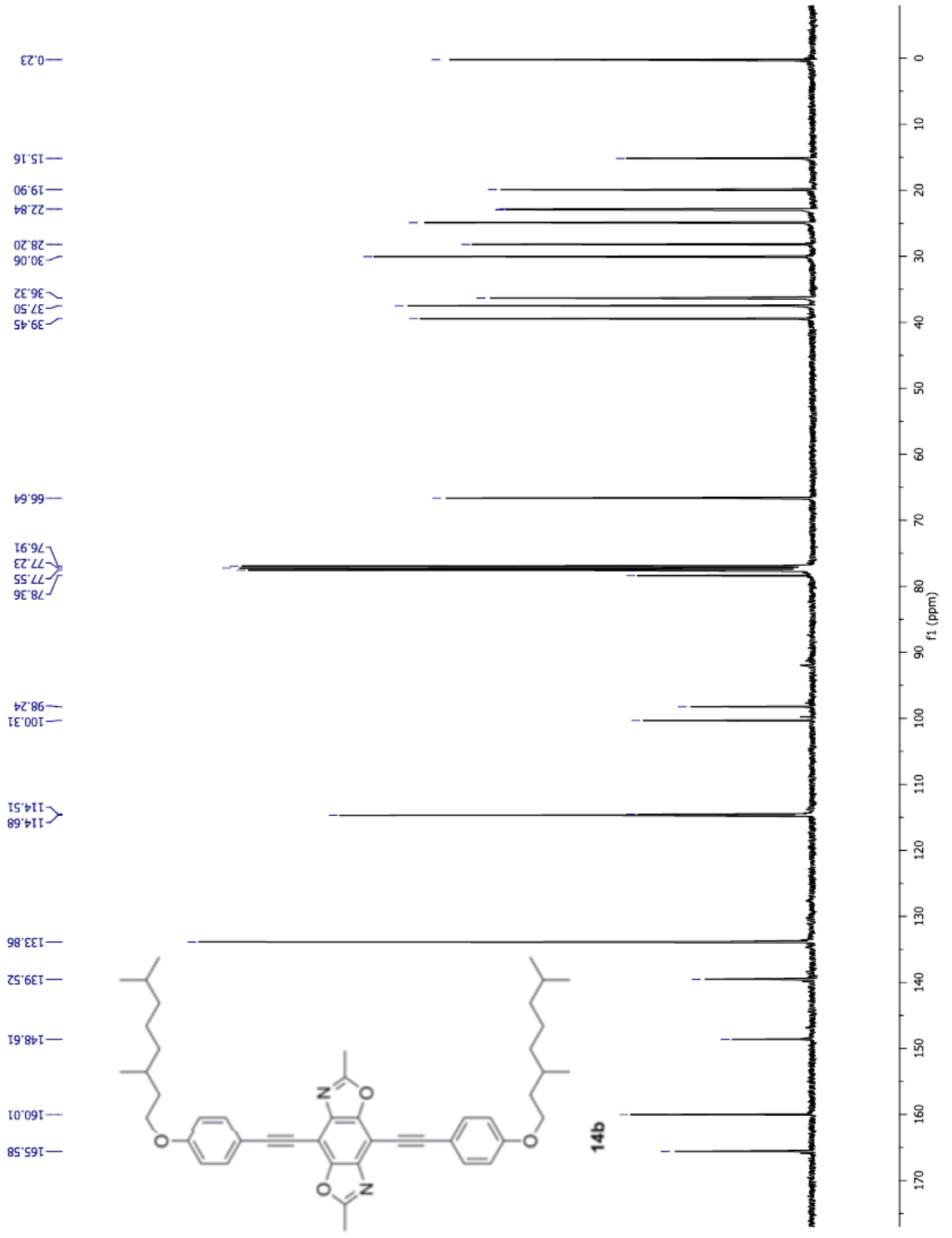

Figure S2.28. ^{13}C NMR of **14b.**

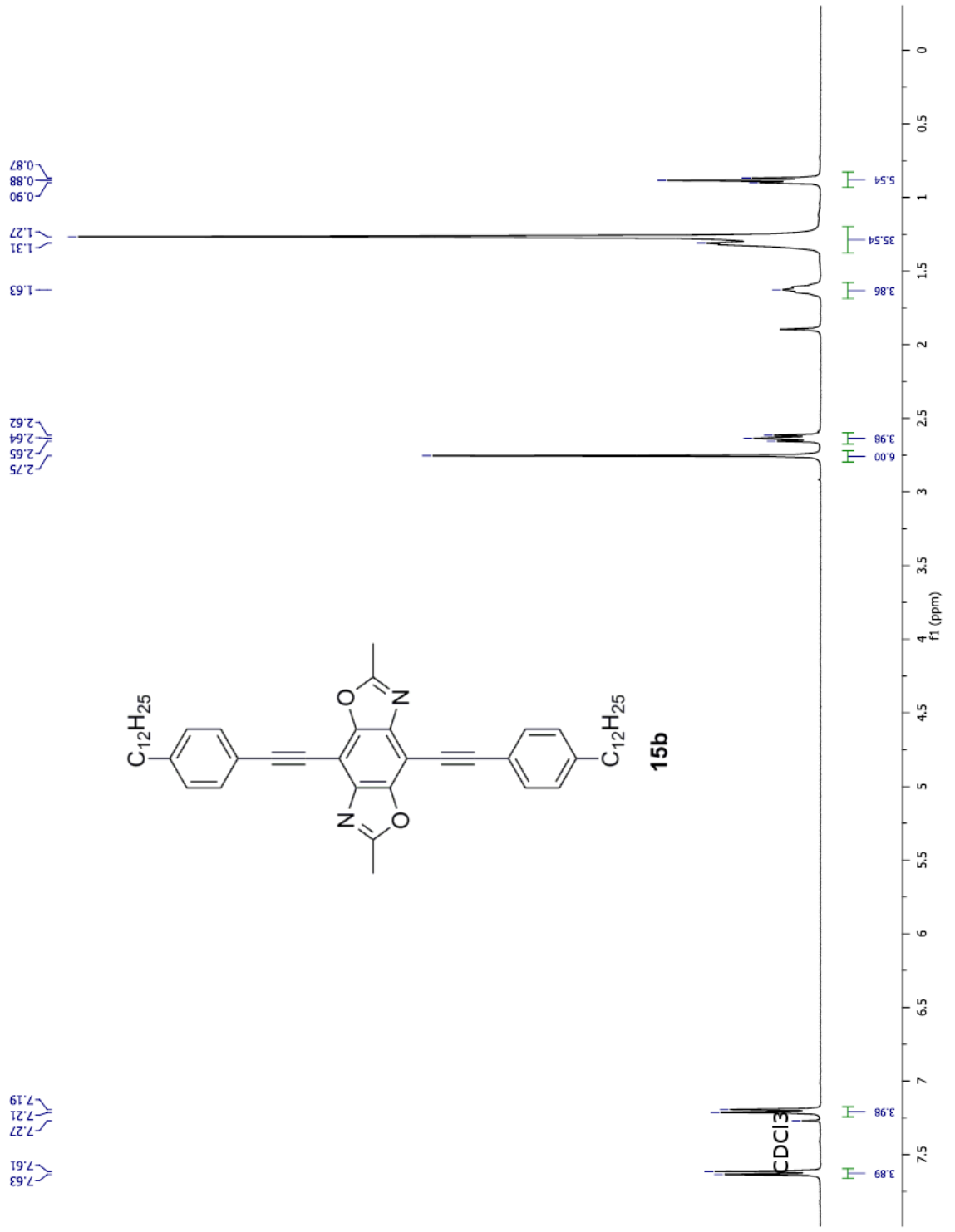

Figure S2.29. ^{1}H NMR of **15b.**

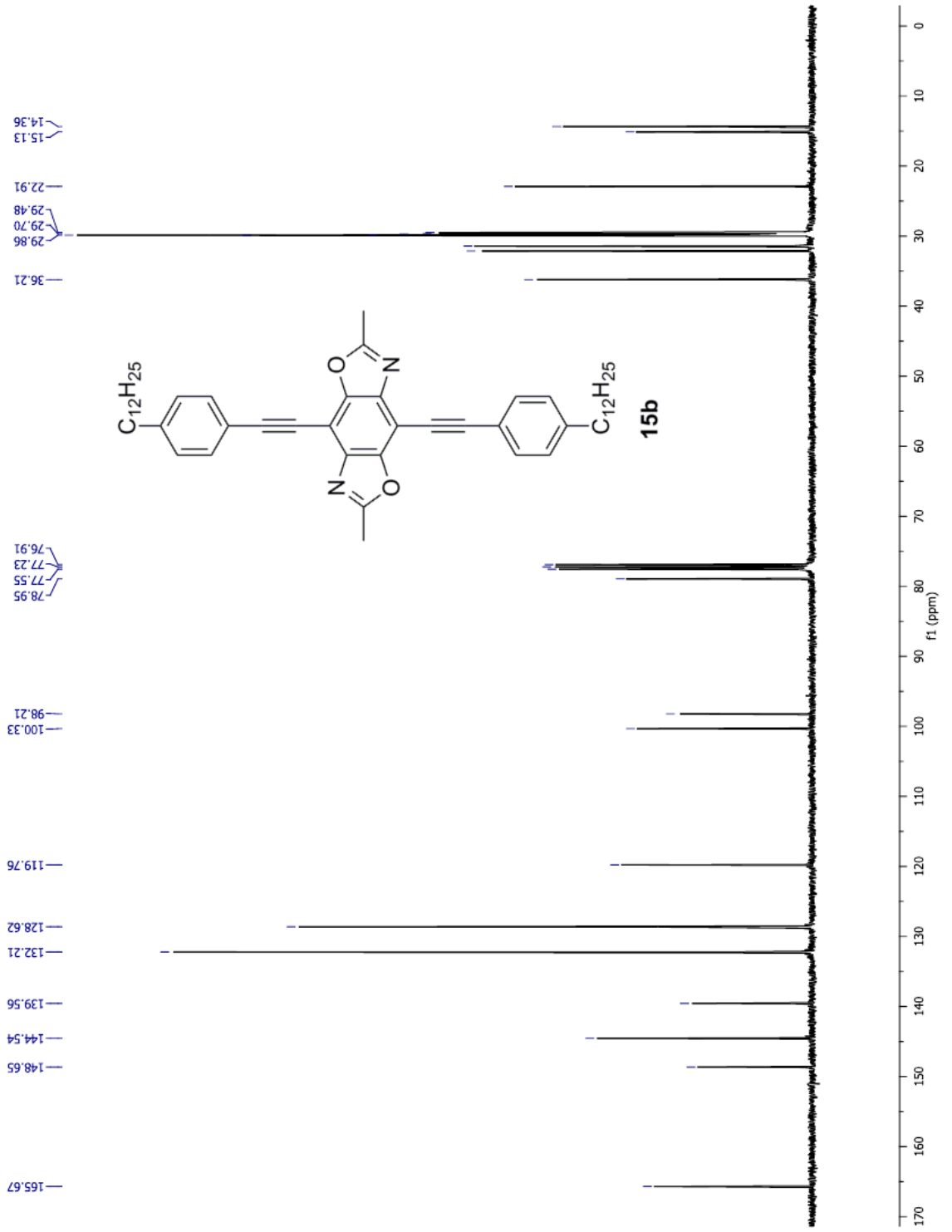

Figure S2.30. ^{13}C NMR of **15b.**

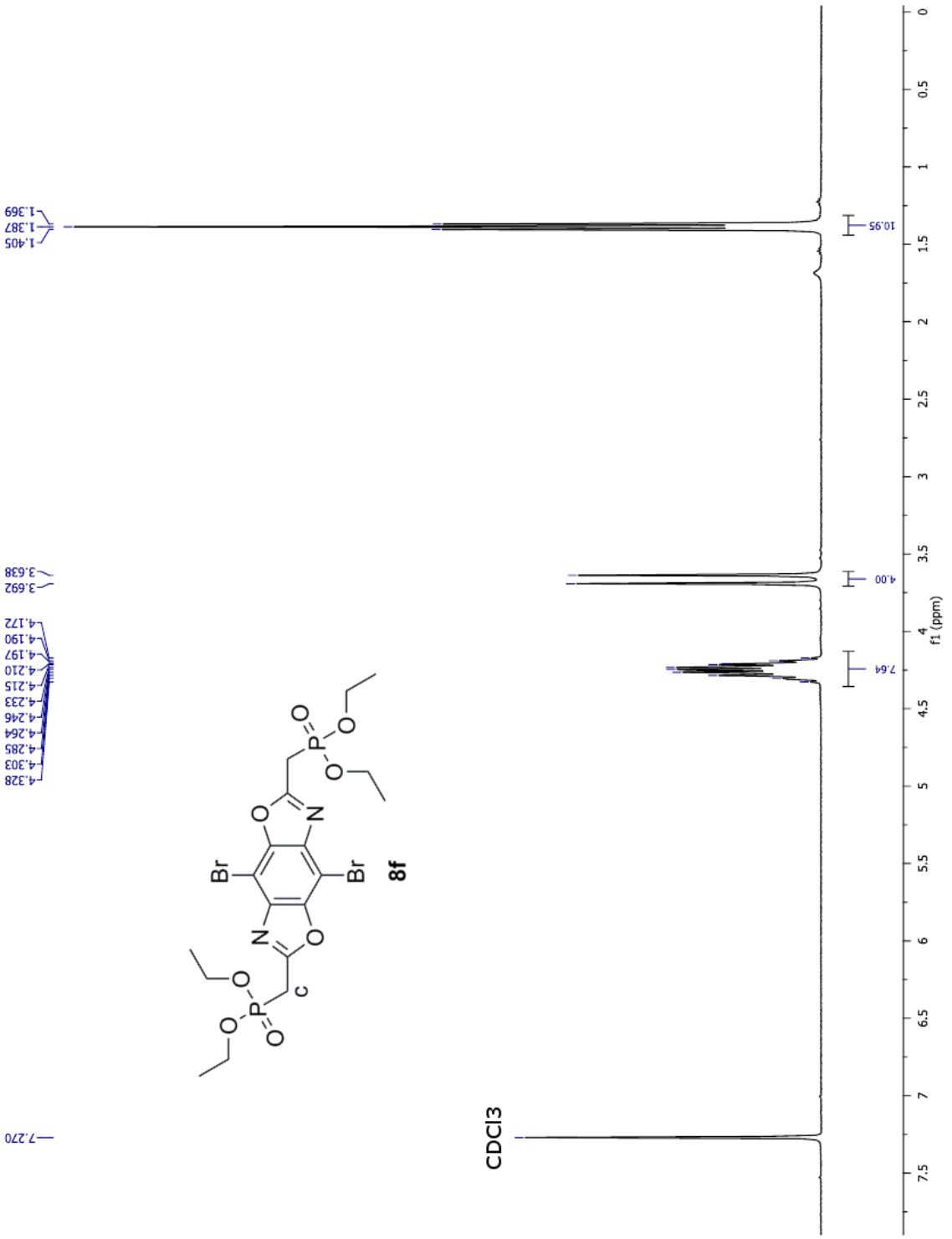

Figure S2.31. ^{1}H NMR of **8f.**

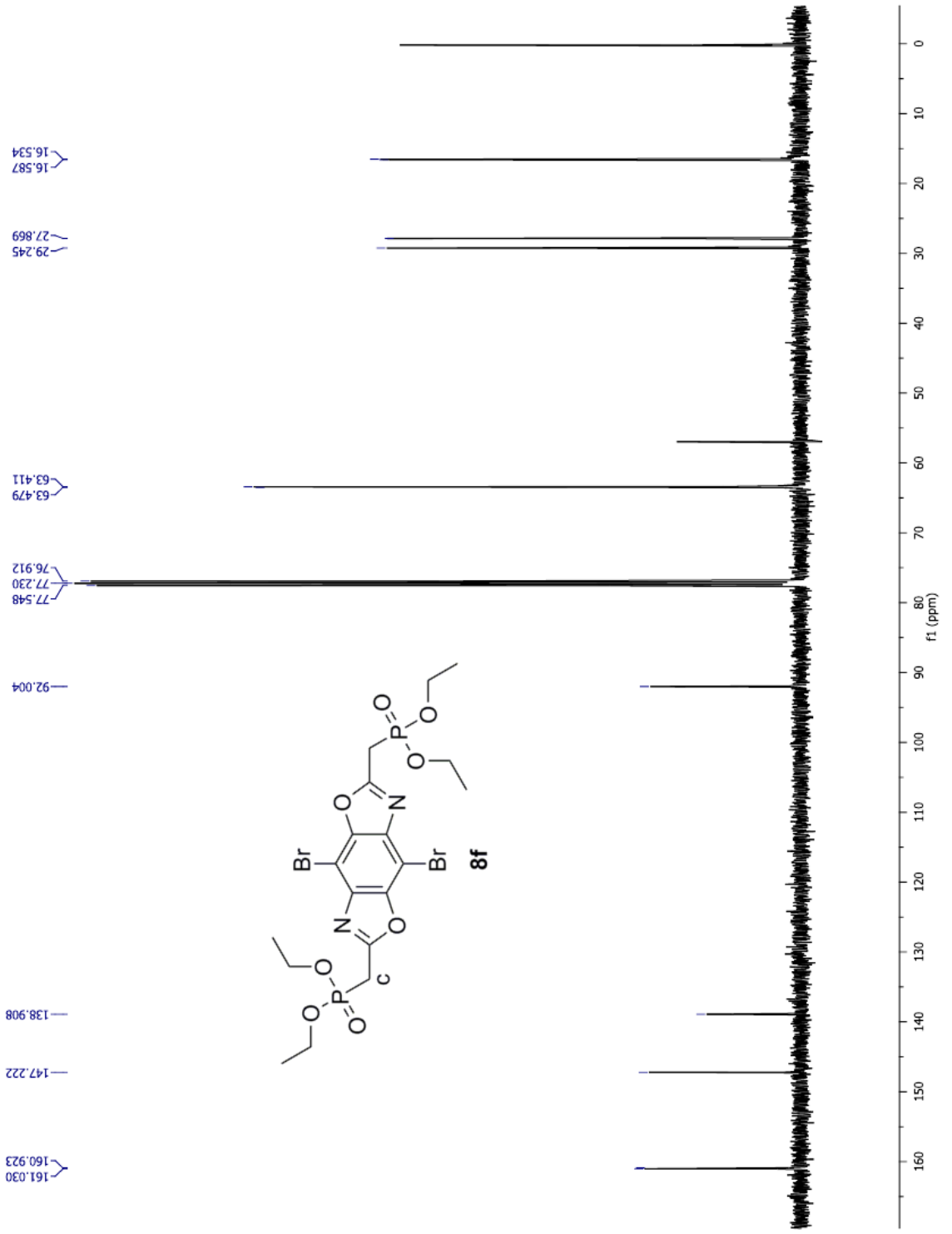

Figure S2.32. ^{13}C NMR of **8f.**

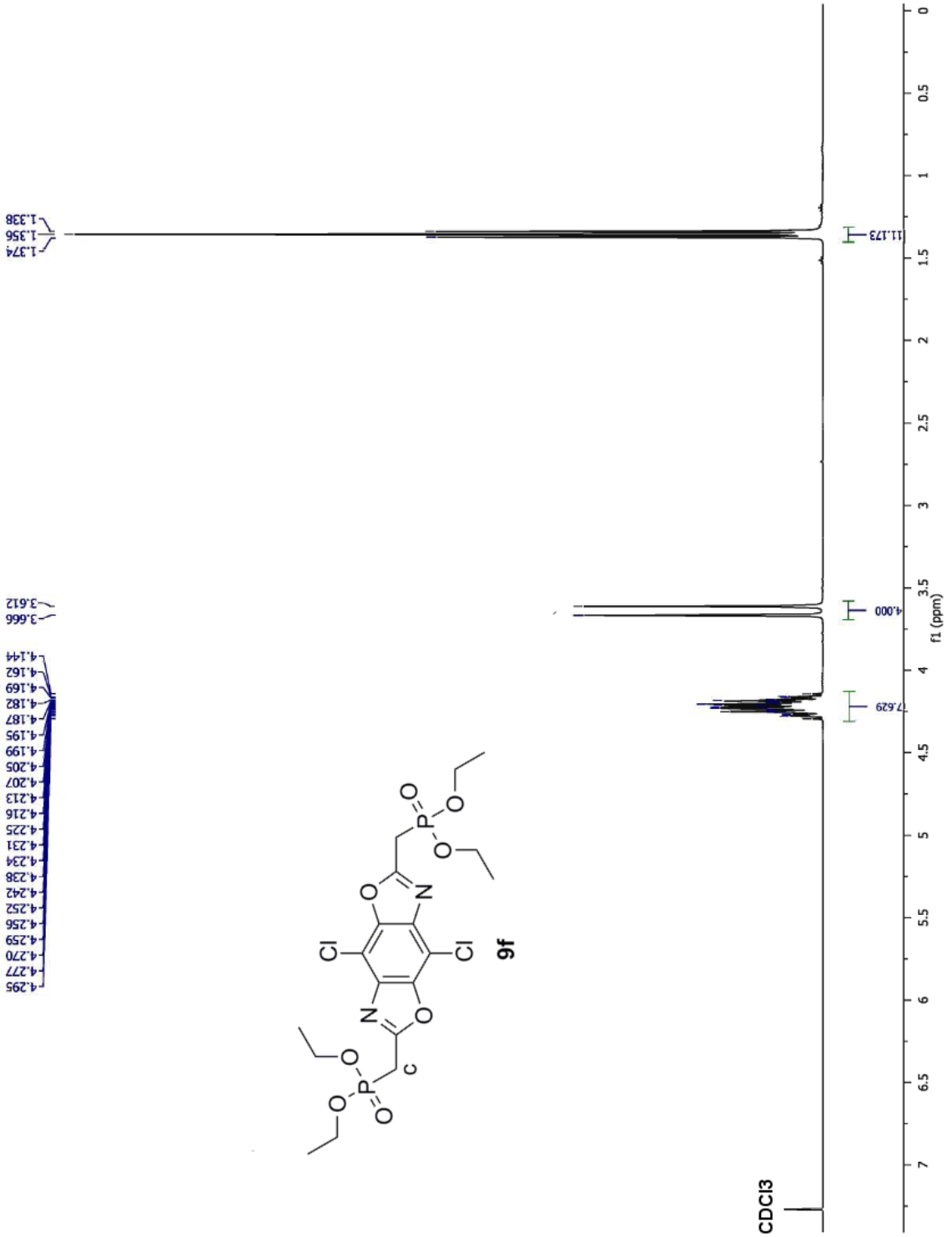

Figure S2.33. ^{1}H NMR of **9f.**

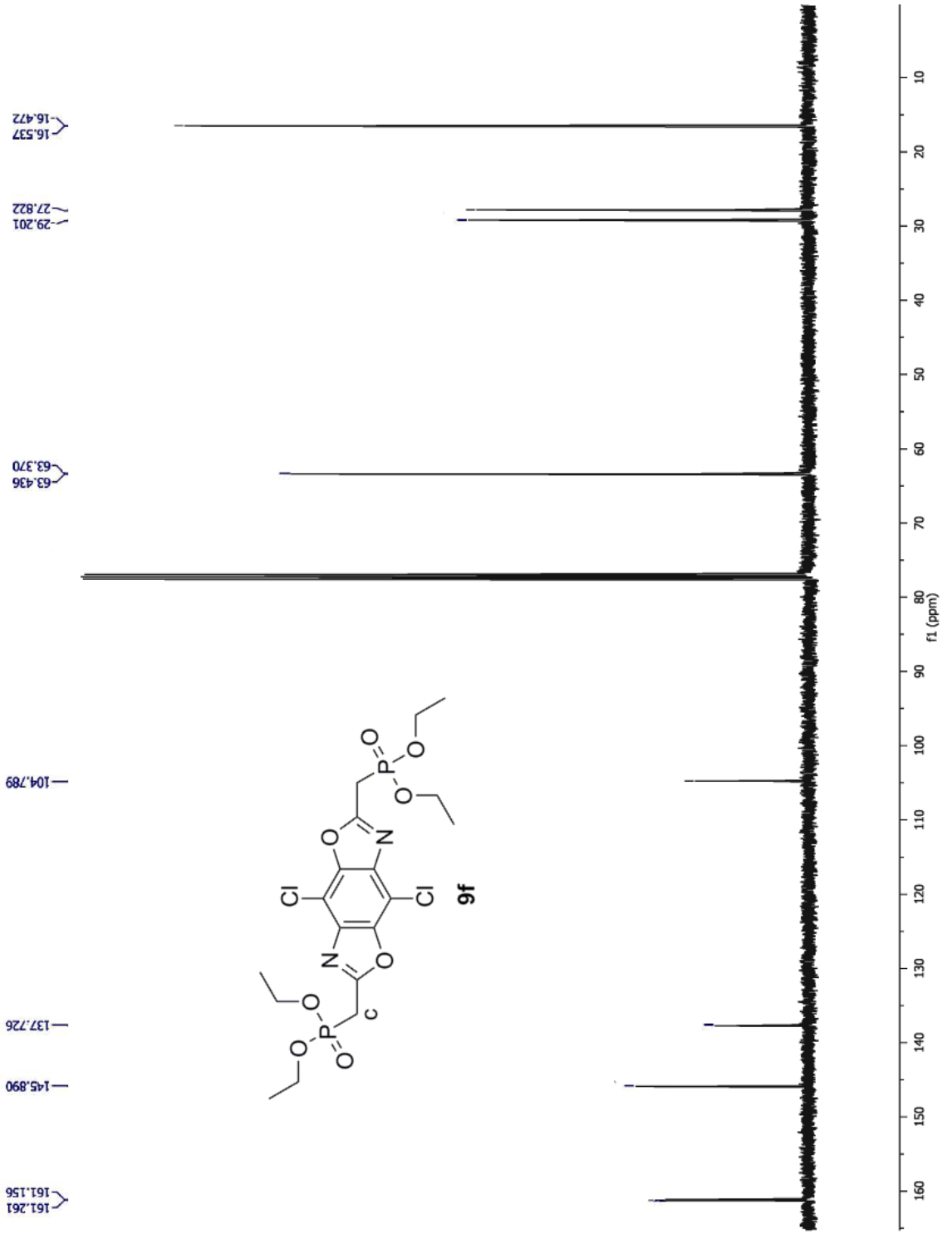

Figure S2.34. ^{13}C NMR of **9f.**

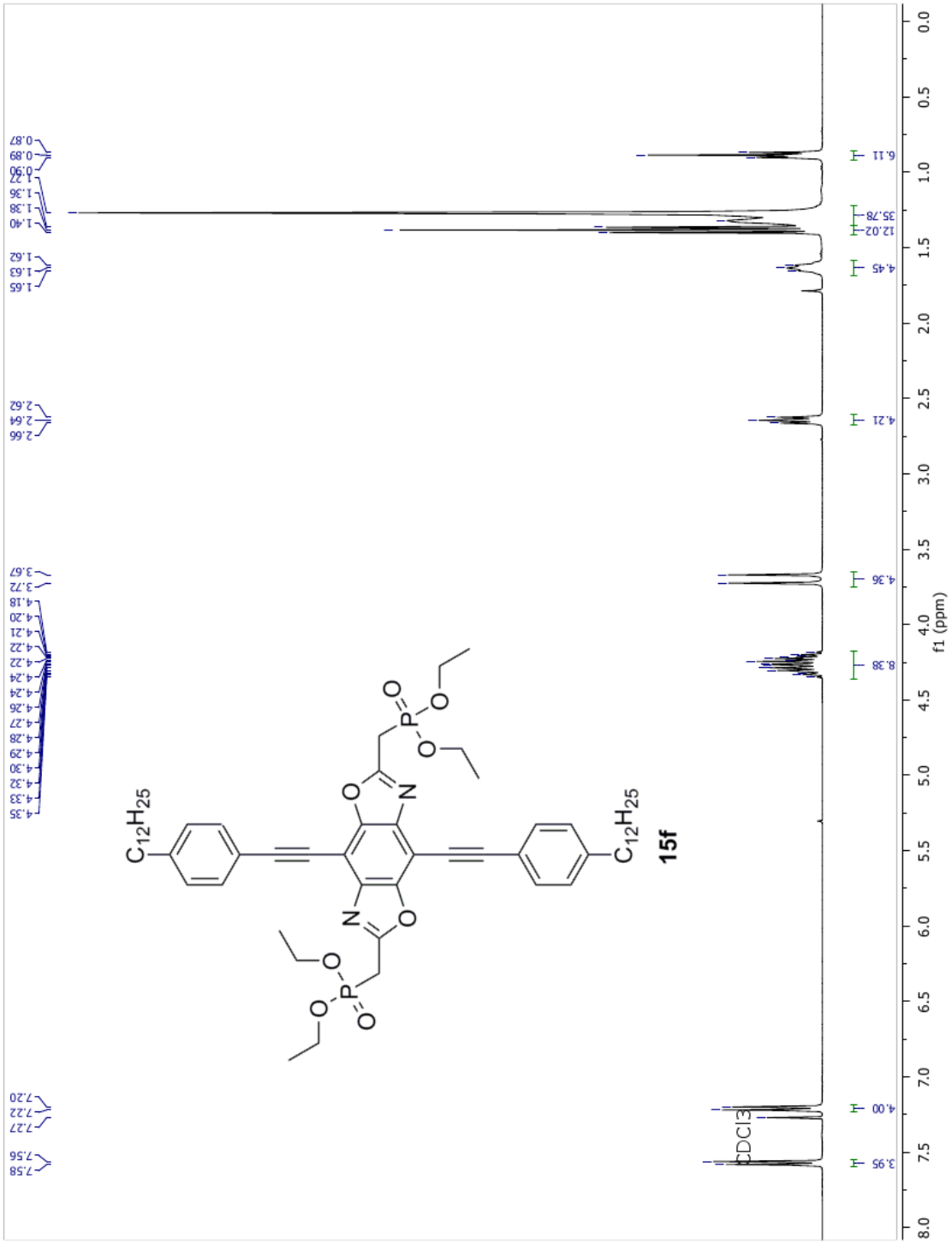

Figure S2.35. ^{13}C NMR of **15f.**

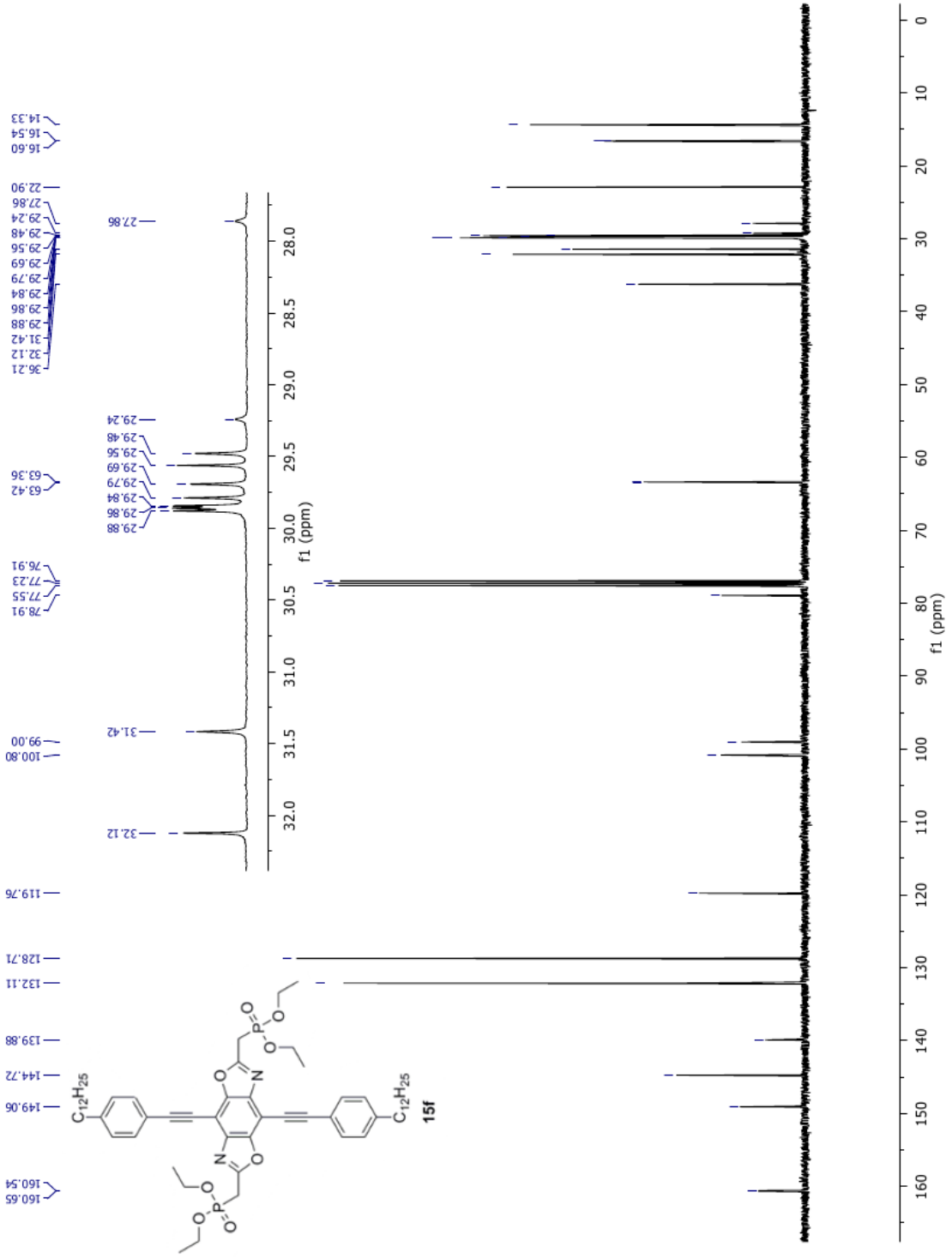

Figure S2.36. ^{13}C NMR of **15f.**

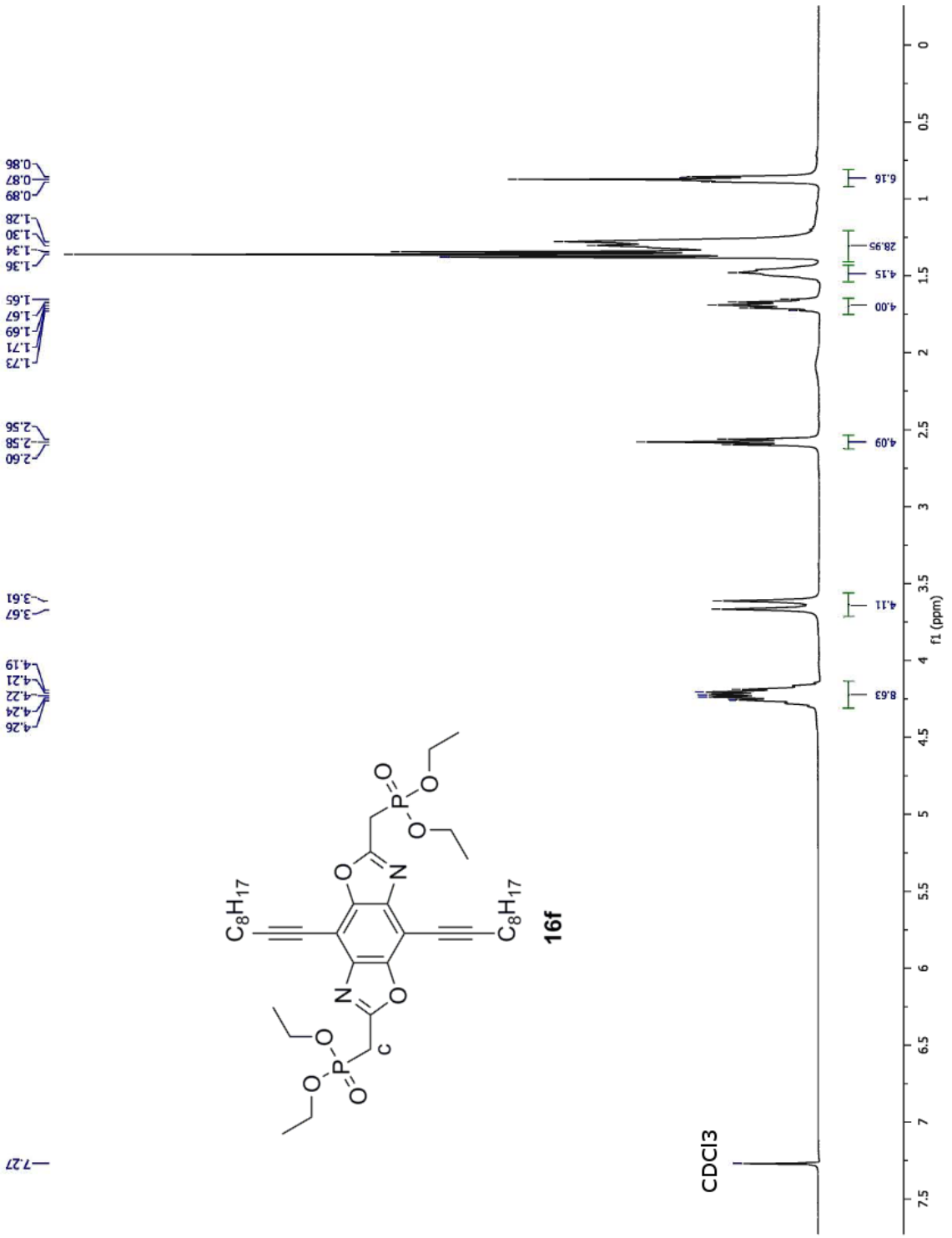

Figure S2.37. ^{1}H NMR of **16f.**

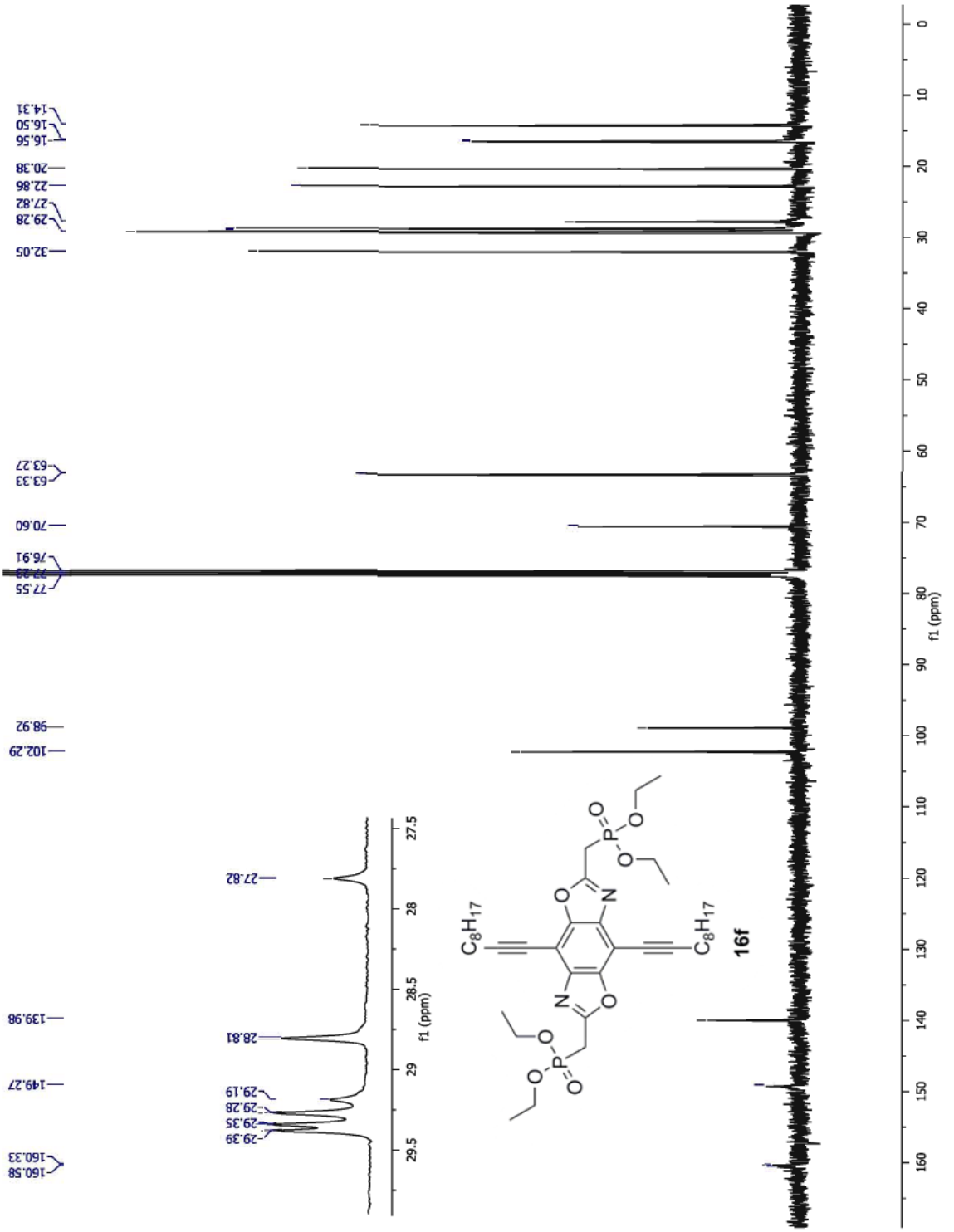

Figure S2.38. ^{13}C NMR of **16f.**

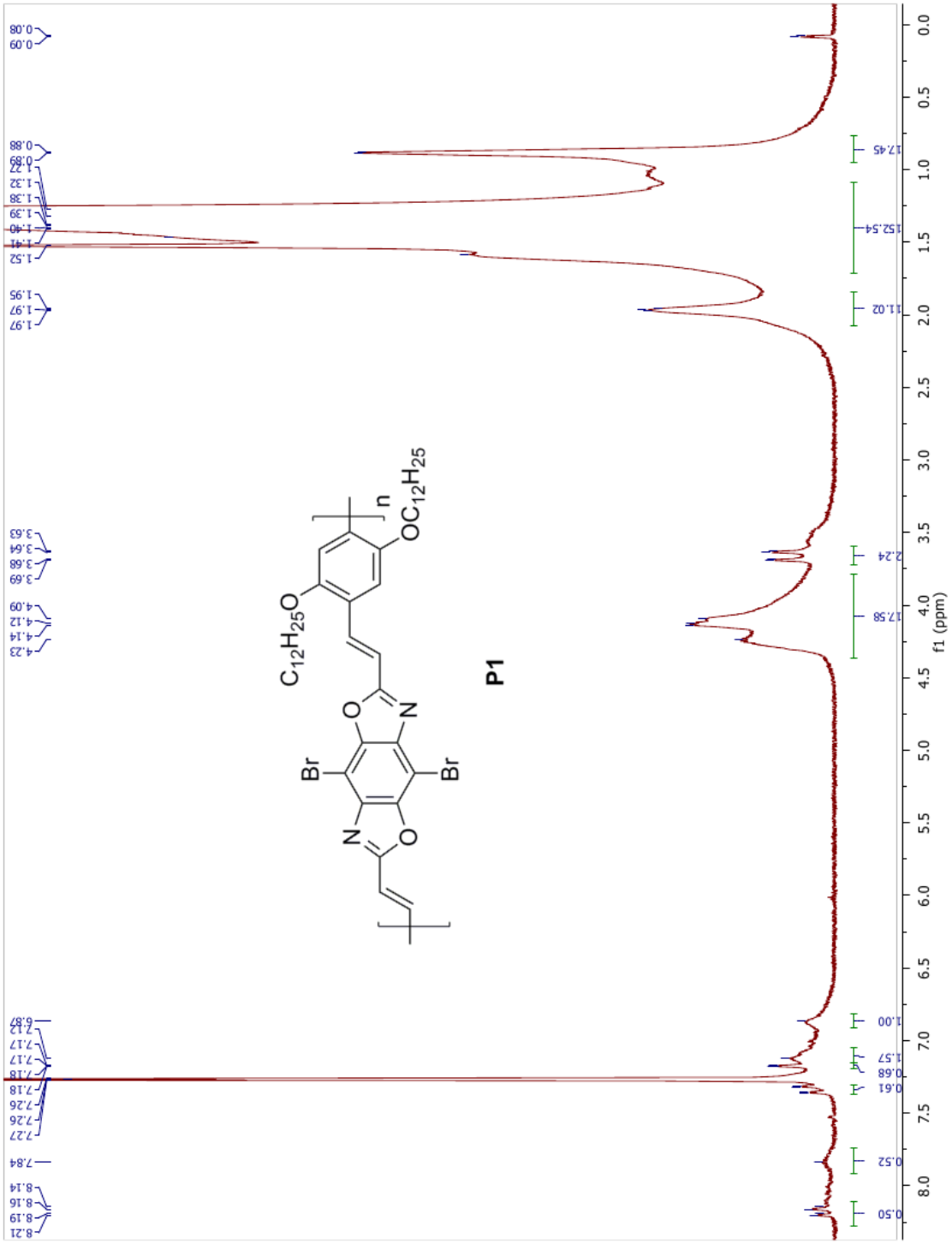

Figure S2.39. ^{1}H NMR of **P1.**

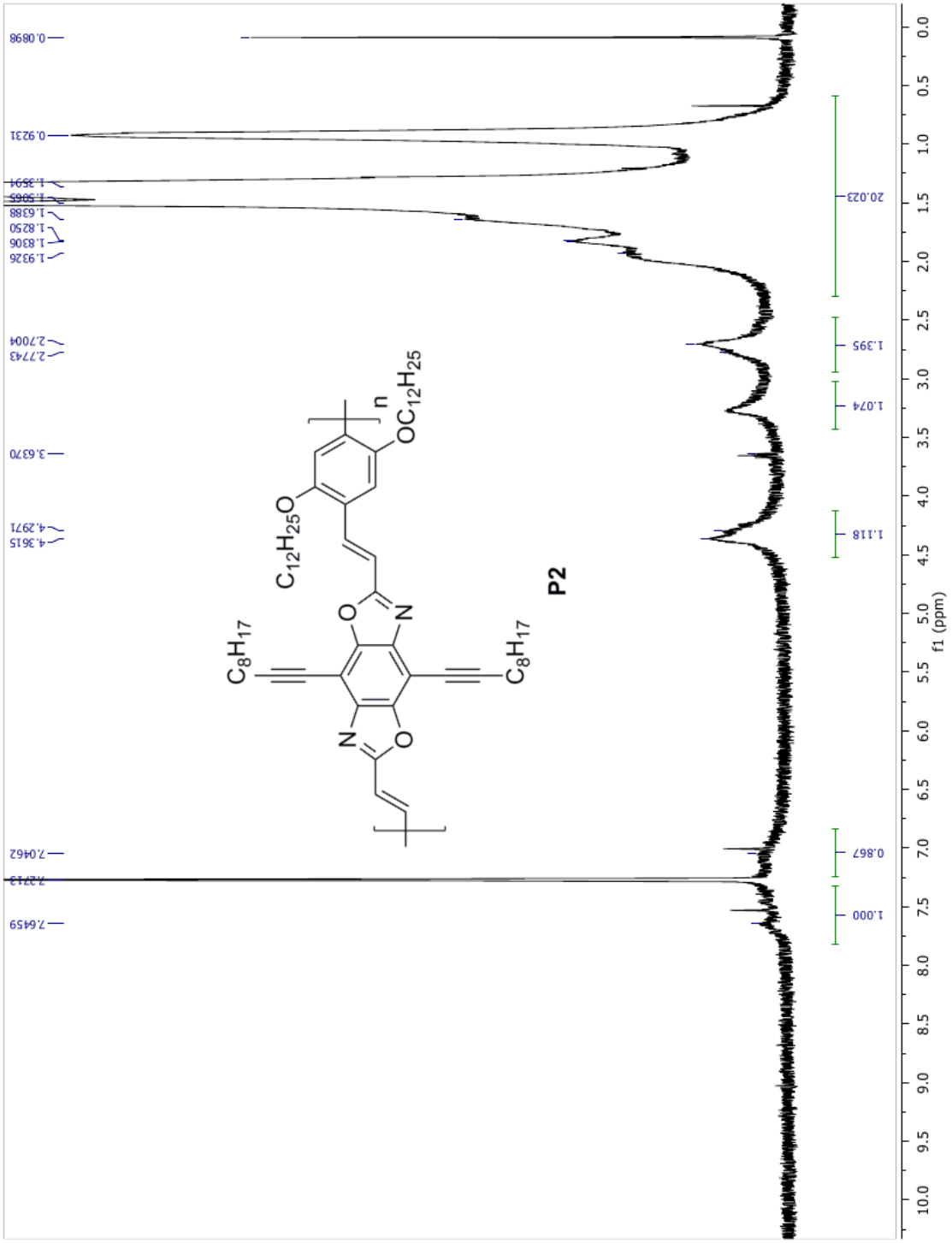

Figure S2.40. ^{1}H NMR of **P2.**

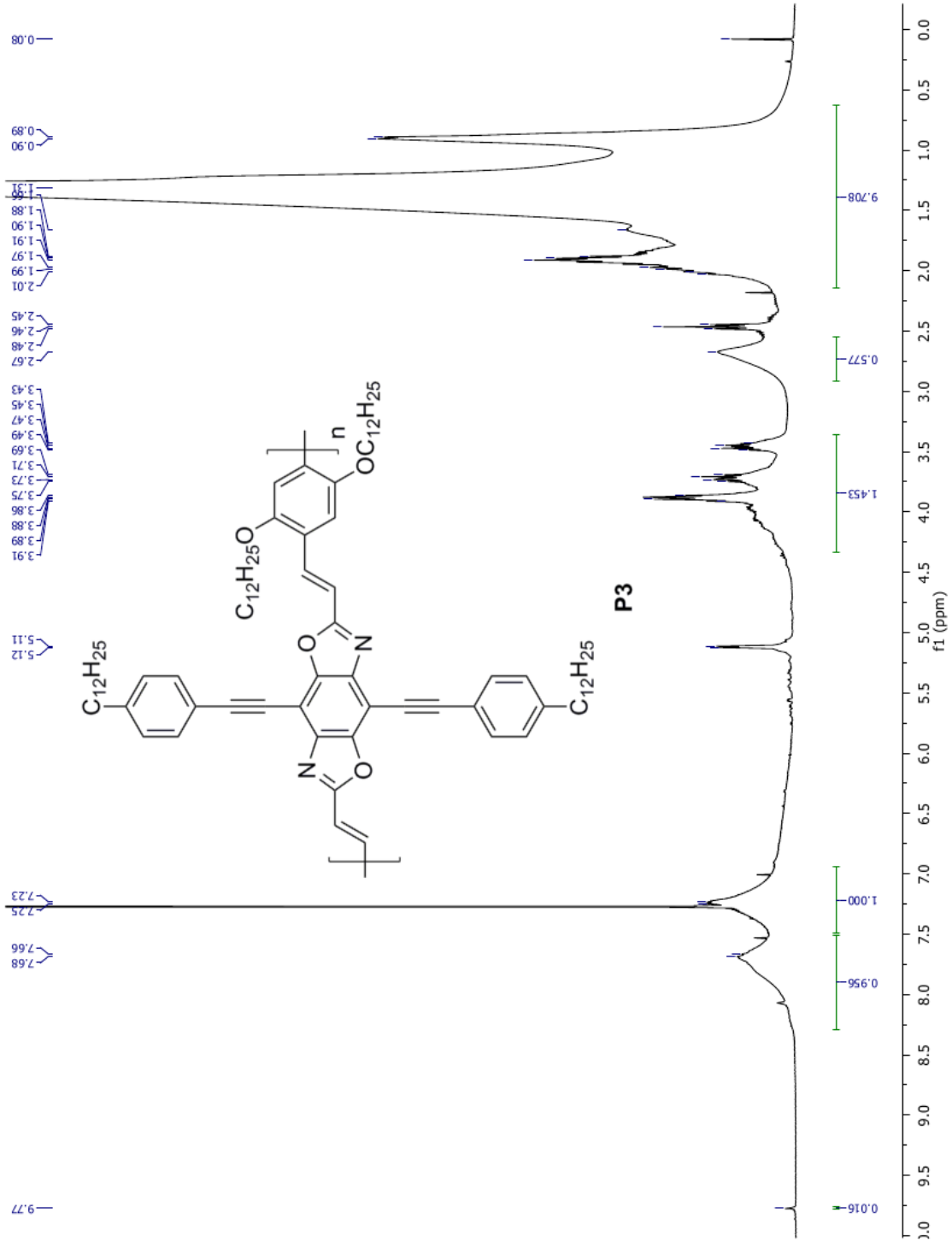

Figure S2.41. ^{1}H NMR of **P3.**

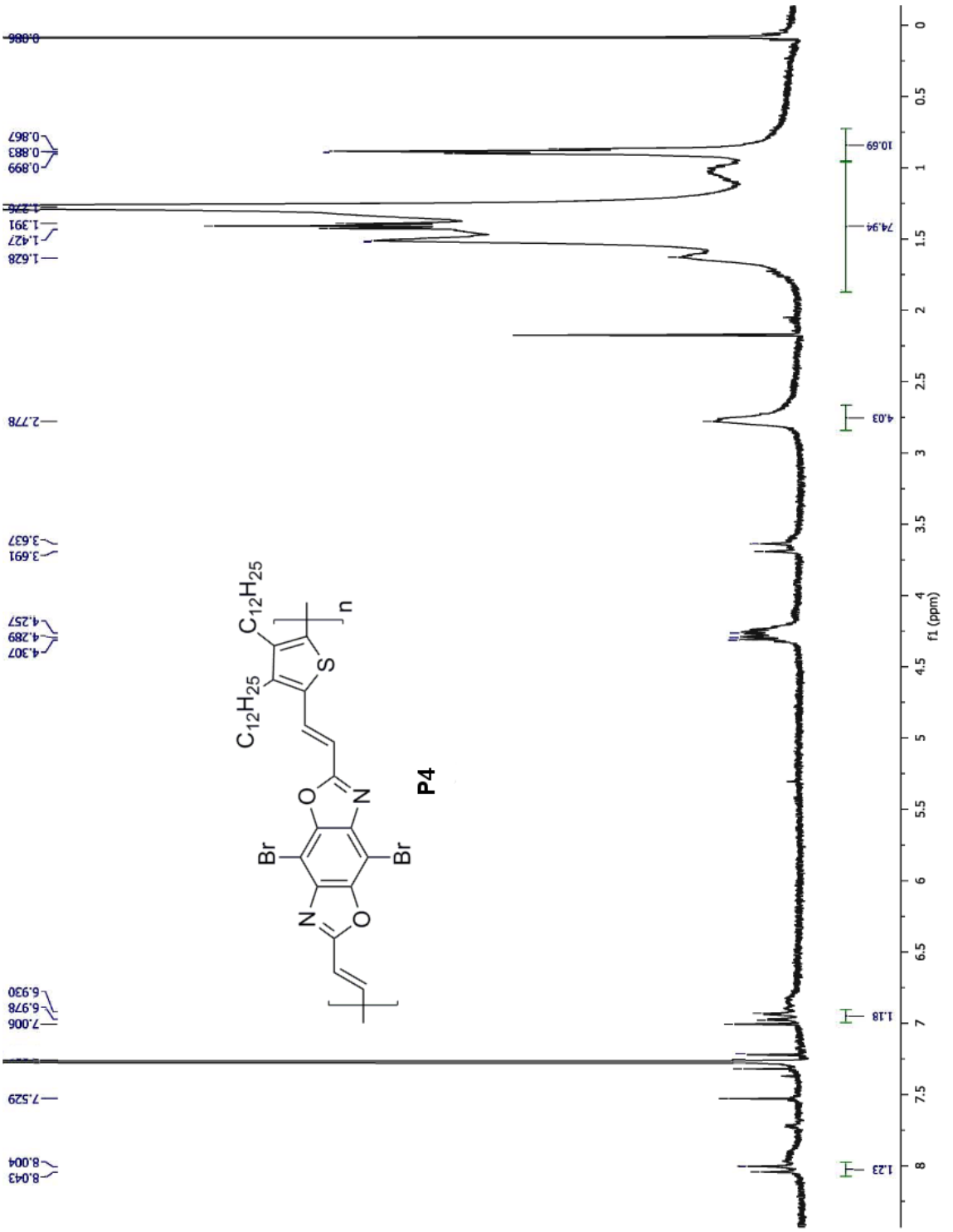

Figure S2.42. ^{1}H NMR of **P4.**

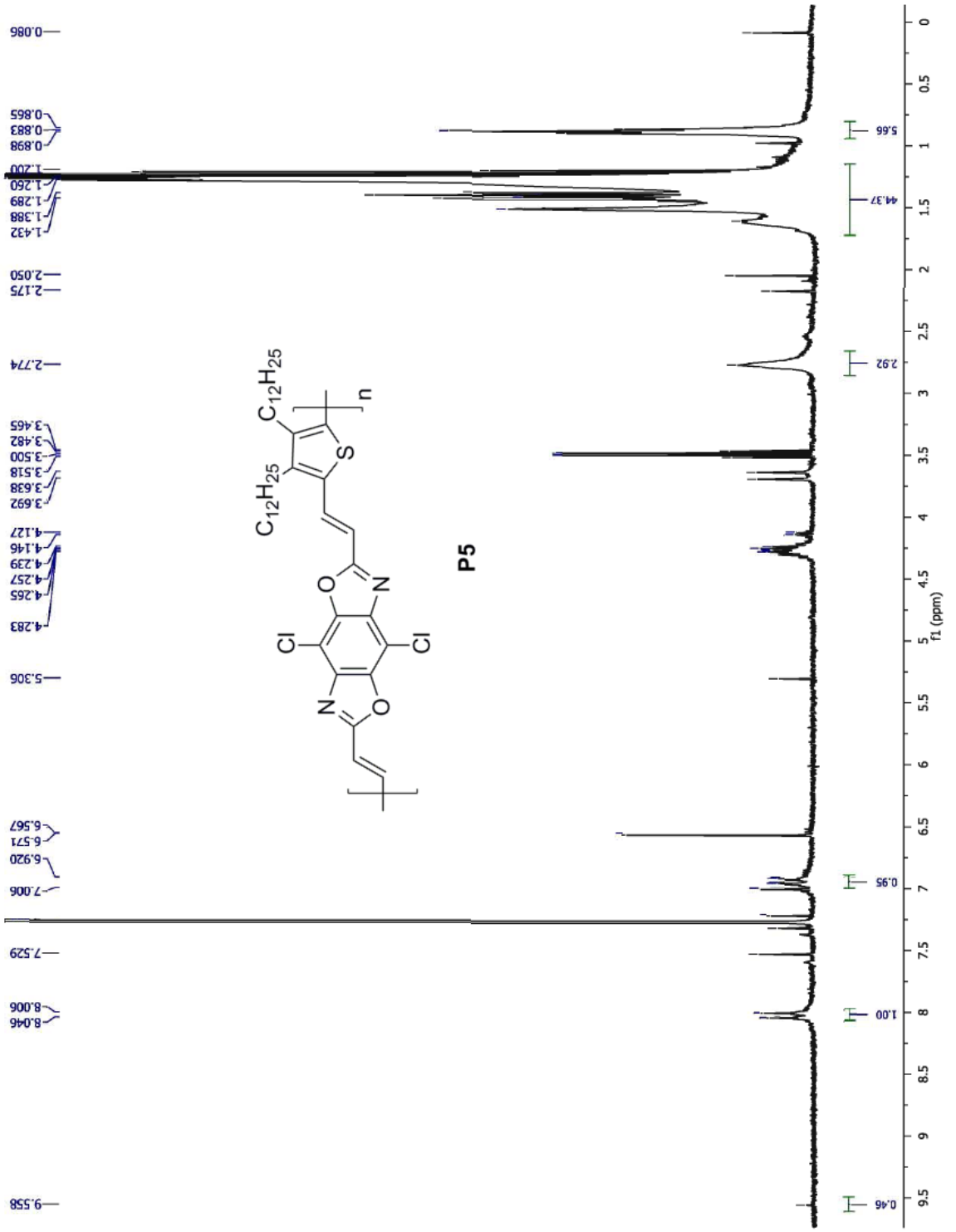

Figure S2.43. ^{1}H NMR of **P5.**

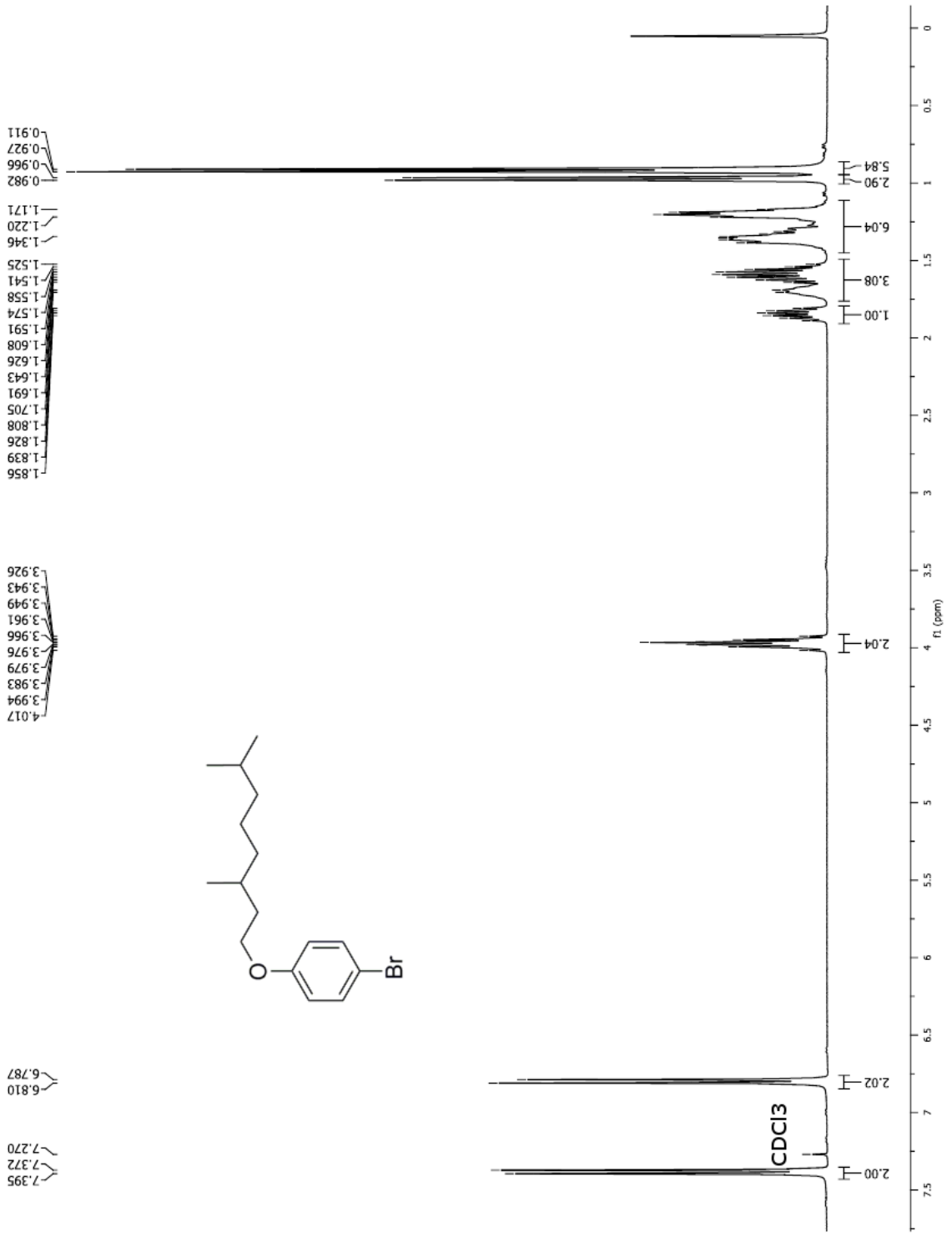

Figure S2.44. ^{1}H NMR of 1-bromo-4-(3,7-dimethyloctyloxy)benzene.

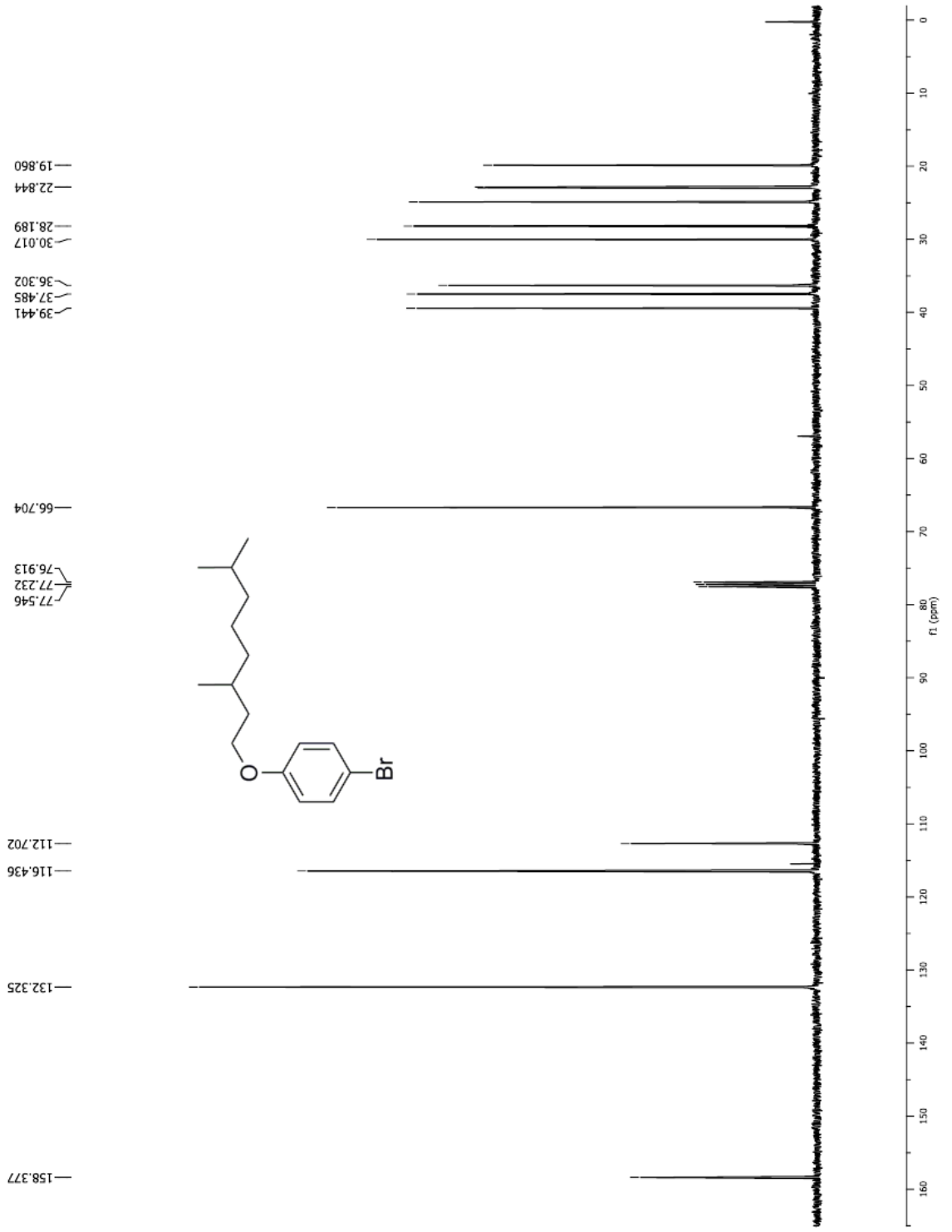

Figure S2.45. ^{13}C NMR of 1-bromo-4-(3,7-dimethyloctyloxy)benzene.

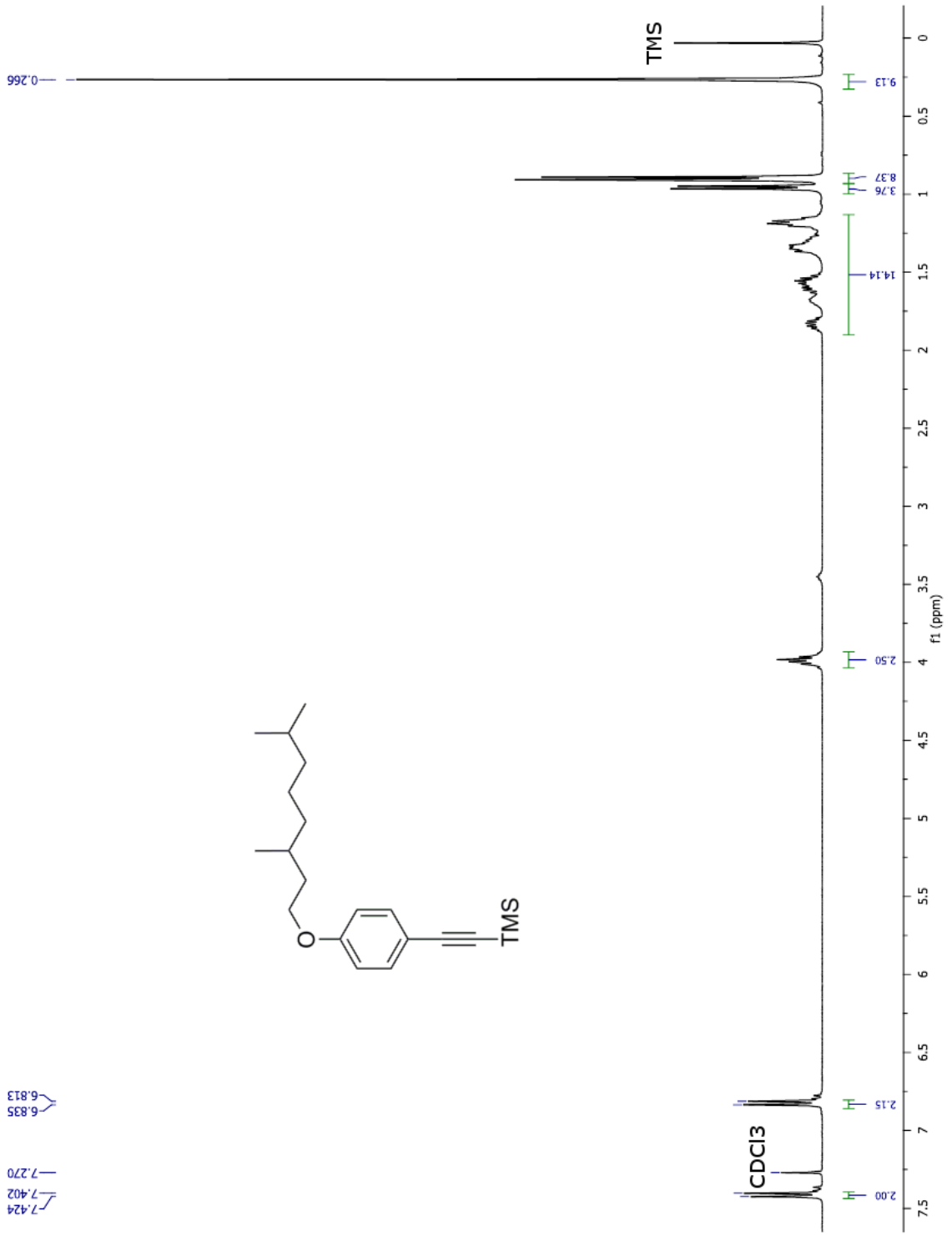

Figure S2.46. ^{1}H NMR of 1-(3,7-dimethyloctyloxy)-4-(trimethylsilylethynyl)benzene.

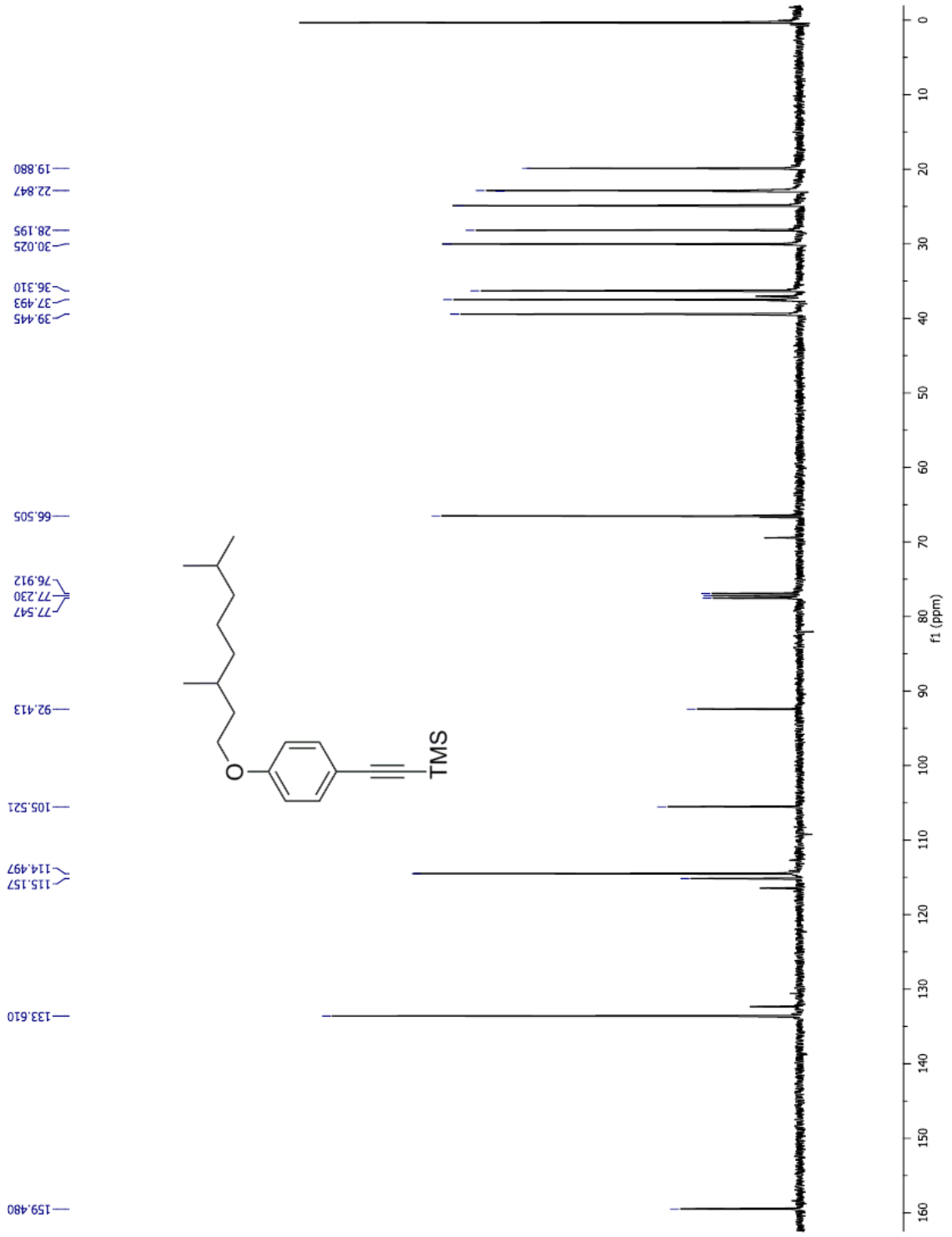

Figure S2.47. ^{13}C NMR of 1-(3,7-dimethyloctyloxy)-4-(trimethylsilylethynyl)benzene.

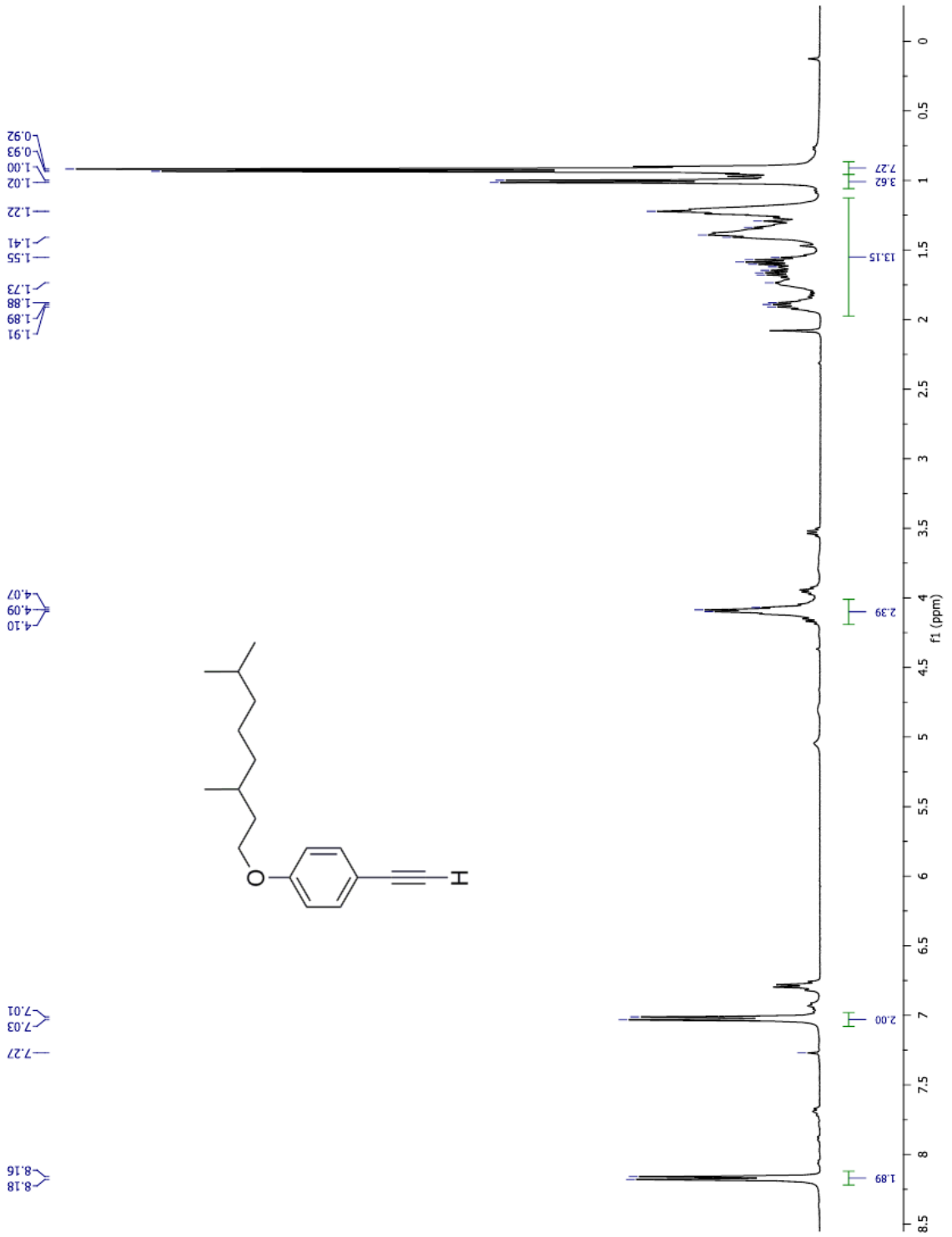

Figure S2.48. ^{1}H NMR of 1-(3,7-dimethyloctyloxy)-4-ethynylbenzene (≈ 90%).

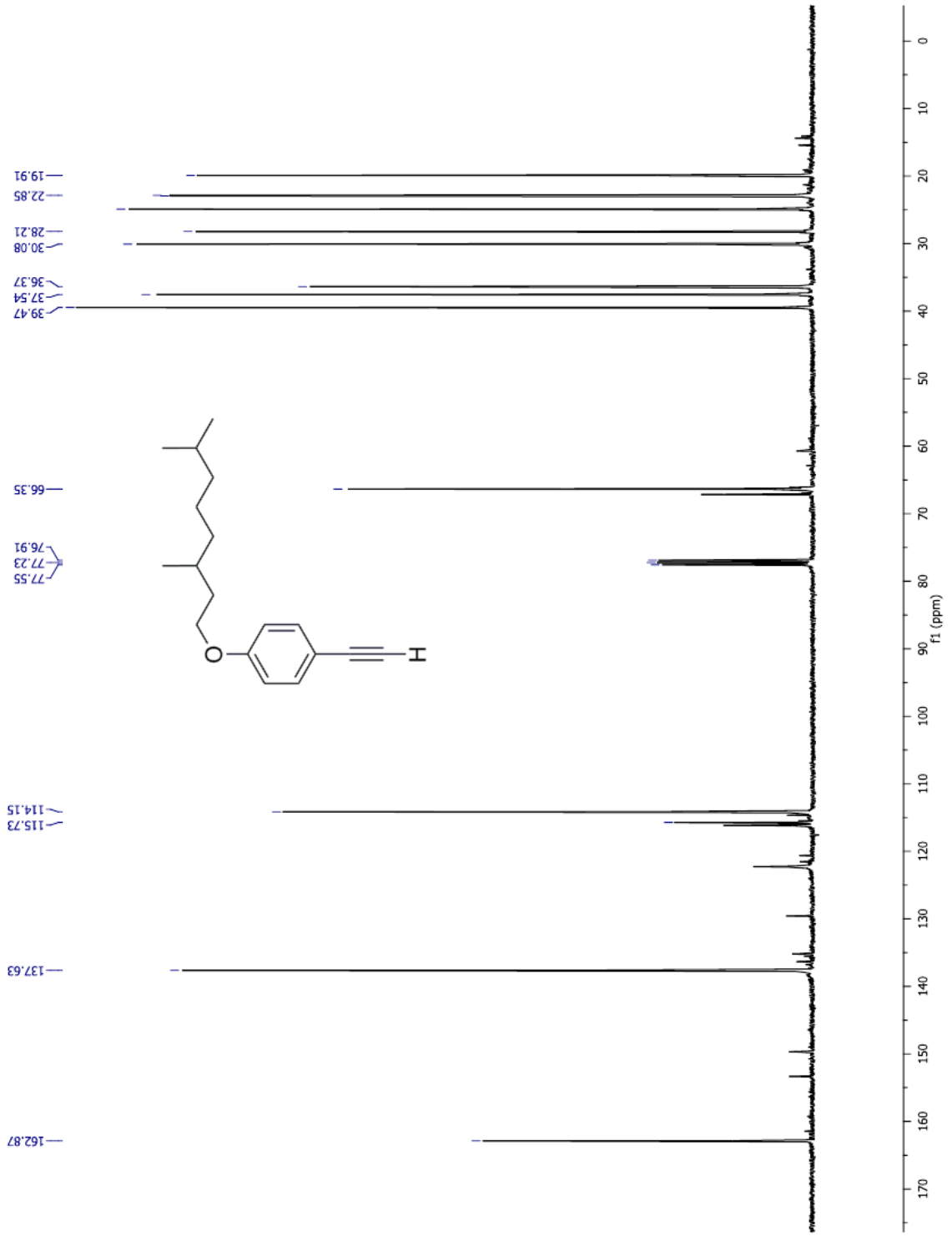

Figure S2.49. ^{13}C NMR of 1-(3,7-dimethyloctyloxy)-4-ethynylbenzene (≈ 90%).

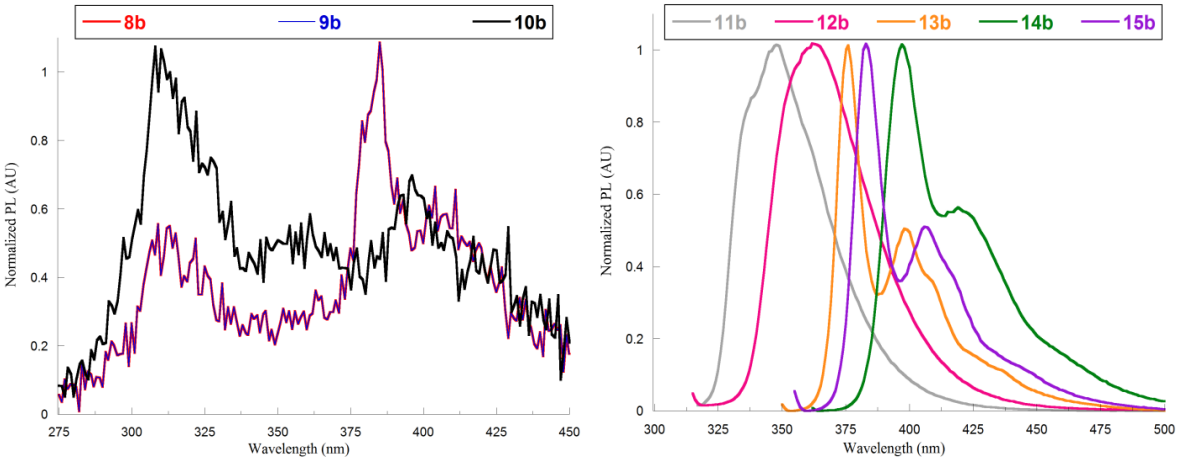

Figure S50. Photoluminesence in THF solution of **8b-10b** (left) and **11b-15b** (right).

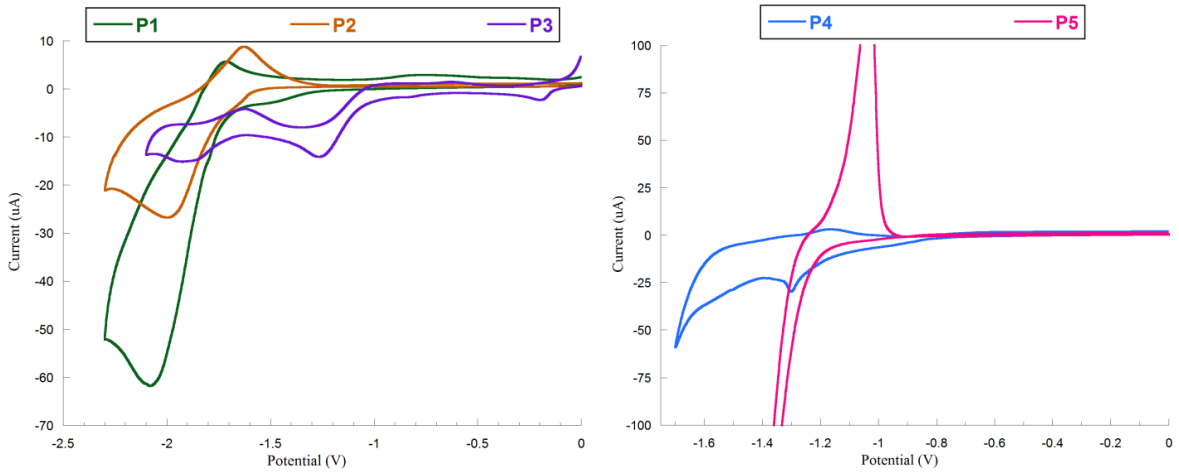

Figure S51. Cyclic voltametry traces of **P1**, **P2**, and **P3** (left) and **P4** and **P5** (left) as thin films. Measurements were carried out in dry/degassed CH_3CN using 0.1 M Bu_4NPF_6 and referenced to Fc/Fc^+ (HOMO level -4.8 eV below vacuum).

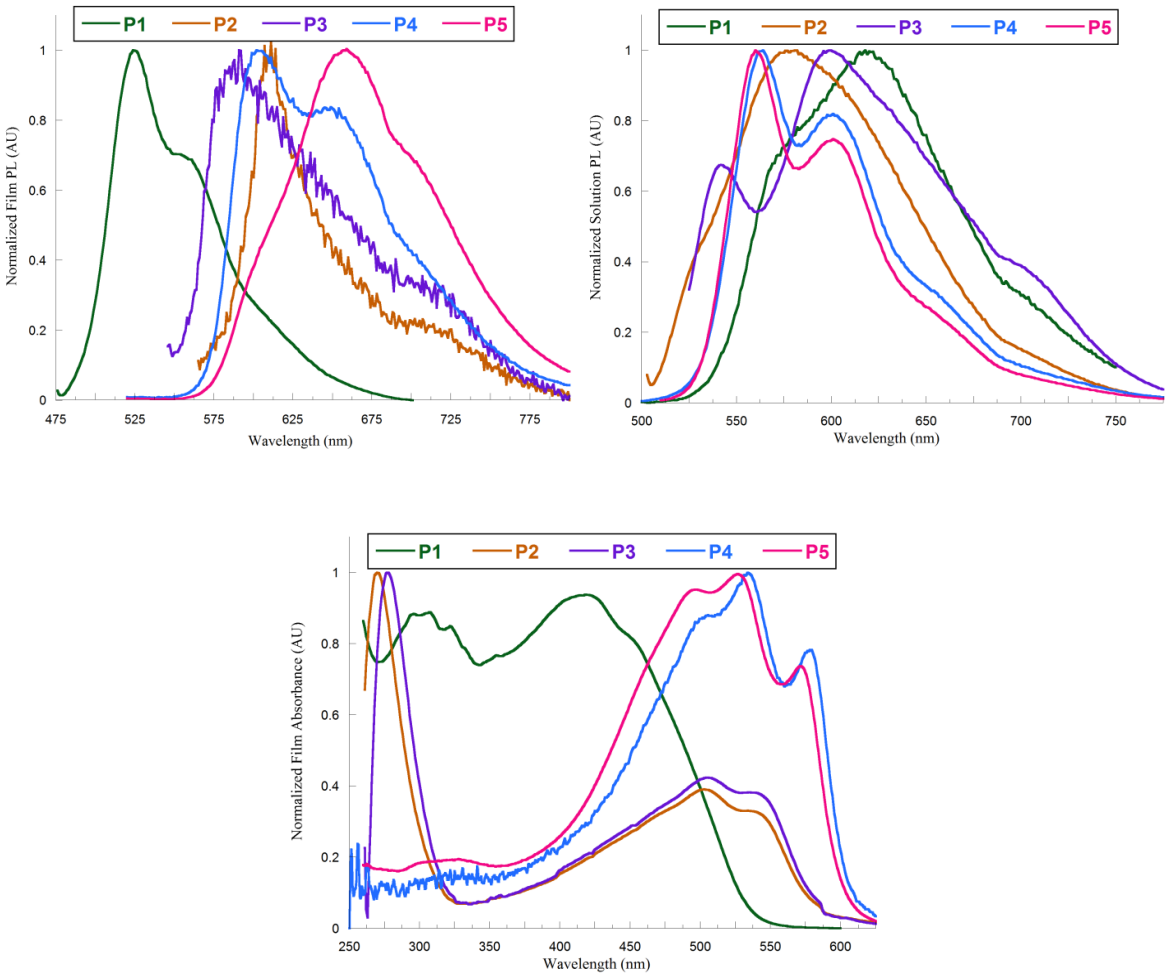

Figure S2.52. Photoluminescence of **P1-P5** in THF solution (left) and thin film (right). UV-Vis data for **P1-P5** in thin film (bottom center).

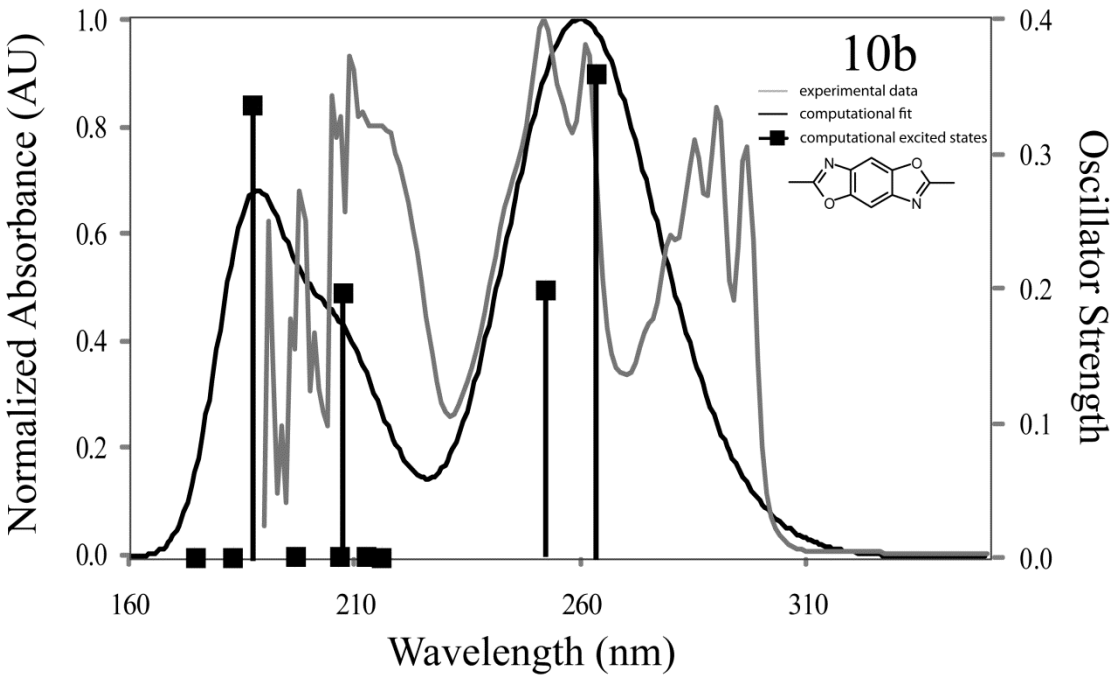

Figure S2.53. A comparison of the experimental UV-Vis spectrum of **10b** with the predicted excited states.

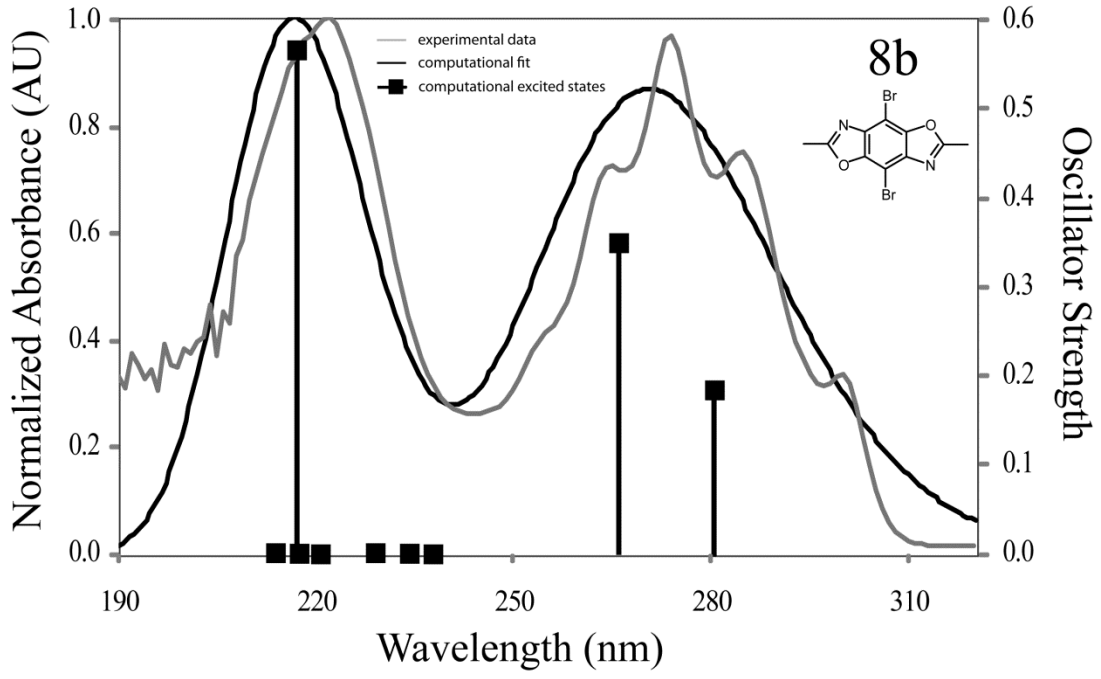

Figure S2.54. A comparison of the experimental UV-Vis spectrum of **8b** with the predicted excited states.

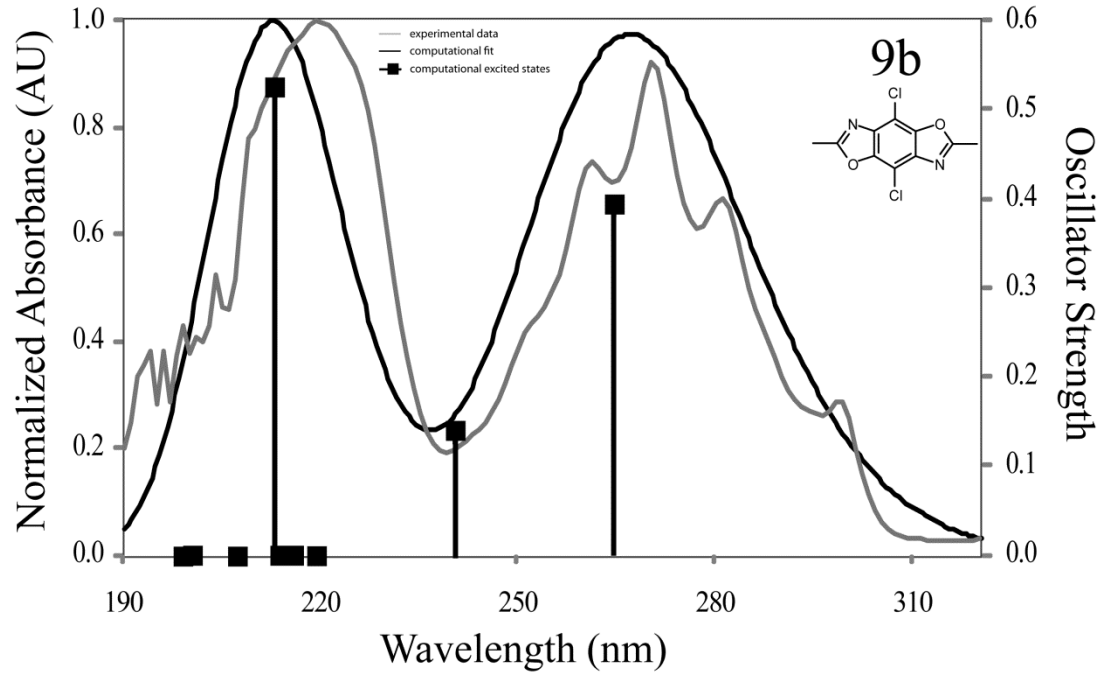

Figure S2.55. A comparison of the experimental UV-Vis spectrum of **9b** with the predicted excited states.

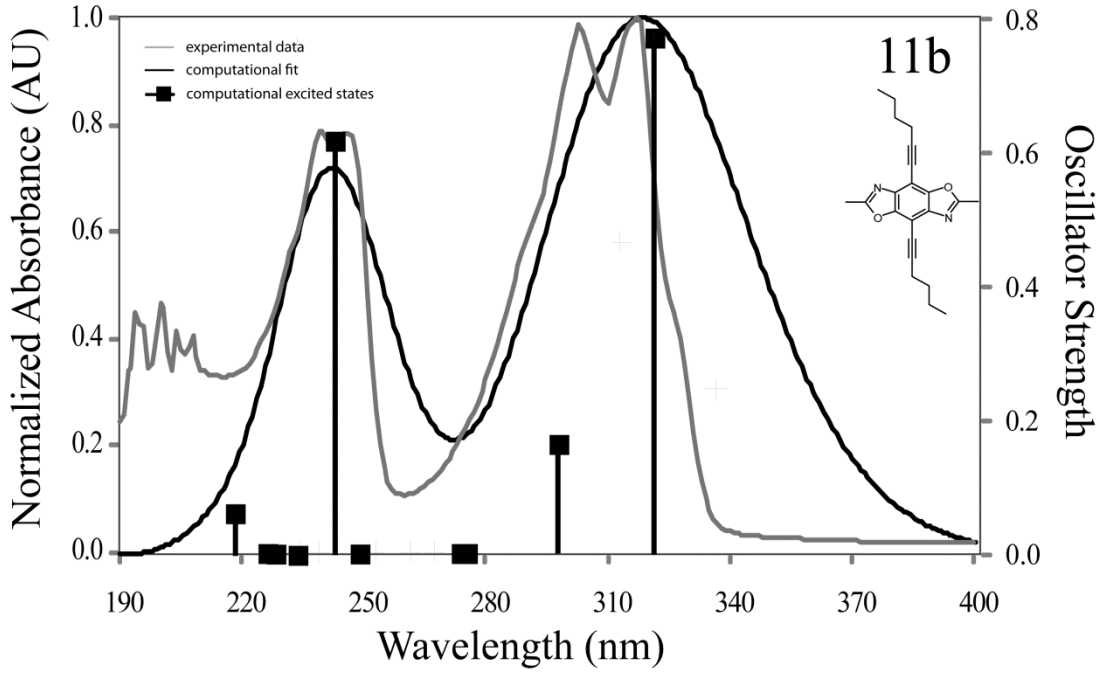

Figure S2.56. A comparison of the experimental UV-Vis spectrum of **11b** with the predicted excited states.

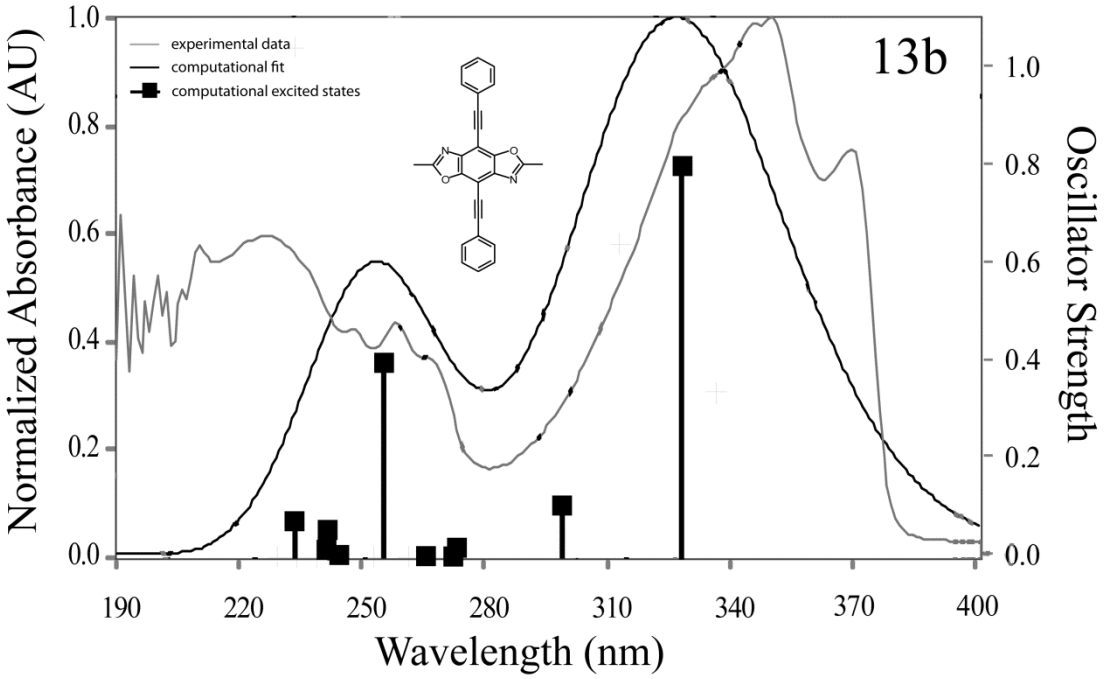

Figure S2.57. A comparison of the experimental UV-Vis spectrum of **13b** with the predicted excited states.

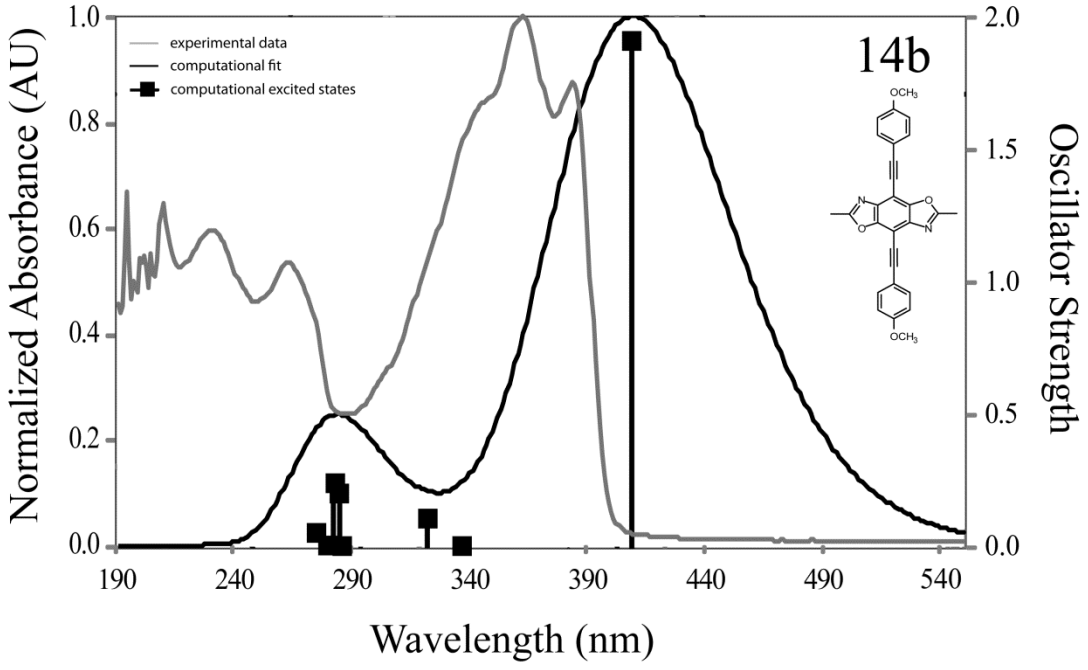

Figure S2.58. A comparison of the experimental UV-Vis spectrum of **14b** with the predicted excited states.

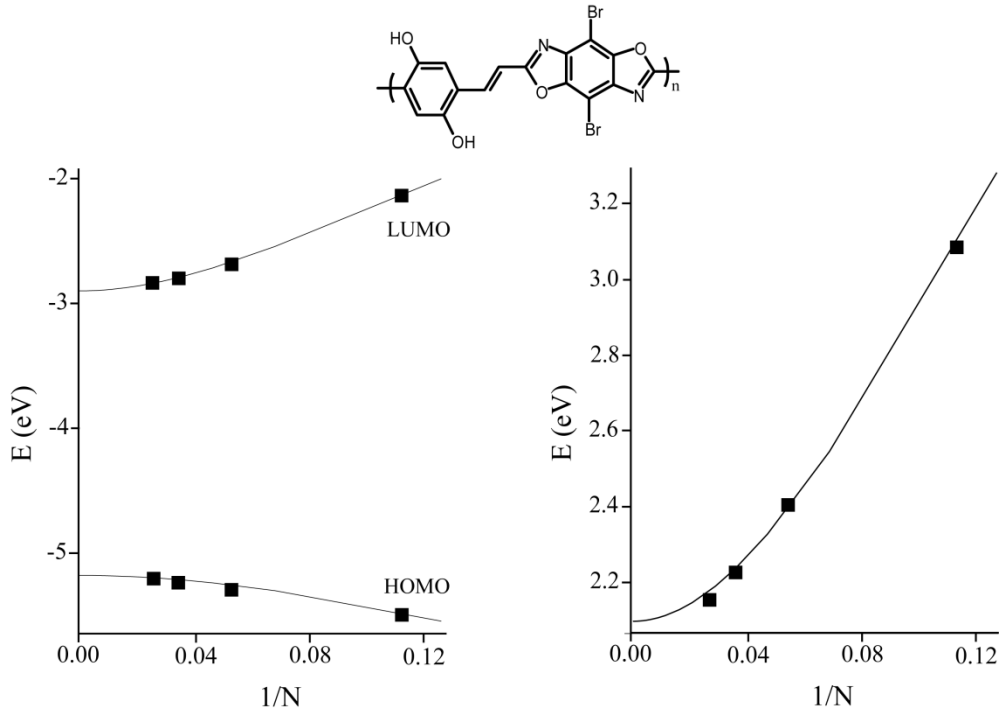

Figure S2.59. The long chain limit of HOMO, LUMO and band gap for polymer **P1**.

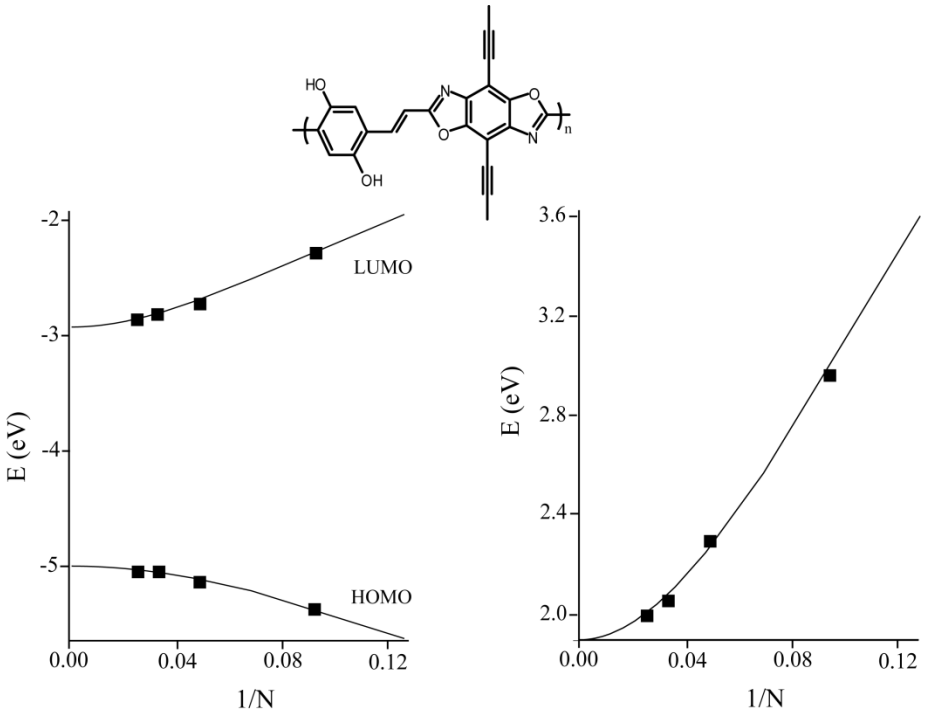

Figure S2.60. The long chain limit of HOMO, LUMO and band gap for polymer **P2**.

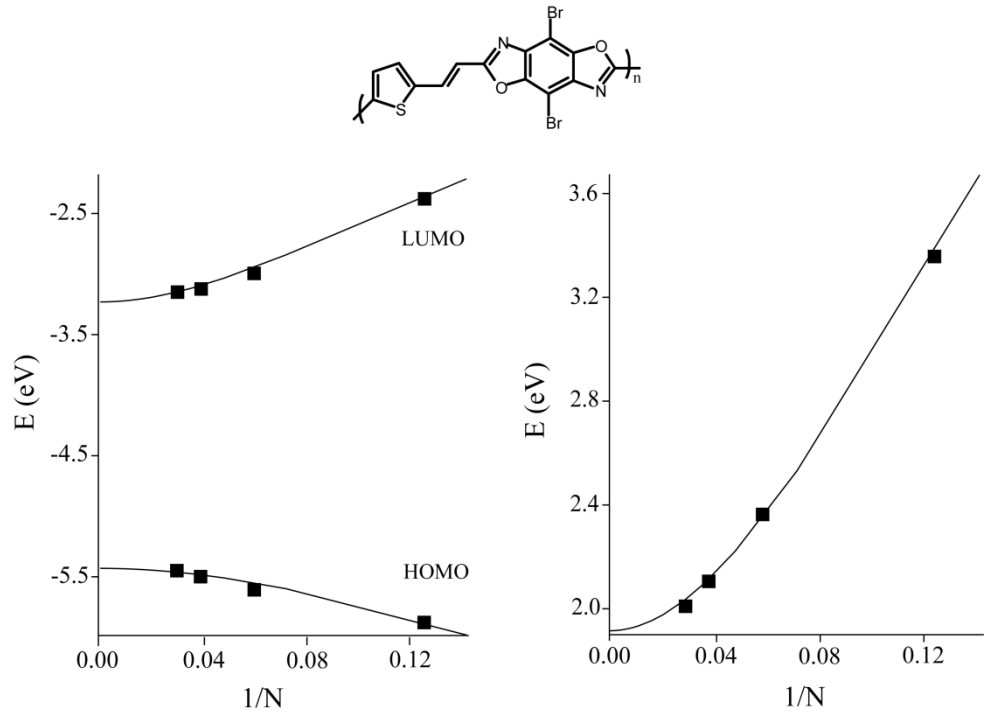

Figure S2.61. The long chain limit of HOMO, LUMO and band gap for polymer **P4**.

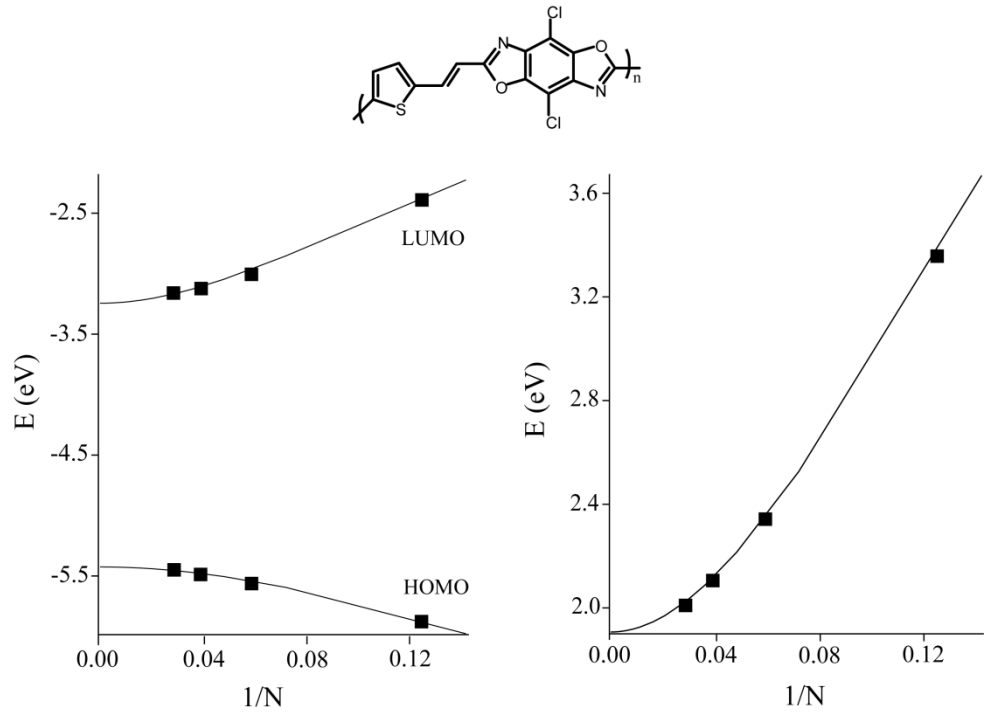

Figure S2.62. The long chain limit of HOMO, LUMO and band gap for polymer **P5.**

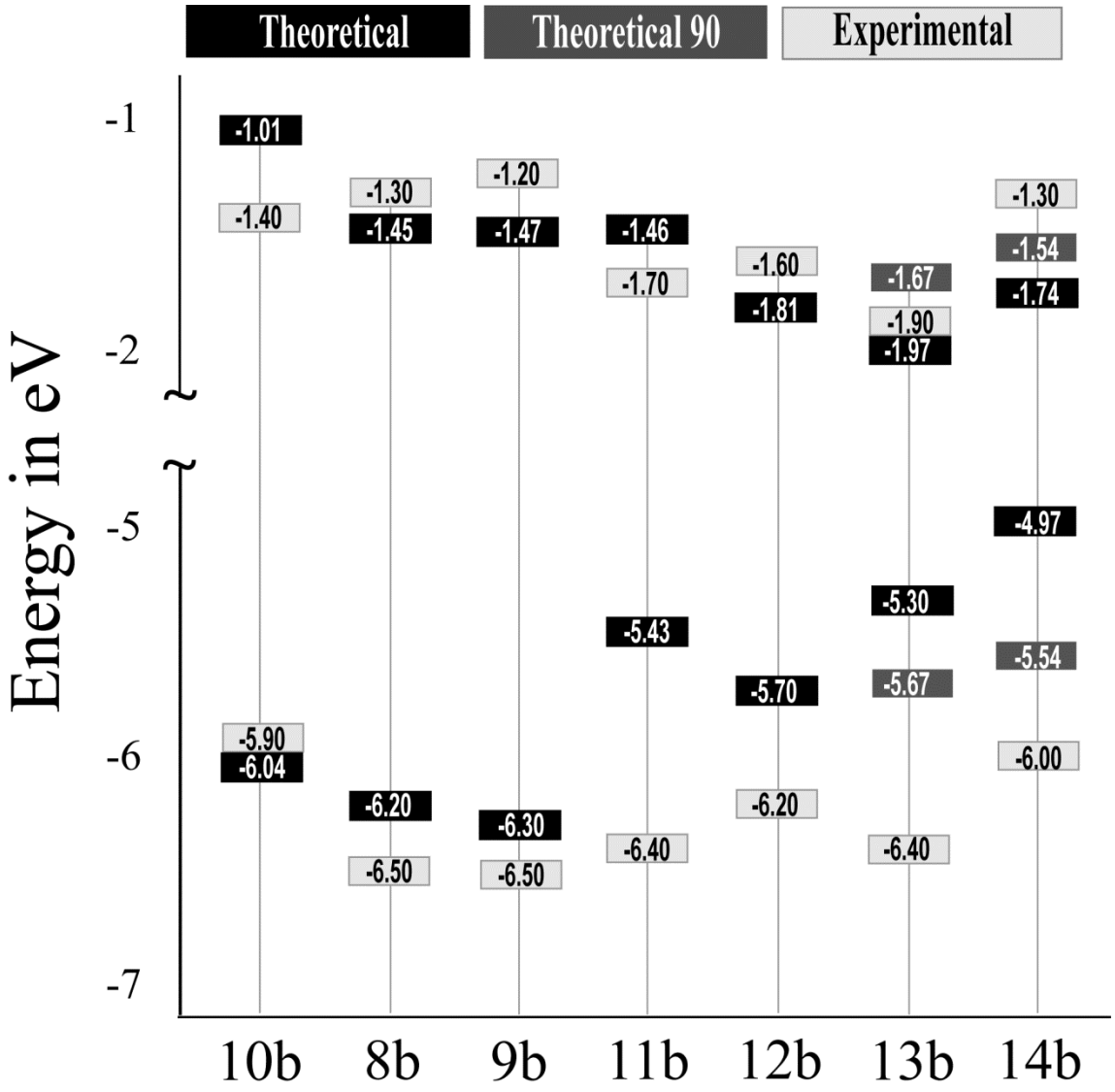

Figure S2.63. A band representation of experimental and theoretical HOMO and LUMO.

Table S2.1. A comparison between TDDFT and observed absorbance data

	Computed λ (nm)	Observed λ (nm)	*f*	Transition Type
10b	187	NA	0.33	H-1 → L+1 (68%), H → L+3 (11%)
	207	209	0.20	H-1 → L (11%), H → L+1 (65%)
	252	252	0.20	H-1 → L (49%), H → L (26%)
	264	285	0.40	H-1 → L (24%), H → L (54%)
8b	217	222	0.57	H-1 → L (18%), H → L+1(70%)
	266	274	0.35	H-1 → L (59%), H → L (25%)
	280	NA	0.18	H-1 → L (20%), H → L (71%)
9b	213	219	0.52	H-1 → L (12%), H → L+1(60%)
	265	270	0.39	H-1 → L (44%), H → L (32%)
	274	NA	0.14	H-1 → L (30%), H → L (48%)
11b	243	243	0.62	H-1 → L (15%), H → L+1(80%)
	298	304	0.16	H-1 → L (79%), H → L+1 (16%)
	321	317	0.77	H → L (96%)
12b	246	242	0.52	H-1 → L (11%), H → L+1(83%)
	309	315	0.14	H-1 → L (85%), H → L+1 (13%)
	331	NA	0.97	H → L (97%)
13b	277	248	0.30	H → L+2 (78%), H-1 → L (9%)
	325	350	0.09	H-1 → L (77%), H → L+2 (15%)
	393	369	1.70	H → L (81%)
14b	271	226	0.03	H-3 → L (78%)
	282	259	0.38	H-2 → L (14%), H → L+2 (69%)
	321	363	0.09	H-2 → L (70%), H → L+2 (23%)
	405	383	1.80	H → L (82%)

H = HOMO and L = LUMO

2.8 References

(1) Horowitz, G. *Advanced Materials* **1998**, *10*, 365.

(2) Mas-Torrent, M.; Rovira, C. *Chemical Society Reviews* **2008**, *37*, 827.

(3) Newman, C. R.; Frisbie, C. D.; daSilva Filho, D. A.; Bredas, J. L.; Ewbank, P. C.; Mann, K. R. *Chem. Mater.* **2004**, *16*, 4436.

(4) Murphy, A. R.; Frechet, J. M. J. *Chemical Reviews* **2007**, *107*, 1066.

(5) Dimitrakopoulos, C. D.; Malenfant, P. R. L. *Advanced Materials* **2002**, *14*, 99.

(6) Tang, C. W.; VanSlyke, S. A. *Applied Physics Letters* **1987**, *51*, 913.

(7) Veinot, J. G. C.; Marks, T. J. *Accounts of Chemical Research* **2005**, *38*, 632.

(8) Friend, R. H.; Gymer, R. W.; Holmes, A. B.; Burroughes, J. H.; Marks, R. N.; Taliani, C.; Bradley, D. D. C.; Dos Santos, D. A.; Bredas, J. L.; Logdlund, M.; Salaneck, W. R. *Nature* **1999**, *397*, 121.

(9) Alam, M. M.; Jenekhe, S. A. *Chemistry of Materials* **2004**, *16*, 4647.

(10) Coakley, K. M.; McGehee, M. D. *Chemistry of Materials* **2004**, *16*, 4533.

(11) Scharber, M. C.; Muehlbacher, D.; Koppe, M.; Denk, P.; Waldauf, C.; Heeger, A. J.; Brabec, C. J. *Advanced Materials* **2006**, *18*, 789.

(12) Tang, C. W. *Applied Physics Letters* **1986**, *48*, 183.

(13) Osaheni, J. A.; Jenekhe, S. A. *J. Am. Chem. Soc.* **1995**, *117*, 7389.

(14) Havinga, E. E.; ten Hoeve, W.; Wynberg, H. *Synthetic Metals* **1993**, *55*, 299.

(15) van Mullekom, H. A. M.; Vekemans, J. A. J. M.; Havinga, E. E.; Meijer, E. W. *Mater. Sci. Eng., R* **2001**, *32*, 1.

(16) Zhou, H.; Yang, L.; Stoneking, S.; You, W. *ACS Appl. Mater. Interfaces* **2010**, *2*, 1377.

(17) Roncali, J. *Chemical Reviews* **1997**, *97*, 173.

(18) Zhu, Y.; Champion, R. D.; Jenekhe, S. A. *Macromolecules* **2006**, *39*, 8712.

(19) So, Y.-H.; Martin, S. J.; Bell, B.; Pfeiffer, C. D.; Van Effen, R. M.; Romain, B. L.; Lefkowitz, S. M. *Macromolecules* **2003**, *36*, 4699.

(20) Klare, J. E.; Tulevski, G. S.; Sugo, K.; de Picciotto, A.; White, K. A.; Nuckolls, C. *J. Am. Chem. Soc.* **2003**, *125*, 6030.

(21) Osowska, K.; Miljanic, O. S. *Chem. Commun.* **2010**, *46*, 4276.

(22) Klare, J. E.; Tulevski, G. S.; Nuckolls, C. *Langmuir* **2004**, *20*, 10068.

(23) Mike, J. F.; Makowski, A. J.; Mauldin, T. C.; Jeffries-El, M. *J. Poly. Sci. A.* **2010**, *48*, 1456.

(24) Mike, J. F.; Nalwa, K.; Makowski, A. J.; Putnam, D.; Tomlinson, A. L.; Chaudhary, S.; Jeffries-El, M. *Phys. Chem. Chem. Phys.* **2011**, *13*, 1338.

(25) Patil, A. V.; Park, H.; Lee, E. W.; Lee, S.-H. *Synthetic Metals* **2010**, *160*, 2128.

(26) Anslyn, E. V.; Dougherty, D. A. *Modern Physical Organic Chemistry*; University Sciences: Sausalito, CA, 2004.

(27) Anthony, J. E.; Brooks, J. S.; Eaton, D. L.; Parkin, S. R. *Journal of the American Chemical Society* **2001**, *123*, 9482. (28) Anthony, J. E.; Eaton, D. L.; Parkin, S. R. *Organic Letters* **2001**, *4*, 15.

(29) Anthony, J. E.; Facchetti, A.; Heeney, M.; Marder, S. R.; Zhan, X. *Advanced Materials* **2010**, *22*, 3876.

(30) Swartz, C. R.; Parkin, S. R.; Bullock, J. E.; Anthony, J. E.; Mayer, A. C.; Malliaras, G. G. *Org Lett* **2005**, *7*, 3163.

(31) Miao, S.; Smith, M. D.; Bunz, U. H. F. *Org. Lett.* **2006**, *8*, 757.

(32) Appleton, A. L.; Miao, S.; Brombosz, S. M.; Berger, N. J.; Barlow, S.; Marder, S. R.; Lawrence, B. M.; Hardcastle, K. I.; Bunz, U. H. F. *Organic Letters* **2009**, *11*, 5222.

(33) Hilger, A.; Gisselbrecht, J.-P.; Tykwinski, R. R.; Boudon, C.; Schreiber, M.; Martin, R. E.; Luethi, H. P.; Gross, M.; Diederich, F. *Journal of the American Chemical Society* **1997**, *119*, 2069.

(34) Rose, B. D.; Chase, D. T.; Weber, C. D.; Zakharov, L. N.; Lonergan, M. C.; Haley, M. M. *Organic Letters* **2011**, *13*, 2106.

(35) Mike, J. F.; Makowski, A. J.; Jeffries-EL, M. *Org. Lett.* **2008**, *10*, 4915.

(36) Liao, J.; Wang, Q. *Macromolecules* **2004**, *37*, 7061.

(37) Destri, S.; Pasini, M.; Pelizzi, C.; Porzio, W.; Predieri, G.; Vignali, C. *Macromolecules* **1999**, *32*, 353.

(38) Rathke, M. W.; Nowak, M. *The Journal of Organic Chemistry* **1985**, *50*, 2624.

(39) Salaneck, W. R. *Journal of Electron Spectroscopy and related Phenomena* **2009**, *174*, 3.

(40) Miyamae, T.; Yoshimura, D.; Ishii, H.; Ouchi, Y.; Miyazaki, T.; Koike, T.; Yamamoto, T.; Muramatsu, Y.; Etori, H.; Maruyama, T.; Seki, K. *Synth. Met.* **1997**, *84*, 939.

(41) Lois, S.; Florès, J.-C.; Lère-Porte, J.-P.; Serein-Spirau, F.; Moreau, J. J. E.; Miqueu, K.; Sotiropoulos, J.-M.; Baylère, P.; Tillard, M.; Belin, C. *European Journal of Organic Chemistry* **2007**, *2007*, 4019.

(42) Becke, A. D. *Journal of Chemical Physics* **1993**, *98*, 5648.

(43) Blouin, N.; Michaud, A.; Gendron, D.; Wakim, S.; Blair, E.; Neagu-Plesu, R.; Belletete, M.; Durocher, G.; Tao, Y.; Leclerc, M. *J. Am. Chem. Soc.* **2008**, *130*, 732.

(44) Belletête, M.; Blouin, N.; Boudreault, P.-L. T.; Leclerc, M.; Durocher, G. *Journal of Physical Chemistry A* **2006**, *110*, 13696.

(45) Belletete, M.; Durocher, G.; Hamel, S.; Cote, M.; Wakim, S.; Leclerc, M. *The Journal of Chemical Physics* **2005**, *122*, 104303.

(46) Zade, S. S.; Bendikov, M. *Org. Lett.* **2006**, *8*, 5243.

(47) Cai, Z.-L.; Sendt, K.; Reimers, J. R. *Journal of Chemical Physics* **2002**, *117*, 5543.

(48) Dreuw, A.; Head-Gordon, M. *Journal of the American Chemical Society* **2004**, *126*, 4007.

(49) Reimers, J. R.; Cai, Z. L.; BiliĆ, A.; Hush, N. S. *Annals of the New York Academy of Sciences* **2003**, *1006*, 235.

(50) Kaur, I.; Jia, W.; Kopreski, R. P.; Selvarasah, S.; Dokmeci, M. R.; Pramanik, C.; McGruer, N. E.; Miller, G. P. *Journal of the American Chemical Society* **2008**, *130*, 16274.

(51) Yasuda, T.; Imase, T.; Nakamura, Y.; Yamamoto, T. *Macromolecules* **2005**, *38*, 4687.

(52) Levitus, M.; Schmieder, K.; Ricks, H.; Shimizu, K. D.; Bunz, U. H. F.; Garcia-Garibay, M. A. *Journal of the American Chemical Society* **2001**, *123*, 4259.

(53) O'Boyle, N. M.; Tenderholt, A. L.; Langner, K. M. *Journal of computational chemistry* **2008**, *29*, 839.

(54) Marsden, J. A.; Miller, J. J.; Shirtcliff, L. D.; Haley, M. M. *Journal of the American Chemical Society* **2005**, *127*, 2464.

(55) Sista, P.; Nguyen, H.; Murphy, J. W.; Hao, J.; Dei, D. K.; Palaniappan, K.; Servello, J.; Kularatne, R. S.; Gnade, B. E.; Xue, B.; Dastoor, P. C.; Biewer, M. C.; Stefan, M. C. *Macromolecules* **2010**, *43*, 8063.

(56) Hundt, N.; Palaniappan, K.; Servello, J.; Dei, D. K.; Stefan, M. C.; Biewer, M. C. *Org. Lett.* **2009**, *11*, 4422.

(57) Zucchero, A. J.; McGrier, P. L.; Bunz, U. H. F. *Acc. Chem. Res.* **2009**, *43*, 397.

(58) Gierschner, J.; Cornil, J.; Egelhaaf, H.-J. *Advanced Materials* **2007**, *19*, 173.

(59) Milian Medina, B.; VanVooren, A.; Brocorens, P.; Gierschner, J.; Shkunov, M.; Heeney, M.; McCulloch, I.; Lazzaroni, R.; Cornil, J. *Chemistry of Materials* **2007**, *19*, 4949.

(60) Mylari, B. L.; Scott, P. J.; Zembrowski, W. J. *Synthetic Communications* **1989**, *19*, 2921.

(61) Jones, R. G. *Journal of the American Chemical Society* **1951**, *73*, 5168.

(62) Hegedus, L. S.; Odle, R. R.; Winton, P. M.; Weider, P. R. *Journal of Organic Chemistry* **1982**, *47*, 2607.

(63) Mike, J. F.; Inteman, J. J.; Ellern, A.; Jeffries-El, M. *Journal of Organic Chemistry* **2010**, *75*, 495.

CHAPTER 3

INFLUENCE OF CONJUGATION AXIS ON THE OPTICAL AND ELECTRONIC PROPERTIES OF ARYL-SUBSTITUTED BENZOBISOXAZOLES

Reproduced with permission from J. Org. Chem., **2013,** *78,* 6570.

DOI: 10.1021/jo4007927

*Brian C. Tlach,[a] Aimée L. Tomlinson,[b] Alden G. Ryno,[b] Dawn D. Knoble,[a] Dana Drochner,[a] Kyle Krager,[a] and Malika Jeffries-EL[a]**

[a] Department of Chemistry, Iowa State University, Ames IA 50010

[b] Department of Chemistry North Georgia College & State University, GA 30597.

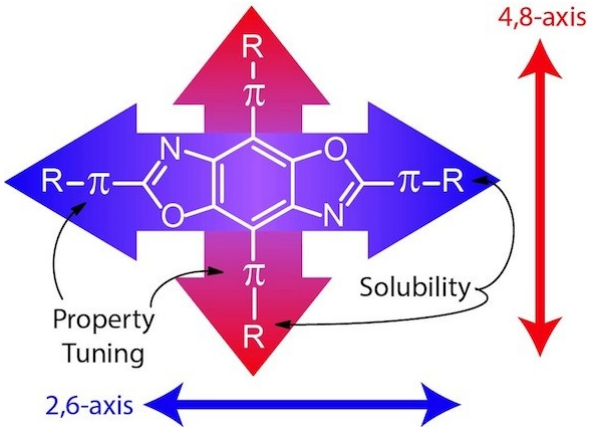

3.1 Abstract

Six different 2,6-diethyl-4,8-diarylbenzo[1,2-*d*:4,5-*d*']bisoxazoles and four different 2,4,6,8-tetraarylbenzobisoxazoles were synthesized in two steps: a Lewis acid-catalyzed orthoester cyclization followed by a Suzuki or Stille cross-coupling with various arenes. The influence of aryl group substitution and/or conjugation axis variation on the optical and electronic properties of these benzobisoxazole (BBO) compounds was evaluated. Structural modifications could be used to alter the HOMO, LUMO and band gap over a range of 1.0, 0.5 and 0.5 eV, respectively. However, depending on the location and identity of the substituent, the HOMO level can be altered without significantly impacting the LUMO level. This is supported by the calculated frontier molecular orbitals. Our results indicate that the FMOs and band gaps of benzobisoxazoles can be readily modified either jointly or individually.

3.2 Introduction

During the past four decades, interest in the development of π-conjugated materials has increased due to their potential use as replacements for inorganic materials in a variety of semiconducting applications including field effect transistors (FET)s,[1-5] organic light emitting diodes (OLED)s,[6-8] and photovoltaic cells (PVC)s.[9-12] In addition to the ability to be processed from solution, organic semiconductors can be modified at the molecular level to optimize the optical and electronic properties of the materials for specific applications. Since the characteristics of π-conjugated systems are strongly influenced by the highest occupied molecular orbital (HOMO) and the lowest unoccupied molecular orbital (LUMO), synthetic

strategies that can alter these parameters are of paramount importance. Unfortunately, most chemical modifications of π-conjugated materials result in changes in the position of both of the frontier molecular orbitals (FMO)s. This is a result of the extensive delocalization of electrons within these systems, rendering selective modification of either the HOMO level or LUMO level difficult. One approach for independently tuning FMOs within π-conjugated materials is through the synthesis of two-dimensional molecules that feature two perpendicular π-conjugated linear "arms" connected through a central aromatic core.[13-23] These so-called "cruciforms" possess spatially segregated FMOs, enabling for strategic tuning of either the LUMO or the HOMO by varying the nature of the substituents and their arrangement around the central molecule. Representative examples include benzobisoxazole-based cruciforms,[13-15] distyrylbis(arylethynyl)benzenes,[16-18] tetrakis(arylethynyl)benzenes,[19-22] and tetrastyrylbenzenes.[23]

Among the aforementioned examples, the benzo[1,2-*d*:4,5-*d*′]bisoxazole (BBO)-based cruciforms are particularly interesting since these molecules have two different conjugation pathways: 2,6-conjugation through the oxazole rings and 4,8-conjugation through the central benzene ring (Scheme 3.1). Since one pathway encompasses heterocyclic rings, the optical and electronic properties can be altered as a function of the substitution pattern around the central benzene ring. Recently, our group[24,25] and that of Miljanić,[13] have shown that the conjugation of BBOs is readily extended via Sonogashira cross-coupling reactions between 4,8-dibromo BBOs and various alkynes. The resulting materials have HOMO and LUMO levels that could readily be tuned by substitution. However, the synthesized cruciforms that were reported feature combinations of triple bonds between the arenes along the 4,8-axis and single bonds between the arenes along the 2,6-axis, so

correlating optical and electronic properties to conjugation pathway was not possible.[16,26,27] The Nuckolls group previously synthesized tetraarylBBO cruciforms; however, since their interest was in developing rigid molecules for self-assembled molecular electronics, the optical and electronic properties of these systems were not fully explored.[15,28]

In order to understand how different substitution patterns will affect the optical and electronic properties of larger BBO structures, we performed a more detailed structure-property relationship study. Modification of the aryl group has previously been used to vary properties through extension of the π-system and inductive effects of their electron-donating or electron-withdrawing nature.[16,26-32] Furthermore, aryl substituents are robust, easily modified, and installed through a variety of methods. First, we evaluated the influence of different aryl groups at the 4- and 8-positions of the BBO moiety using a range of spectroscopic techniques along with computational modeling to gain further insight about the FMO shape and electron distribution. Then, we assessed the impact of conjugation pathway by comparing a pair of 2,6-diarylBBOs to the analogous 4,8-diarylBBOs. Lastly, we compared four BBO cruciforms featuring two different aryl groups to study how properties change upon expanding to a two-dimensional π-system. These structure-property studies provide basic insight on BBO behavior in two-dimensional π-systems as a function of aryl group selection and conjugation axis.

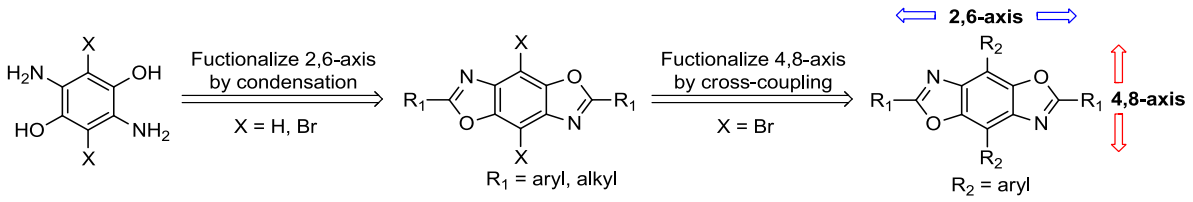

Scheme 3.1. Proposed sequential functionalization of the 2,6- and 4,8-axis of BBO.

3.3 Results and Discussion

3.3.1 Synthesis 4,8-diarylBBOs

The synthesis of compounds **3-8** is shown in Scheme 3.3. Initially, we set out to synthesize the 4,8-diarylBBOs using the Suzuki cross-coupling reaction of various aryl boronic acids and 4,8-dibromo-2,6-dimethylBBO.[24] Suzuki coupling was chosen as boronic acids and esters do not require the use of toxic reagents and are readily purified by standard techniques. Unfortunately, this approach gave low yields of 4,8-diarylBBOs. We hypothesized that the labile methyl protons were being deprotonated under the basic reaction conditions, resulting in undesirable side reactions. The Hegedus group previously decreased the reactivity of the 2,6-position of BBOs by substituting ethyl groups for methyl groups.[33] Therefore we synthesized 2,6-diethyl BBOs **1** and **2** via the Lewis acid catalyzed condensation reaction between the corresponding diamino hydroquinone and triethyl orthopropionate as shown in Scheme 3.2.[34-36]

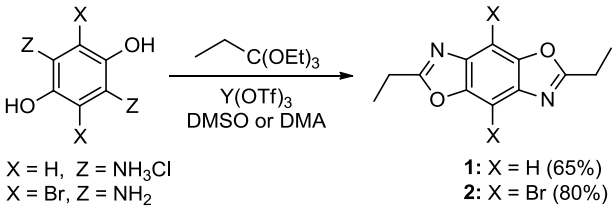

Scheme 3.2. Synthesis of 2,6-diethylBBOs.

The Suzuki cross-coupling reaction of **2** and the appropriate boronic acids or esters afforded **3-7** in yields of 60-83%. Although aryl boronic acids are easier and safer to synthesize, the facile protodeboronation that occurs with thien-2-ylboronic acids[37] required the use of a Stille cross-coupling for the synthesis of 4,8-bis(5-dodecylthien-2-yl)-2,6-diethylBBO **8**. To our knowledge, this is the first report of aryl-aryl cross-coupling of 4,8-dibromoBBOs.

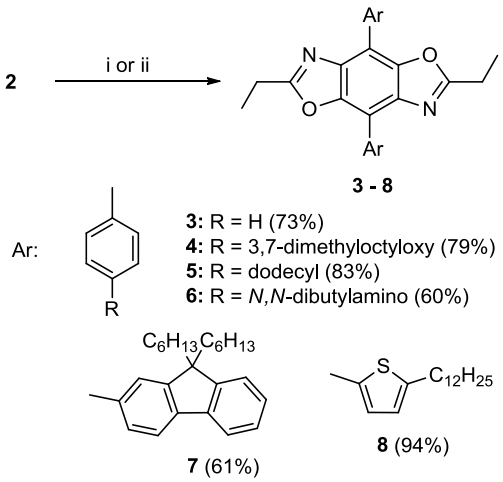

Scheme 3.3. Synthesis of 4,8-diaryl-2,6-diethylBBOs. Reaction conditions: i (**3-7**): $Pd(dppf)Cl_2$, K_2CO_3, TBAB, boronic acid or ester, toluene/H_2O (10:1); ii (**8**): $Pd_2(dba)_3$, $P(^o tolyl)_3$, 5-dodecyl-2-(trimethylstannyl)thiophene, toluene.

3.3.2 Synthesis of 2,6-diarylBBOs

The synthetic approach for the 2,6-diarylBBOs is shown in Scheme 3.5 and the synthesis of the requisite orthoesters is shown in Scheme 3.4. We prepared 5-dodecyl-2-(triethoxymethyl)thiophene in one pot from 2-bromo-5-dodecylthiophene using the method reported by Tschitschibabin.[36,38] The synthesis of 4-dodecyl-1-(triethoxymethyl)benzene proved more difficult as the Tschitschibabin method failed to yield the desired orthoester.

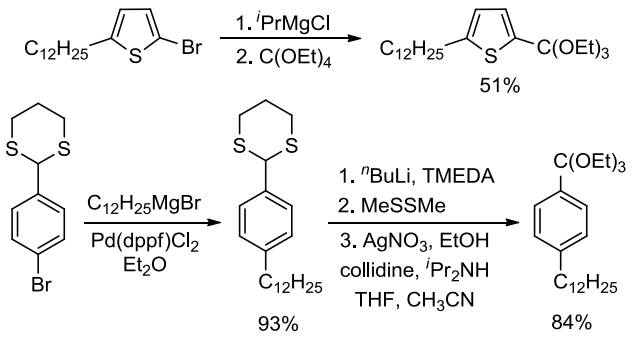

Scheme 3.4. Synthesis of substituted orthoesters.

In search for an alternative approach, we found that aryl orthoesters have been prepared from trithioorthoester intermediates.[39,40] Since the corresponding aldehyde was more readily available, we decided to approach the synthesis of the trithioorthoester intermediate starting from 2-(4-bromophenyl)-1,3-dithiane. This decision proved beneficial as the dithiane protecting group allowed for the addition of a solubilizing alkyl chain via Kumada cross-coupling reaction, and the targeted orthoester was obtained in 84% yield. The 2,6-diarylBBOs **9** and **11** were obtained by the condensation of the corresponding orthoesters and 2,5-diamino-1,4-hydroquinone hydrochloride (DAHQ)[36,41] in yields of 73% and 65%, respectively (Scheme 3.5). Due to their rigid-rod nature, compounds **9** and **11** had noticeably higher melting points and decreased solubility compared to their respective 4,8-diarylBBOs **5** and **7**.

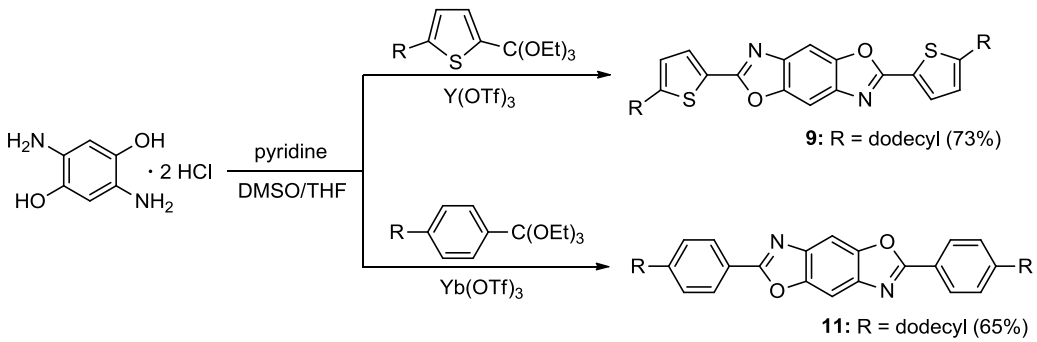

Scheme 3.5. Synthesis of 2,6-diarylBBOs.

3.3.3 Synthesis of 2,4,6,8-tetraarylBBOs

The synthetic approach for the 2,4,6,8-tetraarylBBOs is shown in Scheme 3.6. The Nuckolls group accomplished the synthesis of their tetraarylbenzo[1,2-*d*:4,5-*d*′]bisoxazole cruciforms via a double Staudinger cyclization of substituted bisazidoquinones.[15] Although the reactions occurred in good yields, in their strategy the substituents are introduced early in the reaction sequence. Thus several steps are repeated to make different molecules. A more

versatile approach is to first synthesize 2,6-diaryl-4,8-dibromoBBOs and then extend conjugation across the central benzene ring via cross-coupling chemistry. This approach allows for the synthesis of several BBOs using common intermediates. The condensation reaction of 3,6-diamino-2,5-dibromo-1,4-hydroquinone (Br-DAHQ) with 5-dodecyl-2-(triethoxymethyl)thiophene or 4-dodecyl-1-(triethoxymethyl)benzene afforded compounds **10** and **12** in yields of 75% and 68%, respectively.

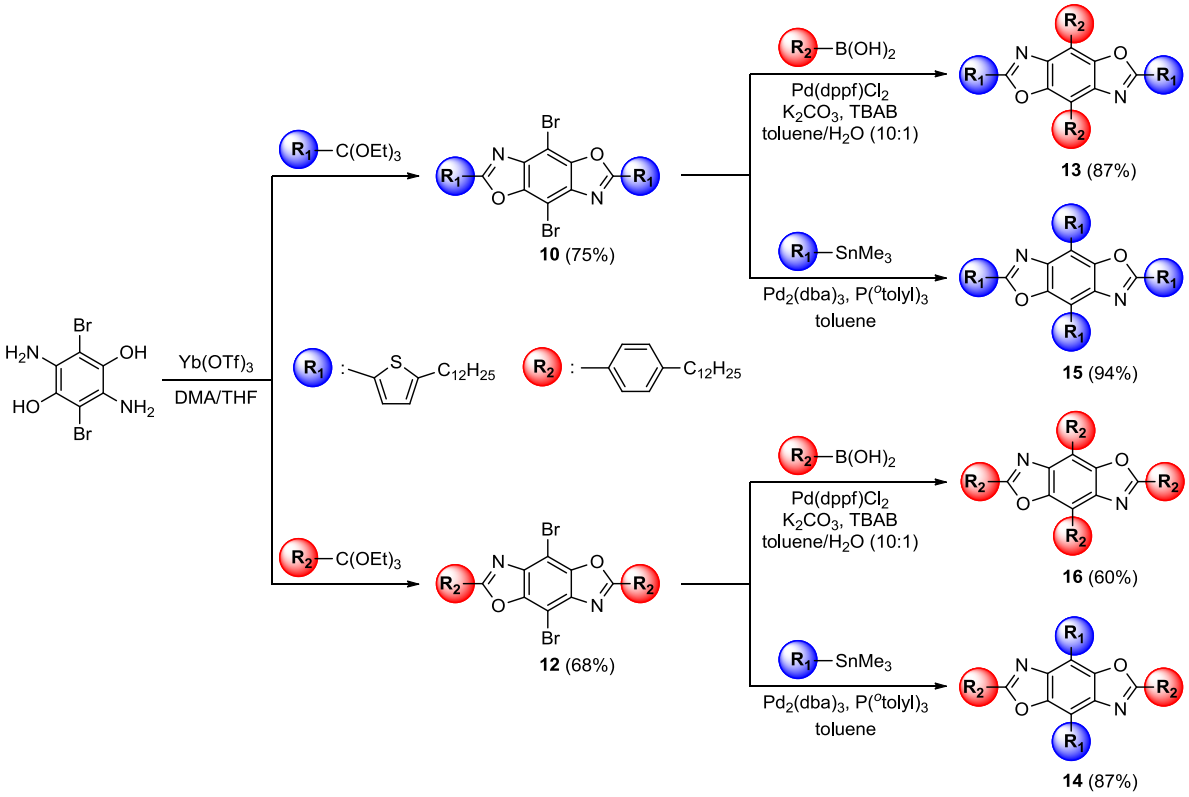

Scheme 3.6. Synthesis of BBO cruciforms.

The subsequent cross-coupling of **10** and **12** with either 5-dodecyl-2-(trimethylstannyl)thiophene or 4-dodecylphenylboronic acid afforded cruciforms **13-16** in 60-94% yield. Purification of these compounds was easily accomplished by first passing through a short silica gel plug to remove polar impurities and residual catalyst followed by recrystallization from an appropriate solvent. The synthesized cruciforms were soluble in

chlorinated solvents and characterized by ^{1}H NMR, ^{13}C NMR, and high-resolution mass spectrometry.

3.3.4 Spectroscopic and Electronic Characterization

4,8-DiarylBBOs. The HOMO levels of the BBOs were investigated using ultraviolet photoelectron spectroscopy (UPS), which provides an absolute determination of the HOMO level.[42-44] We elected to use UPS instead of electrochemistry as many of the compounds were insoluble in acetonitrile and did not have a reduction cycle within the solvent window for the solvent/counter ion blend used. The HOMO values of the BBOs ranged from -4.92 to -5.94 eV. The band gaps were estimated from the intersection of the absorption and emission spectra, and ranged from 3.1 eV to 3.6 eV. The LUMO levels ranged from -2.0 to -2.5 eV and were calculated by adding the optical band gap to the HOMO values, thus these values have a higher degree of uncertainty. These results are summarized in Table 3.1. The electronic properties of the BBOs varied substantially when aryl substituents were incorporated on the 4,8-axis. In general, the extent of the change was dependent on the electron-donating strength of the aryl substituent. BBO **3**, which bears a weakly donating phenyl substituent, has the deepest HOMO at -5.94 eV, whereas BBO **6**, which bears the most electron-rich substituent, has a HOMO level of -4.92 eV. BBO **6** also had the highest-lying LUMO (-2.0 eV) indicating that the incorporation of electron-rich *N,N*-dibutylaniline reduces the acceptor strength of the BBO. Overall, the deepest LUMO, -2.8 eV was observed on the fluorene substituted BBO **7**. This is most likely a result of the greater conjugation length, which increases the acceptor strength of the BBO in the absence of strong electron-donating groups.

The solution UV-Vis absorption of the 4,8-diarylBBOs is shown in Figure 3.1, along with unsubstituted BBO **1**. All of the 4,8-diarylBBOs exhibit high-energy absorptions between 250-275 nm and a second more intense, lower energy absorption in the range of 312-392 nm. The magnitude of this shift varies as a function of the nature of the aryl substituent. Within the 4,8-diphenylBBO series, the maximum absorption (λ_{max}) increases with greater electron-donating strength of the phenyl substituent (H < alkyl < alkoxy < dialkylamino) and thus **3** absorbs at the shortest wavelength (314 nm) and **6** at the longest wavelength (384 nm). Similarly, BBO **8**, which bears thiophene rings also has absorption at longer wavelengths, a result of the electron-rich nature of the substituents and the greater planarity of this molecule relative to the phenyl substituted BBOs. Unlike the 4,8-diphenylBBOs, the main absorption of **8** has visible vibronic coupling likely due to a more planar structure, whereas the spectra of **3-7** all exhibit diminished vibronic detail due to the twisting between the aryl substituent and the BBO core.[45] Surprisingly, further extending the conjugation through the use of fluorene substituents did not display a large bathochromic shift in absorption. This is a result of the fluorene substituents being twisted out of plane due to steric interactions between the BBO core and the hydrogen atoms on fluorene.

The PL quantum yields (Φ_{PL}) of BBOs **3-8** were calculated using anthracene as a standard and an excitation wavelength at 325 nm. The incorporation of bulkier side groups or electron-donating groups results in an increase in Φ_{PL} as seen previously in literature.[30,47,48] Furthermore, thiophene substituents reduce $\Phi_{PL,}$ due to the heavy atom effect of sulfur.

2,6-DiarylBBOs. The electronic properties of the 2,6-diarylBBOs are summarized in Table 3.1. Based on the data obtained from the 4,8-BBOs, we synthesized a pair of 2,6-analogs bearing alkylphenyl or alkylthienyl groups.

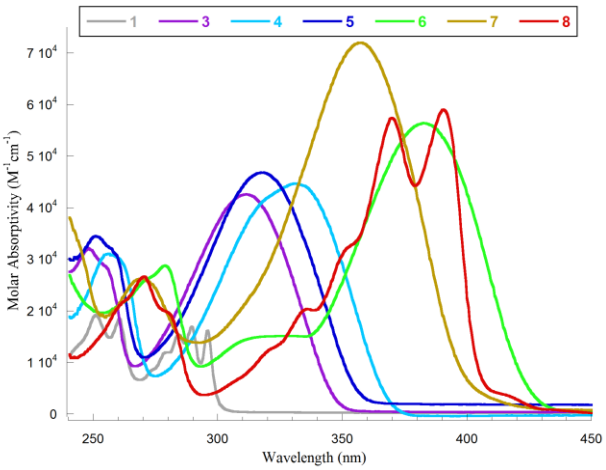

Figure 3.1. Solution UV-Vis spectra of parent BBO **1** and 4,8-diarylBBOs **3-8**.

These groups were selected as representative examples of weak and strong electron-donating substituents, respectively. We did not further evaluate the dialkylamino phenyl group as it resulted in a high-lying HOMO on the 4,8-diarylBBO. Additionally, fluorene was not used due to its longer conjugation length, which would complicate comparisons. The position of the HOMO level exhibits a dependence on the nature of the aryl group and is lowered by 0.24 eV when the aryl group is switched from a thiophene to a phenyl ring. This trend is the result of the increased donor strength of the thiophene in comparison to the phenyl substituent. Due to the uncertainty in the values, we cautiously state that the position of the LUMO level appears to be independent of the aryl group as both **9** and **11** have similar LUMO levels. The band gaps vary proportionally to the HOMO as a result of the independent nature of the LUMO level with respect to the aryl substituent. Additionally, the UV-Vis absorption spectra (Figure 3.2) are consistent with this finding as λ_{max} of **9** is bathochromically shifted relative to that of **11**.

Importance of Substitution Axis. The observed differences in the shape of the UV-Vis spectrum of the BBOs are most likely a result of varying degrees of planarity, which affects

the conjugation length. The steric effects of the ortho-hydrogens on the phenyl ring result in out-of-plane twisting along the 4,8-axis. This is supported by DFT calculations, which predict an out-of-plane twisting between 19-28 degrees for **3-7**. In contrast, thiophene substituted BBOs **8** and **9** are expected to be planar, regardless of which axis the ring is placed on.

Table 1. Optical and electronic data for BBO compounds

	λ_{max} (nm)[a]	λ_{em} (nm)[a]	ε ($M^{-1}\cdot cm^{-1}$)[b]	ϕ[a, c]	HOMO (eV)[d]	LUMO (eV)[e]	E_g^{opt} [eV (nm)][f]
1	252	314	19,200		-6.50	-2.3	4.2
3	314	372	42,600	0.72	-5.94	-2.3	3.6
4	333	379	44,700	0.80	-5.87	-2.5	3.4
5	320	381	46,800	0.59	-5.96	-2.5	3.4
6	384	440	56,400	0.81	-4.92	-2.0	3.0
7	358	404	72,000	0.80	-5.98	-2.8	3.0
8	392	404	59,000	0.34	-5.71	-2.6	3.1
9	369	396	78,000	0.84	-5.51	-2.3	3.2
11	342	386	74,900	0.98	-5.75	-2.3	3.4
13	380	416	85,200	0.72	-5.78	-2.7	3.1
14	374	460	59,600	0.28	-5.49	-2.7	2.8
15	395	448	67,900	0.34	-5.29	-2.5	2.8
16	358	422	71,500	0.74	-5.88	-2.7	3.2

[a] All measurements performed in THF. [b] Extinction coefficients based on absorbance at λ_{max}.

[c] Relative Φ_{PL} were measured using anthracene as a standard. [d] Measured by UPS.

[e] Calculated using HOMO + E_g^{opt}. [f] Measured at intersection of UV-Vis and PL spectra.

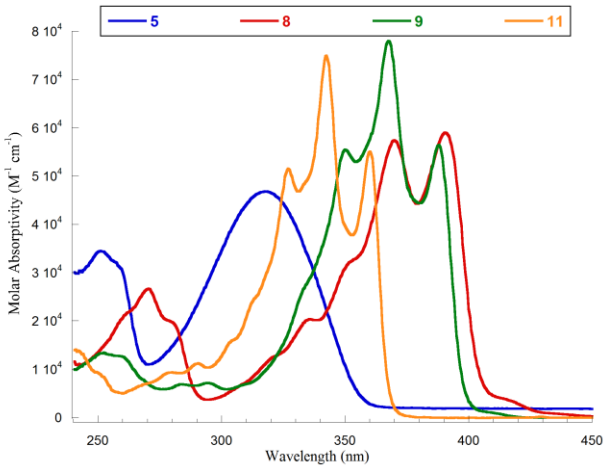

Figure 3.2. UV-Vis spectra of 4,8-diarylBBOs **5** and **8** and the related 2,6-diarylBBOs **9** and **11**.

Phenyl-substituted BBO **11** is also planar since the ring is placed at the 2,6-axis minimizing the steric effects. Thus the 2,6-diarylBBOs **9** and **11** both have similar peak topography, containing vibronic progression in the range of 1310-1410 cm^{-1}, which is characteristic of aromatic ring-stretching modes.[49,50] These features are seen to a small extent in **8** and not observed in **5**. Further analysis of the absorption spectra reveals moving the thienyl group from the 4,8-axis (**8**) to the 2,6-axis (**9**) results in a small bathochromic shift in absorption. Whereas, switching the phenyl group from the 4,8-axis (**5**) to the 2,6-axis (**11**) produces a 22 nm bathochromic shift in λ_{max} and a slight reduction in peak width at half max. This red shift is a result of both the longer conjugation pathway along the 2,6-axis and an increase in planarity. Compounds **5**, **8**, **9**, and **11** show similar PL spectra with Stokes shifts of 61, 12, 27, and 44 nm, respectively (Figure S3.43 in the Supporting Information). The HOMO level is raised by approximately 0.20 eV upon switching the substituents from the 4,8-axis to the 2,6-axis *i.e.* **5** versus **11** or **8** versus **9**, suggesting that the HOMO preferentially aligns along

the 4,8-axis. This decrease in stability was confirmed by the computational studies (Table S3.1 in the Supporting Information).

In order to further compare the effect of substituent type and location, a series 2,4,6,8-tetraarylBBOs were synthesized and characterized. The Φ_{PL} of cruciforms **13** (0.72) and **16** (0.74) are similar while **14** (0.28) and **15** (0.34) were both significantly lower which was expected since Φ_{PL} commonly decreases with narrowing band gap. This has previously been observed in 1,4-bis(phenylethynyl)-2,5-bis(styryl)benzene cruciforms[17] and is a consequence of more accessible non-radiative processes in compounds with narrower band gaps.[51,52] Additionally, the λ_{em} and vibronic detail in the PL spectra of the cruciforms display solvatochromism in which there is a bathochromic shift in λ_{em} as solvent polarity is increased (Figure 3.3 and Figure S3.46 in the Supporting Information). This is more apparent in cruciforms **14** and **15** than in **13** and **16**. The vibronic detail in the PL spectra decreased as the solvent polarity increased for all cruciforms except **13**. Cruciforms **14** and **15** likely have more charge transfer between the two axes than cruciforms **13** and **16**.

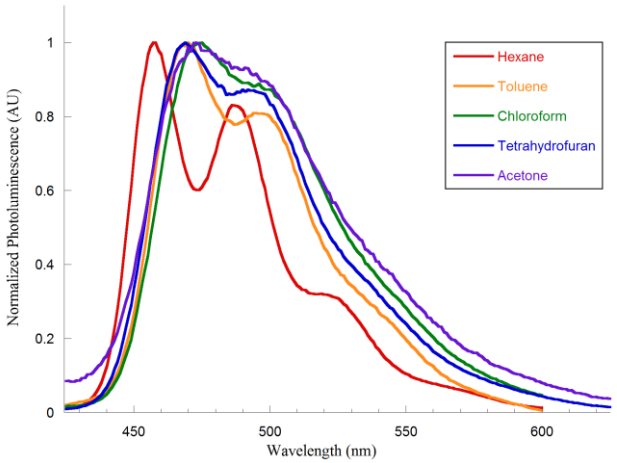

Figure 3.3. Solvatochromism effect of cruciform **15**.

This is further substantiated by the observation of a lower energy shoulder in the UV-Vis spectra and alignment of the FMOs in cruciforms **14** and **15** (*vide infra*). PL spectra of **9** and **11** both exhibit vibronic coupling (Figure S3.43 in the Supporting Information). The Φ_{PL} of the 2,6-diarylBBOs (0.84 for **9** and 0.98 for **11**) are also considerably higher than those for their corresponding 4,8-diarylBBOs (0.34 for **8** and 0.59 for **5**).

An evaluation of cruciforms **15** and **16** demonstrates the influence of the aryl substituents on optoelectronic properties. Cruciform **16**, which bears phenyl substituents in all positions, has the lowest lying HOMO of all the cruciforms at -5.88 eV and the widest band gap at 3.2 eV. Whereas cruciform **15**, which bears electron-rich thiophenes in all positions, has the highest HOMO of all cruciforms at -5.29 eV and the smallest band gap at 2.8 eV. This is consistent with our observations (*vide supra*) that the addition of electron-donating groups at any position destabilizes the HOMO level. The impact of aryl group is substantiated by a comparison of the isomeric cruciforms **13** and **14**. Cruciform **14**, which has the strongly donating thiophene substituents along the 4,8-axis has a HOMO that is nearly 0.3 eV higher and a band gap that is 0.2 eV narrower than that of **13**. This is likely the result of the difference in the planarity of the two structures along with the difference in the electron-donating behavior of the substituents. The origins of this difference may be further explained by comparing the FMO diagrams of the two compounds. Computational studies were carried out to gain further insight into the effect of structural modification by axis and/or aryl group variation. Optimized ground-state geometries were obtained through density functional theory (DFT) employing a B3LYP functional and a SVP basis set. The resulting FMO charge distributions of the optimized structures are shown in Figure 3.4 and the percent distribution along each axis summarized in Table 2.2. The electron density is

focused along the 2,6-axis in the LUMO of cruciforms **13**, **15** and **16**, whereas it is distributed evenly across both axes of **14**. A comparison of the molecular orbital diagrams reveals significant differences in the HOMOs of **13** and **14**. In the case of **13**, the electron density is distributed throughout the entire structure whereas in **14** approximately 96% of the electron density is along the 4,8-axis.. This localization of the HOMO along the more electron-rich axis is consistent with observations made for other cruciforms that contain donor-π-donor conjugation pathways.[16,19,22,32,53-55,] Interestingly, approximately 92% of HOMO is also concentrated along the 4,8-axis in the tetrathiophene-substituted cruciform **15**, indicating that there is a preference for the HOMO to be aligned perpendicular to the benzobisoxazole ring system.[14]

Table 2.2. Calculated percent electronic distribution along each axis for the HOMO and LUMO of the BBO cruciforms.

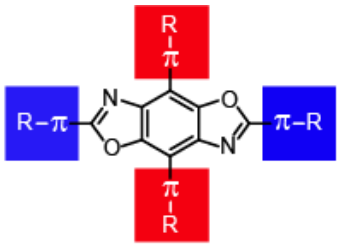

$$\%4,8-axis = \frac{\sum c^2_{4,8-axis}}{\sum c^2_{2,6-axis} + \sum c^2_{4,8-axis}} \qquad \%2,6-axis = \frac{\sum c^2_{2,6-axis}}{\sum c^2_{2,6-axis} + \sum c^2_{4,8-axis}}$$

	HOMO		LUMO	
	4,8-axis	2,6-axis	4,8-axis	2,6-axis
13	58.6	41.4	21.1	78.9
14	95.9	4.1	45.5	54.5
15	91.6	8.4	32.5	67.5
16	79.3	20.7	29.1	70.9

A comparison of the BBO cruciforms to their 1-D building blocks sheds further insights on the impact of aryl substituent location and nature. The UV-Vis spectra of cruciforms **13-16** and their respective 1-D building blocks are shown in Figure 3.5 and the

data is summarized in Table 3.1. Cruciform **13** has phenyl substituents along the 4,8-axis, analogous to BBO **5**, and thiophene substituents along the 2,6-axis, analogous to BBO **9**.

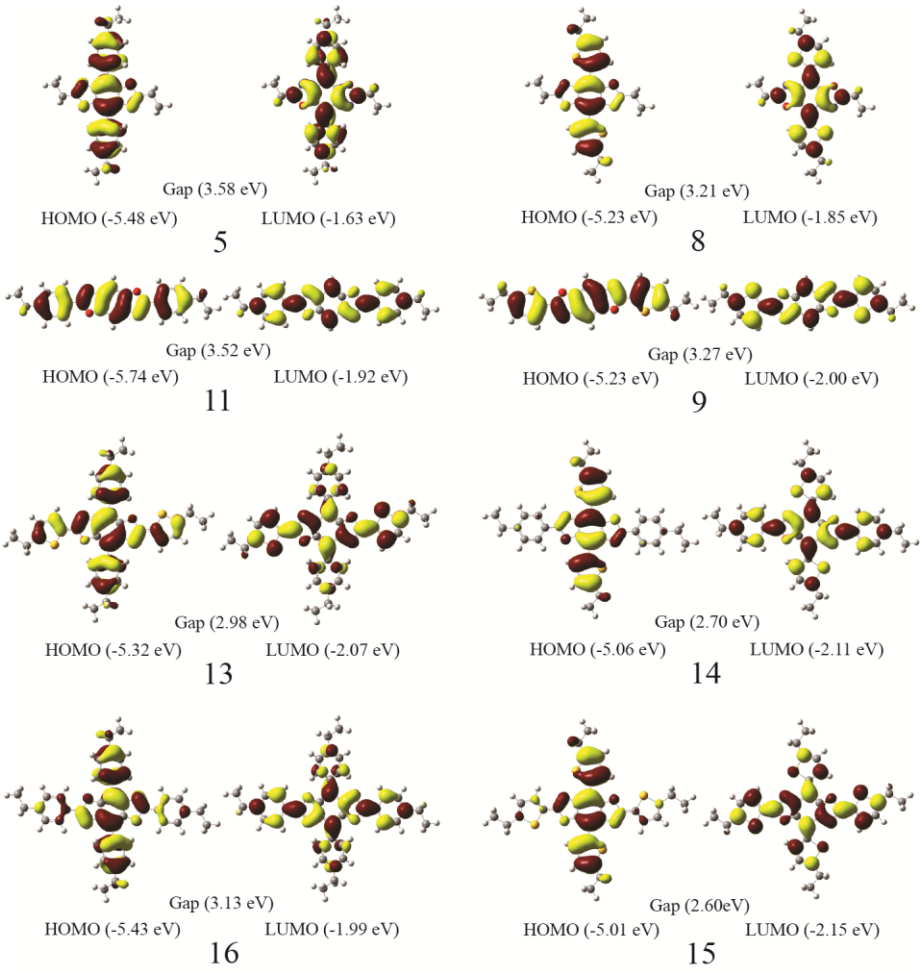

Figure 3.4. FMO diagrams of BBOs **5**, **8**, **9**, **11**, and **13-16**.

The spectrum of **13** has high and low energy absorptions consistent with **5** and **9**, respectively. Additionally, the HOMO level of **13** is between that of **5** and **9**, indicating that **13** behaves as a hybrid of the two compounds. The FMOs show delocalization of electron density along the longest conjugation axis for **5** and **9** whereas **13** shows delocalization throughout the molecule, consistent with our observations. Cruciform **14** has thiophene substituents along the 4,8-axis, analogous to BBO **8**, and phenyl substituents along the 2,6-

axis, analogous to BBO **11**. The overall topography seen in the spectrum of **14** has absorptions consistent with **8** and **11**. However, the spectrum of **14** is significantly broader and has an additional low energy peak around 412 nm suggesting ICT is occurring.[22,56] As a result, the HOMO level of **14** is higher than that of **8** and **11**. The fact that the band gap of **14** is smaller than its structural isomer **13** is further evidence of the importance of aryl substituent placement. The FMO diagram of **14** shows that there is a large amount of electron density localized along the 4,8-axis in the HOMO, providing a suitable environment for charge transfer. These results were somewhat contradictory to those seen for similar 2,6-diaryl-4,8-bis(arylethynyl)BBO cruciforms in which the HOMO, in some cases, is fully localized along the 2,6-axis. In these tetraarylBBOs, full axial "inversion" of the HOMOs and LUMOs does not appear to be prompted by exchanging the aryl groups.[14] However, switching the aryl substituents does appear to have a significant effect on the extent of delocalization in the FMOs.

Cruciform **15** has thiophene substituents along the 4,8- and 2,6-axis, analogous to BBO **8** and BBO **9**, respectively. The spectrum of **15** is broad and lacking in structural detail, thus direct comparisons to **8** and **9** are unclear. Similarly to **14**, there is significant broadening and the appearance of a lower energy shoulder in the spectrum of **15**, which is indicative of ICT. Furthermore, the larger stokes shift and greater influence of solvent polarity on the λ_{em} of **14** and **15** are also indicative of ICT. Collectively, the higher HOMO, narrower band gap, and FMOs of **14** and **15**, support charge transfer is favorable when the 4,8-axis is substituted with thiophene.

Cruciform **16** has phenyl substituents along the 4,8- and 2,6-axis, analogous to BBO **5** and BBO **11**, respectively. As seen in cruciform **15**, the spectrum of **16** is also broad and

lacking in structural detail, thus direct comparisons to **5** and **11** are indeterminate. The diminished vibronic detail in **16**, and to a lesser extent in **13**, is likely a result of the more non-planar structures of these cruciforms compared to **14** and **15** (*vide supra*). This trend also indicates that changes in the spectral topography may be related to the symmetry of these molecules. Of all the cruciforms in this study, **16** has the lowest HOMO and widest band gap. This is a result of a decrease in electron-donating strength and conjugation caused by the phenyl substituents on the 4,8-axis. The FMOs show a slight localization of electron density along the 4,8-axis in the HOMO and the 2,6-axis in the LUMO of **16** consistent with our observations in the other cruciforms.

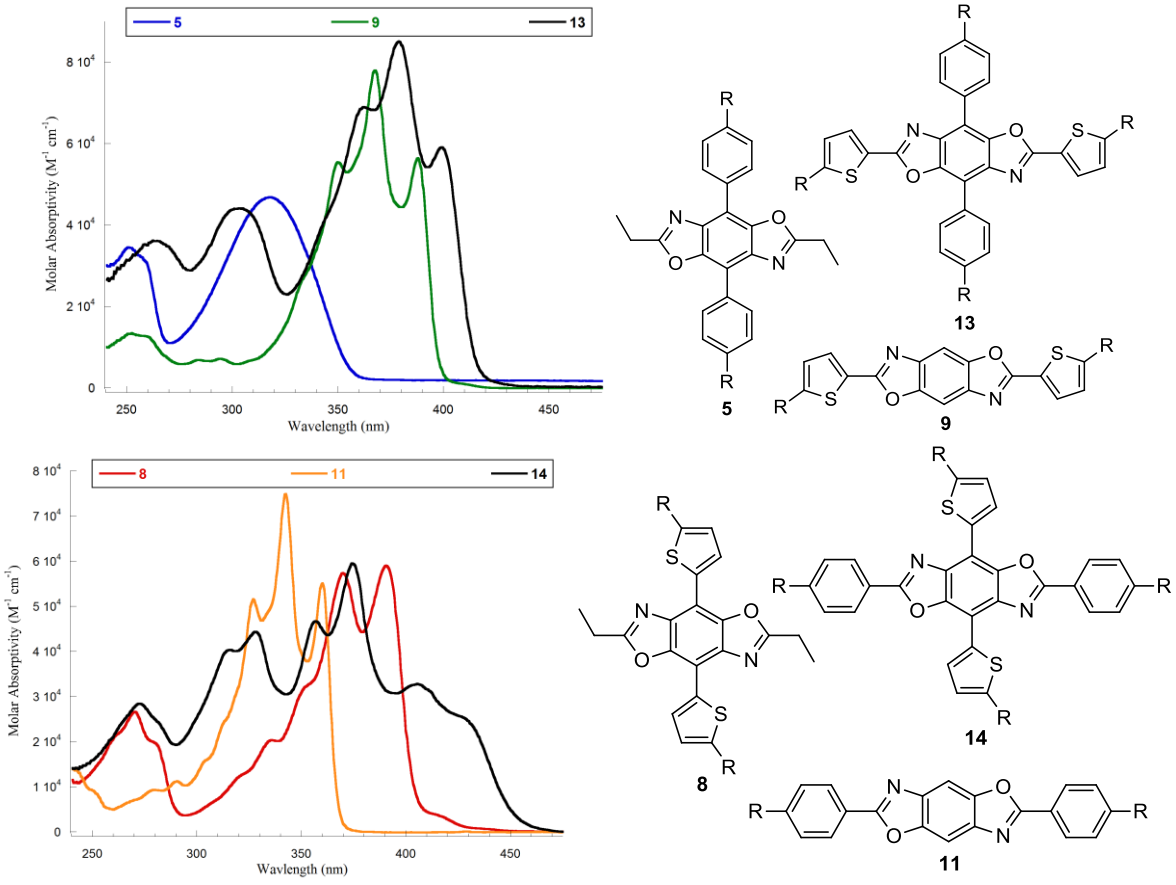

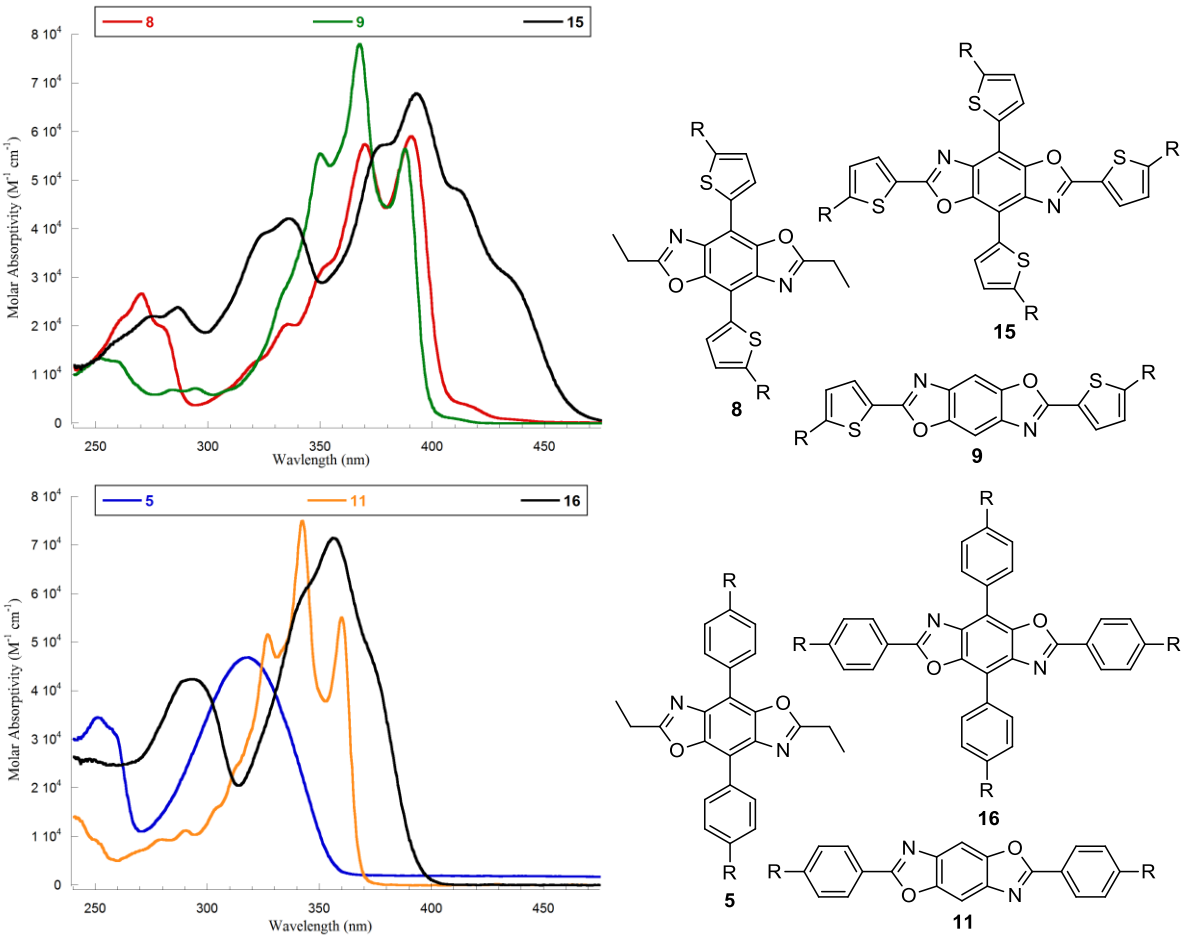

Figure 3.5. UV-Vis spectra of BBO cruciforms **13-16** and their corresponding 1-D building blocks **5**, **8**, **9**, or **11** (left) and the corresponding structures where R = $C_{12}H_{25}$ (right).

3.4 Conclusions

A series of related 4,8-diarylBBOs, 2,6-diarylBBOs and 2,4,6,8-tetraarylBBO cruciforms were readily synthesized in a few high yielding steps. It was observed that the optical and electronic properties of these molecules are dependent on both the electronic nature of the aryl substituent and its location. For linear molecules, as the electron-donating strength of the substituent was increased, the HOMO levels of the BBOs were raised regardless of axis. Additionally, BBOs with an electron-donating group along the 4,8-axis

had lower lying HOMO levels than the analogous 2,6-BBOs. On the other hand the LUMO levels for the related linear BBOs appeared to be unaffected by structural modifications. Similarly, with the mixed cruciforms placing the electron-donating group along the 4,8-axis resulted in a higher HOMO in comparison to placing the substituent on the 2,6-axis. Changing the location of the substituent impacted the LUMO levels for the cruciforms, whereas the bandgaps remained unaffected. Collectively, the UV-Vis, PL and DFT results indicate that the FMOs and bandgaps of benzobisoxazoles can be readily modified either jointly or independently of each other. This result is of significance in the design of new materials for use in a range of organic semiconducting applications. Work is ongoing in our laboratories to develop new two-dimensional oligomers and conjugated polymers.

3.5 Experimental Section

3.5.1 General Methods

Nuclear magnetic resonance (NMR) experiments were carried out in $CDCl_3$ at 400 MHz (^1H) or 100 MHz (^{13}C). ^1H NMR spectra are internally referenced to the residually protonated solvent peak (7.26 ppm), and ^{13}C NMR spectra are referenced to the central carbon peak (77.16 ppm) of $CDCl_3$. In all spectra, chemical shifts are given in δ relative to tetramethylsilane. Coupling constants are reported in hertz (Hz). High-resolution mass spectra were recorded on a double-focusing magnetic sector mass spectrometer using electron impact (EI), electrospray ionization (ESI) or atmospheric pressure chemical ionization (APCI). Melting points were obtained on a melting point apparatus with 260 °C upper limit and are uncorrected. All UV-Vis and fluorescence spectroscopy were obtained using THF solutions unless otherwise noted. Relative solution fluorescence quantum yields

were obtained using anthracene (Φ_{PL} = 0.27 in ethanol)[57] as a standard with excitation at 325 nm. Ultraviolet photoelectron spectroscopy (UPS) measurements were performed on sample films spun from $CHCl_3$. DAHQ,[35] Br-DAHQ,[58] 1-bromo-4-(3,7-dimethyloctyloxy)benzene,[58] 4-dodecyl-1-iodobenzene,[58] 4-dodecylphenylboronic acid,[59] 2-bromo-9,9-dihexylfluorene,[60] 2-(4,4,5,5-tetramethyl-1,3,2-dioxaborolan-2-yl)-9,9-dihexylfluorene,[61] *N,N*-dibutylaniline,[62,63] 4-bromo-(*N,N*-dibutyl)aniline,[63] 4-(*N*-*N*-dibutylamino)phenylboronic acid,[64] 2-bromo-5-dodecanoylthiophene,[65] 2-bromo-5-dodecylthiophene[65,66], 5-dodecyl-2-(trimethylstannyl)thiophene,[67] and 2-(4-bromophenyl)-1,3-dithiane[68] were synthesized according to literature procedures.

3.5.2 Synthetic Procedures

2,6-Diethylbenzo[1,2-*d*;4,5-*d'*]bisoxazole 1. A dry round-bottom flask was placed under an argon atmosphere and charged with 0.054 g (0.05 mmol) $Y(OTf)_3$ and 1.06 g (6.00 mmol) triethylorthopropionate. The flask was fitted with a dry addition funnel and heated to 55 °C with stirring. In the addition funnel, 0.43 g (2.00 mmol) DAHQ was dissolved in 0.33 g (4.20 mmol) pyridine and 2 mL DMSO and the solution added drop-wise to the flask. The mixture was stirred at 55 °C for two hours then allowed to cool to room temperature and diluted with water. The resulting precipitate was collected by filtration washing with water. The crude product was purified by recrystallization from hexanes to yield white needles (0.28 g, 65% yield): mp 95-97 °C; ^{1}H NMR (400 MHz, $CDCl_3$) δ 1.45 (6H, t, J = 8 Hz) 2.96 (4H, q, J = 8 Hz), 7.70 (2H, s, J = 8 Hz); ^{13}C NMR (100 MHz, $CDCl_3$) δ11.0, 22.5, 100.5, 139.2, 148.3, 169.4. HRMS (ESI) *m/z*: Calcd for $C_{12}H_{13}N_2O_2$ 217.0972 $[M + H]^+$, found 217.0972.

4,8-Dibromo-2,6-diethylbenzo[1,2-*d*;4,5-*d'*]bisoxazole 2. A dry round-bottom flask was placed under an argon atmosphere and charged with 0.52 g (0.98 mmol) $Y(OTf)_3$, 21 mL

of DMA, and 10.3 g (58.5 mmol) triethylorthopropionate. The mixture was heated to 55 °C with stirring and 5.81 g (19.5 mmol) freshly prepared Br-DAHQ was added portion-wise over 45 minutes. The reaction was stirred at 55 °C for two hours then allowed to cool to room temperature and diluted with water. The resulting precipitate was collected by filtration and rinsed with water and ethanol. The crude product was further purified by recrystallization from 1:1 chloroform/ethanol to yield small white needles (5.85 g, 80% yield): mp 216-218 °C; ^{1}H NMR (400 MHz, $CDCl_3$) δ 1.50 (6H, t, J = 8 Hz) 3.06 (4H, q, J = 8 Hz); ^{13}C NMR (100 MHz, $CDCl_3$) δ 11.3, 22.8, 91.4, 138.6, 146.7, 170.0. HRMS (ESI) *m/z*: Calcd for $C_{12}H_{11}Br_2N_2O_2$ 372.9182 $[M + H]^+$: found 372.9197.

4,8-Diphenyl-2,6-diethylbenzo[1,2-*d*;4,5-*d'*]bisoxazole 3. A two-neck round-bottom flask was charged with 0.37 g (1.00 mmol) **2**, 0.10 g (1.00 mmol) tetrabutylammonium bromide (TBAB), and 0.33 g (3.0 mmol) phenylboronic acid. The flask was equipped with a reflux condenser and placed under an argon atmosphere. 25 mL of deoxygenated toluene was added followed by 2 mL of deoxygenated 3 M aqueous K_2CO_3. The mixture was further deoxygenated for 10 minutes then 0.036 g (0.05 mmol) $Pd(dppf)Cl_2$ was added, and the reaction heated to reflux with stirring under an argon atmosphere for 36 hours. The mixture was allowed to cool to room temperature, diluted with toluene, and the layers separated. The organic layer was washed with 1 M HCl, H_2O, and brine and dried over $MgSO_4$. The solution was filtered and the solvent removed *in vacuo*. The crude product was taken up in hot hexanes, filtered, and the solvent removed *in vacuo*. The product was further purified by recrystallization from acetone to yield white needles (0.27 g, 73% yield): mp 178-179 °C; ^{1}H NMR (400 MHz, $CDCl_3$) δ 1.50 (6H, q, J = 8 Hz), 3.05 (4H, t, J = 8 Hz), 7.45 (2H, m), 7.58 (4H, m), 8.23 (4H, d, J = 8 Hz); ^{13}C NMR (100 MHz, $CDCl_3$) δ 11.5,

22.8, 114.1, 128.3, 128.8, 130.2, 132.7, 137.2, 146.2, 169.0. HRMS (ESI) *m/z*: Calcd for $C_{24}H_{21}N_2O_2$ 369.1598 $[M + H]^+$, found 369.1603.

4,8-Bis(4-(3,7-dimethyloctyloxy)phenyl)-2,6-diethylbenzo[1,2-*d*;4,5-*d'*]bisoxazole 4.

4-(3,7-Dimethyloctyloxy)phenyl boronic acid. A dry, two-neck round-bottom flask was placed under an argon atmosphere, and charged with 300 mL of dry THF and 9.88 g (30.0 mmol) 4-(3,7-dimethyloctyloxy)-1-bromobenzene. The solution was cooled to -78 °C in a dry ice/acetone bath, 15.0 mL of ^{n}BuLi (2.5 M in hexanes) added drop-wise, and the mixture stirred at -78 °C for one hour. 9.35 g (90.0 mmol) $B(OMe)_3$ was added drop-wise to the solution, stirred at -78 °C for one hour and allowed to warm to room temperature over three hours. The reaction was quenched with 2 M HCl (25 mL) and the mixture extracted with diethyl ether. The combined organic layers were washed with water and brine and dried over $MgSO_4$. The solution was filtered and the solvent removed *in vacuo*. The resulting solid was dried under vacuum overnight to yield an off-white paste that was used without further purification (2.90 g, 35% yield): ^{1}H NMR (400 MHz, $CDCl_3$) δ 0.90 (6H, d, J = 8Hz), 1.00 (3H, d, J = 8 Hz), 1.21-1.88 (10H, comp), 4.09 (2H, m), 7.02 (2H, d, J = 8 Hz), 8.17 (2H, d, J = 8 Hz); ^{13}C NMR (100 MHz, $CDCl_3$) δ 19.9, 22.9, 23.0, 24.9, 28.2, 36.4, 36.5, 37.5, 39.5, 66.4, 114.1, 115.7, 137.6, 162.9.

4,8-Bis(4-(3,7-dimethyloctyloxy)phenyl)-2,6-diethylbenzo[1,2-d;4,5-d']bisoxazole ***4***. Prepared analogously to BBO **3** from BBO **2** (1.00 mmol) and 4-(3,7-dimethyloctyloxy)phenylboronic acid. The product was purified by column chromatography eluting with hexanes/chloroform (3:1 gradient to 1:3) followed by recrystallization from hexanes to yield a white powder (0.54 g, 79% yield): mp 74-76 °C. ^{1}H NMR (400 MHz, $CDCl_3$) δ 0.91 (12H, d, J = 8 Hz), 0.98 (6H, d, J = 8 Hz), 1.2-1.37 (12H, comp), 1.52 (6H, t,

J = 8 Hz), 1.75-1.92 (8H, comp), 3.04 (4H, q, *J* = 8 Hz), 4.11 (4H, m), 7.11 (4H, d, *J* = 8 Hz, 8.21 (4H, d, *J* = 8 Hz); ^{13}C NMR (100 MHz, $CDCl_3$) δ 11.5, 19.9, 22.79, 22.84, 23.0, 25.0, 28.2, 30.1, 36.4, 37.5, 39.5, 66.5, 113.2, 114.8, 125.1, 131.4, 136.8, 146.0, 159.1, 168.6. HRMS (ESI) *m/z*: Calcd for $C_{44}H_{61}N_2O_4$ 681.4626 $[M + H]^+$, found 681.4636.

4,8-Bis(4-dodecylphenyl)-2,6-diethylbenzo[1,2-*d*;4,5-*d'*]bisoxazole 5. Prepared analogously to BBO **3** from BBO **2** (1.00 mmol) and 4-dodecylphenylboronic acid. The product was purified by column chromatography eluting with hexanes/chloroform (3:1 gradient to 1:3) followed by recrystallization from hexanes to yield a white powder (0.59 g, 83% yield): mp 103-105 °C; ^{1}H NMR (400 MHz, $CDCl_3$) δ 0.89 (6H, t, *J* = 8 Hz, 1.28 (36H, comp), 1.47 (6H, t, *J* = 8 Hz), 1.70 (4H, m), 2.70 (4H, t, *J* = 8 Hz), 3.03 (4H, q, *J* = 8 Hz), 7.39 (4H, d, *J* = 8 Hz), 8.15 (4H, d, *J* = 8 Hz); ^{13}C NMR (100 MHz, $CDCl_3$) δ 11.6, 14.4, 22.8, 22.9, 29.6, 29.7, 29.82, 29.87, 29.89, 29.94, 31.7, 32.2, 36.2, 113.9, 128.9, 130.0, 137.0, 143.2, 146.2, 168.8. HRMS (ESI) *m/z*: Calcd for $C_{48}H_{69}N_2O_2$ 705.5354 $[M + H]^+$, found 705.5372.

4,8-Bis(4-*N*,*N*-dibutylaminophenyl)-2,6-diethylbenzo[1,2-*d*;4,5-*d'*]bisoxazole 6. Prepared analogously to BBO **3** from BBO **2** (1.00 mmol) and 4-(*N*,*N*-dibutylamino)phenylboronic acid. The product was purified by column chromatography eluting with 1:1 hexanes/toluene followed by recrystallization from acetone to yield small yellow needles (0.26 g, 60% yield): mp 103-105 °C. ^{1}H NMR (400 MHz, $CDCl_3$) δ 0.99 (6H, t, *J* = 8 Hz, 1.40 (4H, p, *J* = 8 Hz), 1.51 (4H, t, *J* = 8 Hz), 1.65 (4H, m), 3.04 (4H, q, *J* = 8 Hz), 3.36 (4H, t, *J* = 8 Hz), 6.82 (4H, d, *J* = 8 Hz), 8.16 (4H, d, *J* = 8 Hz). ^{13}C NMR (100 MHz, $CDCl_3$) δ 11.7, 14.3, 20.6, 22.8, 29.8, 51.0, 111.7, 113.0, 119.7, 131.0, 136.5, 146.0, 147.8, 168.0. HRMS (ESI) *m/z*: Calcd for $C_{40}H_{55}N_4O_2$ 623.4320 $[M + H]^+$, found 623.4302.

4,8-Bis(9,9-dihexylfluoren-2-yl)-2,6-diethylbenzo[1,2-*d*;4,5-*d'*]bisoxazole 7. Prepared analogously to BBO **3** from BBO **2** (1.00 mmol) and 2-(4,4,5,5-Tetramethyl-1,3,2-dioxaborolan-2-yl)-9,9-dihexylfluorene. The product was purified by column chromatography eluting with hexane/$CHCl_3$ (3:1 gradient to 1:1) followed by recrystallization from hexanes to yield a white solid (0.37 g, 61% yield): mp 157-160 °C; ^{1}H NMR (400 MHz, $CDCl_3$) δ 0.78 (12H, t, J = 8 Hz), 0.86 (8H, m), 1.09-1.17 (24H, comp), 1.55 (6H, t, J = 8 Hz), 2.06 (8H, m), 3.09 (4H, q, J = 8 Hz), 7.33-7.42 (6H, comp), 7.79 (2H, d, J = 8 Hz), 7.91 (2H, d, J = 8 Hz), 8.25(2H, s), 8.29 (2H, d, J = 8 Hz); ^{13}C NMR (100 MHz, $CDCl_3$) δ 11.3, 13.2, 22.86, 22.90, 24.2, 30.1, 31.8, 40.7, 55.3, 114.6, 120.0, 120.1, 123.1, 125.0, 127.0, 127.4, 129.0, 131.4, 137.2, 141.0, 141.1, 146.4, 150.9, 152.6. HRMS (ESI) *m/z*: Calcd for $C_{62}H_{77}N_2O_2$ 881.5980 $[M + H]^+$, found 881.5979.

4,8-Bis(5-dodecylthien-2-yl)-2,6-diethylbenzo[1,2-*d*;4,5-*d'*]bisoxazole 8. A dry, two-neck round-bottom flask was fitted with a reflux condenser, placed under an argon atmosphere, and charged with 0.28 g (0.75 mmol) **2**, 0.70 g (1.67 mmol) 5-dodecyl-2-(trimethylstannyl)thiophene, and 15 mL dry, deoxygenated toluene. The mixture was further deoxygenated for 10 minutes and then charged with 9.1 mg (0.03 mmol) P(^{o}tolyl)$_3$ and 13.7 mg (0.015 mmol) $Pd_2(dba)_3$. The reaction mixture was heated to reflux with stirring under an argon atmosphere for 24 hours, cooled to room temperature, and concentrated *in vacuo*. The crude mixture was dissolved in CH_2Cl_2, passed through a pad of silica gel eluting with CH_2Cl_2, and the solution concentrated *in vacuo*. The product was further purified by recrystallization from hexane to yield small, light-yellow needles (0.51 g, 94% yield): mp 97-99 °C; ^{1}H NMR (400 MHz, $CDCl_3$) δ 0.88 (6H, t, J = 8 Hz), 1.26-1.43 (36H, comp), 1.56 (6H, t, J = 8 Hz), 1.77 (4H, m), 2.91 (4H, t, J = 8 Hz), 3.11 (4H, q, J = 8 Hz), 6.90 (2H, d, J =

4 Hz), 8.11 (2H,d, J = 8 Hz); ^{13}C NMR (100 MHz, $CDCl_3$) δ 11.4, 14.4, 22.89, 22.92, 29.4, 29.58, 29.64, 29.82, 29.87, 29.90, 30.4, 32.0, 32.1, 107.8, 124.8, 128.8, 131.9, 135.4, 144.5, 148.2, 168.4. HRMS (ESI) *m/z*: Calcd for $C_{44}H_{65}N_2O_2S_2$ 717.4482 $[M + H]^+$, found 717.4488.

5-Dodecyl-2-(triethoxymethyl)thiophene. A dry, three-neck round-bottom flask was equipped with a reflux condenser and placed under an argon atmosphere. The flask was charged with 8.28 g (25.0 mmol) of 2-bromo-5-dodecylthiophene and 25 mL dry diethyl ether. 13.8 mL (27.5 mmol) of ^{i}PrMgCl (2.0 M in ether) was added drop-wise, the reaction mixture heated to reflux with stirring for 24 hours, then cooled to room temperature. A solution of 5.53 g (28.8 mmol) of tetraethylorthocarbonate in 20 mL of dry diethyl ether was added drop-wise and the mixture heated to reflux with stirring overnight. The mixture was allowed to cool to room temperature and poured into a saturated aqueous solution of NH_4Cl. The layers were separated and the aqueous layer was extracted with ether. The combined organic layers washed with water and brine and dried over $MgSO_4$. The solution was filtered and the solvent removed *in vacuo*. The low-boiling impurities were removed by vacuum distillation and the resulting red oil was used without further purification (5.05 g, 51% yield): ^{1}H NMR (400 MHz, $CDCl_3$) δ 0.89 (3H, t, J = 8 Hz), 1.20 (9H, t, J = 8 Hz), 1.21-1.40 (18H, comp), 1.67 (2H, m), 2.77 (3H, t, J = 8 Hz), 3.46 (2H, q, J = 8 Hz), 6.64 (1H, d, J = 4 Hz), 6.98 (1H, d, J = 4 Hz); ^{13}C NMR (100 MHz, $CDCl_3$) 14.3, 15.1, 22.9, 29.3, 29.5, 29.6, 29.84, 29.86, 29.88, 30.4, 31.7, 32.1, 58.1, 113.2, 123.4, 126.7, 139.0, 147.0. HRMS (ESI) *m/z*: Calcd for $C_{23}H_{42}NaO_3S$ 421.2747 $[M + Na]^+$, found 421.2753.

2,6-Bis(5-dodecylthien-2-yl)benzo[1,2-*d*;4,5-*d'*]bisoxazole 9. A dry Schlenk flask was placed under an argon atmosphere and charged with 1.59 g (4.00 mmol) 5-dodecyl-2-

(triethoxymethyl)thiophene, 27 mg (0.050 mmol) $Y(OTf)_3$, and 1 mL THF. The solution was deoxygenated for 20 minutes then heated to 55 °C with stirring. Concurrently, a dry 5 mL pear-bottom flask was place under an argon atmosphere and 1 mL DMSO was added and deoxygenated for 20 minutes. The pear-flask was charged with 0.21 g (1.00 mmol) DAHQ and 0.164 g (2.10 mmol) pyridine and the resulting solution added drop-wise to the THF solution at 55 °C. After three hours, the reaction was diluted with 3 mL THF and stirred at 55 °C overnight. The mixture was allowed to cool to room temperature and diluted with methanol. The resulting precipitate was filtered and rinsed with methanol. The product was purified by recrystallization from $CHCl_3$ to yield a yellow solid (0.48 g, 73% yield): mp 190-192 °C; ^{1}H NMR (400 MHz, $CDCl_3$) δ 0.89 (6H, t, J = 8 Hz), 1.27-1.41 (36H, comp), 1.75 (4H, p, J = 8 Hz), 2.90 (4H, t, J = 8 Hz), 6.89 (2H, d, J = 4 Hz), 7.75 (2H, d, J = 4 Hz), 7.80 (2H, s); ^{13}C NMR (100 MHz, $CDCl_3$) δ 14.3, 22.9, 29.3, 29.6, 29.76, 29.85, 29.89, 30.7, 31.7, 32.2, 100.6, 125.9, 127.0, 130.4, 140.5, 148.6, 152.6, 160.6. HRMS (ESI) *m/z*: Calcd for $C_{38}H_{57}N_2O_2S_2$ 661.3832 $[M + H]^+$, found 661.3837.

4,8-Dibromo-2,6-bis-(5-dodecylthien-2-yl)benzo[1,2-*d*;3,4-*d'*]bisoxazole 10. A dry Schlenk flask was placed under an argon atmosphere and charged with 4.78 g (12.0 mmol) 5-dodecyl-2-(triethoxymethyl)thiophene, 5 mL dry DMA, and 5 mL dry THF. The mixture was deoxygenated for 20 minutes, 0.12 g (0.20 mmol) $Yb(OTf)_3$ was added, and the mixture heated to 55 °C. 1.19 g (4.00 mmol) of freshly prepared Br-DAHQ was added portion-wise, the reaction diluted with 5 mL THF after three hours, and stirred at 55 °C overnight. The mixture was allowed to cool to room temperature and diluted with methanol. The resulting precipitate was filtered and rinsed with methanol. The product was purified by recrystallization from $CHCl_3$ to yield pale-yellow needles (2.45 g, 75% yield): mp 190-192

°C; ^{1}H NMR (400 MHz, $CDCl_3$) δ 0.90 (6H, t, *J* = 8 Hz), 1.29-1.43 (36H, comp), 1.77 (4H, p, *J* = 8 Hz), 2.92 (4H, t, *J* = 8 Hz), 6.90 (2H, d, *J* = 8 Hz), 7.87 (2H, d, *J* = 4 Hz); ^{13}C NMR (100 MHz, $CDCl_3$) δ 14.3, 22.9, 29.3, 29.55, 29.57, 29.7, 29.85, 29.86, 29.89, 30.7, 31.6, 32.2, 91.3, 125.9, 126.0, 131.8, 139.8, 146.9, 153.9, 160.7. HRMS (ESI) *m/z*: Calcd for $C_{40}H_{55}Br_2N_2O_2S_2$ 817.2046 $[M + H]^+$, found 817.2066.

4-Dodecyl-1-(triethoxymethyl)benzene

2-(4-dodecylphenyl)-1,3-dithiane. A dry three-neck round-bottom flask was equipped with a reflux condenser and placed under an argon atmosphere. The flask was charged with 7.05 g (25.6 mmol) 2-(4-bromophenyl)-1,3-dithiane, 60 mL dry, deoxygenated ether, and 0.21g (0.256 mmol) $Pd(dppf)Cl_2 \cdot CH_2Cl_2$. The flask was placed in an ice/water bath and 30.7 mL (30.7 mmol) dodecylmagnesium bromide (1.0 M in ether) was added drop-wise. The mixture was allowed to warm to room temperature and then heated to reflux with stirring overnight. The mixture was allowed to cool to room temperature, poured into cold 1 M HCl, and the layers were separated. The aqueous layer was extracted with ether, and the combined organic layers washed with 1 M HCl, water, and brine and dried over $MgSO_4$. The solution was filtered and the solvent was removed *in vacuo*. The crude product was purified by recrystallization from isopropanol to yield ivory-colored needles (9.32 g, 93% yield): mp 52-54 °C; ^{1}H NMR (400 MHz, $CDCl_3$) δ 0.88 (3H, t, *J* = 8 Hz), 1.25-1.35 (18H, comp), 1.60 (2H, p, *J* = 8 Hz), 1.92 (1H, m), 2.16 (1H, m), 2.57 (2H, t, *J* = 8 Hz), 2.90 (2H, dt), 3.06 (2H, td), 5.15 (1H, s), 7.14 (2H, d, *J* = 8 Hz), 7.36 (2H, d, *J* = 8 Hz); ^{13}C NMR (100 MHz, $CDCl_3$) δ 14.3, 22.8, 25.3, 29.49, 29.50, 29.65, 29.73, 29.78, 29.8, 31.5, 32.1, 32.3, 51.4, 127.7, 128.9, 136.4, 143.5. HRMS (APCI) *m/z*: Calcd for $C_{22}H_{37}S_2$ 365.2331 $[M + H]^+$, found 365.2341.

4-Dodecyl-1-(triethoxymethyl)benzene. A dry, two-neck round-bottom flask was placed under an argon atmosphere and charged with 1.82 g (5.00 mmol) 2-(4-dodecylphenyl)-1,3-dithiane, 1.16 g (10.0 mmol) TMEDA and 50 mL dry THF. The flask was cooled to -78 °C in a dry ice/acetone bath and 2.2 mL (5.5 mmol) of ^{n}BuLi (2.5 M in hexane) was added drop-wise. The flask was stirred for one hour at -78 °C and 0.55 mL (6.00 mmol) dimethyl disulfide was added in one portion. The mixture was stirred for 30 minutes at -78 °C and allowed to warm to room temperature over three hours. The reaction was quenched with water and extracted with ether. The combined organic layers were washed with water and brine and dried over Na_2SO_4. The solution was filtered and concentrated *in vacuo*. The remaining residue was dried under vacuum with stirring overnight. The flask was back-filled with argon and charged with 30 mL THF, 6 mL ethanol, 1.05 mL (10.0 mmol) $^{i}Pr_2NH$, and 3.60 mL (27.5 mmol) 2,4,6-collidine. A solution of 4.25 g (25.0 mmol) $AgNO_3$ in dry CH_3CN was added in one portion and the mixture stirred vigorously for 24 hours. The reaction was quenched by stirring with brine for six hours and the solids were filtered and rinsed with large portions of ether. The two layers of the filtrate were separated and the organic layer was washed with water (3x) and brine and dried over Na_2SO_4. The solution was filtered and the solvents were removed *in vacuo*. Low boiling impurities were removed by vacuum distillation and the dark yellow oil was used without further purification (1.64 g, 84% yield): ^{1}H NMR (400 MHz, $CDCl_3$) δ 0.89 (3H, t, J = 8 Hz), 1.78 (9H, t, J = 8 Hz), 1.26-1.35 (18H, comp), 1.62 (2H, m), 2.61, (2H, t, J = 8 Hz), 3.65 (6H, q, J = 8 Hz), 7.16 (2H, d, J = 8 Hz), 7.50 (2H, d, J = 8 Hz); ^{13}C NMR (100 MHz, $CDCl_3$) δ 14.3, 15.1, 22.8, 29.51, 29.52, 29.65, 29.74, 29.80, 29.81, 29.83, 31.5, 32.1, 35.9, 57.6, 114.0, 127.4, 128.0, 135.5, 143.4. HRMS (ESI) *m/z*: Calcd for $C_{25}H_{44}NaO_3$ 415.3183 $[M + Na]^+$, 415.3185.

2,6-Bis(4-dodecylphenyl)benzo[1,2-*d*;3,4-*d'*]bisoxazole 11. Prepared and isolated analogously to BBO **9** from 0.11g (0.50 mmol) DAHQ, 0.63 g (1.60 mmol) 4-dodecyl-1-(triethoxymethyl)benzene, and 43.5 mg $Yb(OTf)_3$. The product was purified by recrystallization from THF to yield white needles (0.21 g, 65% yield): mp >260 °C; ^{1}H NMR (400 MHz, $CDCl_3$) δ 0.90 (6H, t, *J* = 8 Hz), 1.28-1.37 (36H, comp 1.69 (4H, m), 2.71 (4H, t, *J* = 8 Hz), 7.35 (4H, d, *J* = 8 Hz), 7.89 (2H, s), 8.19 (4H, d, *J* = 8 Hz); ^{13}C NMR (100 MHz, $CDCl_3$) 14.2, 22.8, 29.48, 29.50, 29.6, 29.7, 29.81, 29.84, 31.3, 32.1, 36.3, 100.9, 124.9, 127.9, 129.2, 140.7, 147.4, 148.8, 164.7. HRMS (ESI) *m/z*: Calcd for $C_{44}H_{61}N_2O_2$ 649.4728 $[M + H]^+$, found 649.4730.

4,8-Dibromo-2,6-bis(4-dodecylphenyl)[1,2-*d*;3,4-*d'*]bisoxazole 12. Prepared and isolated analogously to BBO **10** from 0.15 g (0.50 mmol) Br-DAHQ, 0.59 g (1.50 mmol) 4-dodecyl-1-(triethoxymethyl)benzene except the reaction mixture was heated to 65 °C. The product was purified by recrystallization from toluene (hot filter, charcoal) to yield white needles (0.27 g, 68% yield): mp 154-156 °C; ^{1}H NMR (400 MHz, $CDCl_3$) δ 0.88 (6H, t, *J* = 8 Hz), 1.26-1.36 (36H, comp), 1.67 (4H, m), 2.70 (4H, t, *J* = 8 Hz), 7.35 (4H, d, *J* = 8 Hz), 8.25 (4H, d, *J* = 8 Hz); ^{13}C NMR (100 MHz, $CDCl_3$) δ 22.8, 29.46, 29.51, 29.6, 29.7, 29.8, 31.2, 32.1, 36.3, 91.8, 123.9, 128.3, 128.4, 129.2, 129.3, 139.9, 147.1, 148.2, 164.9. HRMS (APCI) *m/z*: Calcd for $C_{44}H_{59}Br_2N_2O_2$ 807.2918 $[M + H]^+$, found 807.2922.

4,8-Bis-(4-dodecylphenyl)-2,6-bis-(5-dodecylthien-2-yl)benzo[1,2-*d*;3,4-*d'*]bisoxazole 13. Prepared and isolated analogously to BBO **7** from BBO **10** (0.75 mmol) and 4-dodecylphenylboronic acid. The crude product was dissolved in $CHCl_3$, passed through a pad of silica gel eluting with $CHCl_3$, and the solution concentrated *in vacuo*. The product was further purified by recrystallization from $CHCl_3$ to yield a bright yellow solid

(0.72 g, 84% yield): mp 94-96 °C; ^{1}H NMR (400 MHz, $CDCl_3$) δ 0.91 (12H, comp), 1.29-1.46 (72H, comp), 1.74 (8H, comp), 2.75 (4H, t, *J* = 8 Hz), 2.88 (4H, t, *J* = 8 Hz), 6.85 (2H, d, *J* = 4 Hz), 7.43 (4H, d, *J* = 8 Hz), 7.76 (2H, d, *J* = 4 Hz), 8.29 (4H, d, *J* = 8 Hz); ^{13}C NMR (100 MHz, $CDCl_3$) δ 14.4, 22.92, 22.93, 29.3, 29.57, 29.58, 29.61, 29.75, 29.77, 29.84, 29.86, 29.89, 29.94, 29.95, 30.6, 31.68, 31.73, 32.14, 32.16, 36.2, 113.7, 125.6, 127.1, 128.8, 130.0, 130.3, 138.3, 143.2, 146.2, 152.1, 159.8. HRMS (ESI) *m/z*: Calcd for $C_{76}H_{113}N_2O_2S_2$ 1149.8238 $[M + H]^+$, found 1149.8229.

4,8-Bis(5-dodecylthien-2-yl)-2,6-bis(4-dodecylphenyl)[1,2-*d*;3,4-*d*']bisoxazole 14. Prepared and isolated analogously to BBO **8** from 0.32 g (0.40 mmol) BBO **12** and 0.38 g (0.92 mmol) 5-dodecyl-2-(trimethylstannyl)thiophene. The product was purified by recrystallization from ethyl acetate to yield a yellowish-orange powder (0.40 g, 87% yield): mp 97-100 °C; ^{1}H NMR (400 MHz, $CDCl_3$) δ 0.89 (12H, comp), 1.25-1.51 (72H, comp) 1.70 (4H, p, *J* = 8 Hz), 1.82 (4H, p, *J* = 8 Hz), 2.73 (4H, t, *J* = 8 Hz), 2.98 (4H, t, *J* = 8 Hz), 6.80 (2H, d, *J* = 3 Hz), 7.39 (4H, d, *J* = 8 Hz), 8.31 (4H, d, *J* = 8 Hz), 8.33 (2H, d, *J* = 4 Hz); ^{13}C (100 MHz, $CDCl_3$) δ 14.2, 22.8, 29.44, 29.47, 29.52, 29.63, 29.68, 29.77, 29.83, 29.85, 29.9, 30.5, 31.3, 32.0, 32.1, 36.3, 108.1, 124.8, 124.9, 128.0, 129.1, 129.2, 132.2, 136.8, 144.6, 147.2, 148.2, 163.6. HRMS (APCI) *m/z*: Calcd for $C_{76}H_{113}N_2O_2S_2$ 1149.8238 $[M + H]^+$, found 1149.8259.

2,4,6,8-Tetra(5-dodecylthien-2-yl)[1,2-*d*;3,4-*d*']bisoxazole 15. Prepared and isolated analogously to BBO **8** from 0.41 g (0.50 mmol) BBO **10** and 0.47 g (2.25 mmol) 5-dodecyl-2-(trimethylstannyl)thiophene. The product was purified by recrystallization from ethyl acetate to yield a dark yellow powder (0.55 g, 94% yield): mp 78-80 °C; ^{1}H NMR (400 MHz, $CDCl_3$) δ 0.88 (12H, t, *J* = 8 Hz), 1.27-1.45 (72H, comp), 1.78 (8H, comp), 2.93 (8H,

comp), 6.90 (2H, d, J = 4 Hz), 6.94 (2H, d, J = 4 Hz), 7.86 (2H, d, J = 4 Hz), 8.25 (2H, d, J = 4 Hz); ^{13}C NMR (100 MHz, $CDCl_3$) δ 14.3, 22.9, 29.26, 29.4, 29.5, 29.6, 29.7, 29.80, 29.82, 29.85, 30.4, 30.6, 31.7, 31.95, 32.08, 107.6, 124.8, 125.7, 127.0, 129.0 130.4, 131.9, 136.5, 144.2, 148.2, 152.3, 159.4. HRMS (APCI) *m/z*: Calcd for $C_{72}H_{109}N_2O_2S_4$ 1161.7366 $[M + H]^+$, found 1161.7346.

2,4,6,8-Tetra(4-dodecylphenyl)[1,2-*d*:3,4-*d*']bisoxazole 16. Prepared and isolated similar to **7** from 0.32 g (0.40 mmol) **12** and 0.29 g (2.50 mmol) of 4-dodecylphenylboronic acid. The crude product was dissolved in $CHCl_3$, passed through a pad of silica gel eluting with $CHCl_3$, and the solution concentrated *in vacuo*. The product was purified by recrystallization from ethyl acetate to yield white needles (0.34 g, 60% yield): mp 112-113 °C; ^{1}H NMR (400 MHz; $CDCl_3$) δ 0.89 (12H, comp), 1.27-1.45 (72H, comp), 1.64 (4H, m), 1.74 (4H, m), 2.68 (4H, t, J = 8 Hz), 2.75 (4H, t, J = 8 Hz), 7.31 (4H, d, J = 8 Hz), 7.44 (4H, d, J = 8 Hz), 8.21 (4H, d, J = 8 Hz), 8.35 (4H, d, J = 4 Hz); ^{13}C NMR (100 MHz; $CDCl_3$) δ 14.3, 22.85, 22.86, 29.45, 29.52, 29.54, 29.65, 29.69, 29.75, 29.78, 29.80, 29.82, 29.83, 29.9, 31.4, 31.6, 32.08, 32.10, 36.16, 36.21, 114.0, 124.8, 127.9, 128.8, 129.0, 130.1, 130.2, 138.4, 143.2, 146.4, 147.0. HRMS (APCI) *m/z*: Calcd for $C_{80}H_{117}N_2O_2$ 1137.9110 $[M + H]^+$, found 1137.9139.

3.5.3 Computational Details

All of the calculations on these oligomers studied in this work were studied using the Gaussian 03W with the GaussView 4 GUI interface program package. All electronic ground states geometries were optimized using density functional theory (DFT) employing an SVP functional and a 6-31G* basis set. All computations were performed using Gaussian 09 through the National Science Foundation's Extreme Science and Engineering Discovery

Environment (XSEDE) and San Diego Supercomputer Center's Trestles Cluster. Excited states were generated through time dependent density functional theory (TDDFT) applied to the optimized ground state for each oligomer. The HOMO, LUMO, band gap, first ten excited states, and UV-Vis simulations were generated from these excited computations.

3.6 Acknowledgements

We acknowledge the donors of the Petroleum Research Fund for support of this work. We also thank the 3M Foundation and the National Science Foundation (DMR-0846607) for partial support of this work. We thank Kamel Harrata and the Mass Spectroscopy Laboratory Iowa State University (ISU) for analysis of our compounds. We thank Atta Gueye, Dr. Elena Sheina, and Dr. Christopher Brown of Plextronics for providing UPS measurements. We thank Scott Meester for the synthesis of 1-bromo-4-(3,7-dimethyloctyloxy)benzene. We also thank Dr. William Jenks (ISU), Dr. Jared Mike (Texas A&M University) and Dr. Jeremy Intemann (University of Wisconsin-Green Bay) for helpful discussions on this research.

3.7 Supporting Information

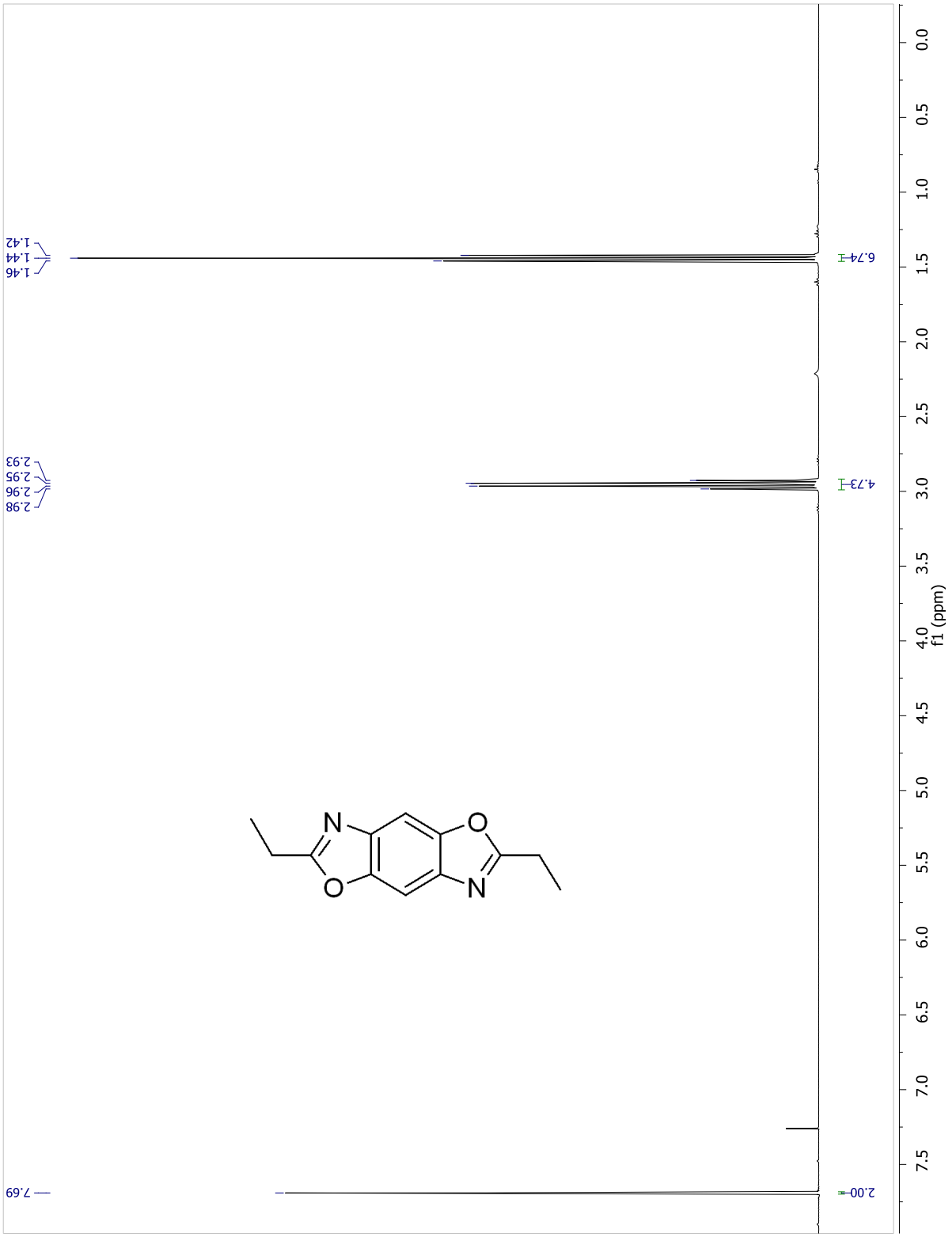

Figure S3.1. ^{1}H NMR spectrum of **1.**

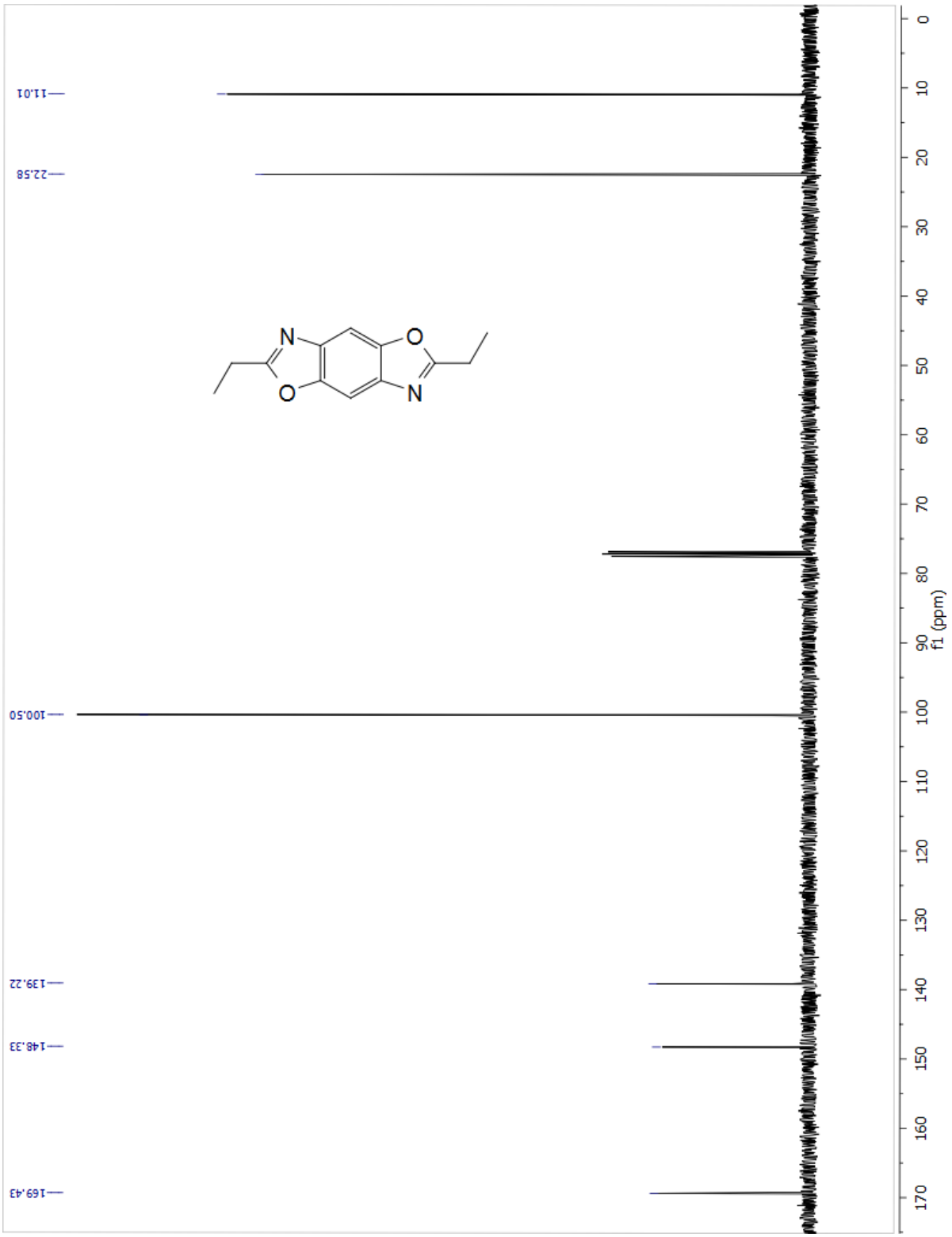

Figure S3.2. ^{13}C NMR spectrum of **1.**

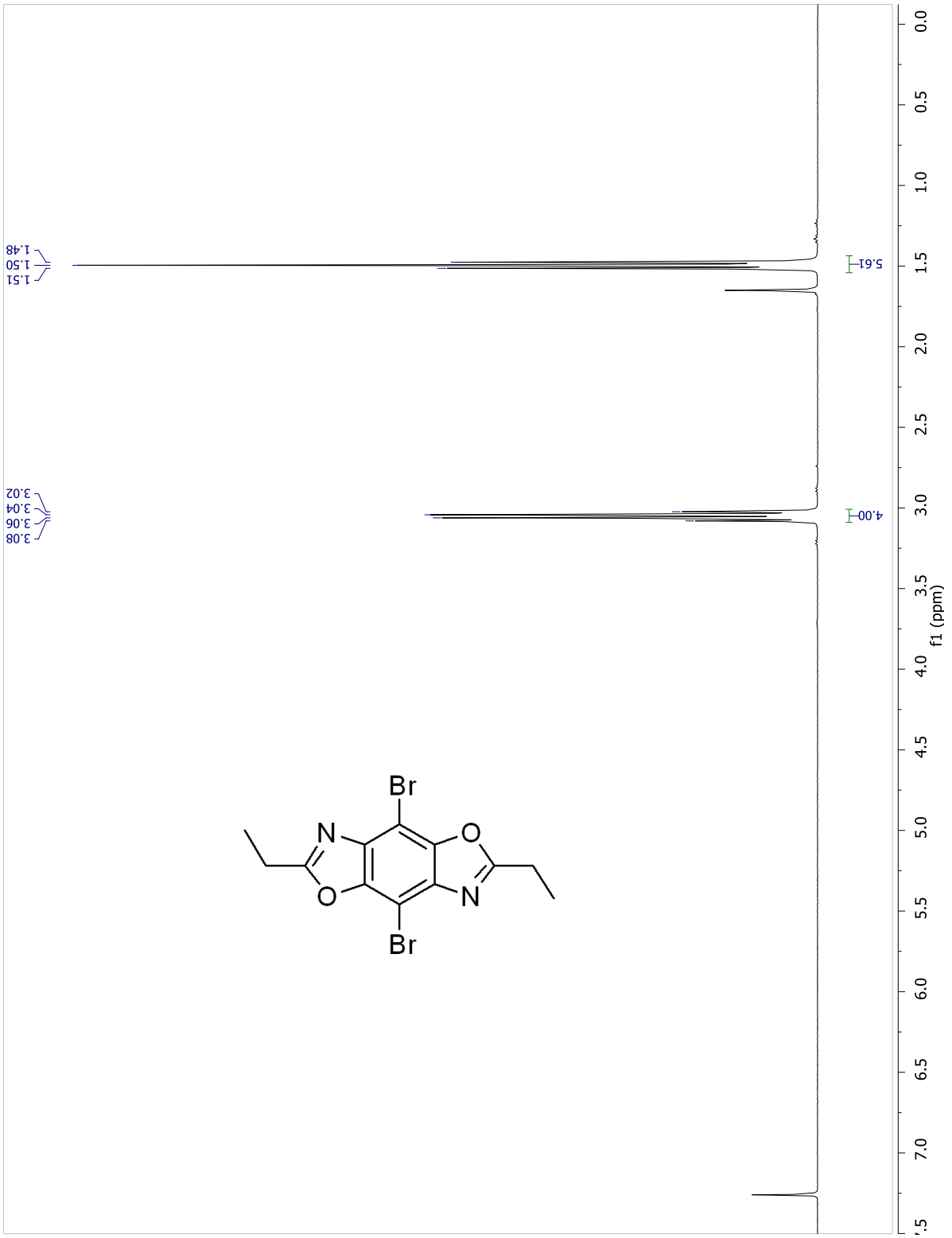

Figure S3.3. ^{1}H NMR spectrum of **2.**

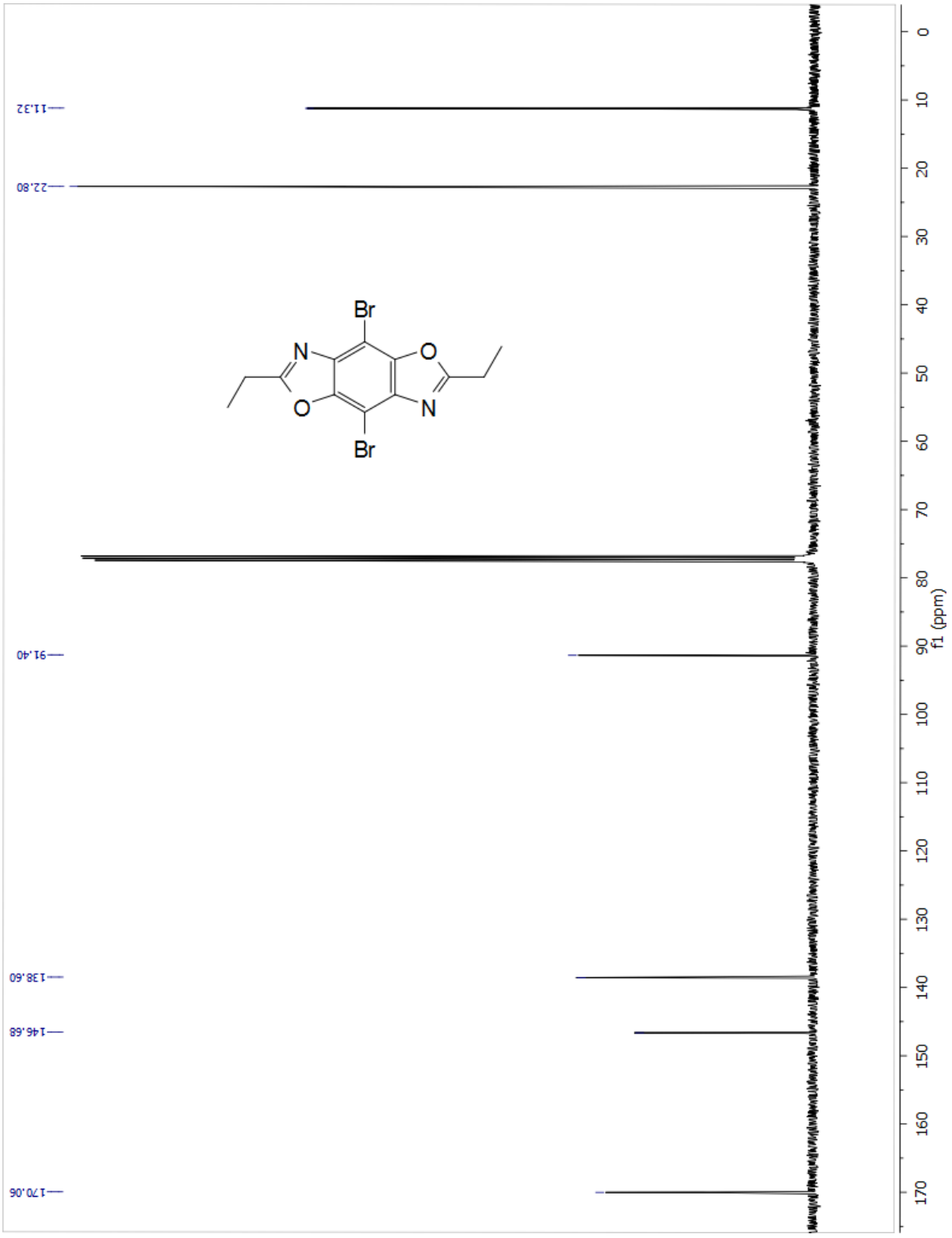

Figure S3.4. ^{13}C NMR spectrum of **2.**

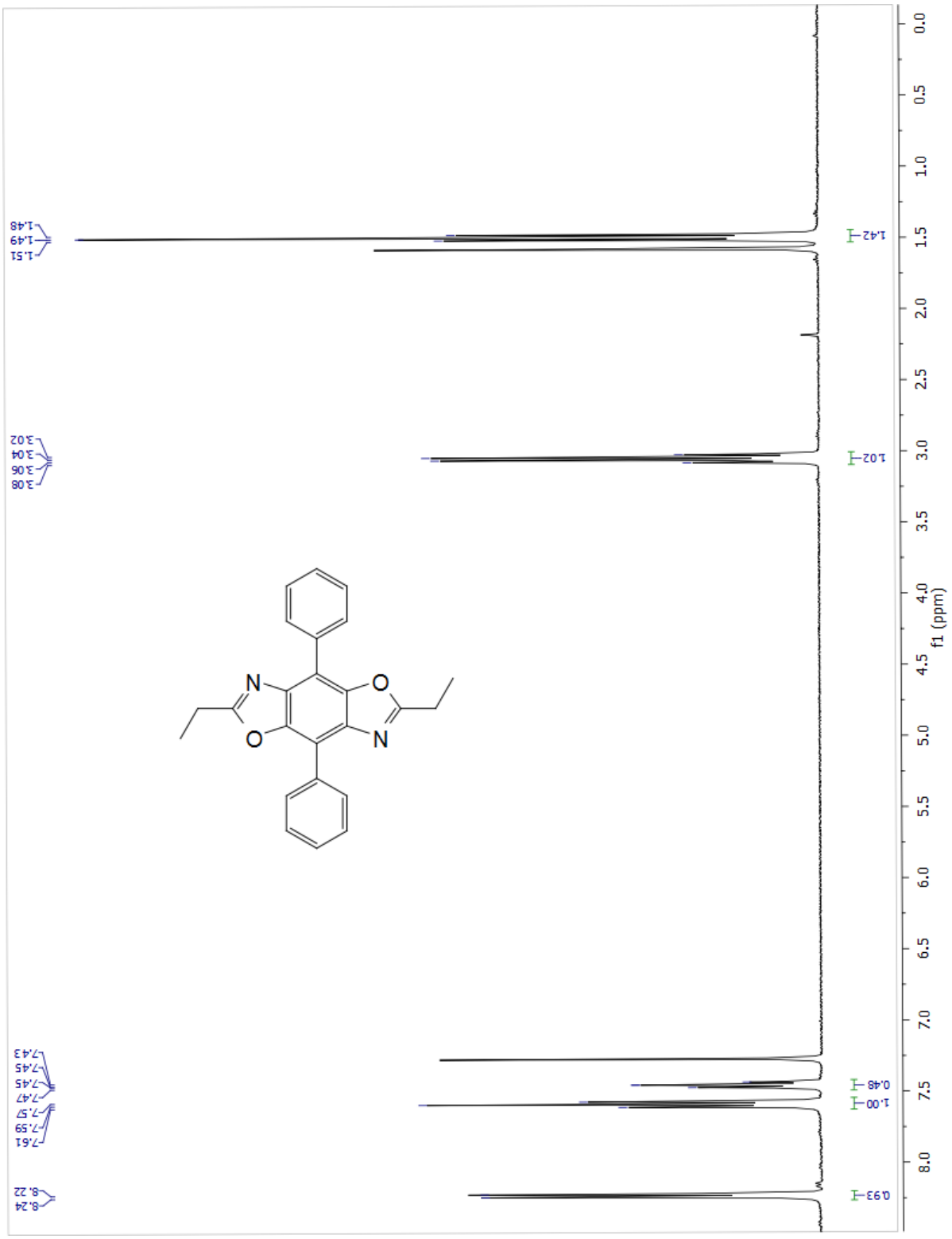

Figure S3.5. ^{1}H NMR spectrum of **3**.

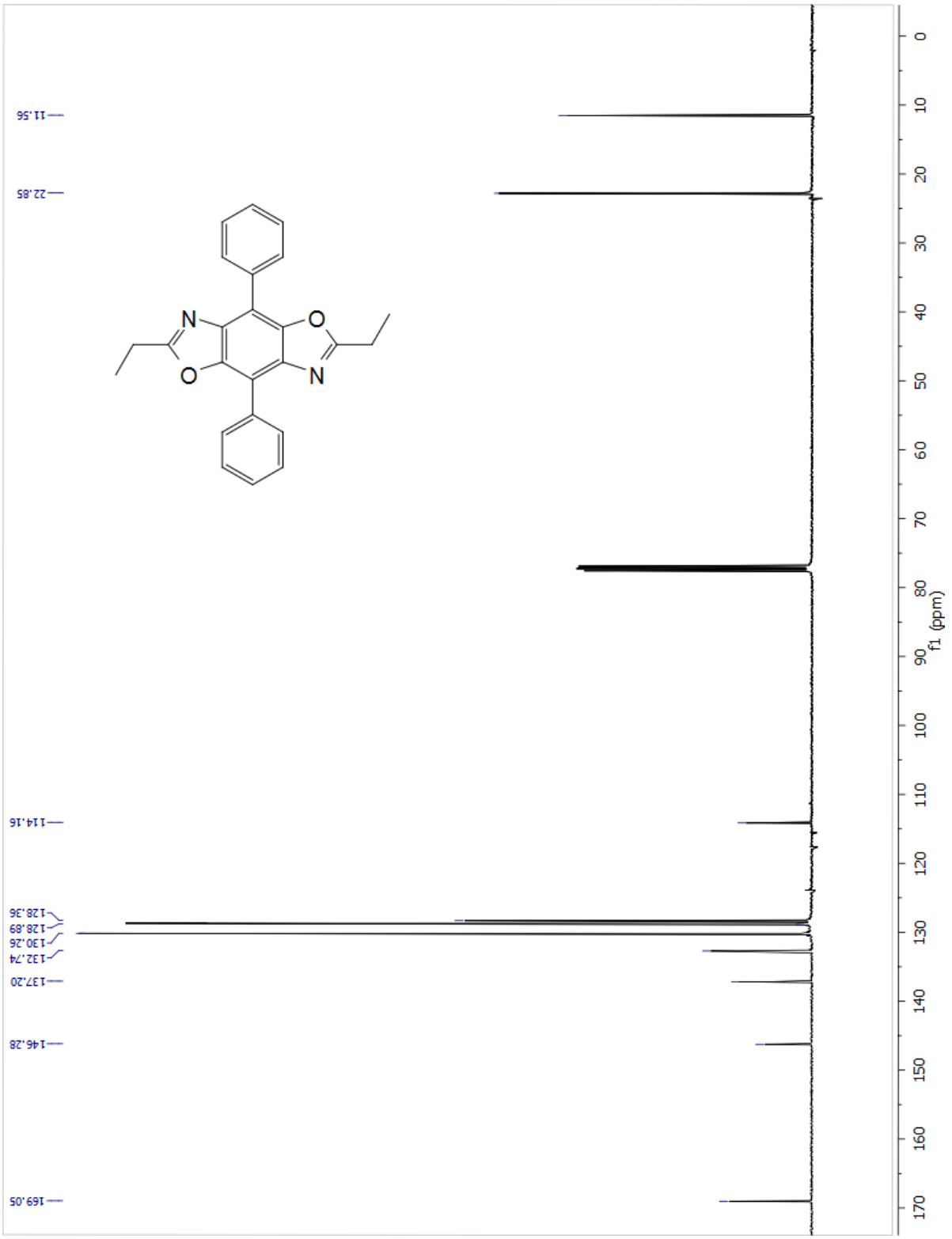

Figure S3.6. ^{13}C NMR spectrum of **3**.

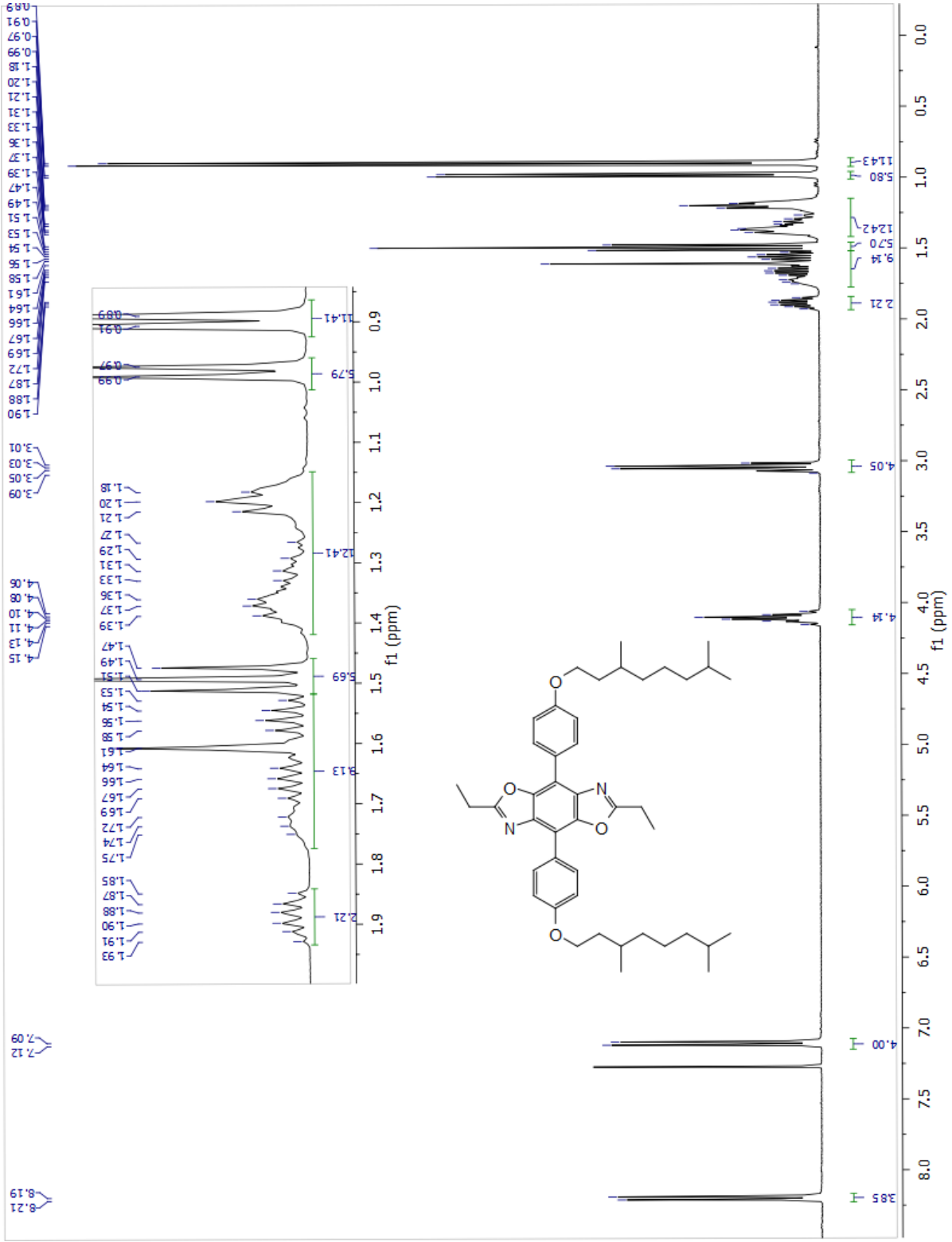

Figure S3.7. ^{1}H NMR spectrum of **4**.

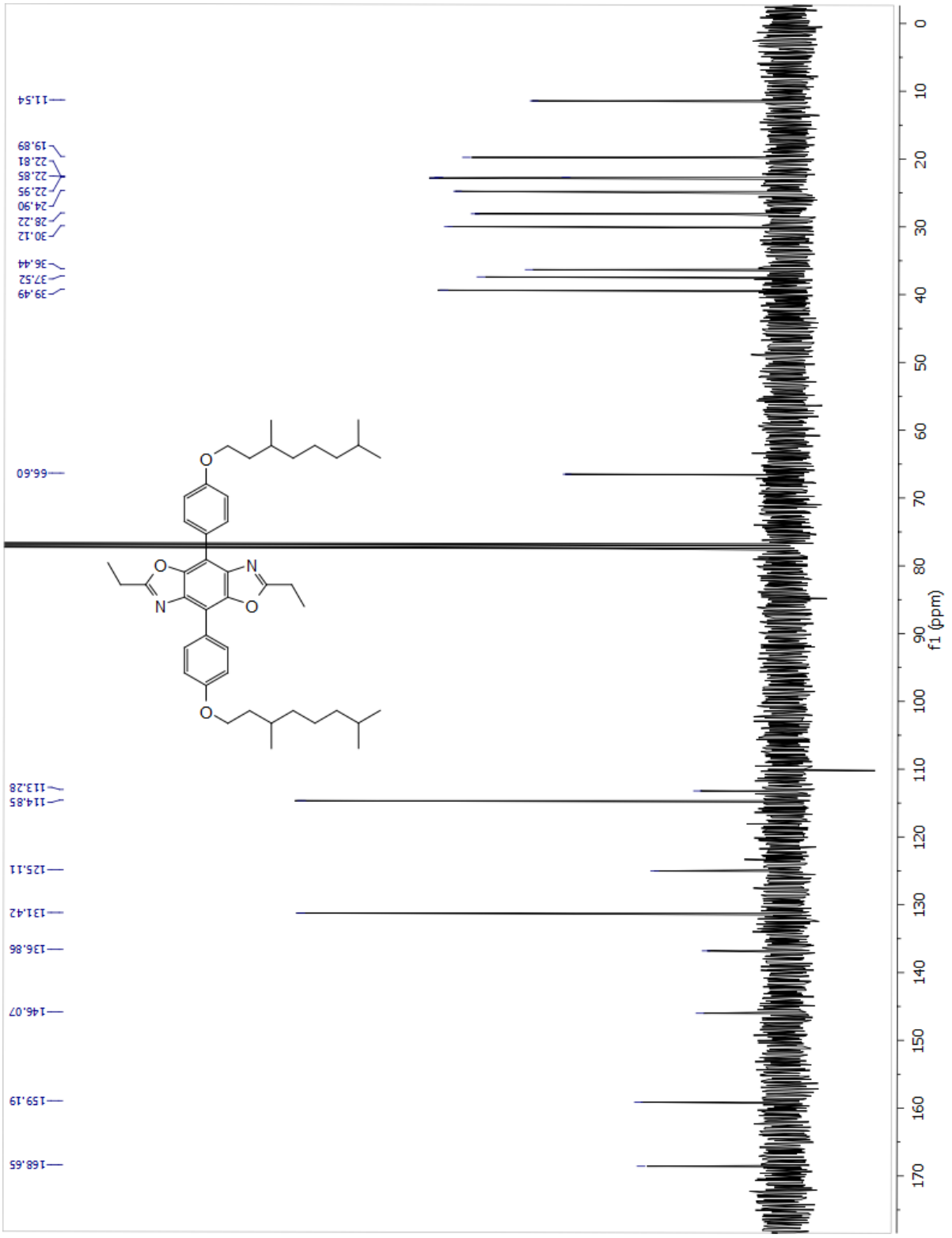

Figure S3.8. ^{13}C NMR spectrum of **4**.

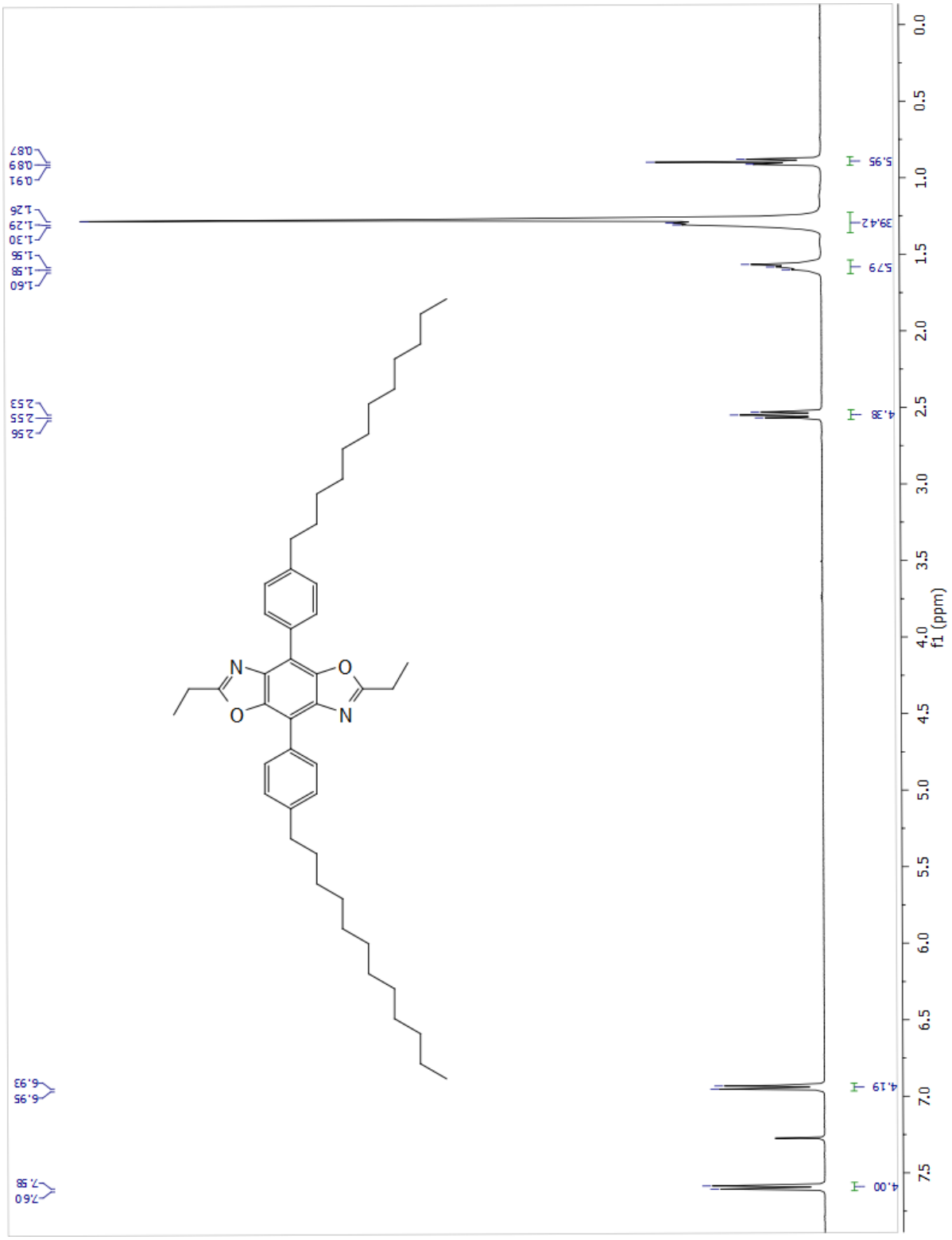

Figure S3.9. ^{1}H NMR spectrum of **5**.

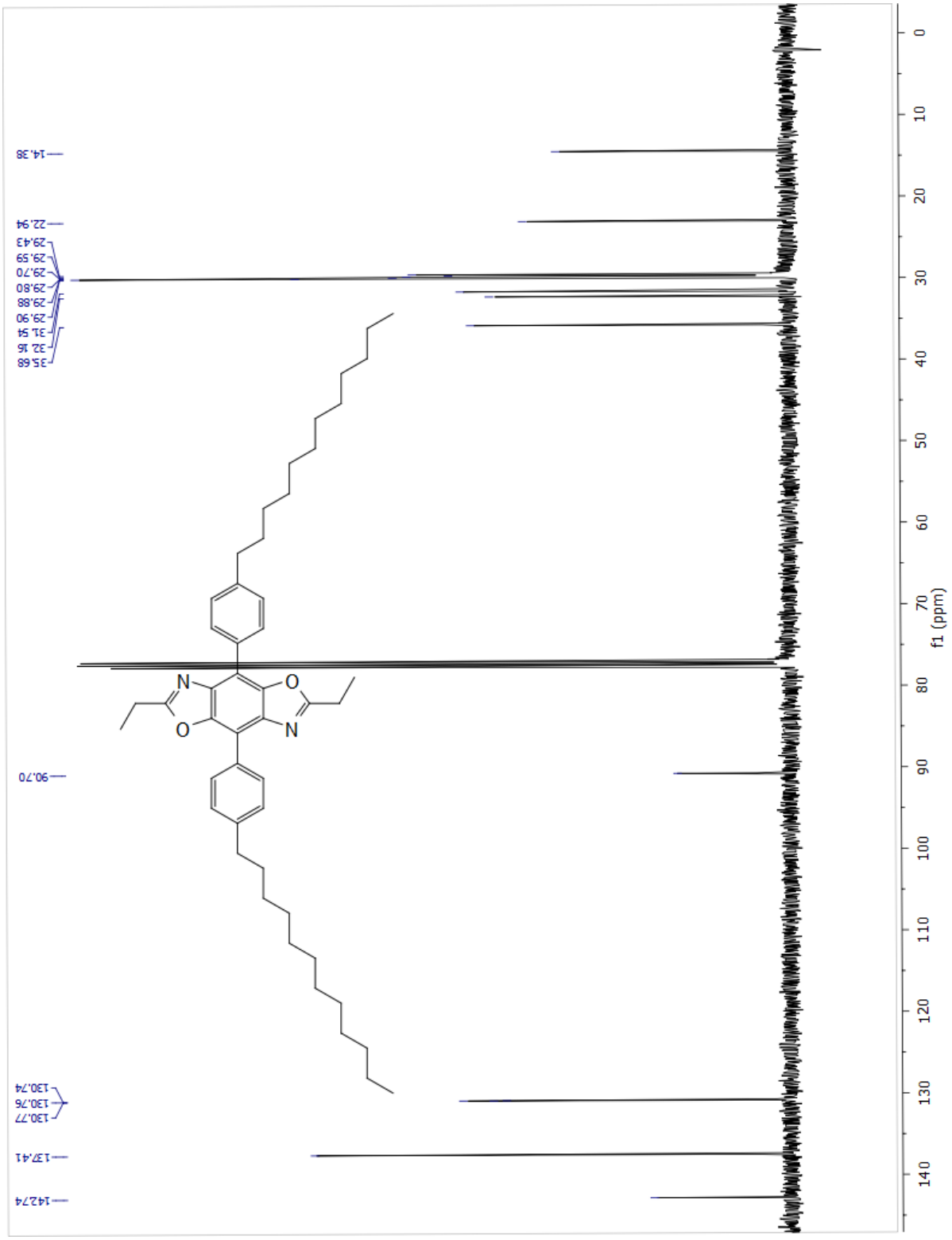

Figure S3.10. ^{13}C NMR spectrum of **5**.

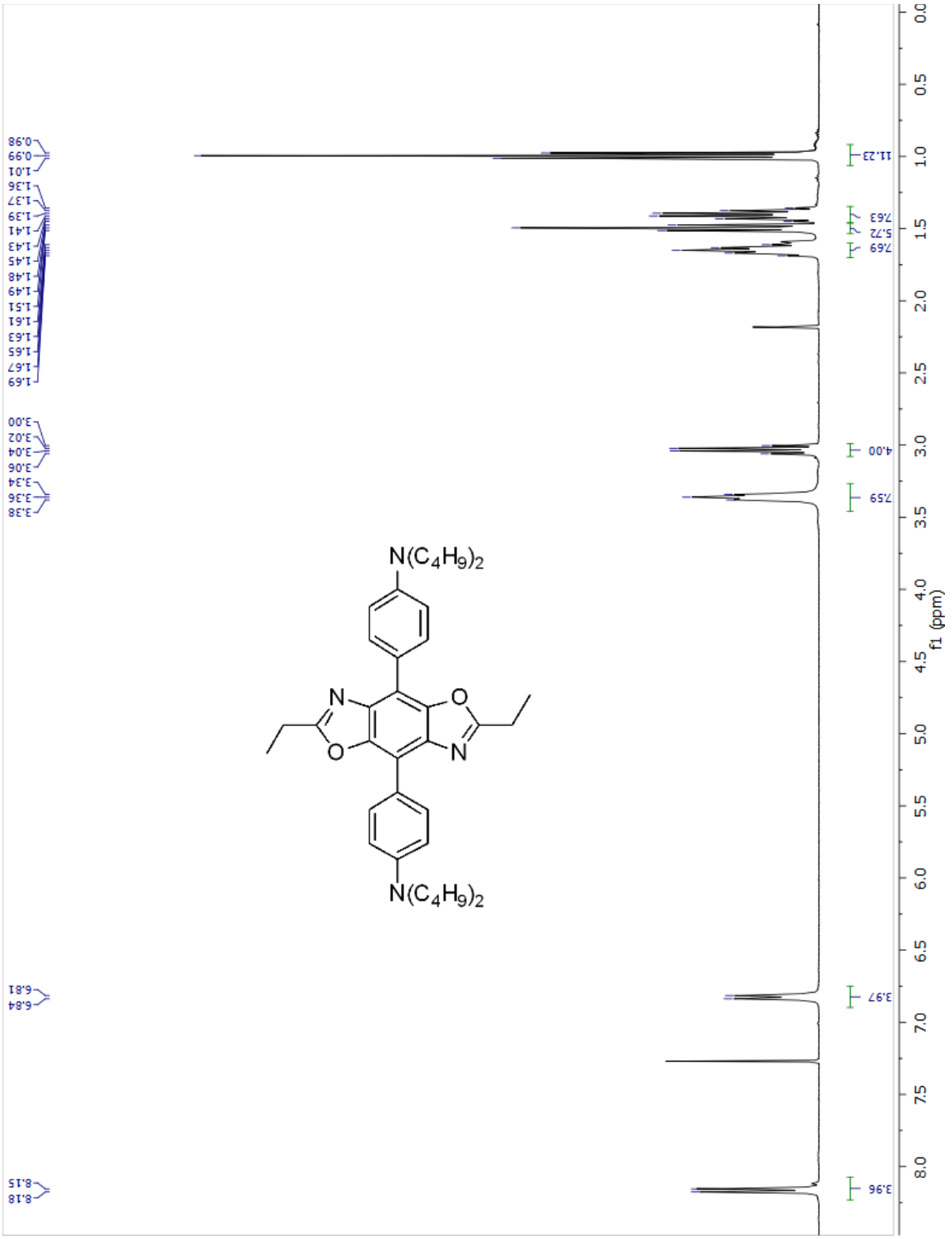

Figure S3.11. ^{1}H NMR spectrum of **6**.

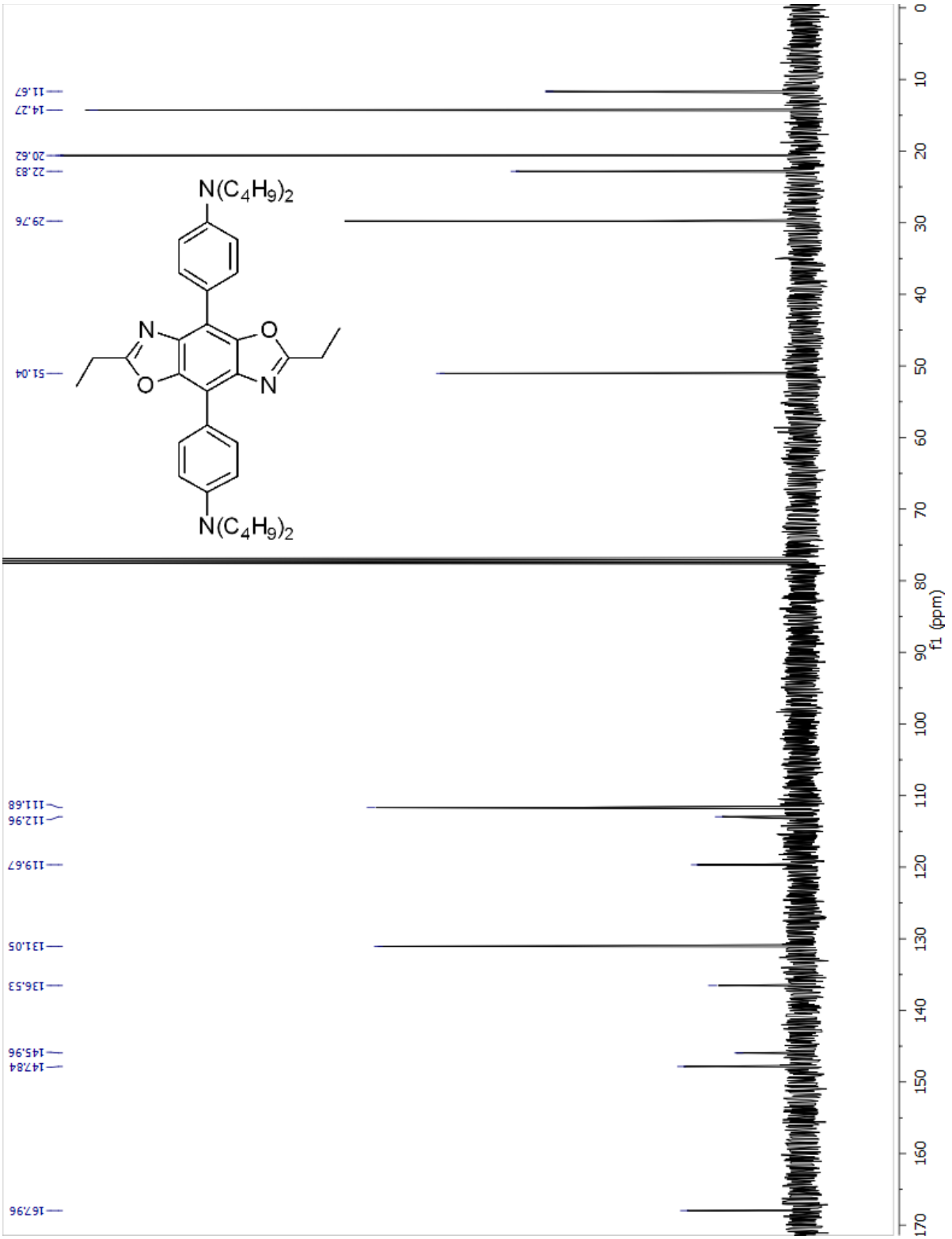

Figure S3.12. ^{13}C NMR spectrum of **6**.

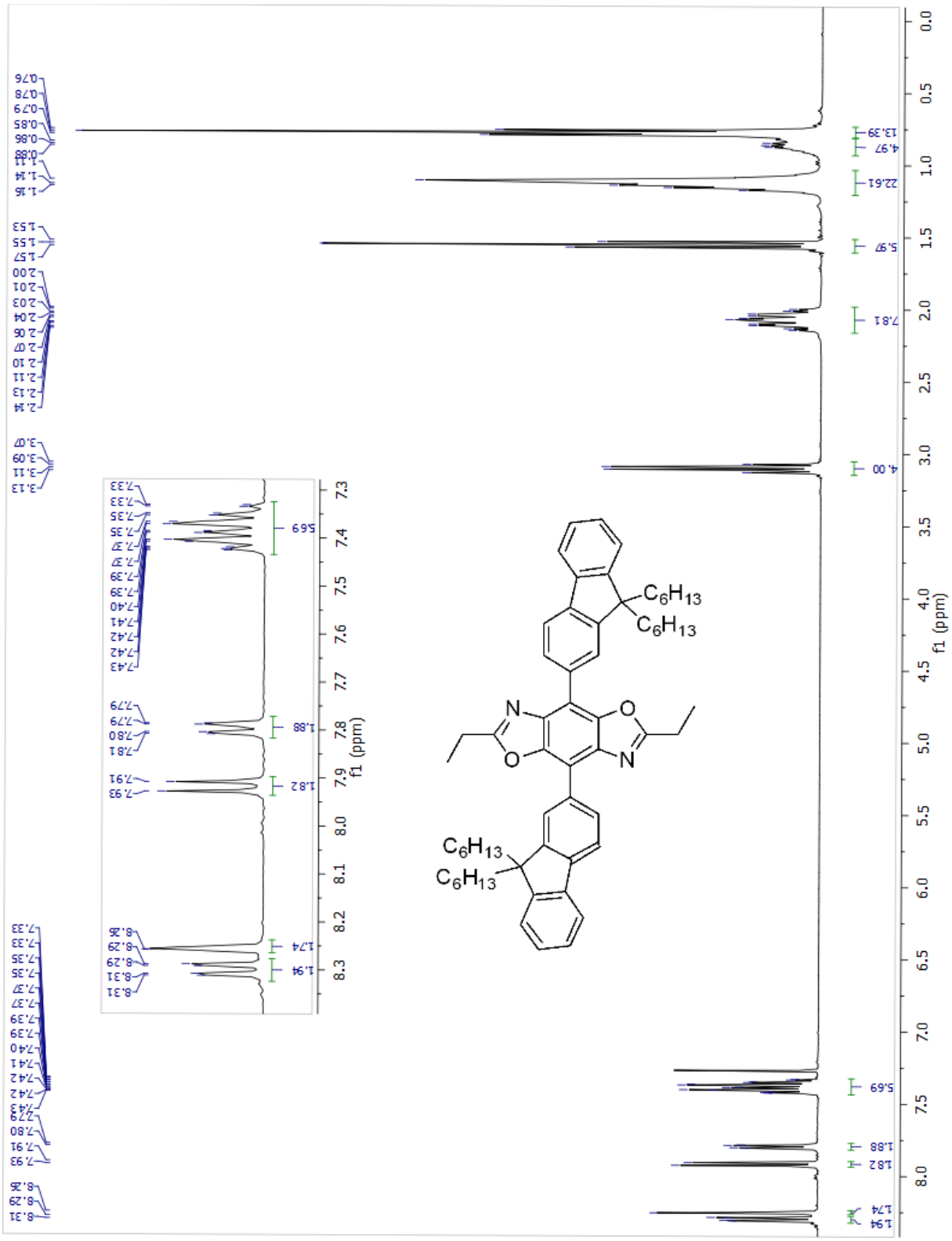

Figure S3.13. ^{1}H NMR spectrum of **7**.

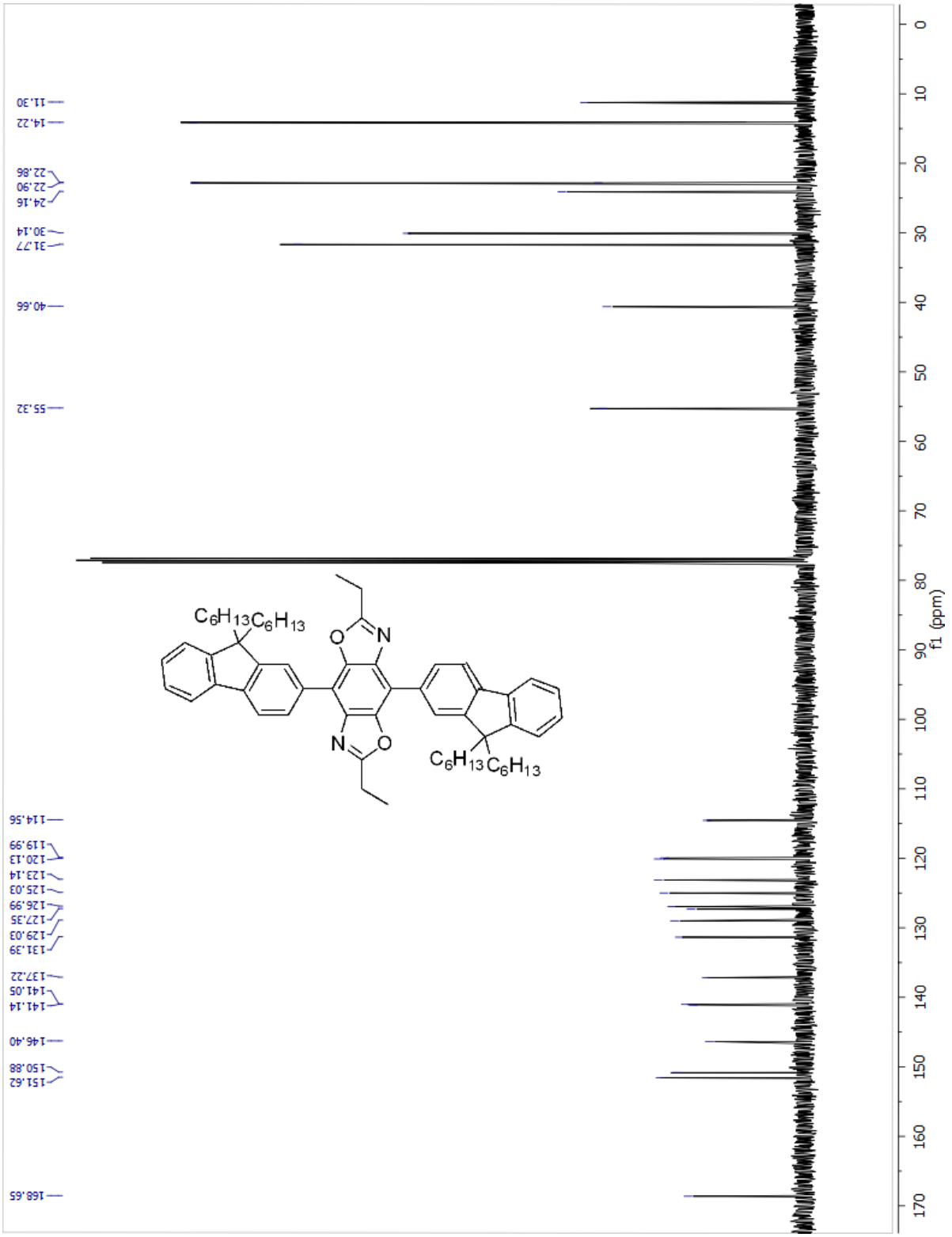

Figure S3.14. ^{13}C NMR spectrum of **7**.

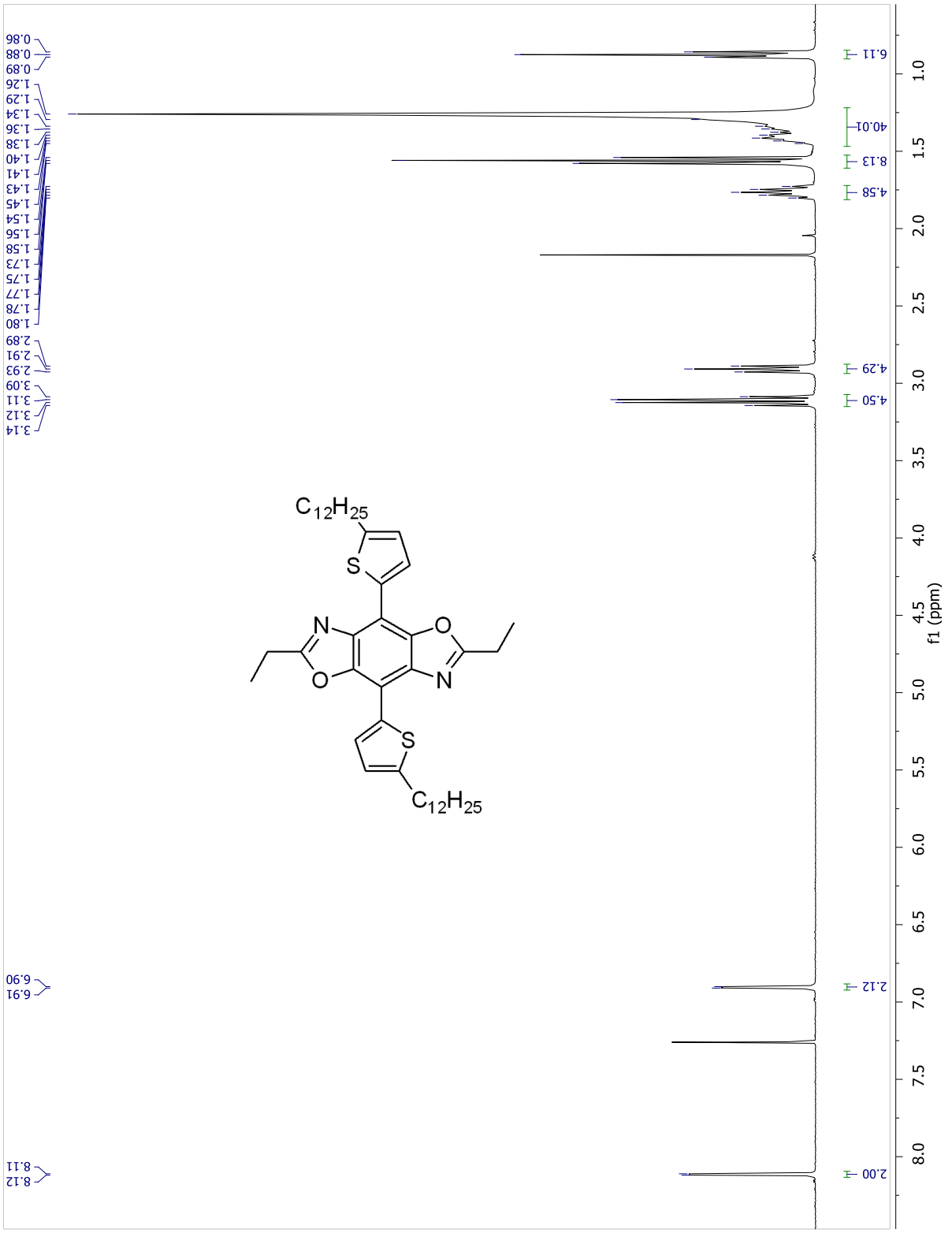

Figure S3.15. ^{1}H NMR spectrum of **8**.

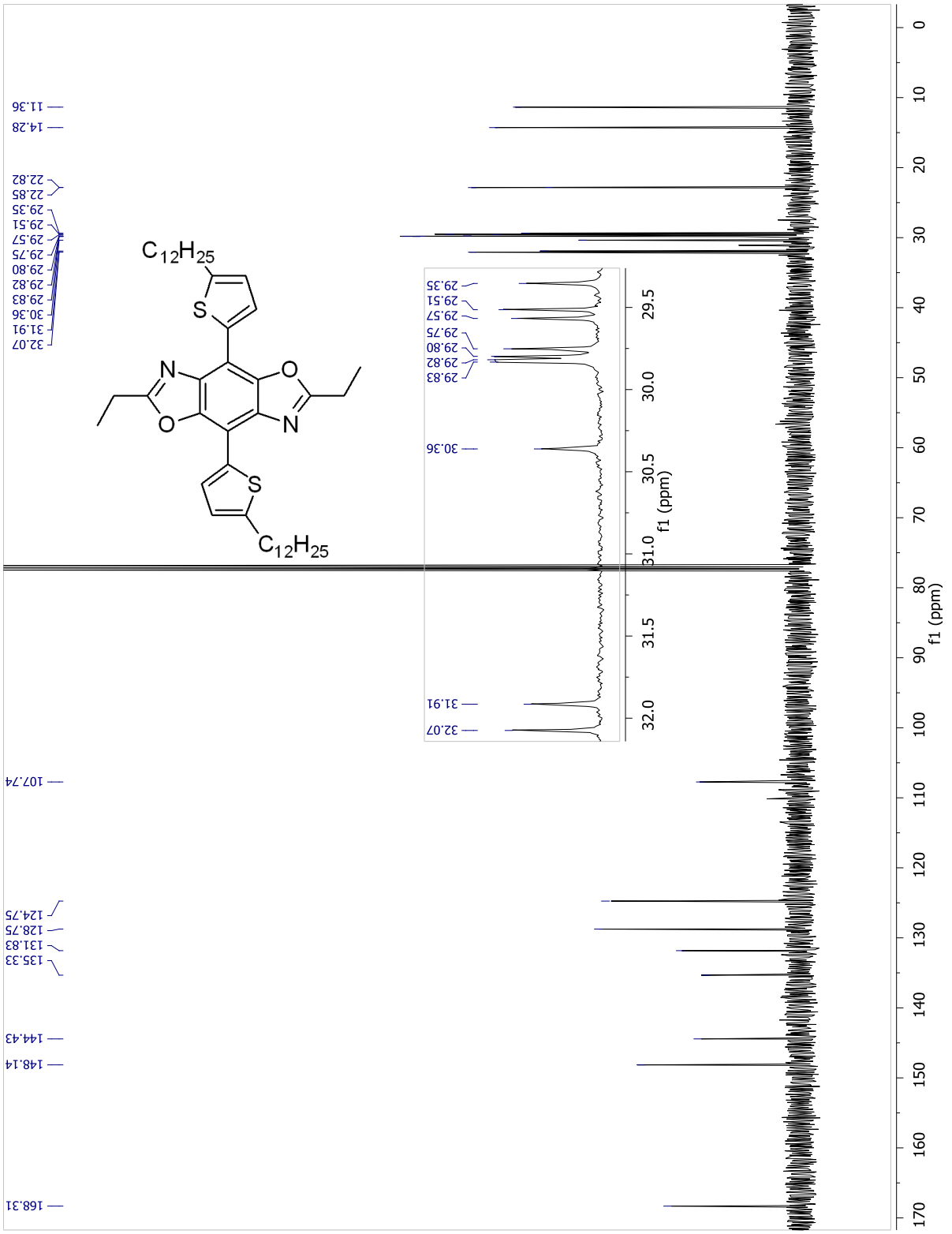

Figure S3.16. ^{13}C NMR spectrum of **8**.

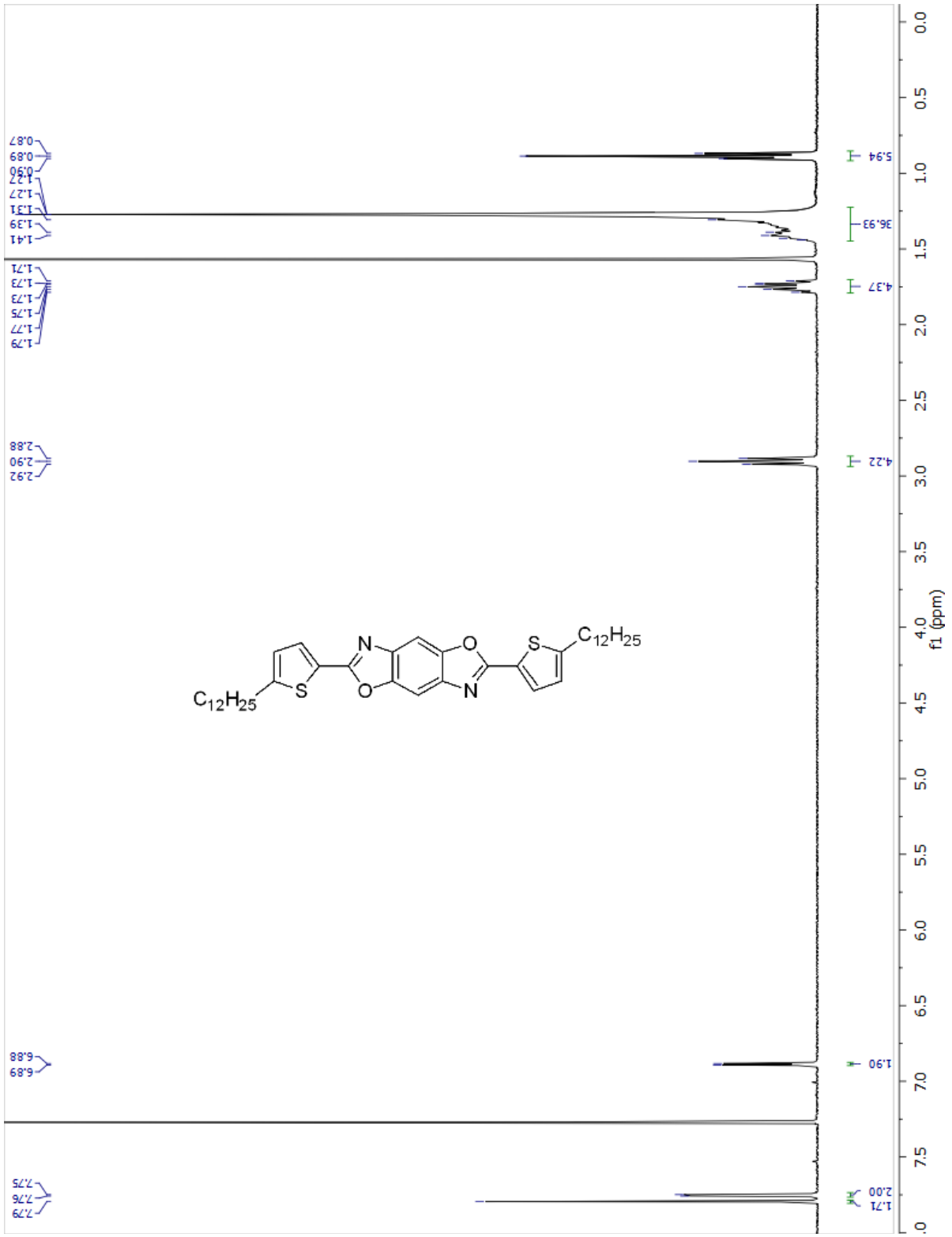

Figure S3.17. ^{1}H NMR spectrum of **9**.

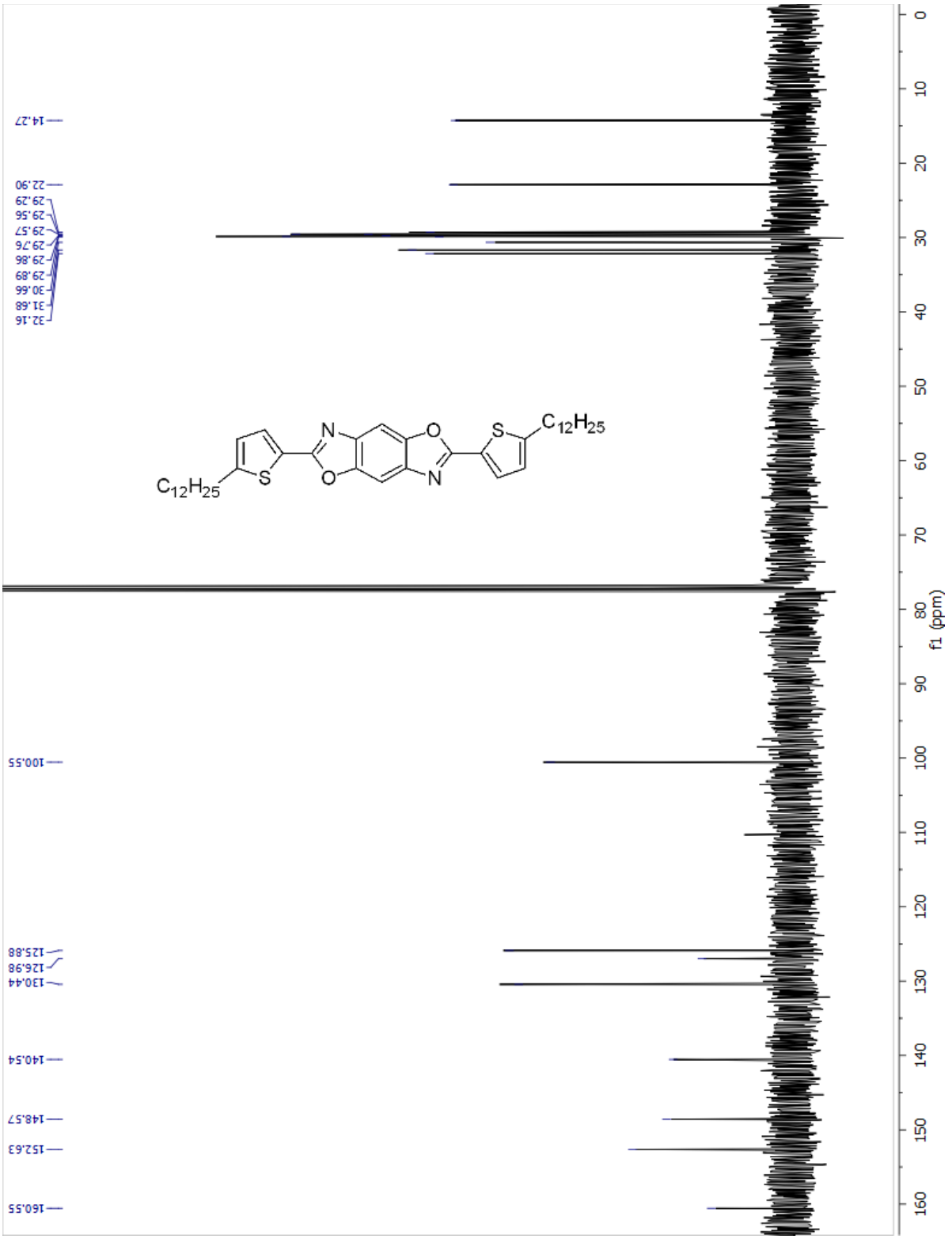

Figure S3.18. ^{13}C NMR spectrum of **9**.

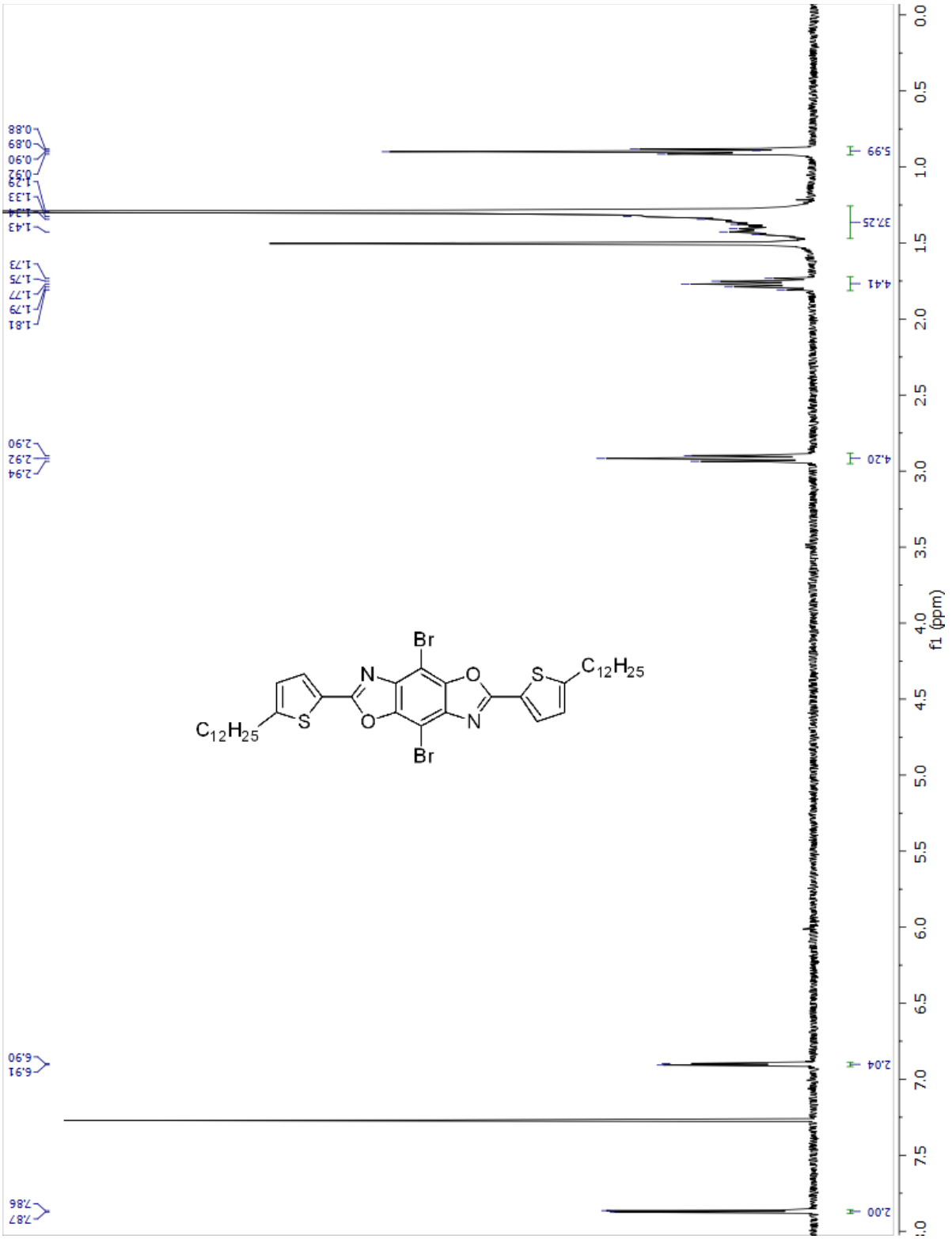

Figure S3.19. ^{1}H NMR spectrum of **10**.

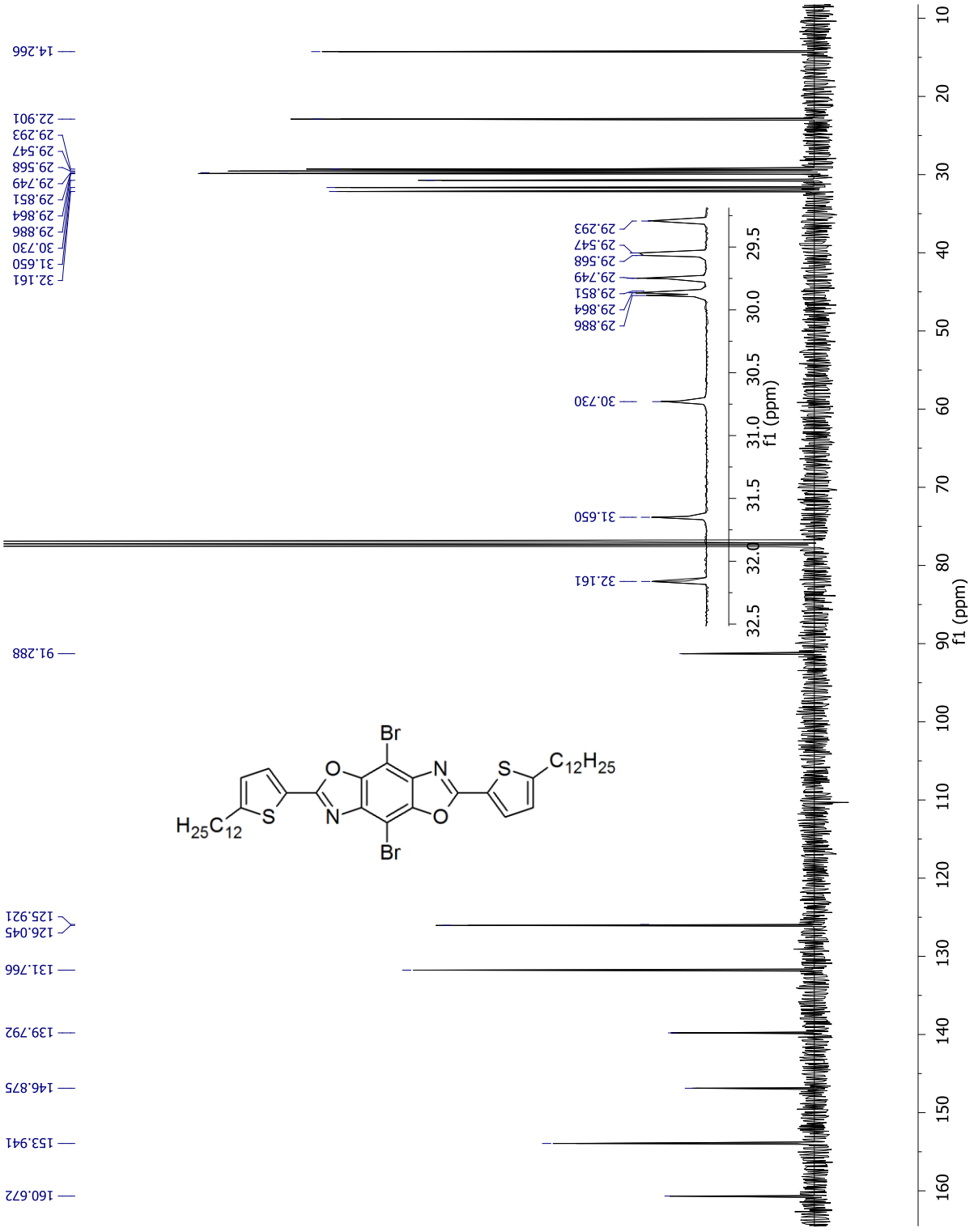

Figure S3.20. ^{13}C NMR spectrum of **10**.

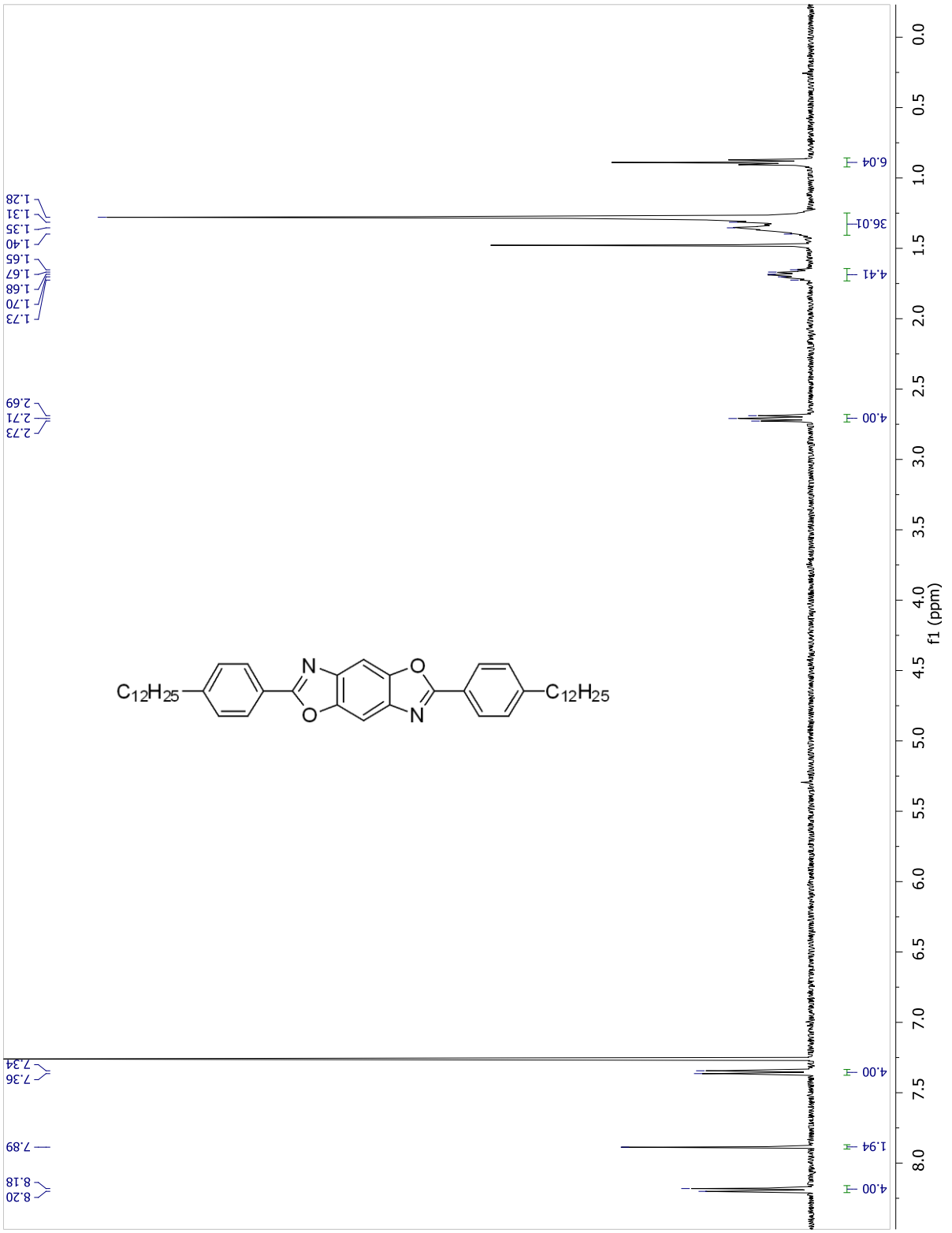

Figure S3.21. ^{1}H NMR spectrum of **11**.

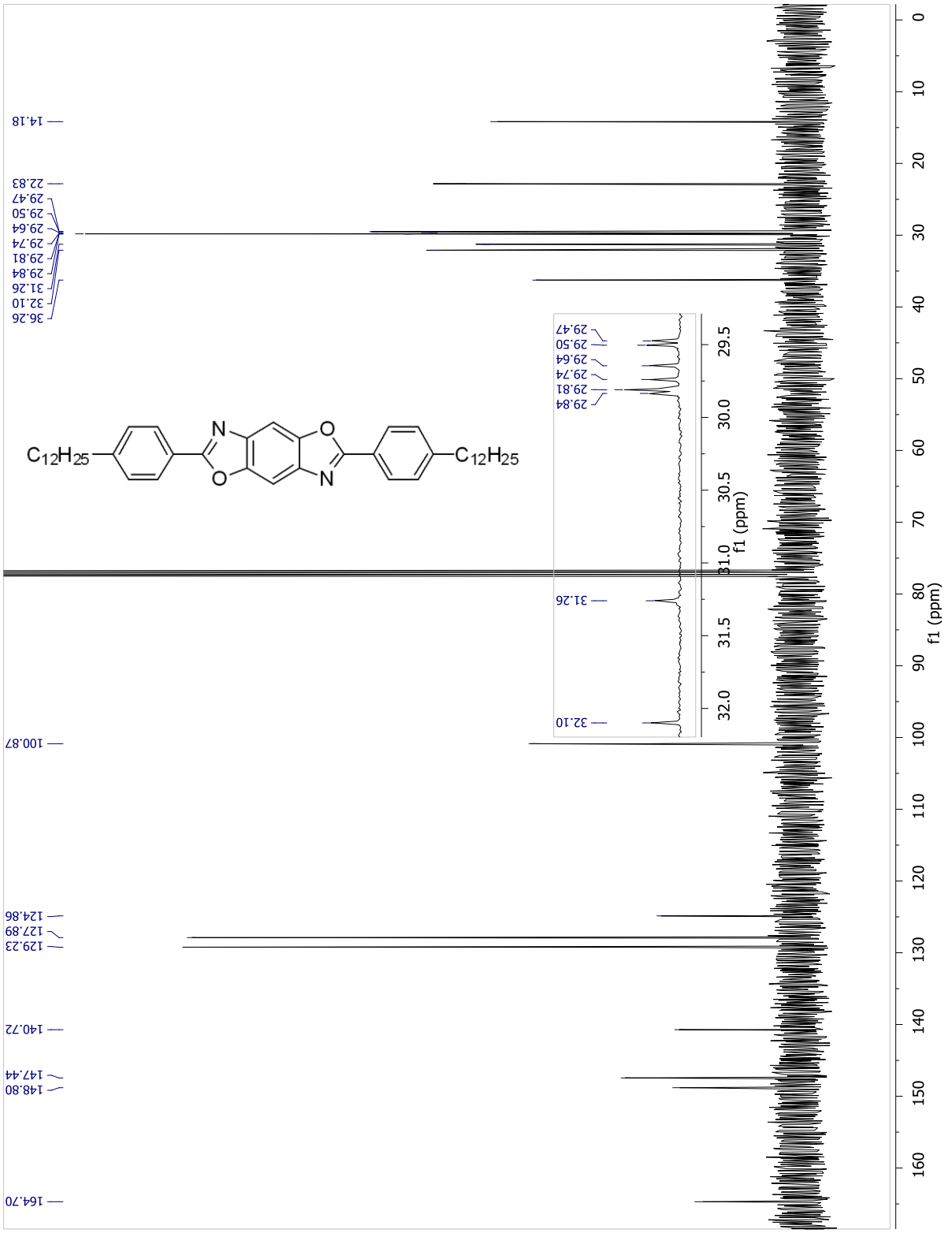

FigureS3.22. ^{13}C NMR spectrum of **11**.

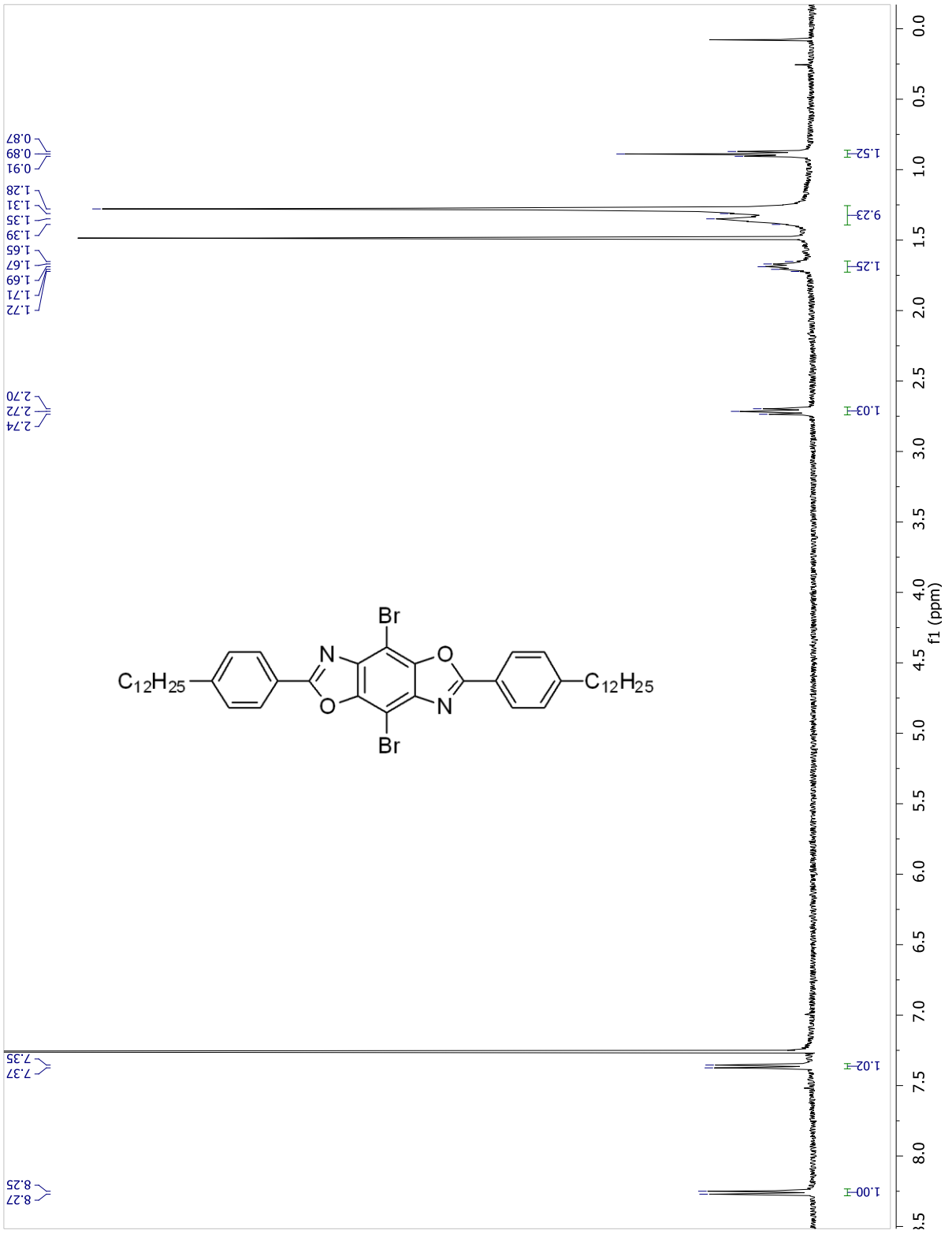

Figure S3.23. ^{1}H NMR spectrum of **12**.

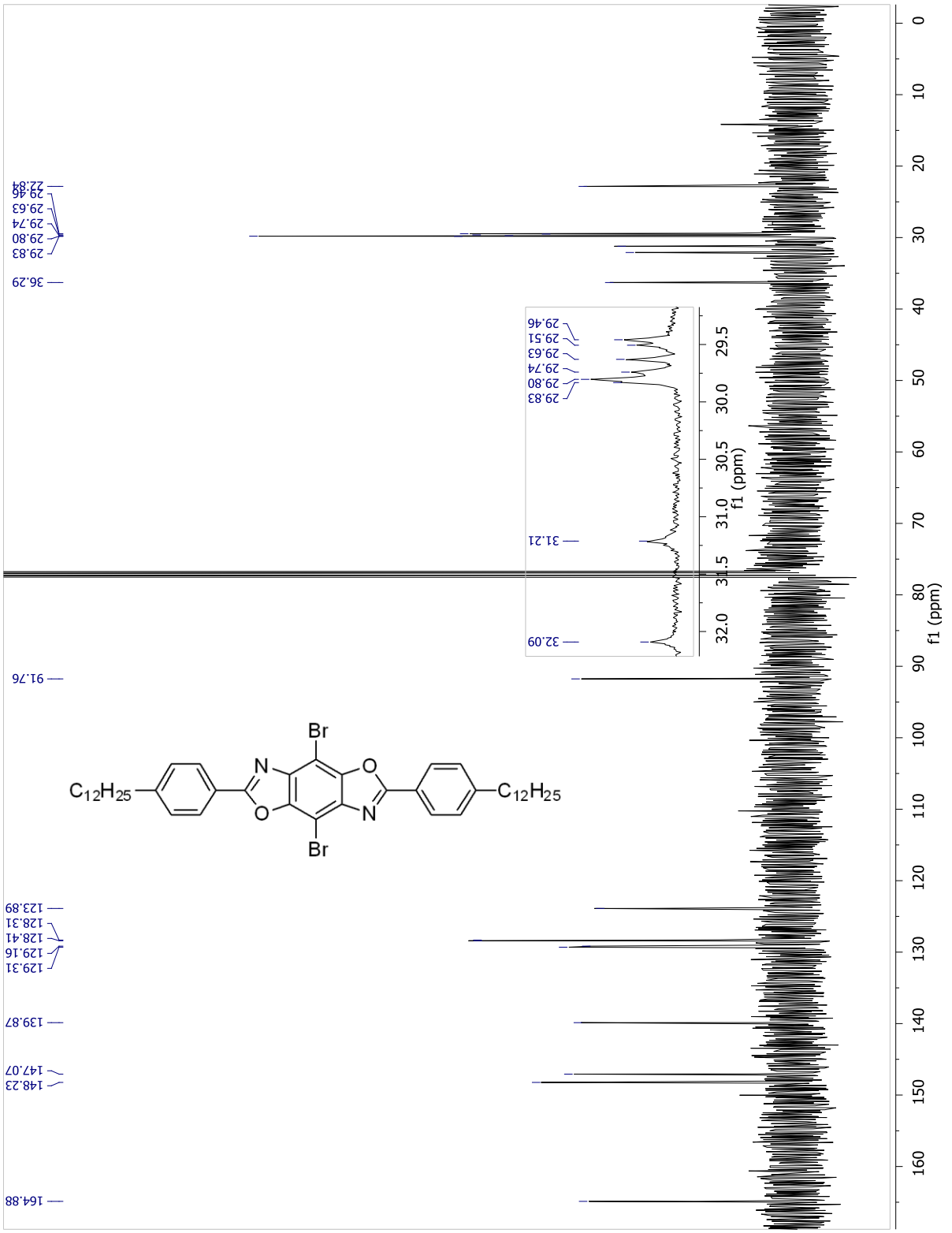

Figure S3.24. ^{13}C NMR spectrum of **12**.

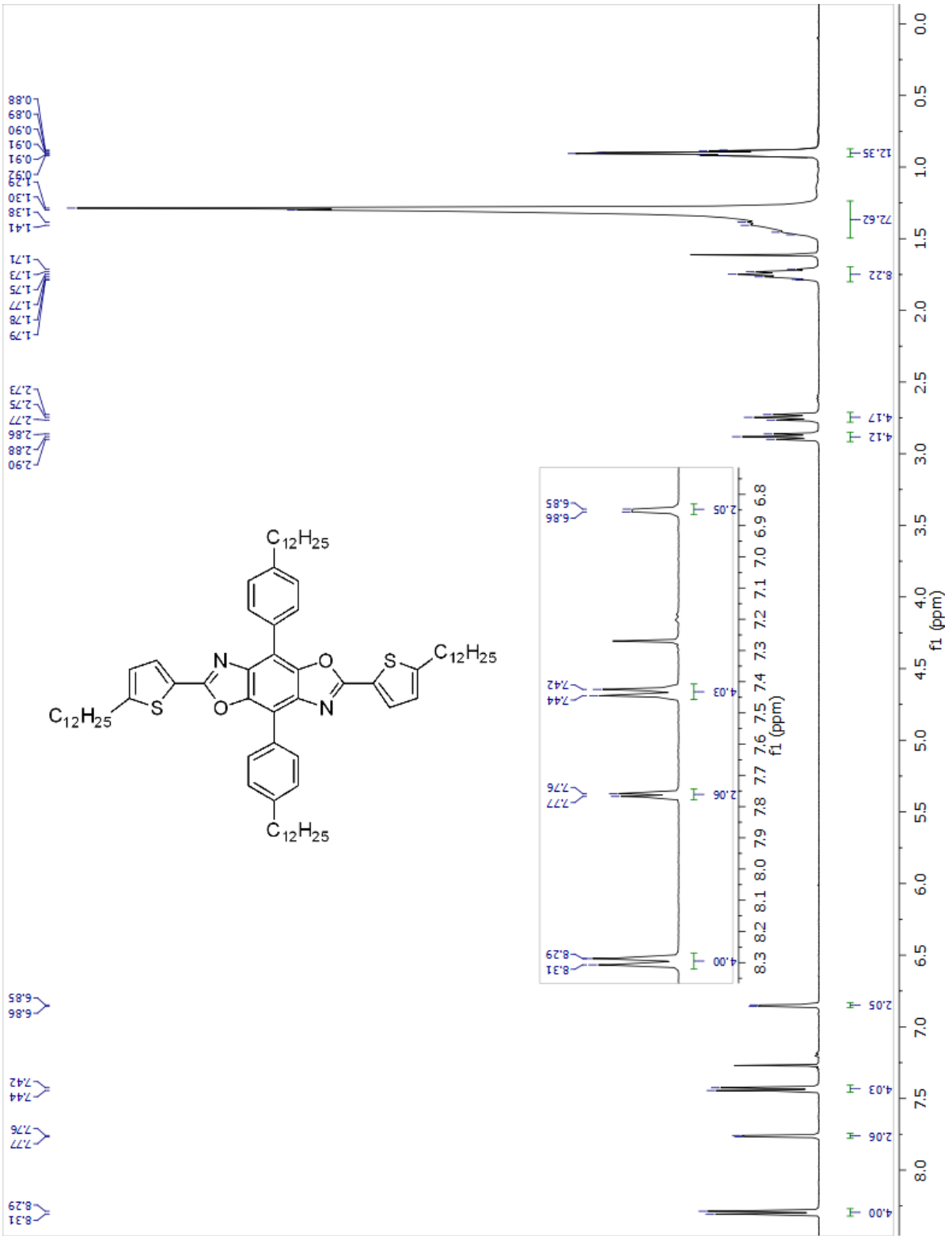

Figure S3.25. ^{1}H NMR spectrum of **13**.

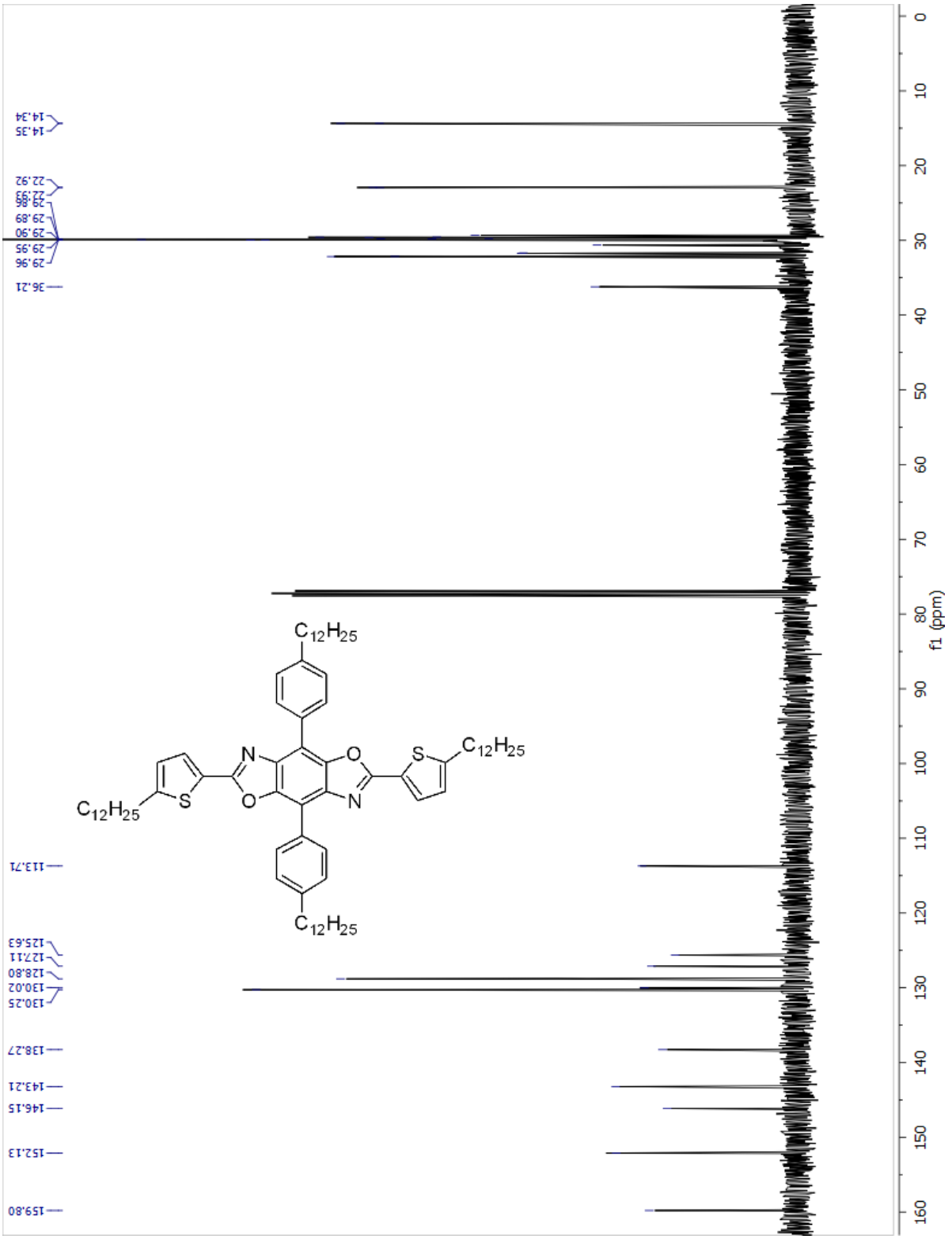

Figure S3.26. ^{13}C NMR spectrum of **13**.

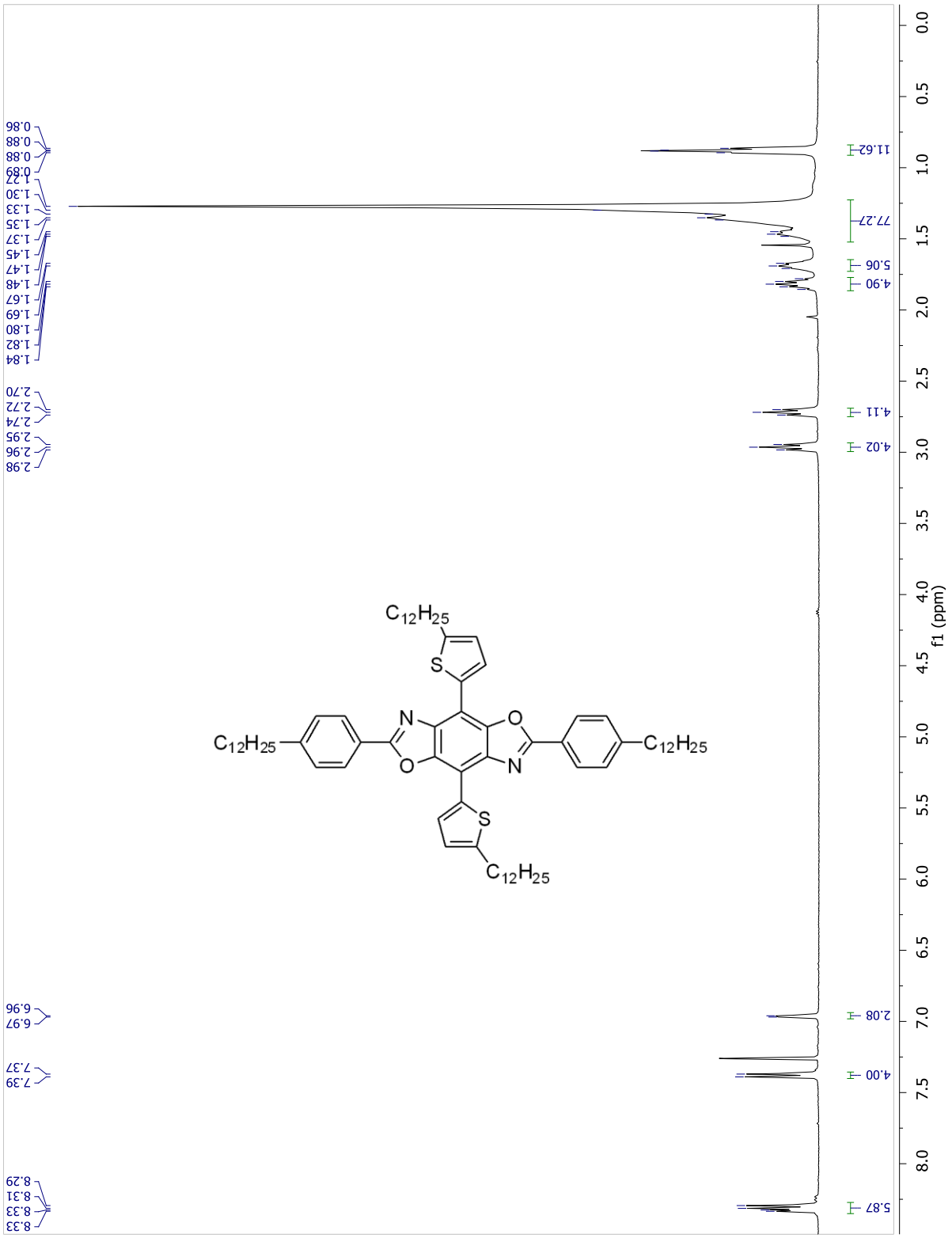

Figure S3.27. ^{1}H NMR spectrum of **14**.

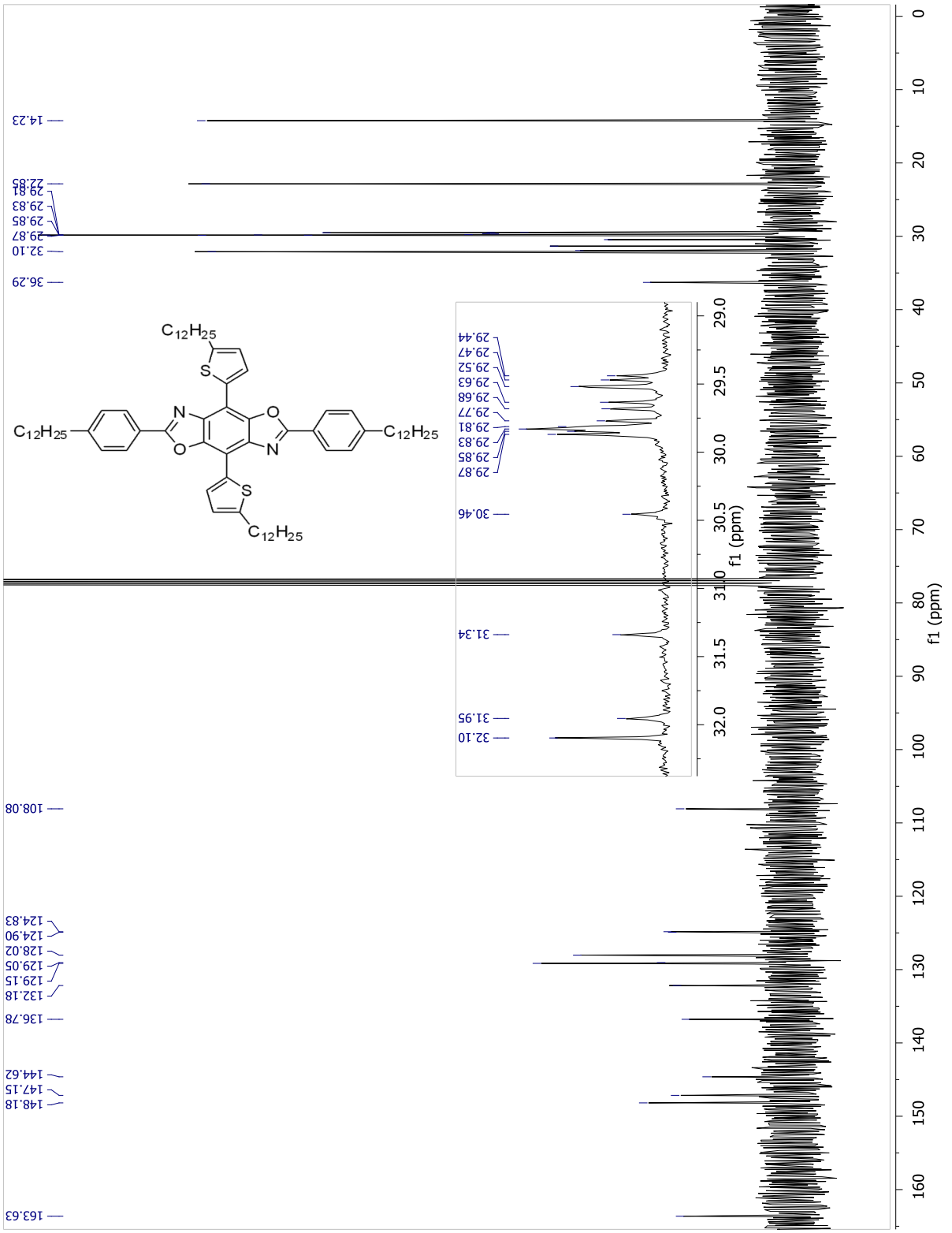

Figure S3.28. ^{13}C NMR spectrum of **14**.

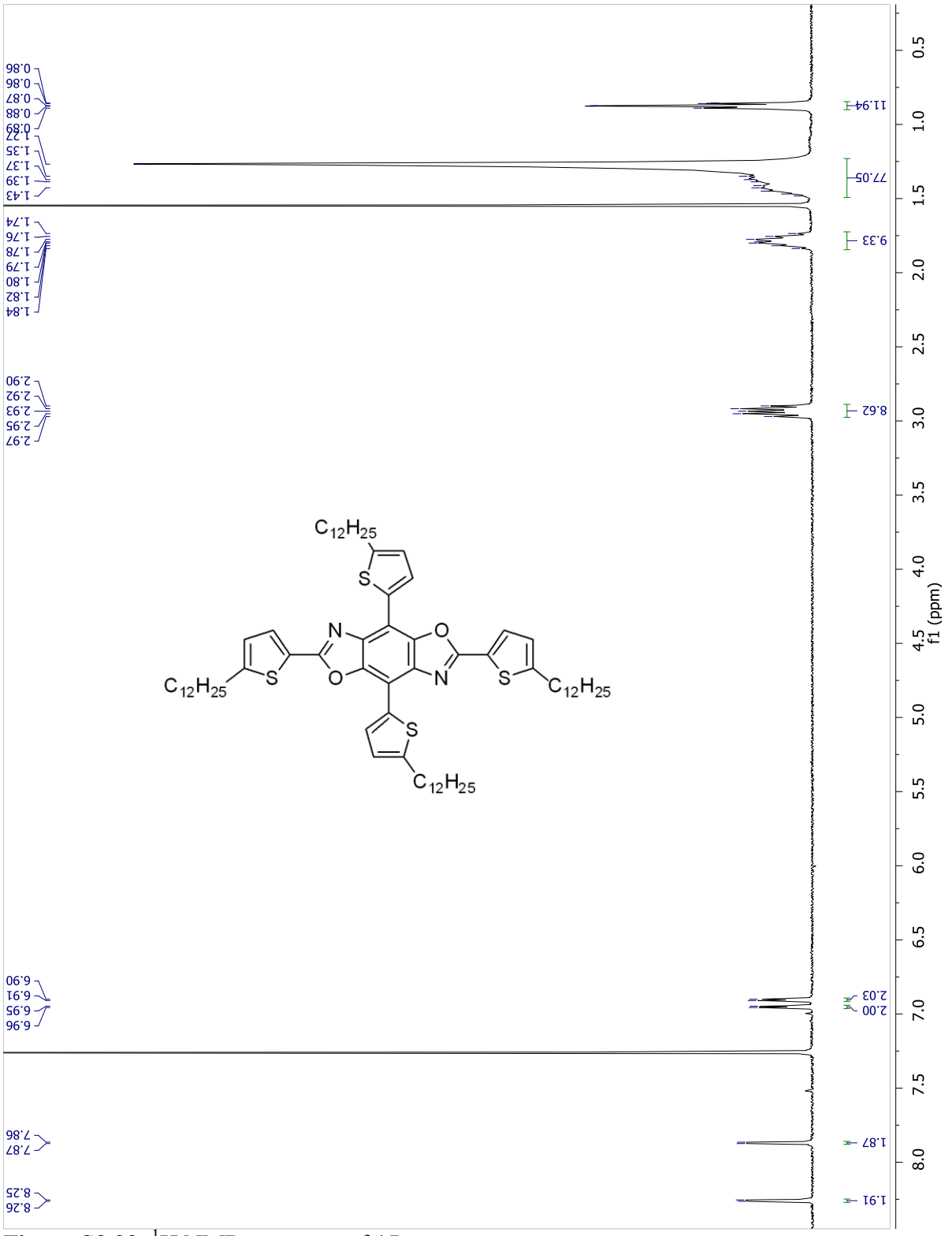

Figure S3.29. ^{1}H NMR spectrum of **15**.

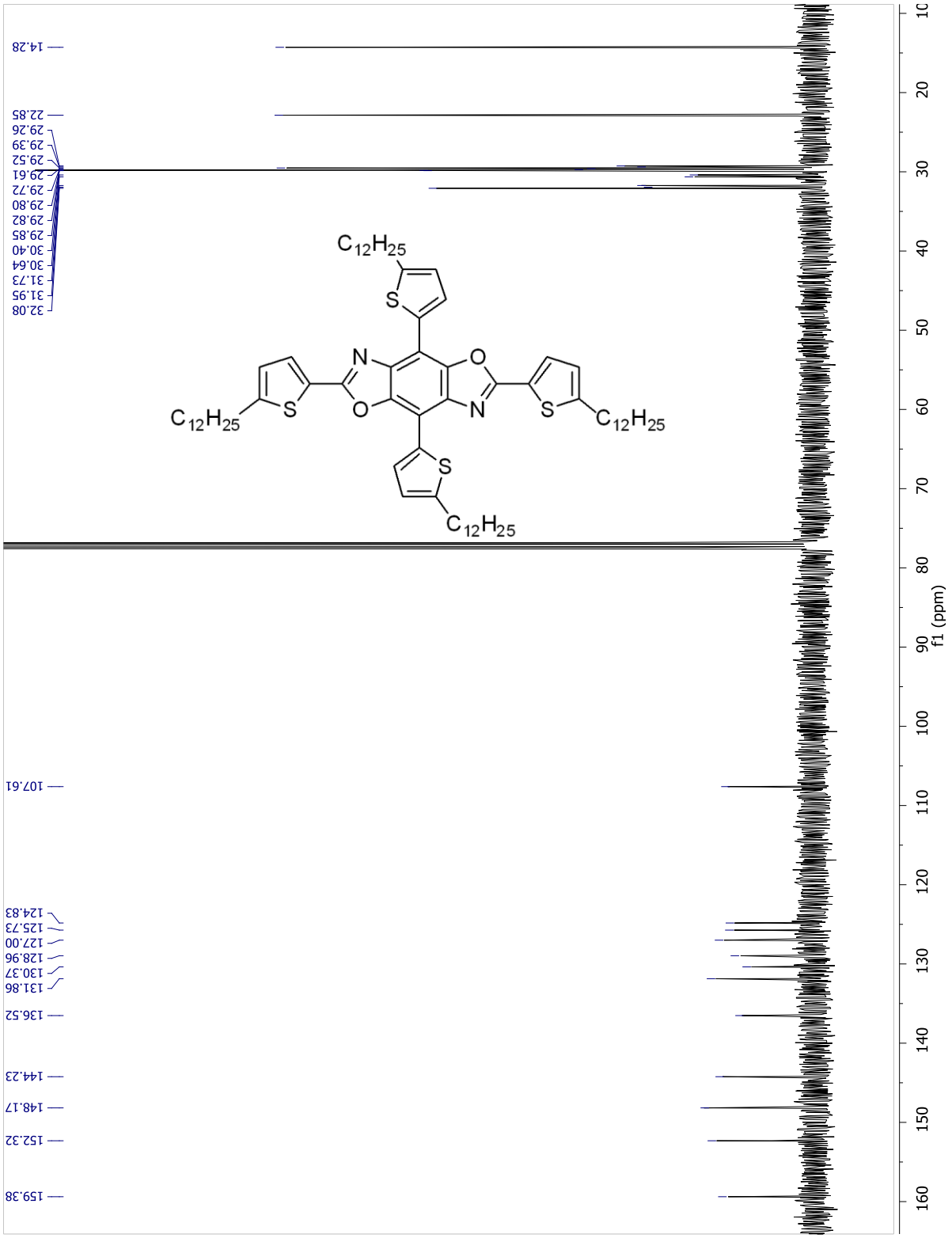

Figure S3.30. ^{13}C NMR spectrum of **15**.

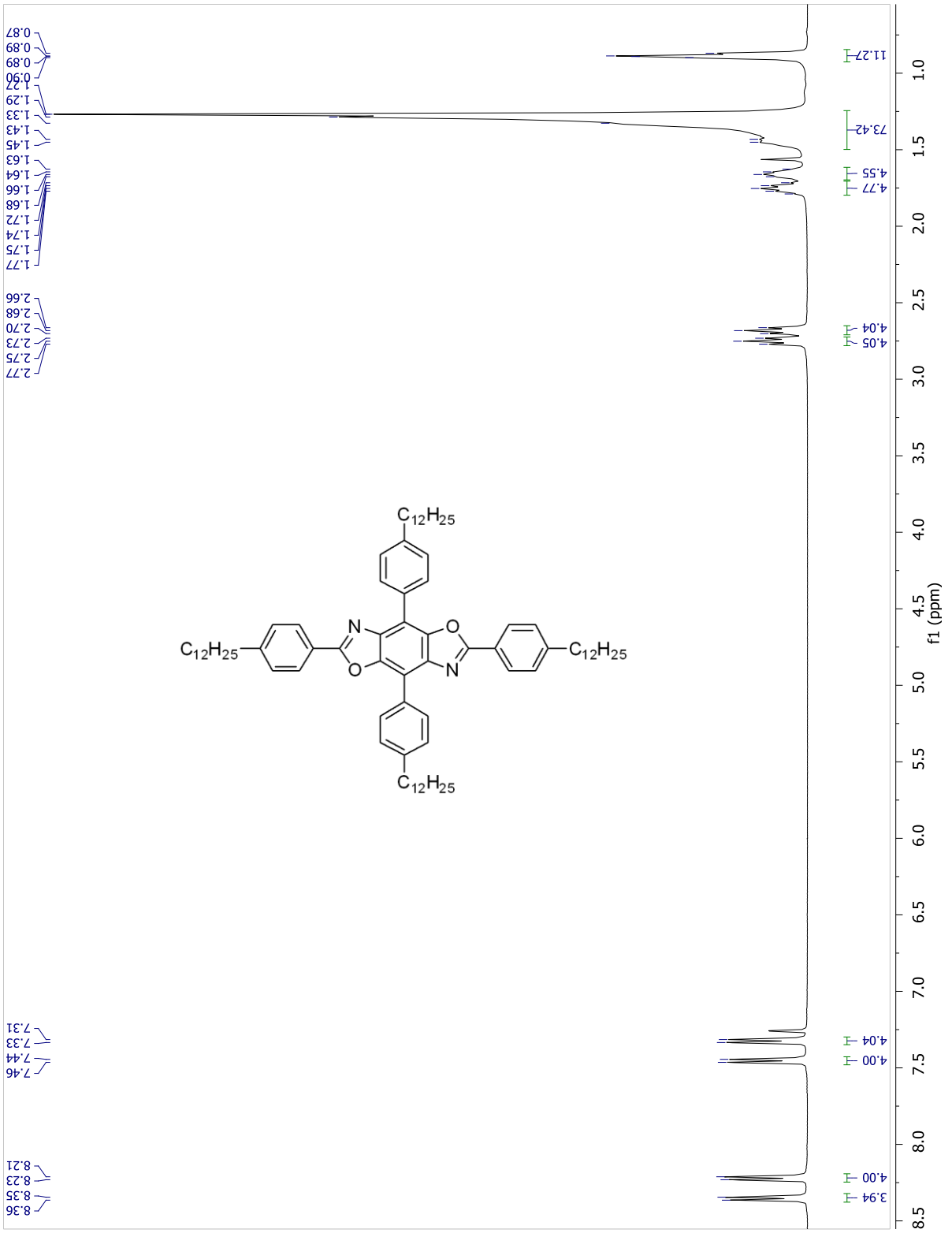

Figure S3.31. ^{1}H NMR spectrum of **16**.

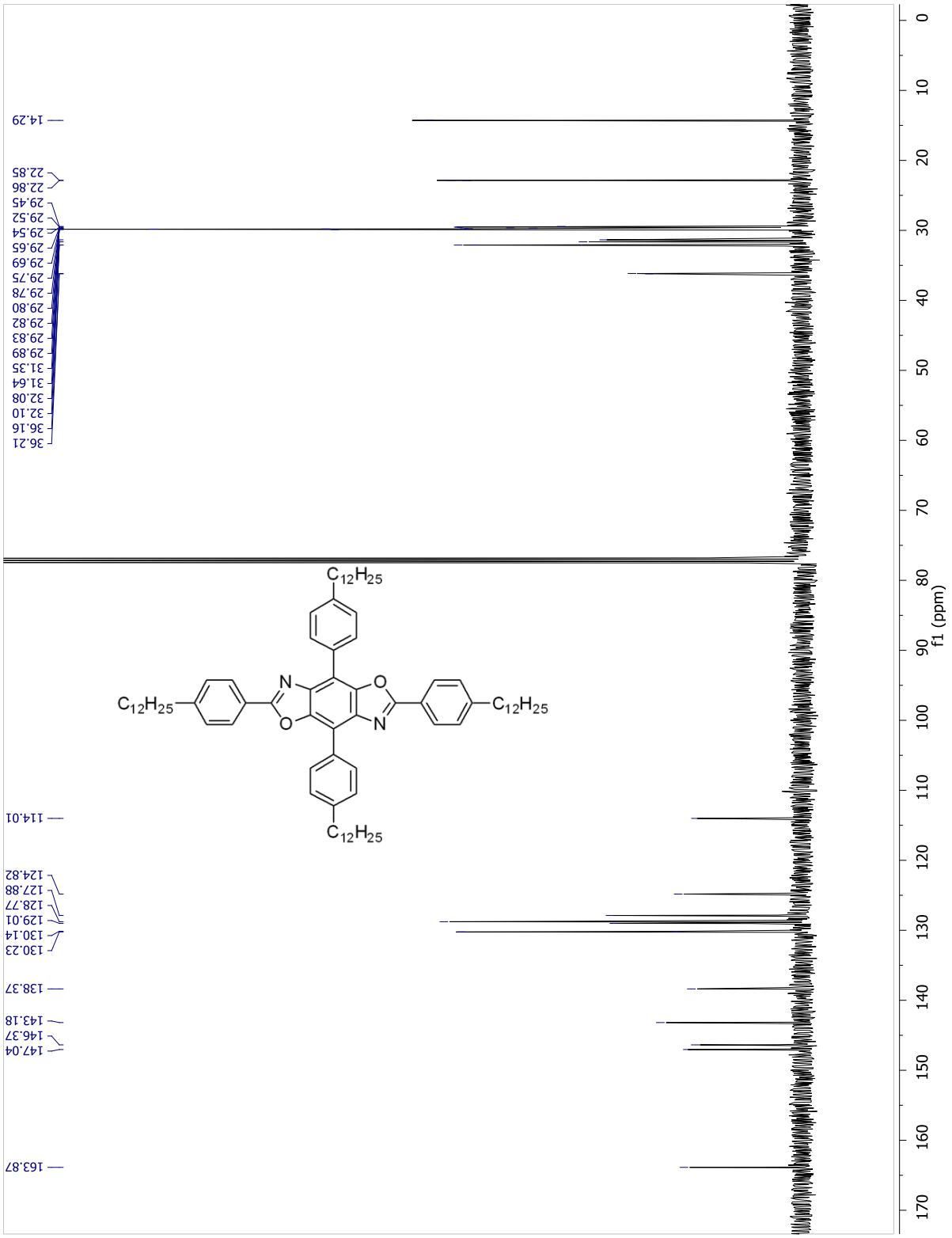

Figure S3.32. ^{13}C NMR spectrum of **16**.

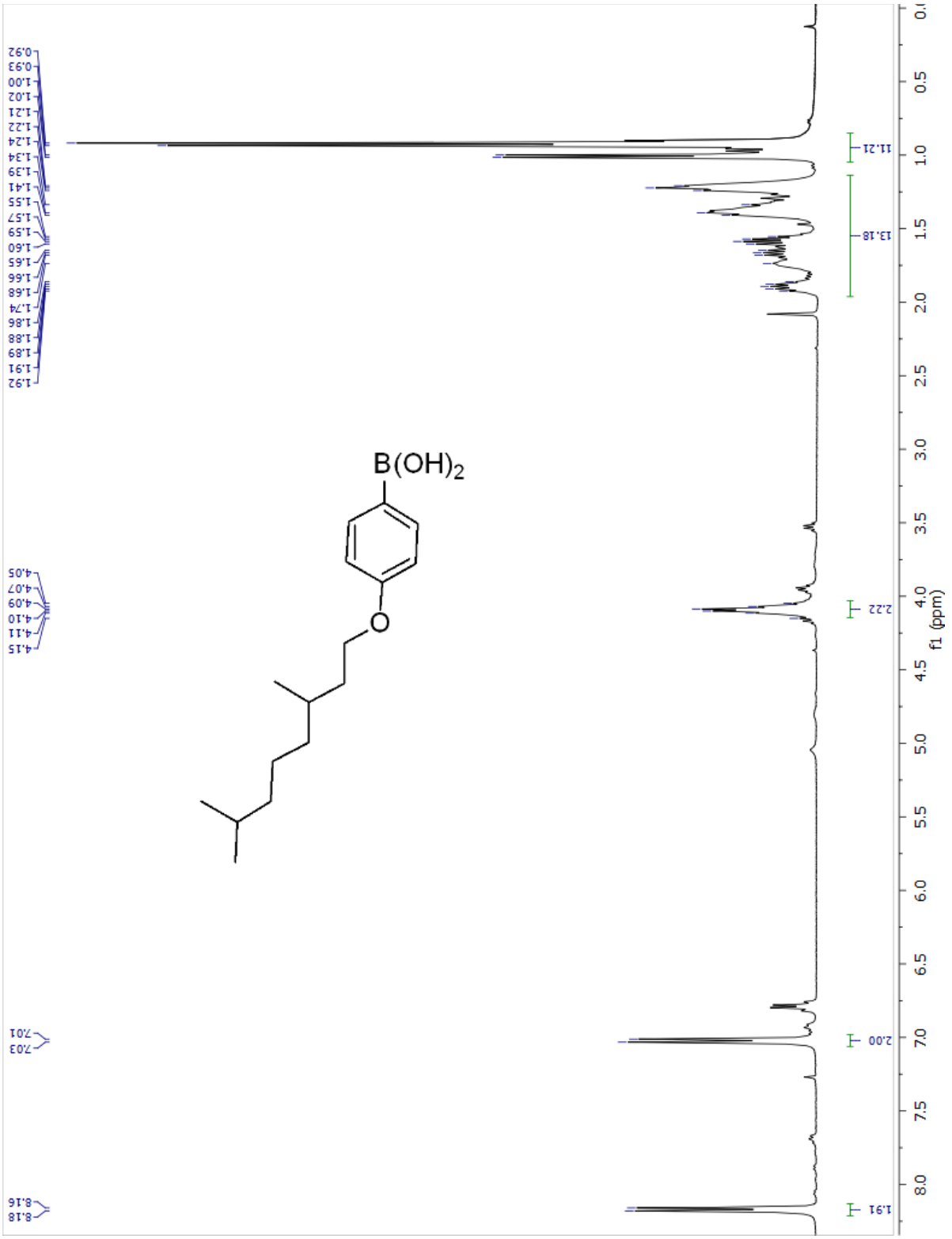

Figure S3.33. ^{1}H NMR spectrum of 4-(3,7-dimethyloctyloxy)phenyl boronic acid.

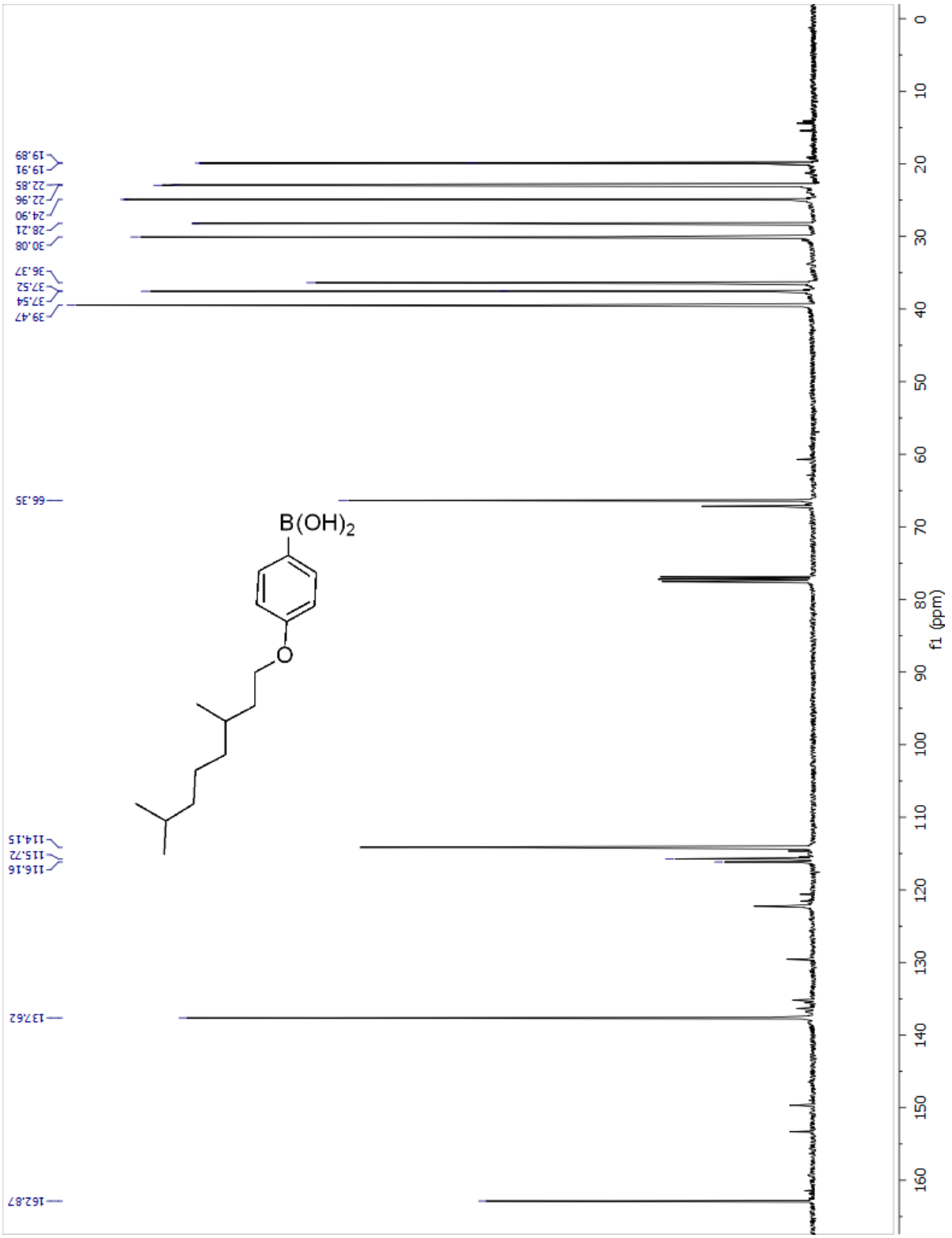

Figure S3.34. ^{13}C NMR spectrum of 4-(3,7-dimethyloctyloxy)phenyl boronic acid.

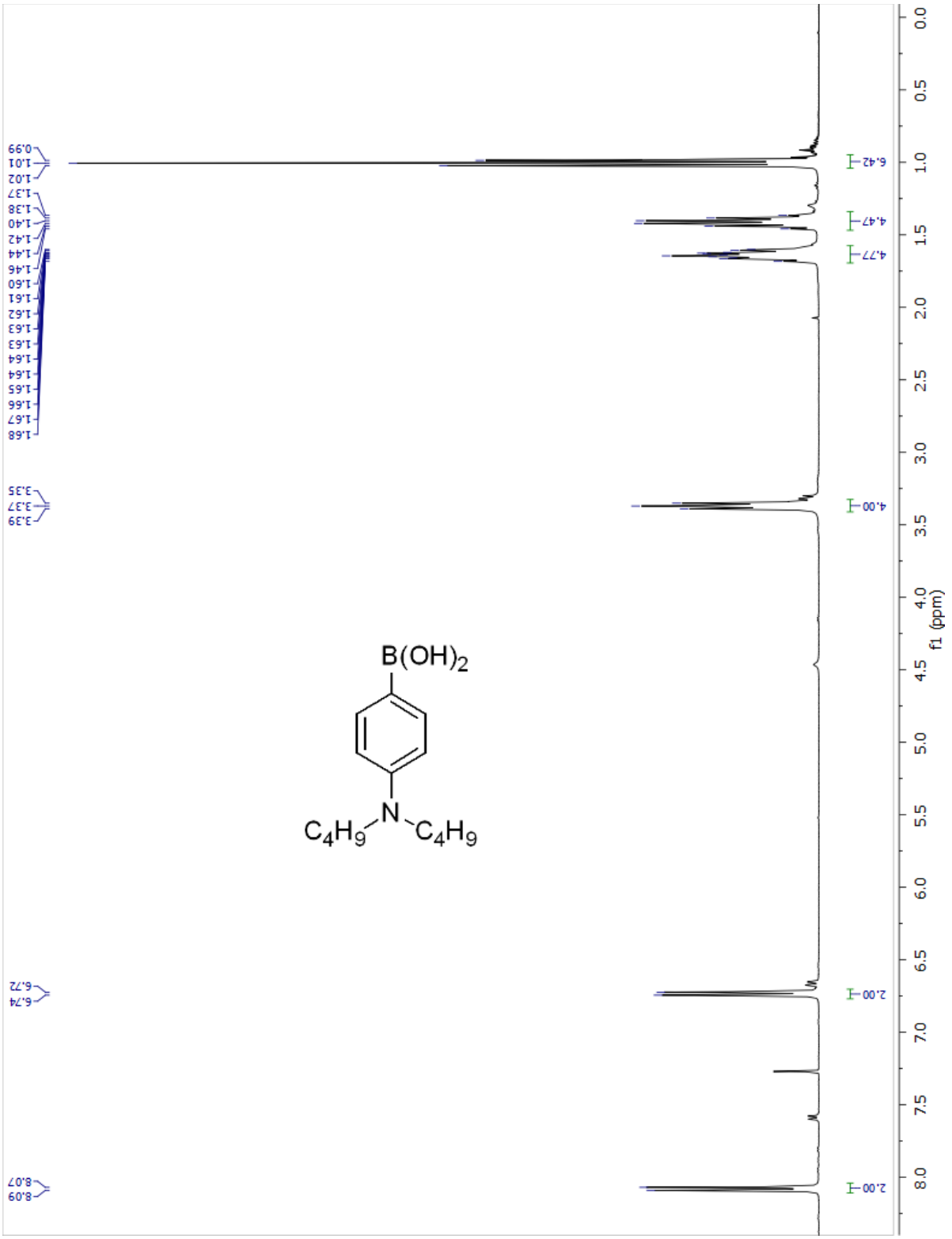

Figure S3.35. ^{1}H NMR spectrum of 4-(*N,N*-dibutylamino)phenyl boronic acid.

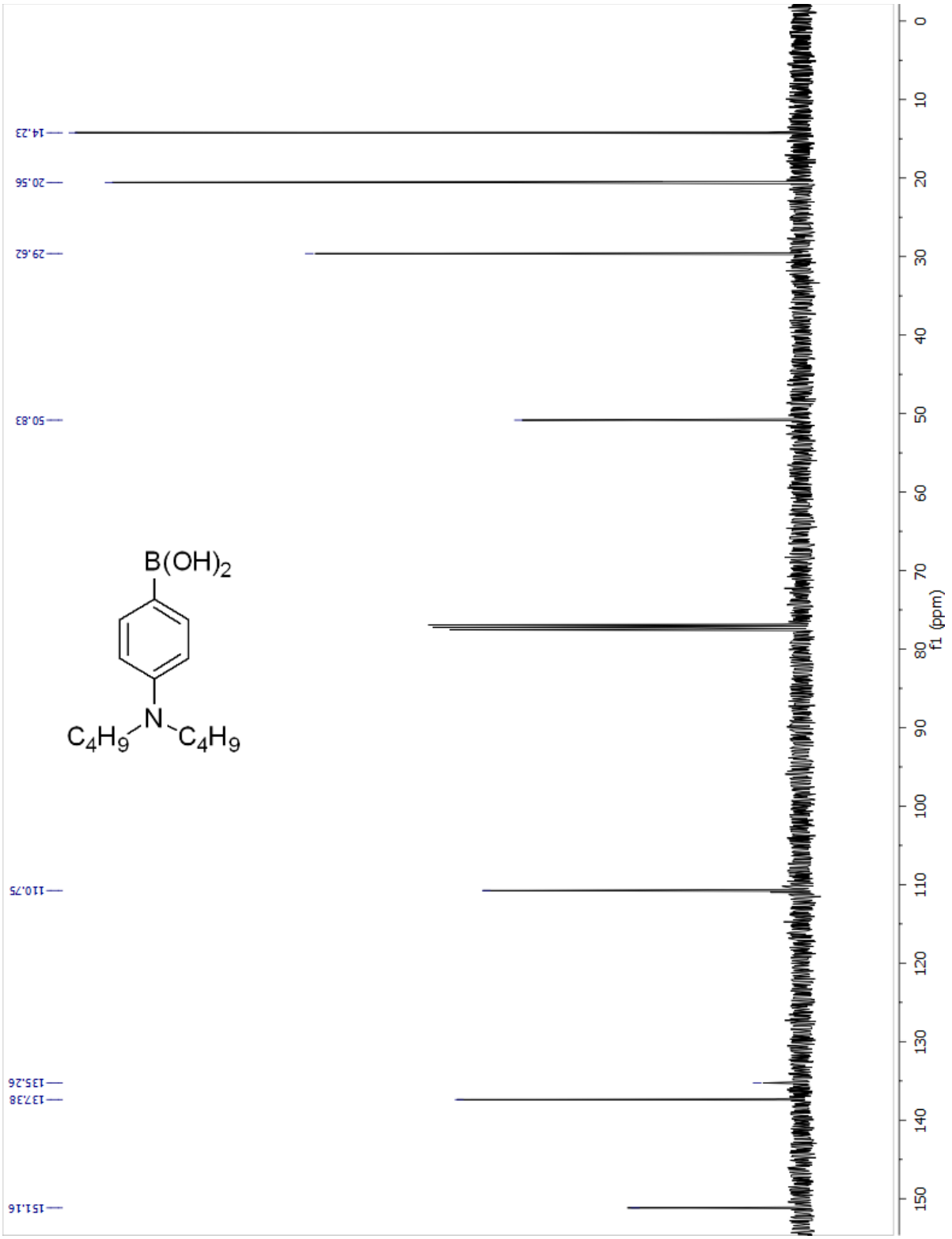

Figure S3.36. ^{13}C NMR spectrum of 4-(*N,N*-dibutylamino)phenyl boronic acid.

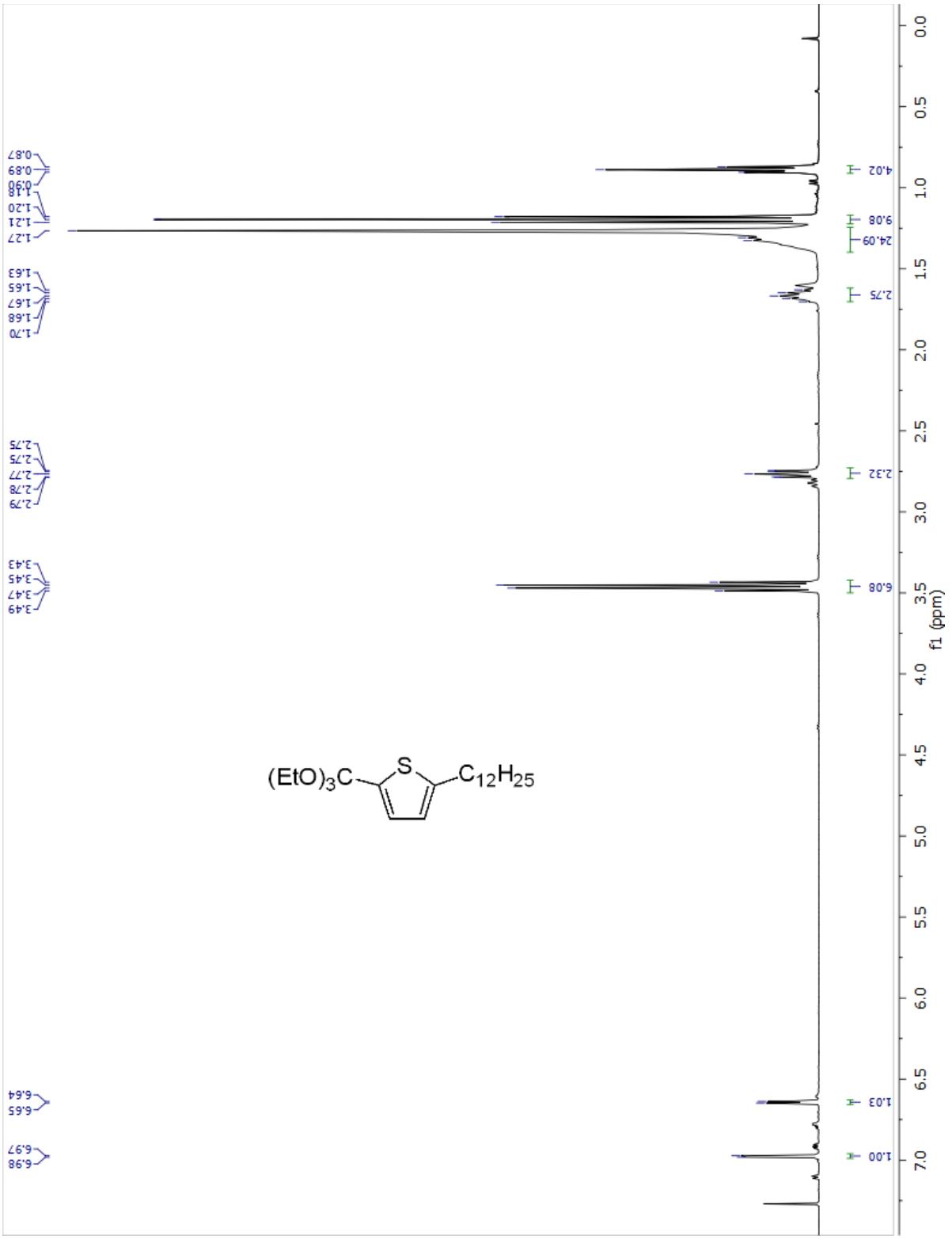

Figure S3.37. ^{1}H NMR spectrum of 5-dodecyl-1-(triethoxymethyl)thiophene.

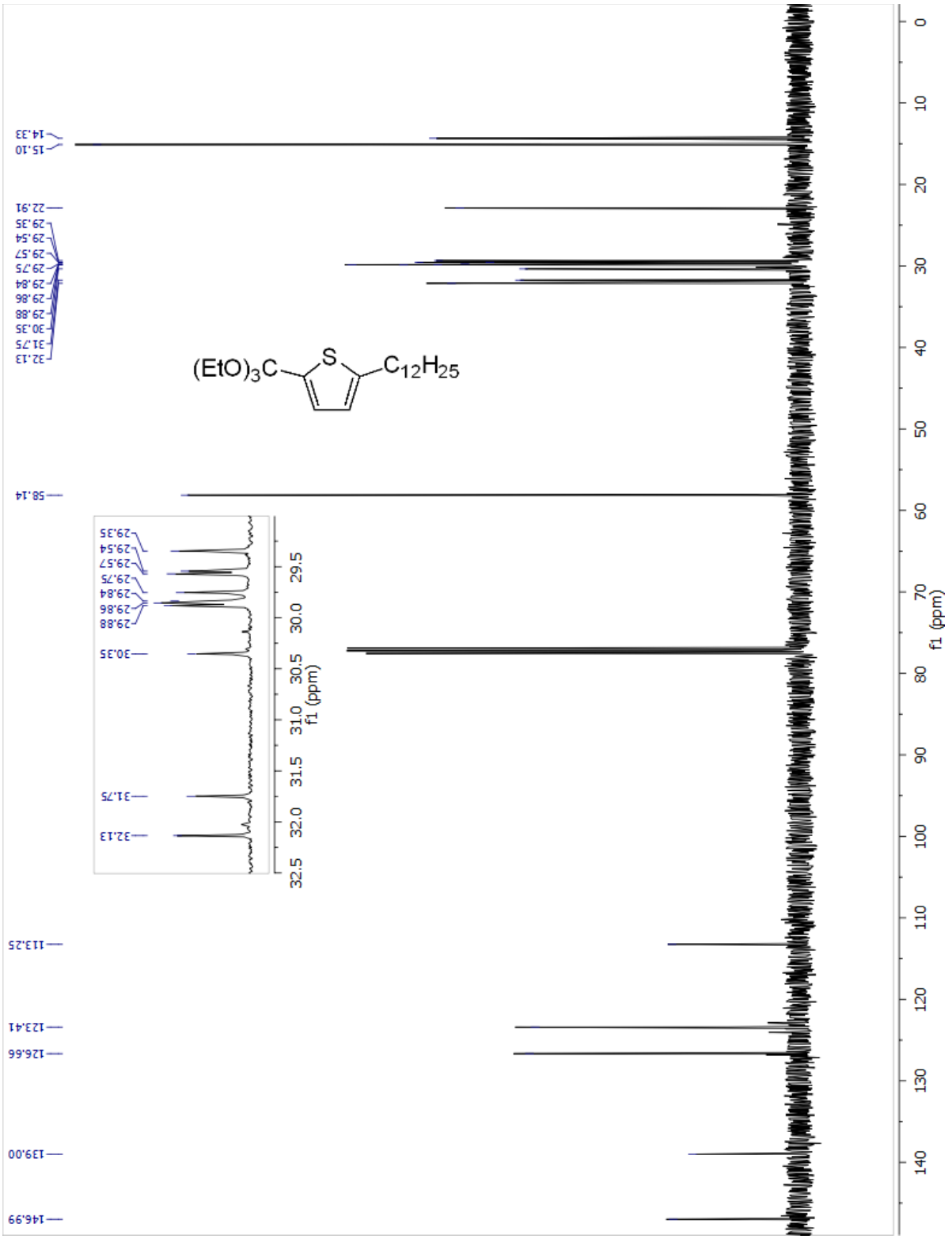

Figure S3.38. ^{13}C NMR spectrum of 5-dodecyl-1-(triethoxymethyl)thiophene.

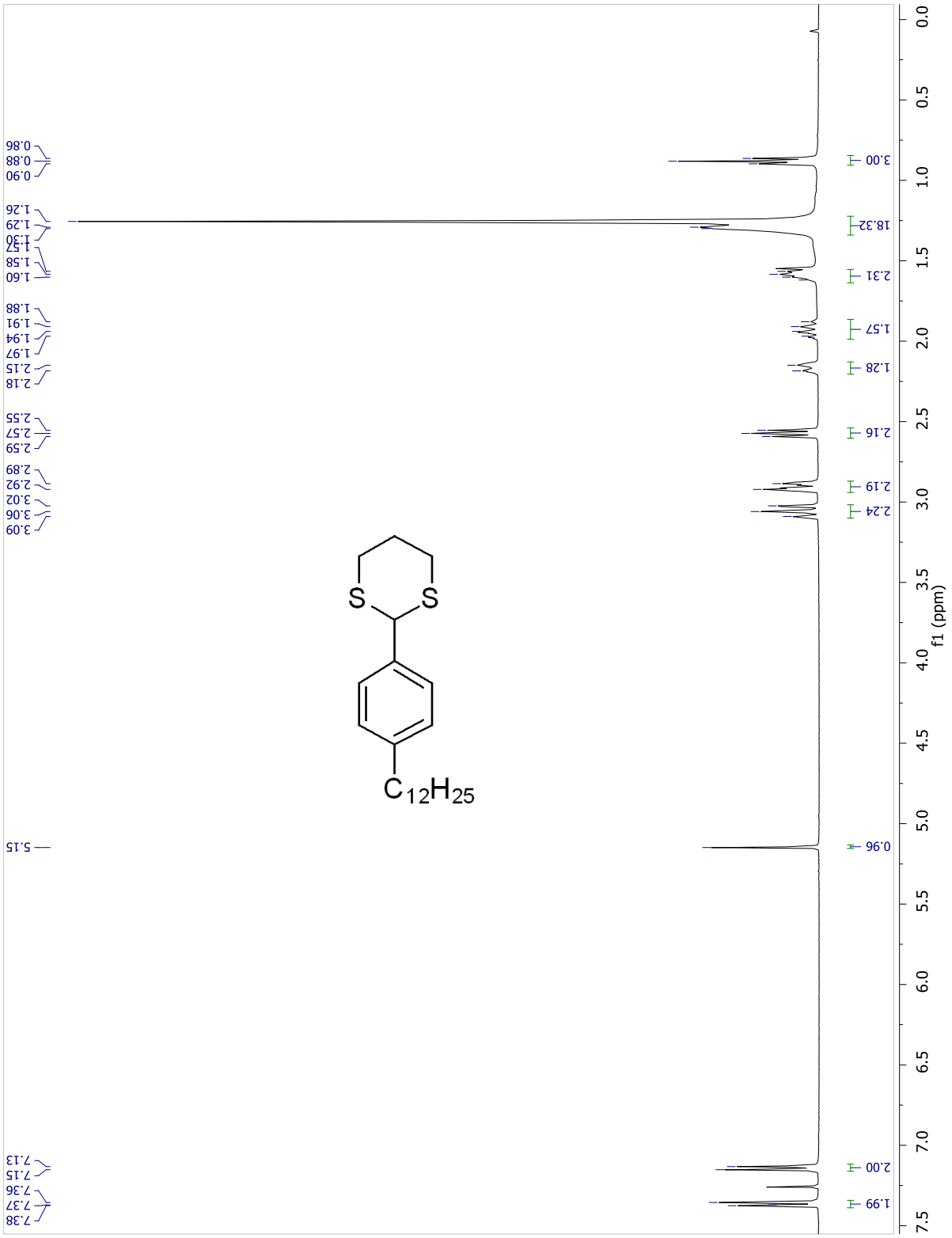

Figure S3.39. ^{1}H NMR spectrum of 2-(4-dodecylphenyl)-1,3-dithiane.

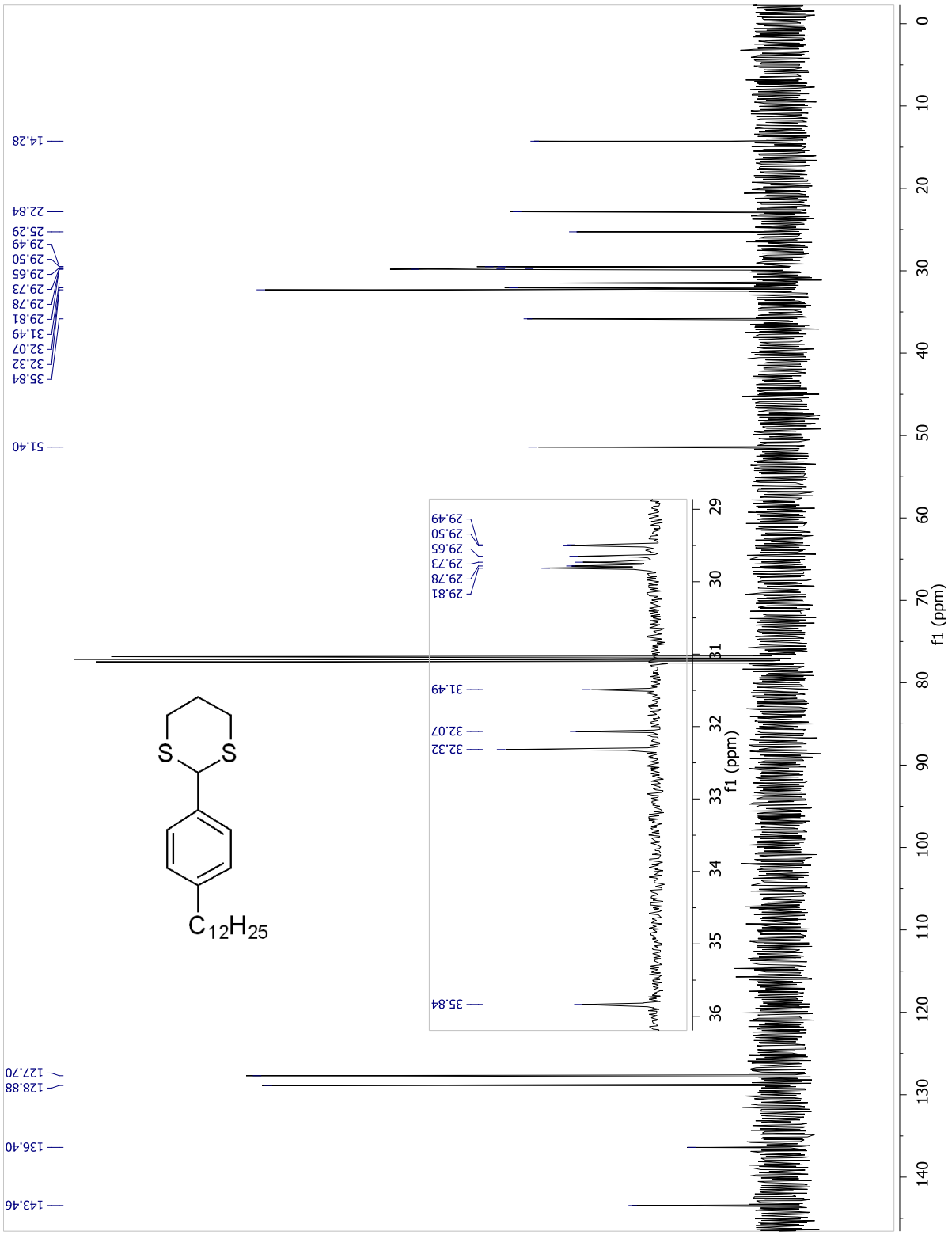

Figure S3.40. ^{13}C NMR spectrum of 2-(4-dodecylphenyl)-1,3-dithiane.

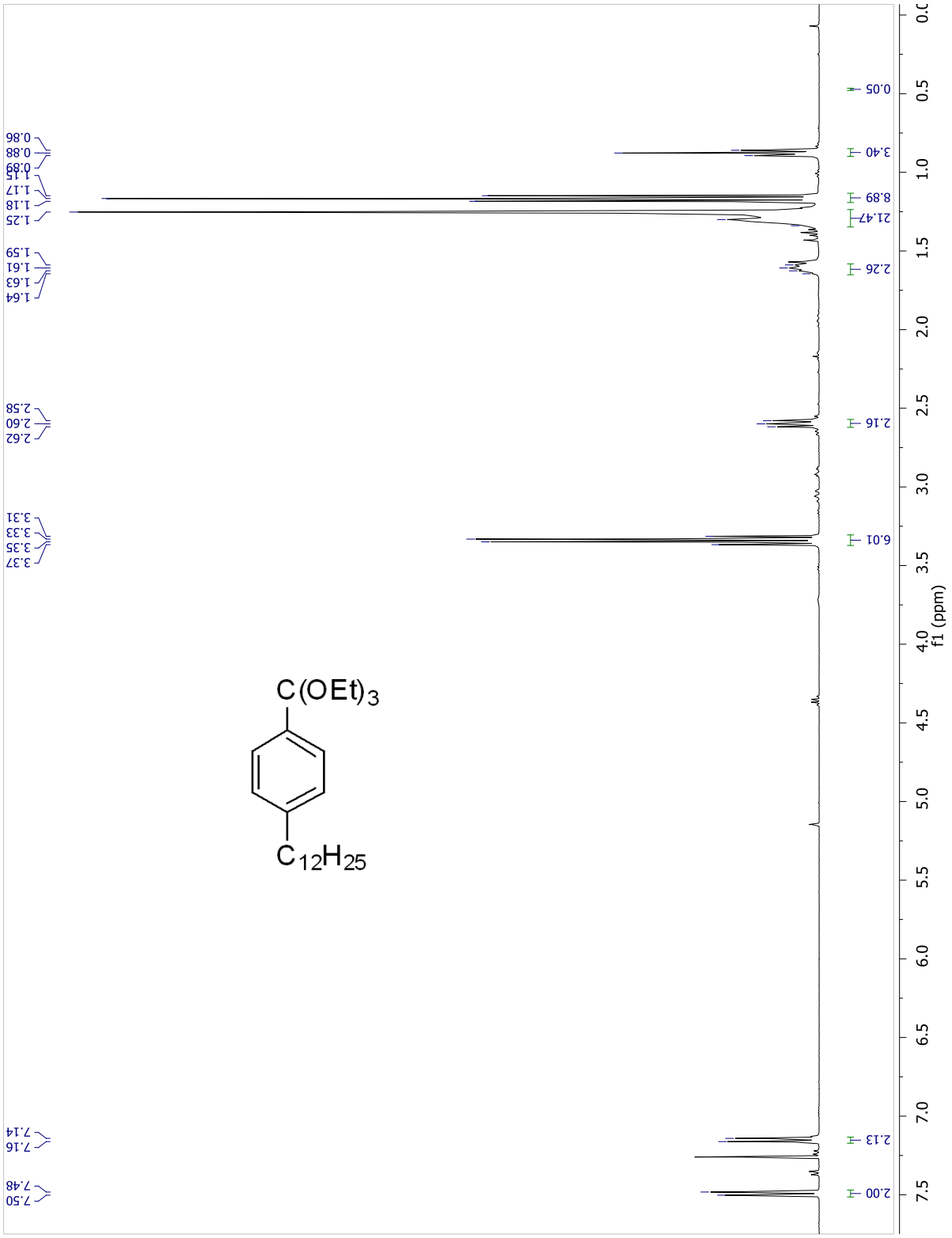

Figure S3.41. ^{1}H NMR spectrum of 4-dodecyl-1-(triethoxymethyl)benzene.

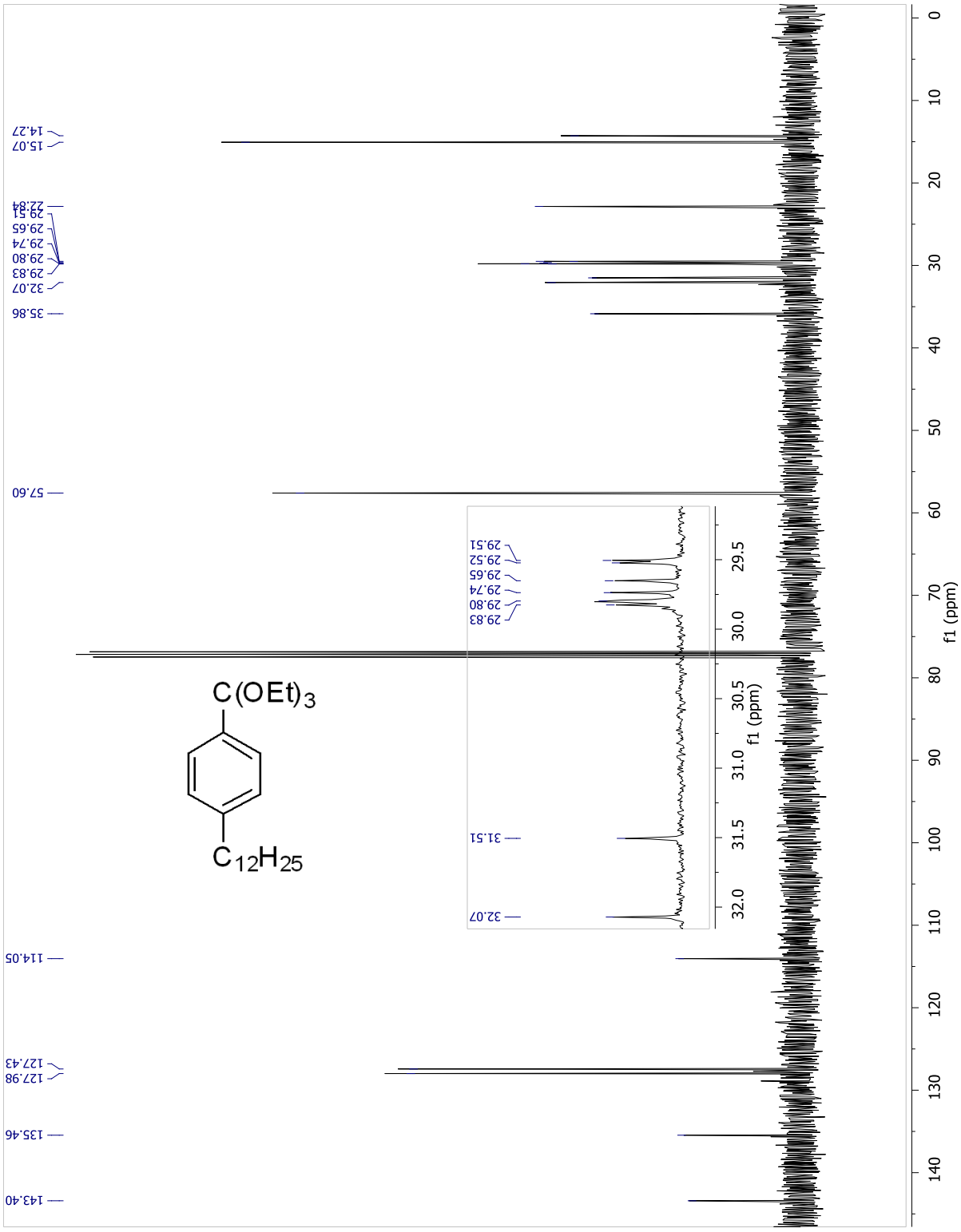

Figure S3.42. ^{13}C NMR spectrum of 4-dodecyl-1-(triethoxymethyl)benzene.

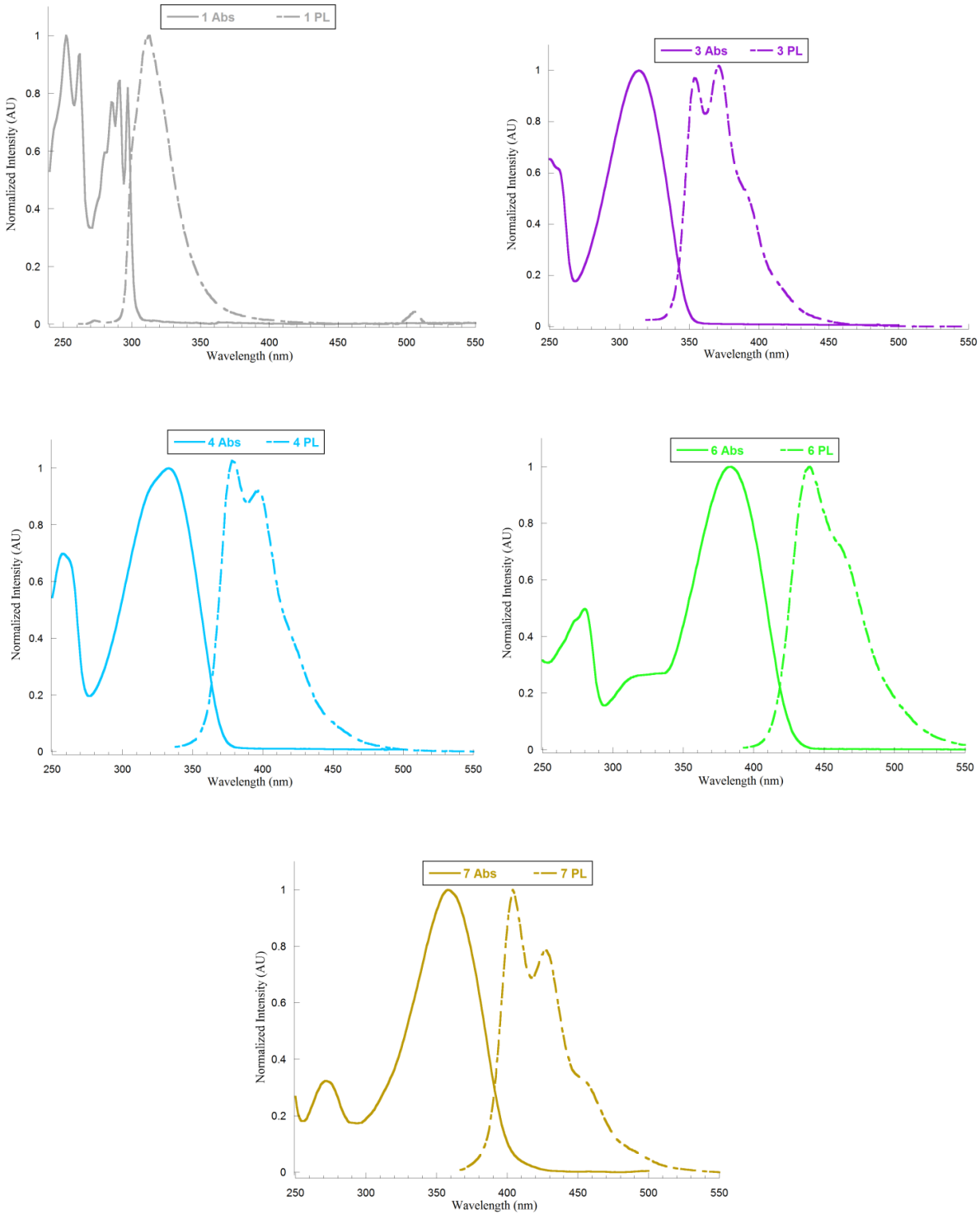

Figure S3.43. Normalized UV-Vis and photoluminescence spectra of **1**, **3**, **4**, **6**, and **7**.

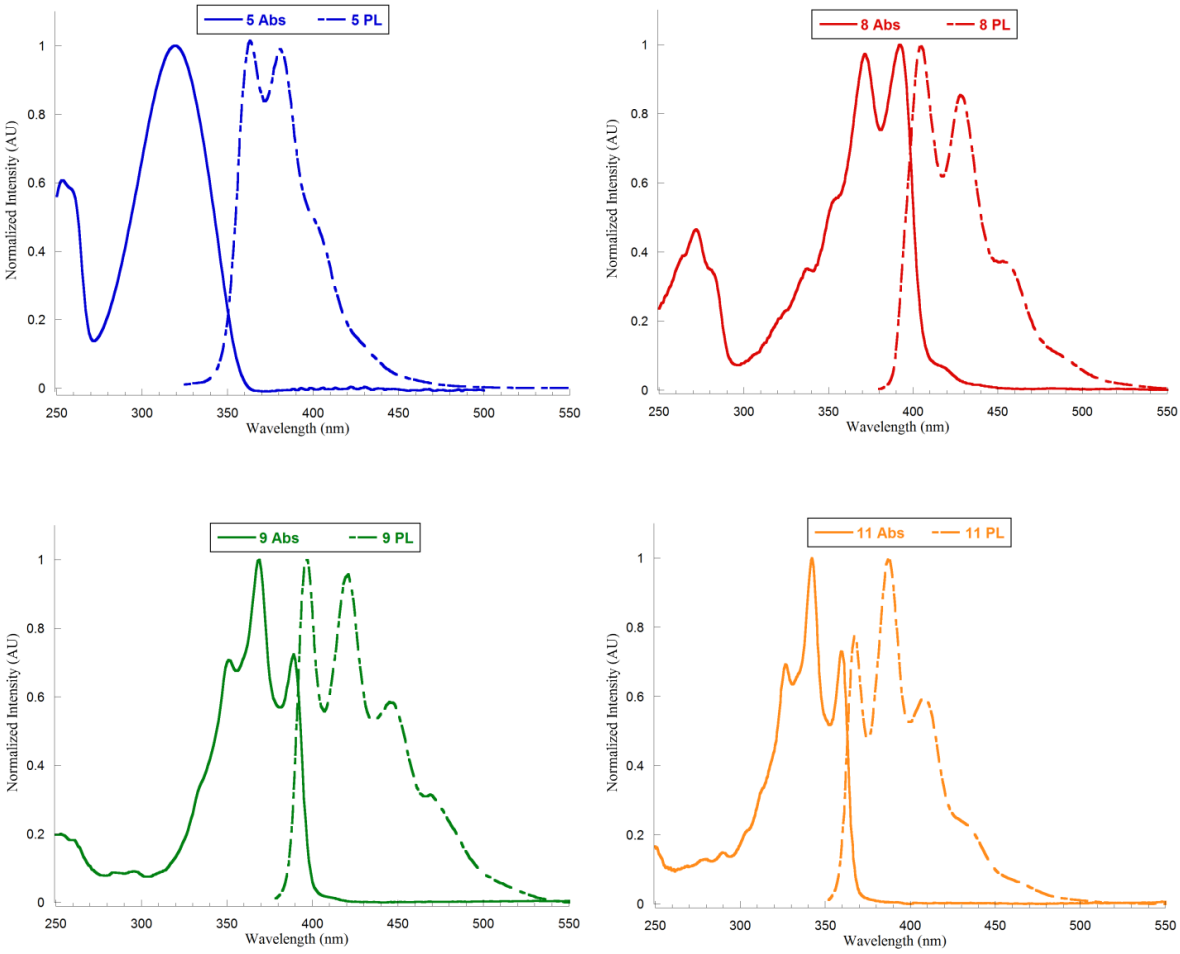

Figure S3.43. Normalized UV-Vis and photoluminescence spectra of **5**, **8**, **9**, and **11**.

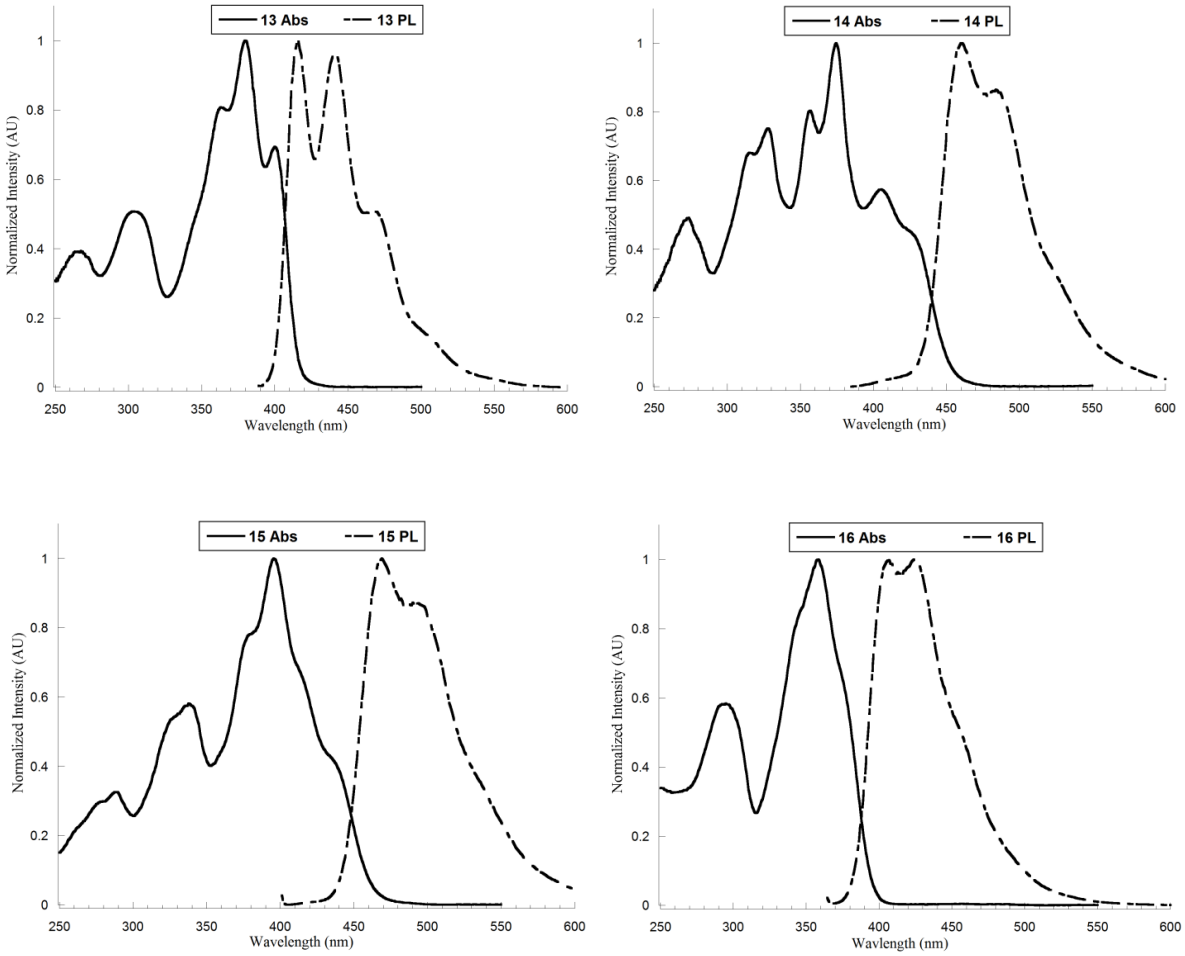

Figure S3.45. Normalized UV-Vis and photoluminescence spectra of **13**, **14**, **15**, and **16**.

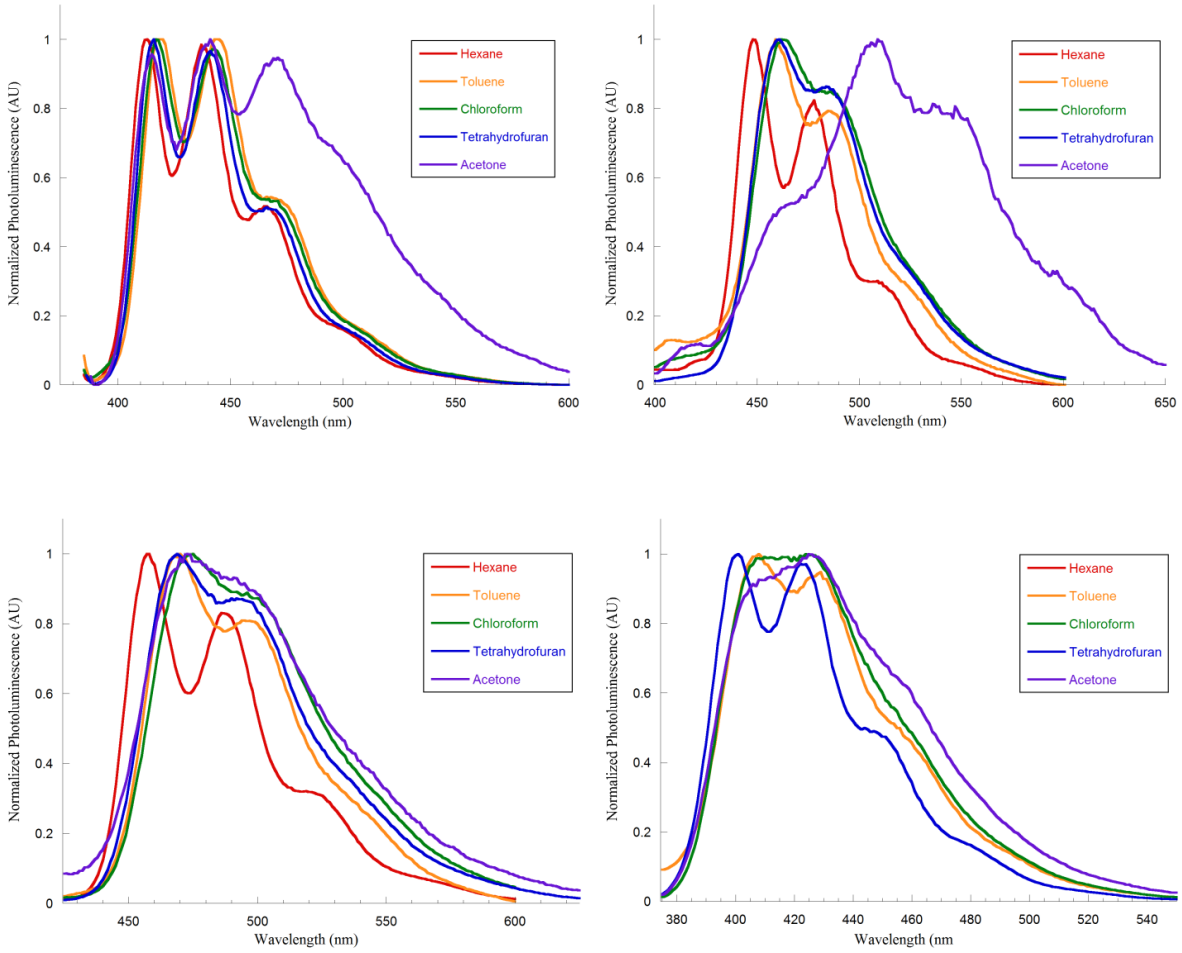

Figure S3.46. Solvochromism effect of cruciforms **13-16**.

Table S1. Comparison of experimental and computional energy levels

	HOMO (eV)		LUMO (eV)		E_g^{opt} (eV)	
	expt[a]	theory	expt[b]	theory	expt[c]	theory
1	-6.50	-6.21	-2.3	-1.21	4.2	4.65
3	-5.94	-5.69	-2.3	-1.74	3.6	3.69
4	-5.87	-5.13	-2.5	-1.59	3.4	3.30
5	-5.96	-5.48	-2.5	-1.63	3.4	3.58
6	-4.92	-4.57	-2	-1.24	3.0	3.05
7	-5.98	-5.36	-2.8	-1.85	3.0	3.17
8	-5.71	-5.23	-2.6	-1.85	3.1	3.21
9	-5.51	-5.52	-2.3	-2.00	3.2	3.27
11	-5.75	-5.74	-2.3	-1.92	3.4	3.52
13	-5.78	-5.32	-2.7	-2.07	3.1	2.98
14	-5.49	-5.06	-2.7	-2.11	2.8	2.70
15	-5.29	-5.01	-2.5	-2.15	2.8	2.60
16	-5.88	-5.43	-2.7	-1.99	3.2	3.13

[a] Measured by UPS. [b] Calculated using HOMO + E_g^{opt}. [c] Measured at intersection of UV-Vis and PL spectra.

3.8 References

(1) Horowitz, G. *Advanced Materials* **1998**, *10*, 365.

(2) Mas-Torrent, M.; Rovira, C. *Chemical Society Reviews* **2008**, *37*, 827.

(3) Newman, C. R.; Frisbie, C. D.; daSilva Filho, D. A.; Bredas, J. L.; Ewbank, P. C.; Mann, K. R. *Chem. Mater.* **2004**, *16*, 4436.

(4) Murphy, A. R.; Frechet, J. M. J. *Chemical Reviews* **2007**, *107*, 1066.

(5) Dimitrakopoulos, C. D.; Malenfant, P. R. L. *Advanced Materials* **2002**, *14*, 99.

(6) Tang, C. W.; VanSlyke, S. A. *Applied Physics Letters* **1987**, *51*, 913.

(7) Veinot, J. G. C.; Marks, T. J. *Accounts of Chemical Research* **2005**, *38*, 632.

(8) Friend, R. H.; Gymer, R. W.; Holmes, A. B.; Burroughes, J. H.; Marks, R. N.; Taliani, C.; Bradley, D. D. C.; Dos Santos, D. A.; Bredas, J. L.; Logdlund, M.; Salaneck, W. R. *Nature* **1999**, *397*, 121.

(9) Alam, M. M.; Jenekhe, S. A. *Chemistry of Materials* **2004**, *16*, 4647.

(10) Coakley, K. M.; McGehee, M. D. *Chemistry of Materials* **2004**, *16*, 4533.

(11) Scharber, M.; Mühlbacher, D.; Koppe, M.; Denk, P.; Waldauf, C.; Heeger, A.; Brabec, C. *Adv. Mater.* **2006**, *18*, 789.

(12) Tang, C. W. *Applied Physics Letters* **1986**, *48*, 183.

(13) Osowska, K.; Miljanic, O. S. *Chem. Commun.* **2010**, *46*, 4276.

(14) Lim, J.; Albright, T. A.; Martin, B. R.; Miljanić, O. Š. *The Journal of Organic Chemistry* **2011**, *76*, 10207.

(15) Klare, J. E.; Tulevski, G. S.; Sugo, K.; de Picciotto, A.; White, K. A.; Nuckolls, C. *J. Am. Chem. Soc.* **2003**, *125*, 6030.

(16) Wilson, J. N.; Josowicz, M.; Wang, Y.; Bunz, U. H. F. *Chemical Communications* **2003**, 2962.

(17) Zucchero, A. J.; McGrier, P. L.; Bunz, U. H. F. *Acc. Chem. Res.* **2009**, *43*, 397.

(18) McGrier, P. L.; Solntsev, K. M.; Miao, S.; Tolbert, L. M.; Miranda, O. R.; Rotello, V. M.; Bunz, U. H. F. *Chemistry – A European Journal* **2008**, *14*, 4503.

(19) Marsden, J. A.; Miller, J. J.; Shirtcliff, L. D.; Haley, M. M. *Journal of the American Chemical Society* **2005**, *127*, 2464.

(20) Ohta, K.; Yamada, S.; Kamada, K.; Slepkov, A. D.; Hegmann, F. A.; Tykwinski, R. R.; Shirtcliff, L. D.; Haley, M. M.; Salek, P.; Gel'mukhanov, F.; Aagren, H. *J. Phys. Chem. A* **2011**, *115*, 105.

(21) Spitler, E. L.; Monson, J. M.; Haley, M. M. *The Journal of Organic Chemistry* **2008**, *73*, 2211. (22) Spitler, E. L.; Shirtcliff, L. D.; Haley, M. M. *The Journal of Organic Chemistry* **2007**, *72*, 86.

(23) Kang, H.; Evmenenko, G.; Dutta, P.; Clays, K.; Song, K.; Marks, T. J. *Journal of the American Chemical Society* **2006**, *128*, 6194. (24) Tlach, B. C.; Tomlinson, A. e. L.; Bhuwalka, A.; Jeffries-El, M. *The Journal of Organic Chemistry* **2011**, *76*, 8670.

(25) Intemann, J. J.; Hellerich, E. S.; Tlach, B. C.; Ewan, M. D.; Barnes, C. A.; Bhuwalka, A.; Cai, M.; Shinar, J.; Shinar, R.; Jeffries-El, M. *Macromolecules* **2012**, *45*, 6888.

(26) Ripaud, E.; Olivier, Y.; Leriche, P.; Cornil, J. r. m.; Roncali, J. *The Journal of Physical Chemistry B* **2011**, *115*, 9379.

(27) Wilson, J. N.; Windscheif, P. M.; Evans, U.; Myrick, M. L.; Bunz, U. H. F. *Macromolecules* **2002**, *35*, 8681.

(28) Klare, J. E.; Tulevski, G. S.; Nuckolls, C. *Langmuir* **2004**, *20*, 10068.

(29) May, J. C.; Biaggio, I.; Bures, F.; Diederich, F. *Applied Physics Letters* **2007**, *90*, 251106.

(30) Gao, B.; Liu, Y.; Geng, Y.; Cheng, Y.; Wang, L.; Jing, X.; Wang, F. *Tetrahedron Letters* **2009**, *50*, 1649.

(31) Würthner, F.; Thalacker, C.; Diele, S.; Tschierske, C. *Chemistry – A European Journal* **2001**, *7*, 2245.

(32) Wilson, J. N.; Hardcastle, K. I.; Josowicz, M.; Bunz, U. H. F. *Tetrahedron* **2004**, *60*, 7157.

(33) Hegedus, L. S.; Odle, R. R.; Winton, P. M.; Weider, P. R. *Journal of Organic Chemistry* **1982**, *47*, 2607.

(34) Mike, J. F.; Inteman, J. J.; Ellern, A.; Jeffries-El, M. *Journal of Organic Chemistry* **2010**, *75*, 495.

(35) Mike, J. F.; Makowski, A. J.; Jeffries-EL, M. *Org. Lett.* **2008**, *10*, 4915.

(36) Mike, J. F.; Intemann, J. J.; Cai, M.; Xiao, T.; Shinar, R.; Shinar, J.; Jeffries-El, M. *Polymer Chemistry* **2011**, *2*, 2299.

(37) Brown, R. D.; Buchanan, A. S.; Humffray, A. A. *Aust. J. Chem.* **1965**, *18*, 1521.

(38) Tschitschibabin, A. E. *Ber.* **1905**, *38*, 561.

(39) Breslow, R.; Pandey, P. S. *J. Org. Chem.* **1980**, *45*, 740.

(40) Mamane, V.; Aubert, E.; Fort, Y. *Journal of Organic Chemistry* **2007**, *72*, 7294.

(41) Bhuwalka, A.; Mike, J. F.; He, M.; Intemann, J. J.; Nelson, T.; Ewan, M. D.; Roggers, R. A.; Lin, Z.; Jeffries-El, M. *Macromolecules* **2011**, *44*, 9611.

(42) Salaneck, W. R. *Journal of Electron Spectroscopy and related Phenomena* **2009**, *174*, 3.

(43) Miyamae, T.; Yoshimura, D.; Ishii, H.; Ouchi, Y.; Miyazaki, T.; Koike, T.; Yamamoto, T.; Muramatsu, Y.; Etori, H.; Maruyama, T.; Seki, K. *Synth. Met.* **1997**, *84*, 939.

(44) Lois, S.; Florès, J.-C.; Lère-Porte, J.-P.; Serein-Spirau, F.; Moreau, J. J. E.; Miqueu, K.; Sotiropoulos, J.-M.; Baylère, P.; Tillard, M.; Belin, C. *European Journal of Organic Chemistry* **2007**, *2007*, 4019.

(45) Nijegorodov, N. I.; Downey, W. S. *The Journal of Physical Chemistry* **1994**, *98*, 5639.

(46) Berlman, I. B. *The Journal of Physical Chemistry* **1970**, *74*, 3085.

(47) Huang, W.; Yin, J. *Polym. Eng. Sci.* **2007**, *47*, 429.

(48) *Principles and Applications of Photochemistry*; Wiley: Hoboken, NJ, USA, 2009.

(49) Dollish, F. R.; Fateley, W. G.; Bentley, F. F. *Characteristic Raman Frequencies of Organic Compounds*; Wiley-Interscience, 1973.

(50) So, Y.-H.; Zaleski, J. M.; Murlick, C.; Ellaboudy, A. *Macromolecules* **1996**, *29*, 2783.

(51) Caspar, J. V.; Meyer, T. J. *The Journal of Physical Chemistry* **1983**, *87*, 952.

(52) Tolbert, L. M.; Nesselroth, S. M.; Netzel, T. L.; Raya, N.; Stapleton, M. *The Journal of Physical Chemistry* **1992**, *96*, 4492.

(53) Zucchero, A. J.; Wilson, J. N.; Bunz, U. H. F. *Journal of the American Chemical Society* **2006**, *128*, 11872.

(54) Zhang, H. C.; Guo, E. Q.; Zhang, Y. L.; Ren, P. H.; Yang, W. J. *Chemistry of Materials* **2009**, *21*, 5125.

(55) Chase, D. T.; Young, B. S.; Haley, M. M. *The Journal of Organic Chemistry* **2011**, *76*, 4043.

(56) Pak, J. J.; Weakley, T. J. R.; Haley, M. M. *Journal of the American Chemical Society* **1999**, *121*, 8182.

(57) Melhuish, W. H. *The Journal of Physical Chemistry* **1961**, *65*, 229.

(58) Tlach, B. C.; Tomlinson, A. L.; Bhuwalka, A.; Jeffries-El, M. *J. Org. Chem.* **2011**, *76*, 8670.

(59) Bo, Z.; Schlüter, A. D. *The Journal of Organic Chemistry* **2002**, *67*, 5327.

(60) Kannan, R.; He, G. S.; Lin, T.-C.; Prasad, P. N.; Vaia, R. A.; Tan, L.-S. *Chemistry of Materials* **2003**, *16*, 185.

(61) Wang, X.; Ng, J. K.-P.; Jia, P.; Lin, T.; Cho, C. M.; Xu, J.; Lu, X.; He, C. *Macromolecules* **2009**, *42*, 5534.

(62) Saikia, G.; Iyer, P. K. *The Journal of Organic Chemistry* **2010**, *75*, 2714.

(63) Zysman-Colman, E.; Arias, K.; Siegel, J. S. *Canadian Journal of Chemistry* **2009**, *87*, 440.

(64) Leermann, T.; Leroux, F. d. r. R.; Colobert, F. o. *Organic Letters* **2011**, *13*, 4479.

(65) Yoon, M.-H.; DiBenedetto, S. A.; Facchetti, A.; Marks, T. J. *Journal of the American Chemical Society* **2005**, *127*, 1348.

(66) Kim, J.-J.; Lim, K.; Choi, H.; Fan, S.; Kang, M.-S.; Gao, G.; Kang, H. S.; Ko, J. *Inorganic Chemistry* **2010**, *49*, 8351.

(67) Ellinger, S.; Kreyes, A.; Ziener, U.; Hoffmann-Richter, C.; Landfester, K.; Möller, M. *European Journal of Organic Chemistry* **2007**, *2007*, 5686.

(68) Firouzabadi, H.; Iranpoor, N.; Hazarkhani, H. *The Journal of Organic Chemistry* **2001**, *66*, 7527.

CHAPTER 4

EVALUATION OF THE IMPACT OF EXTENDED CONJUGATION ON THE OPTOELECTRONIC PROPERTIES BENZO[1,2-*d*:4,5-*d*′] BISOXAZOLE POLYMERS

Reproduced with permission from *J. Aust. Chem.* **2014,** *67,* 711.

DOI: 10.1071/ch13528

Brian C. Tlach,[a] *Aimée L. Tomlinson,*[b] *Kiley D. Morgan,*[b] *Christopher R. Collins,*[b] *Michael D. Zenner,*[a] *and Malika Jeffries-EL*[a]*

[a] Department of Chemistry, Iowa State University, Ames IA 50010

[b] Department of Chemistry/ Biochemistry, University of North Georgia, GA 30597

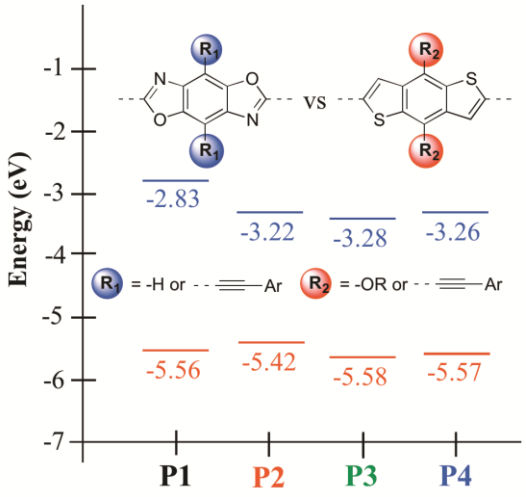

4.1 Abstract

Four copolymers comprised of benzo[1,2-*d*;4,5-*d′*]bisoxazole (BBO) and benzo[1,2-*b*:4,5-*b′*]dithiophene (BDT) units were synthesized. Phenylethynyl substituents were incorporated onto either the BBO moiety, the BDT moiety or both to investigate the influence of two-dimensional conjugation on their optical and electronic properties. The materials were evaluated using cyclic voltammetry, UV-vis spectroscopy, and density functional theory. It was found that the second conjugation axis on the BBO moiety in **P2** resulted in a 0.5 eV decrease in the LUMO level, while the HOMO level was raised by 0.2 eV. However, substitution across the BDT moiety in **P3** also resulted in a 0.5 eV decrease in the LUMO level, and the effect on the HOMO level was negligible. Adding a second conjugation axis on both BBO and BDT in **P4** gave the same results as single substitution across the BDT moiety, while decreasing the solubility of the material. Collectively, these results indicate that cross-conjugation can be used to independently tune the LUMO level within these systems.

4.2 Introduction

In recent years there has been a large amount of research devoted to the development of organic semiconductors (OSC)s as replacements for conventional inorganic materials.[1] These materials are finding use in applications such as field effect transistors (FET)s,[2] organic light-emitting diodes (OLED)s,[3] and photovoltaic cells (OPV)s.[4] OSCs offer a number of advantages over inorganic semiconductors including the opportunity to process them from solution,[5] which can reduce fabrication cost and optoelectronic properties that can be readily tuned by chemical synthesis. Generally, the introduction of flexible side chains

onto the conjugated polymer backbone not only improves the solubility and film-forming characteristics, but also influences the nanoscale morphology, as well as the electronic, optical and physical properties.[6] Varying the electron-donating or electron-accepting strength of the arenes along the polymer backbone can further modify the optical and electronic properties of these materials. Thus in principle, OSCs can be synthesized with highest occupied molecular orbitals (HOMO)s, lowest unoccupied molecular orbitals (LUMO)s, and band gaps that are tailored for specific applications. Unfortunately, in practice, this is often difficult to accomplish due to the complex interplay between the structure of the material and its properties resulting from the extensive delocalization of electrons within the OSCs. Therefore, synthetic strategies that facilitate the independent tuning of the HOMO or LUMO level are highly sought after.

For this reason, 2-dimensional cross-shaped "cruciform" molecules that feature two conjugation axes are especially promising. These compounds have spatially segregated frontier molecular orbitals (FMO)s which facilitate the individual modification of either the LUMO or the HOMO by changing the substituents and their location on the central molecule.[7] Although there have been many reports on the synthesis of cruciform shaped small molecules,[7-8] there have been only a limited number of reports on the effect of extended conjugation in polymeric systems, many of them based on copolymers of benzo[1,2-*b*:4,5-*b'*]dithiophene (BDT) derivatives featuring extended conjugation.[9] BDT is an electron-rich molecule that has been widely investigated for the synthesis of conjugated polymers because it has a planar, conjugated structure that facilitates π–π stacking and promotes charge carrier mobility.[10] As a result, power conversion efficiencies for polymer solar cells have exceeded 9% for BDT copolymers.[10c, 11] Replacing the electron-rich alkoxy

groups with thien-2-yl, aryl, alkynyl, and phenylethynyl substituents, on the 4- and 8-positions of the BDT moiety can be used to lower the HOMO level.

Similarly, benzo[1,2-*d*:4,5-*d*′]bisoxazoles (BBO)s are electron deficient moieties that have been incorporated into polymers with exceptional thermal and chemical stability,[12] efficient electron transport, and blue emission.[13] [14] Like BDT, BBO can also be substituted at the 4- and 8-positions with aryl, alkynyl, and phenylethynyl substitutents.[8a, 15] It has been demonstrated on small molecules that the HOMO and LUMO levels of BBO could readily be tuned by substitution,[7d, 16] and that the impact on the energy levels is a function of the nature and location of the substituent.[8a] However, the effects of extended conjugation on the HOMO, LUMO, and the band gap of the BBO polymers have not been explored. Herein we synthesized four new polymers utilizing combinations of one- and two-dimensional BDT and BBO monomers. The effect of the extended conjugation on the optoelectronic properties was evaluated using cyclic voltammetry, UV-vis spectroscopy, and density functional theory (DFT).

4.3 Results and Discussion

4.3.1 Synthesis of BBO Monomers

Previously we reported the synthesis of 2,6-(dithien-2-yl)BBOs via the Lewis-acid catalyzed condensation of diamino diols and aryl orthoesters.[17] For the synthesis of the BBO monomers in this study, we envisaged a similar approach. The requisite orthoester **1** (Scheme 4.1) was synthesized from 2-bromo-3-(2-ethylhexyl)thiophene[18] in 54% yield using the method first reported by Tschitschibabin.[17, 19] This alkyl substituent was used to increase the solubility of the BBO monomers and allow for easy bromination at the 5-position.

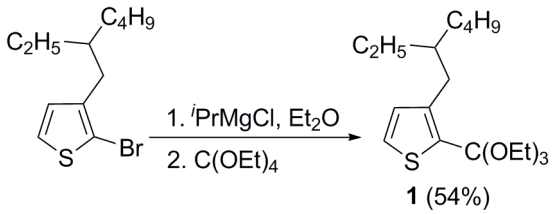

Scheme 4.1. Synthesis of substituted orthoester **1**.

Furthermore, placement of the alkyl chain at the 3-position instead of the 4-position on thiophene should decrease steric interactions between monomer units in the polymer and steric hinderance during the polymerization reaction. The reaction of **1** and 2,5-diamino-1,4-hydroquinone bishydrochloride (DAHQ)[20] afforded BBO **2** in 55% yield (Scheme 4.2). This yield was lower than our previous reports for similar compounds, which is likely due to the steric hinderance caused by the 2-ethylhexyl chain adjacent to the trimethoxymethyl moiety. BBO **2** was then easily brominated in 69% yield to give one-dimensional BBO monomer **3**.

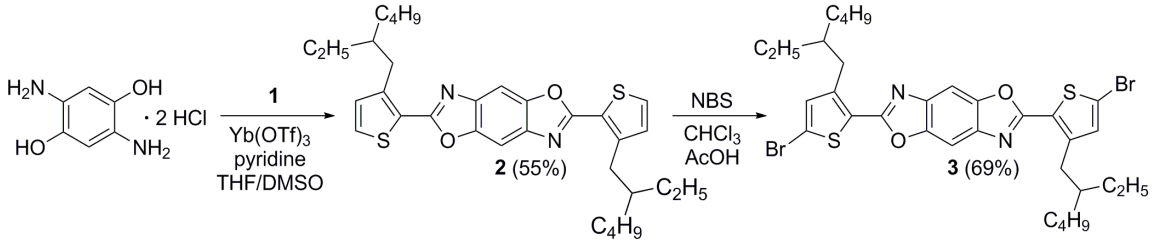

Scheme 4.2. Synthesis of linear BBO **3**.

A similar approach was used to synthesize the two-dimensional BBO monomer and is outlined in Scheme 4.3. The condensation reaction of **1** and 3,6-diamino-2,5-dibromo-1,4-hydroquinone[21] (Br-DAHQ) afforded BBO **4** in 19% yield. The lower yield of the reaction compared to that of **2** is likely a result of the decreased nucleophilicity of Br-DAHQ. The two-dimensional BBO intermediate **5** was obtained from the Sonogashira coupling between **4** and 3,5-di-(2-ethylhexyloxy)-1-ethynylbenzene **6**, in 91% yield (Scheme 4.3). The alkyne

was easily synthesized from 3,5-di-(2-ethylhexyloxy)benzaldehyde[22] via the Corey-Fuchs reaction (Scheme 4.4).

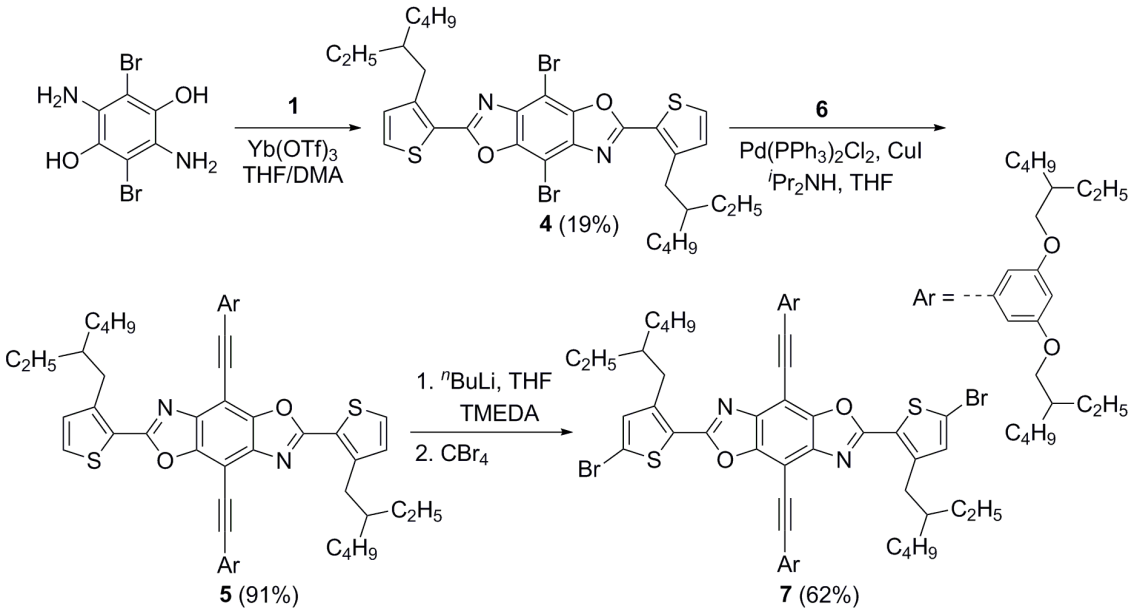

Scheme 4.3. Synthesis of two-dimensional BBO monomer **7**.

This alkyne was used because it allowed for the installation of long-branched alkyl chains for solubility, while the meta substitution pattern prevented the electron-donation from the oxygen atoms into the BBO.

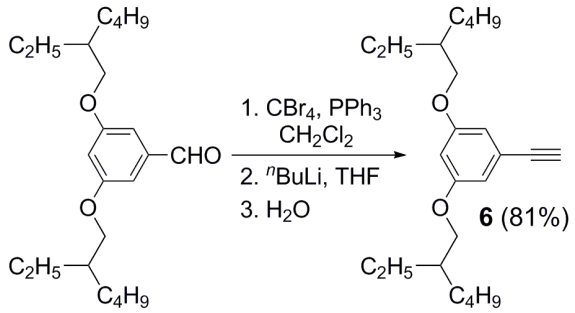

Scheme 4.4. Synthesis of substituted alkyne **6**.

Since electrophilic brominating reagents could not be used on BBO **5**, a double lithium-hydrogen exchange was performed using n-butyl lithium and TMEDA and quenching the

resulting anion with carbon tetrabromide to give the targeted two-dimensional BBO monomer **7** in 62% yield.

4.3.2 Synthesis of BDT Monomers

The synthesis of both the one-dimensional and two-dimensional BDT monomers is shown in Scheme 4.5. The one-dimensional intermediate **8** was synthesized from benzo[1,2-*b*:4,5-*b*']dithiophene-4,8-dione[23] according to the literature procedure.[24] The two-dimensional BDT system was prepared by the nucleophilic addition of lithiated **6** (via n-butyl lithium) to benzo[1,2-*b*:4,5-*b*']dithiophene-4,8-dione. Subsequent stannylation of **8** and **9** afforded monomers **10** and **11** in yields 66% and 86%, respectively. The identity of all the compounds was confirmed using ^{1}H NMR, ^{13}C NMR, and high resolution mass spectroscopy.

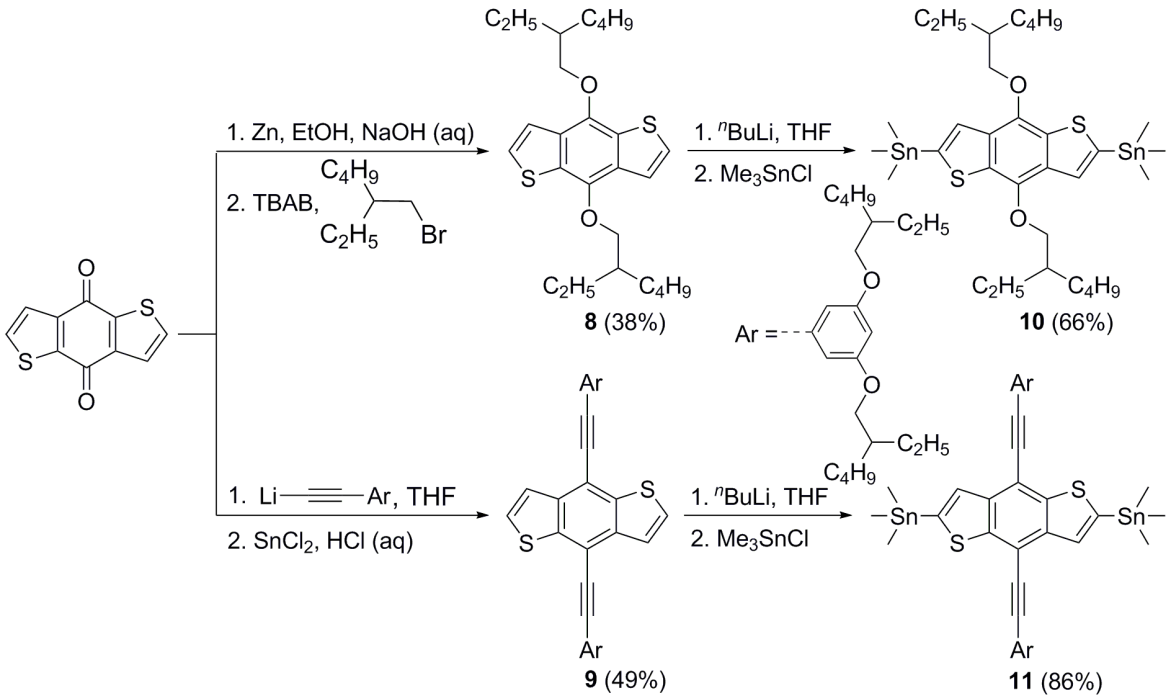

Scheme 4.5. Synthesis of BDT donors.

4.3.3 Synthesis of Copolymers

The copolymers were synthesized using a Stille cross-coupling catalyzed by $Pd(PPh_3)_4$ in toluene/DMF as shown in Scheme 4.6. The isolated polymers **P1 – P4** were obtained in 43 – 80% yield and the structures shown in Figure 4.1. The polymers were characterized by gel permeation chromatography (GPC), UV-vis spectroscopy, and, cyclic voltametry (CV). The ^1H NMR spectra of the four polymers were consistent with the proposed structures. The molecular weight data as determined by GPC is shown in Table 4.1. The polymers showed good solubility in chlorinated solvents and toluene and had moderate to high molecular weights that vary dramatically. **P2** displayed the highest molecular weight (M_n) of 39,000 Da and **P1** had the lowest M_n of 7,000 Da.

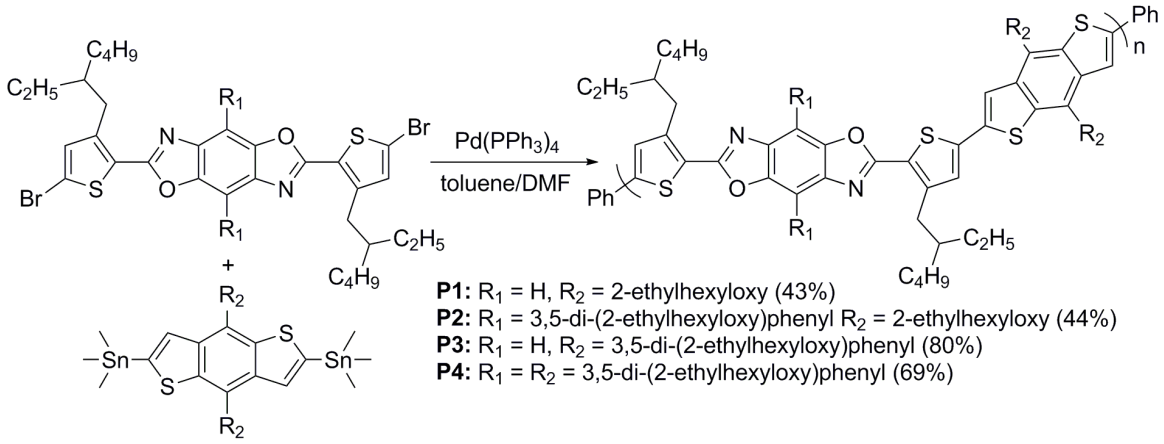

Scheme 4.6. Synthesis of polymers **P1 – P4**.

P1 suffers from lower molecular weights due to decreased number of side-chains and more rigid-rod like structure compared to all other polymers, allowing for increased π-π stacking. In the case of **P4**, the large size of the two-dimensional monomers likely contributes to its limited molecular weight. The general increase in molecular weight for cross-conjugated polymers **P2 – P4** is likely a result from the increased steric bulk of the phenylacetylene side chains and increased side-chain density which disrupt π-π stacking.

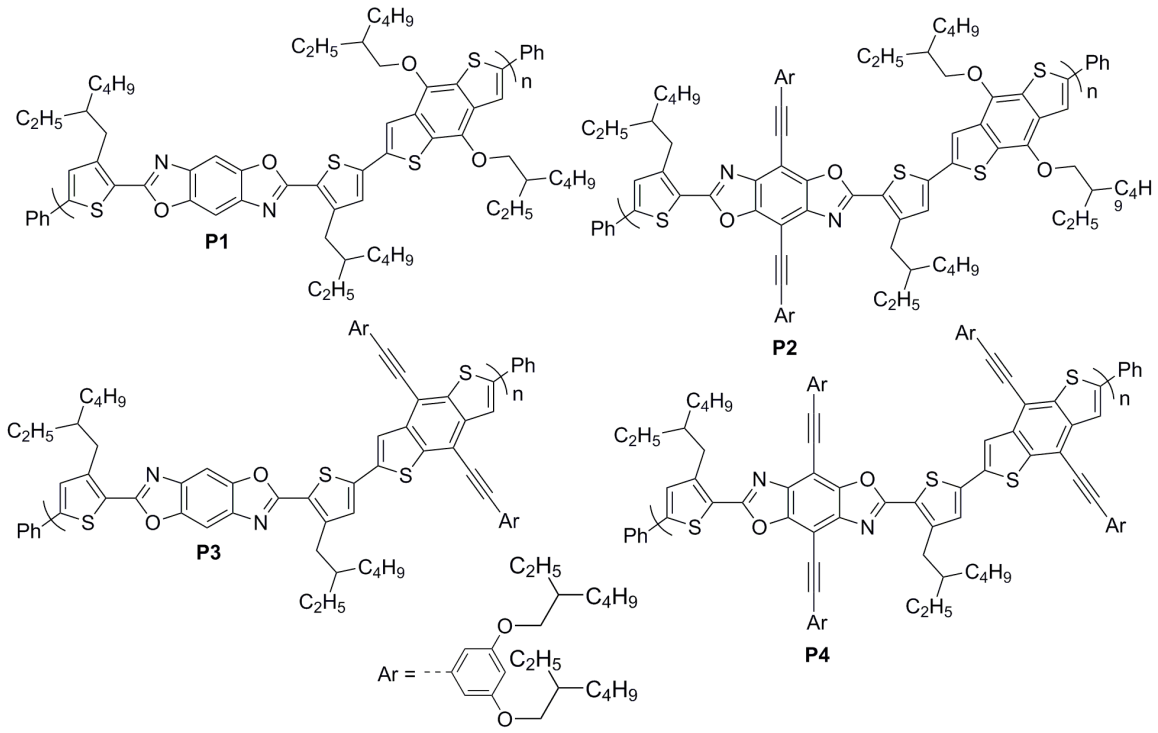

Figure 4.1. Structures of polymers **P1** – **P4**.

Table 4.1. Molecular weight[a] data for polymers **P1 – P4**

	M_n[a] (kDa)	PDI[b]	DP_n[c]	T_d[d] (°C)
P1	7.02	1.17	7	359
P2	39.8	2.31	23	372
P3	28.9	1.44	20	412
P4	19.2	1.55	9	402

[a] M_n: number average molecular weight versus polystyrene in chloroform at 50 °C. [b]PDI: M_w/M_n. [c] DP_n: Degree of polymerization based on M_n.

[d] T_d: 5% weight loss temperature as determined by TGA in air.

The thermal properties of the polymers were studied using differential scanning calorimetry (DSC) and thermogravimetric analysis (TGA). None of the polymers displayed transitions in DSC below 300 °C (Figure S4.29) indicating the amorphous nature of the polymers. The

polymers all showed excellent thermal stability with 5% weight loss temperatures between 359 °C (**P1**) and 412 °C (**P3**) as determined by TGA (Figure S4.30) in air.

4.3.4 Spectroscopic and Electronic Characterization

The normalized absorption spectra of **P1 – P4** both as dilute $CHCl_3$ solutions and as thin films are shown in Figure 4.2 with the optical data summarized in Table 4.2. In comparison to the solution spectra, the thin film spectrum for the unsubstituted polymer, **P1**, exhibits a slight broadening of the absorption band and a slight red shift in the absorption maximum. Whereas the substituted polymers **P2**, **P3**, **P4** show no difference between the solution and film spectra, indicating that the polymers are not π-stacking efficiently in the solid state. This is likely a result of the bulky side chains, which prevent efficient π-stacking. In both solution and film, all four polymers exhibit a single absorption band, with two peaks corresponding to the π-π* transition.

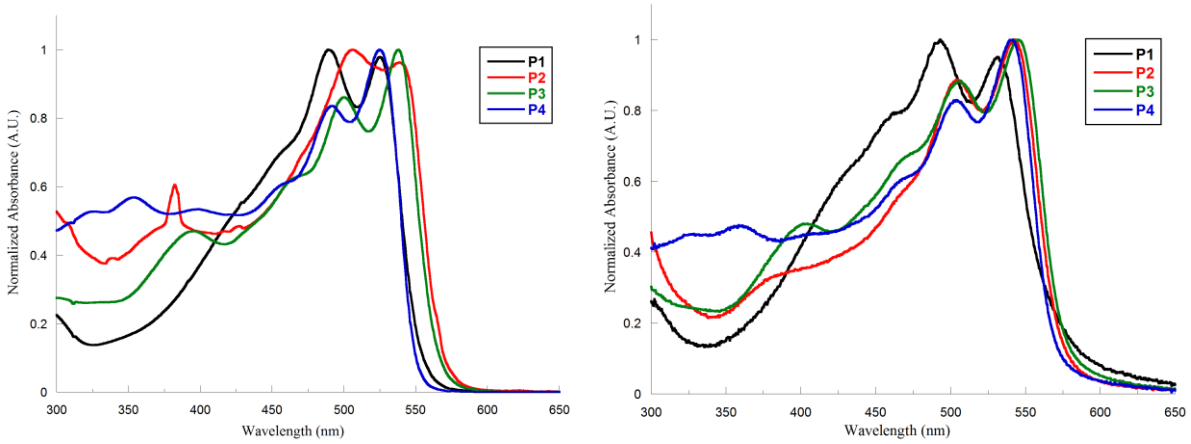

Figure 4.2. UV-vis spectra of **P1 – P4** in chloroform (left) and thin film (right).

However, all of the spectra lack the presence of the low-energy band characteristic of intramolecular charge transfer (ICT) between electron-donating and electron-accepting units within the polymer backbone.[25]

Table 4.2. Optical properties of BBO polymers

	λ_{max}^{soln} (nm)[a]	λ_{max}^{film} (nm)	E_g^{opt} (eV)[b]
P1	489, 525	493, 531	2.3
P2	504, 543	506, 539	2.2
P3	500, 538	506, 545	2.2
P4	492, 525	504, 542	2.2

[a] Performed in dilute chloroform solutions.

[b] Calculated from the intersection of the thin film absorption and emission spectra (Figure S4.25).

The electrochemical properties of the polymers were investigated using cyclic voltametry and the traces can be found in Figure S4.23 in the Supporting Information. All four polymers exhibited measurable and reproducible oxidation and reduction processes. The HOMO and LUMO levels were estimated from the onset of oxidation and the onset of reduction, respectively, using the absolute energy level of ferrocene/ferrocenium (Fc/Fc^+) as 4.8 eV under vacuum and are summarized in Table 4.3.[26] The unsubstituted polymer, **P1** has a HOMO level of -5.6 eV, a LUMO level of -2.8 eV, resulting in an electrochemical bandgap of 2.8 eV. Extension of conjugation across the BBO moiety affords **P2** with a slightly raised HOMO level of -5.4 eV, a lower LUMO level of -3.2 eV, and narrower bandgap of 2.2 eV. Likewise, extension of conjugation across the BDT moiety affords **P3** with an unchanged HOMO level of -5.6 eV, a lower LUMO level of -3.3 eV, and an optical bandgap of 2.3 eV. Interestingly, **P4** that has extended conjugation across both the BBO and the BDT moieties has the same HOMO and LUMO level as **P3**.

Table 4.3. An experimental and theoretical comparison of the electronic properties of BBO polymers

	HOMO[a] (eV)		LUMO[b] (eV)		E_g[c] (eV)	
Polymer	Experiment	Theory	Experiment	Theory	Experiment	Theory
P1	-5.6	-4.98	-2.8	-2.68	2.8/2.3	1.94
P2	-5.4	-4.74	-3.2	-2.58	2.2/2.2	1.86
P3	-5.6	-4.86	-3.3	-2.63	2.3/2.2	1.88
P4	-5.6	-4.83	-3.3	-2.55	2.3/2.2	1.93

[a] Calculated from the oxidation onset using $-4.8 - E_{ox}{}^{onset}$. [b] Calculated from the reduction onset using $-(4.8 + E_{red}{}^{onset})$. [c] Shown as $E_g{}^{EC}/E_g{}^{opt}$ where $E_g{}^{EC} = LUMO - HOMO$ and $E_g{}^{opt}$ was calculated from the intersection of the thin film absorption and emission spectra.

To further elucidate the influence of extended conjugation on the optical and electronic properties of these polymers, ground-state geometry optimizations were performed utilizing density functional theory (DFT) employing a B3LYP[27] functional, a 6-31G* basis and the Gaussian 09 software package.[28] Frontier Molecular Orbital (FMO) diagrams and electrostatic potential maps, as shown in Figure 4.3, were generated from the DFT outputs. In addition a time dependent density functional theory routine with the aforementioned functional and basis set was utilized to generate the excited states and the results are summarized in Table 4.3. According to DFT, the band gaps in increasing size are **P2** < **P3** < **P4** < **P1**, although the difference between the values was only 0.08 eV. The ordering of the calculated HOMO levels from low to high was **P1** > **P3** > **P4** > **P2**, although the difference between **P3** and **P4** was negligible. All of these observations are consistent with the experimental data.

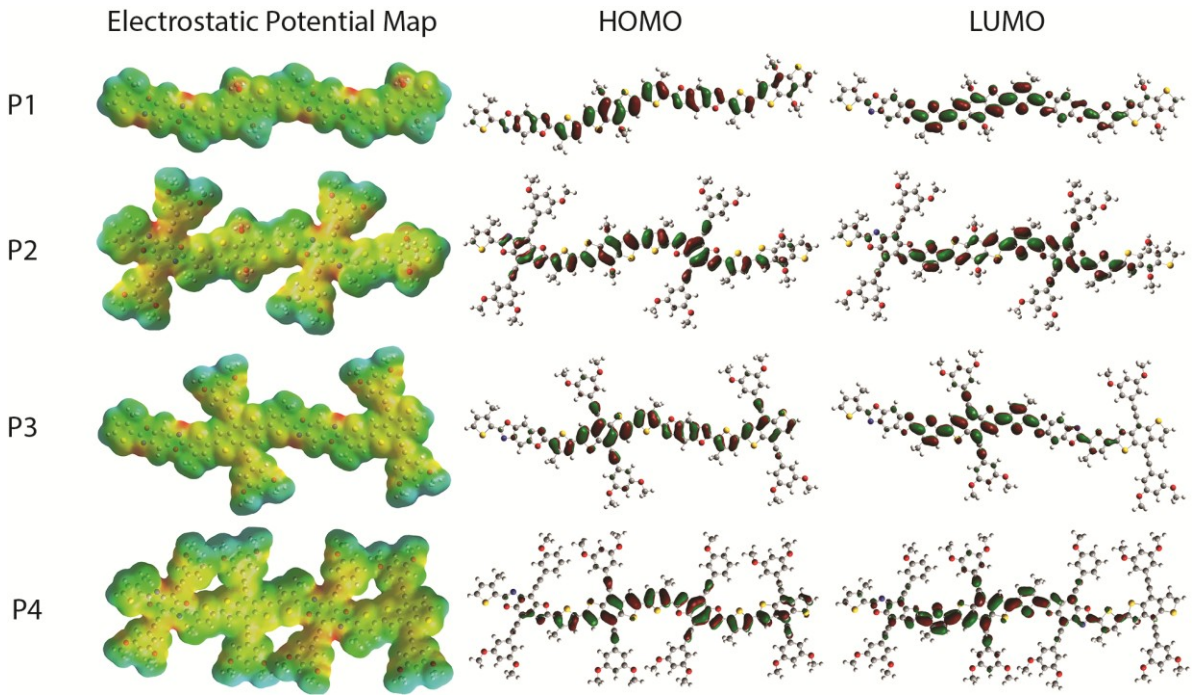

Figure 4.3. Electrostatic potential maps and FMO diagrams of **P1 – P4**.

Copolymers that are comprised of alternating electron-donating and electron-accepting moieties have energy levels that are easily tuned by changing the strength of the donor and acceptor units. In these systems, the LUMO level is primarily related to the acceptor unit, whereas the HOMO level is largely determined by the donor unit.[29] Since the phenylethynyl BBO is a stronger acceptor than the unsubstituted BBO, we anticipated that extending conjugation with an electron accepting phenylethynyl substituent across the BBO would lower the LUMO. Accordingly, **P2** had a lower LUMO (0.5 eV) than **P1** or **P3**, although it also had a slightly higher HOMO level (0.2 eV). This effect is likely a combination of the electron-accepting alkyne and the extended conjugation across the BBO.[15] On the other hand, phenylethynyl BDT is a weaker donor than unsubstituted BDT, thus extending the conjugation along the BDT was expected to lower the HOMO level. Hence, **P3** should have a lower HOMO level than **P1** or **P2**, unfortunately this was not the

case. We believe that this is a result of the twisting along the polymer backbone that occurs in **P3** as demonstrated by the optimized geometry for model dimers of this system. As seen in Figure 4.4, the unsubstituted polymer **P1** is planar, whereas the other polymers are not. Similarly, **P4** that has substituents on both the BDT and BBO has the same HOMO, LUMO and bandgap as **P3**, despite the presence of a second substituent. Again the optimized geometry for model dimers of this system also revealed significant twisting. Thus the resulting energy levels are not merely a function of the increased electron-density around the BBO and BDT moieties, steric effects also play a major role. The latter reduces the planarity of the system and decreases the delocalization of electron density along the polymer backbone.

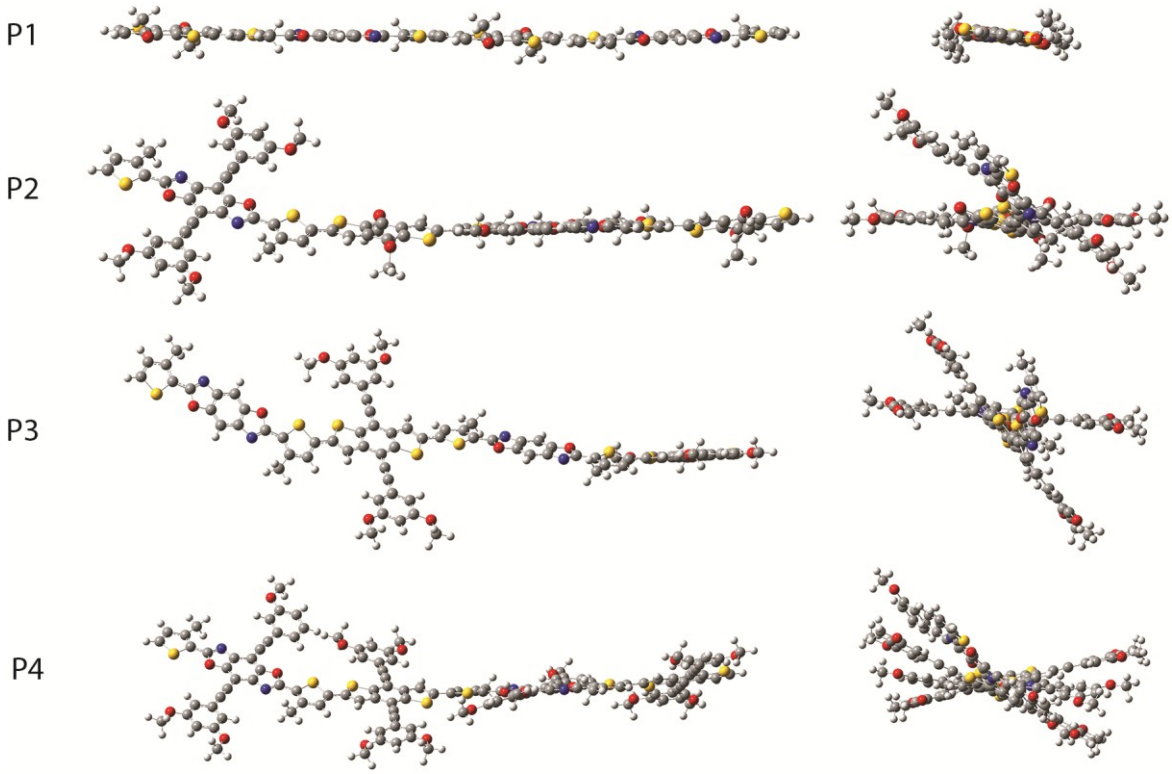

Figure 4.4. Optimized geometries for model dimers of **P1 – P4**.

The FMO diagrams and electrostatic potential maps for all of the polymers indicate that the electron density is uniformly distributed along the polymer backbone. This further supports the experimental and theoretical findings that there is very little difference in the electronic properties of these polymers. Furthermore, the lack of difference between **P3** and **P4** can be attributed to the partial localization of LUMO on the BDT moiety compared to **P1** and **P2** which have complete delocalization of the LUMO. These diagrams are consistent with the observations seen in the UV-vis spectra that ICT is not occurring in these systems due to the delocalization of the FMOs.

4.4 Conclusions

In conclusion, to evaluate the use of cross-conjugation for selectively modifying the FMOs within conjugated polymers, three new two-dimensional polymers were synthesized and compared to the newly synthesized one-dimensional polymer using both experimental and theoretical means. The UV-vis spectra for all of the polymers were similar indicating that there were only minor differences in the optical properties. Additionally, **P2** – **P4** displayed no difference in solution and film spectra indicating there is little to no aggregation in the solid state, most likely due to steric effects introduced by the bulky side chains. However, the spectra for **P1** indicated that ICT was not occurring within the polymer backbone, as a result of relative strength and weakness of the BDT donor and BBO acceptor, respectively. The extended conjugation of **P2** – **P4** failed to increase ICT, as indicated by UV-Vis spectra and the lack of localization of electron density in the FMOs. The absence of donor-acceptor behavior is the cross-conjugated polymers is partially a result of the steric twist along the polymer backbone caused by the large side chains, along with the relative

strength and weakness of the BDT donor and BBO acceptor, respectively. Nonetheless, the fact the HOMO level remained mostly unchanged while the LUMO was altered by structural modifications indicate that cross-conjugation is a promising approach for selectively tuning the LUMO level of OSCs. However, to further evaluate this approach, the polymer design needs to be improved through the use of different substituents to decrease these steric interactions and a more electron rich monomers to promote ICT. Future work will focus on these alterations using experimental and theoretical methods.

4.5 Experimental Section

4.5.1 Characterization

Nuclear magnetic resonance (NMR) experiments were carried out in $CDCl_3$ at 400 MHz (^1H) or 100 MHz (^{13}C) on a Varian MR-400. ^1H NMR spectra are internally referenced to the residually protonated solvent peak (7.26 ppm), and ^{13}C NMR spectra are referenced to the central carbon peak (77.16 ppm) of $CDCl_3$. In all spectra, chemical shifts are given in δ relative to tetramethylsilane. Coupling constants are reported in hertz (Hz). High-resolution mass spectra were recorded on a double-focusing magnetic sector mass spectrometer using electrospray ionization (ESI) or atmospheric pressure chemical ionization (APCI). Melting points were obtained on a melting point apparatus with 260 °C upper limit and are uncorrected. Gel permeation chromatography (GPC) measurements were performed on a separation module equipped with three 5 μm I-gel columns connected in series (guard, HMW, MMW and LMW) with a UV-Vis detector. Analyses were performed at 50 °C using $CHCl_3$ as the eluent with a flow rate of 1.0 mL min^{-1} with calibration based on polystyrene standards. Electrochemistry was performed on a eDAQ e-Corder 410 using 0.01 M $AgNO_3$

in acetonitrile as a reference electrode, platinum wire counter electrode, and platinum button electrode as the working electrode at a scanning rate of 50 mV^{-1} s. All measurements were taken under argon atmosphere in deoxygenated acetonitrile with 0.1 M tetrabutylammonium hexafluorophosphate as the electrolyte. The potentials measured versus the Ag^{+} were externally referenced to Fc/Fc^{+} (-4.8 eV versus vacuum). Thermogravimetric analysis (TGA) measurements were performed over an interval of 25 – 800 °C at a heating rate of 20 °C min^{-1} under ambient atmosphere. Differential scanning calorimetry (DSC) was performed using a first scan heating rate of 10 °C min^{-1} to erase thermal history and a second scan to measure transitions between 0 and 300 °C under nitrogen. All sample films drop-cast from 1,2-dichlorobenzene (^{o}DCB) solutions (2 mg mL^{-1}) and were annealed at 80 °C under vacuum for 6 hours prior to analysis. UV-vis spectroscopy was performed on a Varian Cary-Eclipse spectrometer on dilute chloroform solutions or thin films. Thin films were spin-coated from mixtures of chloroform and ^{o}DCB (5 mg mL^{-1}) onto 25 x 25 x 1 glass slides at 1200 rpm on a Headway Research, Inc. PWM32 spin-coater and annealed at 80 °C under vacuum for 6 hours prior to analysis.

4.5.2 Materials

Tetrabutylammonium hexafluorophospate was purchased from Oakwood Chemical and was recrystallized from methanol prior to use. All other chemicals were purchased from commercial sources and used without further purification. 2,5-diamino-1,4-hydroquinone bishydrochloride (DAHQ)[20], 3,6-diamino-2,5-dibromo-1,4-hydroquinone (Br-DAHQ)[15], 2-bromo-3-(2-ethylhexyl)thiophene (**7**) [18], 3,5-bis(2-ethylhexyloxy)benzaldehyde[22], benzo[1,2-*b*:4,5-*b*']dithiophene-4,8-dione[23], and 2,6-bis(trimethylstannyl)-4,8-bis(2-

ethylhexyloxy)benzo[1,2-*b*:4,5-*b*']dithiophene (**8**)[24] were synthesized according to literature procedures.

4.5.3 General Synthetic Details

Unless otherwise noted, all reactions were carried out in oven-dried glassware, under argon atmosphere, and with stirring using standard Schlenk techniques. Column chromatography was carried out using silica gel (35 – 70 micron) unless otherwise specified.

4.5.4. Synthetic Procedures

*Synthesis of 3-(2-ethylhexyl)-2-(triethoxymethyl)thiophene (**1**).* A dry two-neck flask equipped with an addition funnel and reflux condenser was charged with 1.22 g (50 mmol) magnesium turnings and heated under vacuum for 1 h. The flask was back-filled with argon and a few crystals of iodine added and allowed to sublime for 20 minutes. The flask was cooled to room temperature and charged with 35 mL dry Et_2O. 4.6 mL (50 mmol) of 2-chloropropane in 10 mL dry Et_2O was added drop-wise via addition funnel to maintain a gentle reflux and then refluxed for an additional 1 h. A solution of 6.88 g (20.0 mmol) 2-bromo-3-(2-ethylhexyl)thiophene in 5 mL dry Et_2O was added drop-wise and the solution refluxed for 24 h. The solution was cooled to room temperature, 5.8 g (30 mmol) tetraethylorthocarbonate was added drop-wise and then the reaction heated to reflux for 12 h. The reaction was cooled to room temperature and poured into cold saturated aqueous NH_4Cl and the layers separated. The aqueous layer was extracted with Et_2O and the combined organic layers washed with H_2O and brine and dried over Na_2SO_4. The solution was filtered and the solvent removed *in vacuo*. Low-boiling impurities were removed by Kugelrohr distillation to yield a yellow oil that was used without further purification (3.71g, 54% yield): ^{1}H NMR δ $CDCl_3$ (7.17 (d, J = 4 Hz, 1H), 6.89 (d, J = 4 Hz, 1H), 3.42(q, J = 8 Hz, 6 H), 2.70

(dd, J = 4 Hz, 2H), 1.71 (m, J = 8 Hz, 1H), 1.28 – 1.21 (comp, 8H), 1.21 (t, J = 8 Hz, 9H), 0.87 (t, J = 8 Hz, 6H); ^{13}C NMR ($CDCl_3$) δ 140.5, 134.6, 129.4, 124.4, 113.5, 57.9, 39.5, 32.9, 32.7, 29.1, 26.0, 23.3, 15.0, 14.3, 11.0.

*2,6-bis(3-(2-ethylhexyl)thien-2-yl)benzo[1,2-d;4,5-d']bisoxazole (**2**).* A dry Schlenk flask was charged with 1.03 g (3.00 mmol) **1** and 3 mL dry THF and the solution deoxygenated for 20 minutes. Concurrently, a dry pear flask was charged with 1 mL of DMSO and 180 mg (2.25 mmol) of pyridine and the solution deoxygenated for 20 minutes. 213 mg (1.00 mmol) of DAHQ was added to the pear flask and allowed to dissolve. The Schlenk flask was kept under argon atmosphere, charged with 31 mg (0.05 mmol) of $Yb(OTf)_3$, and warmed to 60 °C. The DAHQ solution was added drop-wise, 1 mL of THF added after 2 h, and stirring continued at 60 °C overnight. The warm mixture was diluted with a small volume of $CHCl_3$ to dissolve the solids and the mixture precipitated into 150 mL methanol at -78 °C. The precipitate was filtered and washed with methanol to yield a white powder (300 mg, 55% yield): mp 102 – 104 °C; ^{1}H NMR ($CDCl_3$) δ 7.81 (s, 2H), 7.46 (d, J = 8 Hz, 2H), 7.02 (d, J = 4 Hz, 2H), 3.15 (d, J = 8 Hz, 4H), 1.75 (m, 2H), 1.39 – 1.29 (comp, 16H), 0.93 (t, J = 8 Hz, 6H), (t, J = 6 Hz, 6H); ^{13}C NMR ($CDCl_3$) δ 160.9, 148.2, 140.1, 131.9, 128.9, 123.9, 100.5, 40.9, 34.2, 33.0, 29.0, 26.1, 23.2, 14.3, 11.1. HRMS (ESI) *m/z*: Calcd for $C_{32}H_{41}N_2O_2S_2$ 549.2604 $[M + H]^+$, found 549.2602.

*2,6-bis(3-(2-ethylhexyl)-5-bromothien-2-yl)benzo[1,2-d;4,5-d']bisoxazole (**3**).* A small flask protected from light was charged with 560 mg (1.02 mmol) **2** and dissolved in 35 mL of 6:1 $CHCl_3$/acetic acid. Upon warming the solution to 40 °C, 540 mg (3.06 mmol) NBS was added portion-wise followed by 2 drops of HBr. The reaction was stirred for 3 days at 40 °C then poured into 300 mL of cold methanol. The precipitate was filtered rinsing with

methanol and the crude product recrystallized from ethyl acetate to yield yellow crystals (500 mg, 69% yield): mp 157 – 159 °C; ^{1}H NMR ($CDCl_3$) δ 7.77 (d, J = 8 Hz, 2H), 6.98 (s, 2H), 3.10 (d, J = 8 Hz, 4H), 1.71 (m, 2H), 1.31 – 1.37 (comp, 16H), 0.92 (t, J = 8 Hz, 6H), 0.89 (t, J = 8 Hz, 6H); ^{13}C NMR ($CDCl_3$) δ 159.7, 148.1, 147.7, 140.1, 135.6, 125.4, 117.0, 100.6, 40.8, 34.2, 32.9, 29.0, 26.0, 23.2, 14.3, 11.0. HRMS (ESI) *m/z*: Calcd for $C_{32}H_{39}Br_2N_2O_2S_2$ 707.0794 $[M + H]^+$, found 707.0798.

*4,8-dibromo-2,6-bis(3-(2-ethylhexyl)thien-2-yl)benzo[1,2-d;4,5-d']bisoxazole (**4**).* A dry Schlenk flask was charged with 3.95 g (11.5 mmol) **1**, 4 mL dry THF, and 4 mL dry DMA and the solution deoxygenated for 20 minutes. The solution was warmed to 55 °C under argon and 119 mg (0.19 mmol) $Yb(OTf)_3$ was added. 1.15 g (3.85 mmol) of freshly prepared Br-DAHQ was added portion-wise over 20 minutes followed by 3 mL of THF after 2 h. Stirring was continued at 55 °C overnight and the warm mixture poured into 200 mL of cold methanol. The precipitate was filtered rinsing with methanol and the crude product recrystallized from ethyl acetate to yield off-white crystals (485 mg, 19% yield): mp 205 – 207 °C; ^{1}H NMR ($CDCl_3$) δ 7.51 (d, J = 8 Hz, 2H), 7.03 (d, J = 4 Hz, 2H), 3.20 (d, J = 8 Hz, 4H), 1.79 (m, 2H), 1.43 – 1.29 (comp, 16H), 0.92 (t, J = 8 Hz, 3H), 0.87 (t, J = 8 Hz, 3H); ^{13}C NMR ($CDCl_3$) 161.0, 148.2, 146.5, 139.4, 132.1, 129.9, 122.9, 91.2, 40.7, 34.5, 32.6, 28.8, 25.7, 23.3, 14.3, 10.8. HRMS (ESI) *m*/z: Calcd for $C_{32}H_{39}Br_2N_2O_2S_2$ 707.0794 $[M + H]^+$, found 707.0798.

*4,8-bis(3,5-di-(2-ethylhexyloxy)phenylethynyl)-2,6-bis(3-(2-ethylhexyl)thien-2-yl)benzo[1,2-d;4,5-d']bisoxazole (**5**).* A dry two-neck round-bottom equipped with a reflux condenser was charged with 887 mg (2.48 mmol) **6**, 1.5 mL (11.0 mmol) $^{i}Pr_2NH$, and 12 mL dry THF and the solution deoxygenated for 30 minutes. The flask was charged with 775 mg

(1.10 mmol) of **4**, 10.5 mg (0.055 mmol) CuI, and 38.6 mg (0.055 mmol) $PdCl_2(PPh_3)_2$, the mixture further deoxygenated for 10 minutes, and then heated to reflux for 48 h. The mixture was allowed to cool to room temperature, filtered through a small pad of celite rinsing with CH_2Cl_2, and the solution concentrated *in vacuo*. The crude product was purified by column chromatography eluting with 90:10 hexanes/CH_2Cl_2 with a slow gradient to 70:30 hexanes/CH_2Cl_2 to yield a viscous red oil (1.26 g, 91% yield): ^{1}H NMR ($CDCl_3$) δ 7.49 (d, J = 8 Hz, 2H), 7.03 (d, J = 4 Hz, 2H), 6.86 (d, J = 4 Hz, 4H), (s, 4H), 6.54 (t, J = 4 Hz, 2H), 3.89 (d, J = 8 Hz, 8H), 3.23 (dq, J_d = 44 Hz, J_q = 8 Hz, 4H), 1.75 (m, 6H), 1.54 – 1.15 (comp, 48H), 0.97 – 0.91 (comp, 30H), 0.77 (t, J = 8 Hz, 6H); ^{13}C NMR ($CDCl_3$) δ 161.1, 160.5, 148.4, 148.5, 140.7, 131.9, 129.4, 124.0, 123.5, 110.4, 103.5, 100.4, 98.2, 79.4, 70.9, 40.8, 39.6, 34.4, 32.5, 30.7, 29.3, 28.7, 26.1, 24.1, 23.2, 23.1, 14.3, 14.2, 11.3, 11.0. HRMS (ESI) *m/z*: Calcd for $C_{80}H_{113}N_2O_6S_2$ 1261.8035 $[M + H]^+$, found 1261.8024.

*3,5-di-(2-ethylhexyloxy)ethynylbenzene (**6**).* In a round-bottom flask, 10.8 g (41.0 mmol) PPh_3 was dissolved in 30 mL CH_2Cl_2, cooled to 0 °C, and then 6.80 g (20.5 mmol) CBr_4 added in one-portion. 3.63 g (10.0 mmol) 1,3-di-(2-ethylhexyloxy)benzaldehyde was dissolved in 20 mL CH_2Cl_2 and added drop-wise via addition funnel to the reaction. The reaction was stirred for 1 h at 0 °C and then warmed to room temperature over 2 h. The solids were filtered rinsing with hexanes and the filtrate concentrated *in vacuo*. The crude mixture was suspended in hexanes, loaded onto a short pad of silica gel, and the product eluted with hexanes. The eluted product was concentrated *in vacuo* and dried under vacuum with stirring. The flask was back-filled with argon, the resulting oil dissolved in 40 mL dry THF, and cooled to -78 °C in a dry ice/acetone bath. 10.3 mL of ^{n}BuLi (2.5 M hexanes) was added drop-wise and the reaction allowed to warm to room temperature overnight. The reaction was

quenched with saturated NH_4Cl (aq) and extracted with hexanes. The combined organic layers were washed with H_2O and brine and dried over Na_2SO_4. The solution was filtered and concentrated *in vacuo*. The product was purified by column chromatography eluting with hexanes to yield a yellow oil (2.90 g, 81% yield): ^{1}H NMR ($CDCl_3$) δ 6.63 (s, 2H), 6.47 (s, 1H), 3.80 (d, J = 8 Hz, 4H), 3.01 (s, 1H), 1.70 (m, 2H), 1.52 – 1.31 (comp, 16H), 0.93 – 0.89 (comp, 12H); ^{13}C NMR ($CDCl_3$) 160.4, 123.2, 110.4, 103.3, 84.0, 78.5, 39.5, 30.6, 29.2, 24.0, 23.2, 14.2, 11.2. HRMS (ESI) *m/z*: Calcd for $C_{24}H_{39}O_2$ 359.2945 $[M + H]^+$, found 359.2948.

*4,8-bis(3,5-di-(2-ethylhexyloxy)phenylethynyl)-2,6-bis(5-bromo-3-(2-ethylhexyl)thien-2-yl)benzo[1,2-d;4,5-d']bisoxazole (**7**).* In a dry Schlenk flask, 1.02 g (0.81 mmol) **5** was dissolved in 20 mL of dry THF and the solution cooled to -78 °C in a dry ice/acetone bath. 1.0 mL of ^{n}BuLi (2.5 M hexanes) was added drop-wise over 10 minutes and stirred for 90 minutes at -78 °C. 940 mg (2.84 mmol) of CBr_4 was added in one portion and the reaction stirred for 3 h at -78 °C and then allowed to warm to room temperature overnight. The reaction was diluted with Et_2O, quenched with saturated NH_4Cl (aq), and the layers separated. The aqueous layer was extracted with Et_2O, the combined organic layers washed with H_2O and brine, and dried over Na_2SO_4. The solution was filtered, concentrated *in vacuo*, and product purified by column chromatography eluting with 95:5 hexanes/CH_2Cl_2 with a slow gradient to 70:30 after the first generation was eluted to yield a sticky red oil (0.71 g, 62% yield): ^{1}H NMR ($CDCl_3$) δ 7.00 (s, 2H), 6.84 (d, J = 4 Hz, 2H), 6.54 (t, J = 4 Hz, 4H), 3.89 (d, J = 8 Hz, 8H), 3.18 (dq, J_d = 40 Hz, J_q = 8 Hz, 4H), 1.75 (comp, 6H), 1.55 – 1.17 (comp, 48H), 0.97 – 0.91 (comp, 30H), 0.78 (t, J = 8 Hz, 6H); ^{13}C NMR ($CDCl_3$) δ 160.5, 148.5, 148.3, 140.6, 134.6, 125.0, 123.8, 117.6, 110.4, 103.6, 100.7, 98.3, 79.1, 70.9,

40.8, 39.6, 34.5, 32.5, 30.7, 29.3, 28.7, 26.0, 24.1, 23.2, 23.1, 14.3, 14.26, 14.17, 11.3, 10.9. HRMS (ESI) *m/z*: Calcd for $C_{80}H_{111}Br_2N_2O_6S_2$ 1417.6245 $[M + H]^+$, found 1417.6204.

*4,8-bis(3,5-di-(2-ethylhexyloxy)phenylethynyl)benzo[1,2-b:4,5-b']dithiophene (**9**).* A dry two-neck round-bottom flask equipped with a reflux condenser was charged with 700 mg (1.95 mmol) **6** and 5.5 mL of dry THF. The flask was cooled to 0 °C and 0.82 mL ^{n}BuLi (2.5 M hexanes) added drop-wise. The reaction was stirred at 0 °C for 1 h, warmed to room temperature, and 187 mg (0.85 mmol) benzo[1,2-*b*:4,5-*b*']dithiophene-4,8-dione added in one-portion. The reaction was heated to reflux for 18 h and then allowed to cool to room temperature. A solution of 770 mg (3.40 mmol) $SnCl_2{\cdot}2H_2O$ dissolved in 3.4 mL of 3 M HCl was added in one portion followed by 5 mL of THF. The mixture was heated to reflux for 6 h then allowed to cool to room temperature. The mixture was extracted with Et_2O and the combined organic layers washed with H_2O and brine and dried over Na_2SO_4. The solution was filtered and concentrated *in vacuo*. The crude product was purified by column chromatography (basic alumina) eluting with 95:5 hexane/CH_2Cl_2 with a gradient to 75:25 after the first generation was eluted to yield a viscous yellow oil (380 mg, 49% yield): ^{1}H NMR ($CDCl_3$) δ 7.73 (d, *J* = 4 Hz, 2H), 7.60 (d, *J* = 4 Hz, 2H), 6.82 (s, 4H), 6.53 (s, 2H), 3.90 (d, *J* = 8 Hz, 8H), 1.75 (m, 4H), 1.56-1.34 (comp, 32H), 0.98 – 0.93 (comp, 24H); ^{13}C NMR ($CDCl_3$) δ 160.6, 140.5, 138.5, 128.3, 124.0, 123.4, 112.1, 110.1, 103.2, 99.6, 85.1, 70.8, 39.6, 30.7, 29.3, 24.1, 23.2, 14.3, 11.3. HRMS (ESI) *m/z*: Calcd for $C_{58}H_{78}O_4S_2$ 903.5414 $[M + H]^+$, found 903.5404.

*2,6-bis(trimethylstannyl)-4,8-bis(3,5-di-(2-ethylhexyloxy)phenylethynyl)benzo[1,2-b:4,5-b']dithiophene (**11**).* In a dry Schlenk flask, 1.41 g (1.56 mmol) **9** was dissolved in 40 mL dry THF and the solution cooled to -78 °C in a dry ice/acetone bath. 1.75 mL ^{n}BuLi (2.5

M hexanes) was added drop-wise and the reaction stirred for 90 minutes at -78 °C. 4.5 mL of trimethyltin chloride (1.0 M in THF) was added in one portion and the reaction allowed to warm to room temperature overnight. The reaction mixture was diluted with hexanes, quenched with H_2O, and the layers separated. The organic layer was washed with H_2O and brine and dried over Na_2SO_4. The solution was filtered, concentrated *in vacuo*, and the crude product dissolved in a minimal volume of warm $CHCl_3$. The solution was precipitated into 400 mL cold methanol and the precipitate filtered rinsing with methanol to yield a yellow powder (1.64 g, 86% yield): mp 101 – 103 °C; ^{1}H NMR ($CDCl_3$) δ 7.73 (s, 2H), 6.84 (d, J = 4 Hz, 4H), 6.53 (d, J = 4 Hz, 2H), 3.90 (d, J = 8 Hz, 8H), 1.75 (m, 4H), 1.57 – 1.34 (comp, 32H), 0.97 – 0.90 (comp, 24H), 0.49 (s, 18H); ^{13}C NMR ($CDCl_3$) δ 160.5, 144.8, 143.7, 139.3, 131.0, 124.3, 110.23, 110.20, 103.1, 98.9, 85.8, 70.9, 39.6, 30.7, 29.3, 24.1, 23.2, 14.3, 11.3, -8.1. HRMS (ESI) *m/z*: Calcd for $C_{64}H_{95}O_4S_2Sn_2$ 1231.4710 $[M + H]^+$, found 1231.4698.

Synthesis of polymers ***P1 – P4***. A dry two-neck flask was equipped with a reflux condenser under argon atmosphere was charged with stannane **3** or **7** and bromide **10** or **11** in equimolar amounts (outlined below). Dry toluene and DMF (8:1) were added and the mixture thoroughly deoxygenated for 30 minutes. $Pd(PPh_3)_4$ (5 mole %) was added, the mixture deoxygenated for an additional 10 minutes, and heated to reflux for 48 h. One drop trimethyl(phenyl)tin and 1 mL toluene was then added and refluxing continued for 6 h. 2 drops of iodobenzene were added followed by refluxing for 12 h to complete polymer end-capping. The warm polymer solution was precipitated into methanol and filtered through a cellulose thimble. The polymer was placed in a Soxhlet extractor and washed with methanol, acetone, hexane, and $CHCl_3$. The solution of polymer from the chloroform fraction was

cooled to 50 °C, stirred with Silicycle DMT® for 8 h to scavenge metal impurities, and the crude polymer concentrated to ca. 5 mL *in vacuo*. The crude polymer solution was filtered through a small pad of silica gel eluting with $CHCl_3$ and the solution concentrated to ca. 5 mL *in vacuo*. The polymer solution was re-precipitated into cold methanol, the solids filtered rinsing with methanol, and the solids dried under vacuum to yield polymers **P1 – P4**.

*Poly[(4,8-bis(2-ethylhexyloxy)benzo[1,2-b:4,5-b']dithiophene)-2,6-diyl-alt-(2,6-bis((2-ethylhexyl)thien-2-yl)benzo[1,2-d;4,5-d']bisoxazole)] (**P1**).* **P1** was synthesized from 177 mg (0.25 mmol) of **3** and 193 mg of **10** (0.25 mmol) to yield an orange-red powder. (107 mg, 43% yield): ^{1}H NMR ($CDCl_3$) δ 7.52 – 7.33 (4H), 7.25 (2H), 6.83 (2H), 4.17 (4H), 3.16 – 3.05 (4H), 1.73-1.10 (60H).

*Poly[(4,8-bis(2-ethylhexyloxy)benzo[1,2-b:4,5-b']dithiophene)-2,6-diyl-alt-(4,8-bis(3,5-di-(2-ethylhexyloxy)phenylethynyl)-2,6-bis((2-ethylhexyl)thien-2-yl)benzo[1,2-d;4,5-d']bisoxazole)] (**P2**).* **P2**was synthesized from 276 mg (0.20 mmol) **7** and 150.3 mg (0.20 mmol) **10** to yield a dark red solid (146 mg, 44% yield): ^{1}H NMR ($CDCl_3$) δ 7.67 (2H), 6.97 – 6.90 (8H), 6.57 (4H), 4.25 (4H), 3.91 (8H), 3.26 (4H), 1.78 – 0.82 (120H).

*Poly[(4,8-bis-(3,5-di-(2-ethylhexyloxy)phenylethynyl)benzo[1,2-b:4,5-b']dithiophene)-2,6-diyl-alt)-(2,6-bis((2-ethylhexyl)thien-2-yl)benzo[1,2-d;4,5-d']bisoxazole)] (**P3**).* **P3** was synthesized from 177 mg (0.25 mmol) **3** and 307 mg (0.25 mmol) **11** to yield a dark red solid (289 mg, 80% yield): ^{1}H NMR ($CDCl_3$) δ 7.82 (2H), 7.38 (2H), 7.00 (2H), 6.90 (4H), 6.65 (2H), 4.04 (8H), 3.19 (2H), 1.83 – 0.97 (90H).

*Poly[(4,8-bis(3,5-di(2-ethylhexyloxy)phenylethynyl)benzo[1,2-b:4,5-b']dithiophene)-2,6-diyl-alt-(4,8-bis(3,5-di-(2-ethylhexyloxy)phenylethynyl)-2,6-bis((2-ethylhexyl)thien-2-yl)benzo[1,2-d;4,5-d']bisoxazole)] (**P4**).* **P4** was synthesized from 240 mg (0.17 mmol) of **7** and 207 mg (0.17 mmol) **11** to yield a red solid (252 mg, 69% yield): 7.87 (2H) 7.35 (2H) 6.87 (8H), 6.53 (d, J = 8 Hz, 4H), 3.90 (q, J = 8 Hz, 16H), 3.23 – 3.33 (4H), 1.87 (2H), 1.72 (8H), 1.52 – 1.21 (80H), 0.97 – 0.79 (60H).

4.5.5 Computational Details

All computations were performed using Gaussian 09 through the National Science Foundation's Extreme Science and Engineering Discovery Environment (NSF-XSEDE) and San Diego Supercomputer Center's Trestles Cluster. Excited states were generated through time dependent density functional theory (TDDFT) applied to the optimized ground state for each polymer's n = 1, 2, 3 and 4 subunits. The long chain limits for the HOMO, LUMO, and band gap were generated from these excited computations and fit using the Kuhn expression.[30]

4.6 Acknowledgements

We acknowledge the donors of the Petroleum Research Fund for support of this work. We also thank the 3M Foundation and the National Science Foundation (DMR-0846607) for partial support of this work. We thank Kamel Harrata and the Mass Spectroscopy Laboratory Iowa State University (ISU) for analysis of our compounds. We would like to thank NSF-XSEDE (TG-CHE-120081) for providing the resources for all the computational work included in this article.

4.7 Supporting Information

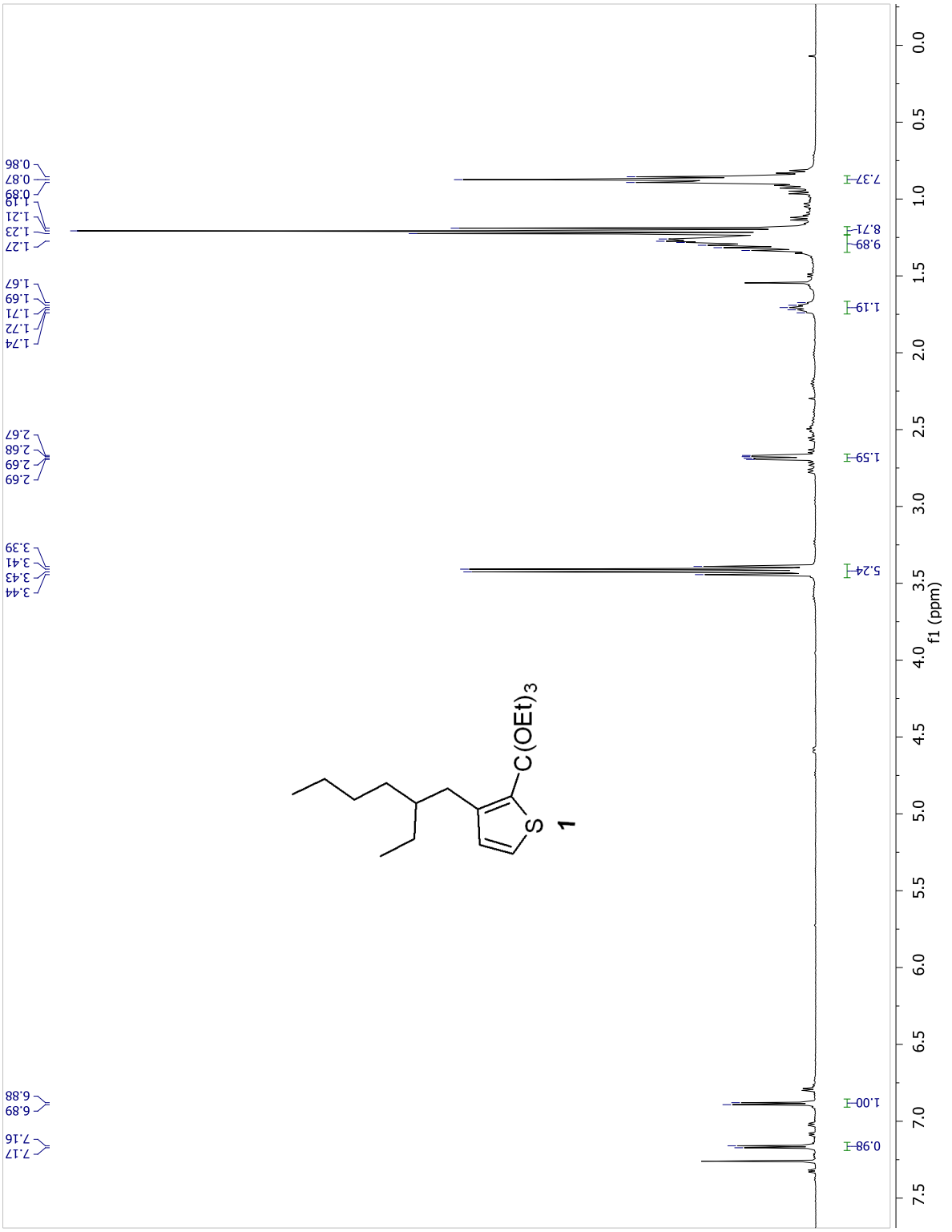

Figure S4.1. ^{1}H NMR spectrum of **1.**

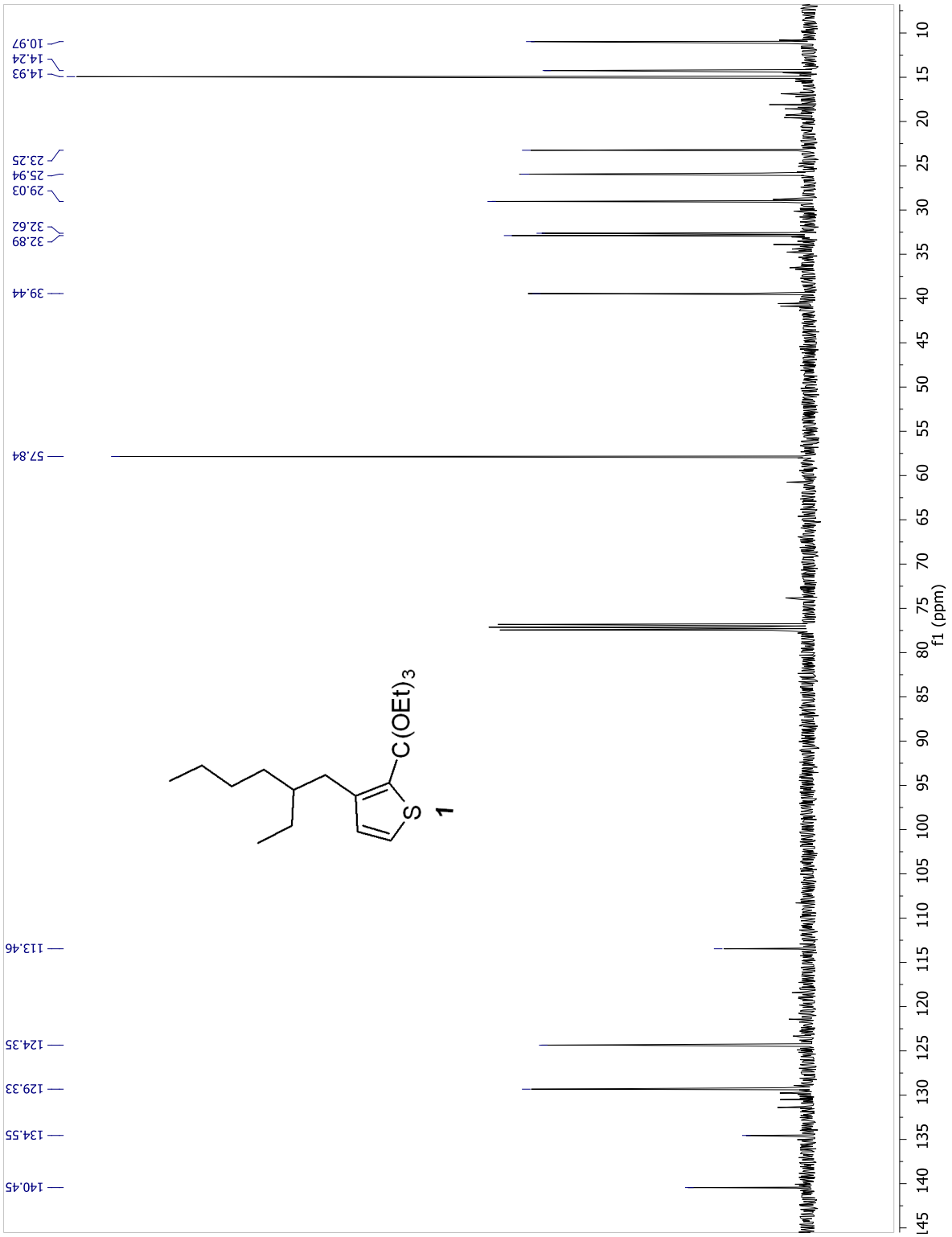

Figure S4.2. ^{13}C NMR spectrum of **1.**

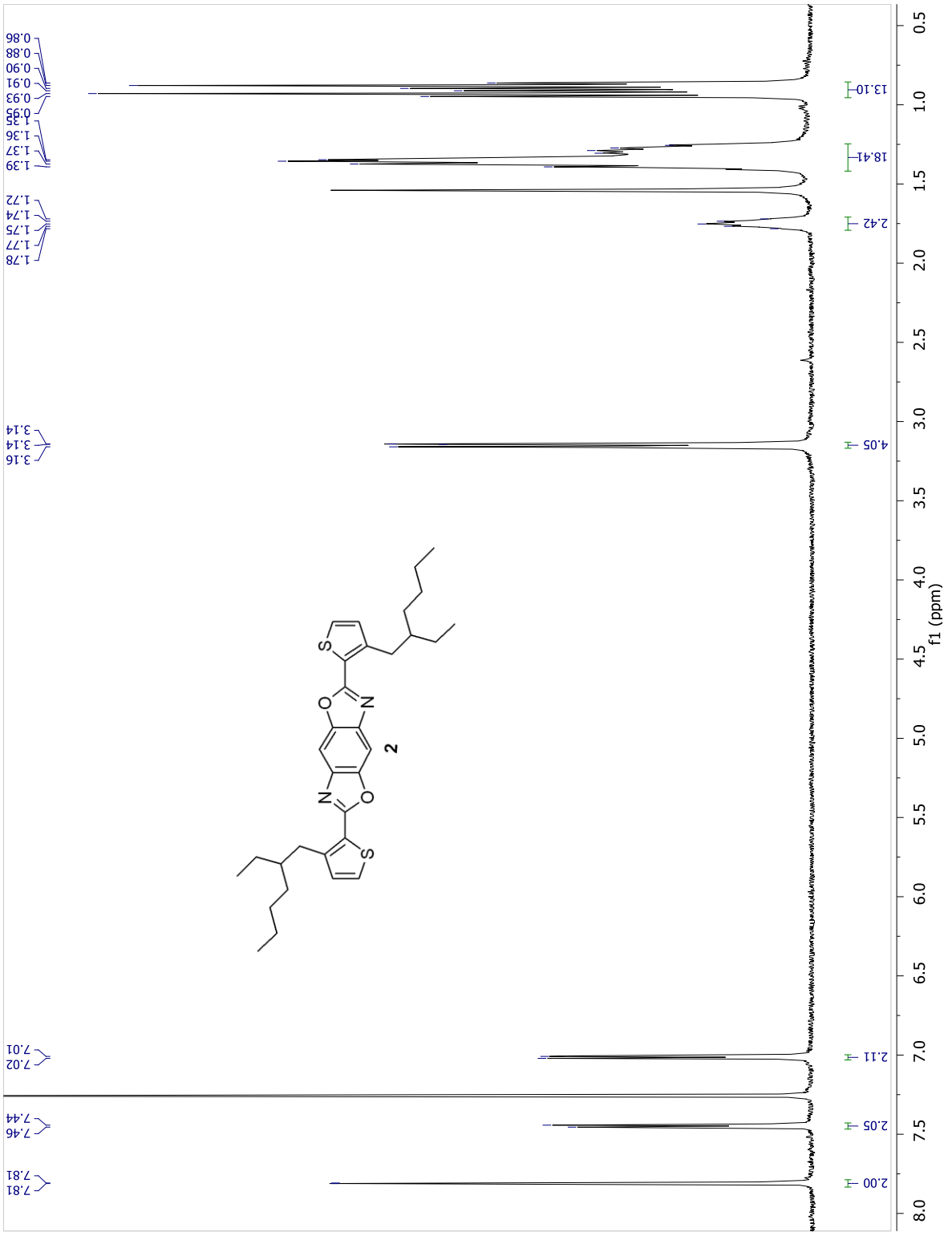

Figure S4.3. ^{1}H NMR spectrum of **2.**

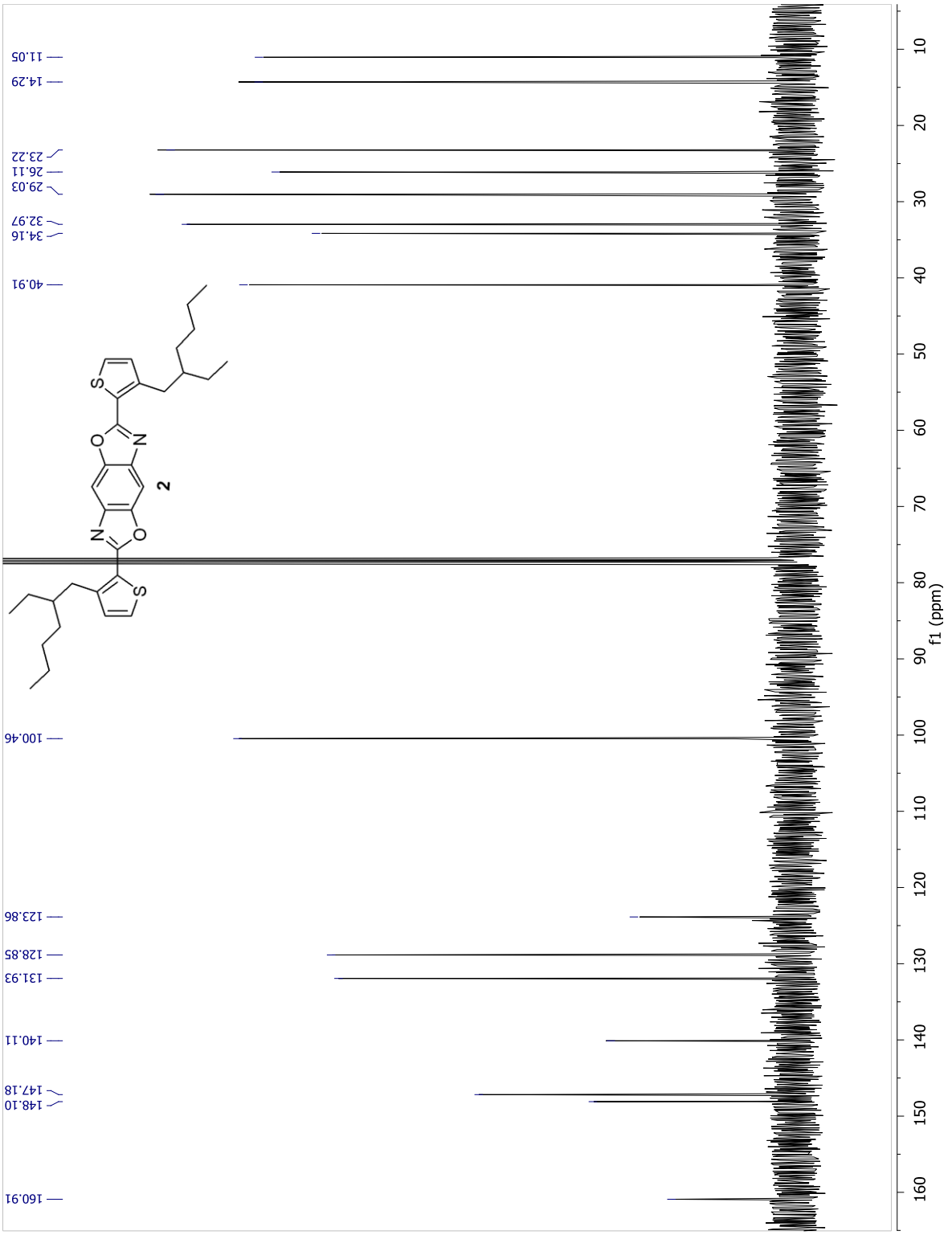

Figure S4.4. ^{13}C NMR spectrum of **2.**

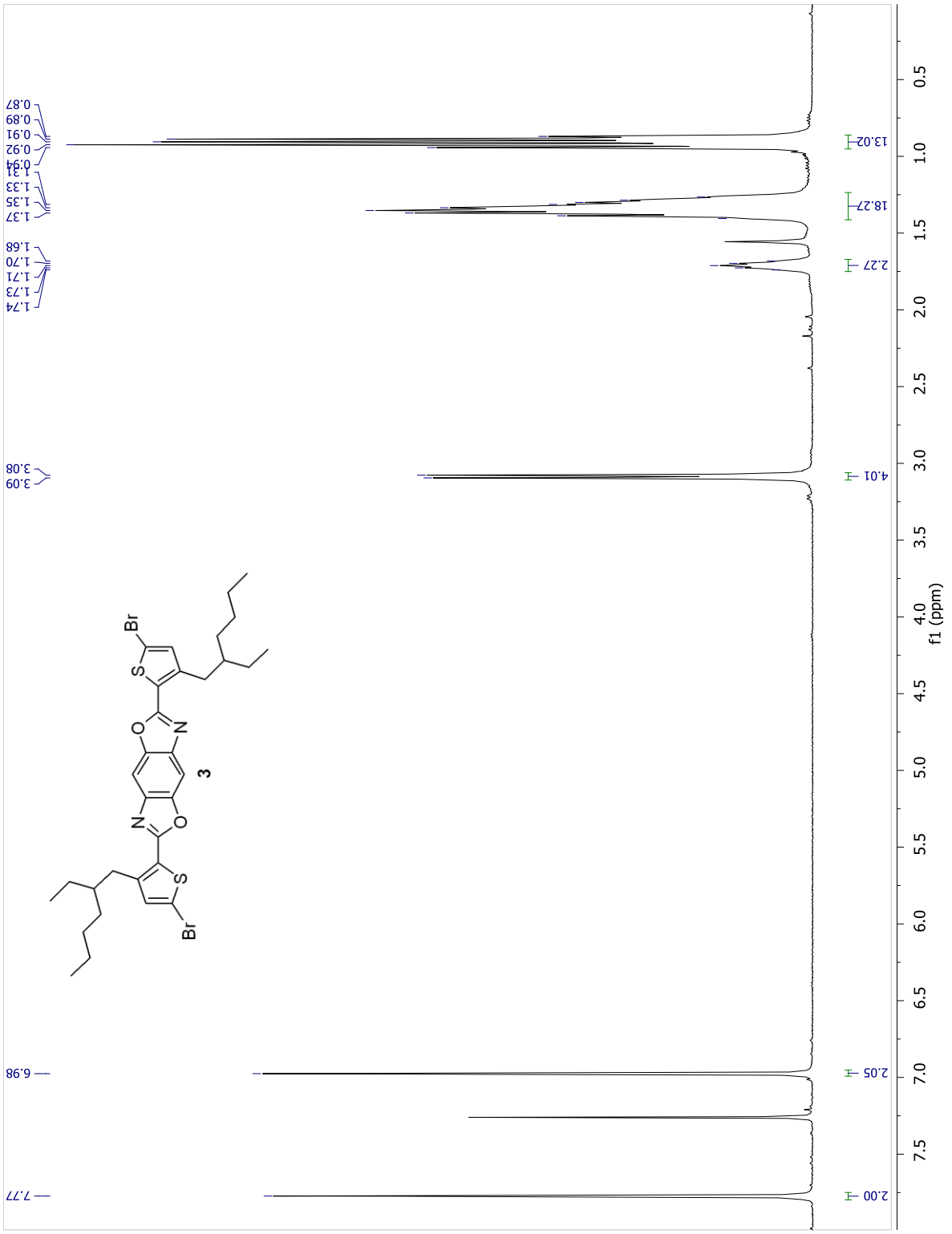

Figure S4.5. ^{1}H NMR spectrum of **3.**

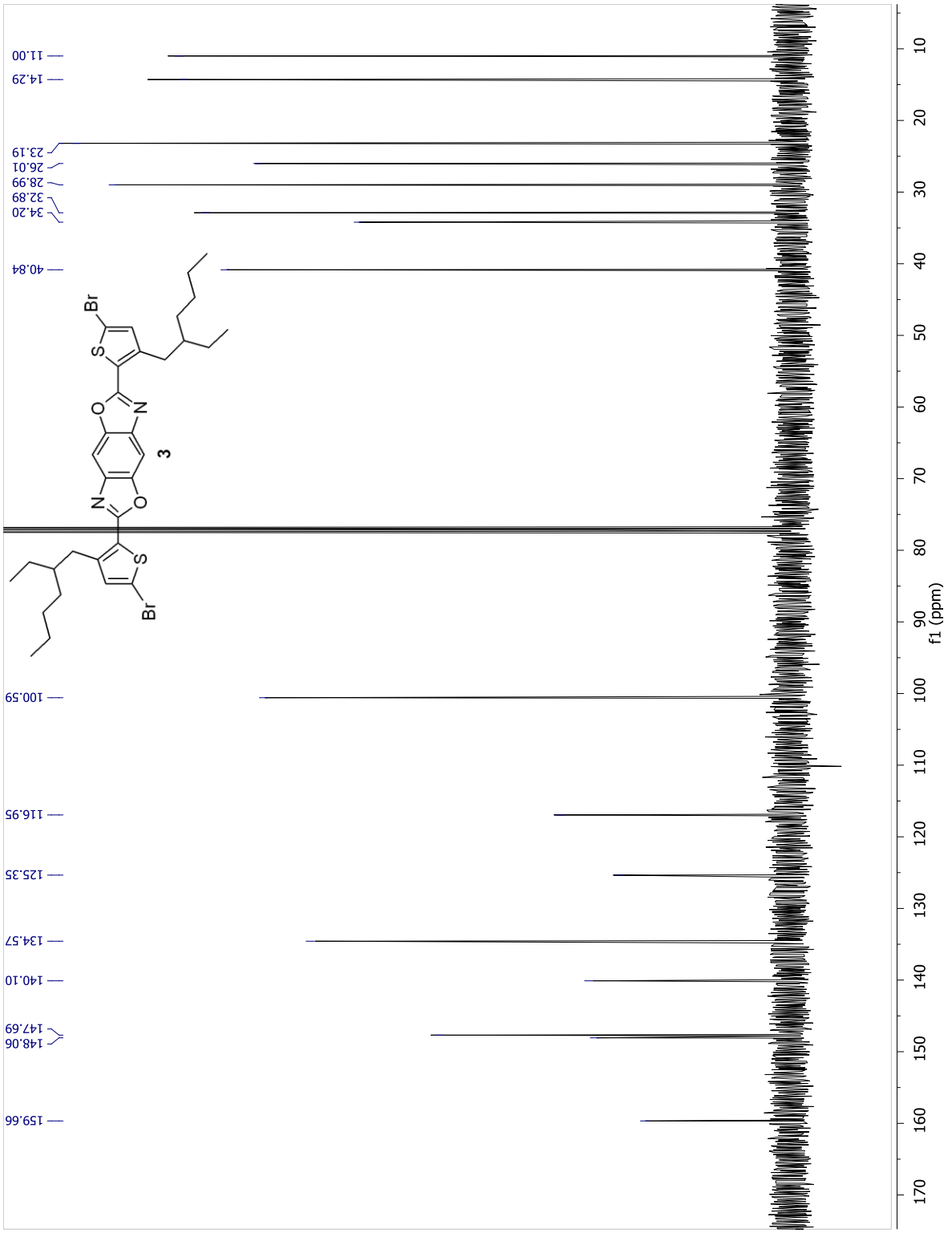

Figure S4.6. ^{13}C NMR spectrum of **3.**

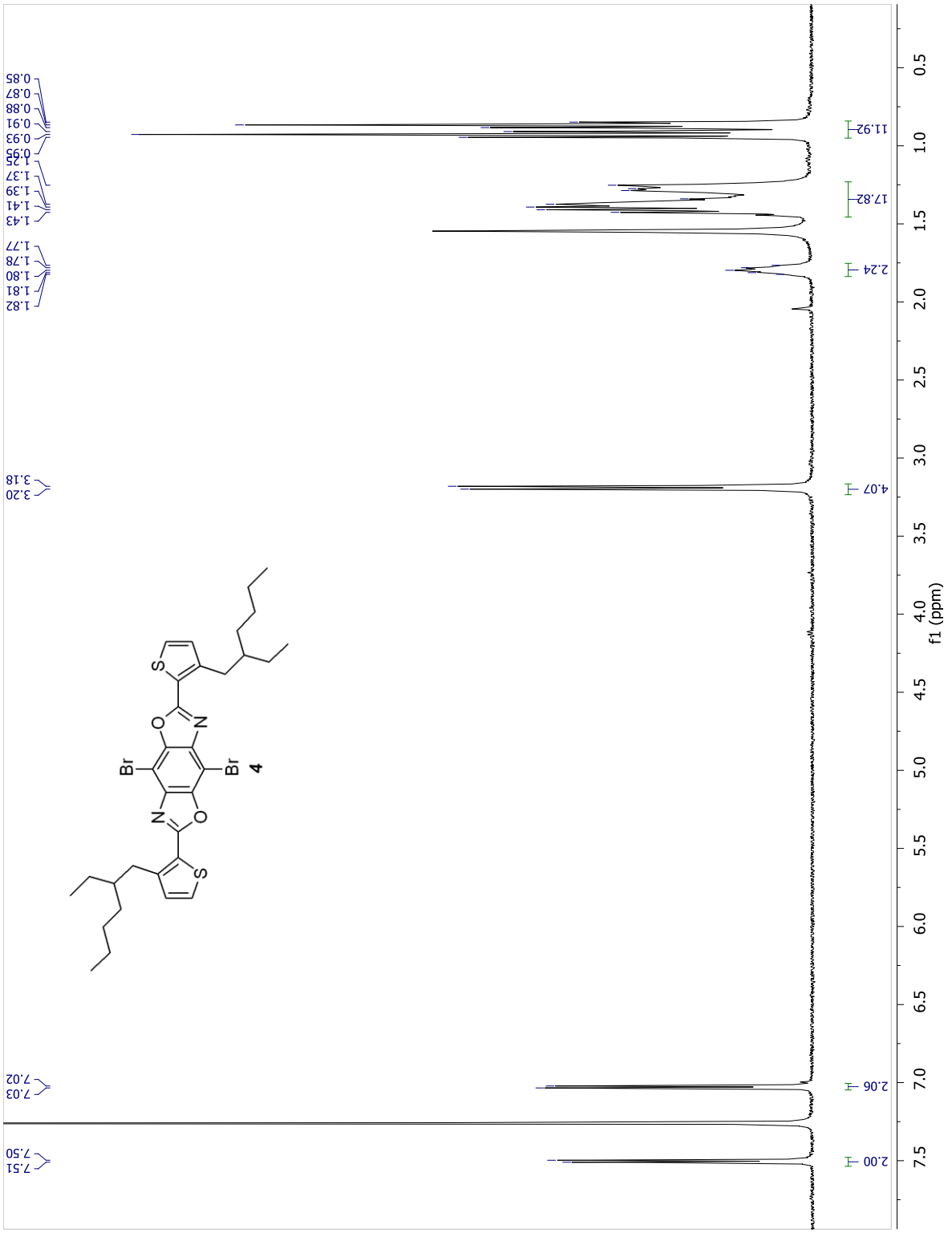

Figure S4.7. ^{1}H NMR spectrum of **4.**

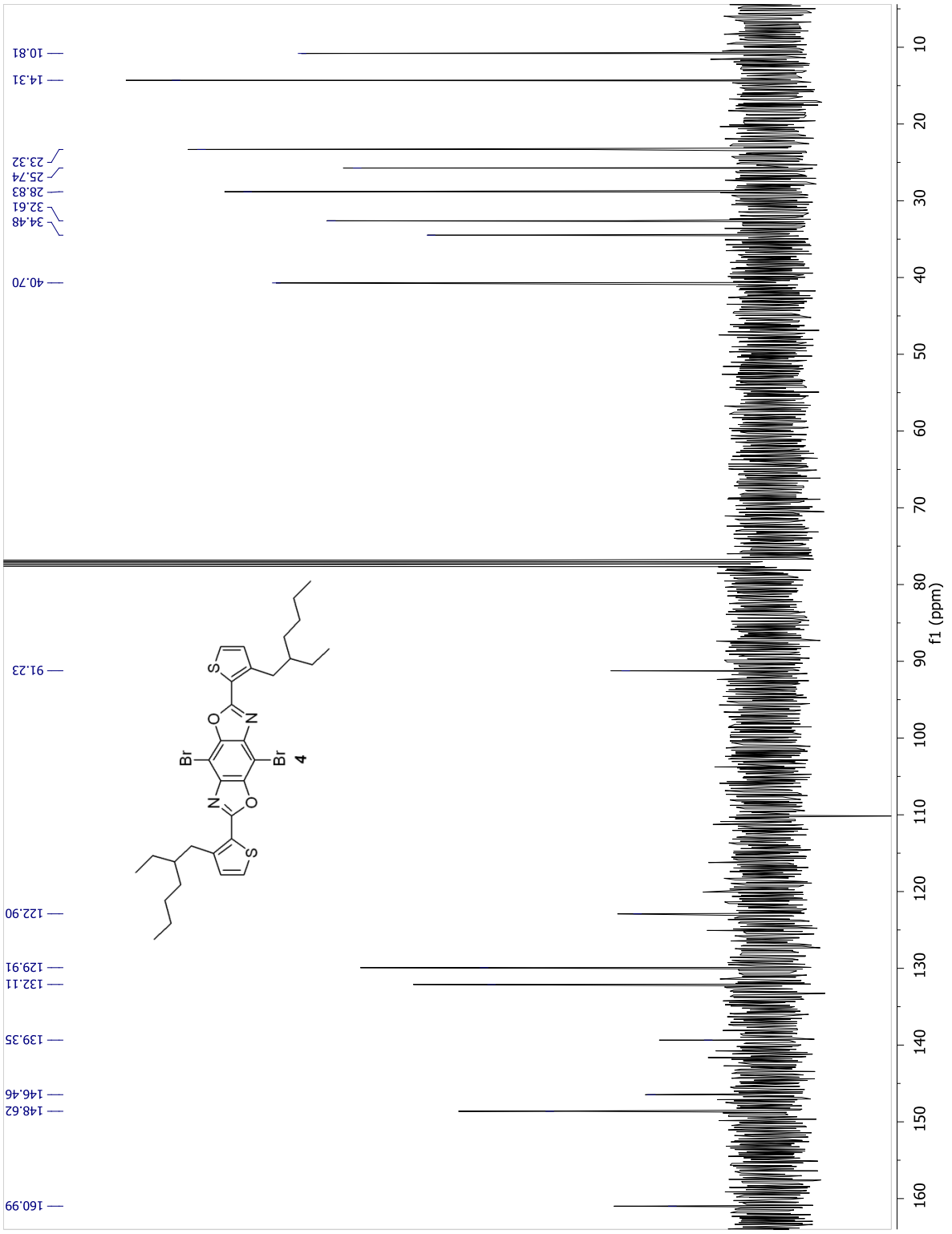

Figure S4.8. ^{13}C NMR spectrum of **4.**

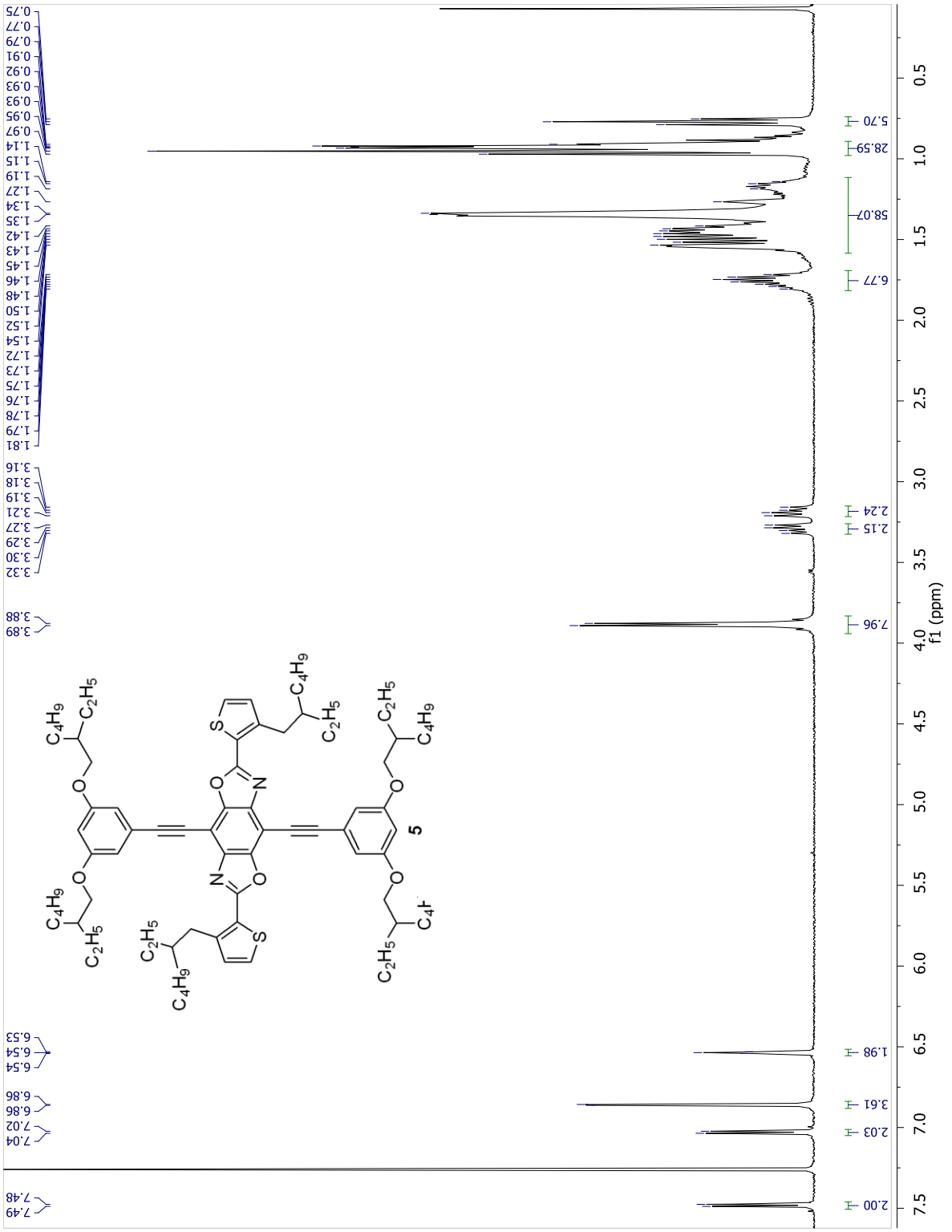

Figure S4.9. ^{1}H NMR spectrum of **5.**

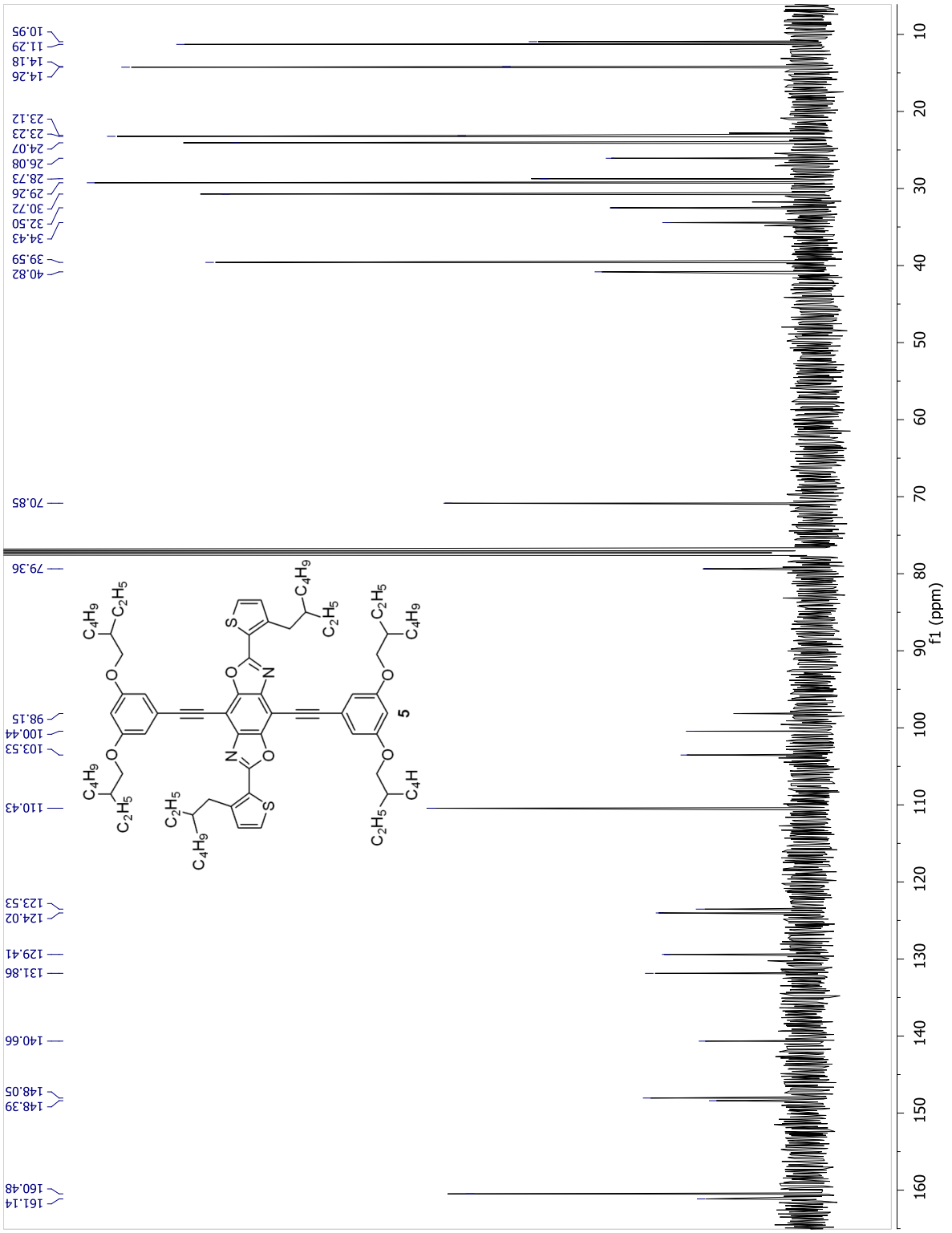

Figure S4.10. ^{13}C NMR spectrum of **5.**

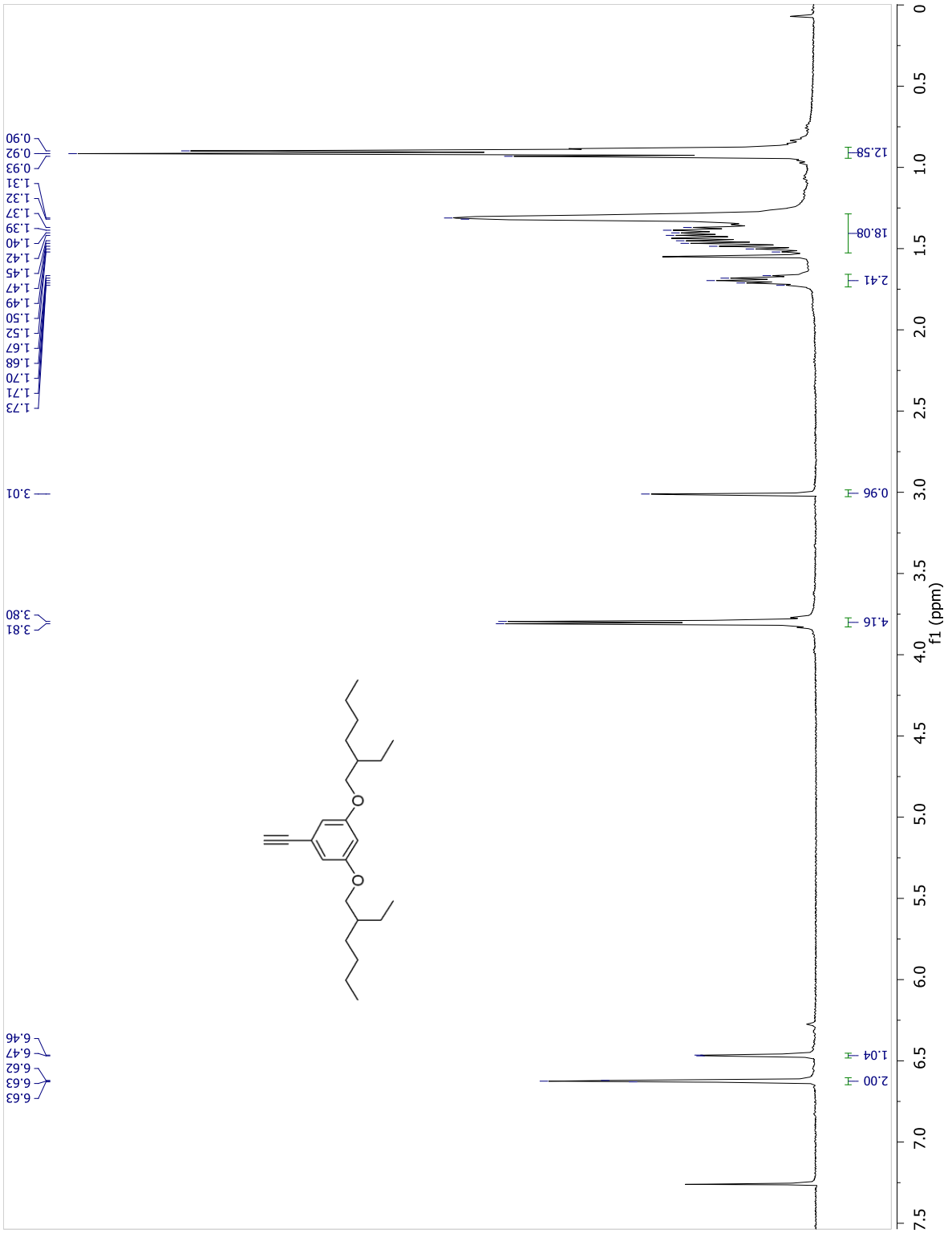

Figure S4.11. ^{1}H NMR spectrum of **6.**

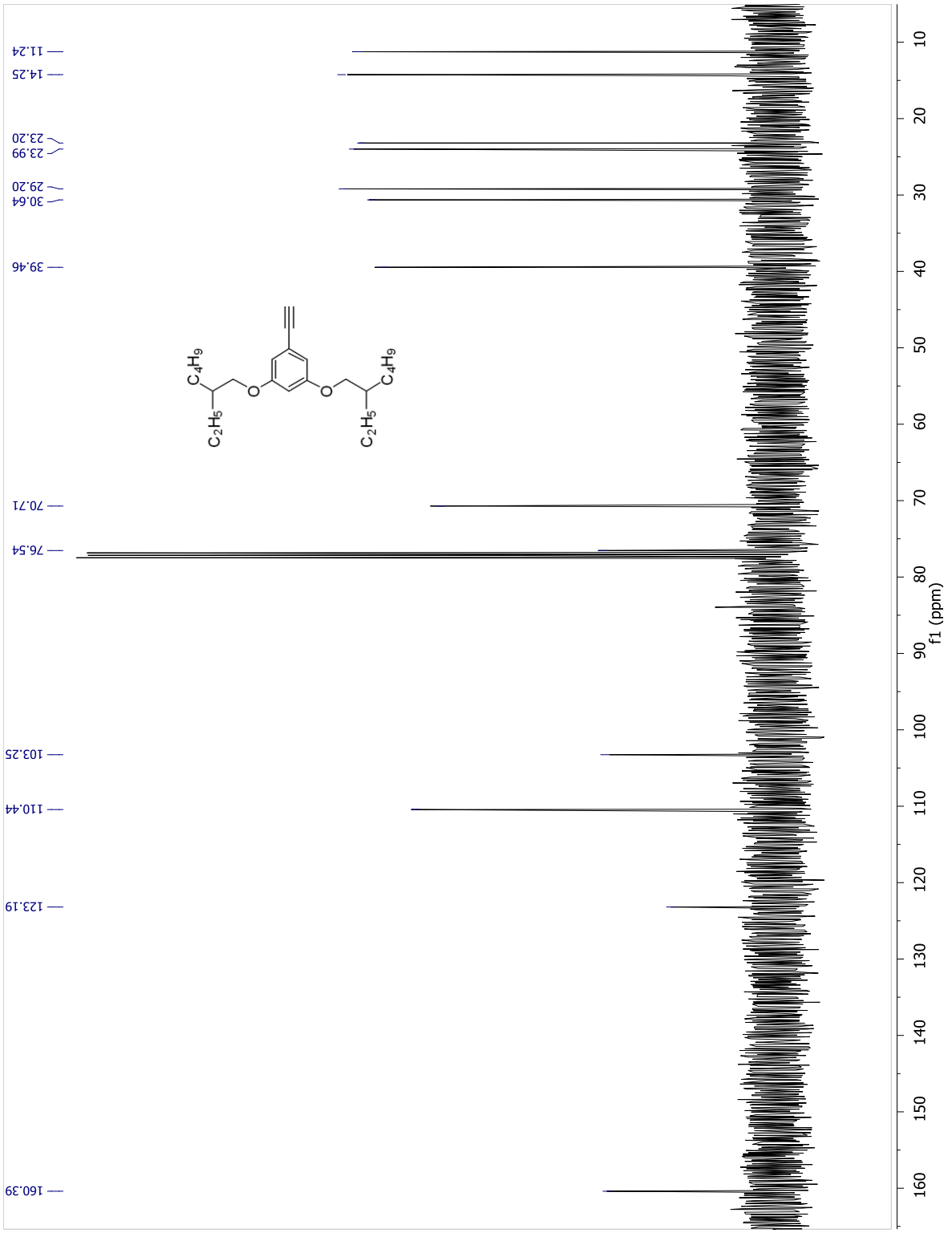

Figure S4.12. ^{13}C NMR spectrum of **6.**

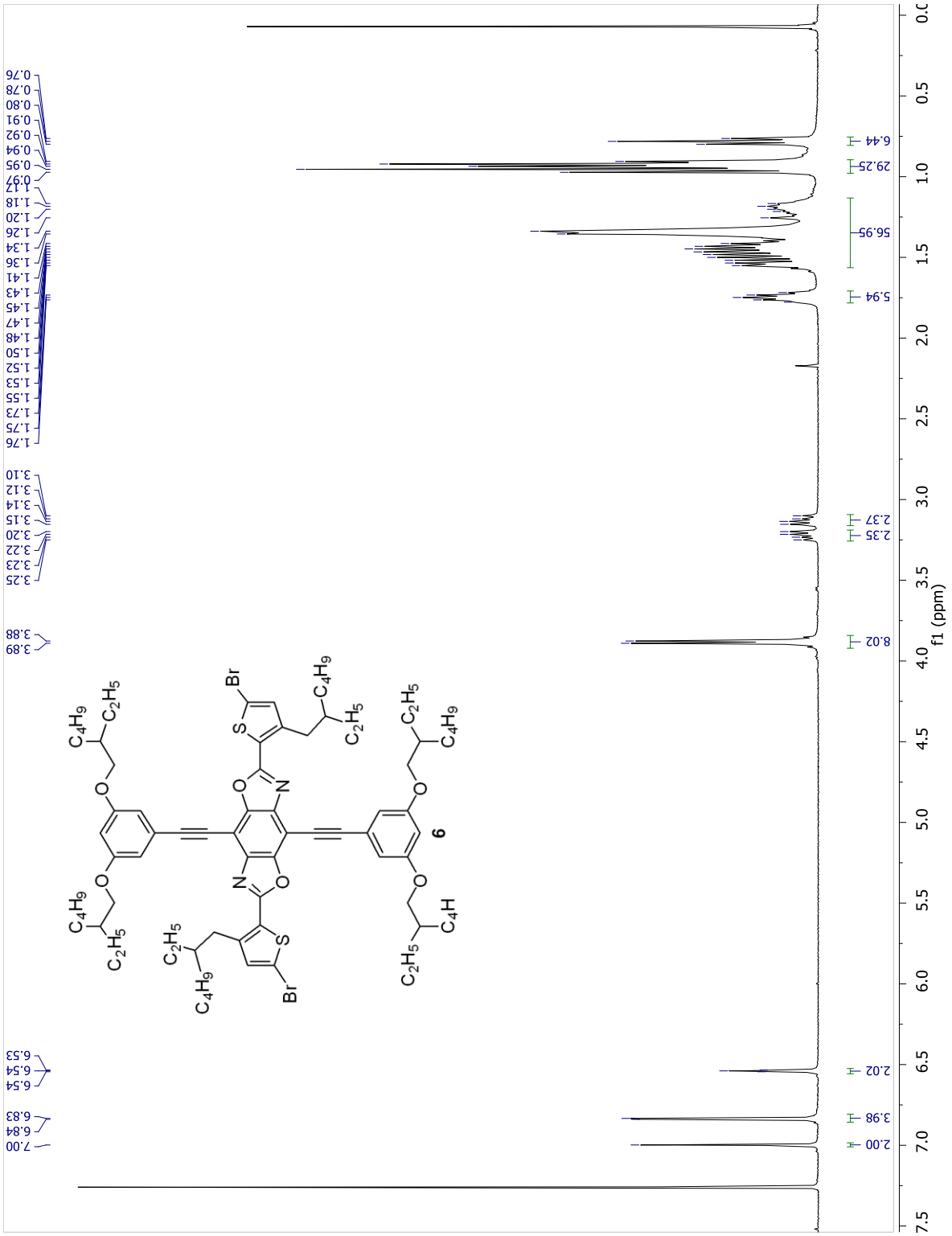

Figure S4.13. ^{1}H NMR spectrum of **7.**

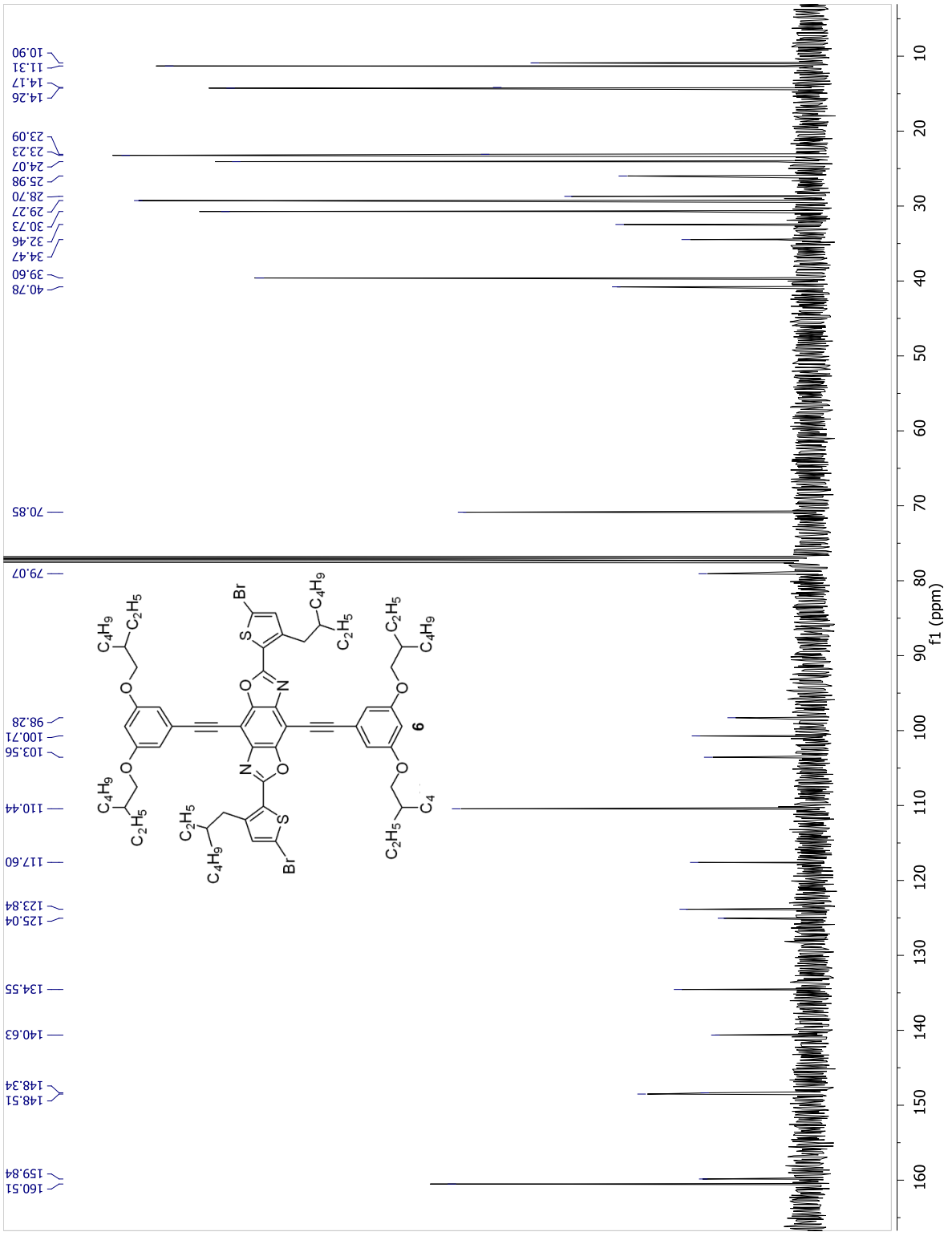

Figure S4.14. ^{13}C NMR spectrum of **7.**

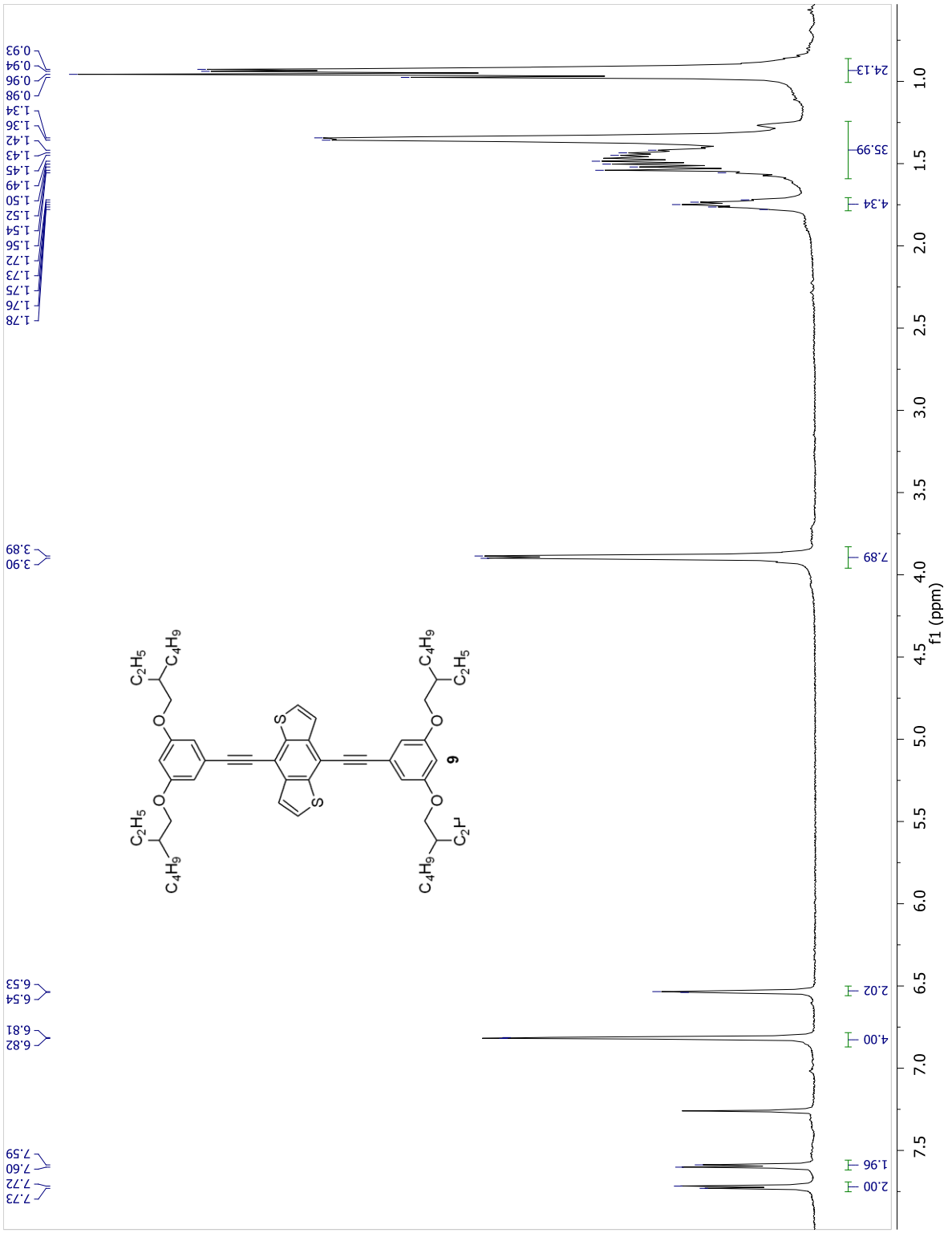

Figure S4.15. ^{1}H NMR spectrum of **9.**

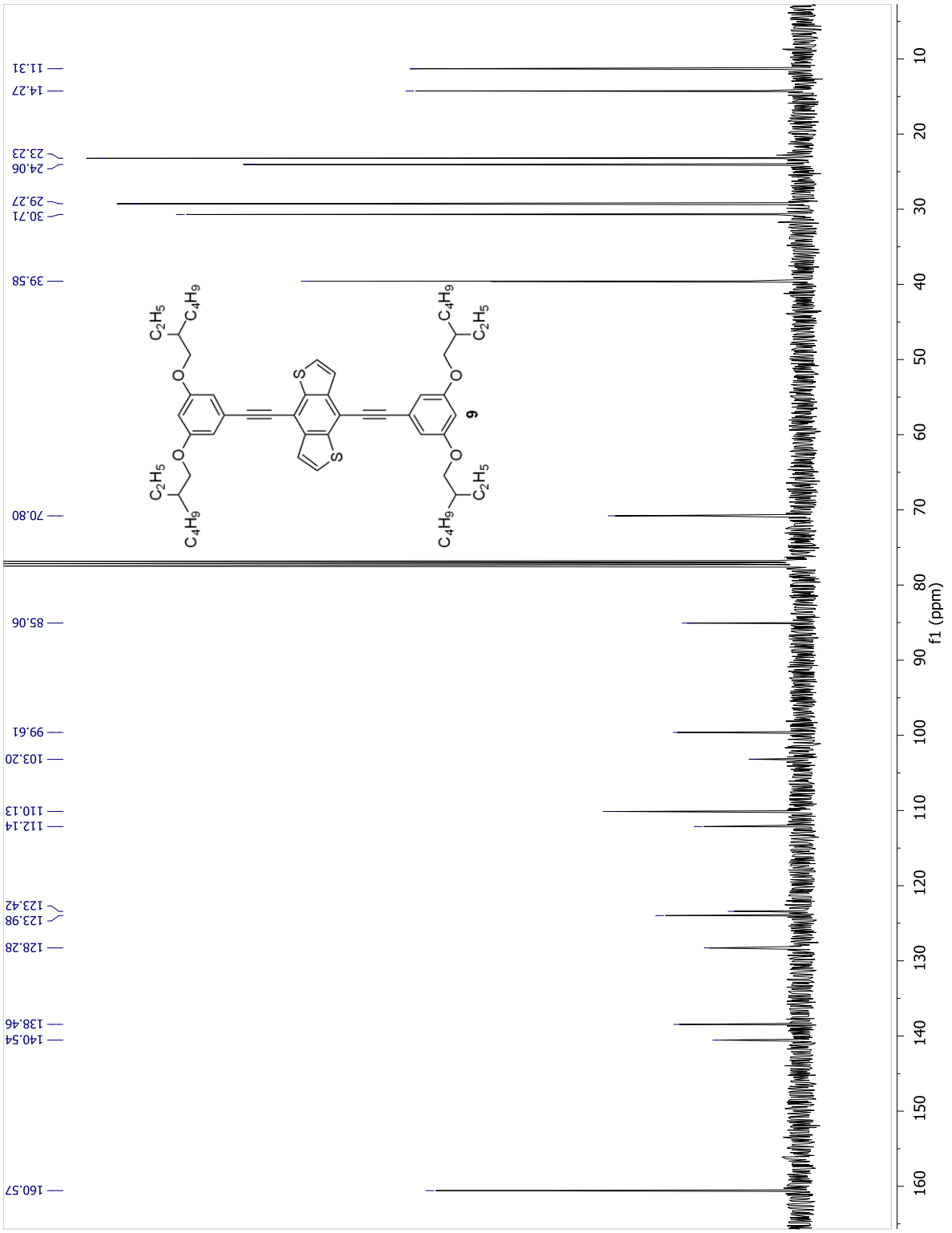

Figure S4.16. ^{13}C NMR spectrum of **9.**

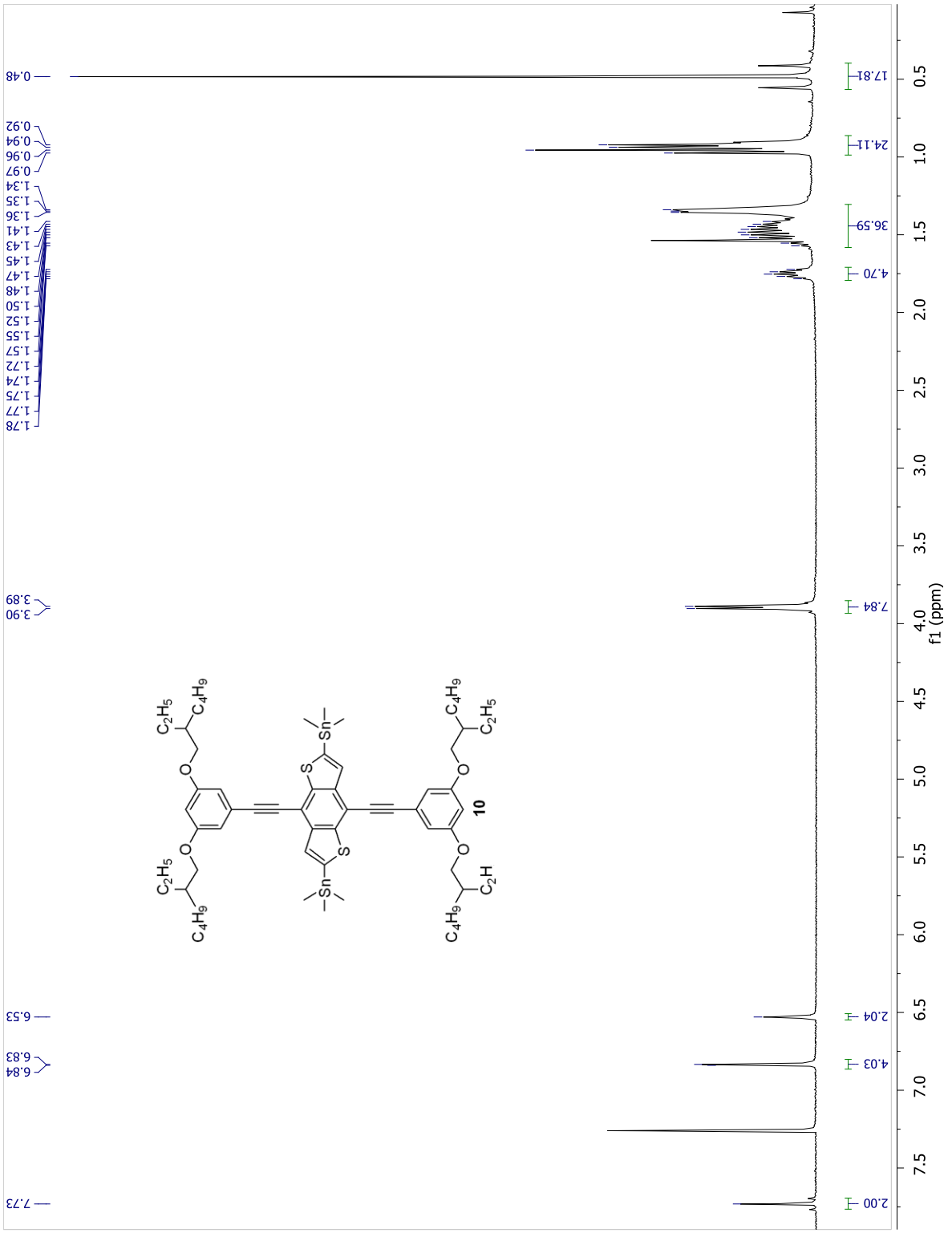

Figure S4.17. ^{1}H NMR spectrum of **11.**

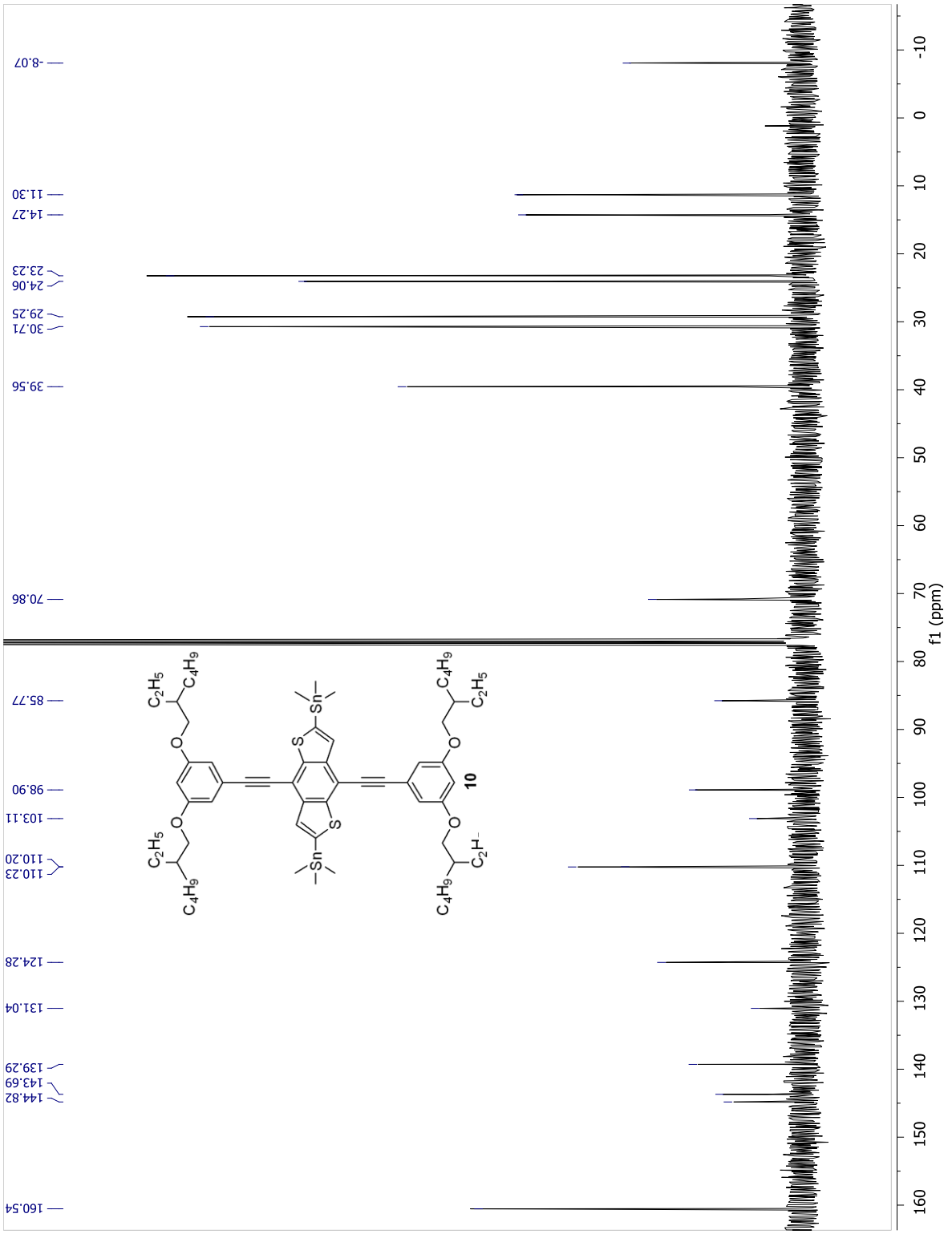

Figure S4.18. ^{13}C NMR spectrum of **11.**

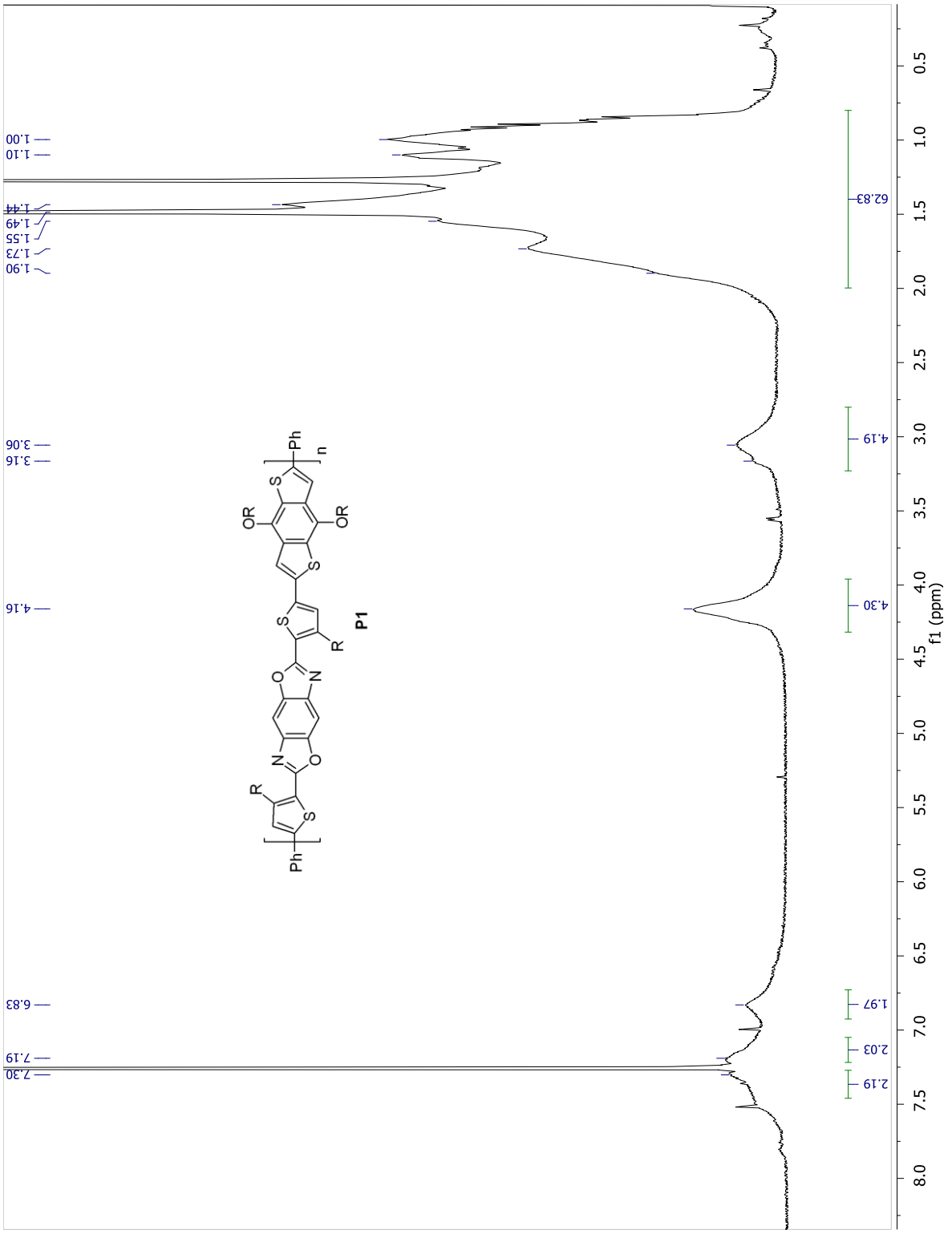

Figure S4.19. ^{1}H NMR spectrum of **P1** (R = 2-ethylhexyl).

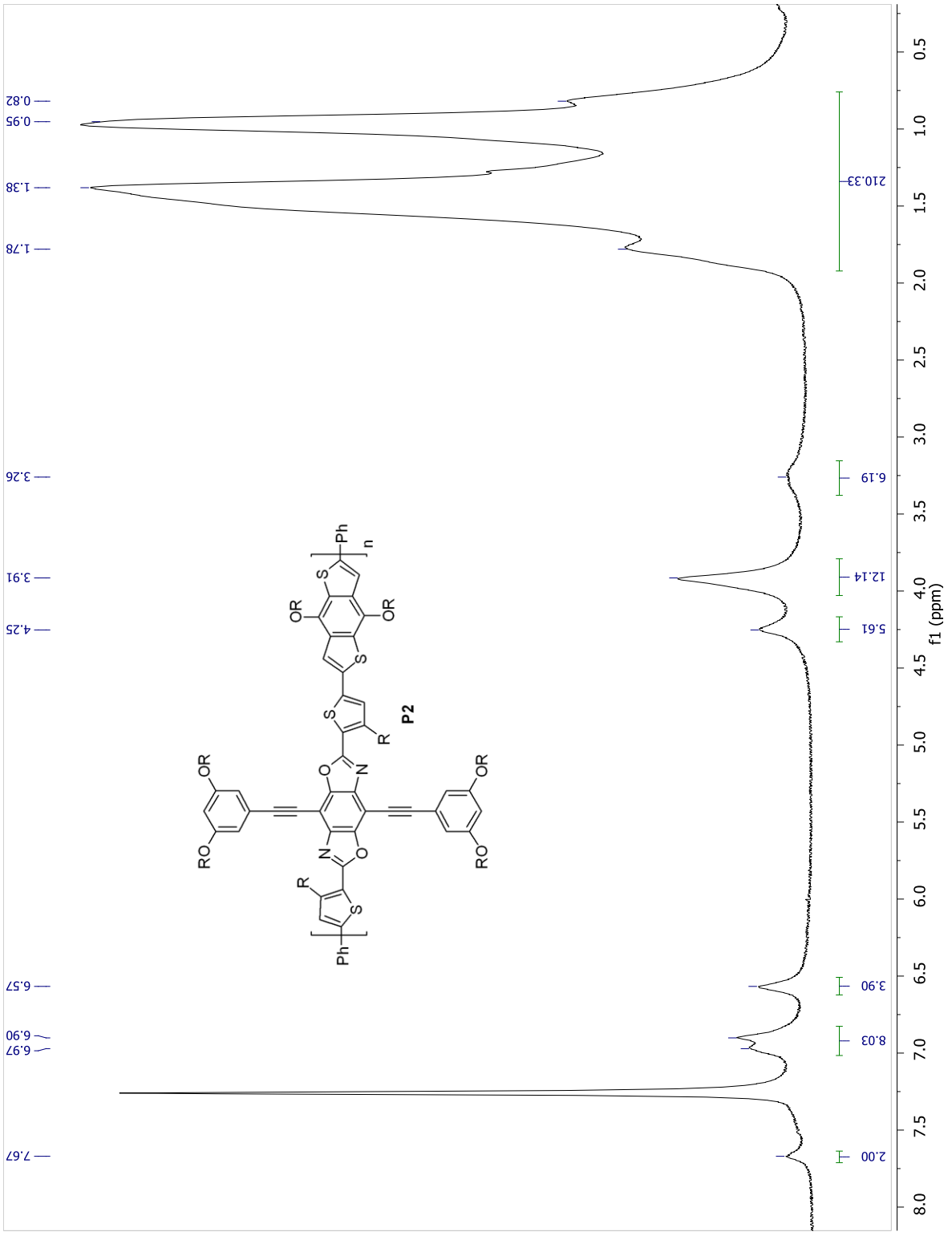

Figure S4.20. ^{1}H NMR spectrum of **P2** (R = 2-ethylhexyl).

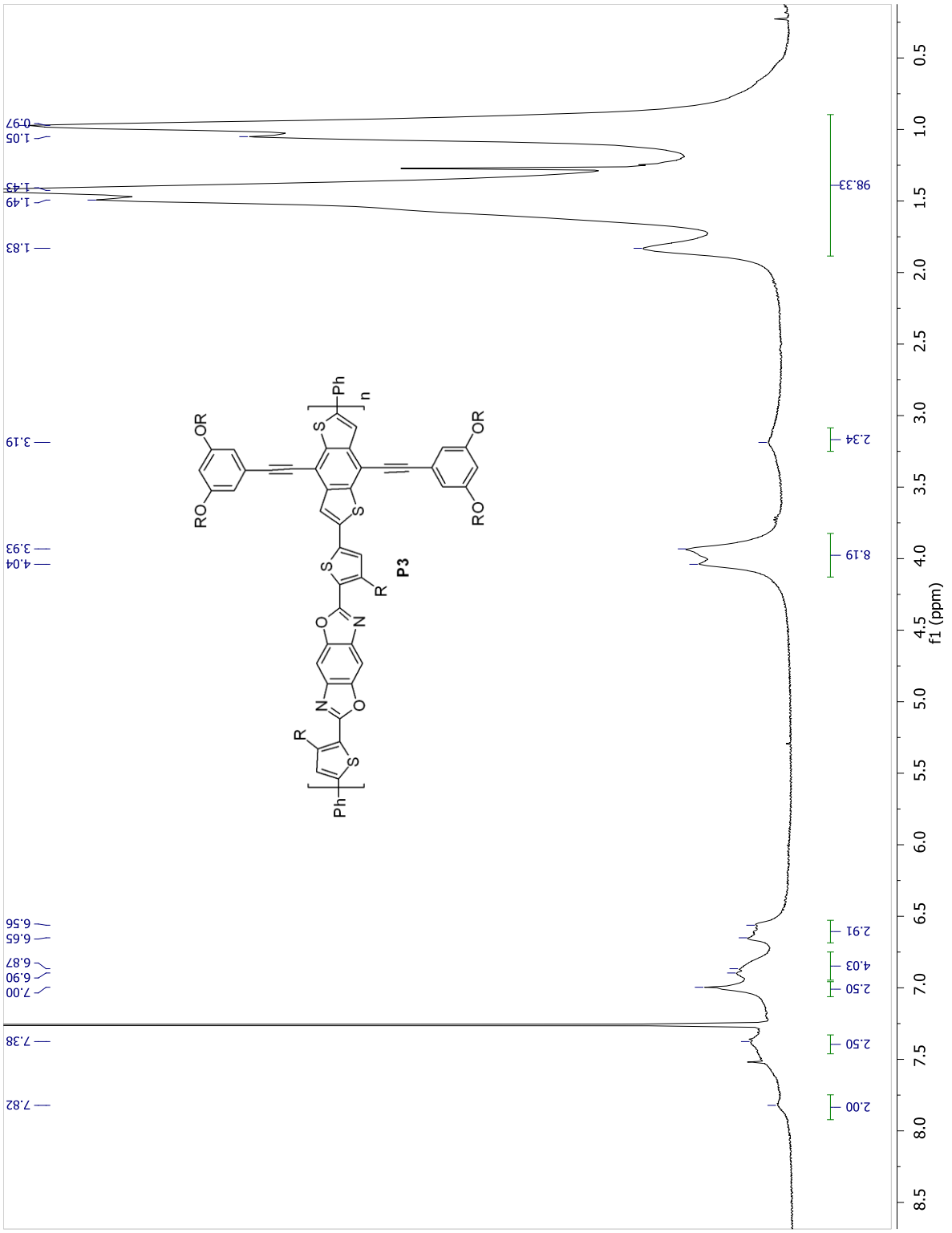

Figure S4.21. ^{1}H NMR spectrum of **P3** (R = 2-ethylhexyl).

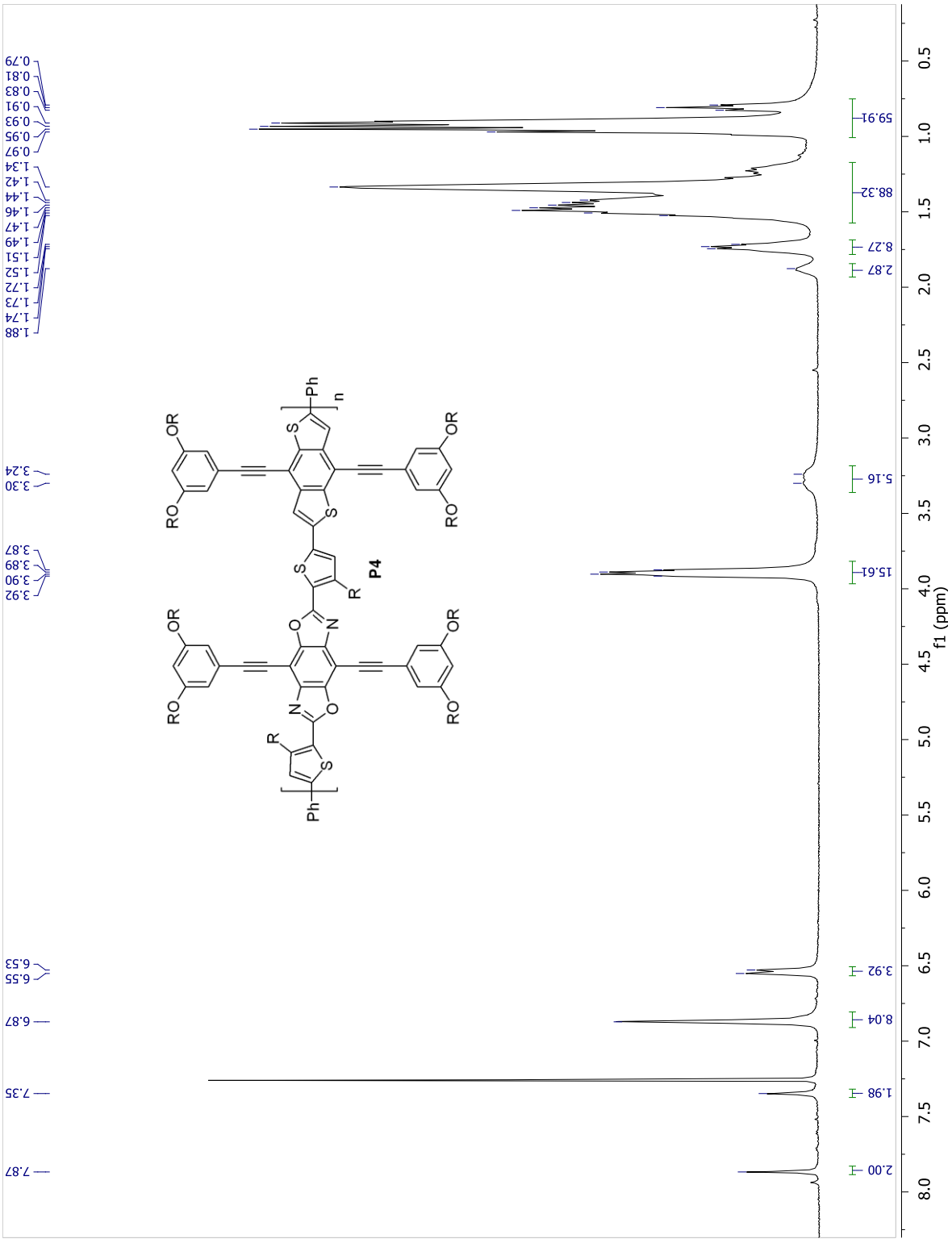

Figure S4.22. ^{1}H NMR spectrum of **P4** (R = 2-ethylhexyl).

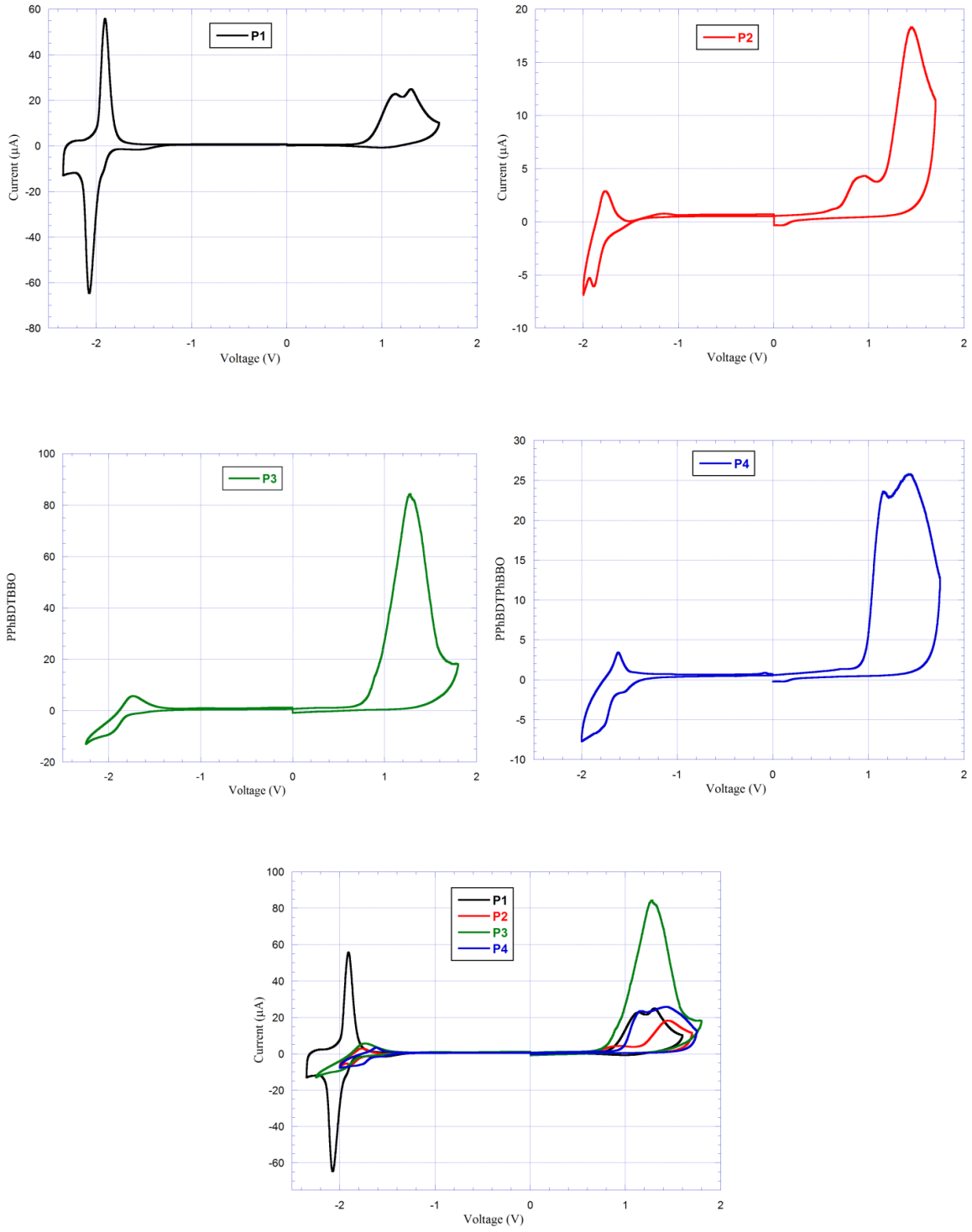

Figure S4.23. Individual and overlay cyclic voltametry traces of polymers **P1 – P4.**

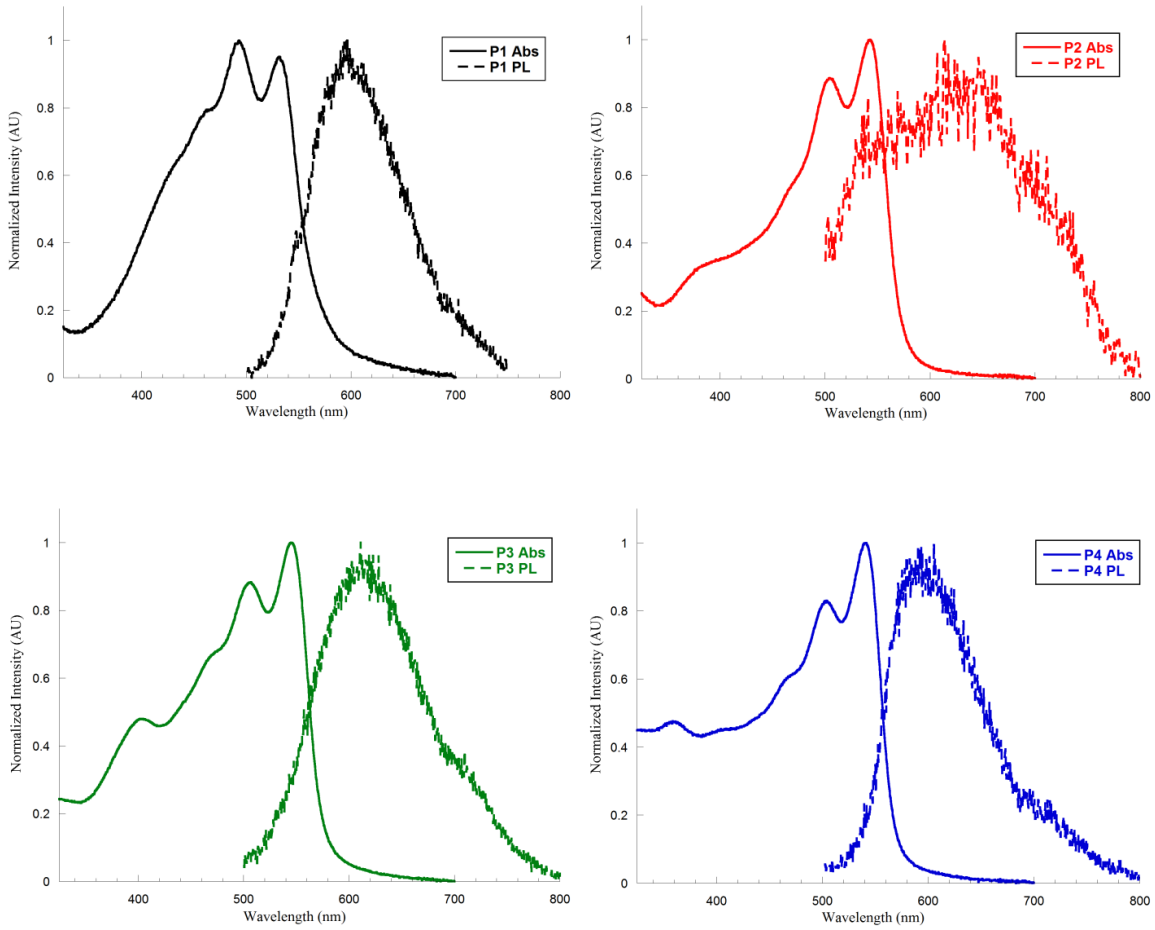

Figure S4.24. Normalized thin film UV-vis and emission spectra of **P1 – P4.**

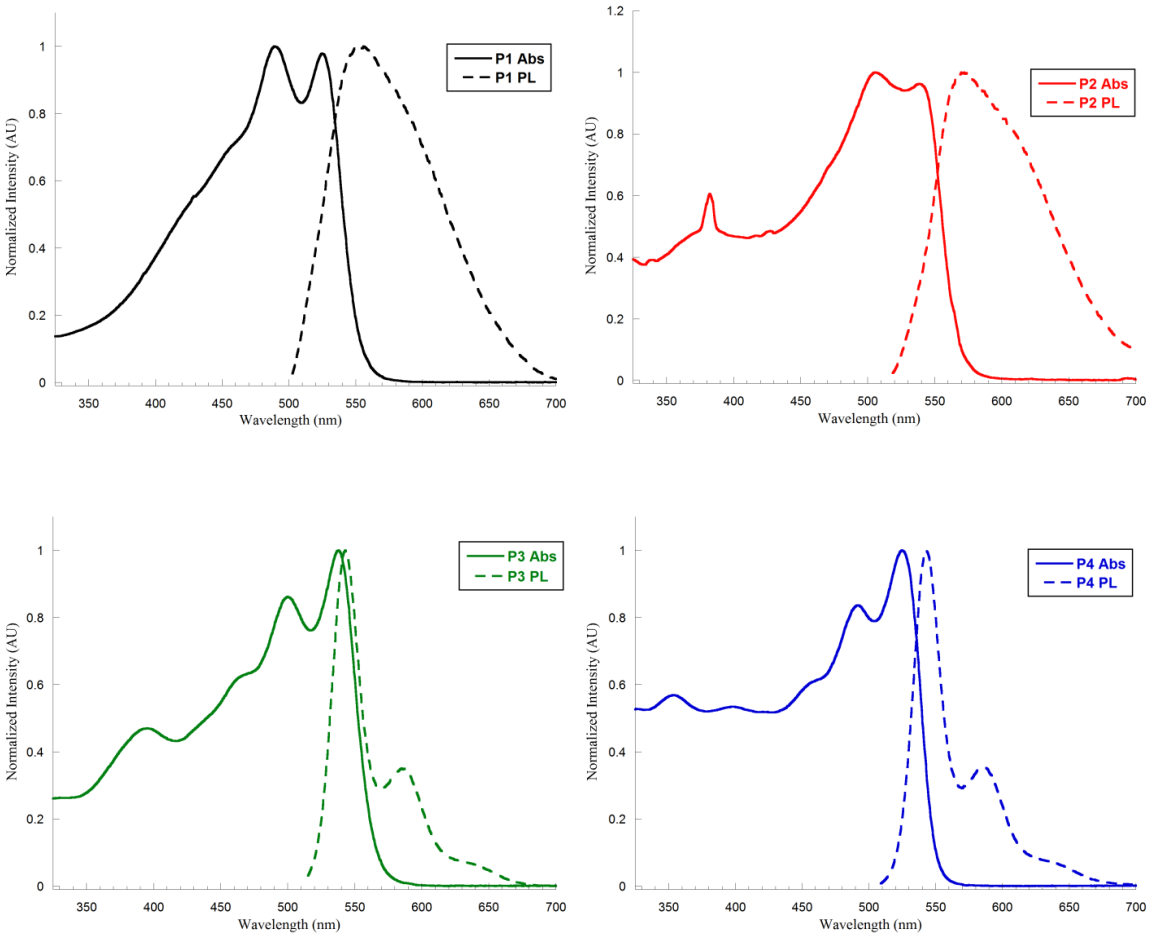

Figure S4.25. Normalized solution UV-vis and emission spectra of **P1** – **P4.**

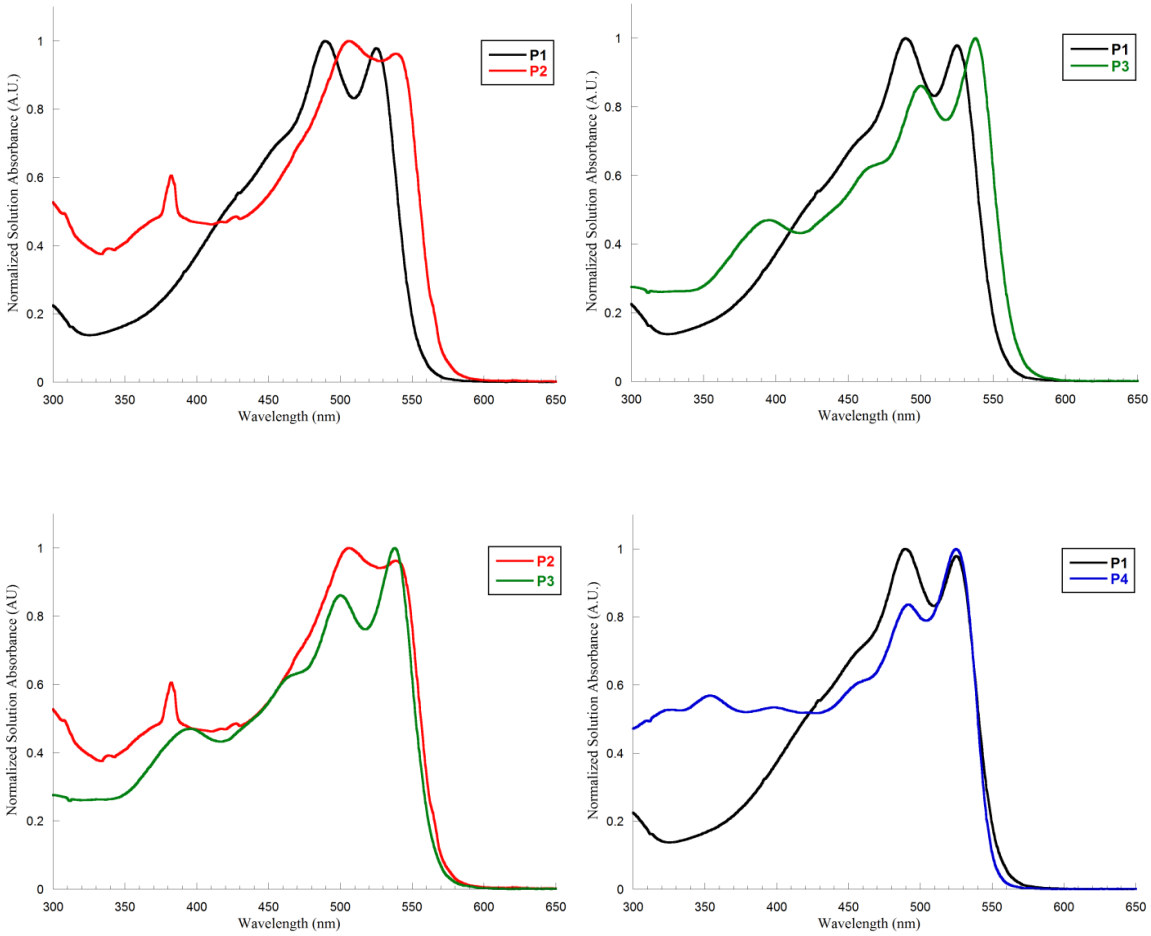

Figure S4.26. Normalized solution UV-Vis spectral comparison of polymers **P1 – P4.**

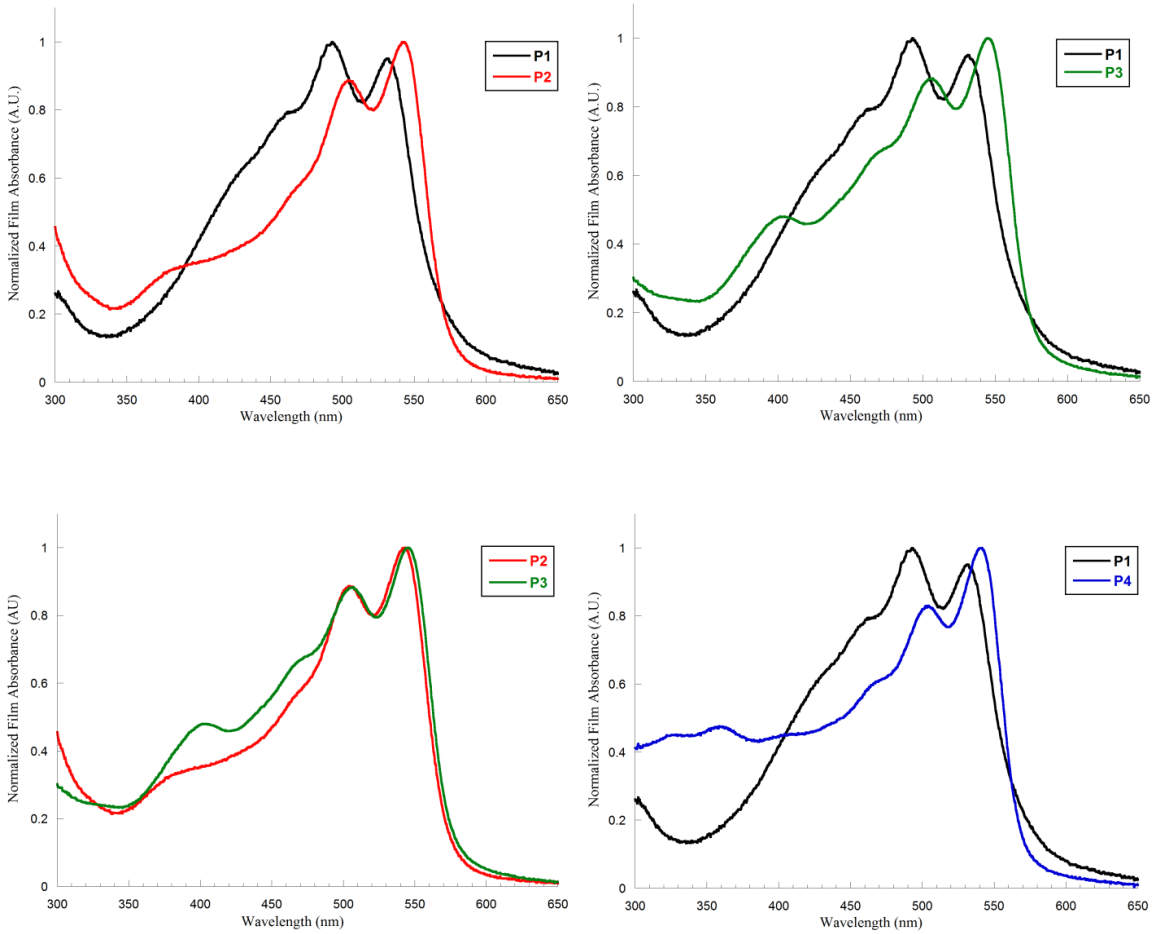

Figure S4.27. Normalized thin film UV-Vis spectral comparison of polymers **P1 – P4.**

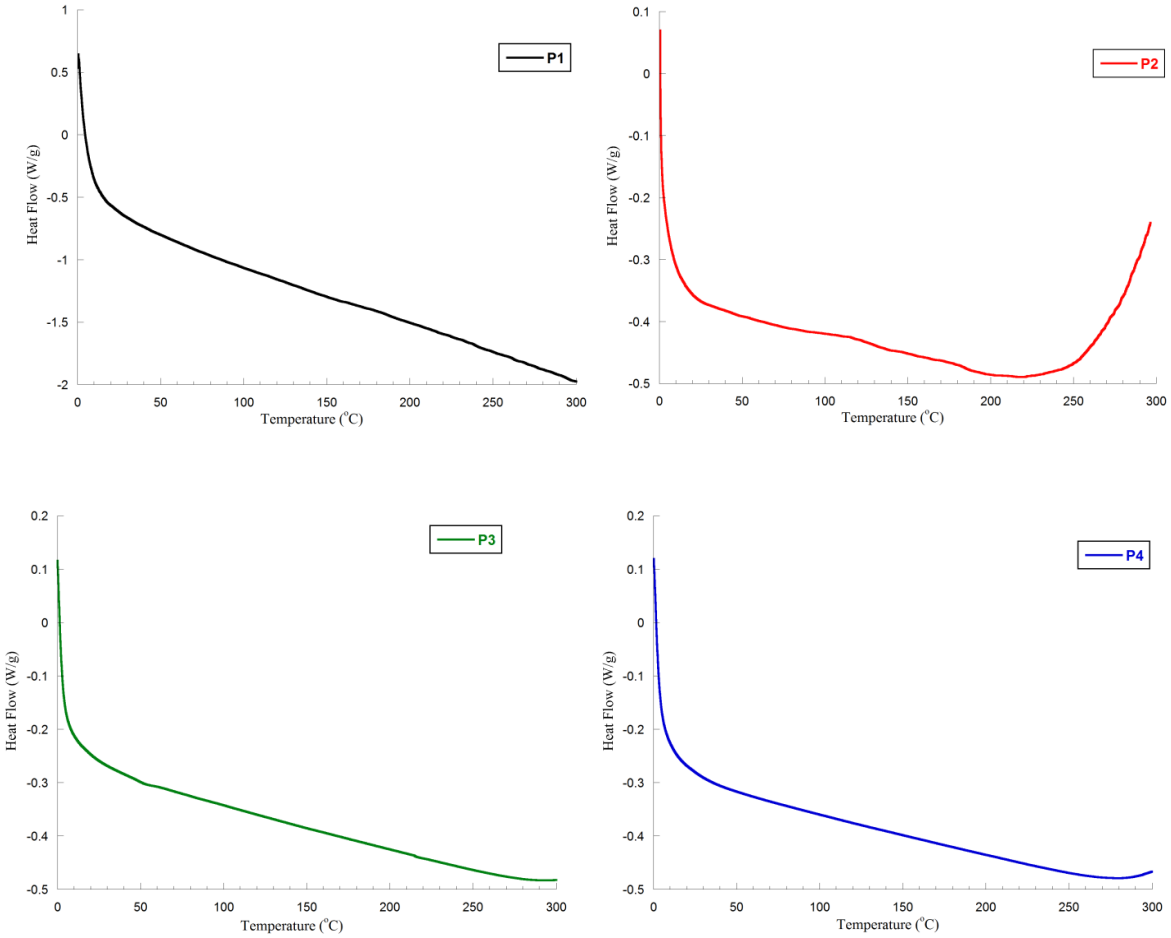

Figure 4.28. Differential scanning calorimetry (DSC) of **P1** – **P4.**

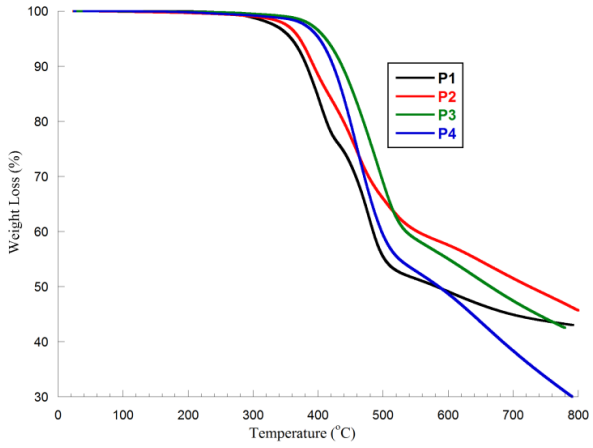

Figure S4.29. Thermogravimetric analysis (TGA) of **P1** – **P4.**

4.8 References

[1] (a) A. Facchetti, *Chem. Mater.*, **2011**, *23*, 733. doi: 10.1021/cm102419z; (b) S. R. Forrest and M. E. Thompson, *Chem. Rev.*, **2007**, *107*, 923. doi: 10.1021/cr0501590

[2] (a) J. Smith, R. Hamilton, I. McCulloch, N. Stingelin-Stutzmann, M. Heeney, D. D. C. Bradley and T. D. Anthopoulos, *J. Mater. Chem.*, **2010**, *20*, 2562. doi: 10.1039/B921674J; (b) A. Facchetti, *Mater. Today*, **2007**, *10*, 28. doi: 10.1016/s1369-7021(07)70017-2; (c) H. E. Katz and J. Huang, *Annu. Rev. Mater. Res.*, **2009**, *39*, 71. doi: 10.1146/annurev-matsci-082908-145433

[3] (a) C. W. Tang and S. A. VanSlyke, *Appl. Phys. Lett.*, **1987**, *51*, 913. doi: 10.1063/1.98799; (b) R. H. Friend, R. W. Gymer, A. B. Holmes, J. H. Burroughes, R. N. Marks, C. Taliani, D. D. C. Bradley, D. A. Dos Santos, J. L. Bredas, M. Logdlund and W. R. Salaneck, *Nature*, **1999**, *397*, 121. doi: doi:10.1038/16393; (c) A. C. Grimsdale, K. Leok Chan, R. E. Martin, P. G. Jokisz and A. B. Holmes, *Chem. Rev.*, **2009**, *109*, 897. doi: 10.1021/cr000013v

[4] (a) C. W. Tang, *Appl. Phys. Lett.*, **1986**, *48*, 183. doi: 10.1063/1.96937 ; (b) M. Scharber, D. Mühlbacher, M. Koppe, P. Denk, C. Waldauf, A. Heeger and C. Brabec, *Adv. Mater.*, **2006**, *18*, 789. doi: 10.1002/adma.200501717; (c) H. Zhou, L. Yang and W. You, *Macromolecules*, **2012**, *45*, 607. doi: 10.1021/ma201648t

[5] M. Singh, H. M. Haverinen, P. Dhagat and G. E. Jabbour, *Adv. Mater.*, **2010**, *22*, 673. doi: 10.1002/adma.200901141

[6] (a) D. Braun and A. J. Heeger, *Appl. Phys. Lett.*, **1991**, *58*, 1982. doi: 10.1063/1.105039; (b) T. Q. Nguyen, I. B. Martini, J. Liu and B. J. Schwartz, *J. Phys. Chem. B*, **2000**, *104*, 237. doi: 10.1021/Jp993190c

[7] (a) K. Osowska and O. S. Miljanic, *Chem. Commun.*, **2010**, *46*, 4276. doi: 10.1039/c0cc00554a; (b) J. Lim, T. A. Albright, B. R. Martin and O. Š. Miljanić, *J. Org. Chem.*, **2011**, *76*, 10207. doi: 10.1021/jo202107w; (c) J. E. Klare, G. S. Tulevski, K. Sugo, A. de Picciotto, K. A. White and C. Nuckolls, *J. Am. Chem. Soc.*, **2003**, *125*, 6030. doi: 10.1021/ja0350942; (d) J. N. Wilson, M. Josowicz, Y. Wang and U. H. F. Bunz, *Chem. Commun.*, **2003**, 2962. doi: 10.1039/B312156A; (e) A. J. Zucchero, P. L. McGrier and U. H. F. Bunz, *Acc. Chem. Res.*, **2009**, *43*, 397. doi: 10.1021/ar900218d; (f) P. L. McGrier, K. M. Solntsev, S. Miao, L. M. Tolbert, O. R. Miranda, V. M. Rotello and U. H. F. Bunz, *Chem. -Eur. J.*, **2008**, *14*, 4503. doi: 10.1002/chem.200800296; (g) J. A. Marsden, J. J. Miller, L. D. Shirtcliff and M. M. Haley, *J. Am. Chem. Soc.*, **2005**, *127*, 2464. doi: 10.1021/ja044175a; (h) K. Ohta, S. Yamada, K. Kamada, A. D. Slepkov, F. A. Hegmann, R. R. Tykwinski, L. D. Shirtcliff, M. M. Haley, P. Salek, F. Gel'mukhanov and H. Aagren, *J. Phys. Chem. A*, **2011**, *115*, 105. doi: 10.1021/jp107044w; (i) E. L. Spitler, J. M. Monson and M. M. Haley, *J. Org. Chem.*, **2008**, *73*, 2211. doi: 10.1021/jo701740n; (j) E. L. Spitler, L.

D. Shirtcliff and M. M. Haley, *J. Org. Chem.*, **2007**, *72*, 86. doi: 10.1021/jo061712w; (k) H. Kang, G. Evmenenko, P. Dutta, K. Clays, K. Song and T. J. Marks, *J. Am. Chem. Soc.*, **2006**, *128*, 6194. doi: 10.1021/ja060185v

[8] (a) B. C. Tlach, A. L. Tomlinson, A. G. Ryno, D. D. Knoble, D. L. Drochner, K. J. Krager and M. Jeffries-EL, *J. Org. Chem.*, **2013**, *78*, 6570. doi: 10.1021/jo4007927; (b) S. Wang, S. Ren, Y. Xiong, M. Wang, X. Gao and H. Li, *ACS Appl. Mater. Interfaces*, **2012**, *5*, 663. doi: 10.1021/am302117k; (c) G. G. Dubinina, R. S. Price, K. A. Abboud, G. Wicks, P. Wnuk, Y. Stepanenko, M. Drobizhev, A. Rebane and K. S. Schanze, *J. Am. Chem. Soc.*, **2012**, *134*, 19346. doi: 10.1021/ja309393c; (d) Y.-L. Wu, F. Bureš, P. D. Jarowski, W. B. Schweizer, C. Boudon, J.-P. Gisselbrecht and F. Diederich, *Chem. -Eur. J.*, **2010**, *16*, 9592. doi: 10.1002/chem.201001051; (e) R. R. Tykivinski, M. Schreiber, P. Seiler, F. Diederich and V. Gramlich, *Adv. Mater.*, **1996**, *8*, 226. doi: 10.1002/adma.19960080308; (f) R. R. Tykwinski and F. Diederich, *Liebigs Annalen*, **1997**, *1997*, 649. doi: 10.1002/jlac.199719970406

[9] (a) Y.-Y. Lai, Y.-J. Cheng, C.-H. Chen, S.-W. Cheng, F.-Y. Cao and C.-S. Hsu, *Polym. Chem.*, **2013**, *4*, 3333. doi: 10.1039/C3PY00168G; (b) S. Zhang, L. Ye, Q. Wang, Z. Li, X. Guo, L. Huo, H. Fan and J. Hou, *J. Phys. Chem. C*, **2013**, *117*, 9550. doi: 10.1021/jp312450p; (c) K. Lu, J. Fang, H. Yan, X. Zhu, Y. Yi and Z. Wei, *Org. Electron.*, **2013**, *14*, 2652. doi: 10.1016/j.orgel.2013.07.006; (d) P. Sista, H. Nguyen, J. W. Murphy, J. Hao, D. K. Dei, K. Palaniappan, J. Servello, R. S. Kularatne, B. E. Gnade, B. Xue, P. C. Dastoor, M. C. Biewer and M. C. Stefan, *Macromolecules*, **2010**, *43*, 8063. doi: 10.1021/ma101709h

[10] (a) J. Hou, M.-H. Park, S. Zhang, Y. Yao, L.-M. Chen, J.-H. Li and Y. Yang, *Macromolecules*, **2008**, *41*, 6012. doi: 10.1021/ma800820r; (b) M. Toba, T. Nakashima and T. Kawai, *J. Poly. Sci. A.*, **2011**, *49*, 1895. doi: 10.1002/pola.24618; (c) Y. Liang, Z. Xu, J. Xia, S.-T. Tsai, Y. Wu, G. Li, C. Ray and L. Yu, *Adv. Mater.*, **2010**, *22*, E135. doi: 10.1002/adma.200903528; (d) A. Najari, S. Beaupré, P. Berrouard, Y. Zou, J.-R. Pouliot, C. Lepage-Pérusse and M. Leclerc, *Adv. Funct. Mater.*, **2011**, *21*, 718. doi: 10.1002/adfm.201001771

[11] H. J. Son, W. Wang, T. Xu, Y. Liang, Y. Wu, G. Li and L. Yu, *J. Am. Chem. Soc.*, **2011**, *133*, 1885. doi: 10.1021/ja108601g

[12] (a) Y.-H. So, S. J. Martin, B. Bell, C. D. Pfeiffer, R. M. Van Effen, B. L. Romain and S. M. Lefkowitz, *Macromolecules*, **2003**, *36*, 4699. doi: 10.1021/ma021045i; (b) J. F. Wolfe, in *Encyclopedia of Polymer Science and Engineering*, John Wiley and Sons, New York, NY, 1988, vol. 11, pp. 601-635.

[13] (a) J. Intemann, J. Mike, M. Cai, S. Bose, T. Xiao, T. Mauldin, R. Roggers, J. Shinar, R. Shinar and M. Jeffries-EL, *Macromolecules*, **2011**, *44*, 248. doi: 10.1021/ma102010s; (b) J. J. Intemann, E. S. Hellerich, B. C. Tlach, M. D. Ewan, C. A. Barnes, A. Bhuwalka, M. Cai, J. Shinar, R. Shinar and M. Jeffries-El, *Macromolecules*, **2012**, *45*, 6888. doi: 10.1021/ma300821m

[14] E. S. Hellerich, J. J. Intemann, M. Cai, R. Liu, M. D. Ewan, B. C. Tlach, M. Jeffries-EL, R. Shinar and J. Shinar, *J. Mater. Chem. C*, **2013**, *1*, 5191. doi: 10.1039/c3tc31019a

[15] B. C. Tlach, A. L. Tomlinson, A. Bhuwalka and M. Jeffries-El, *J. Org. Chem.*, **2011**, *76*, 8670. doi: 10.1021/jo201078w

[16] (a) E. Ripaud, Y. Olivier, P. Leriche, J. r. m. Cornil and J. Roncali, *J. Phys. Chem. B*, **2011**, *115*, 9379. doi: 10.1021/jp203759e; (b) J. N. Wilson, P. M. Windscheif, U. Evans, M. L. Myrick and U. H. F. Bunz, *Macromolecules*, **2002**, *35*. doi: 10.1021/ma025616i

[17] J. F. Mike, J. J. Intemann, M. Cai, T. Xiao, R. Shinar, J. Shinar and M. Jeffries-EL, *Polym. Chem.*, **2011**, *2*, 2299. doi: 10.1039/C1PY00218J

[18] (a) C. H. Woo, B. C. Thompson, B. J. Kim, M. F. Toney and J. M. J. Fréchet, *J. Am. Chem. Soc.*, **2008**, *130*. doi: 10.1021/ja806493n; (b) C. V. Pham, H. B. Mark, Jr. and H. Zimmer, *Synth. Commun.*, **1986**, *16*, 689. doi:

[19] A. E. Tschitschibabin, *Ber. Deusch. Chem. Ges.*, **1905**, *38*, 771. doi: 10.1002/cber.190503801128

[20] J. F. Mike, A. J. Makowski and M. Jeffries-EL, *Org. Lett.*, **2008**, *10*, 4915. doi: 10.1021/ol802011y

[21] L. S. Hegedus, R. R. Odle, P. M. Winton and P. R. Weider, *J. Org. Chem.*, **1982**, *47*, 2607. doi: 10.1021/jo00134a018

[22] (a) W. Li, H. Li, Y. Li and Z. Hou, *Angew, Chem. Int. Ed.*, **2006**, *45*, 7609. doi: 10.1002/anie.200603097; (b) N. Aratani, A. Takagi, Y. Yanagawa, T. Matsumoto, T. Kawai, Z. S. Yoon, D. Kim and A. Osuka, *Chem. -Eur. J.*, **2005**, *11*, 3389. doi: 10.1002/chem.200401306

[23] P. Beimling and G. Kobmehl, *Chem. Ber.*, **1986**, *119*. doi: 10.1002/cber.19861191025

[24] (a) T. E. Kang, H.-H. Cho, C.-H. Cho, K.-H. Kim, H. Kang, M. Lee, S. Lee, B. Kim, C. Im and B. J. Kim, *ACS Appl. Mater. Interfaces*, **2013**, *5*. doi: 10.1021/am302479u; (b) J. Hou, M.-H. Park, S. Zhang, Y. Yao, L.-M. Chen, J.-H. Li and Y. Yang, *Macromolecules*, **2008**, *41*. doi: 10.1021/ma800820r

[25] P. M. Beaujuge, C. M. Amb and J. R. Reynolds, *Acc. Chem. Res.*, **2010**, *43*, 1396. doi: 10.1021/ar100043u

[26] C. M. Cardona, W. Li, A. E. Kaifer, D. Stockdale and G. C. Bazan, *Adv. Mater.*, **2011**, *23*, 2367. doi: 10.1002/adma.201004554

[27] A. D. Becke, *J. Chem. Phys*, **1993**, *98*, 1372. doi: 10.1063/1.464304

[28] M. J. Frisch, G. W. Trucks, H. B. Schlegel, G. E. Scuseria and M. A. C. Robb, J. R.; Montgomery, J. A., Jr.; Vreven, T.; Kudin, K. N.; Burant, J. C.; Millam, J. M.; Iyengar, S. S.; Tomasi, J.; Barone, V.; Mennucci, B.; Cossi, M.; Scalmani, G.; Rega, N.; Petersson, G. A.; Nakatsuji, H.; Hada, M.; Ehara, M.; Toyota, K.; Fukuda, R.; Hasegawa, J.; Ishida, M.; Nakajima, T.; Honda, Y.; Kitao, O.; Nakai, H.; Klene, M.; Li, X.; Knox, J. E.; Hratchian, H. P.; Cross, J. B.; Bakken, V.; Adamo, C.; Jaramillo, J.; Gomperts, R.; Stratmann, R. E.; Yazyev, O.; Austin, A. J.; Cammi, R.; Pomelli, C.; Ochterski, J. W.; Ayala, P. Y.; Morokuma, K.; Voth, G. A.; Salvador, P.; Dannenberg, J. J.; Zakrzewski, V. G.; Dapprich, S.; Daniels, A. D.; Strain, M. C.; Farkas, O.; Malick, D. K.; Rabuck, A. D.; Raghavachari, K.; Foresman, J. B.; Ortiz, J. V.; Cui, Q.; Baboul, A. G.; Clifford, S.; Cioslowski, J.; Stefanov, B. B.; Liu, G.; Liashenko, A.; Piskorz, P.; Komaromi, I.; Martin, R. L.; Fox, D. J.; Keith, T.; Al-Laham, M. A.; Peng, C. Y.; Nanayakkara, A.; Challacombe, M.; Gill, P. M. W.; Johnson, B.; Chen, W.; Wong, M. W.; Gonzalez, C.; Pople, J. A. , Gaussian, Inc.: , Wallingford, CT, , 2004.

[29] (a) H. A. M. van Mullekom, J. A. J. M. Vekemans, E. E. Havinga and E. W. Meijer, *Mater. Sci. Eng., R*, **2001**, *32*, 1. doi: 10.1016/S0927-796X(00)00029-2; (b) E. E. Havinga, W. ten Hoeve and H. Wynberg, *Polym. Bull.*, **1992**, *29*. doi: 10.1007/bf00558045

[30] (a) J. Mike, K. Nalwa, A. Makowski, D. Putnam, A. Tomlinson, S. Chaudhary and M. Jeffries-EL, *Phys. Chem. Chem. Phys.*, **2011**, *13*, 1338. doi: 10.1039/c0cp00353k; (b) B. Milian Medina, A. VanVooren, P. Brocorens, J. Gierschner, M. Shkunov, M. Heeney, I. McCulloch, R. Lazzaroni and J. Cornil, *Chem. Mater.*, **2007**, *19*, 4949. doi: 10.1021/cm071279m

CHAPTER 5

SYNTHESIS AND CHARACTERIZATION OF BULKY BENZOBISOXAZOLE-FLUORENE COPOLYMERS FOR IMPROVED BLUE-EMITTING CONJUGATED MATERIALS

Brian C. Tlach,[a] *Carmen L. Gott,*[a] *and Malika Jeffries-EL*[a]*

[a] Department of Chemistry, Iowa State University, Ames IA 50010

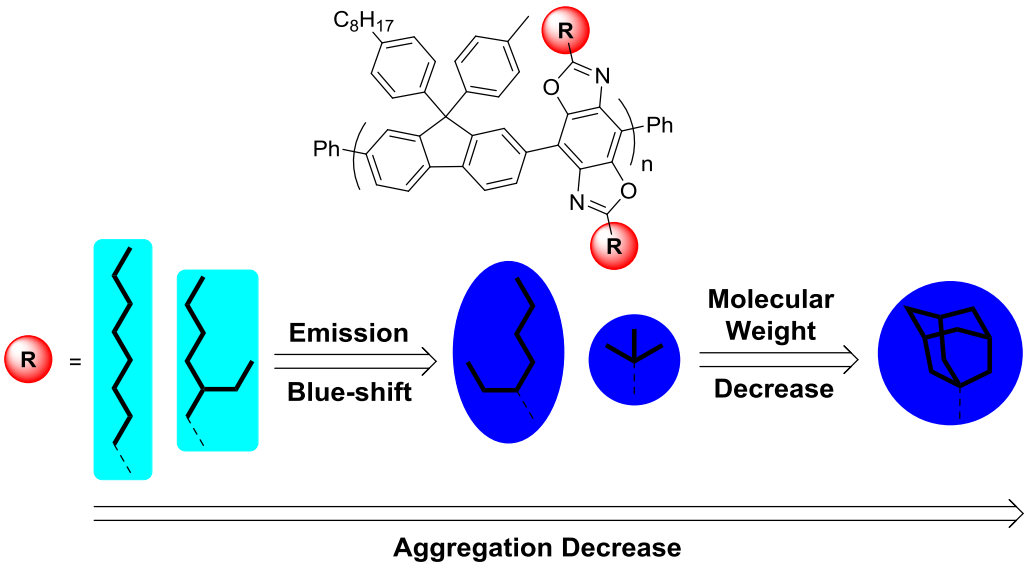

5.1 Abstract

Five new 2,6-dialkyl-4,8-dibromobenzo[1,2-*d*;4,5-*d*']bisoxazoles were synthesized and copolymerized with 9,9-diarylfluorene through a Suzuki cross-coupling on the central 4,8-axis on BBO. These polymers feature alkyl chains of varying steric bulk at the 2,6-

position that decrease π – π stacking and improve solubility of these materials. The BBO monomer imparts high electron affinities for the polymers while the very bulky fluorene monomer suppresses self-quenching by reducing interchain interactions. The polymers all displayed very similar electronic properties but optical properties that had a large dependence on alkyl chain structure. Solid state emission was found to be a function of alkyl chain and varied from 491 nm for long-linear alkyl chains to the 453 nm for the shorter branched chains with aggregation noticeably decreasing as alkyl chain bulkiness increased near the conjugated backbone. These results demonstrate the importance of tuning intermolecular interactions through alkyl chain engineering which can decrease aggregation induced quenching and improve the blue emission of these polymers compared to previous BBO polymers.

5.2 Introduction

Organic semiconductors have been the focus for numerous researchers for their potential to be fabricated using large-scale solution processed methods such as inkjet,[1] roll-to-roll,[2] or screen printing.[3] Of particular interest for organic electronics are organic light emitting diodes (OLED)s for applications in solid-state lighting and flat-panel displays. Although several OLEDs have been developed that utilize metal-centers to efficiently produce the required stable red, green, and blue emission,[4,5] an alternative is the use of polymer LEDs (PLED)s which do not require expensive metals such as platinum.[6-9] However in the past few decades of research on emissive PLEDs, balancing the charge injection of holes and electrons due to differences in mobilities of holes and electrons in the polymers. Most emissive polymers possess a low electron affinity which limit the electron mobility and

has been shown to severely affect the electroluminescent efficiency and thus the overall device efficiency.[7,10]

One method of combating the poor electron mobilities of emissive polymers is the inclusion of electron deficient moieties in the backbone or by addition electron withdrawing substituents. Electron deficient aromatic systems or electron deficient substituents increase the electron affinity of the polymers which typically lead to improvements in electron transport. Benzobisoxazoles are electron-deficient, and when incorporated into polymers, have shown to improve electron affinities,[11] electron mobility,[12-15] fluorescence,[16,17] and thermal stability.[18,19] Our group has previously demonstrated the benefits of copolymerizing various benzobisazoles and flourene derivatives to produce emissive polymers with increased electron affinity.[20-23] The best results were obtained with benzo[1,2-*d*;4,5-*d*']bisoxazole (BBO) and 2,7-diethynyl-9,9-dioctylfluorene to yield polymers which demonstrated stable blue emission (462 nm) in guest-host OLEDs with efficiencies up to 3.4 Cd A^{-1}.[22] However, the polymers still suffered from modest quantum yields and aggregation induced quenching while the alkynyl π-bridge is known degrade in organic semiconductors.

In an effort to improve the stability and efficiency of our previous blue-emitting polymers and to eventually achieve neat PLED devices, we have developed a set of five copolymers utilizing Suzuki cross-coupling through the central benzene ring of various 2,6-dialkyl-4,8-dibromobenzobisoxazoles. This monomer allows ease of introduction of several branched and linear alkyl chains which would prove difficult in most systems and can improve the solubility and disrupt π – π stacking in these polymers. Building on our previous success of blue-emitting materials by co-polymerizing with fluorene, we utilized a 9,9-diarylfluorene monomer. This steric bulk of the 9-position provides increased oxidative

stability of the 9-position while the increased size and rigidity of 4-alkylphenyl substituents perpendicular to the π-system on the sp^3-hybridized 9-position should further disrupt interchain interactions compared to more flexible alkyl chains.[24] The variation of alkyl chains was found to have little impact on the electronic properties of the polymers but significant impact on the intermolecular interactions and optical properties. We found tunable emission from 491 nm to 453 nm in the solid state and improved quantum yields over previous polymers. These polymers are highly soluble and show decreased aggregation in thin film making them excellent candidates for neat PLED devices.

5.3 Results and Discussion

5.3.1 Monomer Synthesis

The synthesis of the BBO monomers is shown in Scheme 5.1. We initially set out to use similar methodology to our previous reports utilizing a Lewis acid catalyzed orthoester condensation.[20,25-30] Since the desired alkyl orthoesters were not commercially available, we attempted to synthesize the desired alkyl orthoesters through the Pinner synthesis[31,32] or Tschitschibabin reaction[25-27,33,34] however, attempts to prepare the desired orthoesters through these methods were unsuccessful. We previously installed alkyl chains at the 2,6-positions of BBO to synthesize 2,6-dihexyl-4,8-dibromobenzobisoxazole[22] in moderate yield through the use of an acid chloride condensation with 3,6-diamino-2,5-dibromo-1,4-hydroquinone (Br-DAHQ) and the dehydration reagent poly(trimethylsilylphosphate) (PPSE). This methodology was synthetically advantageous as the desired acid chlorides were commercially available. Utilizing this methodology, we were able to obtain BBOs **1** – **5** in

moderate yields of 53 – 61% yield. All new compounds were characterized by ^{1}H NMR, ^{13}C NMR, and high-resolution mass spectrometry.

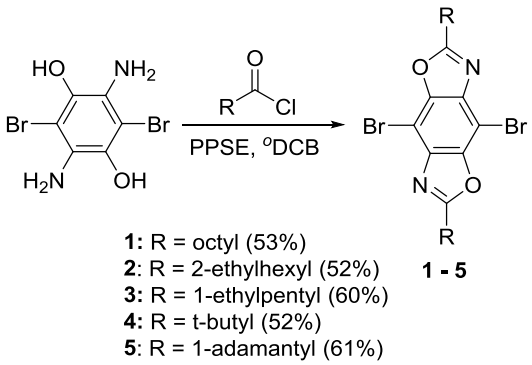

Scheme 5.1. Synthesis of BBO monomers **1 – 5**.

In order to further disrupt aggregation in the polymers, a 9,9-diarylfluorene monomer was chosen as the sp^3 carbon at the 9-position orients the substituents perpendicular to the π-system disrupting π – π stacking and improving solubility while and the aryl groups improving chemical stability of the system. The synthesis of the desired 9,9-diarylfluorene has previously been reported in literature and is shown in Scheme 5.2 starting from 2,7-dibromofluoren-9-one.[35] Nucleophilic addition of 4-octylphenylmagnesium bromide to 2,7-dibromofluoren-2-one yielded **6**. However, the purification provided for **6** was somewhat inefficient on a larger-scale leading us to modify the procedure to remove excess 4-octylbenzene from the crude product prior to column chromatography which provided pure **6** in 88% yield. For the synthesis of **7**, all reaction conditions provided in literature for the Friedel-Crafts type reaction of **6** with triflic acid to form 9,9-diarylfluorene yielded an inseparable mixture of products. However, we found that **7** could be cleanly synthesized by cooling a toluene solution of **6** to -78 °C prior to drop-wise addition of triflic acid and slow warming to room temperature to provide the desired product in 95% yield. **7** was then converted to the boronic ester through metalation of the 2,7-positions followed by quenching

with 2-isopropoxy-4,4,5,5-tetramethyl-1,3,2-dioxaborolane to yield monomer **8** in 68% yield after recrystallization from hexanes.

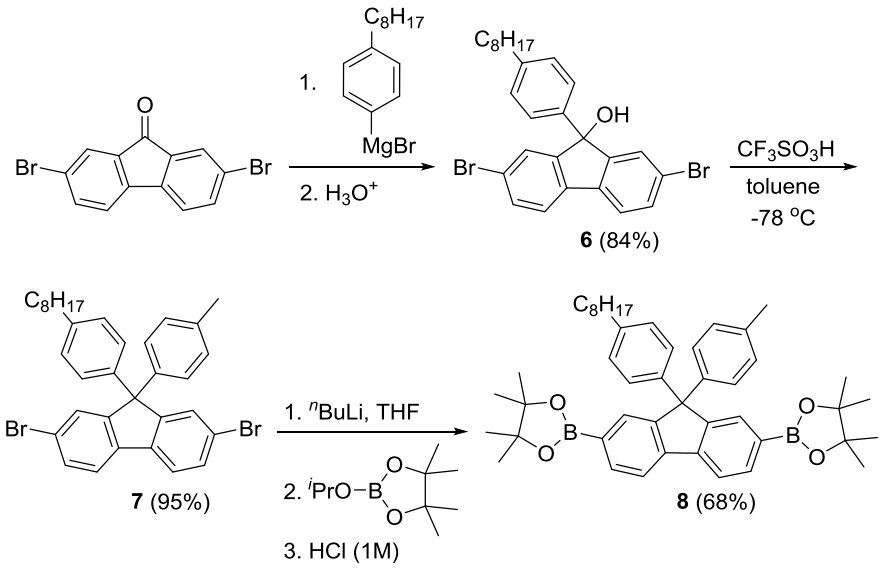

Scheme 5.2. Synthesis of fluorene monomer **8**.

5.3.2 Polymer Synthesis

The BBO-fluorene copolymers **P1 – P5** were synthesized according to Scheme 5.3 in 46 – 71% yield by Suzuki cross-coupling reaction catalyzed by PEPPSI-^{i}Pr™ in a biphasic mixture of toluene and aqueous 2M Na_2CO_3 as shown in Scheme 5.3. $Pd(PPh_3)_4$ was initially chosen as a catalyst, however only oligomers were obtained when employing this catalyst. The appropriate concentration was also find to be critical to obtain the highest molecular weight polymers with a ratio of 5:1 toluene to Na_2CO_3 (aq) providing the best results. The polymers were characterized by gel permeation chromatography (GPC), UV-Vis and fluorescence spectroscopy, and cyclic voltametry. The ^{1}H NMR spectra of the polymers were consistent with the proposed structures. All polymers were soluble in common organic solvents such as THF, chloroform, toluene, and chlorobenzene. Only moderate yields of

isolated polymers were obtained as even higher molecular weight oligomers were removed by acetone during Soxhlet extraction.

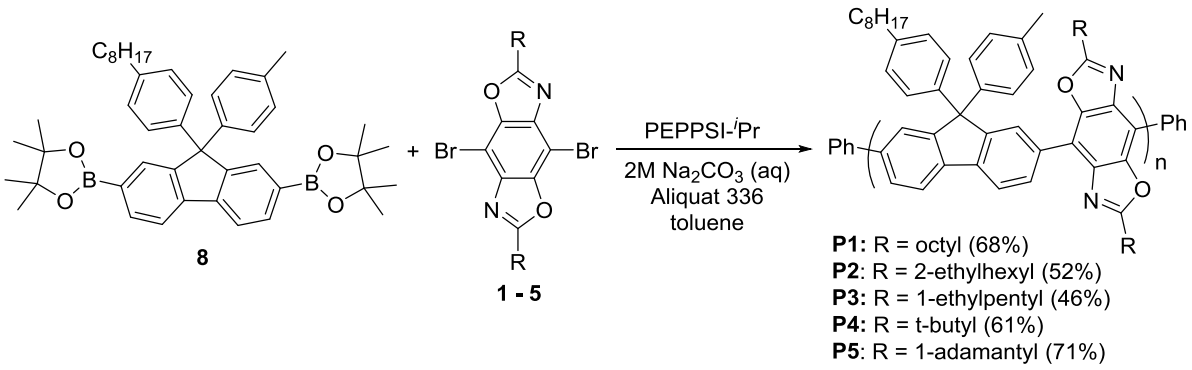

Scheme 5.3. Synthesis of polymers **P1 – P5**.

The molecular weight data for the polymers is summarized in Table 5.1. As a result of the increased solubility, better fractionation of the different molecular weights of the polymers was achieved allowing narrow polydisperity index (PDI) for step-growth polymerizations of 1.12 (**P1**) to 1.69 (**P5**). The polymers showed a broad range of number-average molecular weights (M_n) due to the drastic differences in alkyl chains with **P1** having the highest M_n of 68.5 kdal while **P5**, which bears the much less solubilizing adamantyl group, had a limited M_n of 6.9 kdal.

Table 5.1. Molecular weight data for polymers **P1 – P5**

	M_n (kdal)[a]	PDI[b]	DP_n[c]
P1	68.5	1.12	83
P2	19.8	1.48	24
P3	19.5	1.48	24
P4	17.2	1.54	24
P5	6.94	1.69	8

[a] Molecular weights versus polystyrene in chloroform at 35 °C.

This result is somewhat unexpected as we assumed the branched alkyl chains would afford higher molecular weight polymers, but even after several attempts, higher molecular weights were not achieved for **P2 – P5**. The degree of polymerization (DP_n) was the highest for **P1** of 83 and the lowest for **P5** of 8. Interestingly, all the branched alkyl chain polymers (**P3 – P5**) had the same DP_n of 24. We have not yet been able find a reason for this observation but all the molecular weights are satisfactory for this study.

5.3.3 Optical and Electronic Properties

The electronic properties of the polymers were investigated through cyclic voltametry and the traces shown in Figure S5.16 and the data summarized in Table 5.2. The highest occupied molecular orbital (HOMO) was determined from the oxidation onset (${E_{ox}}^{onset}$) while the lowest unoccupied molecular orbital (LUMO) was calculated from the reduction onset (${E_{red}}^{onset)}$. The electrochemical band gap (E_g^{EC}) was calculated by ${E_g}^{EC} = HOMO - LUMO$. All polymers showed non-reversible oxidation and reduction peaks and were externally referenced to Fc/Fc^+ (-4.8 eV versus vacuum) As expected, the change in alkyl group had very little influence on the electronic properties and the HOMO levels were between -5.94 eV (**P1**) and -5.88 eV (**P4** and **P5**) and are adequate for air stability.[36] The LUMO energy levels had slightly more variation with **P2** having the lowest LUMO of -3.55 eV while **P4** and **P5** had the highest LUMOs of -3.46 eV. The slight variation in the HOMO and LUMO may be due to slightly stronger electron donating ability of a tertiary carbon (**P4** and **P5**) versus secondary (**P3**) or primary (**P1** and **P2**) which would increase the HOMO and LUMO levels. The E_g^{EC} were very similar as well with **P1** having the widest band gap of 2.42 eV while **P4** and **P5** had the narrowest E_g^{EC} of 2.32 eV. The similarity electronic properties of the all the polymers is expected as the alkyl chain structure should have very

little impact on the electronic properties of the polymers. This also indicates that effective conjugation length has been reached in all the polymers and the conjugation length unaffected by alkyl chain structure.

Table 5.2. Electronic properties[a] of **P1 – P5**

	HOMO (ev)[b]	LUMO (ev)[c]	E_g^{EC}(eV)[d]
P1	-5.94	-3.52	2.42
P2	-5.90	-3.55	2.35
P3	-5.90	-3.53	2.37
P4	-5.88	-3.46	2.32
P5	-5.88	-3.46	2.32

[a] Determined by cyclic voltametry of thin films. [b] Calculated from the oxidation onset using $-4.8 - E_{ox}^{onset}$). [c] Calculated from the reduction onset $-4.8 - E_{red}^{onset}$. [d] Calculated by $E_g^{EC} = HOMO - LUMO$.

The absorption properties of the polymers were studied by UV-Vis spectroscopy in dilute chloroform solutions and thin film as shown in Figure 5.1 with corresponding polymer structures and the data summarized in Table 5.3. The solution absorption spectra for all the compounds are fairly similar with aborbance maximum (λ_{max}) that vary from 408 nm for **P1** to 420 nm for **P2**. In general, the λ_{max} of the polymers hypsochromically shift as the bulkiness of the side chains increases with a shoulder starting to appear as the bulkiness of the side-chains increases. In thin film, the spectra are slightly broadened and all of the λ_{max} are within six nanometers between 419 nm (**P4** and **P5**) and 425 nm (**P2**). When comparing solution to thin film, a slight bathochromic shift is seen for polymers with the less bulky chains (**P1 – P3**) of 10 – 14 nm with all spectra being slightly broadened. In general, as the steric bulk increases, the bathochromic shift in λ_{max} from solution to film decreases, the

values became nearly the same (**P4**) or are the same (**P5**). This indicates that the bulky side-chains are effectively disrupting π – π stacking in thin film resulting in less of a red-shift when going from solution and thin film.

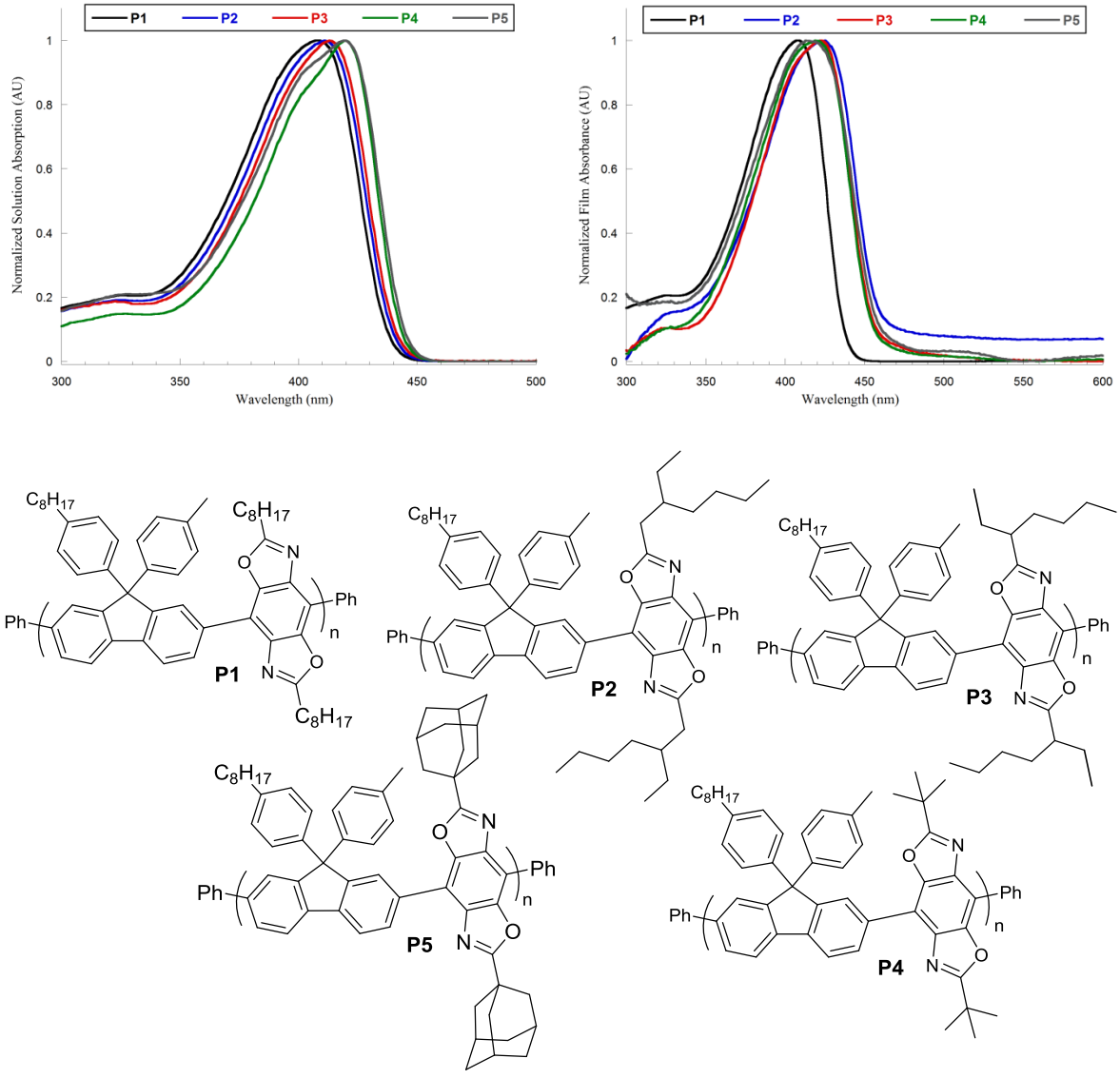

Figure 5.1. UV-Vis spectra in chloroform (top left), thin film (top right) of **P1 – P5** and the corresponding polymer structures (bottom).

The optical band gaps (E_g^{opt}) of the polymers were calculated from the intersection of the thin film absorbance and fluorescence spectra. All the polymers had very similar E_g^{opt}

between 2.80 eV (**P3**, **P4**) and 2.75 eV (**P1**). The E_g^{opt} for all polymers are larger than E_g^{EC} by ca. 0.40 eV. This is unexpected as typically the E_g^{EC} is larger than the E_g^{opt} due to the charge injection barrier between the electrode and polymer film.[37] However, the error may be due to error in the cyclic voltametry measurements as both the oxidation or reduction processes were irreversible which can lead to error that is propagated in the E_g^{EC} calculation.[38]

Table 5.3. Summarized optical data for **P1 – P5**

	λ_{max}^{film} (nm)	λ_{max}^{soln} (nm)[a]	λ_{em}^{film} (nm)	λ_{em}^{soln} (nm)[a]	E_g^{opt} (eV)[b]
P1	422	408	491	442	2.75
P2	425	411	492	443	2.76
P3	423	413	453	443	2.80
P4	419	420	454	444	2.80
P5	419	419	458	445	2.79

[a] Performed in dilute chloroform solutions. [b] Measured from the intersection of the thin film absorption and emission spectra.

The emission properties of the polymers were studied by fluorescence spectroscopy in chloroform and thin films by exciting at their corresponding λ_{max} and the spectra shown in Figure 5.2 and the data summarized in Table 5.3. The solution fluorescence spectra are all nearly the same and all polymers emit in the deep blue region with maximum fluorescence (λ_{em}) between 442 nm and 445 nm. All polymers display the same spectral shape with a main peak and a lower energy shoulder. Conversely, the thin film fluorescence spectra show a higher degree of variation in the energy and shape of the spectra as the alkyl chain structure is changed. The longer and less bulky alky chains of **P1** and **P2** have noticeably

bathochromically shifted thin film fluorescence in the cyan region with λ_{em} of 491 nm and 492 nm, respectively, and broadened spectra compared to **P3 – P4**. **P1** and **P2** both have a higher energy shoulder in the region of **P3 – P4** but the main absorption is red-shifted ca. 35 nm. Also present in **P1** and **P2** is increased vibronic character in the thin film spectra which is likely a result of increased π – π stacking. The changes in spectra also indicate the likely excimer formation within the polymers. **P3 – P4** all emit in the blue region and display very similar fluorescence and have λ_{em} between 453 and 458 nm which are very similar to their respective solution fluorescence with all values bathochromically shifted ca. 10 nm.

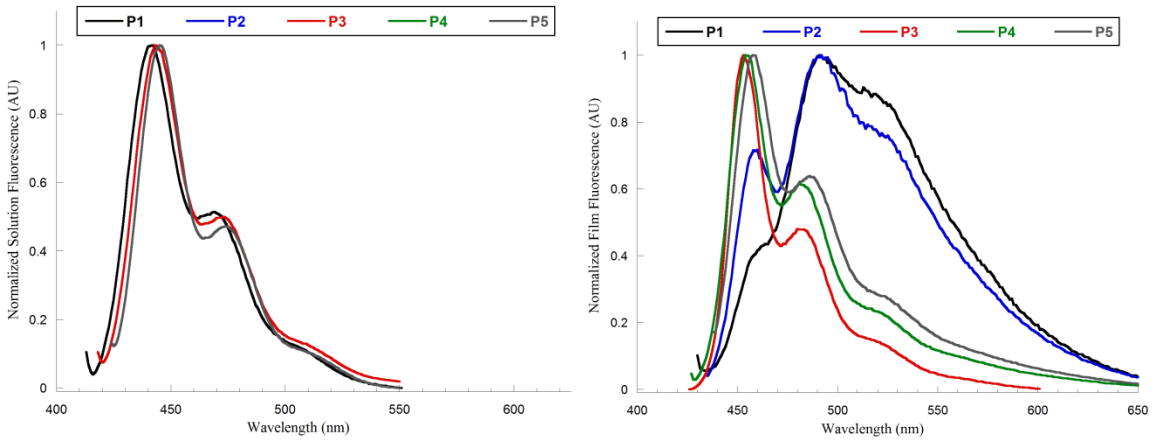

Figure 5.2. Fluorescence spectra of **P1 – P5** in chloroform (left) and thin film (right).

Much like the absorbance spectra, **P3 – P4** display evidence of inefficient π – π stacking in the solid state. More importantly, a structure-property trend appears in that aggregation can be most effectively disrupted by incorporating branching points at the 1-position of the alkyl chain. Furthermore, the large cage structure of the adamantyl side chain does not seem to yield any major benefits in disrupting aggregation while limiting the molecular weight. The additional branching of the 1-position of the *t*-butyl group on **P4** compared to the 1-ethylpentyl group on **P5** does not appear to further disrupt π – π stacking. The decreased

aggregation will hopefully allow the fabrication of neat OLED devices and to improve efficiency over the guest-host devices as we have previously fabricated. The blue emission is also promising that these materials will provide deep blue emission.

5.4 Conclusions

We have synthesized yield five new 2,6-dialkyl-4,8-dibromobenzobisoxazoles in moderate yield using an acid chloride condensation. These monomers were copolymerized with 9,9-diarylfluorene monomers to yield benzobisoxazole-fluorene copolymers with increasingly bulky alkyl side-chains on the 2,6-positions of the benzobisoxazole moiety. The polymers all show similar electronic properties, however, their optical properties are more dependent on the alkyl chain structure. The aggregation in solid state is suppressed upon going from longer-straight to short-branched alkyl chains with the most benefit coming from branching at the one-position of the alkyl chain. Furthermore, all the polymers emit either blue or cyan in the solid state and are great potential materials for blue OLEDs. Fabrication of OLED devices is ongoing along with studies on the effects of increasing the steric bulk of alkyl chains on the thermal properties of the polymers. We are currently investigating the use of bulky aryl substituents at the 2,6-positions to create cross-conjugated emissive polymers that will further disrupt aggregation and tune the $\pi - \pi$ stacking of these materials.

5.5 Experimental Section

5.5.1 Characterization

All nuclear magnetic resonance (NMR) experiments were carried out in $CDCl_3$ with all non-polymer experiments being carried out on a Varian MR-400 at 400 MHz (^1H) or 100

MHz (^{13}C) while all polymer NMR experiments were carried out on a Bruker AVIII-600 at 600 MHz (^{1}H) at 45 °C. All ^{1}H NMR spectra are internally referenced to the residually protonated solvent peak (7.26 ppm) and ^{13}C NMR spectra are referenced to the central carbon peak (77.16 ppm) of $CDCl_3$. In all spectra, chemical shifts are given in δ relative to tetramethylsilane. Coupling constants are reported in hertz (Hz). High-resolution mass spectra were recorded on a double-focusing magnetic sector mass spectrometer using electrospray ionization (ESI) or atmospheric pressure chemical ionization (APCI). Melting points were obtained on a melting point apparatus with 260 °C upper limit and are uncorrected. Gel permeation chromatography (GPC) measurements were performed on a separation module equipped with three 5-mm I-gel columns connected in series (guard, high molecular weight, and medium molecular weight) with a UV–Vis detector. Analyses were performed at 35 °C using $CHCl_3$ as the eluent at a flow rate of 1.0 mL min^{-1} with calibration based on polystyrene standards. Electrochemistry was performed on thin films using an eDAQ e-Corder 410 using 0.01 $AgNO_3$ in acetonitrile as the reference electrode, a platinum wire as the counter electrode, and a platinum button electrode as the working electrode at a scanning rate of 50 mV s^{-1}. All measurements were taken under argon in deoxygenated acetonitrile using 0.1 M tetrabutylammonium hexafluorophosphate as the supporting electrolyte. The potentials were measured versus Ag/Ag^{+} and externally referenced to Fc/Fc^{+} (-4.8 eV versus vacuum). Sample films for electrochemistry were drop-cast onto the working electrode from ca. 2 mg mL^{-1} chlorobenzene solutions and then annealed at 150 °C for 1 h before analysis. All UV-Vis and fluorescence spectroscopy experiments were performed on Cary-Eclipse spectrometers on dilute chloroform solutions or thin films. Thin films were spin coated from mixtures of chloroform and ^{o}DCB (5 – 10 mg mL^{-1}) onto 25x25x1 mm glass

slides at 74 *g* on a Headway Research, Inc. PWM32 spin-coater and annealed at 150 °C for 2 h prior to analysis.

5.5.2 Materials

Tetrabutylammonium hexafluorophosphate was purchased from Oakwood Chemical and was recrystallized from methanol prior to use. Tetrahydrofuran, diethyl ether, and toluene, were dried using an Innovative Technologies solvent purification system. When noted, solvents were deoxygenated by bubbling argon through the solvent for 30 minutes. All other chemicals were purchased from commercial sources and used without further purification. Column chromatography was carried out using silica gel (35 – 70 μm). 3,6-diamino-2,5-dibromo-1,4-hydroquinone (Br-DAHQ),[28] 1-bromo-4-octylbenzene,[40] and 2,7-dibromo-fluoren-9-one[35] were synthesized according to literature procedures.

5.5.3 Monomer Synthesis

4,8-dibromo-2,6-dioctylbenzo[4,5-*d*;4,5-*d'*]bisoxazole (1). PPSE was synthesized according to a modified literature procedure.[41] A dry round-bottom flask was placed under argon atmosphere and then 7.2 g of P_2O_5, 65 mL ^{o}DCB, 10.8 g of hexamethyldisiloxane were added sequentially. The solution was heated to 100 °C for 2 h (solution becomes homogenous) and then allowed to cool to room temperature. The solution was deoxygenated for 30 minutes and then 9.72 g (55.0 mmol) of nonanoyl chloride and 6.55 g (23.0 mmol) of freshly prepared Br-DAHQ were added. The mixture was heat to 100 °C under argon for 72 h and then allowed to cool to room temperature. The crude mixture was concentrated to ca. 10 mL by vacuum distillation and the remaining liquid precipitated into 200 mL cold methanol. The precipitate was filtered and rinsed with methanol. The crude product was further purified by recrystallization from hexanes (hot filter) to yield off-white needles (6.35

g, 53% yield): mp 96 – 98 °C; ^{1}H NMR (400 MHz, $CDCl_3$) δ 0.88 (6H, t, *J* = 8 Hz) 1.27 – 1.36 (16H, comp), 1.42 – 1.47 (4H, m), 1.93 (4H, *J* = 8 Hz, q), 3.01 (4H, *J* = 8 Hz, t); ^{13}C NMR (100 MHz, $CDCl_3$) δ 14.3, 22.8, 27.2, 29.21, 29.28, 29.3, 29.4, 32.0, 91.4, 138.6, 146.7, 169.4; HRMS (ESI) *m/z*: Calcd for $C_{24}H_{35}Br_2N_2O_2$ 543.1034 $[M + H]^+$: found 543.1047.

4,8-dibromo-2,6-di(2-ethylhexyl)benzo[4,5-*d*;4,5-*d′*]bisoxazole (2). This compound was prepared analogously to **1** from Br-DAHQ (10.0 mmol) and 3-ethylheptanoyl chloride. After distillation of the ^{o}DCB the crude was dissolved in 60:40 hexane/chloroform and passed through a pad of silica gel eluting with 60:40 hexane/chloroform. The solution was concentrated *in vacuo* and recrystallized from methanol (hot filter) to yield off-white needles (2.75 g, 52% yield): mp 93 – 96 °C; ^{1}H NMR (400 MHz, $CDCl_3$) δ 0.85 – 0.94 (12H, overlapped triplets, *J* = 8 Hz) 1.29 – 1.44 (16H, comp), 2.04 (2H, p, *J* = 8 Hz), 2.94 (4H, d, *J* = 8 Hz), 3.01 (4H, *J* = 8 Hz, t); ^{13}C NMR (100 MHz, $CDCl_3$) δ 14.3, 22.8, 27.2, 29.21, 29.28, 29.3, 29.4, 32.0 91.4, 138.6, 146.7, 169.4; HRMS (ESI) *m/z*: Calcd for $C_{24}H_{35}Br_2N_2O_2$ 543.1034 $[M + H]^+$: found 543.1041.

4,8-dibromo-2,6-di(1-ethylpentyl)benzo[4,5-*d*;4,5-*d′*]bisoxazole (3). This compound was prepared and isolated analogously to **2** from Br-DAHQ (20.0 mmol) and 2-ethylhexanoyl chloride. The crude product was recrystallized from methanol (hot filter) to give white needles (6.20 g, 60% yield): mp 77 – 80 °C; ^{1}H NMR (400 MHz, $CDCl_3$) δ 0.79, (6H, t, *J* = 8 Hz), 0.86, (6H, t, *J* = 8 Hz), 0.93 (6H, t, *J* = 8 Hz), 1.12 – 1.29 (8H, comp), 1.68 – 1.90 (8H, comp), 2.97 (2H, m); ^{13}C NMR (100 MHz, $CDCl_3$) δ 12.1, 14.1, 22.7, 26.8, 29.8, 33.0, 42.5, 91.5, 138.5, 146.6, 172.0. HRMS (APCI) *m/z*: Calcd for $C_{22}H_{31}Br_2N_2O_2$ 515.0721 $[M + H]^+$: found 515.0733.

4,8-dibromo-2,6-di(2-methylprop-2-yl)benzo[4,5-*d*;4,5-*d′*]bisoxazole (4). This compound was prepared and isolated analogously to **1** from Br-DAHQ (18.0 mmol) and 2,2-dimethylpropanoyl chloride. The crude product was recrystallized from heptane (hot filter) to give glistening white needles (4.01 g, 52% yield): mp >260 °C; ^{1}H NMR (400 MHz, $CDCl_3$) δ 1.56 (18H, s); ^{13}C NMR (100 MHz, $CDCl_3$) δ 28.7, 35.1, 91.6, 138.6, 146.7, 175.3; HRMS (APCI) *m/z*: Calcd for $C_{16}H_{19}Br_2N_2O_2$ 430.9782 $[M + H]^+$: found 430.9791.

4,8-dibromo-2,6-di(adamant-1-yl)benzo[4,5-*d*;4,5-*d′*]bisoxazole (5). This compound was prepared and isolated analogously to **2** from Br-DAHQ (10.0 mmol) and 1-adamantecarbonyl chloride. The crude product was recrystallized from heptane (hot filter) to give small off-white needles (6.35 g, 61% yield): mp >260 °C; ^{1}H NMR (400 MHz, $CDCl_3$) δ 1.82 – 1.84 (12H, m) 2.15 – 2.18 (6H, m), 2.21 – 2.22 (12H, m); ^{13}C NMR (100 MHz, $CDCl_3$) δ 28.1, 36.6, 36.9, 40.3, 91.6, 138.5, 146.4, 174.7; HRMS (APCI) *m/z*: Calcd for $C_{28}H_{31}Br_2N_2O_2$ 587.0721 $[M + H]^+$: found 587.0740.

2,7-dibromo-9-(4-octylphenyl)fluoren-9-ol (6). This compound was synthesized according to a modified literature procedure.[35] A dry round-bottom flask equipped with a condenser was placed under argon, charged with magnesium turnings then heated under vacuum to 90 °C for 30 minutes. The flask was refilled with argon, a few crystals of iodine added, and then allowed to sublime for 20 minutes. The flask was allowed to cool to ca. 70 °C, and 20 mL dry THF added, and the solution refluxed until the iodine color subsided. A THF solution of 4.71 g (17.5 mmol) 1-bromo-4-octylbenzene (in 10 mL THF) was then added drop-wise until the reaction was self-sustaining, the heat source removed, and the remainder of the solution added to maintain a gentle reflux. The reaction was heated to reflux for 2 hours and allowed to cool to room temperature. 3.38 g (10.0 mmol) of 2,7-

dibromofluoren-9-one was added in one portion and the mixture heated to reflux overnight. The solution was then allowed to cool to room temperature, poured into cold, saturated NH_4Cl (aq) and the layers separated. The aqueous layer was extracted with hexanes and the combined organic layers were washed with saturated NH_4Cl, H_2O, and brine, and then dried over Na_2SO_4. The solution was filtered, concentrated *in vacuo*, and excess 4-octylbenzene removed by Kugelrohr® distillation. The crude product was further purified by column chromatography eluting with 98:2 hexane/ethyl acetate with a slow gradient to 80:20 to yield a viscous orange oil (4.63 g, 88% yield): ^{1}H NMR (400 MHz, $CDCl_3$) δ 0.87 (3H, t, J = 8 Hz), 1.26 – 1.30 (10H, comp), 1.57 – 1.62 (2H, m), 2.45 (1H, s), 2.57 (2H, t, J = 8 Hz), 7.10 (2H, d, J = 8 Hz), 7.25 (2H, d, J = 8 Hz), 7.45 (2H, s), 7.49 (4H, d).

2,7-dibromo-9-(4-octylphenyl)-9-(4-methylphenyl)fluorene (7). This compound was synthesized according to modified literature procedure.[35] In a dry round-bottom flask under argon atmosphere, 4.41 g (8.34 mmol) of **6** was dissolved in 75 mL of dry toluene and the solution cooled to -78 °C with vigorous stirring. 2.2 mL (25.0 mmol) of CF_3SO_3H was added drop-wise via syringe and the solution was allowed to warm to room temperature overnight. The reaction mixture was poured into cold saturated $NaHCO_3$, the layers separated, and the organic layer washed with saturated $NaHCO_3$, H_2O, and brine and then dried over Na_2SO_4. The solution was filtered, concentrated *in vacuo*, and the crude product purified by column chromatography eluting with hexanes to yield a yellow oil (4.76 g, 95% yield): ^{1}H NMR (400 MHz, $CDCl_3$) δ 0.88 (3H, t, J = 8 Hz),1.27 – 1.31 (10H, comp), 1.58 – 1.62 (2H, m), 2.31 (3H, s), 2.55 (3H, t, J = 8 Hz), 7.05 (8H, comp), 7.47 – 7.48 (4H, comp), 7.57 (2H, d, J = 8 Hz).

2,7-bis(4,4,5,5-tetramethyl-1,3,2-dioxaborolan-2-yl)2,7-dibromo-9-(4-methylphenyl)-9-(4-octylphenyl)fluorene (8). This compound was synthesized according to modified literature procedure.[35] In a dry round-bottom flask under argon atmosphere, 4.76 g (7.90 mmol) of **7** was dissolved in 100 mL dry THF and cooled to -78 °C. 9.5 mL of ^{n}BuLi (2.5 M hexanes) was added drop-wise and the solution stirred for 2 h at -78 °C. A solution of 8.82 g (47.4 mmol) of 2-isopropoxy-4,4,5,5-tetramethyl-1,3,2-dioxaborolane in 5 mL THF was added drop-wise and the reaction was allowed to warm to room temperature overnight. The reaction mixture was cooled to 0 °C, quenched with 1 M HCl, and stirred for 30 minutes. The layers were separated, the aqueous layer extracted with diethyl ether, and the combined organic layers washed with 1M HCl, H_2O, and brine and dried over Na_2SO_4. The solution was filtered and concentrated *in vacuo*. The crude product was purified by recrystallization from a minimal amount of hexanes followed by cooling to -40 °C. A second crop of crystals was obtained by concentrating the filtrate and cooling to -40 °C to yield a low-melting bright white powder (6.28 g, 68% yield): ^{1}H NMR (400 MHz, $CDCl_3$) δ 0.88 (3H, t, J = 8 Hz) 1.23 – 1.31 (34H, comp), 1.55 – 1.59 (2H, m), 2.28 (3H, s), 2.53 (2H, t, J = 8 Hz), 7.01 (4H, comp), 7.11 (4H, comp), 7.76 – 7.82 (6H, comp).

5.5.4 Polymer Synthesis

General Polymer Synthesis of P1 – P5. A two-neck round bottom flask was charged with 0.25 mmol of **1 – 5** and 0.255 mmol of **8**, and two drops of Aliquat 336. The flask was equipped with a reflux condenser, placed under argon atmosphere, and 10 mL of deoxygenated toluene and 3 mL of deoxygenated of 2M Na_2CO_3 (aq) were added. The mixture was deoxygenated for an additional 15 minutes, 8.5 mg (0.0125 mmol) PEPPSI-^{i}Pr™ was added, and the mixture further deoxygenated for 5 minutes. The reaction mixture

was then heated to reflux under argon with vigorous stirring for 5 days then end-capped sequentially with a 4,4,5,5-Tetramethyl-2-phenyl-1,3,2-dioxaborolane (4 h) and iodobenzene (12 h). The reaction mixture was allowed to cool to room temperature, diluted with water and toluene, and the layers separated. The organic layer was washed with 1M HCl, H_2O, and brine and dried over Na_2SO_4. The solution was filtered, concentrated *in vacuo*, and the crude polymer dissolved in a minimal amount of warm $CHCl_3$. The polymer solution was precipitated into 200 mL of methanol and filtered through a cellulose extraction thimble. The extraction thimble was placed in a Soxhlet extractor and washed with methanol (48 h), acetone (24 h), and finally the polymer extracted with $CHCl_3$. The chloroform extract was concentrated *in vacuo* to ca. 5 mL and passed through a pad of silica gel eluting with $CHCl_3$. The solution was concentrated *in vacuo* to ca. 3 mL and re-precipitated into 200 mL methanol. The precipitate was filtered, rinsed with methanol, and resulting solid dried in the vacuum oven overnight at 50 °C to yield polymers **P1 – P5**.

Poly[(9-(4-octylphenyl)-9-(4-methylphenyl)fluorene-2,7-diyl)-*alt*-(2,6-dioctylbenzo[1,2-d;4,5-d′]bisoxazole-4,8-diyl)] (P1). P1 was synthesized from **1** and **8** to yield a yellow solid (140 mg, 68% yield): ^{1}H NMR (600 MHz, $CDCl_3$) δ 0.84 (3H, t, J = 6 Hz), 0.90 (6H, t, J = 6 Hz), 1.27 – 1.31 (26H, comp), 1.46 – 1.48 (4H, m), 1.58 (2H, m), 1.89 – 1.92 (4H m), 2.30 (3H, s), 2.54 (2H, broad), 2.94 (4H, broad), 7.05 (4H, broad), 7.34 – 7.37 (4H, comp), 8.00 (2H, d, J = 6 Hz), 8.33 – 8.37 (4H, comp).

Poly[(9-(4-octylphenyl)-9-(4-methylphenyl)fluorene-2,7-diyl)-*alt*-(2,6-bis(2-ethylhexyl)benzo[1,2-d;4,5-d′]bisoxazole-4,8-diyl)] (P2). P2 was synthesized from **2** and **8** to yield a bright yellow fluffy solid: (107 mg, 52% yield): ^{1}H NMR (600 MHz, $CDCl_3$) δ 0.84 – 0.92 (15H, comp), 1.24 – 1.30 (18H, comp), 1.40 – 1.46 (10H, comp), 1.54 – 1.59

(2H, m), 2.03 – 2.06 (2H, m), 2.28 (3H, s), 2.53 (2H, t, J = 6 Hz), 2.90 (4H, broad), 7.04 (4H, broad), 7.33 – 7.36 (4H, comp), 7.99 (2H, d, J = 6 Hz), 8.34 – 8.40 (4H, comp).

Poly[(9-(4-octylphenyl)-9-(4-methylphenyl)fluorene-2,7-diyl)-*alt*-(2,6-bis(1-ethylpentyl)benzo[1,2-d;4,5-d′]bisoxazole-4,8-diyl)] (P3). P3 was synthesized from **3** and **8** to yield a very fluffy bright yellow solid (91 mg, 46% yield): ^{1}H NMR (600 MHz, $CDCl_3$) δ 0.86 (9H, broad), 0.93 (6H, broad), 1.27 – 1.32 (20H, comp), 1.58 (2H, broad), 1.74 – 1.86 (10H, comp), 2.28 (3H, s), 2.54 (2H, broad), 2.99 (2H, broad), 7.04 (4H, comp), 7.30 – 7.35 (4H, comp), 8.01 (2H, d, J = 6 Hz), 8.41 (4H, broad).

Poly[(9-(4-octylphenyl)-9-(4-methylphenyl)fluorene-2,7-diyl)-*alt*-(2,6-bis(2-methylprop-2-yl)benzo[1,2-d;4,5-d′]bisoxazole-4,8-diyl)] (P4). P4 was synthesized from **4** and **8** to yield a fluffy yellow solid: (109 mg, 61% yield): ^{1}H NMR (600 MHz, $CDCl_3$) δ 0.86 (3H, broad), 1.27 (10H, comp), 1.49 (18H, s), 1.55 – 1.57 (2H, m), 2.27 (3H, s), 2.53 (2H, broad), 7.04 (4H, broad), 7.30 – 7.34 (4H, comp), 8.00 (2H, d, J = 12 Hz), 8.46 (4H, broad).

Poly[(9-(4-octylphenyl)-9-(4-methylphenyl)fluorene-2,7-diyl)-*alt*-(2,6-bis(1-adamantyl)benzo[1,2-d;4,5-d′]bisoxazole-4,8-diyl)] (P5). P5 was synthesized from **5** and **8** to yield a bright yellow powder (155 mg, 71% yield): ^{1}H NMR (600 MHz, $CDCl_3$) δ 0.85 (3H, broad), 1.25 (10H, broad), 1.82 – 1.85 (12H, comp), 2.13 – 2.18 (18H, comp), 2.26 (3H, s), 2.51 (2H, t, J = 12 Hz), 7.04 (4H, broad), 7.34 (4H, broad), 8.01 (2H, d, J = 8 Hz), 8.49 – 8.51 (4H, comp).

5.6 Acknowledgements

We would like to thank the National Science Foundation (DMR-0846607) for funding support of this work. We would also like to thank the donors of the Petroleum Research Fund and the 3M Foundation for partial support of this work. We would like to thank Kamel Harrata and Iowa State University (ISU) Mass Spectroscopy Laboratory for analysis of our compounds. We would like to thank Dr. Jeremy Intemann (University of Wisconsin – Green Bay), Ramiro Chavez (ISU), and Dana Drochner (ISU) for helpful discussions on this research.

5.7 Supporting Information

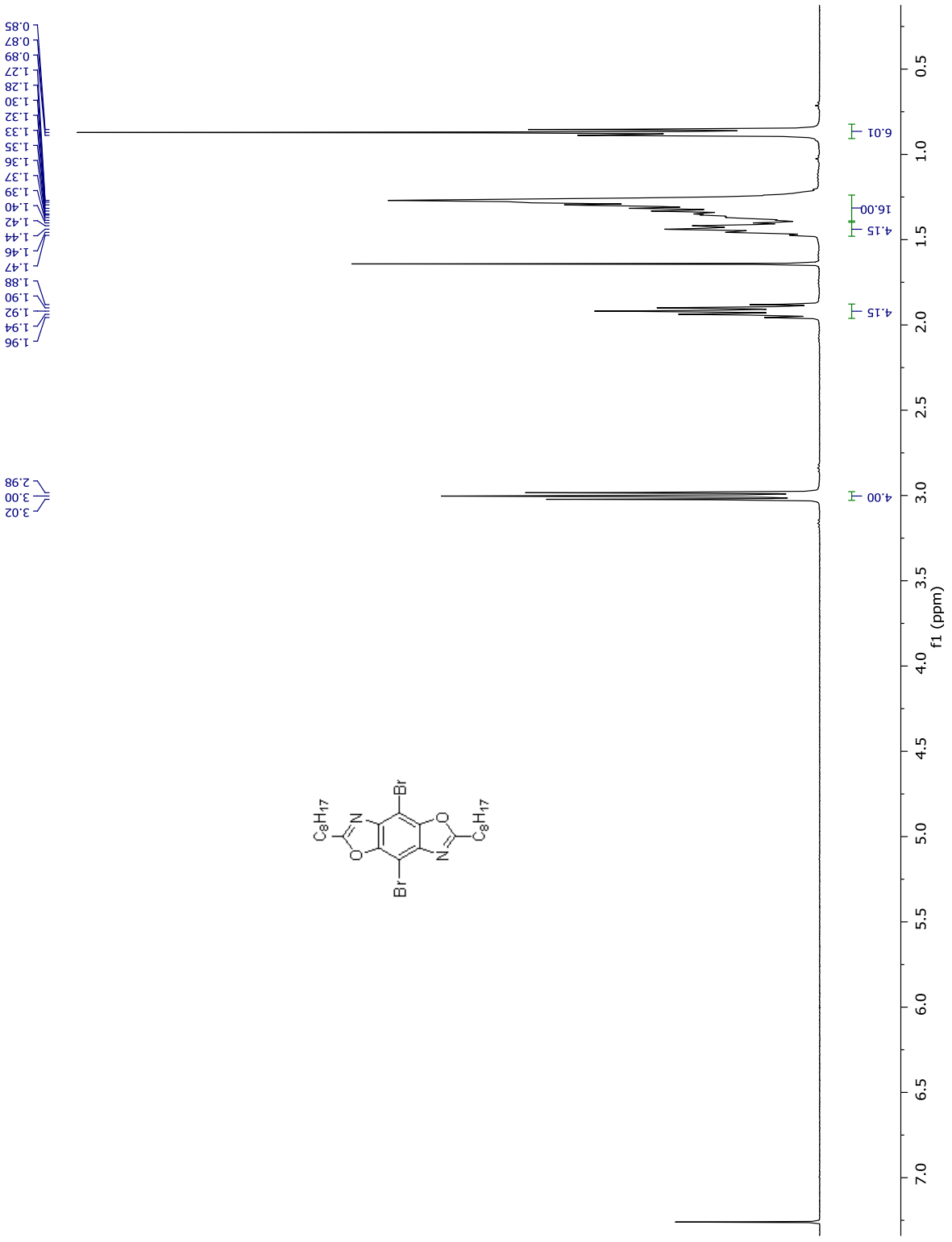

Figure S5.1. ^{1}H NMR spectrum of **1.**

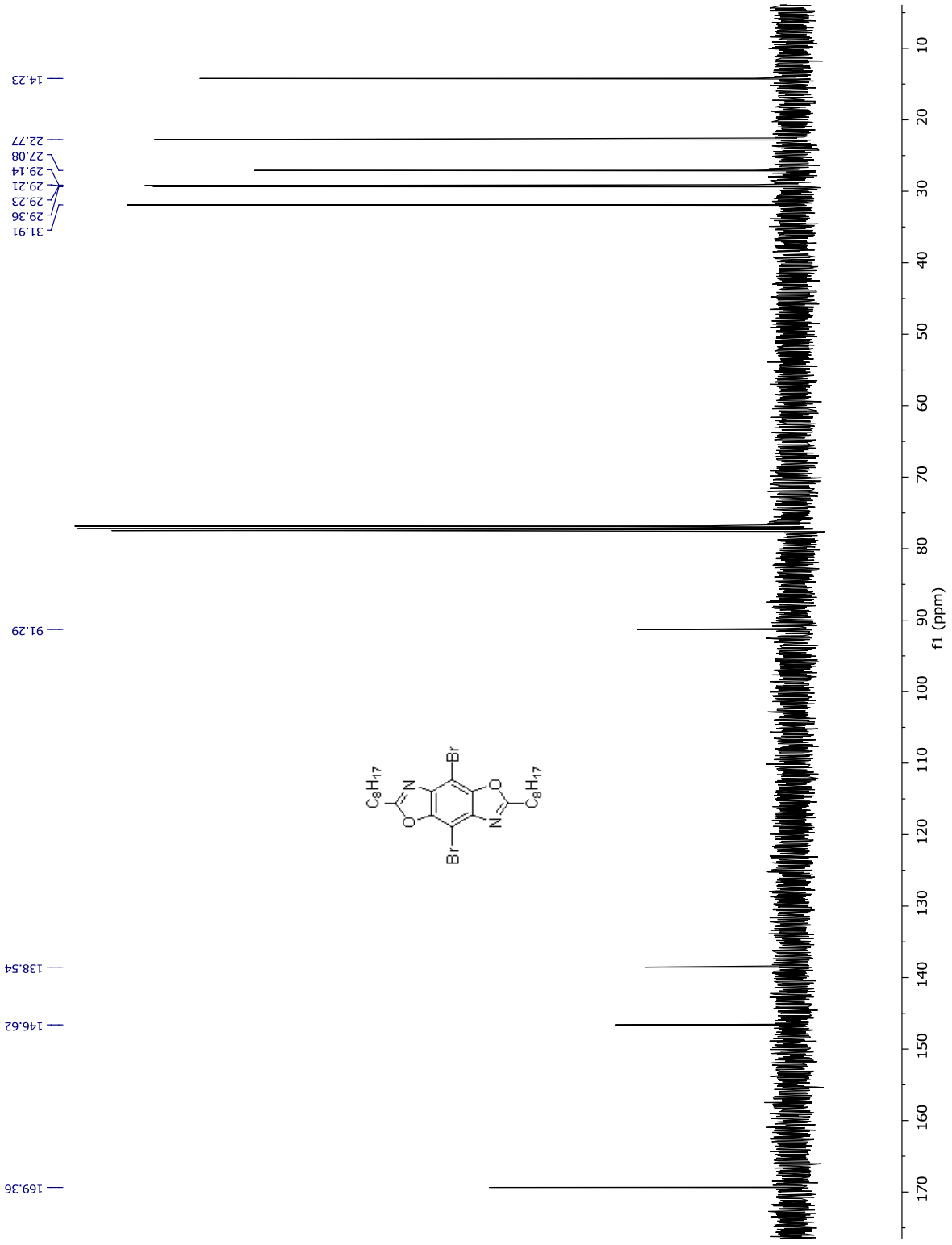

Figure S5.2. ^{13}C NMR spectrum of **1.**

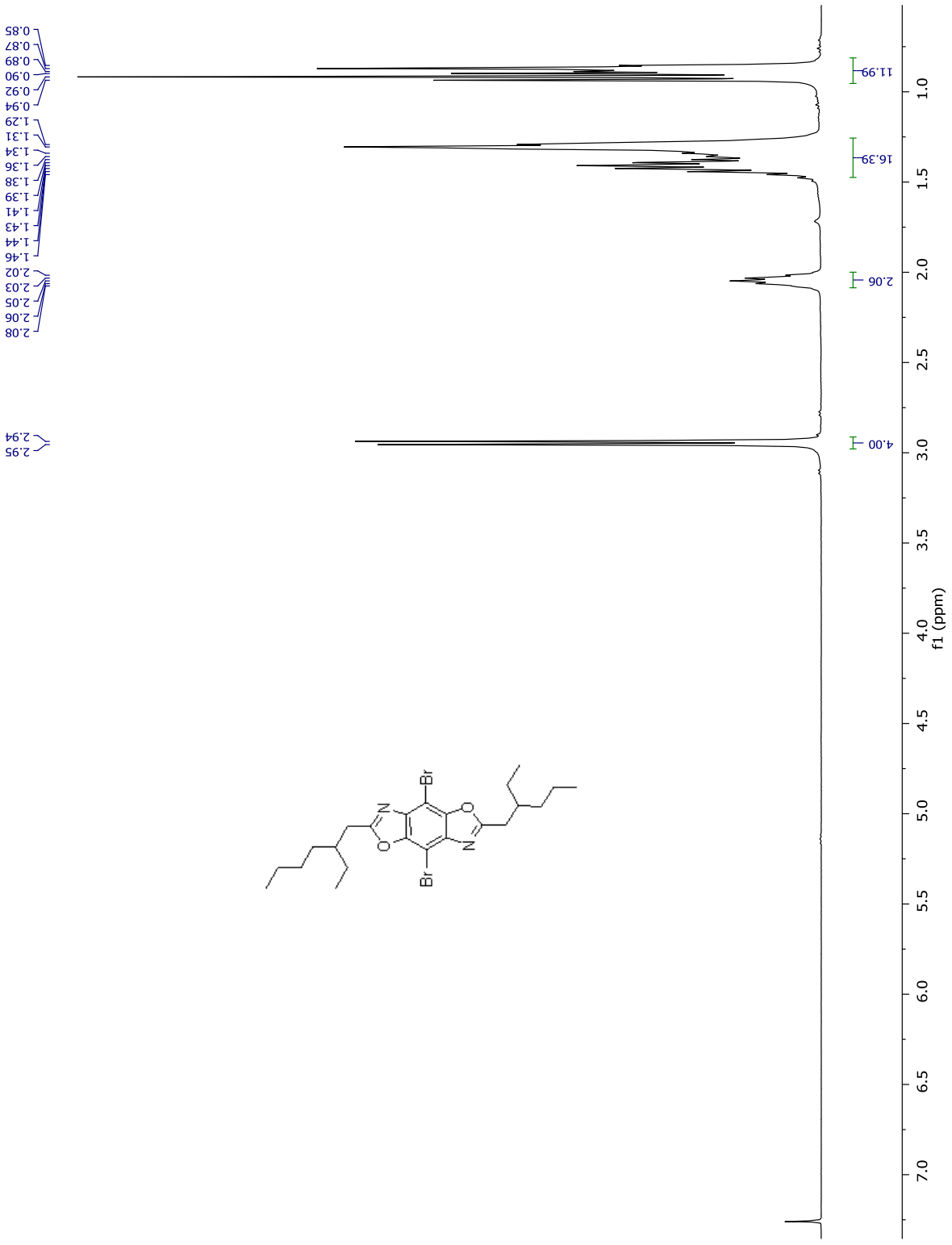

Figure S5.3. ^{1}H NMR spectrum of **2.**

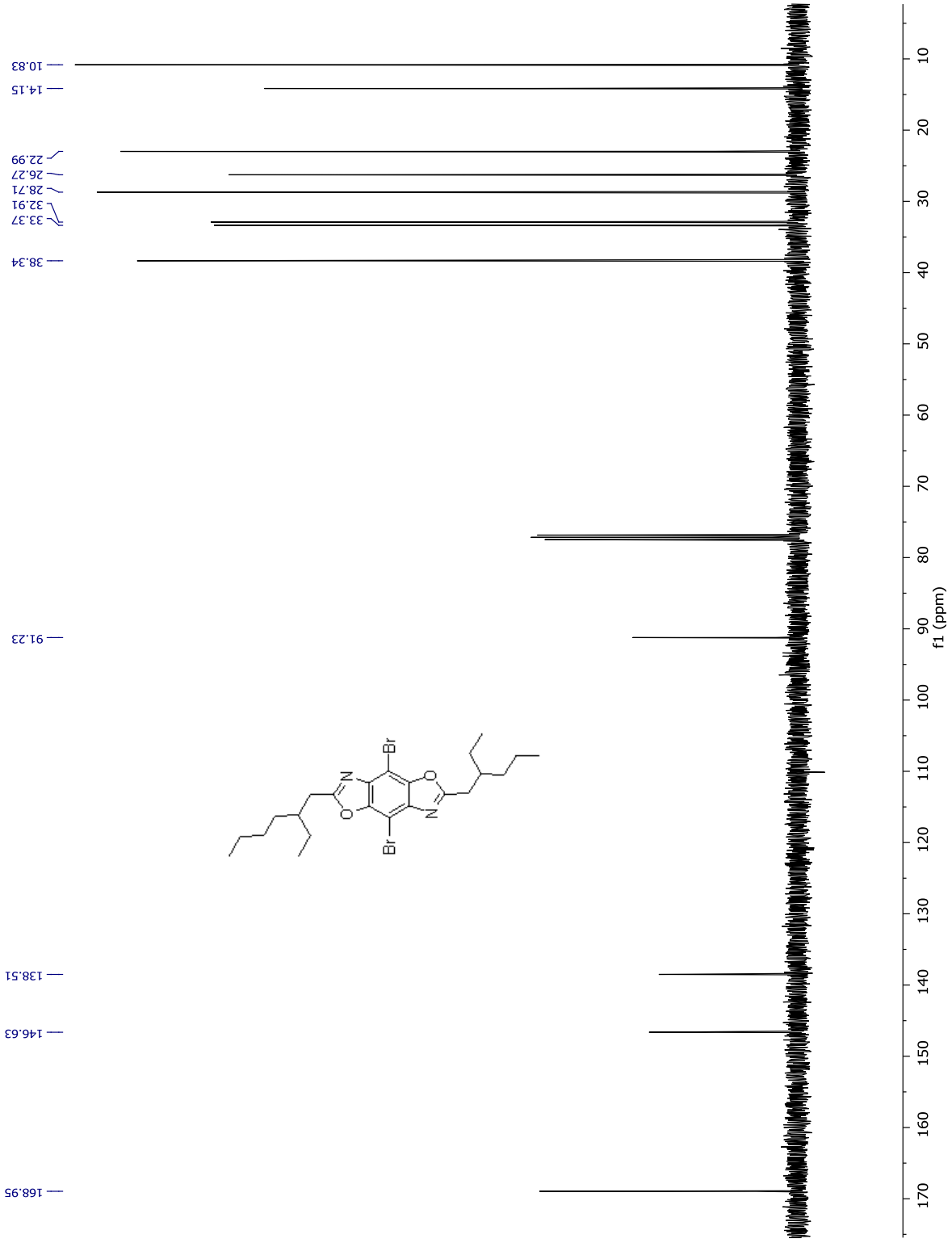

Figure S5.4. ^{13}C NMR spectrum of **2.**

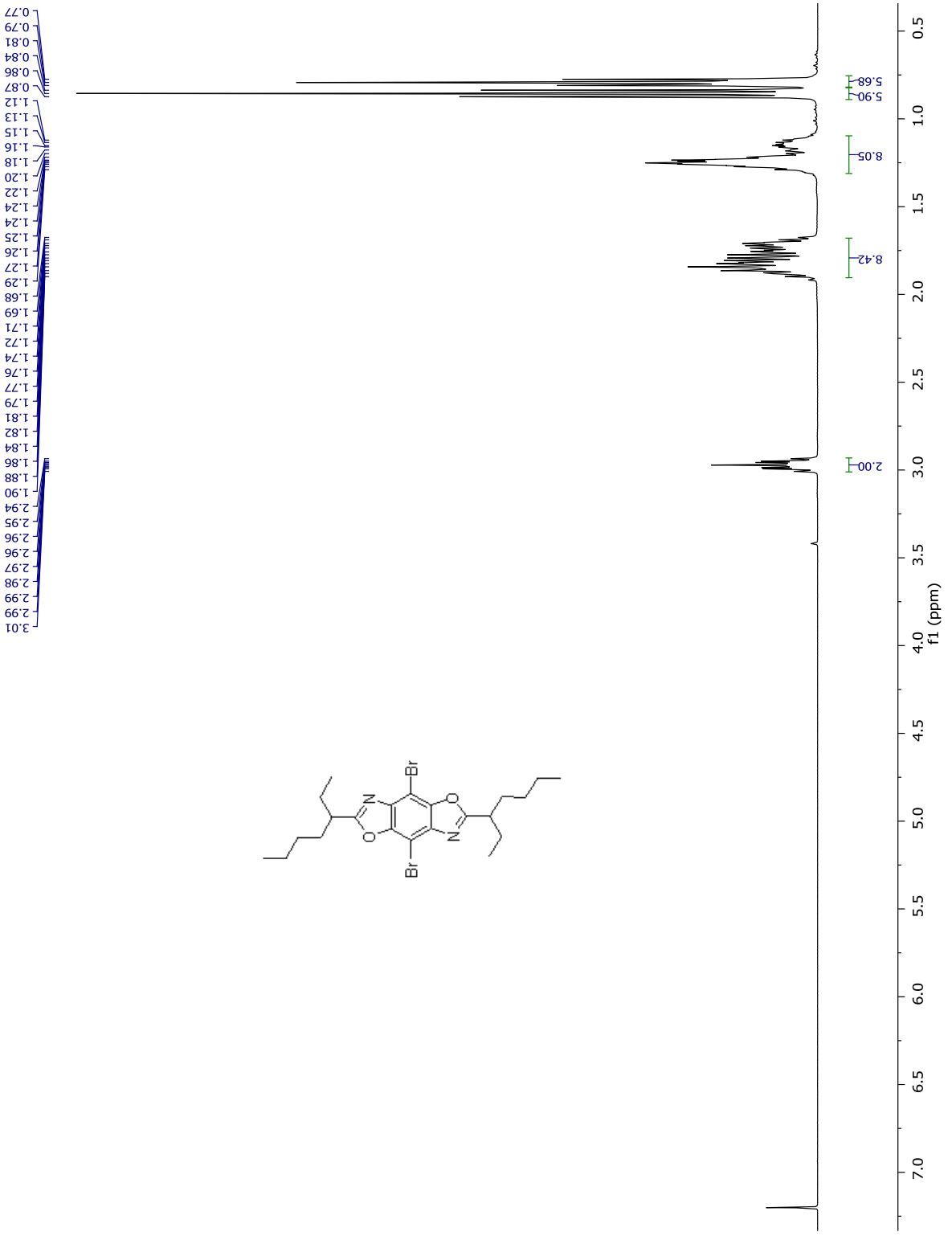

Figure S5.5. ^{1}H NMR spectrum of **3.**

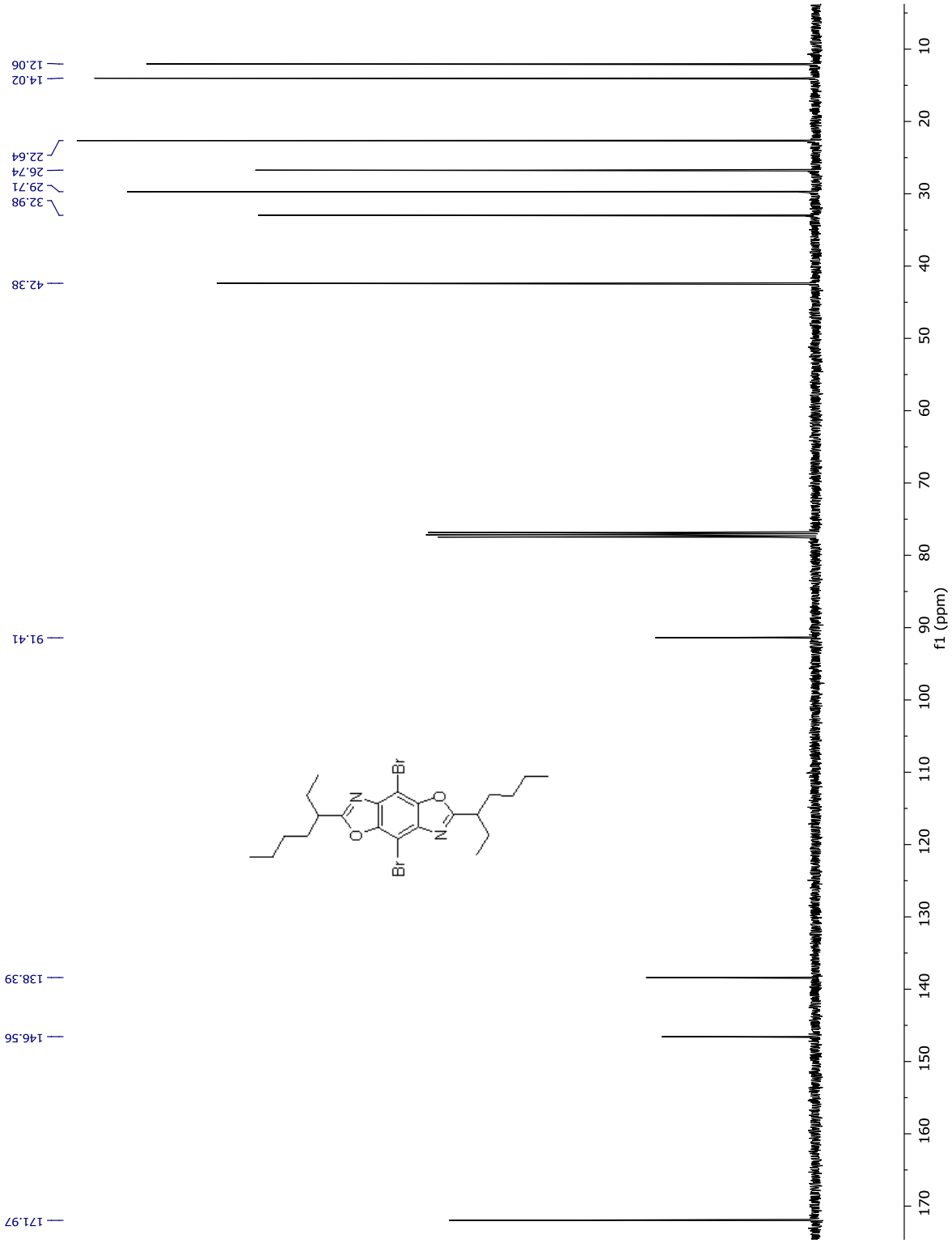

Figure S5.6. ^{13}C NMR spectrum of **3.**

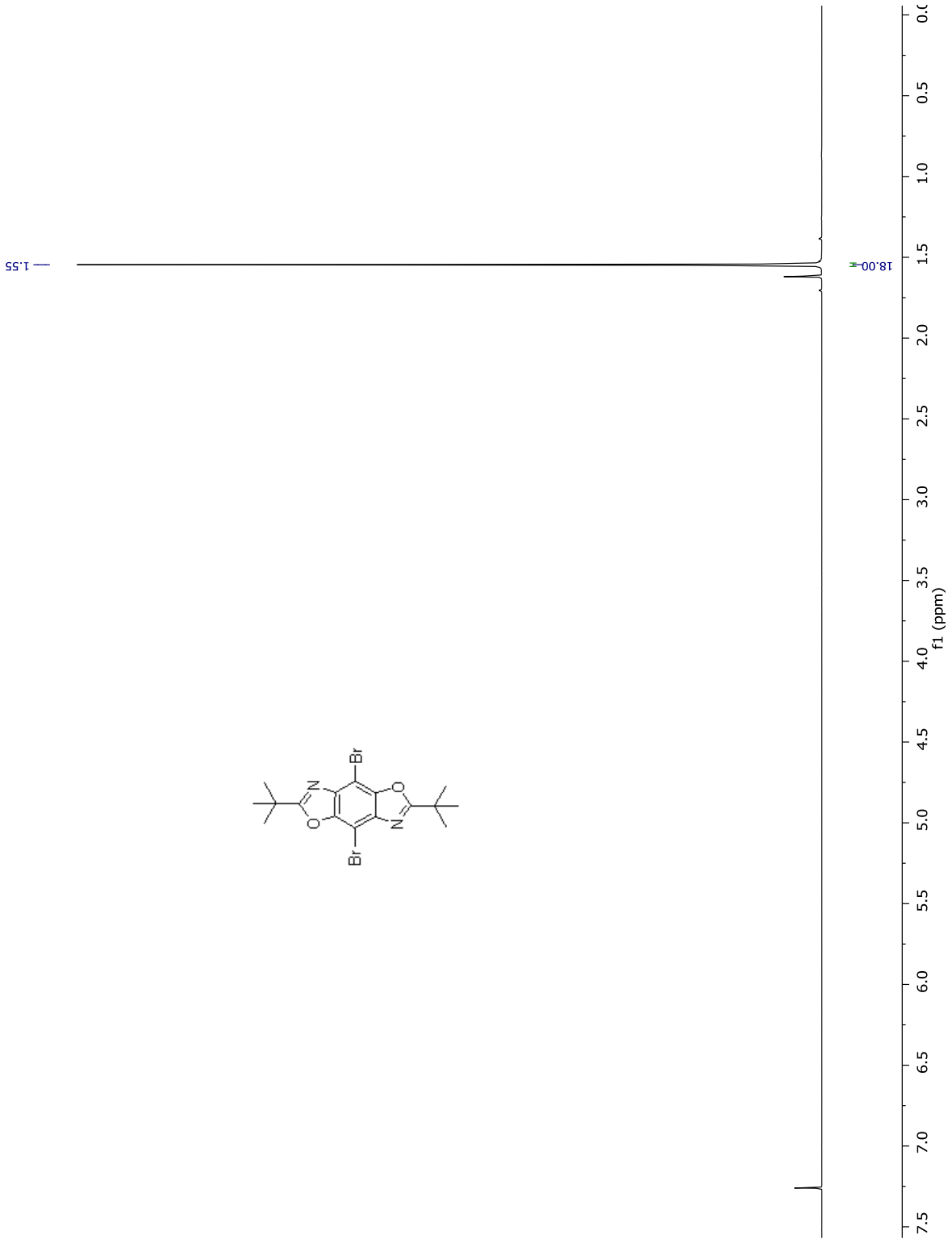

Figure S5.7. ^{1}H NMR spectrum of **4.**

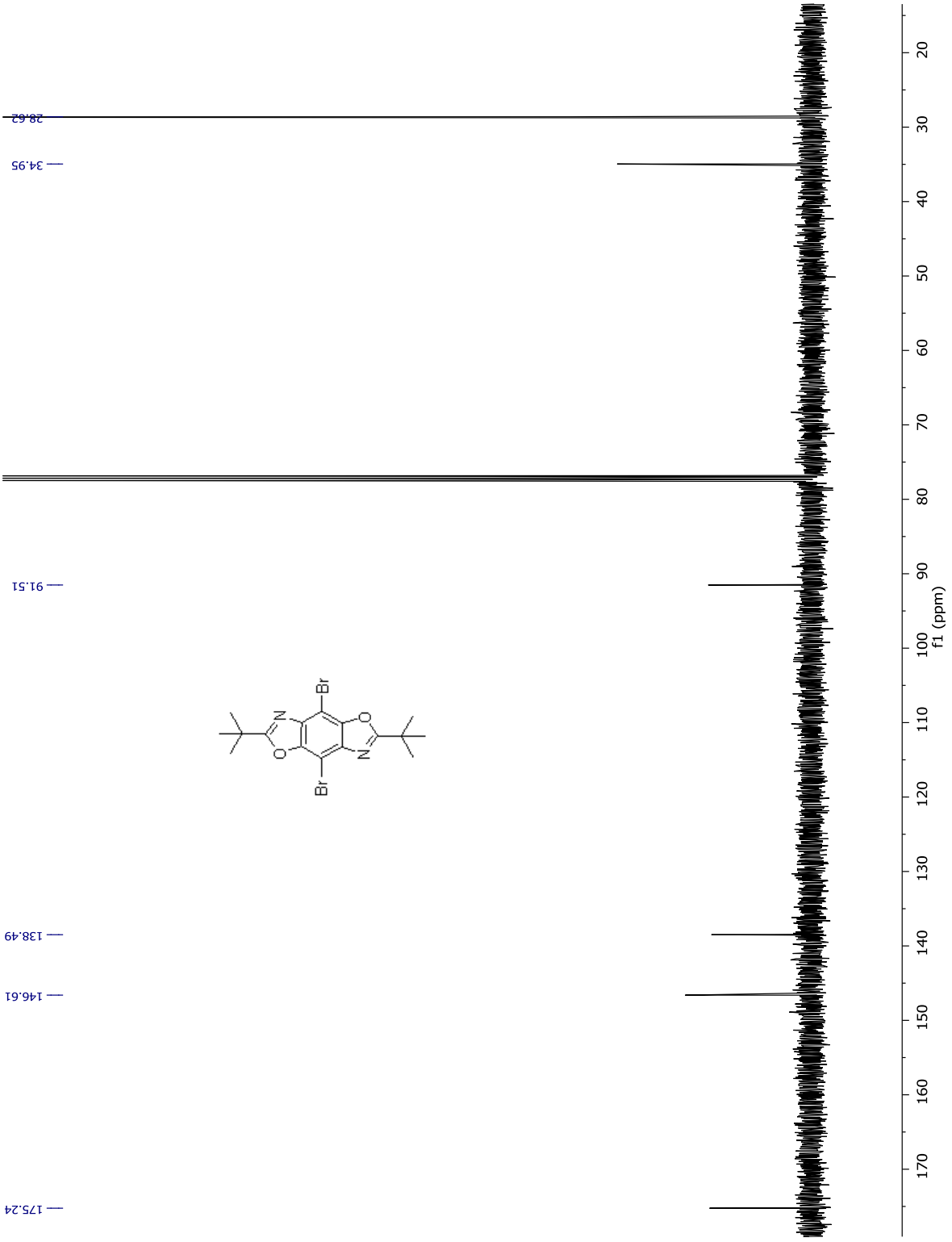

Figure S5.8. ^{13}C NMR spectrum of **4.**

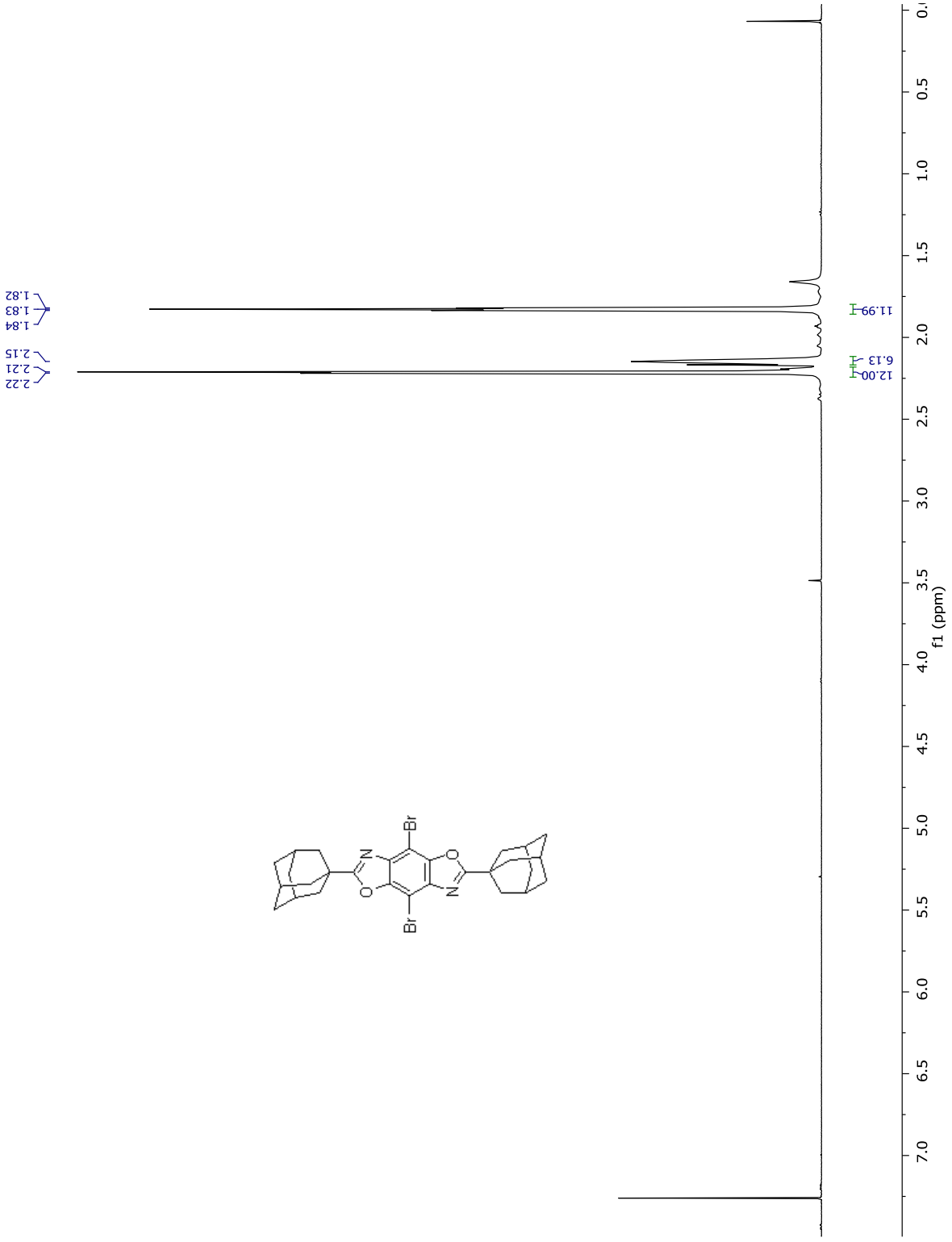

Figure S5.9. ^{1}H NMR spectrum of **5.**

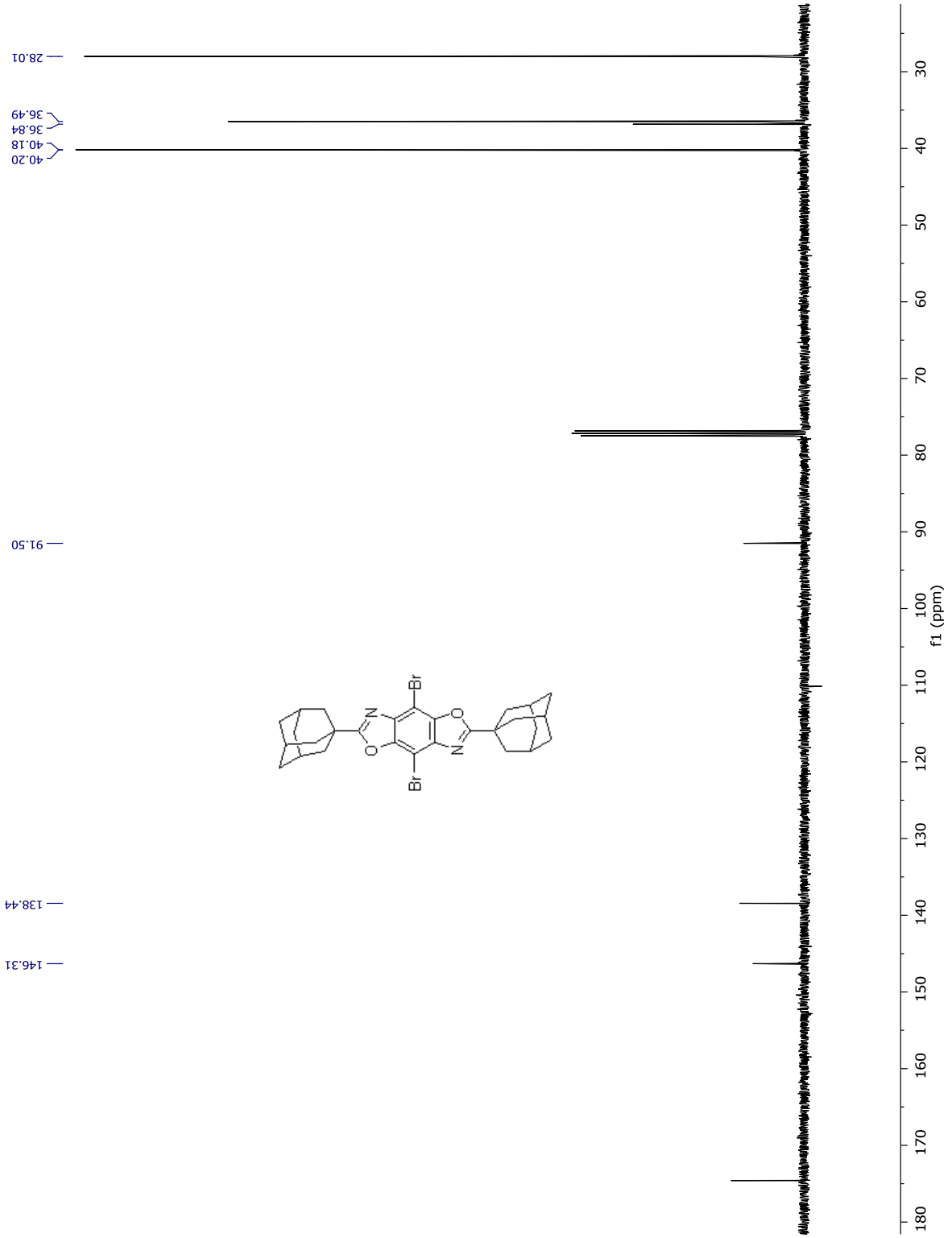

Figure S5.10. ^{13}C NMR spectrum of **5.**

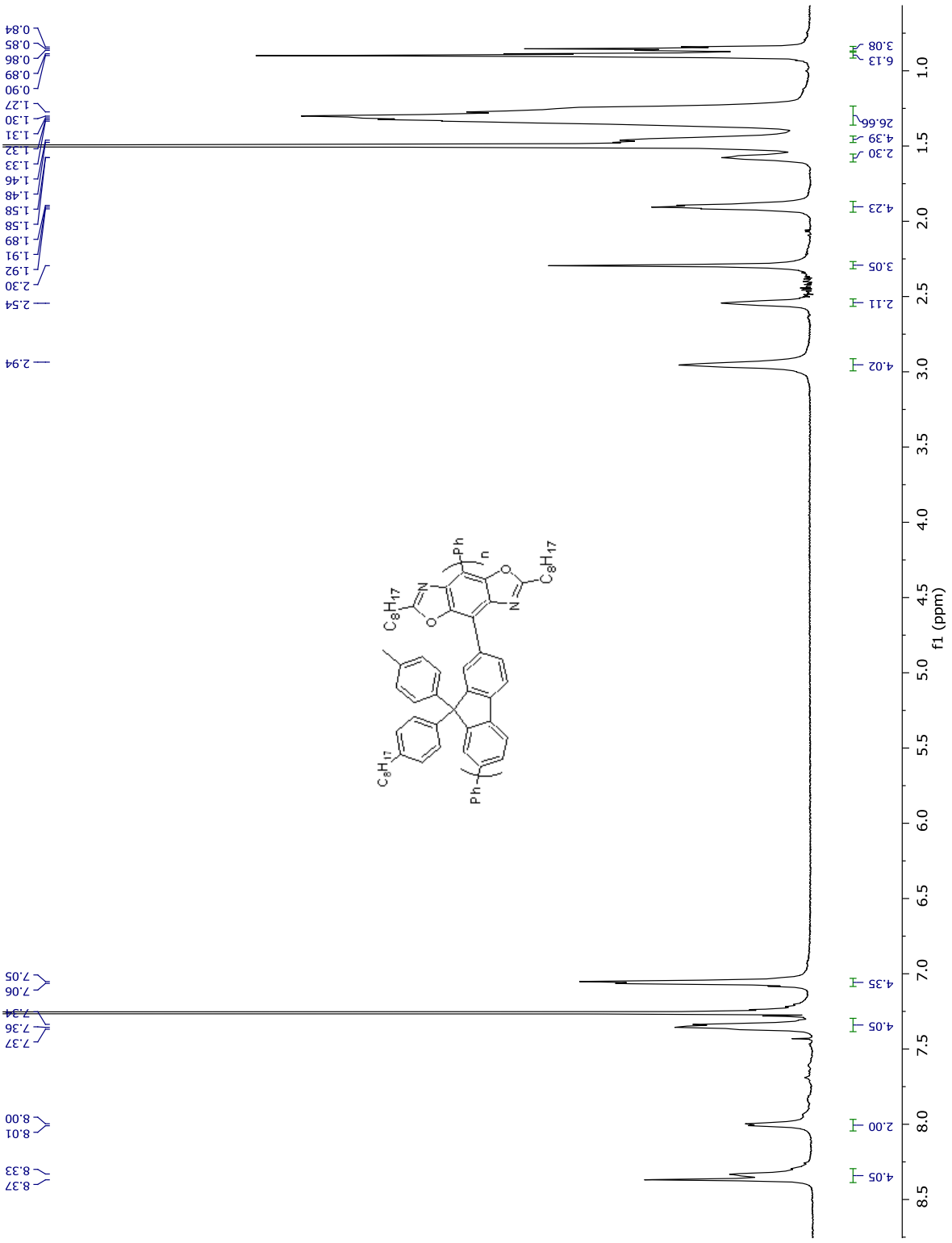

Figure S5.11. ^{1}H NMR spectrum of **P1.**

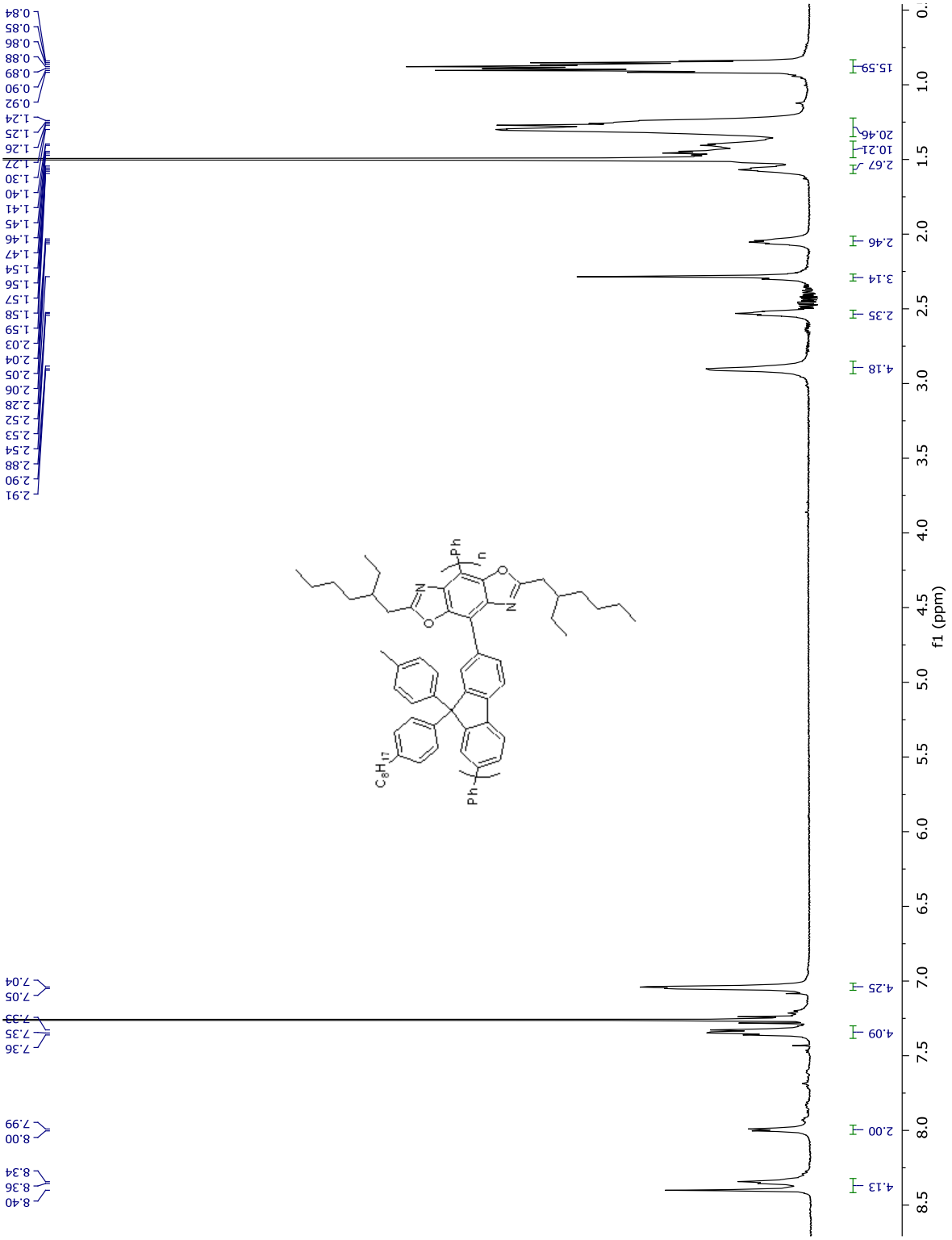

Figure S5.12. ^{1}H NMR spectrum of **P2.**

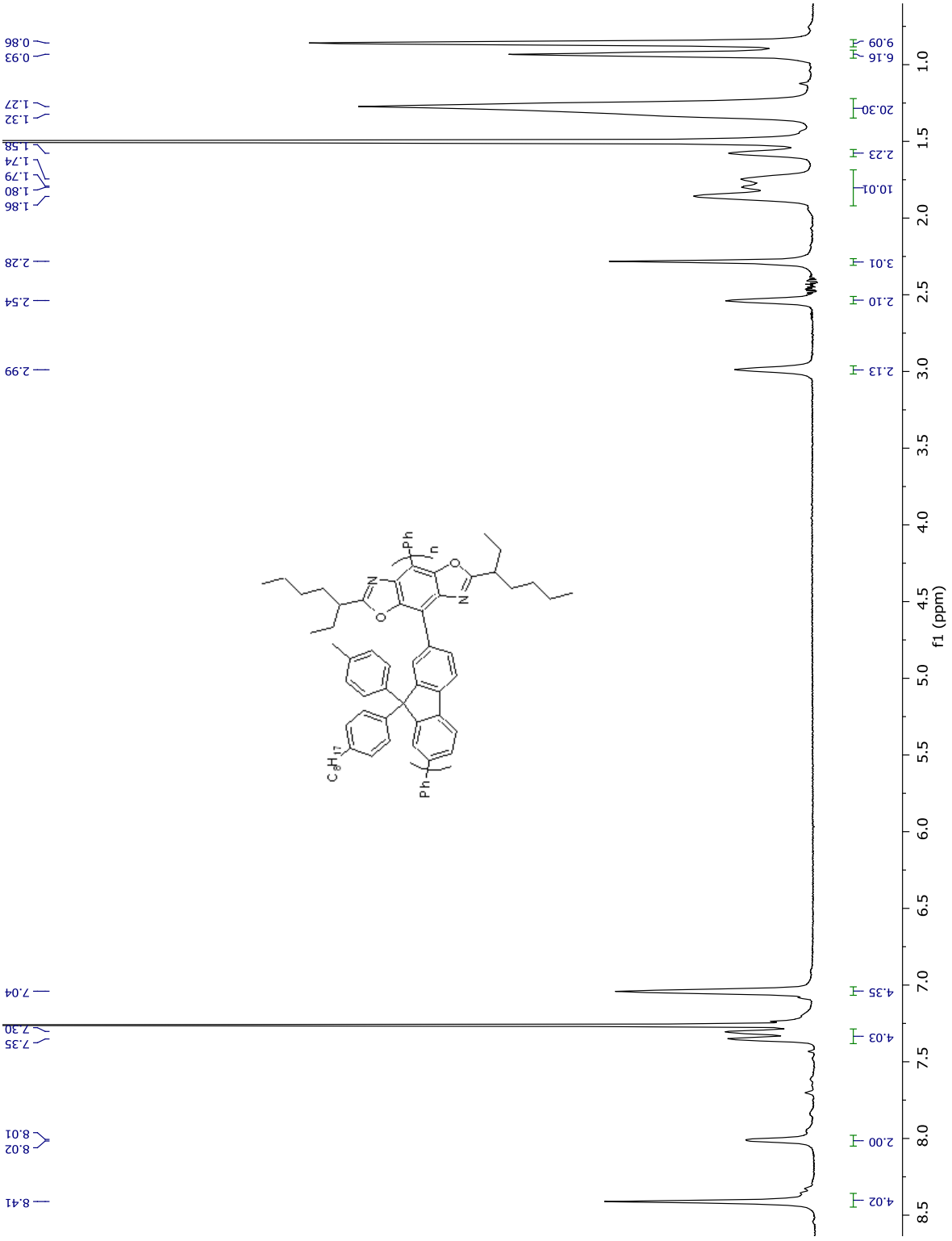

Figure S5.13. ^{1}H NMR spectrum of **P3.**

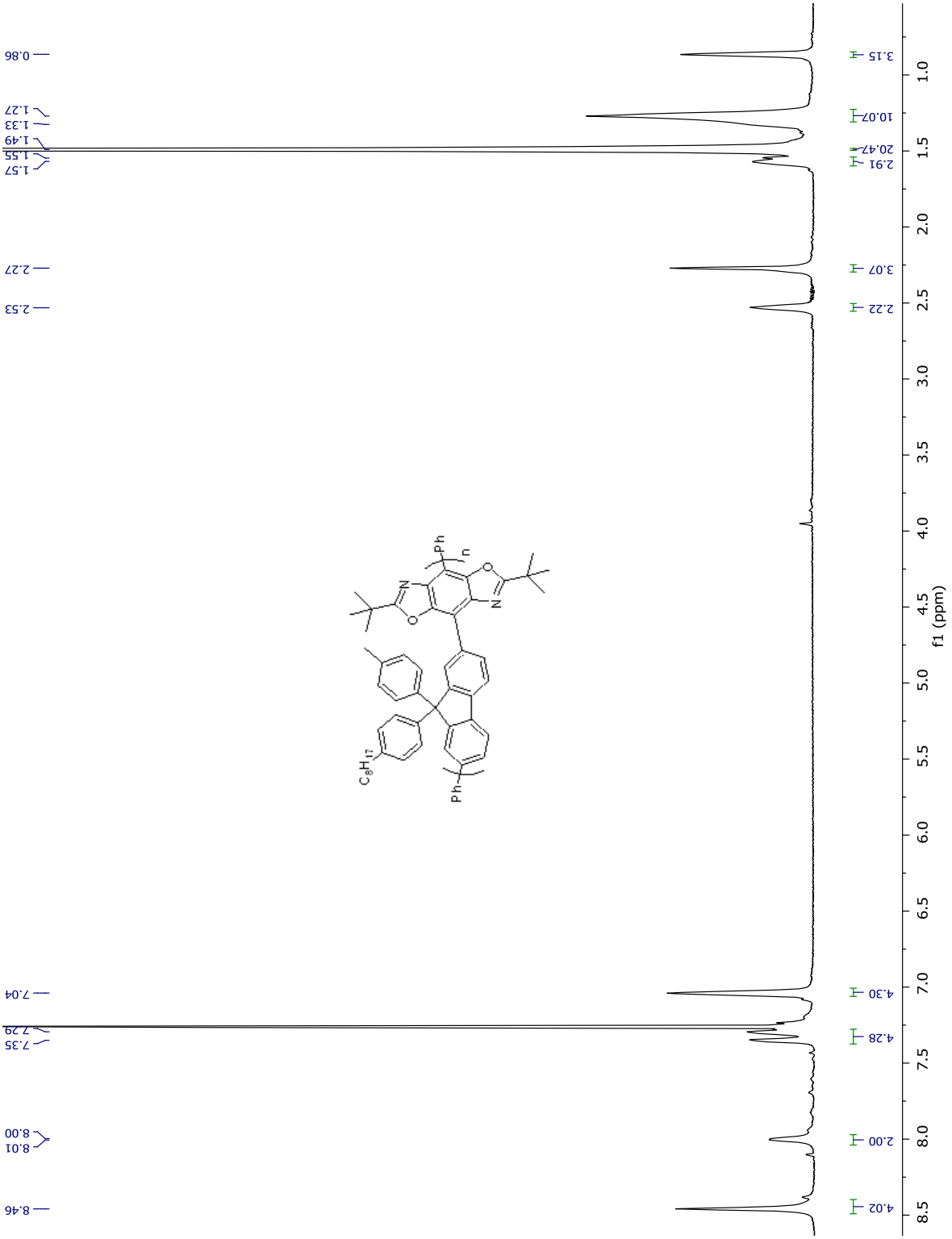

Figure S5.14. ^{1}H NMR spectrum of **P4.**

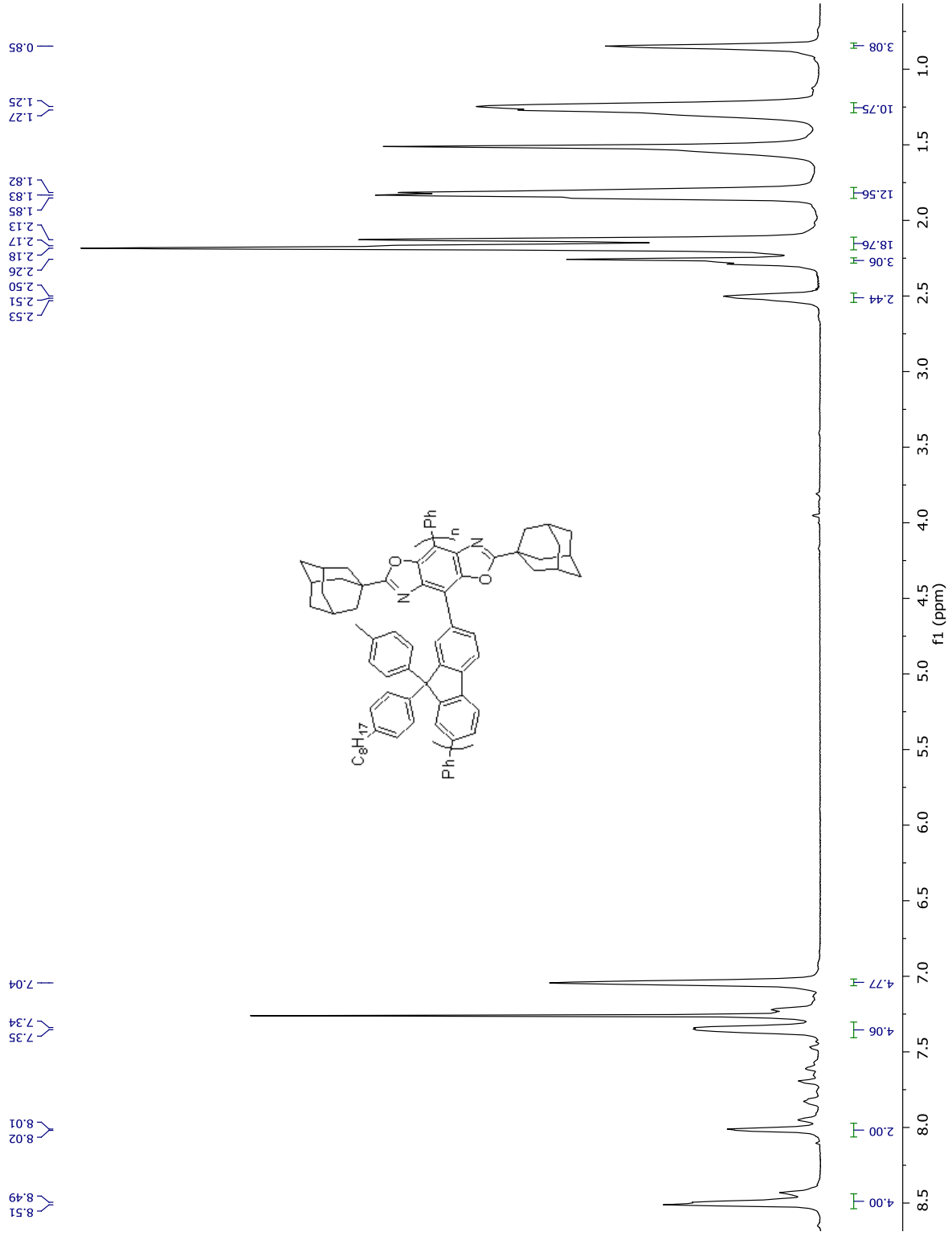

Figure S5.15. ^{1}H NMR spectrum of **P5.**

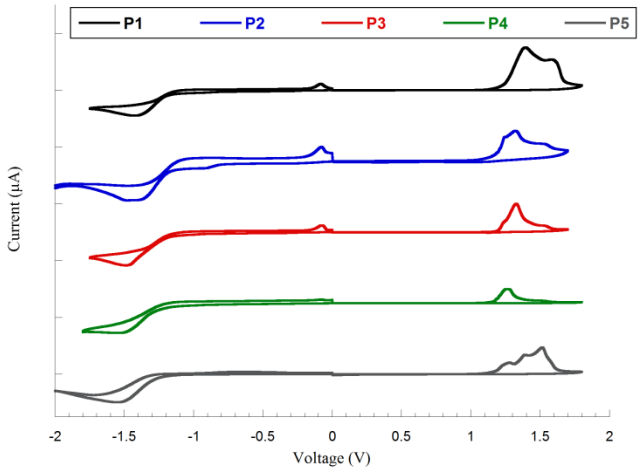

Figure S5.16. Cyclic voltametry traces of **P1 – P5.**

5.8 References

(1) Sirringhaus, H.; Kawase, T.; Friend, R. H.; Shimoda, T.; Inbasekaran, M.; Wu, W.; Woo, E. P. *Science (Washington, D. C.)* **2000**, *290*, 2123. (2) Krebs, F. C.; Tromholt, T.; Jorgensen, M. *Nanoscale* **2010**, *2*, 873.

(3) Mori, K.; Ning, T.; Ichikawa, M.; Koyama, T.; Taniguchi, Y. *Jpn. J. Appl. Phys., Part 2* **2000**, *39*, L942.

(4) Holder, E.; Langeveld, B. M. W.; Schubert, U. S. *Advanced Materials* **2005**, *17*, 1109.

(5) Tsuboyama, A.; Iwawaki, H.; Furugori, M.; Mukaide, T.; Kamatani, J.; Igawa, S.; Moriyama, T.; Miura, S.; Takiguchi, T.; Okada, S.; Hoshino, M.; Ueno, K. *Journal of the American Chemical Society* **2003**, *125*, 12971.

(6) Grimsdale, A. C.; Leok Chan, K.; Martin, R. E.; Jokisz, P. G.; Holmes, A. B. *Chemical Reviews* **2009**, *109*, 897.

(7) Kraft, A.; Grimsdale, A. C.; Holmes, A. B. *Angewandte Chemie International Edition* **1998**, *37*, 402.

(8) Friend, R. H.; Gymer, R. W.; Holmes, A. B.; Burroughes, J. H.; Marks, R. N.; Taliani, C.; Bradley, D. D. C.; Dos Santos, D. A.; Bredas, J. L.; Logdlund, M.; Salaneck, W. R. *Nature* **1999**, *397*, 121.

(9) Bernius, M. T.; Inbasekaran, M.; O'Brien, J.; Wu, W. *Advanced Materials* **2000**, *12*, 1737.

(10) Tseng, S. R.; Chen, Y. S.; Meng, H. F.; Lai, H. C.; Yeh, C. H.; Horng, S. F.; Liao, H. H.; Hsu, C. S. *Synthetic Metals* **2009**, *159*, 137.

(11) Ahmed, E.; Kim, F. S.; Xin, H.; Jenekhe, S. A. *Macromolecules* **2009**, *42*, 8615.

(12) Alam, M. M.; Jenekhe, S. A. *Chemistry of Materials* **2002**, *14*, 4775.

(13) Babel, A.; Jenekhe, S. A. *Advanced Materials* **2002**, *14*, 371.

(14) Babel, A.; Jenekhe, S. A. *The Journal of Physical Chemistry B* **2002**, *106*, 6129.

(15) Jenekhe, S. A.; de Paor, L. R.; Chen, X. L.; Tarkka, R. M. *Chemistry of Materials* **1996**, *8*, 2401.

(16) Feng, D.; Wang, S.; Zhuang, Q.; Wu, P.; Han, Z. *Polymer* **2004**, *45*, 8871.

(17) Chen, Y.; Wang, S.; Zhuang, Q.; Li, X.; Wu, P.; Han, Z. *Macromolecules* **2005**, *38*, 9873.

(18) Wolfe, J. F.; Loo, B. H.; Arnold, F. E. *Macromolecules* **1981**, *14*, 915.

(19) Wolfe, J. F.; Arnold, F. E. *Macromolecules* **1981**, *14*, 909.

(20) Mike, J. F.; Intemann, J. J.; Cai, M.; Xiao, T.; Shinar, R.; Shinar, J.; Jeffries-El, M. *Polymer Chemistry* **2011**, *2*, 2299.

(21) Intemann, J.; Mike, J.; Cai, M.; Bose, S.; Xiao, T.; Mauldin, T.; Roggers, R.; Shinar, J.; Shinar, R.; Jeffries-EL, M. *Macromolecules* **2011**, *44*, 248.

(22) Intemann, J. J.; Hellerich, E. S.; Tlach, B. C.; Ewan, M. D.; Barnes, C. A.; Bhuwalka, A.; Cai, M.; Shinar, J.; Shinar, R.; Jeffries-El, M. *Macromolecules* **2012**, *45*, 6888.

(23) Intemann, J. J.; Mike, J. F.; Cai, M.; Barnes, C. A.; Xiao, T.; Roggers, R. A.; Shinar, J.; Shinar, R.; Jeffries-El, M. *Journal of Polymer Science Part A: Polymer Chemistry* **2013**, *51*, 916.

(24) Grisorio, R.; Allegretta, G.; Mastrorilli, P.; Suranna, G. P. *Macromolecules* **2011**, *44*, 7977.

(25) Mike, J. F.; Makowski, A. J.; Jeffries-EL, M. *Organic Letters* **2008**, *10*, 4915.

(26) Mike, J. F.; Inteman, J. J.; Ellern, A.; Jeffries-El, M. *The Journal of Organic Chemistry* **2009**, *75*, 495.

(27) Mike, J. F.; Makowski, A. J.; Mauldin, T. C.; Jeffries-El, M. *Journal of Polymer Science Part A: Polymer Chemistry* **2010**, *48*, 1456.

(28) Tlach, B. C.; Tomlinson, A. L.; Bhuwalka, A.; Jeffries-El, M. *The Journal of Organic Chemistry* **2011**, *76*, 8670.

(29) Bhuwalka, A.; Mike, J. F.; He, M.; Intemann, J. J.; Nelson, T.; Ewan, M. D.; Roggers, R. A.; Lin, Z.; Jeffries-El, M. *Macromolecules* **2011**.

(30) Tlach, B. C.; Tomlinson, A. L.; Ryno, A. G.; Knoble, D. D.; Drochner, D. L.; Krager, K. J.; Jeffries-El, M. *The Journal of Organic Chemistry* **2013**, *78*, 6570.

(31) De Bo, G.; Marko, I. E. *Eur. J. Org. Chem.* **2011**, 1859.

(32) Bastug, G.; Eviolitte, C.; Marko, I. E. *Org. Lett.* **2012**, *14*, 3502.

(33) Tschitschibabin, A. E. *Ber.* **1905**, *38*, 561.

(34) Intemann, J. J.; Mike, J. F.; Cai, M.; Bose, S.; Xiao, T.; Mauldin, T. C.; Roggers, R. A.; Shinar, J.; Shinar, R.; Jeffries-El, M. *Macromolecules* **2010**, *44*, 248.

(35) Tan, Y.; Gu, Z.; Tsuchiya, K.; Ogino, K. *Polymer* **2012**, *53*, 1444.

(36) Jenekhe, S. A.; Osaheni, J. A. *Science* **1994**, *265*, 765.

(37) Bürgi, L.; Richards, T. J.; Friend, R. H.; Sirringhaus, H. *Journal of Applied Physics* **2003**, *94*, 6129.

(38) Cardona, C. M.; Li, W.; Kaifer, A. E.; Stockdale, D.; Bazan, G. C. *Advanced Materials* **2011**, *23*, 2367.

(39) Morris, J. V.; Mahaney, M. A.; Huber, J. R. *The Journal of Physical Chemistry* **1976**, *80*, 969.

(40) Sista, P.; Nguyen, H.; Murphy, J. W.; Hao, J.; Dei, D. K.; Palaniappan, K.; Servello, J.; Kularatne, R. S.; Gnade, B. E.; Xue, B.; Dastoor, P. C.; Biewer, M. C.; Stefan, M. C. *Macromolecules* **2010**, *43*, 8063.

(41) Imamoto, T.; Matsumoto, T.; Yokoyama, H.; Yokoyama, M.; Yamaguchi, K. *The Journal of Organic Chemistry* **1984**, *49*, 1105.

CHAPTER 6

GENERAL CONCLUSIONS

6.1 Future Research

A focus of this dissertation has been the synthesis of symmetric benzobisazoles. To date, there is no methodology reported for the effective synthesis of asymmetric benzobisazoles due to the difficulty of preparing the required asymmetric starting materials. These systems could be developed for linear donor-acceptor small molecules. Due to the asymmetry, selectively building larger conjugated systems should be simplified compared to other systems and give added versatility to the BBO system. One method of synthesizing oxazoles is a dehydrative condensation of *o*-amidophenols with either PPA or Eaton's Reagent.

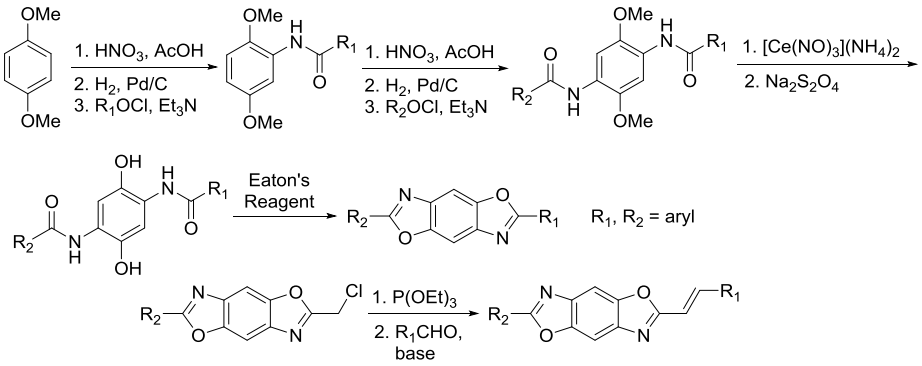

Scheme 6.1. Synthesis of asymmetric BBOs.

Synthesizing 2,5-diamidobenzene-1,4-diol with two different amide groups followed by concurrent condensation of both amides to the oxazole yields an asymmetric BBO (Scheme

6.1). Furthermore if chloroacetyl chloride is utilized, an Arbusov reaction could be performed and conjugation extended through vinyl linkages much like the symmetric dyes[1] and polymers[2-5] designed by our research group. As we have shown, this method is very mild and has good functional group tolerance. Our previously reported vinylene-linked benzobisazole polymers showed moderate efficiencies in PLEDs while other polymers incorporated into OPVs showed very poor efficiency. However, the poor OPV performance was likely a result of poor device engineering and the relatively wide band gaps, low molecular weight, and non-ideal thin film morphology of the polymers.

Several research groups have demonstrated the ability to functionalize the 4,8-axis of BBOs with several alkynes[6-9] and aryl groups[10,11] to create cross-conjugated cruciforms and polymers. The cross-conjugation has shown great ability to tune the properties of small molecules; however, the effect is diminished in conjugated polymers and limits the polymer solubility.

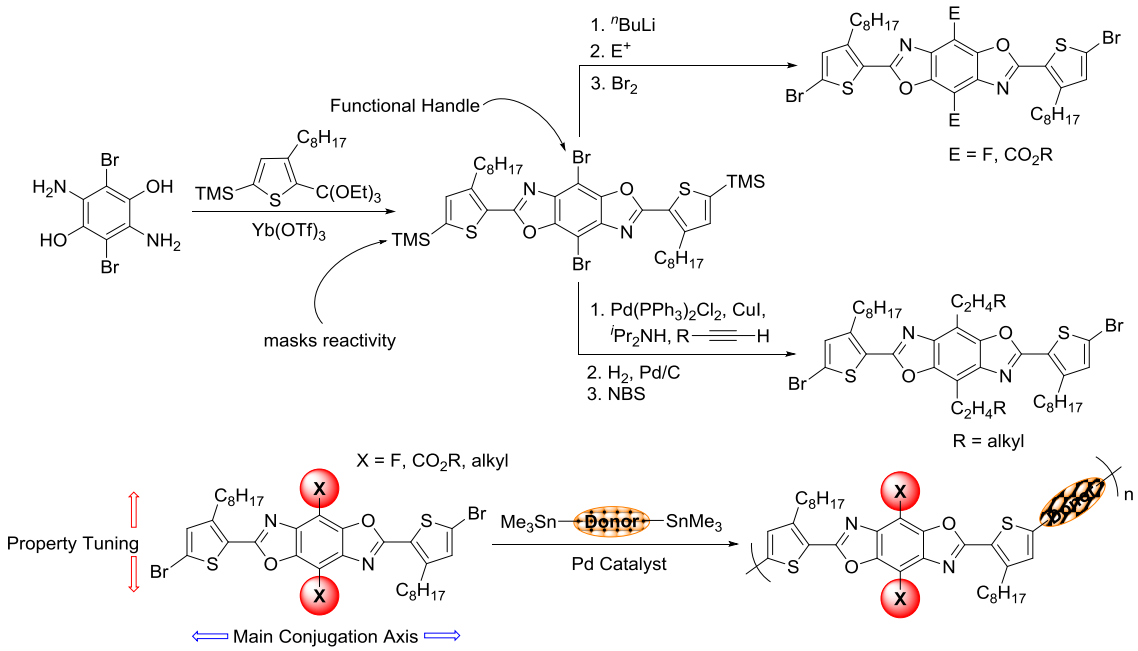

Scheme 6.2. Routes to 4,8-difunctionalized BBOs and their polymerization.

Another method of tuning the optoelectronic properties is through the incorporation of electron-withdrawing or electron-donating substituents. Since BBO is a weak acceptor, functionalization to increase acceptor strength should provide narrower band gap D-A polymers or small-molecules. Hegedus and co-workers were successful in functionalizing the 4,8-position through metal-halogen exchange followed by quenching with electrophiles to yield 4,8-difunctionalized BBOs which were then ring-opened to yield functionalized 1,4-benzoquinones.[12] Utilizing this methodology and foregoing the separate ring-opening step allows the decoration of BBO with electron-withdrawing groups such as fluorines or esters which should increase the acceptor strength of the BBO core. These new BBO acceptors could be polymerized with donor monomers to yield donor-acceptor copolymers as shown in Scheme 6.2.

We have previously reported narrower band gap BBO polymers for use in OPVs and OFETs. Unfortunately most of these materials were low molecular weight due to limited solubility which limits charge mobility, affects thin film morphology, and can lower overall device performance. To improve solubility, additional alkyl chains could be appended to the BBO core. The bromine atoms are excellent functional handles for alkyl chain installation through alkyl-aryl cross-coupling reactions. This has proved difficult in our hands as we have been unsuccessful in performing Suzuki, Kumada, or Negishi alkyl-aryl cross-couplings on 4,8-dibromoBBOs to yield 4,8-dialkylBBOs. However, we have been successful in installing alkylethynyl groups on the 4,8-positions utilizing a Sonogashira cross-coupling. These alkynes could be used as precursors to alkanes through hydrogenation (Scheme 6.2). This type of methodology has proven successful for alkyl chain installation on similar systems.[13,14]

Although conjugated polymers have garnered much attention in OPVs, there has been an increased focus on conjugated small molecules for use in OPVs and OLEDs. Small molecules are monodisperse allowing for batch-to-batch reproducibility, improved solubility, and purification by standard techniques such as recrystallization or column chromatography. Several small molecules for OPVs have been reported with efficiencies in bulk heterojunction solar cells reported as high as 10%.[15] Another possible strategy of building small molecules for OPVs is through the use of two-dimensional cruciform type structures. Cruciforms show tunable optical, electronic, and physical properties through synthetic modification of each arm much like conjugated polymers one-dimensional small-molecules. However, the spatially separated FMOs of cruciforms would allow for several unique design strategies. By careful synthetic design, the HOMO and LUMO of the cruciform can be localized to separate axes which allows for independent tuning of the HOMO and LUMO which modulates the band gap and promotes ICT. This type of molecular structure should allow for straightforward and simple molecular engineering to optimize the band gap, energy levels, and absorption should be very straightforward. BBOs are well-suited for cruciform design as the 4,8-axis shows pre-disposition to isolate the HOMO while the LUMO preferentially aligns along the 2,6-axis. Each axis can be functionalized with orthogonal reactions with the 2,6-axis functionalized through a mild acid chloride or orthoester condensation while the 4,8-axis can be functionalized through a variety of cross-coupling reactions (Scheme 6.3). The side chains of the cruciforms can also be engineered to improve morphology of the materials in neat or blended films by judicious alkyl chain selection that optimize π–π stacking, crystallinity, and solubility.

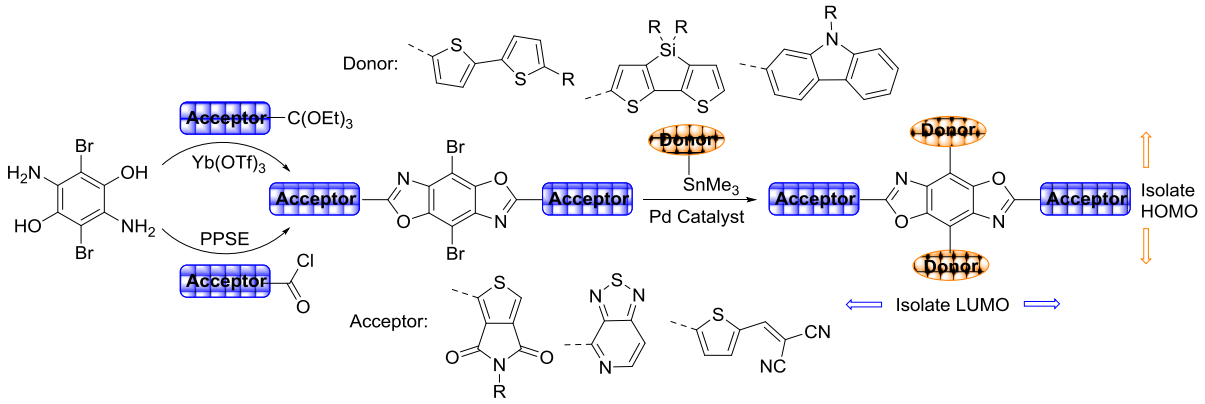

Scheme 6.3. Synthesis of donor-acceptor BBO cruciforms where R = alkyl.

While narrow band gap cruciforms could find applications in OPVs, wider band gap materials have been shown to be excellent chromophores with relatively high quantum yields. Our group has found that fluorene and carbazole containing BBOs can achieve quantum yields in solution as high as 0.68 in polymers[16] and 0.80 in small molecules[10] that emit in the blue region. Dr. Jeremy Intemann also demonstrated that copolymers of BBO and fluorene can be incorporated into blue PLEDs with moderate efficiencies. BBO cruciforms substituted with fluorene, carbazole, or phenyl groups (Figure 6.1) may provide even higher efficiencies as monodisperse materials. Furthermore, the twisting along the 4,8-axis can disrupt the π – π stacking and increase PLED performance by suppressing aggregation induced quenching and exiplex formation. The smaller size of the molecules may further reduce aggregation compared to long polymer chains.

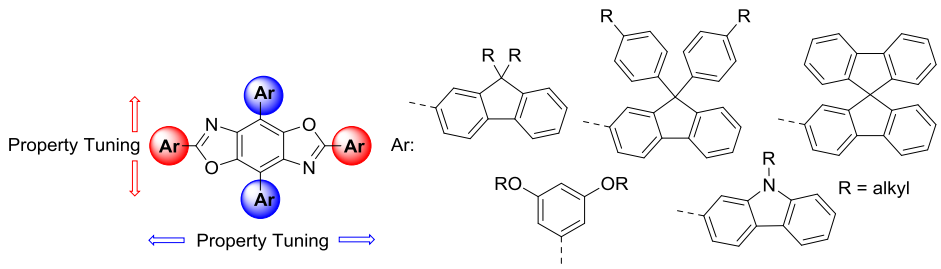

Figure 6.1. Design of wide band gap BBO cruciforms.

To expedite the process of structural design, theoretical modeling could be used to predict the emission of the cruciforms to decrease the number of structural iterations that would need to be synthesized.

6.2 Conclusions

In the past six years, our group has extensively investigated the synthetic versatility and limitations of BBOs as a very versatile rigid-rod aromatic core. The excellent chemical and physical stability of the original PBAs motivated us to investigate this core for organic semiconductor applications. The original methods of synthesizing benzobisazole small molecules and polymers required very harsh reaction conditions, had low functional group tolerance, were insoluble in organic solvents, and in general, inappropriate for organic semiconductor applications. To circumvent this issue, we have developed several methods mildly synthesis and functionalize BBOs with great functional group tolerance to yield a diverse library of organic solvent soluble BBO compounds. The ability to independently functionalize two separate conjugation axes using orthogonal methods makes BBO one of the most versatile aromatic building blocks for conjugated small molecules and polymers. By utilizing the two conjugation axes, materials with very diverse optical, electronic, and physical properties for a broad range of applications have been synthesized.

The functionalization of BBOs leads to changes in their properties, however, the changes of main conjugation axis and type of substituent lead to intricate structure-property relationships. Through studying different series of BBO compounds, we have identified common trends this system. In order to streamline the design of new BBO small molecules and polymers, we have utilized theoretical calculations and modeling to predict the optical

and electronic properties along with the optimized molecular structures. The trends predicted closely match the experimental properties demonstrating its utility in the design of new materials to decrease synthetic time and cost. Furthermore, the modeled FMOs and optimized molecular structures have also been very insightful to understand the trends that were observed experimentally. The ability to functionalize BBOs and their unique properties should make them great candidates for the development of conjugated materials for organic semiconductors.

Our group has shown that BBO-based polymers can be incorporated into OPVs and OLEDs. So far the OLEDs have shown greater improvement than the materials for OPVs, however, both are lower than those reported in literature. From the increased understanding of the BBO system afforded by the trends and properties described in this dissertation, rationally designing higher performing BBO materials should be possible. From our studies, we have also developed the necessary methodology to synthesize new BBO materials and demonstrated unique properties that are not present in other systems. By utilizing our ability to accurately model the systems, we can isolate which derivatives with the greatest potential and focus on the most promising materials. Taking advantage of the versatility of the BBO system, further research should yield promising new materials that provide improved performance in organic semiconductors.

6.3 Acknowledgements

I would like to extend my greatest gratitude to my advisor Dr. Malika Jeffries-EL who has provided guidance, wisdom, and support the last six years and constantly pushed me to find my own answers and make myself better each day. Without her mentoring, I would

not be the scientist and chemist I am today. I would also like to thank my committee members George Kraus, Arthur Winter, Javier Vela, and Sumit Chaudhary for their commitment and guidance in helping me obtain my PhD. I also need to give a tremendous amount of credit to my instructors and professors at West Hancock, Loras College, and Iowa State that have pushed me intellectually and taught me so much. I would also like to thank Iowa State University and the Department of Chemistry for their support and giving me the opportunity to study at such a great university. I would also like to thank the awesome current and past members of the Jeffries-EL researcher group: Dr. Jared Mike, Dr. Jeremy Intemann, Dr. Brandon Kobilka, Dr. Balaji Ganapathy, Achala Bhuwalka, Dana Drochner, Benjamin Hale, Monique Ewan, Ramiro Chavez, Evan Muller, Drew Makowski, Robyn Laskowski, and James Klimavicz. I have learned so much from all of you and I would not want to take this crazy journey with anyone else. I also have to give a great deal of credit to my collaborators, Atta Gueye, Dr. Elena Sheina, and Dr. Christopher Brown at Plextronics, Inc. and special thanks to Dr. Aimée Tomlinson and her cohort of undergraduates at the University of North Georgia. Without the hard-work and knowledge of Dr. Tomlinson's research group, my research would not have been possible. I would like to thank the honorary group member Michael Zenner for the thermal studies on my materials and for making me feel better about my fashion choices. I would also like to thank Kendra Allen for helping me with my job search, always bringing a smile to lab, and is pretty cool for an engineer. I would also like to thank the dedicated undergraduates, Dawn Knoble, Kyle Krager, and Scott Meester, who synthesized numerous building blocks for my projects and I am grateful to have had the opportunity to mentor such great students. I would like to thank my project funding sources: the American Chemical Society – Petroleum Research Fund

(ACS-PRF), the National Science Foundation (NSF), and 3M. I would also like to thank Anna Prisacari for pushing me to become a better person and to become an active student leader at Iowa State and never being afraid to share her time and talents.

Beyond everything I would like to thank my always supportive and very amazing wife Dr. Vicki Tlach. Thank you for the never ending love, support, and motivation over the last six years (and the two years before that) through the weird hours, late nights, and having to deal with a husband who seemed to spend nearly every nice weekend holed up in lab and most of the time distracted by chemistry. You have been my rock and my hope the last few years and I can't even explain how grateful I am to have you in my life and for getting me out of lab to distract me from chemistry for a while. I would also like to thank my family for their love and support throughout my life. I would especially like to thank my parents for teaching the importance of work ethic, respect, politeness, and loyalty that have made me the man and the scientist I am today. I would also like to thank Rajarshi Roychoudhury for all our chemistry talks, coffee breaks, mental breaks, and the lessons on cricket. I also thank Caribou Coffee, Bookends Café, and Mr. Coffee for providing the caffeine to keep me awake during long days, early mornings, and late nights. Of course I also need to acknowledge the fine meats provided by my parent's farm and allowing me to eat better than any graduate student should. I would also like to thank the fine folks at Welch Ave Station and Hy-Vee Wine & Spirits for providing the necessary libations that kept my sanity mostly intact.

6.4 References

(1) Klimavicz, J. S.; Mike, J. F.; Bhuwalka, A.; Tomlinson, A. L.; Jeffries-El, M. *Pure and Applied Chemistry* **2012**, *84*, 991.

(2) Intemann, J. J.; Mike, J. F.; Cai, M.; Bose, S.; Xiao, T.; Mauldin, T. C.; Roggers, R. A.; Shinar, J.; Shinar, R.; Jeffries-El, M. *Macromolecules* **2010**, *44*, 248.

(3) Mike, J. F.; Makowski, A. J.; Mauldin, T. C.; Jeffries-El, M. *Journal of Polymer Science Part A: Polymer Chemistry* **2010**, *48*, 1456.

(4) Mike, J. F.; Nalwa, K.; Makowski, A. J.; Putnam, D.; Tomlinson, A. L.; Chaudhary, S.; Jeffries-El, M. *Physical Chemistry Chemical Physics* **2011**, *13*, 1338.

(5) Intemann, J. J.; Mike, J. F.; Cai, M.; Barnes, C. A.; Xiao, T.; Roggers, R. A.; Shinar, J.; Shinar, R.; Jeffries-El, M. *Journal of Polymer Science Part A: Polymer Chemistry* **2013**, *51*, 916.

(6) Tlach, B. C.; Tomlinson, A. L.; Bhuwalka, A.; Jeffries-El, M. *The Journal of Organic Chemistry* **2011**, *76*, 8670.

(7) Osowska, K.; Miljanic, O. S. *Chemical Communications* **2010**, *46*, 4276.

(8) Lim, J.; Albright, T. A.; Martin, B. R.; Miljanić, O. Š. *The Journal of Organic Chemistry* **2011**, *76*, 10207.

(9) Tlach, B. C.; Tomlinson, A. L.; Morgan, K. D.; Collins, C. R.; Zenner, M. D.; Jeffries-EL, M. *Australian Journal of Chemistry* **2014**, *67*, 711.

(10) Tlach, B. C.; Tomlinson, A. L.; Ryno, A. G.; Knoble, D. D.; Drochner, D. L.; Krager, K. J.; Jeffries-El, M. *The Journal of Organic Chemistry* **2013**, *78*, 6570.

(11) Klare, J. E.; Tulevski, G. S.; Sugo, K.; de Picciotto, A.; White, K. A.; Nuckolls, C. *Journal of the American Chemical Society* **2003**, *125*, 6030.

(12) Heqedus, L. S.; Odle, R. R.; Winton, P. M.; Weider, P. R. *The Journal of Organic Chemistry* **1982**, *47*, 2607.

(13) Kobilka, B. M.; Dubrovskiy, A. V.; Ewan, M. D.; Tomlinson, A. L.; Larock, R. C.; Chaudhary, S.; Jeffries-El, M. *Chemical Communications* **2012**, *48*, 8919.

(14) Kobilka, B. M.; Hale, B. J.; Ewan, M. D.; Dubrovskiy, A. V.; Nelson, T. L.; Duzhko, V.; Jeffries-El, M. *Polymer Chemistry* **2013**, *4*, 5329.

(15) Liu, Y.; Chen, C.-C.; Hong, Z.; Gao, J.; Yang, Y.; Zhou, H.; Dou, L.; Li, G.; Yang, Y. *Sci. Rep.* **2013**, *3*.

(16) Intemann, J. J.; Hellerich, E. S.; Tlach, B. C.; Ewan, M. D.; Barnes, C. A.; Bhuwalka, A.; Cai, M.; Shinar, J.; Shinar, R.; Jeffries-El, M. *Macromolecules* **2012**, *45*, 6888.

APPENDIX

LIST OF ACRONYMS

Acronym	Description
1-D	One-dimensional
2-D	Two-dimensional
A	Acceptor
ACS	American Chemical Society
APCI	Atmospheric pressure chemical ionization
BBO	Benzobis[1,2-*d*-4,5-*d′*]bisoxazole
BBZT	Benzobis[1,2-*d*-4,5-*d′*]bisthiazole
BDT	Benzo[1,2-*b*:4,5-*b′*]dithiophene
BHJ	Bulk heterojunction
BLA	Bond length alteration
Br-DAHQ	2,5-dibromo-3,6-diamino-1,4-hydroquinone
CP	Conjugated polymer
CV	Cyclic voltametry
D	Donor
DABDT	2,5-diaminobenzene-1,4-dithiol
DAHQ	2,5-diaminobenzene-1,4-diol bishydrochloride
DAR	2,4-diaminorescorcinol bishydrochloride
DFT	Density functional theory

DMA	Dimethylacetamide
DMF	Dimethylformamide
DMSO	Dimethyl sulfoxide
DP_n	Degree of polymerization
DSC	Differential scanning calorimetry
E_g^{EC}	Electrochemical band gap
E_g^{opt}	Optical band gap
EI	Electron impact
E_{ox}^{onset}	Oxidation onset potential
E_{red}^{onset}	Reduction onset potential
ESI	Electrospray ionization
ESP	Electrostatic potential
Et_2O	Diethyl ether
Fc/Fc^+	Ferrocene/ferrocenium
FET	Field effect transistor
FMO	Frontier molecular orbital
GPC	Gel permeation chromatography
GTO	Gaussian-type orbital
HF	Hartree-Fock
HMW	High molecular weight
HOMO	Highest occupied molecular orbital
HRMS	High resolution mass spectrometry
HWE	Horner-Wadsworth-Emmons

ICT	Intermolecular charge transfer
ISU	Iowa State University
LMW	Low molecular weight
LUMO	Lowest unoccupied molecular orbital
m/z	Mass to charge ratio
MMW	Medium molecular weight
M_n	Number average molecular weight
MO	Molecular orbital
MP	Melting point
M_w	Weight average molecular weight
NMR	Nuclear magnetic resonance
NSF	National Science Foundation
^{o}DCB	*o*-dichlorobenzene
OFET	Organic field effect transistor
OLED	Organic light emitting diode
OPV	Organic photovoltaic
OSC	Organic solar cell
PBA	Poly(benzobisazole)
PDI	Polydisperity index
PITN	Poly(isothianaphthalene)
PL	Photoluminescence
PLED	Polymer light emitting diode
Poly(BBO)	poly(benzobisoxazole)

PPE	Poly(phenylene-ethynylene)
PPP	Poly(*p*-phenylene)
PPSE	Poly(trimethylsilylphosphate)
PPV	Poly(phenylene-vinylene)
PRF	Petroleum Research Fund
PT	Poly(thiophene)
PVC	Photovoltaic cell
SVP	Split valence, polarization of H-atoms
T_d	Decomposition temperature
TDDFT	Time-dependent density functional theory
T_g	Glass transition temperature
TGA	Thermogravimetric analysis
THF	Tetrahydrofuran
TMEDA	*N*,*N*,*N*′,*N*′-tetramethyl-1,2-diaminoethane
UPS	Ultraviolet photoelectron spectroscopy
UV-Vis	Ultraviolet-visible
XSEDE	Extreme Science and Engineering Discovery Environment
ε	Molar absorptivity
λ_{em}	Maximum emission wavelength
λ_{max}	Maximum Absorption wavelength
π-MO	Pi molecular orbital
Φ_{PL}	Relative photoluminescence quantum yield